



# **Novel Chemical Sensors Based on Boronic Acids for Glucose Detection**

Danielle Bruen, B.A. (Mod.)

*Submission for the Degree Doctor of Philosophy (PhD)*

*July 2018*

Supervisors: Prof. Dermot Diamond

Dr. Larisa Florea

*Insight Centre for Data Analytics, National Centre for Sensor Research,  
School of Chemical Sciences, Dublin City University, Ireland.*

## General Declaration

I hereby certify that this material, which I now submit for assessment on the programme of study leading to the award of PhD is entirely my own work, and that I have exercised reasonable care to ensure that the work is original, and does not, to the best of my knowledge, breach any law of copyright, and has not been taken from the work of others save and to the extent that such work has been cited and acknowledged within the text of my work.

Signed: Danielle Bruen

Date: 13<sup>th</sup> July 2018

(Danielle Bruen; ID: 14212880)



## **Acknowledgements**

First and foremost, many thanks must go to Prof. Dermot Diamond, for this opportunity. To him I am grateful for his guidance and support, as well as the fantastic networking opportunities at home and abroad (especially abroad!). During this degree, I was fortunate to have travelled all over the world and I really appreciated this. In particular, for supporting me on my visit to the University of Wollongong for 3 months. I would also like to thank Prof. Gordon Wallace and Prof. David Officer for all their help and guidance during my visit.

I would like to extend huge thanks to Dr. Larisa Florea. Larisa has been a great friend, mentor and supervisor to look up to. She has always offered great patience, continuous support and encouragement, as well as her immense knowledge for helping me on this journey. I am extremely thankful and indebted to her for this experience.

I would like to extend my sincerest gratitude to Dr. Colm Delaney. Colm has continuously expressed his enthusiasm, valuable expertise and support through this endeavour. His door was always open for any problems I encountered, as well as his valuable comments, suggestions and ideas.

A big thanks must also go to my fellow lab mates, Aishling Dunne, Jennifer Deignan, Wayne Francis, Alex Tudor and Tom Glennon, for all the fun we've had in the last three years, the few scientific discussions and the stress-free distractions! You have made this experience for me.

I would also like to thank the other members of the group Paula Campos, Dr. Margaret McCaul, Dr. Peter McCloskey, Dr. Adam Porter, Andrew Donohoe, Gareth Lacour, Ruairi Barret and undergraduate students who contributed to different aspects of the research, in particular to Adam McColgan, for his hard work, patience and humour.

Last but not least, I would like to thank my family and friends for their continuous support and patience. In particular, thanks to Simon, my sister Robyn and my friends, for their advice, support and friendship throughout. I couldn't have done this without you.

# Contents

<b>General Declaration</b>	<b>(ii)</b>
<b>Acknowledgements</b>	<b>(iii)</b>
<b>Abbreviations</b>	<b>(x)</b>
<b>List of Tables</b>	<b>(xv)</b>
<b>List of Figures</b>	<b>(xvii)</b>
<b>List of Schemes</b>	<b>(xxix)</b>
<b>Thesis Abstract</b>	<b>(xxxix)</b>

<b>Awards and Outputs Generated from this Research</b>	<b>1</b>
--	----------

## **Chapter 1: Literature Survey - Glucose Sensing for Diabetes Monitoring: History and Recent Developments**

<b>1.1 Introduction to Diabetes</b>	<b>8</b>
1.1.1 History of Diabetes Mellitus	9
1.1.2 Types of Diabetes	10
1.1.3 Diabetic Ketoacidosis	12
1.1.4 Treating Diabetes – From Ancient Times to Present	13
1.1.5 Statistics	15
<b>1.2. Glucose Monitoring</b>	<b>17</b>
1.2.1 Glucose Monitoring Methods in Blood From Past to Present	17
1.2.2 Monitoring Glucose in Alternative Physiological Fluids	21
1.2.2.1 <i>Interstitial Fluid</i>	21
1.2.2.2 <i>Urine</i>	25
1.2.2.3 <i>Sweat</i>	26
1.2.2.4 <i>Breath Analysis</i>	31
1.2.2.5 <i>Saliva</i>	33
1.2.2.6 <i>Ocular Fluid</i>	35
<b>1.3 Fluorescence Sensing</b>	<b>40</b>
1.3.1 Phenomena of Fluorescence	40
1.3.2 Mechanisms and Dynamics of Fluorescence Sensing	42
<b>1.4 Boronic Acids</b>	<b>46</b>
1.4.1 Direct Sensing	50
1.4.2 Indirect Sensing	56
<b>1.5 Aim</b>	<b>68</b>
<b>1.6 References</b>	<b>70</b>

<b><u>Chapter 2: Direct Glucose Sensing: Probing Interactions Between Glucose and Fluorescent Boronic Acids</u></b>	<b>83</b>
<b>2.1 Abstract</b>	<b>85</b>
<b>2.2 Introduction</b>	<b>86</b>
<b>2.3 Experimental</b>	<b>88</b>
2.3.1 Materials and Methods	88
2.3.2 General Procedure for the Synthesis of Carboxylic Acid-BA sensors	89
2.3.3 Synthesis of 1-(2-boronobenzyl)-5-carboxyquinolin-1-ium bromide ( <i>o</i> -COOHBA)	90
2.3.4 Synthesis of 1-(3-boronobenzyl)-5-carboxyquinolin-1-ium bromide ( <i>m</i> -COOHBA)	91
2.3.5 Immobilisation of <i>o</i> -COOHBA on to a PDMS ‘Lens’-Like Polymeric Platform	92
<b>2.4 Results and Discussion</b>	<b>93</b>
2.4.1 Glucose Sensing Mechanism	93
2.4.2 Determining the Sensing Range of <i>o</i> -COOHBA and <i>m</i> -COOHBA	94
2.4.3 Fluorescence Glucose-Sensing Using <i>o</i> -COOHBA and <i>m</i> -COOHBA	96
2.4.4 Immobilisation of <i>o</i> -COOHBA on to a PDMS ‘Lens-Like’ Platform and Fluorescence Response to Glucose	98
<b>2.5 Conclusions</b>	<b>100</b>
<b>2.6 Future Work</b>	<b>101</b>
<b>2.6 References</b>	<b>103</b>
<b><u>Chapter 3: Intermolecular Quenching and Recovery of Fluorescence Using Cationic Boronic Acid Derivatives for Indirect Glucose Sensing</u></b>	<b>105</b>
<b>3.1 Abstract</b>	<b>107</b>
<b>3.2 Introduction</b>	<b>108</b>
<b>3.3 Experimental</b>	<b>109</b>
3.3.1 Materials and Methods	109
3.3.2 Synthesis of 1-(2-boronobenzyl)-5-bromopyrimidin-1-ium bromide (BA1) and 1-(3-boronobenzyl)-5-(3-hydroxy-3-methylbut-1-yn-1-yl)pyrimidin-1-ium bromide (BA2)	111
3.3.2.1 <i>Synthesis of BA1</i>	111
3.3.2.2 <i>Synthesis of BA2</i>	112
<b>3.4 Results and Discussion</b>	<b>114</b>
3.4.1 Fluorescence Spectroscopy	114
3.4.1.1 <i>Fluorescence Spectroscopy of BA1</i>	116
3.4.1.2 <i>Fluorescence Spectroscopy of BA2</i>	119
<b>3.5 Conclusion</b>	<b>125</b>
<b>3.6 References</b>	<b>126</b>

<b><u>Chapter 4: Water-Soluble Polymerisable Boronic Acids: Combining an Adaptable One-Step Synthesis with an In-Depth Understanding of pH and Glucose Response</u></b>	<b>128</b>
<b>4.1 Abstract</b>	<b>130</b>
<b>4.2 Introduction</b>	<b>131</b>
<b>4.3 Experimental</b>	<b>133</b>
4.3.1 Materials and Methods	133
4.3.2 Synthesis of BA Monomers ( <i>o</i> -BA, <i>m</i> -BA and <i>p</i> -BA)	134
4.3.2.1 <i>General Synthesis of BA Monomers</i>	134
4.3.2.2 <i>Synthesis of o-BA (N-(2-boronobenzyl)-2-(methacryloyloxy)-N,N-dimethylethan-1-ammonium bromide)</i>	134
4.3.2.3 <i>Synthesis of m-BA (N-(3-boronobenzyl)-2-(methacryloyloxy)-N,N-dimethylethan-1-ammonium bromide)</i>	135
4.3.2.4 <i>Synthesis of p-BA (N-(4-boronobenzyl)-2-(methacryloyloxy)-N,N-dimethylethan-1-ammonium bromide)</i>	136
4.3.3 <sup>11</sup> B NMR Titrations	137
4.3.4 Fluorescence Titrations	138
<b>4.4 Results and Discussion</b>	<b>139</b>
4.4.1 Synthesis of BA Monomers	139
4.4.2 NMR Spectroscopy	139
4.4.2.1 <i><sup>1</sup>H NMR Spectroscopy</i>	139
4.4.2.2 <i><sup>11</sup>B NMR Spectroscopy</i>	140
4.4.3 Fluorescence Spectroscopy	143
4.4.3.1 <i>pH Titrations</i>	143
4.4.3.2 <i>Glucose Titrations</i>	145
<b>4.5 Conclusions and Future Work</b>	<b>148</b>
<b>4.6 References</b>	<b>149</b>
<b><u>Chapter 5: A Two-Component Fluorescent System for Sugar-Sensing</u></b>	<b>152</b>
<b>5.1 Abstract</b>	<b>154</b>
<b>5.2 Introduction</b>	<b>155</b>
<b>5.3 Experimental</b>	<b>157</b>
5.3.1 Materials and Methods	157
5.3.2 Fluorescence Titrations with Hydrogel Cocktails	158
5.3.3 Synthesis of Glucose-Responsive Hydrogels	159
5.3.4 Calculating the Fluorescence Quenching and Sugar Binding Constants	160
<b>5.4 Results and Discussion</b>	<b>161</b>
5.4.1 Fluorescence Quenching with Pyranine with <i>o</i> -BA, <i>m</i> -BA and <i>p</i> -BA	161
5.4.2 Fluorescence Recovery of Pyranine with Monosaccharides	164

<b>5.5 Conclusions</b>	<b>168</b>
<b>5.6 References</b>	<b>169</b>
<b><u>Chapter 6: Future Work: Sugar Sensing Using Boronic Acid Polymers</u></b>	<b>172</b>
<b>6.1 Abstract</b>	<b>175</b>
<b><u>Part A – Indirect Glucose Sensing in Ionogels</u></b>	<b>176</b>
<b>6.2 Introduction</b>	<b>176</b>
<b>6.3 Experimental</b>	<b>179</b>
6.3.1 Materials and Methods	179
6.3.2 Synthesis of Ionogel 1	180
6.3.2.1 <i>Synthesis of Di(trihexyltetradecyl phosphonium) (P<sub>6,6,6,14</sub>) Fluorescein Ionic Liquid (P<sub>6,6,6,14</sub> Fluorescein IL)</i>	180
6.3.2.2 <i>Synthesis of Tetrabutylphosphonium Sulfopropyl Methacrylate (P<sub>4,4,4,4</sub>SPMA) IL Monomer</i>	181
6.3.2.3 <i>Preparation of Ionogel 1</i>	182
6.3.2.4 <i>Synthesis of Cationic BA derivatives, 1-(3-Boronobenzyl)-6-methylquinolin-1-ium bromide (m-MethylBA) and 5-Amino-1-(2-boronobenzyl)quinolin-1-ium bromide (o-AminoBA)</i>	183
6.3.3 Ionogel 1 – Probing Interactions with BAs	184
6.3.4 Synthesis of Ionogel 2	185
6.3.5 Ionogel 2 – Probing Interactions with Glucose	186
<b>6.4 Results and Discussion</b>	<b>187</b>
6.4.1 Ionogel 1	187
6.4.2 Ionogel 2	192
<b>6.5 Conclusions and Future Work</b>	<b>194</b>
<b><u>Part B – Fluorescence Quenching and Recovery Studies in Hydrogel Cocktails</u></b>	<b>195</b>
<b>6.6 Introduction</b>	<b>195</b>
<b>6.7 Experimental</b>	<b>195</b>
6.7.1 Materials and Methods	195
6.7.2 Preparation of Fluorescent Monomeric Cocktails for Fluorescence Titrations	196
<b>6.8 Results and Discussion</b>	<b>197</b>
6.8.1 Monomer Quenching Effect on Pyranine Fluorescence	197
6.8.2 Fluorescence Titrations	200
6.8.2.1 <i>Fluorescence Quenching</i>	200
6.8.2.2 <i>Fluorescence Recovery</i>	203
<b>6.9 Conclusions and Future Work</b>	<b>204</b>

<b><u>Part C – Layer-by-Layer Films Composed of BA Linear Polymers and Poly(vinyl sulfonate)</u></b>	<b>205</b>
<b>6.10 Introduction</b>	<b>205</b>
<b>6.11 Experimental</b>	<b>210</b>
6.11.1 Materials and Methods	210
6.11.2 Preparation of BA Linear Polymers	211
6.11.3 LbL Concept	211
6.11.3.1 LbL Assembly	211
6.11.3.2 Sugar-Induced LbL Disassembly	212
<b>6.12 Results and Discussion</b>	<b>213</b>
<b>6.13 Conclusions and Future Work</b>	<b>215</b>
<b>6.14 References</b>	<b>216</b>
<b><u>Appendix A – Supporting Information for Chapter 2 – Direct Glucose Sensing: Probing Interactions Between Glucose and Fluorescent Boronic Acids</u></b>	<b>220</b>
A.1 Methods	221
A.2 NMR Spectroscopy	222
A.3 Mass Spectrometry	226
A.4 UV-Vis Spectroscopy	226
A.5 Fourier Transform Infrared Spectroscopy	227
<b><u>Appendix B – Supporting Information for Chapter 3 – Intermolecular Quenching and Recovery of Fluorescence Using Cationic Boronic Acid Derivatives for Indirect Glucose Sensing</u></b>	<b>228</b>
B.1 Methods	229
B.2 NMR Spectroscopy	230
B.3 Mass Spectrometry	232
B.4 UV-Vis Spectroscopy	233
B.5 Fluorescence Spectroscopy	233
B.6 Fourier Transform Infrared Spectroscopy	235
<b><u>Appendix C – Supporting Information for Chapter 4 – Water-Soluble Polymerisable Boronic Acids: Combining an Adaptable One-Step Synthesis with an In-Depth Understanding of pH and Glucose Response</u></b>	<b>237</b>
C.1 Characterisation for BA Monomers	238
C.1.1 Spectroscopic Characterisations for <i>o</i> -BA	238
C.1.2 Spectroscopic Characterisations for <i>m</i> -BA	240
C.1.3 Spectroscopic Characterisations for <i>p</i> -BA	243
C.2 Fluorescence pH and Glucose Titrations	245
C.2.1 Fluorescence pH Titrations	245
C.2.2 Fluorescence Glucose Titrations	248

<b><u>Appendix D – Supporting Information for Chapter 5 – A</u></b>	
<b>Two-Component Fluorescence System for Sugar-Sensing</b>	<b>252</b>
D.1 Materials and Methods	253
D.1.1 Materials	253
D.1.2 Synthesis of Fluorescence Acrylamide-BA Hydrogels	253
D.2 Fluorescence	255
D.2.1 Fluorescence Quenching Titrations in Solution	255
D.2.2 Fluorescence Recovery Titrations in Solution	260
D.2.3 Fluorescence Titrations with Hydrogel Cocktails	267
<b><u>Appendix E – Supporting Information for Chapter 6 – Future Work: Sugar</u></b>	
<b>Sensing Using Boronic Acid Polymers</b>	<b>268</b>
<b><u>Part A – Indirect Glucose Sensing in Ionogels</u></b>	<b>269</b>
E.1 Methods	269
E.2 NMR Spectroscopy	270
E.3 Fluorescence Spectroscopy	274
E.4 Fourier Transform Infrared Spectroscopy	275
<b><u>Part B - Fluorescence Quenching and Recovery Studies in Hydrogel</u></b>	
<b><u>Cocktails</u></b>	<b>276</b>
E.5 Fluorescence Spectroscopy	276
<b><u>Part C - Layer-by-Layer Films Composed of BA Linear Polymers and</u></b>	
<b><u>Poly(vinyl sulfonate)</u></b>	<b>285</b>
E.6 Characterisation of BA Linear Polymers	285
E.7 Assembly and Disassembly of (PEI/PVS) <sub>2</sub> (BA LPs/PVS) <sub>5</sub> Films	288

## Abbreviations

3C5NPBA-D	3-Carboxy-5-nitrophenylboronic acid-dendrimer
3CPBA-D	3-Carboxyphenylboronic acid-dendrimer
3D	3-Dimensional
7HC	7-Hydroxycoumarin
AA	Acrylic acid
AD	<i>Anno Domini</i>
ATPS-BuMA	Aminopyrene trisulphonic acid-butylmethacrylate
ATPS-DEGMA	Aminopyrene trisulphonic Acid-diethylene glycol methacrylate
A. U.	Arbitrary units
$\beta$	<i>beta</i>
BA	Boronic acid
BC	Before christ
BF <sub>3</sub>	Boron trifluoride
BINOL	1,1'-Bi-2-naphthol
BODIPY	4,4-Difluoro-4-bora-3a,4a-diaza- <i>s</i> -indacene
BuMA	Butylmethacrylate
°C	Degrees Celsius
cm	Centimetre
cm <sup>-1</sup>	Wavenumber
COOH	Carboxylic acid
COPD	Chronic Obstructive Pulmonary Disease
Cu <sup>+</sup>	Copper(I)
<i>d</i>	Doublet
<i>d</i> -	Deuterated
<i>dd</i>	Double doublet
DBA1	1,3- <i>Bis</i> (2-boronobenzyl)-5-bromopyrimidin-1,3-diiium bromide
DBA2	1,3- <i>Bis</i> (3-boronobenzyl)-5-(3-hydroxy-3-methylbut-1-yn-1-yl)pyrimidin-1,3-diiium bromide
DEGMA	Diethyleneglycolmethacrylate
DI	Deionised
DM	<i>Diabetes Mellitus</i>
DMAEMA	<i>N</i> -(2-(Dimethylamino)ethyl)methacrylate
DMAPMA	<i>N</i> -(3-(Dimethylamino)propyl)methacrylamide
DMF	Dimethylformamide
DMPA	2,2-dimethoxy-2-phenacetophenone
DMSO	Dimethylsulphoxide
DNA	Deoxyribonucleic acid
ECGs	Electrocardiograms
EDGs	Electron-donating groups



EEGs	Electroencephalograms
EMGs	Electromyograms
e-Noses	Electronic-noses
EOG	Electrooculography
eq.	Equivalents
ESI	Electrospray ionisation
EWGs	Electron-withdrawing groups
F	(Measured) Fluorescence intensity
F <sub>0</sub>	Initial fluorescence intensity
FAD <sup>+</sup> or FADH <sub>2</sub>	Flavin adenine dinucleotide
Fluorescein IL	P <sub>44416</sub> fluorescein ionic liquid
FRET	Fluorescence Resonance Energy Transfer
FT-IR	Fourier Transform Infrared
GOx	Glucose oxidase
GC-MS	Gas chromatography mass spectrometry
h	Hours
HEA	2-Hydroxyethyl acrylate
HMPP	2-Hydroxypropiophenone photoinitiator
HOMO	Highest occupied molecular orbital
HPLC	High performance liquid chromatography
HRMS	High resolution mass spectrometry
h <sub>ν<sub>a</sub></sub>	Light absorbed
h <sub>ν<sub>F</sub></sub>	Light emitted as fluorescence
h <sub>ν<sub>P</sub></sub>	Light emitted as phosphorescence
Hz	Hertz
IA-2	Islet antigen-2
ICT	Intramolecular charge transfer
ICT-technologies	Information and communication technologies
IL	Ionic liquid
IR	Infrared
ISC	Intersystem crossing
K <sub>b</sub>	Apparent binding constant
K <sub>s</sub>	Static quenching constant
LbL	Layer-by-layer
LED	Light-emitting diode
λ <sub>ex</sub>	Excitation wavelength
λ <sub>em</sub>	Emission wavelength
λ <sub>max</sub> <sup>ex</sup>	Excitation maximum
λ <sub>max</sub> <sup>em</sup>	Emission maximum
LP	Linear polymer
LUMO	Lowest unoccupied molecular orbital

<i>m</i>	Multiplet
M	Moles per litre
<i>m-</i>	<i>meta</i>
MAA	Methacrylic acid
mBar	Millibars
m-BBV <sup>2+</sup>	<i>Meta</i> diboronic acid-functionalised benzyl viologen
<i>m</i> -BA	<i>N</i> -(3-Boronobenzyl)-2-(methacryloyloxy)- <i>N,N</i> - dimethylethan-1-ammonium bromide
MBIS	<i>N,N'</i> -Methylenebis(acrylamide) crosslinker
<i>m</i> -COOHBA	1-(3-Boronobenzyl)-5-carboxyquinolin-1-ium bromide
<i>m</i> -FBBV <sup>2+</sup>	<i>N,N'</i> -4,4'-bis(benzyl-5-fluoro-3-boronic acid)- bipyridinium dibromide
MHz	Mega Hertz
min	Minute
<i>m</i> -MethoxyBA	1-(3-Boronobenzyl)-6-methoxyquinolin-1-ium bromide
<i>m</i> -MethylBA	1-(3-Boronobenzyl)-6-methylquinolin-1-ium bromide
mL	Millilitre
mm	Millimetre
μm	Micrometre
mM	Millimolar
μM	Micromolar
mmol	Millimole
MΩ.cm <sup>-1</sup>	Molar conductivity
<i>m</i> -OMeBBV <sup>2+</sup>	1,1'- <i>Bis</i> (5-borono-2-methoxybenzyl)-[4,4'-bipyridin]- 1,1'-dium
Mol%	mole %
MS	Mass spectrometry
Na-Acrylate	Sodium acrylate
NH-pyranine	Sodium 8-aminopyrene-1,3,6-trisulphonate
NIR	Near infrared
nL	Nanolitre
nm	Nanometre
NMR	Nuclear magnetic resonance
<i>o-</i>	<i>ortho</i>
<i>o</i> -AminoBA	5-Amino-1-(2-boronobenzyl)quinolin-1-ium bromide
<i>o</i> -BA	<i>N</i> -(2-boronobenzyl)-2-(methacryloyloxy)- <i>N,N</i> - dimethylethan-1-ammonium bromide
<i>o</i> -BBV <sup>2+</sup>	<i>Ortho</i> diboronic acid-functionalised benzyl viologen
<i>o</i> -COOHBA	1-(2-Boronobenzyl)-5-carboxyquinolin-1-ium bromide
OH-pyranine	sodium 8-hydroxypyrene-1,3,6-trisulphonate
<i>o</i> -MethoxyBA	1-(2-Boronobenzyl)-6-methoxyquinolin-1-ium bromide
<i>o</i> -MethylBA	1-(2-Boronobenzyl)-6-methylquinolin-1-ium bromide
<i>o</i> -PBBV <sup>2+</sup>	Diboronic acid-functionalised benzyl viologen
<i>o</i> -PBV	Boronic acid-functionalised benzyl viologen

$\pi$	Pi
<i>p</i> -	<i>para</i>
P <sub>4,4,4,4</sub> Cl	Tetrabutylphosphonium chloride
P <sub>4,4,4,4</sub> SPMA	Tetrabutylphosphonium sulphopropyl methacrylate
P <sub>6,6,6,14</sub> Fluorescein IL	Di(trihexyltetradecyl phosphonium) fluorescein ionic liquid
<i>p</i> -BA	<i>N</i> -(4-boronobenzyl)-2-(methacryloyloxy)- <i>N,N</i> -dimethylethan-1-ammonium bromide
PBPO	Phenyl <i>bis</i> (2,4,6-trimethylbenzoyl)phosphine oxide
PBPYRSO <sub>3</sub> Na	Water-soluble anionic conjugated polyelectrolyte
PDMS	Polydimethylsiloxane
PEDOT	Poly(3,4-ethylene-dioxythiophene)
PEG	Polyethylene glycol
PEI	Poly(ethyleneimine)
PET	Photoinduced electron transfer
PIL	Poly(ionic liquid)
Polymerizable IL ionic	Tetrabutylphosphonium sulphopropyl methacrylate liquid
PPO800	Polypropylene oxide diacrylate
PPD	Poly-orthophenylenediamine
ppm	Parts per million
PP-S-BINOL	Polymer of 1,1'-bi-2-naphthol
<i>p</i> -TBPB	Cationic trispyridine quaternary ammonium salt
PVS	Poly(vinyl sulphonate, sodium salt)
pyranine	8-hydroxypyrene-1,3,6-trisulphonic acid trisodium salt
$\rho$	Density
R <sub>f</sub>	Retention Value
<i>s</i>	Singlet
s	Seconds
s <sup>-1</sup>	per Second
S <sub>0</sub>	Ground electronic singlet state
S <sub>1</sub>	First excited electronic singlet state
S <sub>2</sub>	Second excited electronic singlet state
<i>t</i>	Triplet
T <sub>0</sub>	Ground electronic triplet state
T <sub>1</sub>	First excited electronic triplet state
TB	Pulmonary tuberculosis
TLC	Thin layer chromatography
Tol	Toluene
URTI	Upper respiratory tract infections
UV	Ultraviolet
UV-Vis	Ultraviolet-visible

V  
VOCs

Dynamic quenching constant  
Volatile organic compounds

## List of Tables

### **Chapter 1: Literature Survey - Glucose Sensing for Diabetes Monitoring: History and Recent Developments**

<b>Table 1.1.</b> Summary of glucose concentrations postprandial and pH values measured in physiological fluids of healthy and diabetic patients.	21
<b>Table 1.2.</b> Summary definitions of specialised approaches for glucose sensing in interstitial fluid.	23

### **Chapter 2: Direct Glucose Sensing: Probing Interactions Between Glucose and Fluorescent Boronic Acids**

<b>Table 2.1.</b> Buffer compositions for 200 mL of required pH buffer.	89
---	----

### **Chapter 3: Intermolecular Quenching and Recovery of Fluorescence Using Cationic Boronic Acid Derivatives for Indirect Glucose Sensing**

<b>Table 3.1.</b> Buffer compositions for 200 mL of required buffer.	110
--	-----

### **Chapter 4: Water-Soluble Polymerisable Boronic Acids: Combining an Adaptable One-Step Synthesis with an In-Depth Understanding of pH and Glucose Response**

<b>Table 4.1.</b> <sup>11</sup> B NMR shifts (ppm) for the neutral BA, anionic BA and anionic BA-ester for all BA monomers.	142
<b>Table 4.2.</b> Estimated pK <sub>a</sub> values for the BA and BA-ester forms of the BA monomers.	145

### **Chapter 5: A Two-Component Fluorescent System for Sugar-Sensing**

<b>Table 5.1.</b> Recipe for fluorescent acrylamide- <i>o</i> BA hydrogels.	159
<b>Table 5.2.</b> Recipe for fluorescent acrylamide- <i>m</i> BA hydrogels.	160
<b>Table 5.3.</b> Quenching constants for <i>o</i> -BA and <i>m</i> -BA.	164
<b>Table 5.4.</b> Binding constants (K <sub>s</sub> ) for <i>o</i> -BA and <i>m</i> -BA with all three monosaccharides.	165

### **Chapter 6: Future Work: Sugar-Sensing Using Boronic Acid Polymers**

#### ***Part A – Indirect Glucose Sensing in Ionogels***

<b>Table 6.1.</b> Reagents for Ionogel 1 synthesis.	183
<b>Table 6.2.</b> Reagents for the synthesis of Ionogel 2.	187

***Part B – Pyranine Fluorescence in the Presence of Acrylic Monomers***

**Table 6.3.** Recipe for hydrogel cocktails. 197

**Table 6.4.** Monomer quantities for hydrogel cocktail recipes. 198

## List of Figures

### **Chapter 1: Literature Survey - Glucose Sensing for Diabetes Monitoring: History and Recent Developments**

- Figure 1.1.** World population (%) for people suffering from diabetes in 1980 (left) compared to the revised figures in 2014 (right) for the top ten countries with the highest prevalence of the disease. Adapted from reference 39. 16
- Figure 1.2.** Finger pricking device (left). (A) Lancet needle. (B) Blood sample on test-strip. (C) Glucose meter displaying date and glucose concentration in mmol/L; Continuous glucose monitor (right). Adapted from references 66 and 67. 18
- Figure 1.3.** Schematic of the microneedle glucose-sensing patch. Adapted From reference 80. 24
- Figure 1.4.** SwEatch: watch-sensing platform for sodium analysis in sweat. (1) Electronics. (2) 3D printed casing. (3) Microfluidic chip and ion-selective/ion-specific electrode. (4) 3D printed sweat harvester and sensor connections. Reproduced from reference 92. 27
- Figure 1.5.** Schematic representation of the eyeglasses biosensor system, which integrates a wireless circuit board along the arms of the spectacles and two electrochemical sensors for lactate and potassium on to the nose-bridge pads. A schematic of the lactate sensor (left) and potassium sensor (right), along with the corresponding recognition and transduction events is also shown. Adapted from reference 97. 28
- Figure 1.6.** (A) Flexible glucose sensor. (B) Glucose sensor integrated in to a wearable wristband for non-invasive sensing in sweat. Adapted from reference 100. 29
- Figure 1.7.** Lactate sensing mouthguard for non-invasive continuous lactate sensing in saliva. (A) Mouthguard sensing platform with integrated printable 3-electrode system, with enzyme working electrode. (B) Enzyme coated working electrode with lactate sensing region. Adapted from reference 119. 34
- Figure 1.8.** Glucose-sensing tattoo printed on to a tooth platform as a non-invasive continuous monitoring device. (A) Graphene printed on bioresorbable silk with contacts containing a wireless coil. (B) Biotransfer of sensor on to tooth enamel. (C) Magnified image of the sensing unit with a wireless readout system. (D) Self-assembly of pathogenic bacteria bound by peptides on nanotransducer surface. Adapted from reference 120. 35

- Figure 1.9.** Google and Novartis' smart-contact lens. Adapted from reference 126 and 129. 37
- Figure 1.10.** Sequence of images of the glucose-sensing contact lens during sensor functionalization with GOx, titanium sol-gel film, Nafion membrane and rinsing with DI water, respectively. Reproduced from reference 91. 38
- Figure 1.11.** The Jablonski diagram illustrating the excitation of a ground electronic state  $S_0$  to the excited electronic states  $S_1$ ,  $S_2$  or  $T_1$ , where on returning to the ground state  $S_0$ , energy is emitted in the form of light as fluorescence or phosphorescence, respectively. Adapted from reference 138. 41
- Figure 1.12.** PET fluorescence sensing mechanism. Electron transfer from an electron-donating group/receptor to an electron-accepting fluorophore, which quenches the fluorescence of the fluorophore by PET. Once an analyte binds to the receptor, this electron transfer process is inhibited, which increases the fluorescence of the fluorophore. Adapted from references 138 and 143. 43
- Figure 1.13.** FRET fluorescence mechanism, whereby the emission of one fluorophore must overlap with the absorbance of another in order for the energy to be transferred from one fluorophore to the other. Adapted from reference 138. 44
- Figure 1.14.** ICT fluorescence mechanism, where the fluorescence is quenched based on a conformational change in the molecule altering hybridisation. Adapted from reference 138. 45
- Figure 1.15.** BA equilibrium illustrating the conversion from the neutral trigonal planar  $sp^2$  hybridisation form to the anionic boronate tetrahedral  $sp^3$  hybridised form, on binding glucose in alkaline aqueous media. Adapted from reference 12. 47
- Figure 1.16.** The furanose forms of glucose and fructose sugars binding to a BA derivative, where glucose binds in a bidentate fashion versus the monodentate binding of fructose. Adapted from reference 155. 48
- Figure 1.17.** The first fluorescent BA sensors synthesised by Yoon and Czarnik.<sup>152</sup> 50
- Figure 1.18.** Anthracene-based BA derivative, where its fluorescence is quenched due to aggregation in the absence of fructose (left) and it becomes fluorescent in the presence of fructose due to disaggregation (right). Adapted from reference 158. 51
- Figure 1.19.** Structure of the FRET-BA glucose sensor designed by James *et al.*, using the fluorophores phenanthrene (green) and pyrene (red) (left), where the emission of phenanthrene at 396 nm overlaps with the excitation of pyrene (red) at 342 nm. Upon excitation of the sensor at 299 nm, characteristic to phenanthrene,



only an emission at 417 nm is observed, characteristic to pyrene. Adapted from reference 148.	52
<b>Figure 1.20.</b> Commercially available BODIPY probes ER-Tracker Green and LysoTracker RED. <sup>160</sup>	53
<b>Figure 1.21.</b> Structures of BA-BODIPY glucose sensors synthesised by Hansen <i>et al.</i> <sup>161</sup>	54
<b>Figure 1.22.</b> BA probes synthesised by Badugu <i>et al.</i> , where methyl- and methoxy-groups attached on the quinoline ring are employed and the positioning of the BA moiety is altered between <i>ortho</i> and <i>meta</i> to the N <sup>+</sup> quinoline substituent. <sup>12</sup>	55
<b>Figure 1.23.</b> Scheme showing the charge neutralisation-stabilisation interaction, where the BA derivative is initially fluorescent and on sugar binding, fluorescence quenching occurs. Adapted from references 11, 12, 37 and 134.	55
<b>Figure 1.24.</b> (A) Cationic BA molecules synthesised by Singaram <i>et al.</i> used to quench the fluorescence of pyranine. (B) Pyranine equilibrium at pH 7.4, illustrating the two possible anionic forms. <sup>166</sup>	58
<b>Figure 1.25.</b> Structures of m-BBV <sup>2+</sup> together with –F and –OCH <sub>3</sub> derivatives used to modify viologen fluorescence in the direct glucose sensing approach. <sup>169</sup>	60
<b>Figure 1.26.</b> Components used by Feng <i>et al.</i> in the indirect glucose sensing approach: Pyranine fluorophore and trispyridine-BA. <sup>170</sup>	61
<b>Figure 1.27.</b> Fluorescent graphene quantum dot and BBV <sup>2+</sup> viologen compounds used in the two-component glucose sensing system by Li and co-workers. <sup>164</sup>	62
<b>Figure 1.28.</b> Anionic pyranine fluorophore and BA quencher viologens used in two-component sensing system by Singaram and co-workers. Adapted from reference 166.	63
<b>Figure 1.29.</b> Singaram's cationic BA viologen (blue) and pyranine fluorophore (pink) immobilised in a hydrogel framework.	64
<b>Figure 1.30.</b> Schematic structure of one of the hydrogels synthesised by Singaram <i>et al.</i> , comprising of a derivatised pyranine fluorophore (ATPS-DEGMA: pink) as the fluorescence reporter unit and a cationic BA-viologen compound (blue) as the glucose receptor. The components are immobilised by a single tether to allow for increased mobility within the hydrogel matrix. <sup>177</sup>	65
<b>Figure 1.31.</b> (A) Formation of BA viologen-BINOL fluorophore complex, which is non-fluorescent. (B) Addition of glucose recovers fluorescence.	67

## **Chapter 2: Direct Glucose Sensing: Probing Interactions Between Glucose and Fluorescent Boronic Acids**

**Figure 2.1.** (A) Concept of a smart-contact lens, functionalised with BA sensor. (B) Mobile device is used to capture image of smart-lens while in eye. (C) Non-Invasive and continuous glucose-sensing contact lens is coupled to an ICT application. (D) The application evaluates and maps an optical response in the lens to a specific glucose concentration. (E) Specific glucose concentrations can provide an indication of hypo- or hyperglycaemic levels in diabetic patients, allowing them to personally monitor their condition. 87

**Figure 2.2.**  $^1\text{H}$  NMR assignment for *o*-COOHBA. 91

**Figure 2.3.** Structure of *o*-COOHBA found from mass spectrometry analysis,  $[\text{C}_{18}\text{H}_{17}\text{BNO}_4]^+$ . 91

**Figure 2.4.**  $^1\text{H}$  NMR assignment for *m*-COOHBA. 92

**Figure 2.5.** Glucose sensing using both *o*-COOHBA and *m*-COOHBA in various pH buffer solutions ranging between pH 5.3-11.8. Left: Fluorescence glucose-sensing using *o*-COOHBA (0.5 mM) with 10 mM glucose. Right: Fluorescence glucose-sensing employing *m*-COOHBA with 10 mM glucose, where  $F_0$  is the maximum fluorescence of the COOHBA derivatives in pH 7.4 buffer solution and  $F$  is the measured fluorescence of the COOHBA derivatives in all other solutions. 95

**Figure 2.6.** (A) Excitation (green) and emission (blue) fluorescence spectra for *o*-COOHBA, where the excitation wavelength is 380 nm and the corresponding emission wavelength is 485 nm. (B) Excitation (green) and emission (blue) fluorescence spectra for *m*-COOHBA, where the excitation wavelength is 390 nm and the corresponding emission wavelength is 465 nm. 97

**Figure 2.7.** (A) Fluorescence quenching of *o*-COOHBA (0.5 mM) on sequential additions of glucose (0-50 mM) in pH 7.4 phosphate buffer solution. A decrease in fluorescence intensity by 40% was observed at the emission wavelength 485 nm in the presence of 50 mM glucose. The excitation wavelength was 380 nm. (B) Fluorescence quenching of *m*-COOHBA (0.5 mM) on sequential additions of glucose (0-50 mM) in pH 7.4 phosphate buffer solution. A decrease in fluorescence intensity by 78% was observed at the emission wavelength 460 nm in the presence of 50 mM glucose. The excitation wavelength was 390 nm. The insets for each graph show the COOHBA sensor response to glucose between the concentration range of 0-10 mM. 98

**Figure 2.8.** Fluorescence quenching in the *o*-COOHBA doped PDMS 'lens' on immersing the 'lens' in various pH 7.4 phosphate buffer solutions containing glucose concentrations between 0-5 mM. The excitation wavelength used was 380 nm and the corresponding emission wavelength was 485 nm. 100

**Figure 2.9.** 3D molecular models of COOHBA derivatives, produced using free MolView software, shows the potential conformation of the COOHBA derivatives before and after sugar binding. The N<sup>+</sup>-B<sup>-</sup> interaction is represented by the dotted line. 101

### **Chapter 3: Intermolecular Quenching and Recovery of Fluorescence Using Cationic Boronic Acid Derivatives for Indirect Glucose Sensing**

**Figure 3.1.** Chemical structure of BA1, with labelled <sup>1</sup>H atom assignments. 112

**Figure 3.2.** Chemical structure of compound 4. H atoms are labelled. 113

**Figure 3.3.** Chemical structure of BA2, with labelled <sup>1</sup>H atom assignments. 113

**Figure 3.4.** Excitation and fluorescence emission spectra for 7HC (4 μM) in pH 7.4 buffer solution, where the excitation wavelengths are 328 and 367 nm and the emission wavelength corresponding to both excitation wavelengths is 454 nm. 114

**Figure 3.5.** (A) Schematic for the fluorescence quenching of 7HC with BA1. (B) Excitation spectrum of 7HC (4 μM) with increased concentrations of BA1 (up to 0.48 mM; 120 eq.) in pH 8.12 phosphate buffer solution, showing an excitation wavelength of 367 nm and a shoulder at 328 nm, corresponding to the emission wavelength at 454 nm. (C) Emission spectrum of 7HC with increased concentrations of BA1, displaying an emission at 454 nm when excited at 367 nm. (D) Linear curve of 7HC ( $R^2 = 0.999$ ), where each point on the curve represents the average maximum emission point ( $n = 3$ ) at 454 nm with increased additions of BA1. 117

**Figure 3.6.** (A) Excitation spectrum of 7HC (4 μM) with increased concentrations of BA1 (up to 0.8 mM; 200 eq.) in pH 8.88 phosphate buffer solution, showing an excitation wavelength of 367 nm, corresponding to the emission wavelength of 454 nm (B) Emission spectrum of 7HC, showing an emission wavelength at 454 nm, with increased additions of BA1, when excited at 367 nm. Non-linear curve of 7HC with increased concentrations of BA1 ( $R^2 = 0.980$ ) is shown, where each point on the curve was the maximum emission at 454 nm after each addition of BA1. 118

**Figure 3.7.** (A) Schematic of fluorescence recovery in 7HC, on dissociation of 7HC:BA1-complex in the presence of glucose. (B) Excitation spectrum of 7HC (4 μM) with BA1 (175 eq.; 0.7 mM) and increased concentrations of glucose (0-5 mM) in pH 8.12 phosphate buffer solution, where the blue line indicates the original excitation of 7HC before any BA1 additions. The peak in the excitation spectrum was found at 367 nm, corresponding to an emission at 454 nm. (C) Emission spectrum of 7HC and BA1 (1:175 eq.) with increased

additions of glucose (0-5 mM), displaying an increase in emission intensity by 4%, where the emission wavelength was 454 nm, corresponding to an excitation wavelength of 367 nm. (D) Fluorescence curve of 7HC and BA1 (1:175 eq.) with increased concentrations of glucose (0-5 mM). Each data point curve was taken as the maximum intensity at 454 nm after each addition of glucose.

119

**Figure 3.8.** Fluorescence quenching in neutral 7HC on increased additions of BA2.

120

**Figure 3.9.** (A) Excitation spectrum of 7HC (4  $\mu$ M) with increased concentrations of BA2 (up to 0.3 mM; 75 eq.) in pH 7.4 phosphate buffer solution (containing 40  $\mu$ L CH<sub>3</sub>OH in each 1.5 mL sample). The peak at 328 nm represents the neutral form of 7HC (yellow) and the peak at 366 nm represents the anionic form of 7HC (blue). Both excitation wavelengths correspond to the same emission wavelength at 454 nm. (B) Fluorescence response of 7HC with increased additions of BA2, excited at 328 nm. Each data point was taken at 454 nm corresponding to the maximum emission after addition of BA2 ( $R^2 = 0.977$  and  $0.957$  at 328 and 366 nm, respectively). (C) Emission spectrum of 7HC showing an emission maximum at 454 nm, with increased concentrations of BA2 when excited at 328 nm. (D) Emission spectrum of 7HC showing an emission maximum at 454 nm, with increased additions of BA2 when excited at 366 nm.

121

**Figure 3.10.** (A) Schematic of fluorescence quenching in anionic 7HC on increased interactions with BA2. (B) Excitation spectrum of 7HC (4  $\mu$ M) with increased concentrations of BA2 (up to 1.2 mM; 300 eq.) in pH 7.4 phosphate buffer solution and CH<sub>3</sub>OH (1:1) (measured pH 8.6). The excitation wavelength is shown as 370 nm with a shoulder at 328 nm, corresponding to the emission wavelength 454 nm. (C) Emission spectrum of 7HC with increased additions of BA2, showing an emission wavelength at 454 nm, corresponding to the excitation wavelength at 370 nm. (D) Fluorescence quenching of 7HC with increased concentrations of BA2, where each point on the curve was taken as the maximum fluorescence intensity at 454 nm after the addition of BA2 ( $R^2 = 0.970$ ).

122

**Figure 3.11.** (A) Schematic of the fluorescence recovery in 7HC, on dissociation of fluorophore:BA2-quencher ground-state complex in the presence of glucose. (B) Excitation spectrum of 7HC (4  $\mu$ M) with BA2 (20 eq.; 80  $\mu$ M) and increased concentrations of glucose (up to 100 mM) in pH 7.4 phosphate buffer solution and CH<sub>3</sub>OH (1:1) (measured pH 8.6). The excitation wavelength was 370 nm with a shoulder at 328 nm, corresponding to an emission at 454 nm. (C) Emission spectrum of 7HC and BA2 (1:20 eq.) with increased concentrations of glucose. The emission

wavelength was 454 nm. (D) Fluorescence curve of 7HC and BA2 (1:20 eq.) with increased concentrations of glucose, where each point on the curve was taken as the maximum intensity at 454 nm after the addition of glucose. 123

#### **Chapter 4: Water-Soluble Polymerisable Boronic Acids: Combining an Adaptable One-Step Synthesis with an In-Depth Understanding of pH and Glucose Response**

**Figure 4.1.** Monomeric BA derivatives *o*-BA, *m*-BA and *p*-BA. 133

**Figure 4.2.**  $^{11}\text{B}$  NMR of boric acid in  $\text{D}_2\text{O}$  at pH 3.5 (bottom) and pH 14.2 (top). 138

**Figure 4.3.**  $^1\text{H}$  NMRs for all three BA monomers in  $\text{D}_2\text{O}$ , *o*-BA (top), *m*-BA (middle) and *p*-BA (bottom). 140

**Figure 4.4.**  $^{11}\text{B}$  NMR pH titration in  $\text{D}_2\text{O}$  for *m*-BA (82 mM) in the absence of glucose (A) and in the presence of 10 equivalents glucose (820 mM) (B). The peak at  $\sim 19$  ppm is the impurity boric acid. For details regarding the boric acid peak refer to Figure 4.2. 140

**Figure 4.5.** (A)  $^{11}\text{B}$  NMR pH titration in the absence of glucose for *o*-BA (82 mM). (B)  $^{11}\text{B}$  NMR pH titration in the absence of glucose for *p*-BA (82 mM). (C)  $^{11}\text{B}$  NMR pH titration in the presence of 10 equivalents of glucose (820 mM) for *o*-BA. (D)  $^{11}\text{B}$  NMR pH titration in the presence of 10 equivalents of glucose (820 mM) for *p*-BA. The solvent for all titrations was  $\text{D}_2\text{O}$ . 142

**Figure 4.6.** Fluorescence emission in  $\text{H}_2\text{O}$  of the three BA monomers (1 mM) at approximately pH 4.0, 7.7 and 11.5, where the excitation wavelength was 367, 372 and 370 nm for *o*-BA, *m*-BA and *p*-BA, respectively, corresponding to the anionic form of each BA. 143

**Figure 4.7.** Excitation and fluorescence emission spectra for *m*-BA (1 mM) in  $\text{H}_2\text{O}$ . (A) Excitation spectra as a function of pH showing maxima at 329 nm (low pH) and 372 nm (high pH), and an isosbestic point at 335 nm. (B) Emission spectra as a function of pH with  $\lambda_{\text{ex}} = 372$  nm, showing fluorescence emission intensity increasing with pH, with maximum emission at 466 nm. (C) The  $\text{pK}_a$  for *m*-BA was estimated to be 8.7 from the emission spectra taken at 466 nm. (D) Photo showing the fluorescence increase for *m*-BA solutions under 365 nm irradiation at pH 3.2, 8.0 and 11.5. 144

**Figure 4.8.** Excitation and fluorescence emission spectra for *m*-BA (1 mM) in  $\text{H}_2\text{O}$ . (A) The excitation wavelengths were 329 nm (low pH) and 372 nm (high pH). (B) The emission wavelength was 466 nm. The  $\text{pK}_a$  calibration for *m*-BA (inset B) was estimated to be 8.5. 144

**Figure 4.9.** Experimental emission values taken at the emission wavelengths for *o*-BA, *m*-BA and *p*-BA at 460, 466 and 460 nm respectively, as a function of pH and fit to a sigmoid model, to estimate the pK<sub>a</sub> for each BA derivative (1 mM) in H<sub>2</sub>O; *F* is the measured fluorescence intensity at excitation wavelengths 367, 372 and 370 nm for the BA derivatives, respectively, in the presence of glucose (10 mM), *F*<sub>min</sub> and *F*<sub>max</sub> are the minimum and maximum fluorescence intensities measured in each case. 145

**Figure 4.10.** Fluorescence emission spectra (A) and relative fluorescence increase (B) for *o*-BA (1 mM) with glucose (0-150 mM) in H<sub>2</sub>O at pH 8.0; The emission at 460 nm was recorded using the corresponding excitation wavelength ( $\lambda_{\text{max}}^{\text{ex}}$ ) of 367 nm, showing a fluorescence increase of 13% in the presence of 150 mM glucose. Fluorescence emission spectra (C) and relative fluorescence increase (D) for *m*-BA (1 mM) with glucose (0-150 mM) in H<sub>2</sub>O at pH 7.5; The emission at 466 nm was recorded using the corresponding excitation wavelength ( $\lambda_{\text{max}}^{\text{ex}}$ ) of 372 nm, showing a fluorescence increase of 47% in the presence of 150 mM glucose. Fluorescence emission spectra (E) and relative fluorescence increase (F) for *p*-BA (1 mM) with glucose (0-150 mM) in H<sub>2</sub>O at pH 8.0; The emission at 460 nm was recorded using the corresponding excitation wavelength ( $\lambda_{\text{max}}^{\text{ex}}$ ) of 370 nm, showing a fluorescence increase of 177% in the presence of 150 mM glucose. Inset F Shows a photo of the samples before (blue fluorescent) and after the addition of 150 mM glucose (green fluorescent). *F*<sub>0</sub> is the initial fluorescence of the BA in the absence of glucose and *F* is the measured fluorescence intensity of the BA in the presence of glucose (0-150 mM). 147

## **Chapter 5: A Two-Component Fluorescent System for Sugar-Sensing**

**Figure 5.1.** Indirect sensing system components; pyranine (left) and the general structure of the BA monomers (right). 157

**Figure 5.2.** Absorbance spectra for pyranine (4  $\mu$ M) (blue), pyranine and *o*-BA (1:50) (pink) and pyranine, *o*-BA (1:50) and glucose (100 mM) (green) in pH 7.4 buffer. 161

**Figure 5.3.** Excitation and emission spectra for pyranine (4  $\mu$ M) with increasing concentrations of *o*-BA (0-200  $\mu$ M), *m*-BA (0-160  $\mu$ M) and *p*-BA (0-1000  $\mu$ M) in pH 7.4 buffer solution. The inset for *m*-BA shows an image of this change under 365 nm UV irradiation. 163

**Figure 5.4.** Fluorescence quenching of pyranine (4  $\mu$ M) with *o*-BA (0-200  $\mu$ M), *m*-BA (0-100  $\mu$ M) and *p*-BA (0-160  $\mu$ M). 164

**Figure 5.5.** Left: Fluorescence recovery of pyranine (4  $\mu$ M) and *o*-BA

(1:50), Right: Fluorescence recovery of pyranine and *m*-BA (1:20). 165

**Figure 5.6.** Left: Fluorescence emission spectra of the hydrogel cocktail; containing acrylamide (100 mol%), MBIS (1 mol%) and pyranine (0.001 mol%) after titration with *o*-BA (0-5 mM) and right: normalised ( $F_0/F$ ) fluorescence emission of both hydrogel cocktails after titrations with *o*-BA (0-1.5 mM) and *m*-BA (0-1.5 mM) in DI H<sub>2</sub>O fitted with a model using Equation 5.1. 166

**Figure 5.7.** Normalised emission data ( $n = 3$ ) of hydrogel disks containing pyranine (0.001 mol%) and *o*-BA (15 eq.) or *m*-BA (10 eq.) with varied glucose concentrations (0-100 mM). (A) Shows the excitation and emission spectra for the *o*-BA hydrogels with increased fluorescence by 35% with 100 mM glucose and (B) shows the emission calibration at 490 nm. (C) Shows the excitation and emission spectra for the *m*-BA hydrogels with increased fluorescence by 45% with 100 mM glucose and (D) shows the emission calibration at 520 nm. The insets in (B) and (D) show images of the quenched hydrogel under 365 nm UV light. The points on the curve represent the mean  $\pm$  standard deviation. 167

## **Chapter 6: Future Work: Sugar-Sensing Using Boronic Acid Polymers**

### ***Part A – Indirect Glucose Sensing in Ionogels***

**Figure 6.1.** (A) Prototype holder; plastic slide holder with glass coverslip sealed with parafilm, the ionogel sits inside with pH 7.4 phosphate buffer. (B) 3D-printed cuvette style holder with fluorescein ionogel in pH 7.4 phosphate buffer solution. 180

**Figure 6.2.** <sup>1</sup>H NMR assignment for *m*-MethylBA. 184

**Figure 6.3.** <sup>1</sup>H NMR assignment for *o*-AminoBA. 184

**Figure 6.4.** Ionogel 1 mobile components: P<sub>6,6,6,14</sub> fluorescein IL and cationic BA derivatives used for screening. 185

**Figure 6.5.** Structure of Ionogel 2 in pH 7.4 conditions, where X:Y:Z is 1:3:1 187

**Figure 6.6.** Proposed two-component glucose-sensing mechanism using Ionogel 1. (A) Ionogel 1 in its initial fluorescent state; (B) Cationic BA derivative diffuses in to Ionogel 1 to form a non-fluorescent ground-state complex by electrostatic and  $\pi$ - $\pi$  stacking interactions; (C) Glucose diffuses inside Ionogel 1 and binds to the BA derivative. BA group binds glucose, leading to dissociation in BA-fluorophore complex to recover fluorescence. 189

**Figure 6.7.** Immersion of Ionogel 1 in a solution of *o*-AminoBA (10 mM) in pH 7.4 phosphate buffer, resulted in a decrease in fluorescence (left). Sequential addition of a glucose containing solution in pH 7.4 phosphate

buffer (10 mM) caused restoration of fluorescence (right). 190

**Figure 6.8.** (A) Excitation and emission spectra of Ionogel 1 in pH 7.4 phosphate buffer solution, where the excitation wavelength is 505 nm and the corresponding emission wavelength is 565 nm. (B) Initial emission spectrum for Ionogel 1 in pH 7.4 phosphate buffer solution (red), Ionogel 1 was immersed in a solution of *o*-AminoBA in pH 7.4 phosphate buffer (10 mM), demonstrating a decrease in the emission intensity by 26% after 12h (blue), Ionogel 1 was placed in a solution of glucose in pH 7.4 phosphate buffer (10 mM), exhibiting an increase in fluorescence intensity by 16% after 12h (yellow). 190

**Figure 6.9.** Emission spectrum of Ionogel 1 when immersed in a solution of *m*-MethylBA in pH 7.4 phosphate buffer (10 mM) at room temperature, showing a fluorescence decrease by 72% over 4h (left). Emission spectrum of Ionogel 1 when placed in a solution of glucose in pH 7.4 phosphate buffer (44 mM) showing a fluorescence increase by 32% (right). 191

**Figure 6.10.** Immersion of Ionogel 2 (initially fluorescent, left) in a glucose containing solution of pH 7.4 phosphate buffer (100 mM) resulted in a decrease in fluorescence (right), where X:Y:Z is 1:3:1. 193

**Figure 6.11.** (A) Emission spectrum of Ionogel 2 when immersed in 100 mM glucose solution in pH 7.4 phosphate buffer over 4 hours; the excitation wavelength was 448 nm and the corresponding emission wavelength was 557 nm. (B) Evolution of the emission at 557 nm in the presence of 100 mM glucose over ~4h, where the initial blue points represent stabilisation of the hydrogel in buffer before the addition of glucose. A decrease in fluorescence intensity by 44% was recorded.  $F_0$  represents the initial fluorescence of fluorescein and  $F$  corresponds to the measured fluorescence after the addition of glucose. 193

### ***Part B – Pyranine Fluorescence in the Presence of Acrylic Monomers***

**Figure 6.12.** Fluorescent pyranine monomeric cocktails in DI H<sub>2</sub>O, where the colours range from green to blue depending on the acidic nature of the solution. Left to right: pyranine, *N*-(3-(dimethylamino)propyl)methacrylamide (DMAPMA), *N*-(2-(dimethylamino)ethyl)methacrylate (DMAEMA), sodium acrylate (Na-Acrylate), acrylamide, methacrylic acid (MAA), acrylic acid (AA) and 2-hydroxyethylacrylate (HEA). 198

**Figure 6.13.** Pyranine acid-base equilibrium indicating switching from blue to green fluorescent state. Adapted from reference 29. 199

**Figure 6.14.** Fluorescence quenching of pyranine (0.1 mM) in monomeric cocktails with cross-linker MBIS (1 mol%) and acrylic monomers (100 mol%); acrylamide, DMAEMA, DMAPMA, HEA and MAA, with



increased concentrations of *o*-BA (top) and *m*-BA (bottom) in DI H<sub>2</sub>O, fitted with a model using Equation 5.1. The solution sample contains pyranine (0.1 mM) and increased equivalents of the BA co-monomer only in DI water. The emission wavelengths for the monomeric cocktails were; 510, 440, 517, 515, 436 and 440 nm for acrylamide, AA, DMAEMA, DMAPMA, HEA and MAA cocktails, respectively. For spectral data on the excitation and emission wavelengths see Appendix E. 201

**Figure 6.15.** Fluorescence emission curves for the acrylamide, AA and HEA cocktails comparing the *o*-BA and *m*-BA monomer fluorescence quenching efficiency in pyranine (0.1 mM) in H<sub>2</sub>O. The acrylamide cocktail is shown in blue, the AA cocktail is shown in green and the HEA cocktail is shown in red. The *o*-BA equivalents to pyranine is represented by the triangle and the *m*-BA equivalents is represented by the square. The emission wavelengths were 510, 440 and 436 nm for the acrylamide, AA and HEA cocktails, respectively. The data is fitted with a model using Equation 5.1. 203

**Figure 6.16.** Fluorescence recovery in HEA cocktails with *o*-BA (5 mM; top, A-C) and *m*-BA (2 mM; bottom, D-F) in DI H<sub>2</sub>O. (A) Fluorescence emission spectrum with emission peak at 492 nm, corresponding to an excitation wavelength at 419 nm, showing fluorescence increase by 52% with 100 mM glucose. (B) Fluorescence emission curve at 492 nm, where  $F_0$  is the initial fluorescence of the cocktail before the addition of *o*-BA and  $F$  is the measured fluorescence after the addition of *o*-BA. (C) Shows an image of the HEA cocktail before (left) and after the addition of *o*-BA (middle) and after the addition of 100 mM glucose (right). (D) Fluorescence emission spectrum with emission peak at 492 nm, corresponding to an excitation wavelength at 419 nm, showing fluorescence increase by 25% with 100 mM glucose. (E) Fluorescence emission curve at 492 nm. (F) Shows an image of the HEA cocktail before (left) and after the addition of *m*-BA (middle) and after the addition of 100 mM glucose (right). 203

***Part C – Layer-by-Layer Films Composed of BA Linear Polymers and Poly(vinyl sulfonate, sodium salt)***

**Figure 6.17.** LbL assembly (A) and destruction (B) processes for insulin drug delivery systems stimulated by glucose. 207

**Figure 6.18.** Assembly process of bilayers on to a quartz slide, where the poly-BA is the BA linear polymer and the polyanion is PVS. 211

**Figure 6.19.** Disassembly process of the bilayers in saccharide containing solutions. 212

**Figure 6.20.** Absorbance spectra for the assembly of the (PEI/PVS)<sub>2</sub>(pBA LP/PVS)<sub>15</sub> film (left) and the average (n = 3) linear growth

at 230 nm (right). 213

**Figure 6.21.** Assembly of the (PEI/PVS)<sub>2</sub>(oBA LP/PVS)<sub>5</sub> film (Red circle ●), (PEI/PVS)<sub>2</sub>(mBA LP/PVS)<sub>5</sub> (green square ■), and the (PEI/PVS)<sub>2</sub>(pBA LP/PVS)<sub>5</sub> film (blue triangle square ▲), in triplicate, when monitored at 230 nm (left). 214

**Figure 6.22.** Normalised absorbance ( $A/A_0$ ) at 230 nm for the disassembly of The BA films; oBA (◆), mBA (■) and pBA (▲) with 10 mM fructose at pH 7.4, where the blue circle (●) is the initial measurement for each film. The red points represent stabilisation of the films in buffer before the addition of fructose, where  $A_0$  is the last stable measurement in buffer and  $A$  is the measured absorbance after the addition of fructose 215

## List of Schemes

### **Chapter 1: Literature Survey - Glucose Sensing for Diabetes Monitoring: History and Recent Developments**

**Scheme 1.1.** Production pathways of ketone bodies occurring in urine and exhaled breath. Adapted from reference 44. 13

**Scheme 1.2.** Conversion of glucose to gluconic acid using glucose oxidase. Adapted from reference 58. 18

### **Chapter 2: Direct Glucose Sensing: Probing Interactions Between Glucose and Fluorescent Boronic Acids**

**Scheme 2.1.** Synthesis of novel BA sensor (*o*-COOHBA). (i) Anhydrous DMF, N<sub>2</sub>, 80 °C for 4 days. 90

**Scheme 2.2.** Synthesis of novel BA sensor (*m*-COOHBA). (ii) Anhydrous DMF, N<sub>2</sub>, 66 °C for 4 days (61%). 91

**Scheme 2.3.** Fabrication steps taken for producing a doped PDMS ‘lens’ with *o*-COOHBA. 93

**Scheme 2.4.** Charge neutralisation-stabilisation interaction on glucose binding to the fluorescent *o*-COOHBA sensor, forming the non-fluorescent boronate-sugar complex. (i) Addition of glucose. (ii) Removal of glucose or addition of acid. 94

**Scheme 2.5.** Doped PDMS ‘lens’ with *o*-COOHBA. The ‘lens’ is fluorescent due to the presence of neutral BA group. When the ‘lens’ is then immersed in a solution containing glucose, the ‘lens’ becomes non-fluorescent due to the conformational change in boron to the anionic boronate form producing the boronate-glucose complex. (i) Addition of glucose (ii) Removal of glucose or addition of acid. 99

### **Chapter 3: Intermolecular Quenching and Recovery of Fluorescence Using Cationic Boronic Acid Derivatives for Indirect Glucose Sensing**

**Scheme 3.1.** Synthesis of BA1. (i) Diethyl ether, 20 °C for 24h. 111

**Scheme 3.2.** Synthesis of BA2. (i) PdCl<sub>2</sub>(PPh<sub>3</sub>)<sub>2</sub>, CuI, diethylamine, Ar, stirred at RT for 24h. (ii) Anhydrous THF, N<sub>2</sub>, reflux at 80 °C for 5 days. 112

### **Chapter 4: Water-Soluble Polymerisable Boronic Acids: Combining an Adaptable One-Step Synthesis with an In-Depth Understanding of pH and Glucose Response**

**Scheme 4.1.** Synthesis of *o*-BA. (i) CH<sub>2</sub>Cl<sub>2</sub>, N<sub>2</sub>, 35 °C, 24h (60%). 134

<b>Scheme 4.2.</b> Synthesis of <i>m</i> -BA. (i) CH <sub>3</sub> CN, N <sub>2</sub> , 20 °C, 24h (63%).	135
<b>Scheme 4.3.</b> Synthesis of <i>p</i> -BA. (i) CH <sub>2</sub> Cl <sub>2</sub> , N <sub>2</sub> , 20 °C, 24h (65%).	136

## **Chapter 6: Future Work: Sugar-Sensing Using Boronic Acid Polymers**

### ***Part A – Indirect Glucose Sensing in Ionogels***

<b>Scheme 6.1.</b> Synthesis of P <sub>6,6,6,14</sub> fluorescein ionic liquid.	181
<b>Scheme 6.2.</b> Synthesis of tetrabutylphosphonium sulfopropyl methacrylate IL monomer.	182
<b>Scheme 6.3.</b> Synthesis of <i>m</i> -MethylBA. (i) Anhydrous acetonitrile, N <sub>2</sub> , 24h.	184
<b>Scheme 6.4.</b> Synthesis of <i>o</i> -AminoBA. (i) Anhydrous acetonitrile, N <sub>2</sub> , 24h.	184

### ***Part C – Layer-by-Layer Films Composed of BA Linear Polymers and Poly(vinyl sulfonate, sodium salt)***

<b>Scheme 6.5.</b> Radical polymerisation of the BA monomers to form the linear polymers. (i) DMSO, PBPO (2 mol%) and THF, white light irradiation for 1h.	212
--	-----

Danielle Bruen

## **Novel Chemical Sensors Based on Boronic Acids for Glucose Detection**

### ***Thesis Abstract***

Boronic acid (BA) derivatives have been exploited for their strong and reversible interactions with diol-containing compounds for the recognition of saccharides, such as glucose. Combining BA groups and fluorescent moieties can allow for sugar concentrations to be monitored by changes in fluorescence. In this thesis, two approaches based on BA sensing capabilities are investigated. In a direct sensing approach, the BA group is covalently attached to the fluorescent reporter group. Conversely, in an indirect sensing approach, a two-component system is created when the BA group and fluorophore are incorporated in to separate molecules.

A direct sensing approach is described in Chapter 2, where the BA derivatives employed contain a quinoline-5-carboxylic acid functionality. These BA fluorescent sensors were investigated for their glucose sensing capabilities in solutions of various pH and when immobilised on to a 'lens-like' platform.

An indirect sensing approach is described in Chapter 3, where a BA-cationic pyrimidinium molecule, induced fluorescence quenching in an anionic fluorophore (7-hydroxycoumarin). On introducing glucose, the fluorescence was recovered. This sensing system was investigated in solutions of various pH.

Chapter 4 details the synthesis of a new family of BA-monomers. These monomers were characterised by  $^{11}\text{B}$  NMR and fluorescence in the absence and presence of glucose.

In Chapter 5, the BA-monomers described in Chapter 4 were investigated for indirect sensing with the anionic fluorophore pyranine in solution and in hydrogels.

Finally, in Chapter 6, additional strategies for the integration of a two-component sensing in to hydrogel matrices are investigated.

The aim of this research is the development of novel sensing systems that could be integrated in to a continuous glucose-monitoring device. Such a platform could offer diabetics personal control over monitoring their glucose levels, to aid the prevention of the side effects associated with the disease.

## Awards and Outputs Generated from this Research

### Awards

#### *Bursary Travel Awards*

1. Royal Society of Chemistry Researcher Mobility Award, worth £5000, awarded by The Royal Society of Chemistry, Cambridge, United Kingdom, to undertake a three-month research visit to the Australia Research Council (ARC) Centre of Excellence for Electromaterials Sciences (ACES) and the Intelligent Polymer Research Institute (IPRI), University of Wollongong, Australia, to work under the supervision of Prof. Gordon Wallace.

**“3-Dimensional (3D) Printing of Glucose-Sensing Boronic Acid Polymers”**, Danielle Bruen, Colm Delaney, Gordon Wallace, Dermot Diamond and Larisa Florea

2. Travel Grant Award, worth €400, awarded by The European Biophysical Societies' Association (EBSA), to attend the 4<sup>th</sup> Edition Conference on Analytical and Nanoanalytical Methods for Biomedical and Environmental Sciences, Transylvania University of Brasov, Romania, 29 June-1 July 2016.

**“Two-component Fluorescent Sensing of Saccharides”**, Danielle Bruen, Colm Delaney, Larisa Florea and Dermot Diamond.

#### *Best Poster Presentation*

**“Boronic Acid Derivatives for Indirect Fluorescent Glucose Sensing”**, Danielle Bruen, Colm Delaney, Larisa Florea, Dermot Diamond, *Insight Student Conference 2016, Dublin City University, Ireland, 14 Sept 2016.*

#### *Best Oral Presentation*

**“Applications of Fluorescent Biosensors for Non-Invasive Glucose Monitoring”**, Danielle Bruen, Colm Delaney, Larisa Florea and Dermot Diamond, *68th Irish Universities Chemistry Research Colloquium, University College Cork, Ireland, 23-24 June 2016.*

## Publications

1. Danielle Bruen,\* Paula Campos,\* Colm Delaney, Marystela Ferreira, Dermot Diamond and Larisa Florea, Boronic Acid Linear Homopolymers as Effective Polycations for Sugar-Responsive Layer-by-Layer Assemblies, *ACS Applied Materials and Interfaces*, **2018** (In preparation).
2. Danielle Bruen, Colm Delaney, Dermot Diamond and Larisa Florea, Water-Soluble Polymerisable Boronic Acids: Combining an Adaptable One-Step Synthesis with an Understanding of pH and Glucose Response, *Organic Letters*, **2018** (Submitted).
3. Danielle Bruen, Colm Delaney, Dermot Diamond and Larisa Florea, A Two-Component Fluorescent System for Sugar-Sensing, *Journal of the American Chemical Society*, **2018** (Submitted).
4. Colm Delaney, Larisa Florea, Danielle Bruen, Dermot Diamond, Boronic Acid Derivatives for Sugar-Sensing Hydrogels, GB Patent, GB1805226.6, 29 March 2018.
5. Danielle Bruen, Colm Delaney, Larisa Florea and Dermot Diamond, Glucose Sensing for Diabetes Monitoring: Recent Developments, *Sensors*, **2017**, *17*, 1866-1887.

\* *Authors who contributed equally to this work*

## Conference Contributions

### *Oral Presentations*

*(First author of the contribution represents the presenting author)*

- [1] **“Biomimetic microfluidics and stimuli responsive materials: new solutions to old problems in bio-chemical sensing”**, Dermot Diamond, Aishling Dunne, Danielle Bruen, Colm Delaney, Peter McCluskey, Margaret McCaul and Larisa Florea, *Invited Seminar and Research Meetings, University of Granada, Spain*, 18 Oct 2017.
- [2] **“Bioinspired Microfluidics”**, Dermot Diamond, Aishling Dunne, Danielle Bruen, Colm Delaney, Peter McCluskey, Margaret McCaul, Larisa Florea, (2017), *Biodetection & Biosensors 2017, Cambridge, UK*, 10-11 Oct 2017.
- [3] **“Novel Chemical Sensors Based on Boronic Acids for Glucose Detection”**, Danielle Bruen, Colm Delaney, Larisa Florea and Dermot Diamond, *2<sup>nd</sup> DCU Chemistry Day, Dublin City University, Ireland*, 12 May 2017.
- [4] **“Fluorescence Sensing for Non-Invasive and Continuous Glucose Detection”** Danielle Bruen, Adam McColgan, Colm Delaney, Larisa Florea and Dermot Diamond, *American Advanced Materials Congress 2016, The Caribbean Sea, Miami, Florida, USA*, 4-9 December 2016.
- [5] **“Two-Component Fluorescent Sensing of Saccharides”**, Danielle Bruen, Colm Delaney, Larisa Florea and Dermot Diamond, *4th Edition Conference Analytical and Nanoanalytical Methods for Biomedical and Environmental Sciences, Transylvania University of Brasov, Romania*, 29 June-1 July 2016.
- [6] **“Stimuli-Responsive Materials for Self-Reporting Micro-Fluidic Devices”**, Larisa Florea, Aishling Dunne, Wayne Francis, Danielle Bruen, Alexandru Tudor and Dermot Diamond, *4th Edition Conference Analytical and Nanoanalytical Methods for Biomedical and Environmental Sciences, Transylvania University of Brasov, Romania*, 29 June-1 July 2016.
- [7] **“Applications of Fluorescent Biosensors for Non-Invasive Glucose Monitoring”**, Danielle Bruen, Colm Delaney, Larisa Florea and Dermot Diamond, *68th Irish Universities Chemistry Research Colloquium, University College Cork, Ireland*, 23-24 June 2016.



- [6] **“From Finger Prick Sampling to On-Body and Ultimately Implantable Chem/Bio-Sensors: The Key Role of Active Fluidics in Realising the Long-Term Functional Platforms of the Future”**, Larisa Florea, Danielle Bruen, Wayne Francis, Aishling Dunne, Simon Coleman, Aymen BenAzouz and Dermot Diamond, *CIMTEC 2016, Perugia, Italy*, 8 June 2016.
- [8] **“Boronic Acid Derivatives for Saccharide Sensing”**, Danielle Bruen, Colm Delaney, Larisa Florea and Dermot Diamond, *8<sup>th</sup> Conference on Analytical Science Ireland (CASi) 2016, Dublin City University, Ireland*, 14-15 April 2016.
- [9] **“Bio-Inspired Active Fluidic Systems Based on Stimuli-Responsive Materials”**, Dermot Diamond, Larisa Florea, Wayne Francis, Alexandru Tudor and Danielle Bruen, *67th Irish Universities Chemistry Research Colloquium, National University of Ireland Maynooth, Ireland*, 25-26 June 2015.

*Poster Presentations*

- [1] **“Novel Chemical Sensors Based on Boronic Acids for Glucose Detection“**, Danielle Bruen, Colm Delaney, Larisa Florea and Dermot Diamond, *69<sup>th</sup> Irish Universities Chemistry Research Colloquium, Dublin City University, Ireland, 22-23 June 2017.*
- [2] **“Indirect Optical Glucose Detection Using a Two-Component Sensing System”** Danielle Bruen, Colm Delaney, Larisa Florea and Dermot Diamond, *Next Generation Analytical Platforms for Environmental Sensing (NAPES) 2017 – Sensing in our Environment: From Innovative Materials to Autonomous Sensors and Earth Observation, Croke Park, Dublin, Ireland, 27-28 March 2017.*
- [3] **“Boronic Acid Derivatives for Indirect Fluorescent Glucose Sensing”**, Danielle Bruen, Colm Delaney, Larisa Florea, Dermot Diamond, *3<sup>rd</sup> Insight Student Conference 2016, Dublin City University, Ireland, 14 Sept 2016.*
- [4] **“Fluorescent Boronic Acid Derivatives for Glucose Biosensing”**, Danielle Bruen, Larisa Florea and Dermot Diamond, *Europt[r]ode XIII 2016, University of Graz, Graz, Austria, 20-23 March 2016.*
- [5] **“Ocular Glucose Biosensing Using Boronic Acid Fluorophores”**, Danielle Bruen, Larisa Florea, Dermot Diamond, *2<sup>nd</sup> Insight Student Conference 2015, National University of Ireland Galway, Ireland, 30 October 2015.*
- [6] **“Glucose Sensing in Real-Time Using Boronic Acid Derivatives”**, Danielle Bruen, Larisa Florea, Dermot Diamond, *NanoNet Ireland 2015, University of Limerick, Ireland, 21-22 Oct 2015.*
- [7] **“Fabrication of Non-Enzymatic Optical Glucose Sensors Based on Boronic Acid Derivatives”**, Danielle Bruen, Larisa Florea, Dermot Diamond, *XIV Brazil Materials Research Meeting 2015, Sul America Convention Centre, Rio de Janeiro, Brazil, 27-30 Sept 2015.*
- [8] **“Contact Lenses for Real-Time Colorimetric Sensing of Glucose”**, Danielle Bruen, Rami Albatal, Larisa Florea, Dermot Diamond, *Advanced Materials World Congress 2015, The Baltic Sea, Stockholm, Sweden, 23-26 Aug 2015.*
- [9] **“Boronic Acid Derivatives for Sugar Sensing”**, Danielle Bruen, Larisa Florea, Dermot Diamond, *67<sup>th</sup> Irish Universities Chemistry Research Colloquium, National University of Ireland Maynooth, Ireland, 25-26 June 2015.*

# Chapter 1

---

## Literature Survey

### **Glucose Sensing for Diabetes Monitoring: History and Recent Developments\***

---

\*Part of this chapter has been published as “Glucose Sensing for Diabetes Monitoring: Recent Developments”, [Danielle Bruen](#), Colm Delaney, Larisa Florea and Dermot Diamond, *Sensors*, 2017, *17*, 1866-1887.

## Contents

### Chapter 1: Literature Survey - Glucose Sensing for Diabetes Monitoring: History and Recent Developments

<b>1.1 Introduction to Diabetes</b>	<b>8</b>
1.1.1 History of Diabetes Mellitus	9
1.1.2 Types of Diabetes	10
1.1.3 Diabetic Ketoacidosis	12
1.1.4 Treating Diabetes – From Ancient Times to Present	13
1.1.5 Statistics	15
<b>1.2 Glucose Monitoring</b>	<b>17</b>
1.2.1 Glucose Monitoring Methods in Blood From Past to Present	17
1.2.2 Monitoring Glucose in Alternative Physiological Fluids	21
<i>1.2.2.1 Interstitial Fluid</i>	21
<i>1.2.2.2 Urine</i>	25
<i>1.2.2.3 Sweat</i>	26
<i>1.2.2.4 Breath Analysis</i>	31
<i>1.2.2.5 Saliva</i>	33
<i>1.2.2.6 Ocular Fluid</i>	35
<b>1.3 Fluorescence Sensing</b>	<b>40</b>
1.3.1 Phenomena of Fluorescence	40
1.3.2 Mechanisms and Dynamics of Fluorescence Sensing	42
<b>1.4 Boronic Acids</b>	<b>46</b>
1.4.1 Direct Sensing	50
1.4.2 Indirect Sensing	56
<b>1.5 Aim</b>	<b>68</b>
<b>1.6 References</b>	<b>70</b>

## 1.1 Introduction to Diabetes

*Diabetes mellitus* is an incurable disease<sup>1-3</sup> resulting from an insufficiency of insulin.<sup>4</sup> This disease causes classic elevated blood-glucose levels, known as hyperglycaemia or reduced glucose concentrations known as hypoglycaemia due to an insufficient insulin supply.<sup>5</sup> Insulin is a hormone that is synthesised and secreted by the pancreas to mediate metabolic reactions with glucose.<sup>1, 2, 6-9</sup> In doing so, it signals to cells around the body that require energy to uptake glucose, hence reducing glucose concentrations in blood.<sup>4, 10</sup> The malformation in these metabolic processes can progress, regress or stay the same in the case of diabetes, meaning that early diagnosis is imperative for preventing grave lasting side effects. As a result, diabetes is associated with many complications including coeliac disease, cystic fibrosis, tuberculosis and heart disease, promoting acute and chronic complications that can result in retinopathy leading to blindness, nephropathy giving rise to renal failure, peripheral nerve damage with increasing risks of foot ulcers, amputation, cardiovascular diseases, cancer or kidney failure.<sup>3, 4, 11-16</sup> Diabetes has been described as a “silent epidemic” in a review detailing the origin of the disease by C. Nwaneri<sup>17</sup> and since its discovery, great efforts have been made to understand the disease in order to achieve efficient diagnosis, monitoring and treatment. In the current chapter, a review of diabetes summarising the history and treatments of the disease from past to present is described.

A plethora of biosensors have been developed to provide diagnostic information regarding a patient’s health status. Many different types of sensors have been investigated, and a 2010 review by Toghil and Compton provides a great insight into enzymatic and non-enzymatic electrochemical glucose sensing approaches studied over the past decade.<sup>18</sup> Spectroscopic methods for non-invasive glucose detection have also been growing in popularity, with Raman and infrared spectroscopy being of particular attention.<sup>19-21</sup> For applications of clinically relevant biosensors, the reader is directed to excellent reviews by Corrie *et al.*<sup>22</sup> and Yoo *et al.*<sup>23</sup> However, the real challenge that remains is the creation of biosensors for daily use by patients for personalised monitoring.<sup>22</sup>

In order to fabricate a personalised monitoring device, the device design must be fully understood and characterised. Several reviews focusing on sensor integration in to wearable platforms have been published recently.<sup>24-26</sup> Therefore, this present

review chapter will focus solely on recent advances made for monitoring glucose in alternative biological fluids, such as interstitial fluid, sweat, breath, saliva and ocular fluid, towards the aim of producing a non-invasive and continuous glucose monitoring device for diabetics.

### 1.1.1 History of Diabetes Mellitus

The history of *diabetes mellitus* dates back to ancient Egypt circa 1500 BC.<sup>12, 17, 27</sup> Although the Egyptians were the first to discover the disease, it was around this time that physicians in India generated a crude test for distinguishing diabetic urine.<sup>12</sup> They were descriptive in noting that ants and flies were attracted to the sweetness of diabetic patients' urine,<sup>17</sup> where this condition was referred to as 'honey urine'.<sup>12, 27</sup> The name *diabetes mellitus* originated from the Greeks, where diabetes is the Greek word for 'siphon' or 'drain',<sup>27</sup> referring to the frequent 'draining' of urine from the body, which was one of the main symptoms of the disease noted at the time.<sup>17, 27</sup> The disease kept this name until the late 18<sup>th</sup> century, when a Scottish trained surgeon of the British army paired diabetes with 'mellitus', meaning 'honey' and from then on the disease was known as *diabetes mellitus*.<sup>17, 27</sup>

It wasn't until around 30 BC-50 AD that the first symptoms of diabetes were recognised and reported by A. C. Celsus of Greece.<sup>28</sup> He observed that excessive urination in frequency and volume, as well as weight loss were the obvious side effects of this disease. An Egyptian physician correlated these symptoms to Celsus' analysis of excessive urination to the kidneys almost 180 years later and it was around this time that the main characteristics of diabetes were labelled as excessive thirst, increased urination and over eating.<sup>17</sup>

The first crude treatment for the disease was publicized around this time as dehydration and phlebotomy (bloodletting), due to a lack of information for understanding the disease.<sup>17</sup> These severe treatments increased further awareness of diabetes and progressed research of the disease in to the mid-6<sup>th</sup> century, where the use of emetic medicines for inducing vomiting or the use of laxatives, as well as narcotics,<sup>17</sup> like opium, were prescribed for the next 200 years.<sup>27</sup> During the period between 980-1037, an Arabian clinical physician described that diabetes related to complications of the nervous system as well as liver dysfunction. He encouraged his patients to use emetic medicines as well as exercises to help manage the symptoms.

This slow evolution of diagnosing and treating diabetes only reached the UK in 1674, almost 2500 years later from the first discovery in ancient Egypt.<sup>29,30</sup> In 1674 an Oxford-qualified British physician, Thomas Willis, re-focused attention towards the sweet urine of diabetic patients.<sup>29-31</sup> At the time, the sweet substance was still unknown and it was only in 1766 that Matthew Dobson in Liverpool, confirmed that the sweet substance was sugar.<sup>30</sup> Nearly 50 years later in Paris, Chevreul tagged this sugar to be glucose.<sup>12,17</sup> He proposed that glucose was not synthesised in the kidneys, as previously thought, but in fact was used by the blood and it was the misuse of glucose by the blood that resulted in its accumulation in urine.<sup>32</sup>

In 1840, a breakthrough was made by the physiologist Claude Bernard, who concluded that glucose production was linked to the pancreas.<sup>17, 33</sup> Bernard determined that glucose was absorbed from the intestines in to the liver where the reversible conversion to glycogen was possible.<sup>34</sup> Bernard also reported that sugar was present in the blood of normal animals, even when fasting, as well as “enormous quantities” of a starch-like substance in the liver. When tested, this substance was not a true sugar, but found it could be transformed into one and therefore, it was named glycogen.<sup>34</sup> Bernard was the first to report on glucose metabolism, where he stated that glycogen was produced from glucose in the liver, introducing the “glycogenic theory”.<sup>17</sup> The Bernard hypothesis resulted in an escalation of research in the areas of diabetic ketoacidosis and diagnosing, as well as monitoring and treating diabetes, which were all imperative for today’s understanding of the disease. Currently there is no cure available for this life-threatening disease.<sup>17,35</sup>

### 1.1.2 Types of Diabetes

Diabetes mellitus can be classified by three different types; type 1, type 2 and type 3, respectively, and it is known to affect people of all ages worldwide.<sup>4, 11, 36, 37</sup> Type 1 diabetes is more commonly known as juvenile onset or insulin-dependent diabetes, which has been correlated to an autoimmune dysfunction.<sup>4,38</sup> In this case, the diabetic patient can’t produce insulin due to an attack by antibodies on the islet  $\beta$ -cells of the pancreas, known to stimulate insulin release.<sup>16, 38</sup> Antibodies for islet cells, namely insulin, glutamic acid decarboxylase and tyrosine phosphate IA-2 and IA-2  $\beta$  are known to initiate attack on the islet  $\beta$ -cells.<sup>4</sup> As a result, diabetic ketoacidosis can more easily manifest due to stress or infection.<sup>5</sup> This immune-mediated disease has a genetic correlation as well as environmental relations, where insulin is necessary to

survive.<sup>4</sup> Approximately 5-10% of all diabetics suffer from type 1 diabetes,<sup>16</sup> where the strong genetic influences are mostly from Asian or African origin.<sup>4, 39</sup>

Conversely, in type 2 diabetes, the body can produce insulin, but can't use the insulin effectively, either by deficiencies in insulin resistance or secretion.<sup>1-4, 6, 8</sup> Type 2 diabetes is known as non-insulin dependent diabetes or adult-onset diabetes, where in most cases diabetics don't require insulin to survive. Around 90-95% of people suffering from diabetes are type 2 diabetics,<sup>16, 38</sup> where these patients quite often suffer with obesity and have some predisposition to diabetes.<sup>4</sup> Obesity can develop from a diet of increased glucose intake and little exercise, where studies have shown that a healthy diet and physical exercise can contribute to better management of the disease.<sup>40, 41</sup> The build-up of adipose tissue in the abdominal region resulting in obesity can cause type 2 diabetes, however when accompanied by an infection or stress, ketoacidosis in these patients can be triggered.<sup>4</sup> On the other hand in patients suffering from type 1 diabetes, although these patients are rarely obese, obesity can lead to worsening of the disease.<sup>4</sup> In type 2 diabetes, the pancreas can become over stimulated for insulin, due to the constant elevated levels of glucose present in the blood. Failing to sufficiently produce these required heightened insulin levels, increases the risk of vascular complications hence inducing cardiovascular disease.<sup>4</sup>

Type 3 diabetes is another branch of the disease relating to insulin resistance.<sup>5</sup> Type 3 is suspected to link diabetes with neurodegeneration, which can ultimately lead to complications such as Alzheimer's disease.<sup>5</sup> Evidence in the literature has become increasingly suggestive that insulin resistance and Alzheimer's disease are strongly related, although this phenomenon has yet to be widely accepted.<sup>5</sup>

Gestational diabetes occurs more predominantly during the third trimester of pregnancy.<sup>4, 38</sup> It is described as the onset or first recognition of glucose intolerance in pregnant women, dismissing whether or not insulin or diet are factors for treatments. Approximately 4% of all pregnancies in the U.S. are complicated by gestational diabetes, which sums to near 135,000 pregnancies per year.<sup>4</sup> It has also been shown that these women and their children are more likely to suffer from diabetes disease later in life.<sup>38</sup>

Other types of diabetes may be induced from a number of environmental or genetic circumstances. Common genetic predispositions that increase the risk of diabetes include endocrinopathies, mutations in the insulin-producing  $\beta$ -cell and genetic



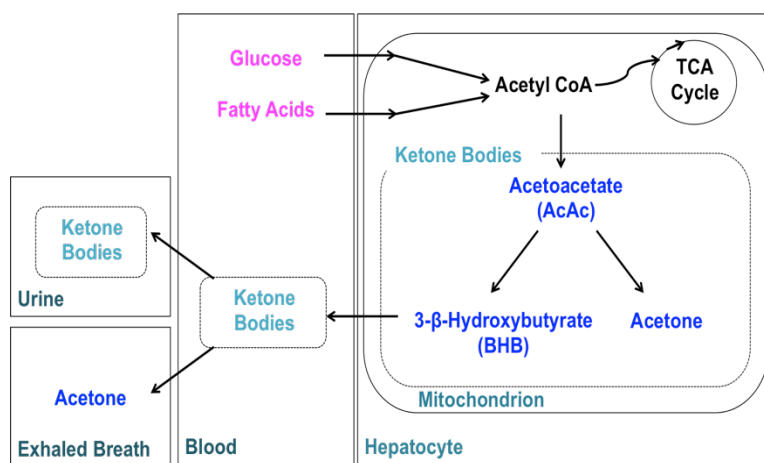
syndromes such as Down's syndrome and Leprechaunism, that can lead to insulin resistance.<sup>4</sup> Mutations in transcription factors during DNA replication can result in abnormal glucokinase formation. Glucokinase has an important role in glucose metabolism, converting glucose to glucose-6-phosphate for energy release and stimulating insulin secretion.<sup>4</sup> Environmental factors such as contracting infections and drug use are known to inhibit  $\beta$ -cell functioning, where this can lead to diabetes.<sup>42</sup> Many drugs or medications, such as steroids or pentamidine, a medicine prescribed for pneumonia, are known to impair insulin activity. This becomes an issue when some patients are predisposed to having an intolerance level for glucose referred to as "pre-diabetes", which could advance to the diagnosis of diabetes.<sup>4</sup>

### 1.1.3 Diabetic Ketoacidosis

Diabetic Ketoacidosis is commonly presented in diabetic patients that exhibit a deficiency in insulin.<sup>4, 5, 35, 43</sup> It was discovered by William Prout in 1848 and since then has been an important factor to consider in treating and monitoring the symptoms of diabetes. Elevated levels of regulatory hormones such as glucagon, catecholamines, cortisol and growth hormones, simultaneously result in an insulin deficiency due to stress or infection.<sup>4, 35</sup> This combination of increased regulatory hormones and insulin deficiency creates a catabolic state of gluconeogenesis and glycogenolysis, resulting in heightened glucose levels in the kidneys and liver. Excessive production of glucose combined with the breakdown of fatty acids generates elevated concentrations of ketone bodies as by-products (Scheme 1.1).<sup>35, 43, 44</sup> These raised levels of ketone bodies can then enter into the bloodstream, where they migrate to adipose tissue for storage or are expelled in urine or exhaled breath as volatile organic compounds (VOCs).<sup>43, 44</sup> By entering the bloodstream, these VOCs can inhibit glycation of insulin, where this is thought to explain insulin resistance<sup>5</sup> and also lower the pH of blood, making it more acidic,<sup>43</sup> where the pH of blood is normally in the range of pH 7.35-7.45.<sup>22</sup> The main symptoms associated with diabetic ketoacidosis are very similar to *diabetes mellitus*, although since some of the ketone bodies have the ability to cross the blood-brain barrier, these molecules can also affect the nervous system. The three main ketone bodies produced in the liver are acetone, beta-hydroxybutyrate and acetoacetate.<sup>5, 43, 44</sup>

Beta-Hydroxybutyrate is the most prevailing ketone body. It is produced from the reduction of acetoacetate (Scheme 1.1).<sup>44</sup> Ketone bodies are known to be present in

high levels in the blood during fasting and prolonged exercise in both normal and diabetic patients.<sup>5</sup>



**Scheme 1.1.** Production pathways of ketone bodies occurring in urine and exhaled breath. Adapted from reference 44.

Diabetic ketoacidosis is a common pathological cause of elevated blood-glucose levels in diabetic patients, resulting from lipolysis in hypoinsulinemic conditions. When this occurs, the ratio between beta-hydroxybutyrate and acetoacetate increases from 1:1 to 10:1.<sup>5</sup> This can be detected in the blood of diabetic patients and has the potential to be used as a diagnosis tool for diabetic ketoacidosis and *diabetes mellitus*.<sup>35</sup>

Acetone is another ketone body that has been investigated for diabetes detection. It is a colourless, sweet VOC that is exhaled in breath or excreted in urine.<sup>43, 45</sup> The body naturally produces this 3-carbon ketone in a basal state, where it is formed from the decarboxylation of acetoacetate by acetoacetate decarboxylase and from the oxidation of non-esterified fatty acids.<sup>43, 44</sup> A linear relationship between the breath and blood acetone levels has been established, where breath analysing devices for acetone levels have been considered for diabetes diagnosis (see Section 1.2.2.4).<sup>43</sup>

#### 1.1.4 Treating Diabetes – From Ancient Times to Present

As previously mentioned, several distressing methods for ‘treating’ *diabetes mellitus* were employed in ancient times.<sup>17</sup> Initially narcotics and laxatives were prescribed, however they fell short of showing any benefits. It wasn’t until the early 19<sup>th</sup> century that diet and exercise were discovered to alleviate some of the symptoms

of diabetes.<sup>17, 27</sup> Towards the end of this century and in to the early 20<sup>th</sup> century, pancreatic extracts containing insulin-producing islet cells were used in an attempt to improve the quality of life for patients suffering from this disease. This idea first originated from an experiment carried out by Mering and Minkowski in 1889, when they surgically removed the pancreas of a dog. They found that the dog developed diabetes without a pancreas.<sup>17, 27</sup> Mering and Minkowski's experiment confirmed that the pancreas played an important role in the disease. Thus, this discovery led to another experiment whereby a pancreatic component of a codfish was injected in to a dog, which was carried out by Rennie and Fraser in Aberdeen, in 1902. The dog died soon after of suspected severe hypoglycaemia or anaphylactic shock, or both.<sup>17, 27</sup> George Ludwig Zeuler, a German physician, also carried out similar experiments on dying diabetic patients. In 1908 he proved that the patient could be 'cured' of any symptoms of diabetes, although high mortality rates accompanied when this approach was performed on comatose patients.<sup>17</sup> Tests were carried out weeks post-treatment, which showed that the insulin-producing islet cells were still viable, although enzyme destruction of the pancreatic duct post-transplantation was the main reason this was not an applicable solution.<sup>17, 27</sup> Other pancreas extracts for transplantation in dogs were also attempted, however none of these approaches led to a cure for the disease.

Up until the early 1900s, insulin was described in scientific procedures but not named or discovered.<sup>17, 27</sup> Banting and colleagues coined this term in 1921 when they extracted and purified insulin by an acid-ethanol extraction from a dog's pancreas, making it available for the first time to people suffering with diabetes.<sup>17</sup> This important discovery was built on previous knowledge from different research groups including Kleiner, at the Rockefeller Institute and New York Medical College in 1919, Baron in Minneapolis in 1920, the works of Paulescu in Bucharest in 1916-1920 and the discovery of the 'islet cells of Langerhans' by Paul Langerhans in 1869.<sup>17</sup> This research won the Nobel Prize in Physiology and Medicine in 1923, after a boy was successfully treated for diabetes using insulin.<sup>27</sup> The results showed a reduction in ketone body concentration and glucose concentration in the boy's blood and urine.<sup>17</sup>

This astounding revelation lead to the explosive development of drugs in an attempt to control glycaemic blood levels.<sup>17</sup> A wide variety of insulin-based drugs were commercially identified that would revolutionise diabetes care. Insulin was extracted from animals, such as cows, where this bovine insulin could be used to

control glycaemic levels in humans over a prolonged period of time.<sup>17, 27</sup> This led to the establishment of diabetic clinics, first in London, launched by the endocrinologist Robert Lawrence, which further contributed to the establishment of insulin pharmaceutical companies like Novo Company and Nordisk Insulinlaboratorium in Denmark. These companies merged in 1923 to form Novo Nordisk, which is currently the largest Insulin pharmaceutical company in the world.<sup>17</sup>

In the 1950s, the first oral drugs to combat diabetes were produced.<sup>27</sup> They were a class of sulphonylureas and were discovered by serendipity. When investigating the antibiotic properties of sulphonamides on animals, these drugs demonstrated a hypoglycaemic effect.<sup>17</sup> The introduction of carbutamide, a well-known hypoglycaemic agent, to the market in 1955 caused research on additional medications (*e.g.* phenformin and metformin, types of glucosidase inhibitors and insulin sensitizers) to exponentially increase.<sup>27</sup> It took another 30 years for the first human insulin manufacture, by Graham Bell and a further two years for the first biocompatible insulin known as humulin to be fabricated. Insulin could be administered intravenously, where the elusive goal was to produce insulin in an orally available drug.<sup>27</sup> In the 1950s the production of hypoglycaemic agents was at its peak, however since then no new medications have been developed. Due to the polypeptide nature of insulin and its immediate metabolism by enzymes when orally digested, producing a form of insulin that can be orally administered remains a major challenge. Currently, an oral insulin drug for diabetes treatment is still desired to replace repeated invasive injections of insulin.<sup>17</sup>

### 1.1.5 Statistics

Between 1980 to 2014 the prevalence of diabetes was monitored (Figure 1.1).<sup>39</sup> Research shows that in 1980, approximately 108 million people suffered from this disease, where this number has nearly quadrupled to 422 million by 2014, demonstrating its epidemic nature. It is thought that by 2025 diabetes will affect over 700 million people worldwide.<sup>39</sup> Men currently exceed the amount of women suffering from diabetes, where it is thought that men acquire higher risk factors for the disease due to environmental habits such as smoking, little exercise and high body mass index rates, leading to increased adiposity in the abdominal region.<sup>39, 49</sup>

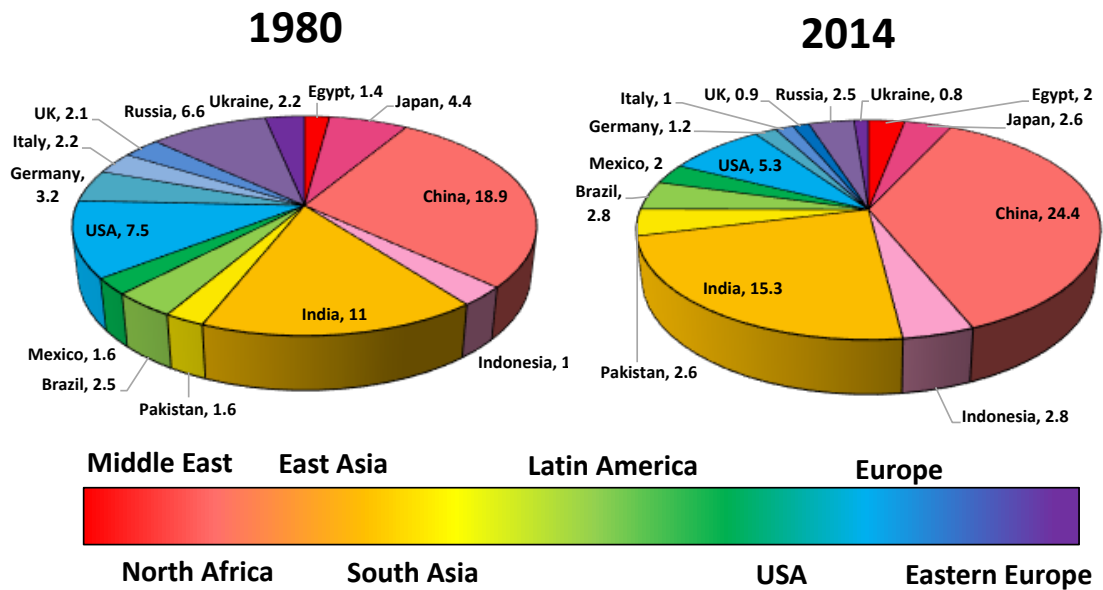


**Figure 1.1.** World population (%) for people suffering from diabetes in 1980 (left) compared to the revised figures in 2014 (right) for the top ten countries with the highest prevalence of the disease. Adapted from reference 39.

The regions of the world most affected by this disease are Polynesia and Micronesia (the thousands of islands found in the sub region of the South and West Pacific Ocean), The Middle East and North Africa, followed by India and China.<sup>39</sup> The latter are speculated due to their ever-increasing populations.<sup>50</sup> Currently, the U.S. territory American Samoa, located in the South Pacific Ocean, holds the title for the highest national prevalence of diabetics.<sup>39</sup> Half of the world's population, comprising China, India, USA, Brazil and Indonesia accounted for half of the world's diabetic populations in 2014, where this number is continually growing.<sup>39</sup>

As predicted, diabetes has escalated in countries with low and middle-incomes compared to that of countries with higher revenues.<sup>39</sup> Recently, Indonesia, Pakistan, Mexico and Egypt were deemed in the top ten countries with the highest number of adults with diabetes, over European countries such as Germany, Ukraine, Italy and the UK in previous years.<sup>39, 50</sup> The main reasons for this is thought to result from a number of factors, such as obesity, availability of medical supplies, genetic susceptibility, dietary habits and physical activity.

Lifestyle choices and genetic influences are the two main factors known to affect the predisposition to diabetes. Obesity is a major side effect of the disease, as mentioned before, in particular for type 2 diabetics. High calorific intake and poor dietary patterns can lead to adiposity. The lack of physical exercise can also play a

role, where the rate of fat storage overcomes the rate of fat conversion to energy. The second risk factor for susceptibility to this disease is a genetic influence, where certain regions of the world are known for an earlier onset of the disease due to environmental effects like poor nutrition in early-foetal and childhood development stages, for example in Asian populations. A reason for this is thought to rise from a lack of available medical services, where identifying  $\beta$ -cell dysfunction could act as a preventative or earlier diagnosis test.<sup>50</sup> Only few developed countries offer clinical aid towards developing countries for the treatment of diabetes. This means that in developing countries identifying the disease at an early stage, treatments and lifestyle alteration guidelines are scarce, which could account for the high prevailing rate of the disease. Monitoring diabetes for early detection and diagnosis has shown to be expensive, especially in developing countries.<sup>39</sup>

## **1.2 Glucose Monitoring**

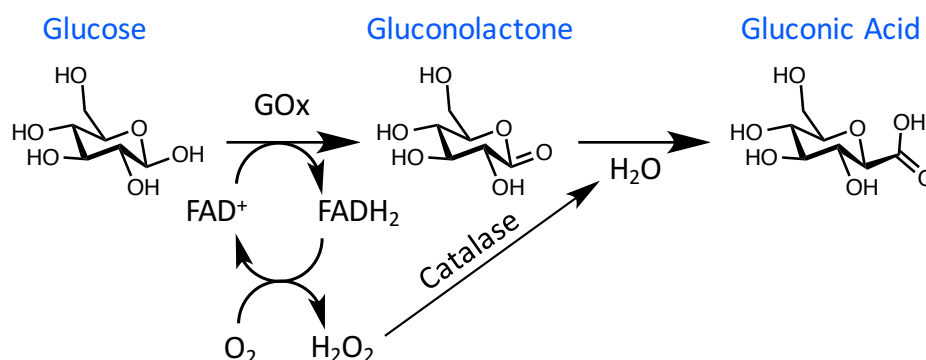
### **1.2.1 Glucose Monitoring Methods in Blood from Past to Present**

As a preventative treatment or cure for diabetes is yet to be developed, managing the life-impeding conditions of this disease is currently the most successful means for its control. Monitoring glucose levels in blood, as a disease marker, has proven to prolong life expectancy by enabling diabetics to manage episodes of hypo- or hyperglycaemia, hence providing better control over their condition and preventing some of the debilitating side effects.<sup>16,38</sup> In addition, glucose monitoring can be used to optimise patient treatment strategies, and provide an insight into the effect of medications, exercise and diet on the patient.<sup>23</sup> Although blood-glucose monitoring is the gold-standard medium for glucose sampling, measurements carried out in this fluid are invasive.<sup>25,38</sup> Blood-glucose concentrations are typically in the range of 4.9–6.9 mM for healthy patients, increasing to up to 40 mM in diabetics after glucose intake.<sup>4, 12, 16, 38, 51</sup>

Clark and Lyons at the Children's Hospital in Cincinnati proposed in 1962 the first-generation of glucose biosensors.<sup>52</sup> These sensors were initially based on an electrochemical approach, which used the enzyme glucose oxidase (GOx).<sup>23</sup> Electrochemical sensors were chosen for blood-glucose measurements due to their high sensitivity, on the order of  $\mu\text{M}$  to mM, good reproducibility and ease of fabrication at relatively low cost.<sup>38</sup> GOx was employed as the enzymatic basis for the

sensor, owed to its high selectivity for glucose. Less common enzymes, such as hexokinase and glucose-1-dehydrogenase were also used for glucose measurements,<sup>53, 54</sup> but GOx can tolerate extreme changes in pH, temperature and ionic strength in comparison with other enzymes. Withstanding these conditions can be important during any manufacturing processes, making it a prime candidate for glucose monitoring devices.<sup>55, 56</sup>

GOx catalyses the oxidation of glucose to gluconolactone in the presence of oxygen, while producing hydrogen peroxide ( $H_2O_2$ ) and water as by-products (Scheme 1.2).<sup>23</sup> Gluconolactone further undergoes a reaction with water to produce the carboxylic acid product, gluconic acid. GOx requires a redox cofactor to carry out this oxidation process, where flavin adenine dinucleotide ( $FAD^+$ ) is employed.  $FAD^+$  is an electron acceptor which becomes reduced to  $FADH_2$  during the redox reaction.<sup>57</sup> Subsequent reaction with oxygen to produce  $H_2O_2$  regenerates the  $FAD^+$  cofactor. This reaction occurs at the anode, where the number of transferred electrons can be correlated to the amount of  $H_2O_2$  produced and hence the concentration of glucose.<sup>57</sup>



**Scheme 1.2.** Conversion of glucose to gluconic acid using glucose oxidase. Adapted from reference 58.

In the sensor design presented by Clark and Lyons, indirect quantification of glucose concentrations was achieved by placing a thin layer of the GOx enzyme on a platinum electrode via a semipermeable dialysis membrane. This sensor measured the decrease in oxygen concentration and the liberation of hydrogen peroxide, which was proportional to the glucose concentration.<sup>52</sup> The main obstacle to overcome with this approach was the interference of other electroactive species present in blood, such as ascorbic acid and urea.<sup>23, 59</sup> This approach was further developed in 1975, when the first successful commercial sensor based on GOx was made available.<sup>23</sup> This sensor

directly measured glucose concentrations by amperometric detection of hydrogen peroxide. The electrochemical signal required a high operating potential and due to the expensive nature of the platinum electrode used, the use of this device was strictly confined to clinical settings.<sup>23</sup> This led to the second generation of glucose-biosensors in the 1980s.<sup>59</sup>

In the design of first generation sensors, oxygen was employed as the electron-acceptor, which can result in errors from variations in oxygen tension and limitations, known as the oxygen deficit.<sup>60</sup> This deficit is caused by oxygen concentrations being one order of magnitude lower than measured glucose concentrations. In order to overcome these challenges, oxygen was replaced with a synthetic electron redox mediator in second generation sensors.<sup>60</sup> The evolution of this sensing approach also led to the development of disposable enzyme electrode strips, which were accompanied by a pocket-size blood-glucose meter.<sup>61, 62</sup> Each strip housed miniaturised screen-printed working and reference electrodes, where the working electrode was coated with the required sensing components; glucose oxidase, an electron-shuttle redox mediator, stabilizer and linking agent. These revolutionary second-generation glucose sensors directly resulted in the advent of self-monitored glucose management, known as the “finger-pricking” approach.

Currently, the most widely used self-monitoring method involves this ‘finger-pricking’ approach. It is enzymatic-based and involves sampling blood from a finger via pricking, to be analysed by *in vitro* methods using test strips and a glucometer (Figure 1.2).<sup>2, 10, 36, 51, 63, 64</sup> The effectiveness of this method relies on strict compliance, which can be negatively influenced by time constraints, pain, and inconvenience.<sup>65</sup> It is also not a continuous monitoring approach and needs to be carried out at multiple intervals throughout the day to help manage elevated glucose levels,<sup>38, 57</sup> especially after meals,<sup>2</sup> exercise<sup>2, 12</sup> and dosing of insulin medication.<sup>2, 12, 37, 65</sup> Moreover, a non-continuous method such as this can overlook periods of hyper- or hypoglycaemia which occur outside of the sampling window.<sup>65</sup> Recent developments in implantable sensors, on the other hand, can be used to incorporate insulin pumps, which allow for immediate insulin administration.<sup>12, 36, 37, 64, 65</sup>



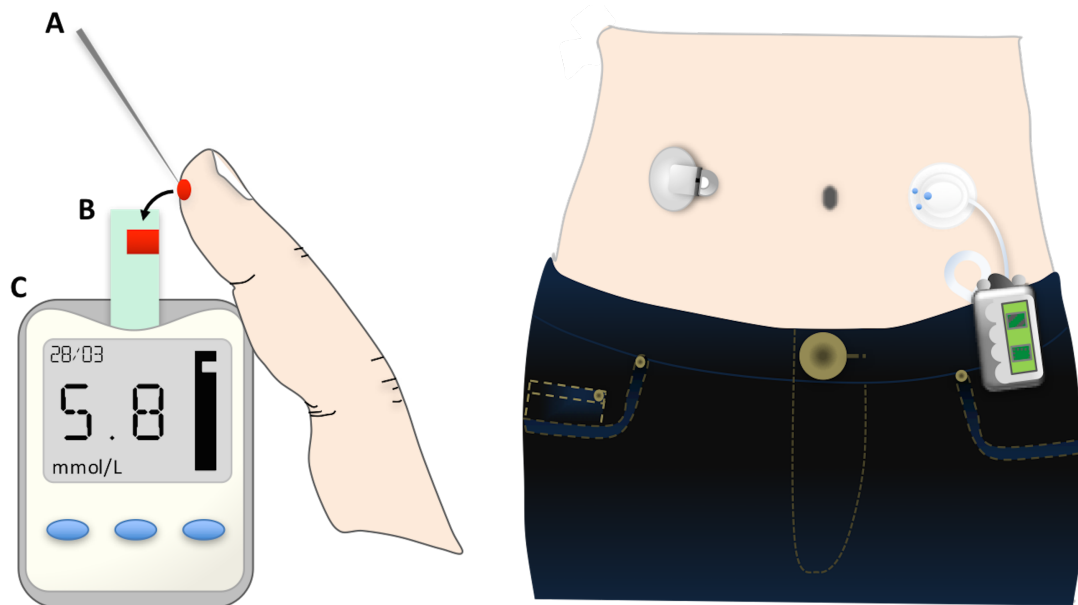


**Figure 1.2.** Finger pricking device (left). (A) Lancet needle. (B) Blood sample on test-strip. (C) Glucose meter displaying date and glucose concentration in mmol/L; Continuous glucose monitor (right). Adapted from references 66 and 67.

In the early 1970s, Albisser *et al.*<sup>46</sup> and Shichiri *et al.*<sup>47</sup> first introduced *in vivo* continuous glucose monitoring using an artificial pancreas. The artificial pancreas design was based on continuous glucose monitoring, where the device would remove blood from the body to an external benchtop analyser that was connected to an insulin pump. As this suggests, the device was not implanted and therefore not portable, although it was named the ‘artificial pancreas’. This led to the development of a third generation of glucose biosensor, which was subcutaneously implanted (Figure 1.2). Although the device could analyse glucose concentrations in blood using GOx, this was considered an invasive method.<sup>68</sup> It wasn’t until the late 1990s that the first commercially available personalised *in vivo* glucose monitor was launched by Medtronic Minimed Inc. (Sylmar, CA, USA).<sup>59</sup> Unfortunately, the device could not provide real-time information, with data being accessed every 3 days by a physician.<sup>23</sup> Although implantable glucose monitoring systems offer regular glucose level readings, this approach isn’t recommended for all diabetics, due to its invasive nature<sup>38</sup> and some continuous glucose monitoring methods have been reported to show inaccuracies of up to 21%.<sup>69</sup> These inaccuracies are often attributed to sensor drift, caused by changes in the catalytic performance of the enzyme. This requires the device to be periodically recalibrated via the finger-pricking method.<sup>70</sup> Despite current commercially available glucometers, such as the Freestyle-Navigator by

Abbott (Abbott Park, IL, USA), providing real-time measurements every 1–5 minutes, the longest working model without calibration is approximately two weeks. Consequently, there is high consumer demand for a continuous glucose monitoring system, which can quantify glucose concentrations without frequent calibration. Although blood remains the most studied body fluid for such measurements, other more accessible biological fluids such as interstitial fluid, ocular fluid, sweat, breath, saliva or urine have been investigated as alternative sample media for non-invasive continuous monitoring (Table 1.1).<sup>16, 25, 26, 38</sup> It is likely that the development of a device for glucose sensing with a working model of more than two weeks may target one of these more accessible fluids.

**Table 1.1.** Summary of glucose concentrations postprandial and pH values measured in physiological fluids of healthy and diabetic patients.

Physiological Fluid	Biomarker	Concentration for Healthy Patients <sup>7</sup>	Concentration for Diabetic Patients <sup>7</sup>	pH
Blood	Glucose	4.9–6.9 mM <sup>16</sup>	2–40 mM <sup>12, 63</sup>	7.35–7.45 <sup>22</sup>
Interstitial Fluid	Glucose	3.9–6.6 mM <sup>71</sup>	1.99–22.2 mM <sup>72</sup>	7.2–7.4 <sup>22</sup>
Urine	Glucose	2.78–5.55 mM <sup>38</sup>	>5.55 mM <sup>38</sup>	4.5–8 <sup>22</sup>
Sweat	Glucose	0.06–0.11 mM <sup>73</sup>	0.01–1 mM <sup>73</sup>	4.5–7 <sup>74</sup>
Saliva	Glucose	0.23–0.38 mM <sup>75</sup>	0.55–1.77 mM <sup>75</sup>	6.2–7.6 <sup>76</sup>
Ocular Fluid	Glucose	0.05–0.5 mM <sup>51</sup>	0.5–5 mM <sup>12, 51</sup>	6.5–7.6 <sup>38</sup>
Breath	Acetone	0.1–2 ppm <sup>77</sup>	0.1–103.7 ppm <sup>77</sup>	7.4–8.1 <sup>78</sup>

## 1.2.2 Monitoring Glucose in Alternative Physiological Fluids

### 1.2.2.1 Interstitial Fluid

Interstitial fluid is the extracellular fluid which surrounds tissue cells. It has significant potential for medical diagnostics as it possesses a similar composition of a number of clinically important biomarkers to blood.<sup>22, 24</sup> Blood and the surrounding vascularised tissue readily exchange biological analytes and small molecules by diffusion with the interstitial fluid.<sup>22</sup> As a result, the interstitial fluid can offer valuable information about a patient's health and has been used for minimally invasive determination of inherited metabolic diseases, organ failure or drug efficacy.

Consequently, substantial efforts have focused on non-invasive glucose sensing in this physiological fluid to provide information regarding a patient's glycaemic state.

Methods for monitoring glucose via the skin have become very popular in recent years, where these approaches have been developed to counteract the challenges associated with patient compliance and invasive monitoring.<sup>24</sup> Some of these approaches include sensing by optical detection such as light absorption or fluorescence detection, ultrasound or sonophoresis, polarimetry, heat or thermal emission, electromagnetic techniques, photoacoustic detection, Raman or bioimpedance spectroscopy, electrochemical methods and reverse iontophoresis-based electrochemical sensing, among others (Table 1.2).<sup>16, 24, 79-81</sup> A limitation of reverse iontophoresis is that typically stable measurements can only be reliably recorded for a period of 24h before calibration of the device is required. This is thought to result from the initiation of the skin healing process as interstitial fluid sampling is achieved by breaching the skin barrier.<sup>80</sup> The GlucoWatch was developed as a wearable device, which was initially brought to market for non-invasive continuous monitoring of glucose.<sup>3, 12, 36, 37, 82</sup> This technique used reverse iontophoresis to extract interstitial fluid through the skin, and measure glucose levels<sup>3, 82</sup> in a pH range of pH 7.2–7.4.<sup>22</sup> Although the GlucoWatch was a considerable advancement towards non-invasive and continuous glucose monitoring, the approach was hampered by the need for periodic recalibration by the pricking method,<sup>23, 36, 83</sup> thereby resulting in an increase in costs for testing equipment and patient care.<sup>37</sup> Other drawbacks included long warm-up times, sweating and skin rash with irritation,<sup>36</sup> which subsequently resulted in this product's removal from the market in 2008.<sup>23, 24, 79</sup>

**Table 1.2.** Summary definitions of specialised approaches for glucose sensing in interstitial fluid.

Sensing Technique	Explanation	Reference
Reverse Iontophoresis	Reverse iontophoresis is the passing of a current over the skin to drive ions from the interstitial fluid and on to the surface of the skin, where they can be analysed. This results due to the increased negative charge across the skin driving cations to the skin's surface.	84
Thermal Emission	Thermal emission, infrared thermography, infrared imaging or thermal imaging is a non-contact tool that uses the surface body temperature to gain insight in to the detection of diseases, flow of blood or muscular performance of an individual.	85
Photoacoustic Detection	Photoacoustic spectroscopy uses a form of light absorption to detect an analyte concentration in a biofluid, such as blood. Light from a laser source is absorbed by blood which generates heat in a localised region. The heat induces ultrasonic pressure waves in blood, which can be detected by an ultrasonic transducer and directly related to an analyte concentration that absorbs at the laser wavelength.	19
Sonophoresis	Transdermal delivery of drugs by ultrasound.	86

Sode *et al.*<sup>87</sup> have also developed a self-powered implantable continuous monitoring device called the BioRadioTransmitter for use in an artificial pancreas. In this instance, the device is composed of a capacitor, radio transmitter and receiver. In the presence of glucose, the capacitor of the BioRadioTransmitter device discharges a radio signal, which is received and amplified by the radio receiver. The change in transmission frequency is then related to the glucose concentration.<sup>87</sup>

Microneedles and microneedle arrays have also garnered a lot of interest over recent years for interstitial fluid sensing, since this approach can offer minimally invasive methods for bio-sensing. This concept was used in the development of a glucose-sensing patch by Jina *et al.*<sup>80</sup> The device was designed in two compartments; the first containing the microneedle array and glucose biosensor with the second containing the electronics (Figure 1.3). This miniaturised device spans a total area of 6 × 6 mm in which it contains 200 hollow microneedles (300 µm in length with a 50 × 50 µm lumen).<sup>80</sup> Three screen-printed electrodes were used for quantifying glucose concentrations in the interstitial fluid, including a Pt-C working electrode covered with a layer of cross-linked bovine albumin serum and glucose oxidase. The sensing device was attached to the skin by an adhesive layer contouring the perimeter of the

sensing pod. Detection was performed upon glucose diffusion into the microneedle array, wherein GOx could react to produce hydrogen peroxide. The production of hydrogen peroxide detected by the working electrode was proportional to the glucose concentration.<sup>80</sup> The electronics module of this device required the use of an external potentiostat, a microprocessor and a battery to power the device.<sup>80</sup>

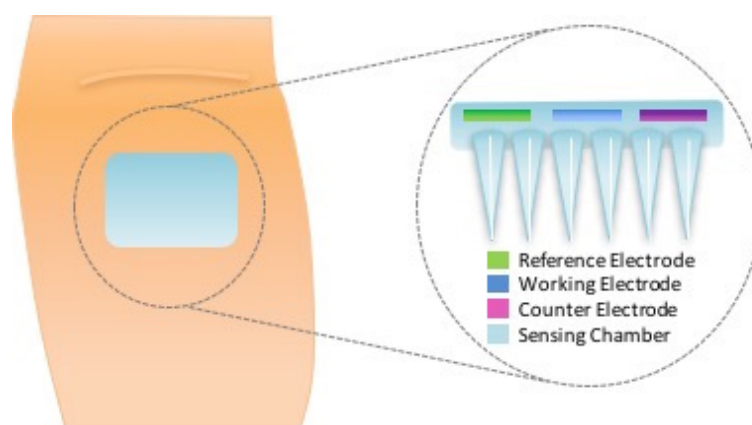


**Figure 1.3.** Schematic of the microneedle glucose-sensing patch. Adapted from reference 80.

A microneedle patch platform allows the device to be in constant contact with the skin, providing permanent access to the interstitial fluid, and enabling this device to operate continuously.<sup>25</sup> In this particular case, the short length of the microneedles means that penetration is optimal for interstitial fluid sampling, as the microneedles do not reach the dermis layer. This minimises any damage to blood-capillaries and nerve endings found in the dermis layer. Moreover, as the microneedles penetrate the skin, contamination by sweat is avoided.<sup>25</sup> Tests have shown that this device can operate successfully for up to 72h with only a 17 min lag time caused by the passive diffusion of analytes from blood in to the interstitial fluid matrix.<sup>80</sup> To increase the lifetime of the device, the skin healing process must be inhibited. This could potentially be achieved by designing a sensing patch with microneedles of optimal length, width, tip and pitch characteristics, and by coating the microneedles with a biocompatible material exhibiting similar mechanical properties to that of biological tissue. Currently, the device must be recalibrated daily by the finger-prick approach.<sup>80</sup> Potential clogging of the microneedles and the distortion of their shape upon penetration of the skin can also affect the dynamics of sampling. Despite these

shortcomings, this novel device holds great potential as a non-invasive continuous glucose monitor.

Russell *et al.*<sup>88</sup> were the first to introduce a tattoo sensing technology using hydrogel glucose-sensing microspheres. Zhi *et al.*<sup>81</sup> further developed this technology by encapsulating the sensors in a thin film, which offered the advantage of fast analyte transport through the device. This was achieved by fabricating microvesicles through a layer-by-layer approach, which encapsulated a fluorescent labelled protein as the glucose receptor. When glucose bound to the protein, a conformational change was induced in the protein, which increased the polarity of the sensing environment. As a result, the fluorescence became increasingly quenched as the concentration of glucose increased.<sup>81</sup> These microvesicles were then implanted in to the dermis layer of the skin in a mouse ear, and the fluorescence lifetime was measured for glucose concentrations between the range of 1–100 mM. An advantage of measuring fluorescence lifetime meant that important issues such as light scattering and photobleaching could be avoided. This approach could also be designed for pancreatic islet transplants, which are a known treatment procedure for type 1 diabetes patients. It is commonly seen that these cells are subject to early destruction or rejection from the innate host immune systems upon transplantation. To overcome this challenge, a biocompatible encapsulation method using fluorophores with excitation wavelengths in the NIR region holds the potential for improving the efficacy of this transplantation approach. As cellular tissues are transparent to NIR light, measurements taken via the surface of the skin could facilitate continuous non-invasive sensing.<sup>81, 89</sup> Other methods for interstitial fluid sensing, which are currently under development, include sensors based on impedance spectroscopy (Pendra, by Pendragon Medical Ltd., Zurich, Switzerland) and optical transducers (C8 MediSensors Optical Glucose Monitor™ System, by C8 MediSensors, Inc., San Jose, CA, USA).

#### 1.2.2.2 Urine

Since 1841, urine has been used as a diagnostic fluid for diabetes.<sup>90</sup> It has been extensively studied, as it can be easily and non-invasively collected.<sup>22, 38</sup> Urine is composed of metabolites, such as glucose, proteins and nitrates, as well as other dissolved salts, such as sodium and potassium. As a result, the pH of urine fluctuates between acidic pH 4.5 to basic pH 8.0.<sup>22</sup> Due to the intermittent nature of this fluid, where collection is required for sampling, it cannot be incorporated into a continuous

glucose-monitoring device.<sup>91</sup> Glucose can be found in urine when it is excreted from blood in elevated levels and as a result, this fluid has been investigated for the diagnosis of diabetes. A positive result occurs when the glucose levels in urine are in the 2.78–5.55 mM range.<sup>38</sup>

### *1.2.2.3 Sweat*

Sweat is one of the most accessible body fluids, where its primary biological role is for thermoregulation.<sup>92</sup> Conveniently, for sampling purposes, eccrine glands that excrete sweat can be found all over the body, where they are particularly concentrated in multiple locations, for example in the hands, feet, lower back and underarm.<sup>74</sup> Sweat has been exploited for diagnostic purposes, in particular for the detection of disease markers such as sodium, potassium, calcium, phosphate and glucose.<sup>25</sup> It is also known that small-molecule drugs and their metabolites are present in sweat, thereby allowing the evaluation of drug efficacy.<sup>93</sup> Sweat can be continuously accessed and its production can be stimulated on-demand at certain locations, for example by iontophoresis.<sup>74</sup> By placing sensors in close contact with the skin, sweat samples can be processed rapidly without contamination.<sup>74</sup> For many years, sweat has been used as a sampling medium of interest in sensing devices for confirming diseases, such as cystic fibrosis and for gaining other valuable information, relating to electrolyte balance, diet, injury, stress, medications and hydration. The hydration status of individuals has become a relatively new area of interest for monitoring human performance, resulting in an increase in wearable smart devices on the global market.<sup>25, 94</sup> Most analytes contained in sweat tend to vary significantly between basal and exercising states, as well as between individuals. The reported glucose level in sweat for healthy patients is between 0.06 and 0.11 mM and between 0.01 and 1 mM for diabetics.<sup>73</sup> The fluctuations in analyte concentrations result in a broad pH range of sweat, typically between pH 4.0–6.8 during exercise,<sup>95, 96</sup> which can impact on the effectiveness of chemical-sensing or bio-sensing techniques chosen for disease diagnosis or monitoring.<sup>22</sup>

An example of a device developed for sweat sensing is SwEatch by Diamond and co-workers.<sup>92</sup> This device was designed for sodium analysis in sweat and was fabricated using 3D-printing methods for the sensor casing and sensor connections (Figure 1.4). The device was powered by a lithium battery that allowed the device to

function continuously for up to 3h.<sup>92</sup> This approach could be easily adapted for glucose sensing in sweat by introducing a glucose sensor into the platform.

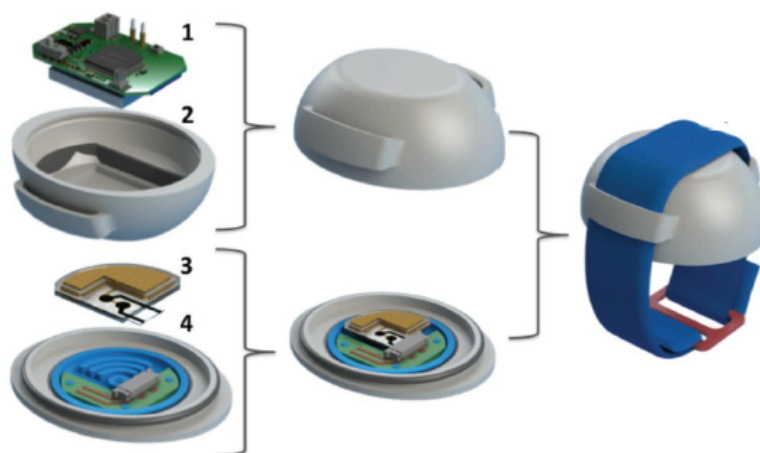


**Figure 1.4.** SwEatch: watch-sensing platform for sodium analysis in sweat. (1) Electronics. (2) 3D printed casing. (3) Microfluidic chip and ion-selective/ion-specific electrode. (4) 3D printed sweat harvester and sensor connections. Reproduced from reference 92.

In 2010, Heikenfeld *et al.*<sup>94</sup> began fabricating sweat-sensing patches that could stimulate sweat production, measure analyte concentrations in sweat wirelessly, and transmit that information to a smartphone. This research aimed to determine physical fatigue in athletes by measuring their dehydration status using their sweat. Dehydration is known to be a reoccurring problem for professional athletes and by alerting an athlete of their oncoming over-exertion, instances such as cramping and electrolyte imbalance could be avoided, while simultaneously prompting the uptake of fluids.<sup>94</sup> Heikenfeld has written many reviews in this area, and his outlook for the future suggests that technology is advancing towards glucose sensing in sweat.<sup>74, 93, 94</sup>

Wang *et al.*<sup>97-99</sup> have also recently been working towards the development of a continuous and non-invasive sensing device for detecting specific analytes in sweat using electrochemical sensing. In their approach, they have investigated a range of innovative sensing platforms, including wristbands,<sup>98</sup> stick-on flexible sensors<sup>99</sup> and traditional eyeglasses (Figure 1.5).<sup>97</sup> By adapting spectacles, Wang *et al.* have created a device that can be easily integrated into an individual's lifestyle. This device contains an amperometric lactate biosensor connected on to one of the nose-bridge pads and a potentiometric potassium ion-selective electrode on to the other (Figure 1.5).<sup>97</sup> Both sensors were interfaced with an electronic backbone on the glasses' arms. The device could successfully sense lactate and potassium ions in sweat for a few



hours continuously. The positioning of the sensors on separate nose pads also minimised cross-talk and facilitated separate fabrication and replacement. These instrumented eyeglasses were coupled by Bluetooth wireless data to a remote mobile host device for data analysis and visualisation. In this approach, the nose-bridge pads were designed so that the pads could be interchanged with others for multifunctional sensing applications.<sup>97</sup> Wang and co-workers also demonstrated that by interchanging the lactate sensing pad for a glucose sensitive one, the spectacles could be used to monitor glucose concentrations in human sweat. The results showed good blood-sweat glucose correlations in healthy individuals when the blood levels were compared with a commercially available blood-glucose meter.<sup>97</sup>

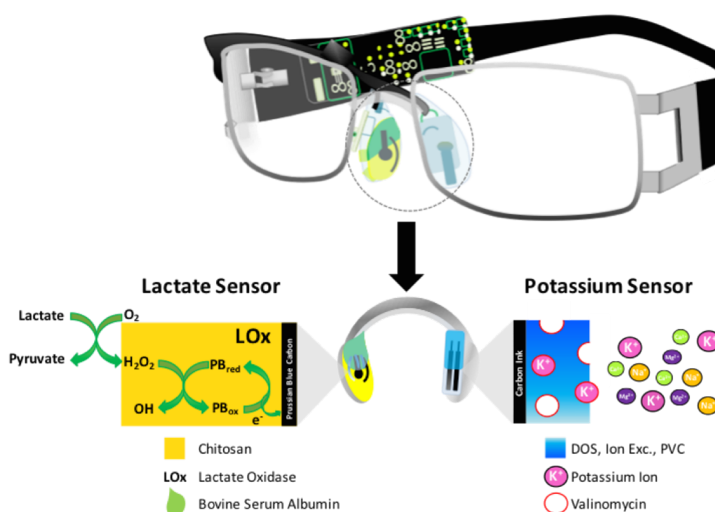


**Figure 1.5.** Schematic representation of the eyeglasses biosensor system, which integrates a wireless circuit board along the arms of the spectacles and two electrochemical sensors for lactate and potassium on to the nose-bridge pads. A schematic of the lactate sensor (left) and potassium sensor (right), along with the corresponding recognition and transduction events is also shown. Adapted from reference 97.

Gao *et al.*<sup>100</sup> recently reported a non-invasive and continuous wearable glucose-sweat sensing device (Figure 1.6). Sensors integrated in to this Bluetooth-enabled wristband detect skin temperature, sodium, potassium, lactate and glucose concentrations in sweat.<sup>100</sup> An advantage of this approach is the use of multiple sensors which overcomes limitations of single, stand-alone sensors.<sup>93, 100</sup> Due to the complex nature of sweat, multiple sensors are required to provide a more comprehensive profile of sweat composition and enable data cross-comparisons. For example, it is known that the potassium concentration in sweat is quite stable during basal and exercising states. As a result, potassium levels can be used as a reference for

comparing the fluctuating concentrations of other analytes, such as glucose and enable real fluctuations to be distinguished from artefacts.<sup>100</sup> This device was designed to exhibit similar form factors of existing devices, such as the fitness wristbands by Fitbit Inc. (San Francisco, CA, USA), thereby encouraging user uptake to create a pathway to commercialisation. The sensors were tested individually *in situ* and collectively in the device. The device analyte readings showed good correlations to the normal concentration ranges in sweat during exercise and the sensors could be used for continuous operation for up to 2h before the glucose and lactate sensing units were interchanged for fresh sensor arrays. A minimum of 10  $\mu\text{L}$  of sweat was required before any sweat analysis could be achieved.<sup>100</sup> The sensors were placed close to the skin, to allow for immediate analysis of sweat as it emerged. Sweat was absorbed into a water-absorbent thin rayon pad for stable and reliable glucose readings, placed between the electrode sensors and skin. This flexible wearable sensing system is a promising platform for tracking multiple physiological analytes during exercise.

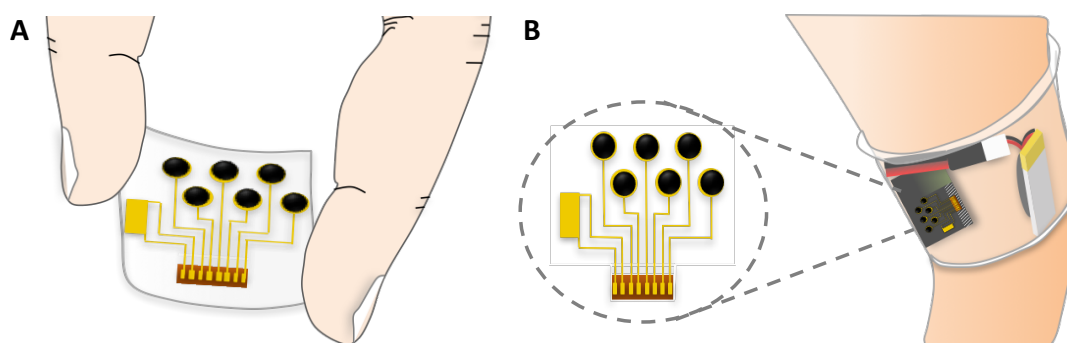


**Figure 1.6.** (A) Flexible glucose sensor. (B) Glucose sensor integrated into a wearable wristband for non-invasive sensing in sweat. Adapted from reference 100.

Rogers and co-workers,<sup>101</sup> have examined a range of porous materials that can be used for optimising epidermal characterisation of sweat with the aim of developing thin (1 mm thick), wireless, stretchable sensors for continuous monitoring. Some of the soft materials investigated include recycled cellulose sponge, polyurethane sponge, polyvinyl alcohol sponge, cellulose paper and silicone sponge. These materials were chosen for their ability to absorb and retain sweat by capillary forces when in contact with the skin, in order to optimise the handling and analysis of the biofluid, by eliminating the need for complex microfluidic systems.<sup>101</sup> The substrate is

skin-like in nature, which makes it conformable and comfortable to wear during monitoring periods. It also is simple to integrate with a range of electronic sensors and communication platforms, such as a smart phone for simple colorimetric measurements.<sup>101</sup> Moreover, by employing soft skin-like polymeric materials, irritation during long-term monitoring sessions could be reduced as direct contact of the electrodes with the skin is prevented, by having the hydrogel sandwiched between the skin on one side and the metal electrode substrate on the other. The device developed by Rogers *et al.*<sup>101</sup> could successfully monitor the volume and pH of sweat, as well as the physiologically relevant concentrations of copper ( $\text{Cu}^+$ ) and iron ( $\text{Fe}^{2+}$ ) ions (0.8–1 mg/L) for a period of 2h.

Rogers and co-workers,<sup>102</sup> have also investigated soft ferromagnetic materials for skin-interfaced electrodes. This material was designed for intimate and adhesive contact with skin, ensuring a device that is conformable and robust enough for continuous operation compared to conventional hydrogel-based alternatives. The device is also paired with a separate standing platform, to which the electrodes are magnetically attached to facilitate cleaning or replacement of sensor units.<sup>102</sup> The main advantages of this approach included the conformability and resilience of the sensors to allow for natural movements on body during sensing periods and direct integration of the wireless electronics for data collection and communication. Moreover, the sensors minimised noise from motion artefacts by incorporating a magnetic bi-layer material.<sup>102</sup> In comparison to conventional hydrogels, which are known to shrink or swell in response to certain analytes, this magnetic material retained its shape when exposed to biofluids or air. Continuous operation of the device was demonstrated for a period of two days (50h).<sup>102</sup> Measurements performed included electroencephalograms (EEGs) to monitor electrical activity of the brain,<sup>103</sup> electromyograms (EMGs) to detect electrical activity in muscles,<sup>104</sup> electrocardiograms (ECGs)<sup>105</sup> and electrooculography (EOG).<sup>106</sup> The designs are compatible with the most sophisticated electrode potential monitoring systems that are currently commercially available. The authors also suggest that the material can be readily adapted for detecting other epidermal analytes of interest.<sup>102</sup>

Overall, although sweat sensing for diagnostic data is very promising, there are also some concerns associated with this sensing fluid.<sup>74</sup> The main challenges include (1) limited fundamental knowledge about the sensing fluid, compared to other physiological fluids, such as blood which are much better understood; (2) sampling

issues associated with sweat production by exercising, iontophoretic stimulation; heat or carbon dioxide;<sup>95</sup> (3) the skin surface can also act as a contaminant; as sweat traveling across the skin can mix with fresh emerging sweat and contaminate the sample; (4) the pH range of sweat fluctuates over a wide range between pH 4.0–6.8, which can interfere with some sensing approaches<sup>96</sup> and; (5) the rate of sweat production is variable and can be quite low (1 nL/min/mm<sup>2</sup>).<sup>74</sup> However, this low sweat rate can be compensated for by increasing the area sampled for sweat analysis. Although most of these effects can be adjusted for in prototype technology innovations, some biological factors such as the variable nature of sweat pH, and variable concentrations of ions such as sodium and chloride remain a significant hurdle. Broad pH ranges can affect enzymatic sensors and influence the concentration of weak acids or weak bases in sweat, such as phosphates, chlorides or salts of organic acids, such as lactic acid. Therefore, these concentrations may be observed at slightly higher concentrations in comparison to other fluids, such as blood.<sup>74, 107</sup>

#### *1.2.2.4 Breath Analysis*

Breath analysis is another means of tracking the health status of an individual.<sup>22, 45</sup> Volatile organic compounds (VOCs) are generated as by-products from metabolic pathways within the body. These biomarkers migrate throughout the body via the circulatory system, pass over the alveolar interface and are exhaled in breath.<sup>108</sup> A molecular breath signature can be established by measuring the ratio between VOCs in breath.<sup>43, 108</sup> This signature is composed of over 3500 VOCs, consisting of hydrocarbons, ketones, aldehydes, alcohols, esters, nitriles and aromatic compounds, whose concentrations can be affected by specific diseases.<sup>108</sup> For example, 112 of these VOCs have been found to be specifically related to cancer.<sup>43</sup>

Nanomaterials can be incorporated into sensing elements for monitoring acetone concentrations in breath, as an alternative to glucose monitoring for diabetes.<sup>109</sup> Ethanol and methyl nitrite have also been identified as biomarkers for diabetes.<sup>108</sup> Acetone levels in blood are approximately 330 times higher than in breath, at 0.1–2 ppm for healthy individuals' post-glucose loading and reaching to up to 103.7 ppm in critically ill diabetic patients.<sup>77</sup> Therefore, the sensing units must have a high sensitivity to detect VOCs in the nanomolar to picomolar concentration ranges, where recent examples of such devices lack specificity for concentrations of biomarkers relating solely to diabetes.<sup>77</sup> Jiang and co-workers have reported a breath acetone

analyser, which can detect acetone levels in diabetic patients.<sup>77</sup> Unfortunately, the device requires a controlled external atmosphere in order to diagnosis diabetes accurately, where the reported diagnosis accuracy is estimated at 74%. However, other factors can affect acetone levels, including fasting, exercising, dieting and intra-individual variation, thereby limiting the use of acetone as a specific biomarker for diagnosing and monitoring diabetes.<sup>44</sup>

For this technology to be fully efficient, the sensor must also integrate easily into a portable meter, and provide a means for non-invasive, inexpensive and qualitative monitoring to be implemented in to a rapid response tool for early-diabetes diagnosis.<sup>43, 45, 108</sup> Although breath can be more readily evaluated in comparison to blood or urine, there are some shortcomings when attempting to design a device with fast analytical responses to breath. The analysis of VOCs in breath is more challenging due to external air interferents and the wide complex range of VOCs detectable, although more comprehensive analysis techniques can be incorporated, such as GC-MS, to provide rich-information regarding the breath composition.<sup>25, 43-45</sup> However, the device currently remains expensive and non-portable, although significant advances in miniaturisation have occurred.

Electronic-nose (e-nose) technology has also been applied to continuous monitoring of breath. These portable sensors were designed to mimic olfactory sensing by breath analysis using sensor arrays that generate response patterns that can be related to the composition of breath.<sup>77</sup> E-noses have been primarily designed for assessing volatile mixtures of biomarkers or VOCs in breath for lung diseases. The e-nose generates response patterns when exposed to the breath samples, and these patterns are compared to database libraries of molecular breath signatures for known diseases, such as chronic obstructive pulmonary disease (COPD),<sup>110</sup> upper respiratory tract infections (URTI)<sup>111</sup> and pulmonary tuberculosis (TB).<sup>112</sup> Currently these devices have found applications in the food,<sup>113</sup> environmental and chemical industries,<sup>114</sup> as well as in clinical trials for the recognition of lung cancer,<sup>115</sup> asthma,<sup>116</sup> pulmonary arterial hypertension<sup>117</sup> and diabetes.<sup>77</sup> However, a major obstacle, which must be overcome before these devices reach the consumer market is the elimination of issues involving external air contaminants. In order to standardise the sampling procedure for accurate detection, stringent control to remove any external air contaminants is necessary for background correction of the device. This is not only related to the dead-space in the device, but also the atmosphere the patient is

exposed to.<sup>45</sup> In order to reach its full commercial potential, further development and standardisation must be implemented. Moreover, controversy still exists regarding the reliability of this approach for accurate correlation of response patterns to underlying health conditions.<sup>25, 45</sup>

#### 1.2.2.5 Saliva

Saliva is a complex fluid containing many analytes that permeate from blood, thereby in principle providing a useful insight into a person's emotional, hormonal, metabolic and nutritional state.<sup>24, 118</sup> As a result, saliva has been investigated as an alternative fluid for non-invasive glucose sensing, with glucose levels for a healthy individual ranging from 0.23 to 0.38 mM and between 0.55 and 1.77 mM for diabetics.<sup>75</sup> Although a relationship between glucose levels in blood and saliva obviously exists, it is not well understood, and relating saliva concentration to therapeutic intervention is therefore more challenging. However, saliva offers many advantages for diagnostics, the main benefit being that saliva can be collected in a non-invasive fashion. As a result, there have been many emerging technologies reported for continuous and non-invasive glucose detection in saliva, using everyday dental platforms, including mouth guards and dentures, as well as novel devices, such as dental tattoos.<sup>24, 119</sup>

Several research groups, including that of Kim *et al.*,<sup>22, 119</sup> have investigated the potential use of a mouth guard as a minimally invasive continuous monitoring platform for metabolite sensing in saliva. This sensing platform encompasses a printable enzymatic electrode, based on lactate oxidase, for the detection of salivary lactate (Figure 1.7) with high sensitivity, selectivity and stability in human saliva samples.<sup>119</sup> This amperometric electrochemical sensing approach uses a poly-orthophenylenediamine (PPD)/lactate oxidase reagent layer with a printable Prussian-blue transducer, where the Prussian-blue reagent acts as the 'artificial peroxidase' to offer a highly selective detection approach for hydrogen peroxide in the catalytic reaction.<sup>119</sup> The Prussian-blue reagent was previously used for oral treatment of heavy metal poisoning, such as thallium and caesium, for which it is widely accepted as safe under physiological conditions and at high oral dosages. PPD has also been commonly used for electropolymeric entrapment of oxidases, and its relatively low oxidation potential in comparison to other electroactive species, such as ascorbic acid or urea, facilitates protection of the biosensor surface, and enhances stability of the sensing

components.<sup>119</sup> This sensing approach also has the potential to be used for glucose biosensing, by replacing the lactate sensor with a glucose sensor, as the sensing principles of these electrochemical biosensors and their associated electronics are very similar.

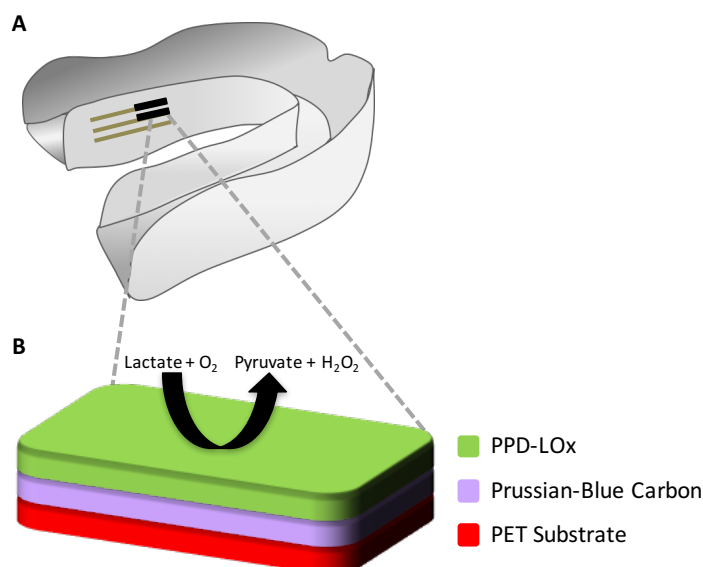


**Figure 1.7.** Lactate sensing mouthguard for non-invasive continuous lactate sensing in saliva. (A) Mouthguard sensing platform with integrated printable 3-electrode system, with enzyme working electrode. (B) Enzyme coated working electrode with lactate sensing region. Adapted from reference 119.

Intraoral dental accessories have also been of interest for non-invasive and continuous monitoring to provide information regarding a patient's health status. A tooth has the potential to act as a continuous monitoring device as it is in constant contact with the patient's saliva. Mannoor *et al.*<sup>120</sup> have developed a bacterial detection approach whereby a graphene-based nanosensor was printed on to water-soluble silk and transferred on to tooth enamel (Figure 1.8). This sensing tooth incorporates a resonant coil to prevent the need for a power source and external connections. The device operates by the self-assembly of antimicrobial peptides on to the single sheet of graphene, where the bio-selective analysis of bacteria can be performed at a single cellular level. Preliminary results showed great specificity, response time and single-molecule detection abilities for this sensor, however this sensing application must still be tested on-body for real-time analysis.<sup>120</sup> This approach could potentially be adapted for detection of other analytes such as glucose,

by means of a chemical glucose sensor immobilised on to a water-soluble silk layer attached to the tooth enamel.

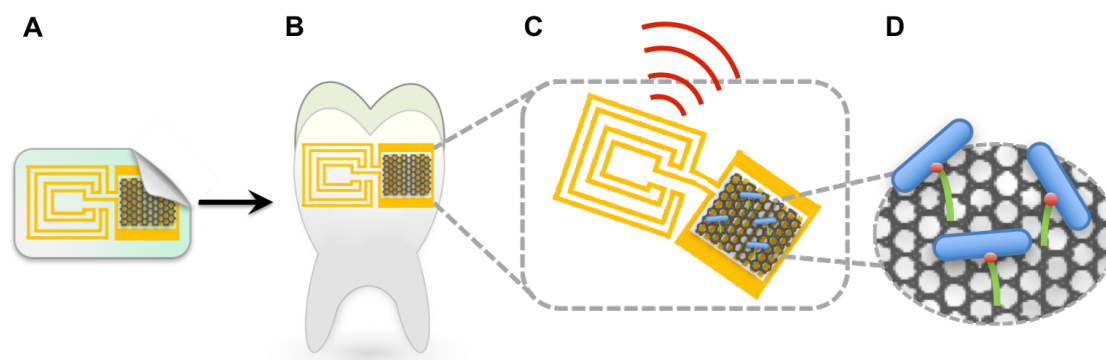


**Figure 1.8.** Glucose-sensing tattoo printed on to a tooth platform as a non-invasive continuous monitoring device. (A) Graphene printed on bioresorbable silk with contacts containing a wireless coil. (B) Biotransfer of sensor on to tooth enamel. (C) Magnified image of the sensing unit with a wireless readout system. (D) Self-assembly of pathogenic bacteria bound by peptides on nanotransducer surface. Adapted from reference 120.

Zhang and co-workers<sup>90</sup> have fabricated a disposable microfluidic device that has been developed as a diagnostic tool for quantifying saliva-glucose concentrations by electrochemical methods. The glucose-sensing chip houses a working electrode, a counter electrode and reference electrode.<sup>90</sup> The intricate device design consisted of a working electrode functionalised with single-walled carbon nanotubes, to promote electron transfer for the glucose oxidase reaction. Gold nanoparticles were incorporated to enhance this signal sensitivity, as well as to promote increased enzyme attachment. Chitosan, a non-toxic biocompatible polysaccharide, was also employed for promoting film formation and adhesion characteristics in order to enhance glucose oxidase immobilisation.<sup>90</sup> This device showed impressive linearity for glucose detection in the range of 0.017–0.8 mM,<sup>90</sup> correlating to saliva-glucose levels in healthy patients.

#### 1.2.2.6 Ocular Fluid

The fluid surrounding the eye and ocular tissue, also known as the aqueous humour, contains many analytes present in blood. This complex fluid can be excreted from the body as an extracellular fluid in the form of tears. Analytes found in this fluid, such as glucose, ascorbic acid, lactate, proteins, peptides, hormones, carbohydrates, electrolytes, lipids and chloride, can offer great insight into an



individual's health status.<sup>24, 121</sup> As a result, this fluid has been investigated for non-invasive and continuous glucose monitoring.

Recently, the Google[X] lab (Mountain View, CA, USA) and Novartis (Basel, Switzerland) have collaborated on the development of glucose sensing technologies in the aqueous humour. The Google[X] lab was founded to “find new solutions to big global problems” with diabetes in this category.<sup>122</sup> In 2014, they announced their goal to create a smart-contact lens, which they hoped would overcome glucose-monitoring obstacles associated with current methods, which are either invasive, in the case of implanted wearable devices or non-continuous, in the case of the finger-pricking approach. This novel technology incorporates an electrochemical battery-operated enzymatic glucose sensor, utilising the enzyme glucose oxidase (GOx), in a microchip sandwiched between two layers of a soft contact lens, as represented in Figure 1.9.<sup>122, 123</sup> A tiny sensor relays data to a mobile device, from which the patient or medical practitioner can read the corresponding glucose levels in the ocular fluid.<sup>124-126</sup> This redox reaction is monitored through the production of hydrogen peroxide at the working electrode to quantify the glucose concentration in the ocular fluid.<sup>127</sup> However, there are disadvantages to an electrochemical sensing approach, which can be related to the use of enzymes leading to the production of corrosive hydrogen peroxide as a by-product or interference from electroactive species in the ocular fluid, such as ascorbic acid, lactate or urea.<sup>121, 125</sup> Blinking may also stimulate a movement artefact in the wireless sensor signal. In addition to the battery source embedded in the lens, an external power source must be provided for enabling efficient sensor function and to facilitate wireless communication of the data. This is a very active area of research, with multiple approaches under investigation in to the production of a safe biocompatible battery powered device.<sup>128</sup> These include additional power sources external to the device that would wirelessly transmit power, for example through radio frequency induction, using solar cells to harvest energy, or using biofuel cells. Biofuel cells could be used in a second wearable device to supply chemical energy, which would be converted to electrical energy, to power the biosensor. This separate power source would need to be within close proximity of the eye in order for the smart-contact lens to function efficiently.<sup>128</sup>

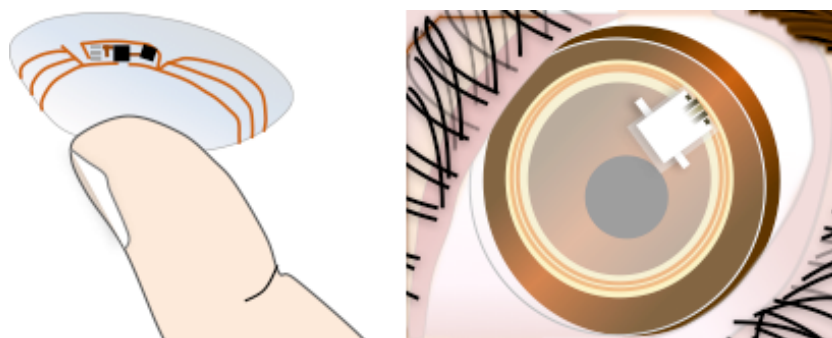


**Figure 1.9.** Google and Novartis' smart-contact lens. Adapted from references 126 and 129.

Using a contact lens as a sensing platform does hold many advantages, including real-time continuous and non-invasive glucose monitoring, as the lens would be in constant contact with the aqueous ocular fluid.<sup>12, 121, 130</sup> Disposable contact lenses are typically replaced every 24h, which is a reasonable period for reliable continuous biosensor operation. Blinking and tear secretion also allow for natural, fresh sample replenishment for accurate glucose concentration measurements throughout the day.<sup>121</sup> By incorporating a glucose sensor in to a commercially available lens, not only could this lens provide a form of corrective vision but a monitoring function too.<sup>12, 121, 126</sup> It is well known that critical side effects associated with diabetes are eye damage or blindness,<sup>12</sup> due to glycation of proteins in the blood vessels of the eye.<sup>11</sup> To account for such ocular deteriorations a detection function, potentially based on imaging, for glycation of vascularised tissues could later be incorporated in to the lens.

Other research groups, such as Yao *et al.*<sup>91</sup> have worked with Google, to investigate the use of contact lenses as a biosensing platform for quantifying glucose concentrations in the ocular humour. GOx was the enzyme employed in an amperometric glucose sensor for this purpose. The sensor was immobilised as a screen-printed structure on to a polymeric substrate in the shape of a lens (Figure 1.10).<sup>91</sup> An amperometric sensing method was chosen since the oxidation and reduction potentials of this reaction can be directly associated with a measurable current signal, which is proportional to the concentration of the analyte being quantified.<sup>121</sup> The preliminary results showed some promise, with the lens reported to sense glucose in the range of 0.1–0.6 mM.<sup>91</sup> This correlates with ocular glucose levels of 0.05–0.5 mM for healthy individuals, increasing to up to 5 mM for critically ill diabetics.<sup>12</sup> The ocular glucose levels in comparison to blood-glucose levels are

approximately 10 times smaller with a lag time of about 10 min.<sup>22, 121, 131</sup> Although this smart lens showed rapid response time of up to 20 s and good reproducibility,<sup>91</sup> it did not manage to demonstrate non-invasive and continuous glucose-monitoring. Many issues associated with tear fluid interference and challenges related to powering the device are still under development.<sup>121</sup> Kagie *et al.*<sup>132</sup> and Iguchi *et al.*<sup>131</sup> proposed an alternatively designed sensor, using the same glucose sensing methodology, which was inserted into the tear canal. Kagie *et al.*<sup>132</sup> showed that the sensor could be fabricated by screen-printing approaches and Iguchi *et al.*<sup>131</sup> demonstrated the sensor production by microfabrication techniques. The sensors fabricated by both approaches were reported to have high selectivity for ocular-glucose, but further tests are required to determine the effects of interfering electroactive species such as ascorbic acid, lactate or urea, all of which are present in the aqueous humour.<sup>131, 132</sup>

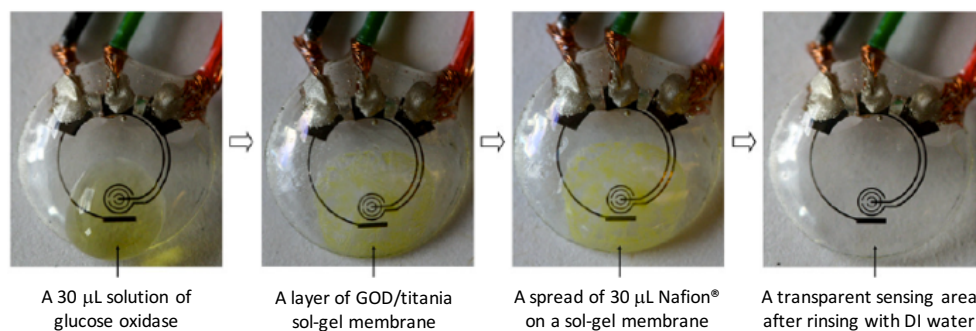


**Figure 1.10.** Sequence of images of the glucose-sensing contact lens during sensor functionalization with GOx, titanium sol-gel film, Nafion membrane and rinsing with DI water, respectively. Reproduced from reference 91.

Recently, Badugu *et al.*<sup>12</sup> introduced an optical chemical sensor for glucose detection in the ocular fluid. In this case, they used boronic acids (BAs) attached to a fluorescent component to directly sense glucose by optical means.<sup>7, 12-14, 37, 51, 133, 134</sup> On interaction of the fluorescent BA sensors with increasing saccharide concentrations, a decrease in the fluorescence intensity of the BA sensors occurred. For example, when using a fluorescent quinoline moiety a decrease of ~30% was observed upon introduction of 100 mM glucose.<sup>12, 51</sup> This sensing mechanism was attributed to fluorescence quenching via a charge neutralisation-stabilisation mechanism. The anionic boronate ester formed on glucose binding was stabilised by a positively charged N<sup>+</sup> atom in the quinoline structure, which consequently quenched the fluorescence of the BA sensor.<sup>12, 51</sup> The main advantage for using chemical

sensors over enzymatic sensors is that the sensing detection and communication mechanisms do not require any power. Chemical sensing by optical means, eliminates the need for external energy sources to power the device when the material is coloured and self-reporting. The concentration changes detected by the sensor induce an optical change in the material, which are used to communicate the analytical response. As a result, by using a chemical sensing approach the sensing components can be greatly simplified. Moreover, the production of corrosive hydrogen peroxide when using GOx is eliminated, overcoming a significant disadvantage of the electrochemical sensing approach.<sup>12</sup>

Other groups working towards non-invasive monitoring of glucose in the ocular fluid include Jeong, *et al.* and Microsoft Inc. (Redmond, WA, USA) in collaboration with Evans and co-workers. Jeong *et al.*<sup>135</sup> have developed Raman sensitive, silver plasmonic, nanostructures that are responsive to glucose. These nanostructures used solvent-assisted nanotransfer printing to attach the plasmonic glucose sensing material on to a commercially available contact lens. Nanotransfer printing in this way created narrow passageways or 'hot spots' in the nanostructure, to take advantage of the surface-enhanced Raman scattering in the sensing material to detect small molecules, such as glucose, non-invasively in the ocular fluid. The approach is clever in that it uses retina-safe laser excitation to measure glucose concentrations within the range of 0.1–10 mM.<sup>135</sup>

Microsoft, in collaboration with Drew Evans' group from the University of South Australia (Mawson Lakes, SA, Australia), have designed hydrophilic organic electrodes that could be incorporated in to flexible hydrogels, such as a contact lens.<sup>136</sup> In their approach, they have fabricated polymeric coatings that were engineered to be biocompatible and conducting, which could be grown directly on to a contact lens. Evans and co-workers, deposited the conductive polymer poly(3,4-ethylene-dioxythiophene) (PEDOT) on to the lens using oxygen plasma techniques. This lens was designed to advance the development of silicone hydrogels with technologically relevant properties, such as conductivity, to pave the way for conductive hydrogel electrodes.<sup>136</sup> Ultimately, this lens would self-report relating optical changes to glucose concentrations. An advantage of this passive device is that no batteries or wireless connections are required to receive and transmit crucial information. Currently, work is underway in the group to test the robustness of the coatings, to further develop the lens towards disease diagnosis and monitoring, and

other alternative applications for military camouflage apparel, where an electrical current would induce a reversible colour change in the polymer from brown to green.<sup>137</sup>

Wearable sensors have the potential to play a major role in the continuous and non-invasive monitoring of biomarkers for diabetes and other disease conditions. The majority of sensors described so far in this chapter still require further clinical evaluation before they can be approved for medical use. The interest of companies such as Google, Novartis and Microsoft suggest there is really significant market potential for new approaches to self-monitoring and diagnosing. A key enabling step will be to create a clearer understanding of the relationship between the diagnostically relevant concentrations of key disease markers in blood compared to other physiological fluids. Existing wearable devices such as fitness bands and smartwatches, which already dominate the consumer technology market, provide an information base that can be expanded to encompass disease monitoring or diagnosis, and provide a tangible impact on health and wellness. However, unless these wearable technologies can provide additional insights into the wearer's health, be integrated in to clinical practices and promote actionable behavioural change, their positive impact may continue to be limited.

## **1.3 Fluorescence Sensing**

### **1.3.1 Phenomena of Fluorescence**

Fluorescence is a type of luminescence, which is the emission of light from an electronically excited state of a substance.<sup>138</sup> The Jablonski diagram illustrates various molecular processes that can occur from excited states, where fluorescence and phosphorescence are the most dominant processes of luminescence. Light is commonly used as an excitation source for these processes when a large energy gap exists between the ground electronic state and the excited electronic state.<sup>138</sup>

The process of fluorescence begins with a molecule that exists in a singlet-ground state ( $S_0$ ) (Figure 1.11). In this state the electrons are paired by opposite spin.<sup>138</sup> When a molecule is excited, the molecule absorbs this energy and is promoted in to the singlet-excited state ( $S_1$ ). The excited state can then undergo relaxation by internal conversion to the lowest energy vibrational state in the thermally equilibrated electronic state of  $S_1$ .<sup>138</sup> As a result of this spin pairing, this allowed process returns

the excited state to the ground state accompanied by the swift emission of a photon. The energy of this photon can be related to the excitation energy used to promote the electron from  $S_0$  to  $S_1$ . This process is known as fluorescence (Figure 1.11).<sup>138</sup>

Phosphorescence is another type of luminescence. This type of photon emission occurs when electrons in the  $S_1$  state undergo a spin conversion by intersystem crossing to a lower energy excited-triplet state ( $T_1$ ).<sup>138</sup> This process is recognised as a forbidden transition. As a result, on transitioning back to the  $S_0$  ground state, the light energy emitted is shifted to longer wavelengths of lower energy, corresponding to the phosphorescence emission. Since both electrons have the same spin orientation as the  $T_1$  state, the emission process of the photon is considerably slower in the form of phosphorescence.<sup>138</sup> Molecules containing heavy atoms, for example halides such as ethyl iodide, often induce phosphorescence in rigid aromatic molecules, for example in pyrene.<sup>139</sup> This is due to the spin-orbit coupling within these molecules that induce a quantum mechanical mixing of states, resulting in states of mixed multiplicity. Consequently, large increases in the rates of spin-forbidden transitions occur in the presence of molecules containing halides. As a result, the fluorescence intensity decreases and the phosphorescence capability increases.<sup>140</sup> Fluorescence and phosphorescence processes are depicted in the Jablonski diagram (Figure 1.11).<sup>138</sup>

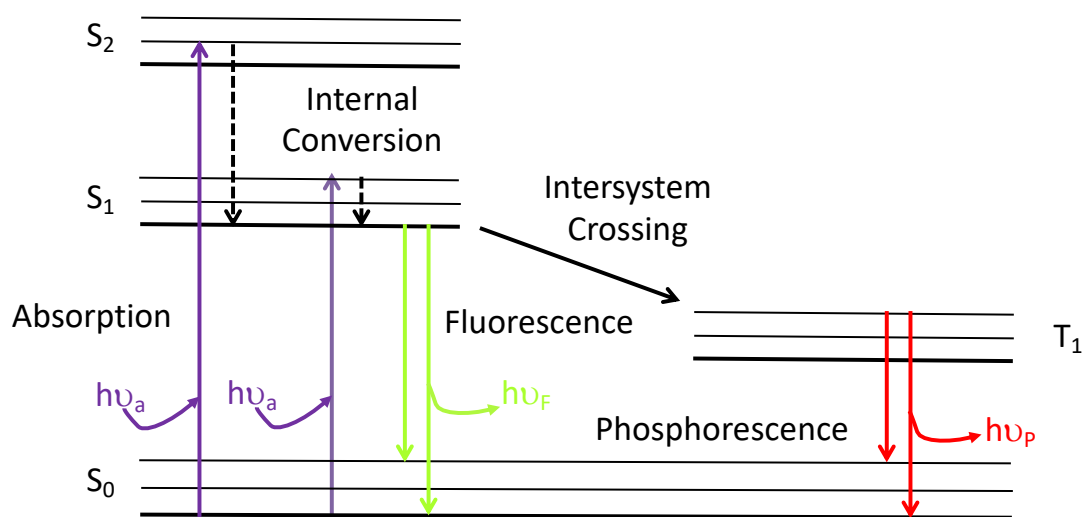


**Figure 1.11.** The Jablonski diagram illustrating the excitation of a ground electronic state  $S_0$  to the excited electronic states  $S_1$ ,  $S_2$  or  $T_1$ , where on returning to the ground state  $S_0$ , energy is emitted in the form of light as fluorescence or phosphorescence, respectively. Adapted from reference 138.

The excitation and emission processes are normally mirror images of each other since the nuclear geometry of the material is not altered. The difference between the excitation maxima ( $\lambda_{ex}$ ) and the emission maxima ( $\lambda_{em}$ ) is known as the Stokes shift. A Stokes shift greater than 100 nm has been proven to be ideal for sensing applications, since minimal overlap between the excitation wavelength and emission wavelength occur, meaning that energy loss is minimised.<sup>138</sup>

Emissive rates for fluorescence and phosphorescence differ due to the type of transitions (allowed or forbidden) that occur. Since the transitions for fluorescence are allowed, the typical emissive rates are near  $10^{-8}$  s and the emissive rates for phosphorescence are much greater, since these transitions are normally forbidden, in the range of milliseconds to seconds.<sup>138</sup> Fluorescent lifetimes can also be measured and these values range in the nanosecond region at approximately  $1 \times 10^{-9}$  s.<sup>138</sup> The lifetime of a fluorophore is the average time a molecule spends in the excited state, where it can diffuse or interact with its environment. The lifetime measurement provides information on the emissive rate of the fluorophore and the non-radiative decay.

### 1.3.2 Mechanisms and Dynamics of Fluorescence Sensing

It is important to note that not all of the energy absorbed is emitted in the form of light as fluorescence or phosphorescence. Some of this energy can be lost through non-radiative deactivation, by photoinduced electron transfer (PET),<sup>141, 142</sup> fluorescence resonance energy transfer (FRET),<sup>138</sup> internal charge transfer (ICT) or by static quenching or dynamic quenching.<sup>138</sup>

Non-radiative deactivation is the relaxation of an electron through vibrational states and in doing so thermal energy is released. Since the difference between these energy levels is minimal, this process occurs much faster compared to that of radiative decay by light emission. Solvent and environmental effects are the main causes for this type of quenching.<sup>138</sup>

PET often results in a quenched state of fluorescence in a fluorophore.<sup>138</sup> A typical PET sensor is composed of a fluorophore-spacer-receptor system (Figure 1.12).<sup>141</sup> One of the most popular fluorophores used for this sensing system is anthracene, commonly linked to a receptor molecule, such as an aliphatic amine by a methylene spacer. The length of this spacer is critical for the communication between the fluorescent and receptor components and so this linker is generally short consisting of

a one-carbon unit.<sup>138</sup> The process of electron transfer originates from the receptor. When the receptor interacts with its target analyte, this can cause the transfer of an electron from the lone pair on the aliphatic amine to the fluorophore, thus inducing quenching in the fluorophore. This causes an ‘*off*’-state of fluorescence.<sup>141, 142</sup> The fluorescence can be restored to an ‘*on*’-state by protonating the aliphatic amine or by an analyte binding to the receptor to make it electron-accepting. In this case, the electron from the lone pair may be transferred to the electron-accepting receptor, hence causing an increase in the fluorescence intensity, by inhibiting the transfer of an electron to the fluorophore (Figure 1.12).<sup>138</sup>

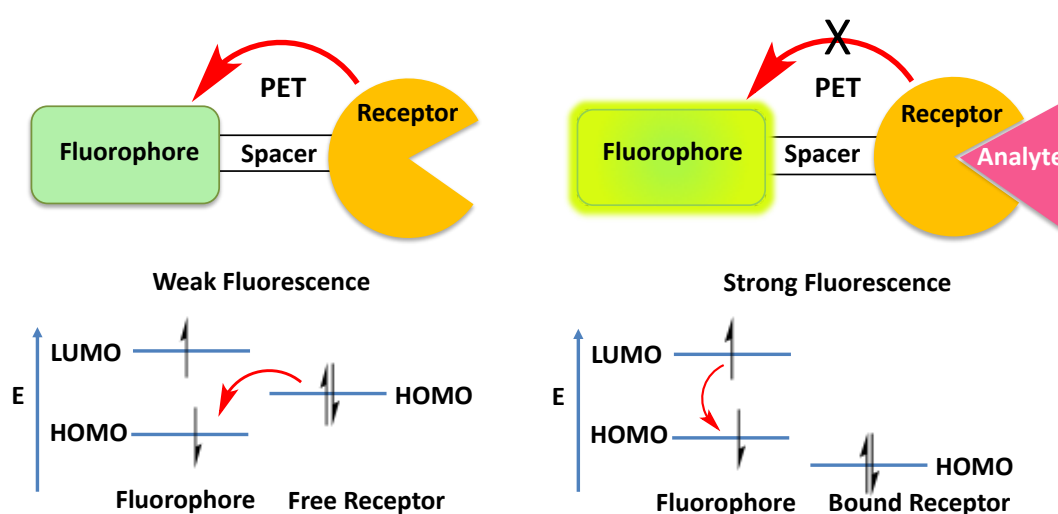


**Figure 1.12.** PET fluorescence sensing mechanism. Electron transfer from an electron-donating group/receptor to an electron-accepting fluorophore, which quenches the fluorescence of the fluorophore by PET. Once an analyte binds to the receptor, this electron transfer process is inhibited, which increases the fluorescence of the fluorophore. Adapted from references 138 and 143.

Fluorescence resonance energy transfer (FRET) is another form by which energy can be lost from a fluorescent species. In this case, the nonradiative energy is transferred from a donor fluorescent species to another acceptor molecule by collisional or dynamic quenching.<sup>138, 144</sup> This process transfers energy during the lifetime of the excited state through contact with another molecule.<sup>144</sup> This process is dependent on the concentration of the acceptor molecule in solution, where the donor and acceptor can be coupled by dipole-dipole interactions.<sup>138</sup> On contact between the donor and acceptor (Figure 1.13), the donor species then returns to the ground state, without the release of a photon and without fluorescence emission. A fluorescence



emission in this case is only possible if transfer of energy between the donor and acceptor molecules becomes disrupted.<sup>144</sup> An example includes the energy transfer from fluorescent electron rich fluorescein to electron deficient Rhodamide.<sup>138</sup> More examples of this type of quenching can be found in Section 1.4.1.

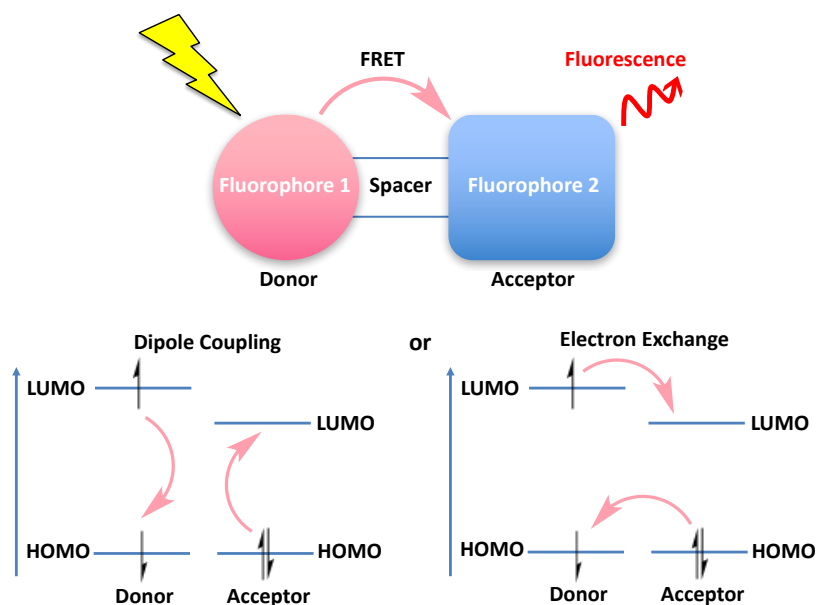


**Figure 1.13.** FRET fluorescence mechanism, whereby the emission of one fluorophore must overlap with the absorbance of another in order for the energy to be transferred from one fluorophore to the other. Adapted from reference 138.

For ICT, the receptor and fluorophore are covalently attached in a manner that allows for efficient orbital overlap for electronic coupling (Figure 1.14).<sup>144</sup> As a result of a ligand binding to the receptor, the wavelength of excitation and emission of the fluorophore may be altered. Another example of ICT occurs if an electron is transferred to a 2-(boronobenzyl)-6-methoxyquinolinium fluorophore; this causes the fluorescence to become quenched due to a conformational change altering hybridization around the boronic acid sugar receptor (Figure 1.14). However, if the electron is not accepted, for example by 2-(boronobenzyl)-6-methoxyquinolinium, the fluorescence remains unchanged.<sup>138</sup> This type of charge transfer can be seen in boronic acid sensors that are discussed later in Section 1.4.1.

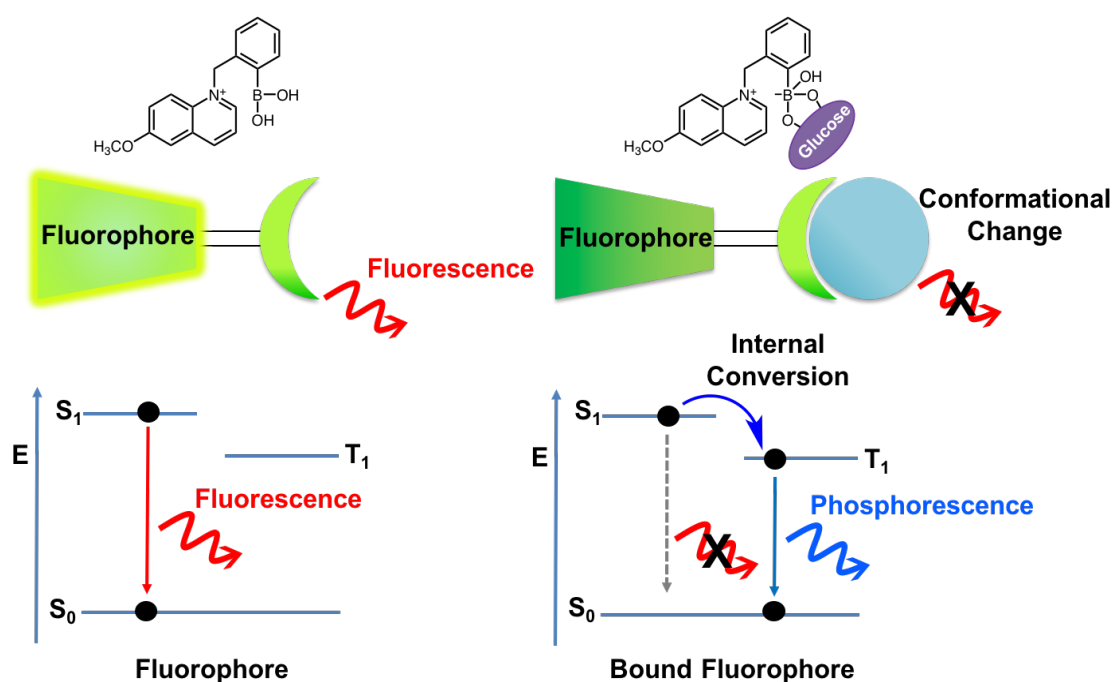


**Figure 1.14.** ICT fluorescence mechanism, where the fluorescence is quenched based on a conformational change in the molecule altering hybridisation. Adapted from reference 138.

Static and dynamic quenching are other types of quenching processes that may occur in solution.<sup>145</sup> For static quenching, a ground-state complex forms between the fluorophore and quencher molecule, most commonly by  $\pi$ - $\pi$  stacking interactions but also through electrostatic interactions.<sup>138, 145</sup> The formation of this complex leads to a stable non-fluorescent species. Dynamic quenching on the other hand causes quenching by collisions between molecules based on diffusion. These collisions occur in the excited state of the fluorophore, which deactivate the fluorescence upon contact. One of the best-known quenchers for dynamic quenching is molecular oxygen ( $O_2$ ).<sup>138</sup> Since  $O_2$  is paramagnetic, meaning that it houses two unpaired electrons, on collision of the fluorophore with  $O_2$  an electron may be transferred to initiate a quenched state of fluorescence.  $O_2$  can also cause the fluorescent species to undergo intersystem crossing to the excited-triplet state that immediately becomes quenched in aqueous solutions, rendering the fluorescent species non-emissive.<sup>138</sup> Examples of this type of quenching can occur between cationic boronic acids quenchers and anionic fluorophores.<sup>145</sup> More examples will be discussed later in Sections 1.4.1 and 1.4.2.

## 1.4 Boronic Acids

Boronic acids (BAs) are related to boric acid, belonging to a class of organoboranes. They are unique acids due to their Lewis acidic properties, which lends to numerous applications in a variety of different areas ranging from purification of glycoproteins by affinity chromatography to acting as protecting groups in carbohydrate chemistry. An interesting application is the use of BAs as chemoreceptor molecules for sugars.<sup>146</sup> The boron-sugar bond is unique in that although the interaction between the boronic acid and sugar forms strong covalent hydrogen bonds, it is completely reversible, which allows for the development of reversible and continuous sugar sensors.<sup>146</sup>

BAs are composed of an electron deficient boron atom with two attached hydroxyl groups.<sup>14</sup> BAs are Lewis acidic molecules due to the vacant *p*-orbital in boron, rendering this atom electron-deficient.<sup>144</sup> As a result of their Lewis acidic properties, BAs form strong interactions with Lewis basic diol-containing compounds, like glucose, to form *cis*-1,2- or *cis*-1,3-diols (5 or 6 membered cyclic-boronate esters).<sup>3, 147-151</sup> Reversible binding is desired for sensing since the analyte is not consumed in the sensing process.<sup>147</sup> The typical  $pK_a$  of a BA in aqueous media is  $\sim 9$ ,<sup>14</sup> meaning that sugar interactions preferentially occur under basic pH conditions.<sup>146</sup> In comparison to the BA moiety, the sugar bound form shows a higher acidity with a reduced  $pK_a$  of  $\sim 6$ . This is a result of the greater electron-withdrawing effect of the sugar in comparison to a hydroxyl group.<sup>144, 150</sup> Therefore, BAs with a reduced  $pK_a$  would allow for the detection of glucose molecules in solutions closer to physiological pH.<sup>150</sup> This concept allows for BA-fluorescent compound systems to be used as attractive chemoreceptors for the optical sensing of sugars within a pH range of pH 6-9 (Figure 1.15), which is well suited for physiological applications.<sup>152</sup>

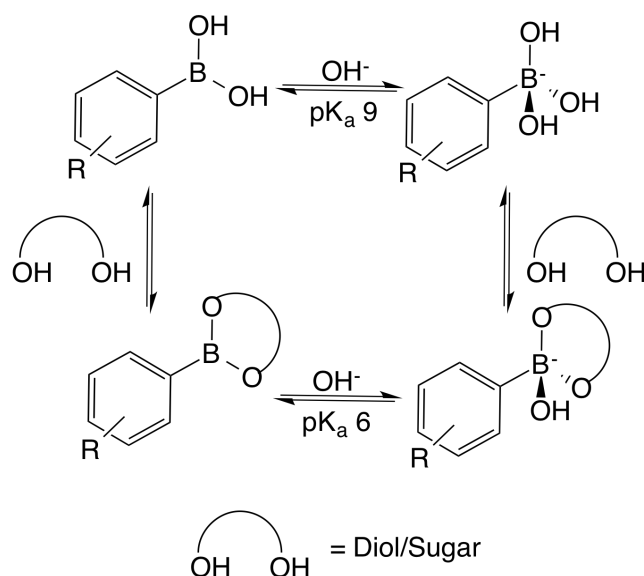


**Figure 1.15.** BA equilibrium illustrating the conversion from the neutral trigonal planar  $sp^2$  hybridisation form to the anionic boronate tetrahedral  $sp^3$  hybridised form, on binding glucose in alkaline aqueous media. Adapted from reference 12.

As BA groups bind diol-containing compounds, they are not selective for one sugar over another. Various physiological sugars exist, and some examples include, glucose, fructose, galactose, sucrose, lactose and mannose. The binding strength between specific saccharides and the BA moiety depend greatly on the orientation of the electron-withdrawing hydroxyl groups on the sugar in aqueous solutions,<sup>153</sup> as well as the aromatic moiety to which the BA group is attached.<sup>14</sup> BAs can bind to furanose and pyranose saccharides, to form *cis*-1,2- and *cis*-1,3-diols in this order of affinity (Figure 1.16).<sup>153</sup> *Trans*-1,2-diols can also form, however this formation is least favoured due to steric hindrance between axial atoms and ring strain. For this reason, BA binding to fructose can only occur 1:1, whereas a 2:1 binding with glucose is possible.<sup>154</sup> Different orientations in the sugar can allow for stronger affinities to certain diols. It is known that mono-BA groups preferentially bind with a higher affinity to furanose sugars over pyranose sugars, where monosaccharides such as fructose can bind preferentially over others like galactose, mannose and glucose, in this order.<sup>153</sup> The selectivity towards particular sugars is tuneable through the incorporation of other functionalities,<sup>14, 144, 151, 153, 155</sup> for example, by altering the aromatic group to which the BA is attached.<sup>14</sup> This information is particularly useful for designing a sensor with enhanced binding to a specific saccharide. Another design tactic could incorporate more BA moieties, which would increase the sensor

selectivity towards glucose. By introducing more BA groups, the number of sugar binding sites becomes increased, which would allow for enhanced interactions to glucose, as shown by Shinkai *et al.*<sup>153</sup> This allows the design of the BA sensors to be tailored to applications for sensing glucose in the millimolar range, corresponding to blood-glucose concentrations and the micromolar range, correlating to ocular-glucose levels.

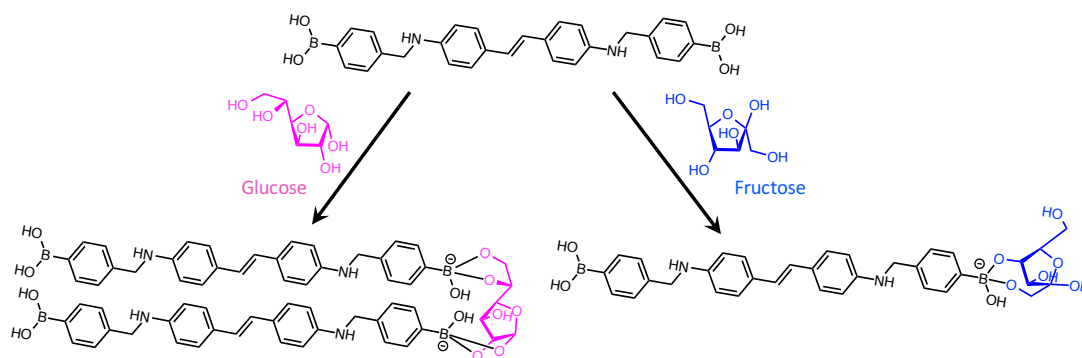


**Figure 1.16.** The furanose forms of glucose and fructose sugars binding to a BA derivative, where glucose binds in a bidentate fashion versus the monodentate binding of fructose. Adapted from reference 155.

BA derivatives that possess two or more BA groups can be tailored for glucose specificity over other sugars (Figure 1.16).<sup>149-151, 155</sup> This has been shown to depend on the linker length connecting the BA groups as well as the distance in space between the two groups, where a carbon-chain of 6 or 7 units has been determined for optimal glucose selectivity, while shorter or longer linkers are more suited towards fructose or galactose binding.<sup>144, 150, 151, 155</sup> As mentioned previously, on coupling with sugars, the  $pK_a$  of the BA moiety is reduced, which can increase the binding affinity towards glucose. This can lead to cooperative binding of glucose molecules, where the binding of one glucose molecule will facilitate the binding a second, if multiple BA groups are available for interaction.<sup>156</sup> Reducing the  $pK_a$  of the BA group can also be achieved by including electron withdrawing groups (EWGs) in the structure of the BA derivative.<sup>144</sup> In molecular biological systems, multivalent recognition sites are utilised to transform weak binding-interactions into strong binding-interactions, similar to that of the chelate effect in coordination chemistry. The chelate effect states that a tridentate ligand can bind preferentially over three monodentate ligands.<sup>153</sup> With emphasis on cumulative binding, a weak interaction can result in a greater binding

affinity from the same molecule, creating a strong and favoured binding interaction. Shinkai and coworkers showed this concept in 1994, when they fabricated a *bis*-phenylBA derivative that was designed for a glucose-sensing patch to monitor blood-glucose concentrations.<sup>153</sup> Although ditopic BA sensors aren't commonly described as 'multivalent' due to the divalent BA active sites, two BA moieties can bind to four hydroxyl groups forming a 1:1 cyclic boronate ester with glucose. This cooperative glucose binding can manifest as a multivalent interaction, which occurs in a greater affinity for glucose compared to fructose.<sup>153</sup>

Boronic acid-containing polymers, nanomaterials and higher order boronic acid-containing scaffolds have also been presented to show multivalent interactions with monosaccharides, demonstrating an increased affinity for glucose over fructose.<sup>3, 11-14, 37, 51, 133, 134, 146</sup> This proves that the orientations of the BA moieties play a critical role in sugar-selectivity on binding. A conformational change on glucose binding to a BA derivative also plays a key role in terms of selectivity. This conformational change differentiates the selective nature of sensors for specific monosaccharides, which has been exploited throughout the years in the development of physiological based glucose sensors.<sup>3, 11-14, 37, 51, 133, 134</sup> Some of the characteristic methods used to quantify this diol-sugar interaction include <sup>11</sup>B NMR, X-Ray crystallography, UV-vis and fluorescence spectroscopy.<sup>146</sup>

Fluorescent sugar sensing using boronic acids could be categorised in to *direct* and *indirect* sensing systems. In a direct sensing approach, the BA moiety and the fluorophore are included in the same structure, where the fluorescence becomes quenched on glucose introduction. Conversely, in an indirect sensing approach, the BA moiety and fluorophore are on separate molecules. A known fluorophore acts as the fluorescent reporter group, which is typically negatively charged. The BA group is typically attached to another positively charged molecule, which induces quenching in the fluorophore on forming a non-fluorescent ground state complex by electrostatic interactions. When glucose is then introduced in to the indirect sensing system, a conformational change in the BA group is induced, which renders the BA group anionic. As a result, the interaction between the fluorophore and BA derivative is weakened on sugar binding, initiating dissociation in the ground-state complex to release the fluorophore, therefore restoring the fluorescence.

### 1.4.1 Direct Sensing

Incorporating BAs in to fluorescent moieties, for intra-molecular sensing is a common approach for monitoring BA-sugar binding.<sup>3, 11-14</sup> The main three types of mechanisms used for fluorescence sensing in the direct approach are internal conversion, fluorescence resonance energy transfer (FRET) and internal charge transfer (ICT), where these processes were first introduced in Section 1.3.2.

The first fluorescent BA sensors were synthesised by Yoon and Czarnik in 1992 and it was composed of a BA functionalised anthracene moiety (Figure 1.17).<sup>3, 152</sup> In this case, the BA group acted as the receptor and anthracene as the fluorophore. As small polyol molecules, such as glucose, interacted with the BA receptor, the fluorescence of anthracene decreased by a charge transfer mechanism. Boronic acids in their neutral form possess a vacant *p*-orbital, which attributes to their Lewis acidity. As a result, the BA group could readily accept electrons. On interacting with electron-rich diol groups, the BA moiety became anionic. This caused a reduction in the pK<sub>a</sub> of the BA group to ~6 and altered the hybridisation of the boron to tetrahedral sp<sup>3</sup> hybridised.<sup>152</sup> Consequently, this hybridisation change of the BA group prevented electron transfer from anthracene to boron, which led to a quenched state of fluorescence in anthracene. This new conformation created an enhanced dipole moment, which increased the affinity for dipole-dipole interactions with solvent molecules. As a result, this interaction is highly dependent on the surrounding environment, where the solvent can influence the stabilisation of the sensor leading to significant fluorescent changes.<sup>150</sup> Consequently, the hybridisation change in boron resulted in the quenched state of fluorescence by 30% on saccharide binding.<sup>152</sup> Shinkai and co-workers then built on this work by synthesising a second sensing system based on an internal conversion quenching mechanism.<sup>3, 157, 158</sup>

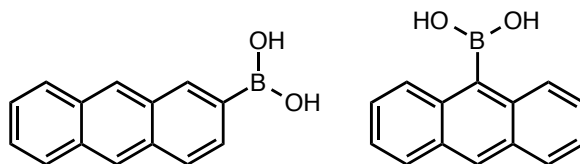


**Figure 1.17.** The first fluorescent BA sensors synthesised by Yoon and Czarnik.<sup>152</sup>

Two years later, another anthracene-based fluorescence system was developed by Shinkai *et al.*,<sup>3</sup> where they strategically placed an amino group in a 1,5-relation to the

BA group (Figure 1.18). By positioning the amino group close to the BA group, it was thought that internal B-N dative bond formation could stabilise sugar binding and further lower the  $pK_a$  of the BA group.<sup>153, 159</sup> In this sensing approach, the fluorophore is attached to a BA receptor through an amine-spacer moiety.<sup>141</sup> Recently, this sensing approach has undergone scrutiny where the fluorescence signal was previously believed to result from a PET sensing mechanism, however now it is believed that an internal conversion mechanism accounts for the enhanced fluorescence in the presence of sugars.<sup>158</sup> James and Anslyn *et al.*<sup>158</sup> have proved this sensing approach through solvent isotope-effects. Above the  $pK_a$  of the boronic acid, solvent molecules become inserted to transform the BA group to its  $sp^3$  hybridised form. In water -OH groups are inserted, however with sugars, in methanol or in  $D_2O$ , - $OCH_3$  groups or -OD groups can be inserted, respectively. Upon replacing the hydroxyl groups, the vibrational states in -OH become reduced, which leads to suppressed internal conversion and enhanced fluorescence.<sup>158</sup> Aggregation of the BA sensors in solution, as well as collisional quenching, also contribute to the initial quenched state of fluorescence. In the presence of sugars disaggregation results to enhance fluorescence (Figure 1.18).<sup>158</sup> This change was large enough to produce an *on/off* fluorescence response.<sup>142</sup>

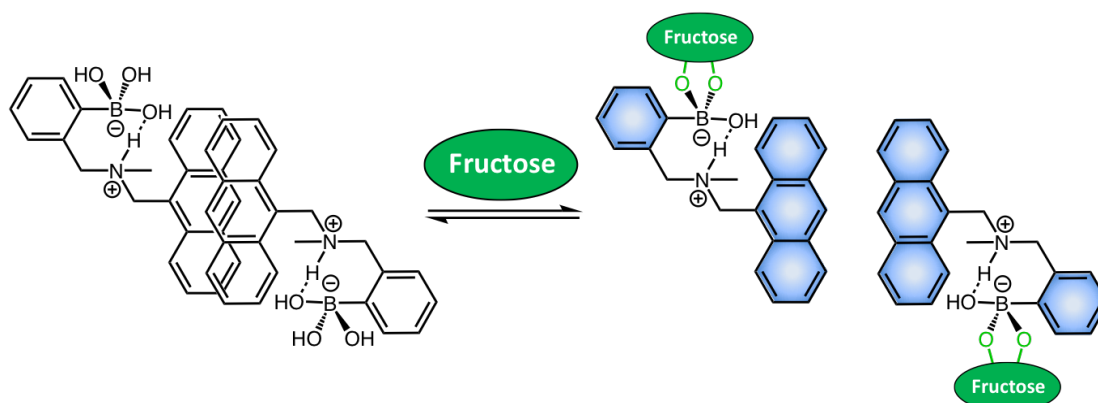


**Figure 1.18.** Anthracene-based BA derivative, where its fluorescence is quenched due to aggregation in the absence of fructose (left) and it becomes fluorescent in the presence of fructose due to disaggregation (right). Adapted from reference 158.

Fluorescence resonance energy transfer (FRET) has also been employed to modulate fluorescence of BA systems upon glucose binding. This sensing mechanism requires the emission of one fluorophore to overlap with the absorbance of another, in order for non-radiative energy to be passed from one fluorophore's excited state



(donor) to another fluorescent acceptor molecule's ground state.<sup>144</sup> For this process to occur, both fluorophores must be in close proximity, where they are usually attached to the same structure through a spacer.<sup>144</sup> James *et al.*<sup>148</sup> developed a *bis*-BA sensor based on the fusion of two different BA-functionalised fluorophores, namely phenanthrene and pyrene (Figure 1.19). The system operates based on the overlap of the emission of phenanthrene with the excitation of pyrene, where phenanthrene acts as the donor and pyrene as the acceptor.<sup>3, 148</sup> On binding to glucose in a 1:1 ratio, the structure of the sensor becomes more rigid, which assists the transfer of energy from phenanthrene to pyrene to enhance the fluorescence.<sup>3, 148</sup> As a result of exciting the sensor at 299 nm, characteristic to phenanthrene, an emission wavelength of 417 nm was observed, unique to pyrene.<sup>148</sup> Consequently, the fluorescence could be enhanced by ~3.9 times on glucose binding. Moreover, this *bis*-BA sensor exhibited increased fluorescence with glucose relative to fructose, due to the fact that glucose binds to the sensor in a 1:1 ratio forming a cyclic complex, whereas fructose binds in a 2:1 ratio forming an acyclic complex.<sup>148</sup>

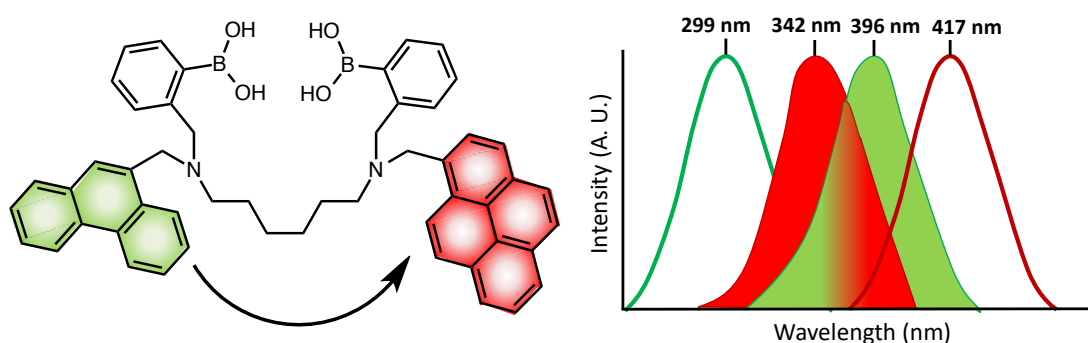


**Figure 1.19.** Structure of the FRET-BA glucose sensor designed by James *et al.*, using the fluorophores phenanthrene (green) and pyrene (red) (left), where the emission of phenanthrene at 396 nm overlaps with the excitation of pyrene (red) at 342 nm. Upon excitation of the sensor at 299 nm, characteristic to phenanthrene, only an emission at 417 nm is observed, characteristic to pyrene. Adapted from reference 148.

4,4-difluoro-4-bora-3a,4a-diaza-*s*-indacene (BODIPY)-based dyes have also been of interest, where Kikuchi *et al.*<sup>160</sup> have recently published a review based on the current state of BODIPY-based probe developments for imaging of biomolecules in living cells. BODIPY dyes are favourable for imaging purposes because they possess relatively high photostability, a total neutral charge, high fluorescence quantum yields and the controllability of their fluorescence by either PET or FRET fluorescence approaches.<sup>160</sup> A challenge for bio-imaging using BODIPY-dyes remains their high

hydrophobicity.<sup>160</sup> Nevertheless, some BODIPY-based probes have even emerged commercially, such as ER-Tracker Green, valuable for mammalian cell tracking and LysoTracker Red, used for labelling and monitoring the movement of acidic-based cell organelles (Figure 1.20).<sup>160</sup>

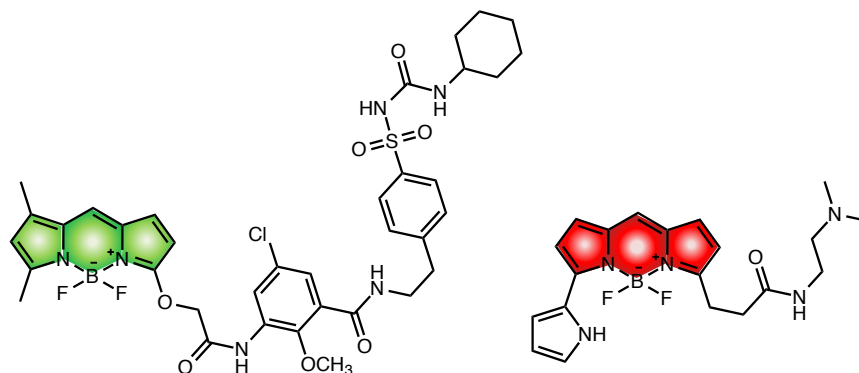


**Figure 1.20.** Commercially available BODIPY probes ER-Tracker Green and LysoTracker RED.<sup>160</sup>

Various BODIPY dyes have also been modified to contain phenylBA functionality, where these probes have been implemented for glucose sensing applications.<sup>144, 149, 161, 162</sup> Hansen *et al.*<sup>161</sup> synthesised pinacol ester-BODIPY-BA derivatives (Figure 1.21), where with increased sugar concentrations, an increase in fluorescence intensity of the dye was observed. Similar to the PET quenching mechanism described earlier, electrons can be transferred from the phenylBA ring in to the BODIPY rings to quench the fluorescence. However, on coupling to sugars, this process is inhibited by the electronic configuration change in boron to the anionic boronate form. As a consequence, the fluorescence intensity increases.<sup>161</sup> The pitfall with this sensor design is that monophenylBA derivatives are more selective for fructose over glucose. Consequently, these sensors were not very receptive to glucose within the clinical range, where the blood-glucose levels for diabetics are known to be between 2-40 mM.<sup>149, 161</sup> The sensor, however, showed slight sensitivity to glucose in the hypoglycaemic range (0-1.6 mM) displaying a 20% fluorescence increase in buffered solutions.<sup>161</sup>

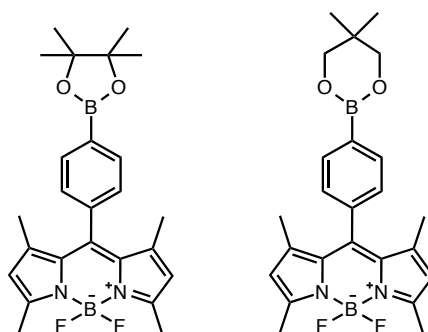


**Figure 1.21.** Structures of BA-BODIPY glucose sensors synthesised by Hansen *et al.*<sup>161</sup>

Further development in the BODIPY-BA sensor design by Hansen *et al.*, showed the effect of *ortho* substituents on the BA group. Using the BA version of the pinacol ester-BODIPY probes previously employed, methyl- and fluoro-groups were used as substituents in the *ortho* position to the BA moiety.<sup>149</sup> It wasn't surprising to find that the fluoro-group showed an increased fluorescence response to glucose. This came as a consequence of the electron-withdrawing ability of fluorine to decrease the  $pK_a$  of the BA group to 7.3, which ultimately enhanced its affinity for glucose.<sup>149</sup> On the other hand, the BA-BODIPY probe with the methyl substituent attained an increased  $pK_a$  of 10.7, which explained the low fluorescence increase on binding glucose.<sup>149</sup> Importantly, the fluoro-probe showed to bind glucose in physiological relevant concentrations as a result of the reduced  $pK_a$ . It was also concluded that although large EWGs, such as  $CF_3$ -group, can further decrease the  $pK_a$  of the BA group relative to fluorine when *ortho* to the BA moiety, the attachment of bulky groups can interfere by sterically hindering the binding of glucose.<sup>149</sup> As a result, achieving a balance between the electron-withdrawing effect and size of the *ortho* substituent is crucial in the BA probe design.

Glucose sensors displaying intramolecular charge transfer (ICT) fluorescence have also been of interest, where Badugu *et al.* have developed a family of BA probes for glucose detection that rely on this mechanism.<sup>7, 11-14, 37, 51, 133, 134</sup> Typically, quinoline was the fluorophore employed and this was covalently bonded to a phenylBA group via a methyl-linker (Figure 1.22). The sensors were investigated for any fluorescence effect on the quinoline moiety by changing the positioning of the BA group in the *ortho*, *meta* or *para* orientations as well as interchanging methyl- and methoxy-substituents in the 6-position on the quinoline ring.<sup>7, 11-13, 37, 51, 133, 134</sup> On interaction with increasing sugars concentrations, a decrease in the fluorescence intensity of the

BA sensors occurred.<sup>11-14</sup> As glucose binds to the BA moiety, the hybridisation around boron conforms to the anionic boronate form.<sup>7, 12, 13, 37, 51, 133</sup> This induces a geometry alteration in the BA group from trigonal planar to tetrahedral on converting the BA moiety in to its anionic boronate form. This renders the BA group as no longer electron withdrawing and as a result, an optical fluorescence response is observed due to the ICT nature of the excited state.<sup>14</sup> The negative charge on boron interacts with the cationic charge on nitrogen in the quinoline ring to stabilise glucose binding and neutralise the charge on boron. This is known as a charge-neutralisation stabilisation interaction (Figure 1.23). The electron transfer from B<sup>-</sup> to N<sup>+</sup> consequently quenches the fluorescence. Similarly, the fluorescence is quenched with increased solution basicity.<sup>7, 12, 13, 37, 51, 133</sup>

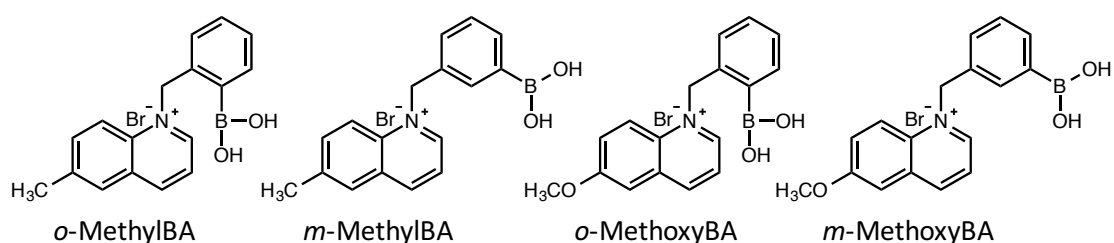


**Figure 1.22.** BA probes synthesised by Badugu *et al.*, where methyl- and methoxy-groups attached on the quinoline ring are employed and the positioning of the BA moiety is altered between *ortho* and *meta* to the N<sup>+</sup> quinoline substituent.<sup>12</sup>

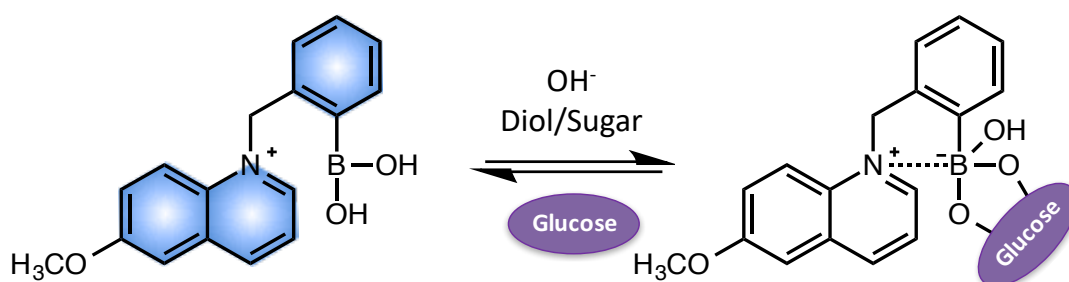


**Figure 1.23.** Scheme showing the charge neutralisation-stabilisation interaction, where the BA derivative is initially fluorescent and on sugar binding, fluorescence quenching occurs. Adapted from references 11, 12, 37 and 134.

Importantly, these BA-probes could detect glucose in solution, within an appropriate physiological range relative to blood-glucose concentrations. Although a fluorescence decrease by approximately 30% was shown, both probes concurred similar findings.<sup>7, 11-13, 37, 51, 133</sup> This wasn't surprising since the pK<sub>a</sub> of the BA probes

was reduced to  $< 7$ , to afford a higher affinity for glucose binding.<sup>37</sup> However, possessing only monophenylBA functionality, the sensors were more receptive to fructose over glucose. *o*-MethoxyBA exhibited the greatest fluorescence quenching by ~32% in the presence of 50 mM glucose and by ~14% with 5 mM glucose, relevant for physiological blood and ocular glucose concentrations, respectively. This improved sensitivity of the *o*-MethoxyBA compared to the *m*-MethoxyBA is possibly owed to the increased ability for B<sup>-</sup>-N<sup>+</sup> interactions when the BA is present in the *ortho* position to the N<sup>+</sup> quinoline substituent.<sup>12</sup>

To this end, glucose-sensing investigations have been carried out in solution. Badugu *et al.* also determined the probes' sensitivity to glucose using commercially available contact lenses that were doped in a solution of the sensor. In this context, the sensor was adsorbed to the surface of the lens.<sup>12, 37, 134</sup> The BA probes best responded to increased sugar concentrations by a decrease in fluorescence intensity in pH buffer solutions between pH 6-9. This could be attributed to the difference in equilibria between the pK<sub>a</sub> of the BA and the pK<sub>a</sub> of the sugar-bound boronate-diester form. *o*-MethylBA probe was reported to have an optimal response to glucose in the lens, where a quenched state of fluorescence by ~10% was observed with 1.6 mM glucose, corresponding to hypoglycaemic glucose concentrations in diabetics.<sup>12, 37</sup> It was also determined that considerable amounts of the fluorophore leached from the lens due to non-covalent doping, which also contributed to the low fluorescence intensity.<sup>12, 37</sup> Consequently, the *o*-BA probes exhibited an optimised glucose response in contrast to the *m*-BA counterparts, which was thought to reflect on the more accessible B<sup>-</sup>-N<sup>+</sup> interaction.

#### 1.4.2 Indirect Sensing

Inter-molecular sensing using BAs has also gained attention in recent years for modulating fluorescence as a function of saccharide concentration.<sup>144, 145, 163-169</sup> Incorporation of a BA component into charged molecules can be used to induce quenching in the emission of a fluorophore, thereby creating a two-component sensing system. Cationic BA derivatives have been modelled as quenchers for known fluorophores, such as pyranine derivatives,<sup>145, 163, 169, 170</sup> fluorescent graphene quantum dots<sup>164</sup> and PP-*S*-BINOL.<sup>167</sup> The signal transduction operates based on the initial interaction between the fluorophore and BA quencher molecule, where the fluorescence of the fluorophore becomes quenched.<sup>145, 163, 164, 166, 167, 169, 170</sup> The change

in fluorescence intensity of the system is achieved via the formation of a ground-state complex that is non-fluorescent, through electrostatic and  $\pi$ - $\pi$  stacking interactions between the fluorophore and BA-quencher. In the presence of saccharides, the formation of a boronate diester results in the dissociation of the BA-quencher and fluorophore ground-state complex, leading to a sequential recovery of fluorescence.<sup>145, 163, 164, 166, 167, 169, 170</sup>

In 2001, Singaram and co-workers were the first to introduce this indirect sensing approach for applications in real-time glucose monitoring *in vivo*.<sup>145, 163, 169</sup> They reported pyranine derivatives as the anionic fluorescent reporter and a cationic BA-appended viologen functioning both as a fluorescence quencher and sugar receptor molecule. With increased concentrations of the BA quencher relative to the fluorophore, a decrease in the fluorescence intensity of the fluorophore was observed. On sequential addition of glucose, fructose or galactose, the fluorescence of the fluorophore could be recovered, correlating to the specific sugar concentration.<sup>145, 163, 169</sup> Singaram *et al.* proved this two-component sensing mechanism by UV-visible spectroscopy. Firstly, Singaram *et al.* showed the ionic formation of a ground state complex, as a photo-inactive compound, on electrostatic interactions between the fluorophore and BA-derivative.<sup>168</sup> Using UV-visible spectroscopy, the presence of a neutral zwitterionic species from the dicationic BA-viologen compound on sugar binding was characterised.<sup>168</sup> On forming this zwitterionic species the loss of electrostatic attraction between the fluorophore and BA viologen resulted in dissociation in the non-fluorescent ground-state complex. Consequently, this restored the fluorescence in pyranine.<sup>168</sup> It's important to note that this system is limited to the photochemical properties of the fluorophore chosen, in terms of photostability and excitation wavelength.<sup>168</sup> The  $pK_a$  of the substituents in the structure of the fluorophore is also a consideration, since the pH of the sensing solution would determine whether or not the fluorophore is present in its neutral or anionic state. It is in one's best interest when designing such a system for glucose sensing that uses BAs to choose a fluorophore with a  $pK_a$  within the range of pH 6-9.

Two years later, Singaram *et al.*<sup>166</sup> reported on further developments on the same bimolecular sensing system. Cationic viologen BA-derivatives were employed with the same anionic fluorophore, pyranine, in a pH 7.4 buffer solution.<sup>165</sup> Figure 1.24 depicts the structure of pyranine and the BA molecules screened for the initial

fluorescence quenching process. In this example, the quenched state of fluorescence in pyranine was measured upon incorporation of the cationic BA molecule.<sup>166</sup> A non-fluorescent ground-state complex resulted by electrostatic and  $\pi$ - $\pi$  stacking interactions between these two-components.<sup>166</sup> A maximum of 92% and 83% quenched state of fluorescence was observed in o-PBBV<sup>2+</sup> and o-BBV<sup>2+</sup>, when molar ratios of 1:30 and 1:42.5 of fluorophore to BA species were employed, respectively.<sup>166</sup> On addition of glucose to the system, which bound to the BA moiety, the BA group was rendered negatively charged. As a result, a neutral zwitterionic component formed.<sup>166</sup> This initiated dissociation in the complex due to the loss of electrostatic attractions between the fluorescent and BA components, to release the fluorophore and restore the fluorescence intensity in pyranine on glucose addition by 4% using o-BBV<sup>2+</sup> and 45% using o-PBBV<sup>2+</sup>.<sup>166</sup> o-PBBV<sup>2+</sup>, in this case is shown to be more selective for glucose compared to o-BBV<sup>2+</sup> since the geometry of the BA groups allows for cooperative bidentate glucose binding over monodentate binding between o-BBV<sup>2+</sup> and glucose.<sup>166</sup> It is known that the binding of multiple BA groups to one glucose molecule is preferential to a 1:1 binding between a BA group and a glucose molecule.<sup>3, 157, 171, 172</sup> For this reason, o-PBBV<sup>2+</sup> can sense glucose more selectively compared to o-BBV<sup>2+</sup>.

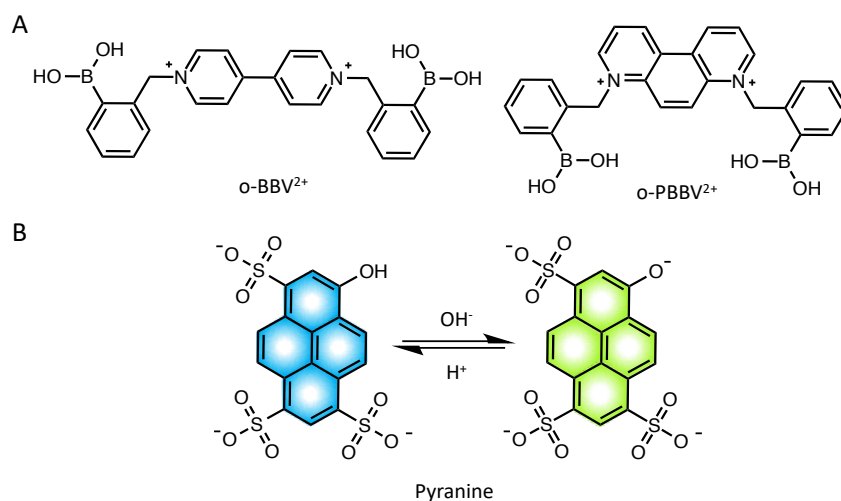


**Figure 1.24.** (A) Cationic BA molecules synthesised by Singaram *et al.* used to quench the fluorescence of pyranine. (B) Pyranine equilibrium at pH 7.4, illustrating the two possible anionic forms.<sup>166</sup>

In 2007, the Singaram group investigated the effect of substituents on the BA component.<sup>169</sup> In this example, they attached different substituents on to the BBV<sup>2+</sup> molecule, as shown in Figure 1.25. Both an electron-donating group *e.g.* methoxy group and an electron withdrawing group *e.g.* fluoride group, were attached to the m-BBV<sup>2+</sup> component in an attempt to understand the fluorescent quenching mechanism, based on how the pK<sub>a</sub> of the BA group changed.<sup>169</sup> Electron withdrawing groups bonded to the same phenyl ring as the BA group were expected to pull electron density away from the BA group. As a result, the BA group became more acidic, with a reduced pK<sub>a</sub>,<sup>172, 173</sup> which enhanced the electrostatic attraction with the anionic fluorophore and improved fluorescence quenching.<sup>169</sup> Conversely, electron-donating groups increased electron density around the B atom, making it more basic. As a result of this increased pK<sub>a</sub>,<sup>173</sup> the fluorescence intensity increased due to weakened electrostatic attraction with the anionic fluorophore.<sup>169</sup> Similarly, when the electron-donating methoxy-group was positioned *para* to the BA group (in m-OMeBBV<sup>2+</sup>), the pK<sub>a</sub> of the BA group was increased relative to m-BBV<sup>2+</sup>. In comparison, by adding an alternative electron withdrawing group to form m-FBBV<sup>2+</sup>, the net effect of both the N<sup>+</sup> moiety and the fluoro group lowered the pK<sub>a</sub> of the BA group,<sup>170</sup> whereas the methoxy-group by donating electron density counteracted the N<sup>+</sup> electron-withdrawing effect.<sup>169</sup> However, the attachment of both –F and –OCH<sub>3</sub> substituents hindered the ground state complex formation, which interfered with fluorescence quenching of the system.<sup>169</sup> Singaram *et al.* concluded that any change associated with the electron affinity in the viologen would make the compound less efficient at quenching the fluorescence of the fluorophore. This change for the most part can be related to sterics, where it was thought that the attachment of the –F group sterically hindered the efficient formation of the non-fluorescent ground state complex.<sup>169</sup> Consequently, the glucose recovery in both m-FBBV<sup>2+</sup> and m-OMeBBV<sup>2+</sup> was also lower in comparison to the m-BBV<sup>2+</sup> derivative. This was attributed to a stronger non-fluorescent ground state complex formation between pyranine and m-BBV<sup>2+</sup> in comparison to m-FBBV<sup>2+</sup> and m-OMeBBV<sup>2+</sup>, although the m-FBBV<sup>2+</sup> compound showed a greater binding affinity for glucose, due to the lowered pK<sub>a</sub> effect on the BA group.<sup>169</sup>



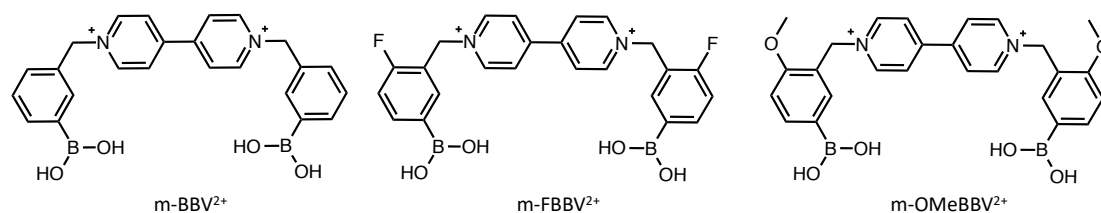


**Figure 1.25.** Structures of  $m\text{-BBV}^{2+}$  together with  $-\text{F}$  and  $-\text{OCH}_3$  derivatives used to modify viologen fluorescence in the indirect glucose sensing approach.<sup>169</sup>

Structural differences between the BA derivatives affect the extent of quenching and glucose recovery in this two-component sensing system. For an optimal quenching interaction, the BA moiety must be covalently bonded to an electron acceptor molecule.<sup>166</sup> From the work presented by Singaram *et al.*, the viologen structural framework was desired since it possesses two positive  $\text{N}^+$  atoms (Figure 1.25). These charges facilitate two types of processes that are necessary for the quenching of fluorescence by electron transfer and Coulombic or electrostatic attraction.<sup>166, 170</sup> Incorporating electron withdrawing groups or increasing the conjugation in the BA derivatives structure can improve the electron-accepting ability of the molecule.<sup>166, 172</sup> By incorporating electron-withdrawing substituents, a decrease in the electron density around the  $\text{N}^+$  atom rendering it more electron accepting, can result due to mesomeric effects. This is desired to enhance the extent of electrostatic attraction between the anionic fluorophore and cationic BA group. This would allow for a maximised quenching interaction, but also a reduction in the  $\text{pK}_a$  of the B atom, to enhance glucose binding<sup>172</sup> and restore fluorescence.<sup>166, 169</sup>

The orientation of the BA group in the *ortho* or *meta* position can also play a role in the fluorescence restoration of the system.<sup>157</sup> It is known that the more acidic the BA group, the greater the extent of glucose binding at neutral pH.<sup>166</sup> Fluorescence recovery can be maximised in this way by attaching the BA group in an *ortho* position, so that interaction with the positively charged nitrogen is permitted. On forming the B-N interaction, the  $\text{pK}_a$  of the BA group becomes even more acidic, with an approximate  $\text{pK}_a \sim 3.7$ , since the B atom is directly connected to the electron withdrawing pyridinium ring.<sup>166</sup> This accounts for enhanced glucose binding which is necessary to restore the fluorescence intensity.

In 2013, Feng *et al.*<sup>170</sup> progressed to screen another BA-derivative for its ability to quench the fluorescence of the same pyranine derivative employed by Singaram *et al.*

The structures of both the fluorescent and BA components can be seen in Figure 1.26. Noting the design of the *tris*-pyridine BA component (*p*-TBPB), the BA groups are directly attached to the pyridine rings containing the electron-withdrawing N<sup>+</sup> moiety. This structural design had a considerable impact on lowering the pK<sub>a</sub> of the BA group, and it aimed to enhance the electrostatic attraction between the anionic fluorophore and cationic BA derivatives and also to improve glucose binding for fluorescence recovery.<sup>170</sup> On investigating the initial quenching interaction using a ratio of 1:4.4 fluorophore to BA derivative, Feng *et al.* found an exponential decay in the Stern-Volmer plot, indicating an amplified fluorescence quenching response by ~95%.<sup>170</sup> The fluorescence recovery was calculated at ~28% with 100 mM D-glucose, when 0.02 mM of the BA component with 4.0 mg/mL of pyranine-like polymer was employed.<sup>170</sup> Feng *et al.* also screened a range of saccharides with this pyranine fluorophore and *p*-TBPB in a two-component fluorescence switch, where they found that this two-component sensing system was the most selective towards fructose.<sup>170</sup> Overall, this sensing system showed optimum quenching and recovery results, since only 0.02 mM of the BA component was required to quench the fluorescence by ~95%,<sup>168</sup> which is a considerable smaller quantity in comparison to other reports from Singaram *et al.* and others.<sup>166, 169</sup>

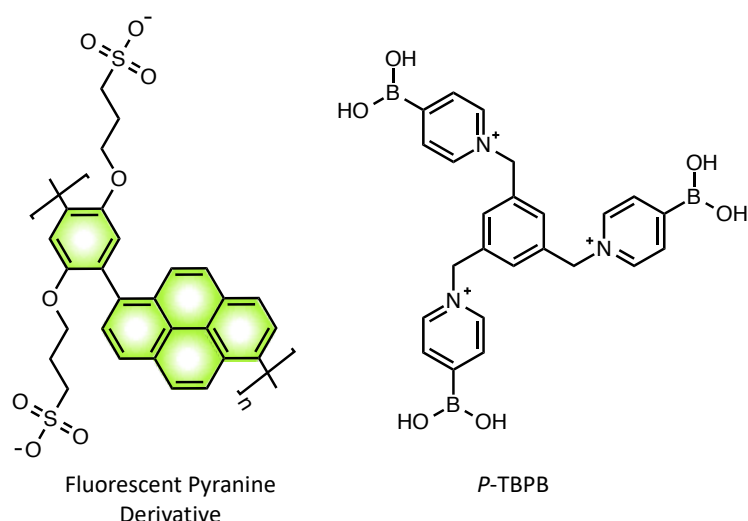


**Figure 1.26.** Components used by Feng *et al.* in the indirect glucose sensing approach: Pyranine fluorophore and trispyridine-BA.<sup>170</sup>

In 2013, Li *et al.*<sup>164</sup> used fluorescent graphene quantum dots for bimolecular glucose detection with Singaram's BBV<sup>2+</sup> molecule. The structures are depicted in

Figure 1.27. Fluorescent graphene quantum dots were chosen since they consist of a single atomic layer of carbon with many unique characteristics that can easily be tailored to a device design.<sup>164</sup> These carbon dots have a diameter < 10 nm, meaning they possess strong quantum confinement, since their electronic and optical properties differ greatly from the bulk material in which they are situated, providing them with wavelength-dependant fluorescent properties.<sup>164</sup> As a result, these quantum dots exhibit a high surface area, better surface grafting using a  $\pi$ - $\pi$  conjugated network or other surface groups,<sup>164, 174</sup> as well as those unique physical properties of graphene such as biocompatibility, low toxicity and chemical inertness.<sup>174, 175</sup> Quenching by 80% in the fluorescence of the quantum dots on addition of 0.5 mM BBV<sup>2+</sup> was observed under UV light illumination.<sup>164</sup> This fluorescence was then restored by 33% on sequential additions of glucose, when a ratio of 1:20 fluorophore:BBV<sup>2+</sup> was employed.<sup>164</sup> This two-component sensing system was most sensitive to glucose within a concentration range of 0-60 mM,<sup>164</sup> which corresponds to the blood-glucose concentration ranges in diabetic patients.<sup>12</sup>

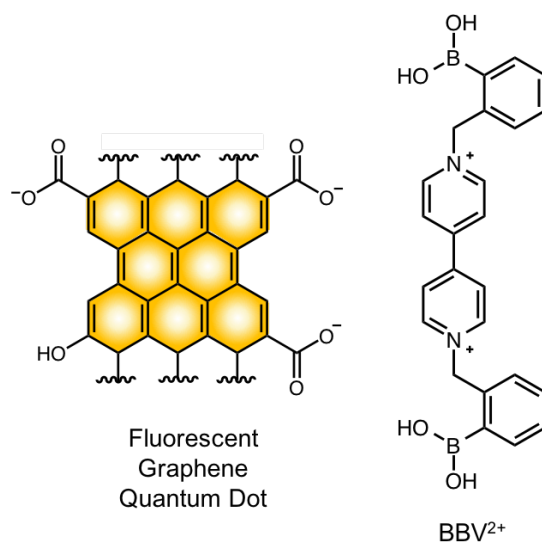


**Figure 1.27.** Fluorescent graphene quantum dot and BBV<sup>2+</sup> viologen compounds used in the two-component glucose sensing system by Li and co-workers.<sup>164</sup>

The only important disadvantage to Singaram's approach is that viologens are known to be very toxic<sup>176</sup> and are therefore not suitable towards *in vivo* glucose monitoring. This flexible two-component approach is very advantageous in that the components can be modified individually to optimise the saccharide response in the system. It is also beneficial for tailoring the synthetic design of the BA quenchers.

The BA compounds could be fabricated so that they would possess water-solubility properties for biological applications, anchoring groups for surface modifications or polymerising groups for incorporation into polymeric substrates and gels.<sup>170</sup>

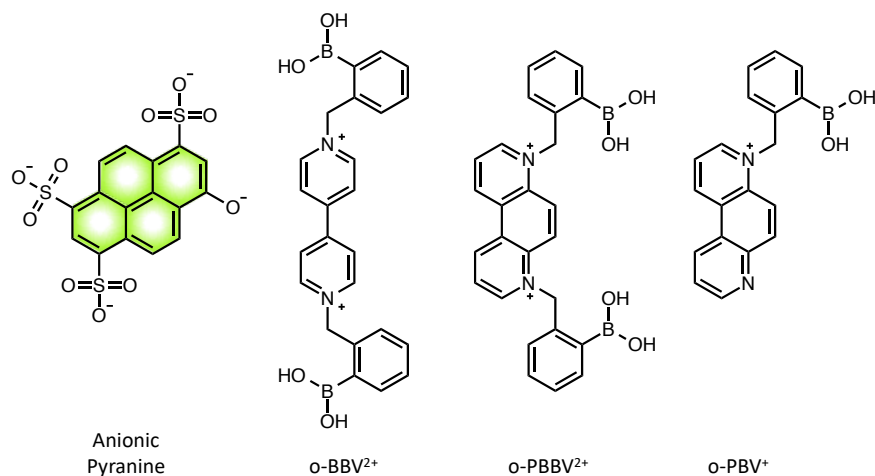


**Figure 1.28.** Anionic pyranine fluorophore and BA quencher viologens used in two-component sensing system by Singaram and co-workers. Adapted from reference 166.

Singaram *et al.*, have also built on their initial work by fabricating fluorescent hydrogel glucose sensors using the same viologen compounds.<sup>163</sup> They fabricated a thin-film hydrogel consisting of a co-polymerised fluorophore and BA compound.<sup>145</sup> Pyranine was employed as the fluorescent component and a cationic viologen BA derivative (o-BBV<sup>2+</sup>) was used as the glucose receptor (Figure 1.29). Glucose (20 mM) was successfully detected demonstrating a recovery of fluorescence of ~18%.<sup>145</sup> As a result of covalently immobilising the fluorescent and BA components, their local interactions were sufficient to form the non-fluorescent ground-state complex, which dissociated upon binding with glucose. Moreover, they also found that in the gel matrix these fluorescent changes were reversible, although the response was slow (~30 minutes).<sup>163</sup> The only disadvantage was that the fluorophore was found to be pH sensitive within the physiological glucose sensing range.<sup>177</sup> This challenge was later overcome by making a small modification to the fluorophore.<sup>177</sup>

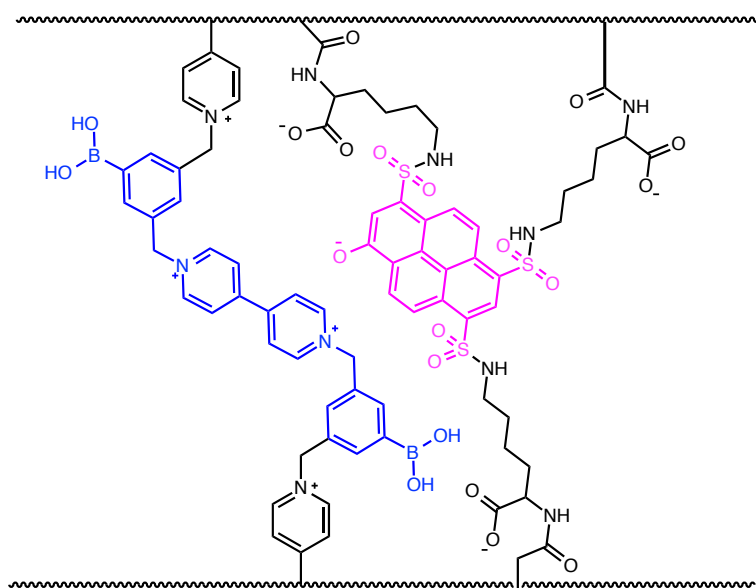


**Figure 1.29.** Singaram's cationic BA viologen (blue) and pyranine fluorophore (pink) immobilised in a hydrogel framework.

In 2009, Singaram *et al.*<sup>177</sup> developed this system further. By interchanging the -OH substituent in pyranine for an amine (-NH<sub>2</sub>) Singaram *et al.* produced a fluorophore that was pH insensitive within the relevant pH range.<sup>177</sup> Moreover, they found that simpler chemistry enabled them to attach a linker through the -NH<sub>2</sub> substituent in comparison to the -OH substituent (Figure 1.30). Similarly, by immobilising the fluorophore via a single tether in the -NH<sub>2</sub> gel, enhanced mobility of the fluorophore inside the hydrogel matrix was permitted, in contrast to the hydrogel depicted in Figure 1.29, which is immobilised through three linkers. This increased flexibility allowed for improved interaction between o-BBV<sup>2+</sup> and the fluorophore. As a result, the o-BBV<sup>2+</sup> component was modified to contain extra cationic pyridine moieties for enhanced electrostatic interaction with anionic pyranine and a single linker was incorporated in to the o-BBV<sup>2+</sup> moiety to increase mobility (Figure 1.30).

Two different linkers were employed for immobilising the amine-derivatised pyranine fluorophore inside the hydrogel matrix; pyranine-BuMA and pyranine-DEGMA.<sup>177</sup> Pyranine-BuMA was tethered with a butylmethacrylate chain, whereas pyranine-DEGMA possessed a diethyleneglycolmethacrylate chain.<sup>177</sup> Figure 1.30 shows the structures for the pyranine-DEGMA:BA-viologen hydrogel, where this combination exhibited optimal fluorescence responses. The fluorescence recovery response of each pyranine fluorophore was compared when a ratio of 1:10 pyranine:o-BBV<sup>2+</sup> was polymerised inside the hydrogel matrix. The pyranine-BuMA fluorophore

showed a fluorescence increase by 1.7 fold and the pyranine-DEGMA fluorophore displayed the optimal fluorescence recovery by 2.8 fold, on addition of 20 mM glucose.<sup>177</sup> The pyranine-DEGMA fluorophore was thought to respond better to glucose due to its more hydrophilic polyethyleneglycol tether.<sup>177</sup>

Finally, Singaram and co-workers optimised the fluorescence modulation by varying the ratios between the pyranine-DEGMA fluorophore and the viologen BA. Hydrogels comprising of pyranine-DEGMA:BA-viologen 1:30 were synthesised. Consequently, this gel exhibited a lower initial fluorescence in comparison to the other hydrogels, due to the increased concentration of the BA-viologen. As expected, a weaker fluorescence recovery of  $F/F_0 = 1.9$  was measured for the same concentration of glucose (20 mM).<sup>177</sup> In this case, in order to observe an increased fluorescence recovery, a higher concentration of glucose was required to overcome the quenched state of fluorescence. This shows that the molar ratios between the fluorophore, BA derivative and glucose are imperative for optimum sensing.

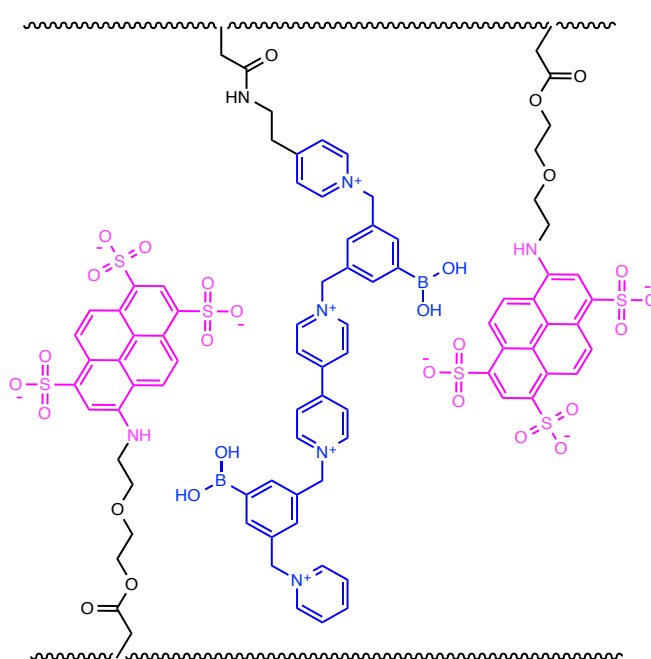


**Figure 1.30.** Schematic structure of one of the hydrogels synthesised by Singaram *et al*, comprising of a derivatised pyranine fluorophore (ATPS-DEGMA: pink) as the fluorescence reporter unit and a cationic BA-viologen compound (blue) as the glucose receptor. The components are immobilised by a single tether to allow for increased mobility within the hydrogel matrix.<sup>177</sup>

A disadvantage to Singaram *et al.*'s results were the long equilibrium times on introducing glucose.<sup>177</sup> The shortest time encountered per addition of glucose was

0.66h and the longest time was 2h.<sup>177</sup> The dimensions of the thin-film gels in this case were 1 cm x 3 cm with a thickness of 0.25 cm. Equilibrium response times could be accelerated by synthesising gels with smaller dimensions or increased pore sizes.<sup>177,</sup>

178

In comparison to the solution based studies,<sup>165</sup> using the pyranine-OH fluorophore and the o-BBV<sup>2+</sup> viologen derivative, the BA-viologen showed improved fluorescence recovery with glucose when immobilised within the hydrogel.<sup>177</sup> The BA-viologen when investigated in solution exhibited a maximum glucose recovery of  $F/F_0 = 1.35$  with the pyranine-OH fluorophore containing three polymerizable groups.<sup>165</sup> Previously, when other similar BA-viologen compounds were investigated for fluorescent glucose detection in solution the fluorescence intensity was much higher in comparison to the hydrogel counterparts. On comparing the fluorescence response of the immobilized pyranine-NH<sub>2</sub> and pyranine-OH fluorophores in the hydrogels, pyranine-NH<sub>2</sub> was tethered by a single chain as opposed to pyranine-OH that was secured by three polymerizable chains. The enhanced mobility of pyranine-NH<sub>2</sub>, in comparison to pyranine-OH, allowed for optimised fluorescence quenching with the BA-viologen compound. Consequently, the fluorescence recovery could also be maximised from  $F/F_0 = 1.18$  for pyranine-OH to  $F/F_0 = 2.8$  for the pyranine-NH<sub>2</sub>, when approximately the same concentration ratios of the fluorophores and BA-viologen were employed.<sup>145, 177</sup>

In 2011, the Singaram group continued using thin-film hydrogels for indirect glucose detection by fluorescence. These gels were polymerised in a multi-well plate and the fluorescence could then be conveniently read using a plate reader, allowing for rapid fluorescence measurements. This approach meant that multiple assays could be analysed in parallel for label-free high throughput assays or bioprocess monitoring applications.<sup>163</sup> The initial quenching interaction between pyranine with varying concentrations of the BA-viologen (0-0.2 mM) was determined by synthesising multiple gels with differing concentrations of the BA-viologen. A maximised decrease in fluorescence of 93% using 8 equivalents of the BA-viologen was established with 0.025 mM pyranine.<sup>163</sup> Glucose recovery was then measured between a glucose concentration range of 0-20 mM, corresponding to blood-glucose levels for a healthy individual,<sup>12</sup> where an optimum recovery of ~32.5% was observed with 0.2 mM BA-viologen and 20 mM glucose.<sup>163</sup> The fluorescence response stabilised after ~30 minutes and remained unchanged for 8h.<sup>163</sup> Overall, Singaram *et al.* developed a

method for the manufacture of glucose-sensitive hydrogels under ambient conditions, where the fluorescence response can be read rapidly using a plate-reader.

In 2011, Feng *et al.*, have also used Singaram's viologen compound (o-BBV<sup>2+</sup>) for two-component sensing, where they employed 1,1'-*bi*-2-naphthol (BINOL) polymer as the water-soluble fluorescent moiety (Figure 1.31).<sup>167</sup> The fluorescence of BINOL was modulated by a decrease in fluorescence with increased concentrations of the BA-viologen.<sup>167</sup> A quenched state of fluorescence occurred due to electron-transfer from the anionic PP-S-BINOL to the cationic BA-viologen. The fluorescence could then be restored with glucose. Anionic sulphates and a polymerisable group were incorporated in to the BINOL fluorophore, so that the fluorophore could be immobilised inside a hydrogel. By assimilating anionic sulphate groups in the fluorophore design, enhanced quenching in the fluorescence of pyranine was observed due to increased electrostatic attraction with the o-BBV<sup>2+</sup> component. These groups also increased the hydrophilicity of the sensor. The extended  $\pi$ -system of BINOL was also desired for  $\pi$ - $\pi$  stacking interactions, which were required for enhanced fluorescence quenching on interacting with the o-BBV<sup>2+</sup> derivative. On increased concentrations of the cationic o-BBV<sup>2+</sup> component to the anionic fluorescent BINOL polymer, a decrease of 97% was observed with 20 equivalents of the o-BBV<sup>2+</sup> component.<sup>167</sup> Approximately, 100 mM (25,000 equivalents) of glucose was then required to restore the fluorescence intensity by 25%.<sup>167</sup> Although this sensing system showed sensitivity towards glucose, the system was in fact more responsive towards other monosaccharides such as fructose > galactose > glucose, in this order.<sup>167</sup>

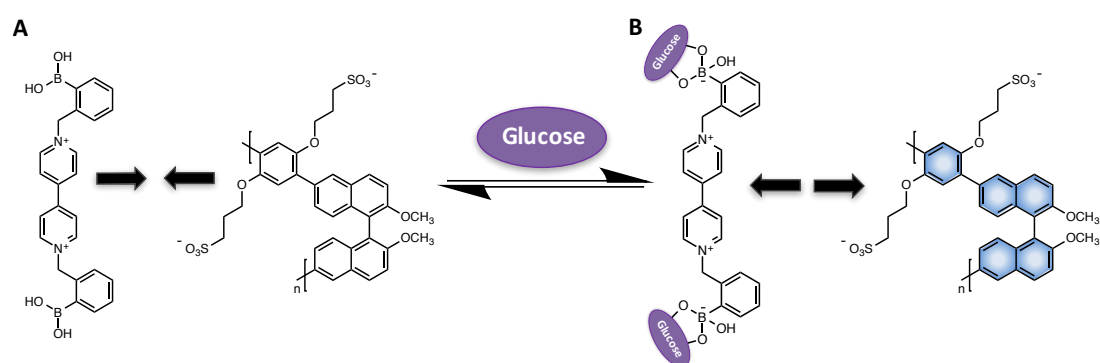


**Figure 1.31.** (A) Formation of BA viologen-BINOL fluorophore complex, which is non-fluorescent. (B) Addition of glucose recovers fluorescence.



## 1.5 Aim

To this end, chemical BA sensors have shown they can be used to monitor glucose concentrations by changes in fluorescence. Two approaches have been described, a direct and an indirect sensing approach. In the direct sensing approach glucose concentrations are accompanied by a quenched state of fluorescence and conversely, in the indirect sensing approach an increase in fluorescence is proportional to increased concentrations of glucose.

In this context, my work, described in the next chapters of this thesis comprises the synthesis and characterisation of novel BA sensors for direct and indirect glucose monitoring.

In Chapter 2, a direct sensing approach is described, built on the work carried out by Badugu and co-workers. In this approach, the BA moiety was directly attached to a fluorescent quinolinium framework, where the fluorescence of these BA-derivatives becomes quenched in the presence of glucose. The BA derivatives were investigated for their direct glucose sensing capabilities in aqueous media of various pH.

In Chapter 3, indirect glucose sensing is realised upon integration of a BA moiety and fluorophore into a two-component system. In this case, the BA moiety is attached to a cationic molecule, which induces quenching in a commercially available anionic fluorophore, namely 7-hydroxycoumarin (7HC). Novel *bis*-BA derivatives have been synthesised that contain cationic pyrimidine nuclei in their structures, which would allow for enhanced electrostatic interactions with 7HC. The BA glucose receptors have shown to cause a quenched state of fluorescence in 7HC, where the fluorescence can be effectively switched-off. This fluorescence can be recovered on introducing glucose.

In Chapter 4, the synthesis of a novel family of polymerisable BA derivatives and their characterisation with glucose is described in terms of  $^{11}\text{B}$  NMR and fluorescence. The monomers differ in the positioning of the BA group, in the *ortho*, *meta* and *para* position (*o*-BA, *m*-BA and *p*-BA). The  $\text{pK}_a$  for each monomer was determined by fluorescence, where this information is imperative for optimising glucose sensing. All monomers displayed dramatic differences in excimer fluorescence with increased concentrations of glucose that can be directly linked to the positioning of the BA group, where *p*-BA showed optimum glucose-sensing capabilities. Moreover, these BA derivatives contain polymerisable handles, which

would allow for these glucose responsive molecules to be covalently polymerised inside a hydrogel matrix.

In Chapter 5, the BA monomers (*o*-BA, *m*-BA and *p*-BA) described in Chapter 4 were investigated for their response towards different monosaccharides, such as glucose, fructose and galactose, in a two-component sensing system. In this indirect sensing approach, the fluorescence of pyranine was monitored. Initially, the optimum fluorescence quenching of pyranine was determined by interchanging the BA monomers. *o*-BA and *m*-BA exhibited the most efficient fluorescence quenching responses and were therefore further investigated for fluorescence recovery measurements with the monosaccharides. Thereafter, this two-component system was studied in a hydrogel matrix and later optimised in Chapter 6.

Finally, in Chapter 6, additional strategies for the integration of a two-component sensing system in to hydrogel matrices were investigated. In Part A, an indirect sensing approach is described, where a two-component sensor is incorporated inside an ionogel matrix. A known fluorophore (fluorescein) is employed, which was immobilised by electrostatic charges within the ionogel matrix. In Part B, monomeric cocktails were screened with pyranine to optimise fluorescence quenching interactions and hence, to maximise fluorescence recovery with monosaccharides. In Part C, linear polymers obtained from the BA monomers described in Chapter 4 are employed in the construction of sugar-sensitive layer-by-layer films.

In this thesis, both direct and indirect sensing approaches are compared for their glucose sensing capabilities, where this project aims to incorporate BA derivatives on to flexible polymeric substrates for continuous non-invasive glucose sensing. Such platforms include sensing patches or smart contact lenses, where the design of the BA sensors would allow for simple integration into wearable devices. Such a device could offer diabetics personal control over monitoring their glucose levels, to aid the prevention of the side effects associated with the disease.

## 1.6 References

1. Honda, M.; Katoka, K.; Seki, T.; Takeoka, Y. Confined Stimuli-Responsive Polymer Gel in Inverse Opal Polymer Membrane for Colorimetric Glucose Sensor. *Langmuir*, **2009**, *25* (14), 8349-8356.
2. Larin, K. V.; Motamedi, M.; Ashitkov, T. V.; Esenaliev, R. O. Specificity of Noninvasive Blood Glucose Sensing using Optical Coherence Tomography Technique: A Pilot Study. *Phys. Med. Biol.*, **2003**, *48*, 1371-1390.
3. Fang, H.; Kaur, G.; Wang, B. Progress in Boronic Acid-Based Fluorescent Glucose Sensors. *J. Fluoresc.*, **2004**, *14* (5), 481-489.
4. American Diabetes Association. Diagnosis and Classification of Diabetes Mellitus. *Diabetes Care*, **2004**, *27* (1), 5-10.
5. Sabokdast, M.; Habibi-Rezaei, M.; Moosavi-Movahedi, A. A.; Ferdousi, M.; Azimzadeh-Irani, E.; Poursasan, N. Protection by Beta-Hydroxybutyric Acid Against Insulin Glycation, Lipid Peroxidation and Microglial Cell Apoptosis. *DARU J. Pharm. Sci.*, **2015**, *23* (42).
6. Wang, X. D.; Zhou, T.-Y.; Chen, X.; Wong, K.-Y.; Wang, X.-R. An Optical Biosensor for the Rapid Determination of Glucose in Human Serum. *Sens. Actuators, B.*, **2008**, *129*, 866-873.
7. Geddes, C. D.; Badugu, R.; Lakowicz, J. R. Quaternary Nitrogen Heterocyclic Compounds for Detecting Aqueous Monosaccharides in Physiological Fluids. **2007**.
8. Torpy, J. M.; Lynn, C.; Glass, R. M. Diabetes. *J. Am. Med. Assoc.*, **2009**, *301* (15), 1620.
9. Li, R.; Zhen, M.; Guan, M.; Chen, D.; Zhang, G.; Ge, J.; Gong, P.; Wang, C.; Shu, C. A Novel Glucose Colorimetric Sensor based on Intrinsic Peroxidase-Like Activity of C<sub>60</sub>-Carboxyfullerenes. *Biosens. Bioelectron.*, **2013**, *47*, 502-507.
10. Bratlie, K. M.; York, R. L.; Invernale, M. A.; Langer, R.; Anderson, D. G. Materials for Diabetes Therapeutics. *Adv. Healthcare Mater.*, **2012**, *1* (3), 267-284.
11. Badugu, R.; Lakowicz, J. R.; Geddes, C. D. Ophthalmic Glucose Sensing: A Novel Monosaccharide Sensing Disposable and Colourless Contact Lens. *Analyst*, **2004**, *129*, 516-521.
12. Badugu, R.; Lakowicz, J. R.; Geddes, C. D. Ophthalmic Glucose Monitoring using Disposable Contact Lenses - a review. *J. Fluoresc.*, **2004**, *14* (5), 617-633.
13. Badugu, R.; Lakowicz, J. R.; Geddes, C. D. Boronic acid Fluorescent Sensors for Monosaccharide Signalling Based on the 6-Methoxyquinolinium Heterocyclic Nucleus: Progress Toward Noninvasive and Continuous Glucose Monitoring. *Bioorg. Med. Chem.*, **2005**, *13*, 113-119.
14. Badugu, R.; Lakowicz, J. R.; Geddes, C. D. Noninvasive Continuous Monitoring of Physiological Glucose using a Monosaccharide-Sensing Contact Lens. *Anal. Chem.*, **2004**, *76*, 610-618.

15. Pickup, J. C.; Hussain, F.; Evans, N. D.; Rolinski, O. J.; Birch, D. J. S. Fluorescence-Based Glucose Sensors. *Biosens. Bioelectron.*, **2005**, *20*, 2555-2565.
16. Ferrante do Amaral C. E.; Wolf, B. Current Development in Non-Invasive Glucose Monitoring. *Med. Eng. Phys.*, **2008**, *30* (5), 541-549.
17. Nwaneri, C. Diabetes Mellitus: A Complete Ancient and Modern Historical Perspective. *WebmedCentral Diabetes*, **2015**, *8* (2), WMC004831.
18. Toghill, K. E.; Compton, R. G. Electrochemical Non-Enzymatic Glucose Sensors: A Perspective and an Evaluation. *Int. J. Electrochem. Sci.*, **2010**, *5*, 1246-1301.
19. Yadava, J.; Rani, A.; Singh, V.; Murari, B. M. Prospects and Limitations of Non-Invasive Blood Glucose Monitoring using Near-Infrared Spectroscopy. *Biomedical Signal Processing and Control*, **2015**, *18*, 214-227.
20. Pandey, R.; Paidi, S. K.; Valdez, T. A.; Zhang, C.; Spegazzini, N.; Dasari R. R.; Barman, I. Noninvasive Monitoring of Blood Glucose with Raman Spectroscopy. *Acc. Chem. Res.*, **2017**, *50*, 264-272.
21. Spegazzini, N.; Barman, I.; Dingari, N. C.; Pandey, R.; Soares, J. S.; Ozaki, Y.; Dasari, R. R. Spectroscopic Approach for Dynamic Bioanalyte Tracking with Minimal Concentration Information. *Sci. Rep.*, **2014**, *4*, Article number: 7013.
22. Corrie, S. R.; Coffey, J. W.; Islam, J.; Markey, K. A.; Kendall, M. A. F. Blood, Sweat, and Tears: Developing Clinically Relevant Protein Biosensors for Integrated Body Fluid Analysis. *Analyst*, **2015**, *140* (13), 4350-4364.
23. Yoo, E.-H.; Lee, S.-Y. Glucose Biosensors: An Overview of Use in Clinical Practice. *Sensors*, **2010**, *10*, 4558-4576.
24. Bandodkar, A. J.; Wang, J. Non-Invasive Wearable Electrochemical Sensors: A Review. *Trends Biotechnol.*, **2014**, *32* (7), 363-371.
25. Coyle, S.; Curto, V. F.; Benito-Lopez, F.; Florea, L.; Diamond, D. Wearable Bio and Chemical Sensors. In *Wearable Sensors*, Elsevier Inc.: **2014**; pp 65-83.
26. Matzeu, G.; Florea, L.; Diamond, D. Advances in Wearable Chemical Sensor Design for Monitoring Biological Fluids. *Sens. Actuators, B.*, **2015**, *21* (1), 403-418.
27. Lakhtakia, R. The History of Diabetes Mellitus. *Medical History*, **2013**, *13* (3), 368-370.
28. Medvei, V. C. The Greco-Roman Period. In *The History of Clinical Endocrinology: A Comprehensive Account of Endocrinology from Earliest Times to Present Day.*, Medvei, V.C., ed.; Parthenon Publishing: New York, USA, **1993**; pp 34-37.
29. Willis, T. *Practice of Physick: Pharmaceutical Rationalis*. T. Dring, C. Harper and J. Leigh: London, United Kingdom., 1684.
30. Eknoyan, G.; Nagy, J. A History of Diabetes Mellitus or How a Disease of the Kidneys Evolved into a Kidney Disease. *Adv. Chronic Kidney Dis.*, **2005**, *12* (2), 223-229.

31. McGrew, R. E. *Encyclopedia of Medical History*. First ed.; McGrew-Hall Book Company: London, United Kingdom, 1985.
32. Barnett, D. M.; Krall, L. P. *The History of Diabetes*. Fourth ed.; A. Wolters Kluwer Company: Massachusetts, USA, 2005.
33. Grmek, M. D. Bernard Claude, *Complete Dictionary of Scientific Biography* [Online], 2017.
34. Tattersall, R. Frederick Pavy (1829-1911) and his Opposition to the Glycogenic Theory of Claude Bernard. *Ann. Sci.*, **1997**, *54* (4), 361-374.
35. Raghupathy, P. Diabetic Ketoacidosis in Children and Adolescents. *Indian J. Endocrinol. Metab.*, **2015**, *19* (1), 55-57.
36. Wang, J. Electrochemical Glucose Biosensors. *Chem. Rev.*, **2008**, *108*, 814-825.
37. Badugu, R.; Lakowicz, J. R.; Geddes, C. D. A Glucose-Sensing Contact Lens: from Bench Top to Patient. *Curr. Opin. Biotechnol.*, **2005**, *16*, 100-107.
38. Makaram, P.; Owens, D.; Aceros, J. Trends in Nanomaterial-Based Non-Invasive Diabetes Sensing Technologies. *Diagnostics*, **2014**, *4*, 27-46.
39. Ezzati, M.; et al. Worldwide Trends in Diabetes Since 1980: A Pooled Analysis of 751 Population-Based Studies with 4.4 Million Participants. *Lancet*, **2016**, *387*, 1513-1530.
40. Barnard, N. D.; Cohen, J.; Jenkins, D. J. A.; Turner-McGrievy, G.; Gloede, L.; Jaster, B.; Seidl, K.; Green, A. A.; Talpers, S. A Low-Fat Vegan Diet Improves Glycemic Control and Cardiovascular Risk Factors in a Randomised Clinical Trial in Individuals with Type 2 Diabetes. *Diabetes Care*, **2006**, *29* (8), 1777-1783.
41. Boulé, N. G.; Haddad, E.; Kenny, G. P.; Wells G. A.; Sigal, R. J. Effects of Exercise on Glycemic Control and Body Mass in Type 2 Diabetes Mellitus. *JAMA*, **2001**, *286* (10), 1218-1227.
42. Gittoes, N. J. L.; Ayuk, J.; Ferner, R. E. *Textbook of Diabetes*. 4th ed.; Blackwell Publishing: 2010.
43. Mathew, T. L.; Pownraj, P.; Abdulla, S.; Pullithadathil, B. Technologies for Clinical Diagnosis Using Expired Human Breath Analysis. *Diagnostics*, **2015**, *5*, 27-60.
44. Yamada, K.; Ohishi, K.; Gilbert, A.; Akasaka, M.; Yoshida, N.; Yoshimura, R. Measurement of Natural Carbon Isotopic Composition of Acetone in Human Urine. *Anal. Bioanal. Chem.*, **2016**, *408*, 1597-1607.
45. Hill, D.; Binions, R. Breath Analysis for Medical Diagnosis. *Int. J. Smart Sens. Intell. Syst.*, **2012**, *5* (2), 401-440.
46. Albisser, A. M.; Leibel, B. S.; Ewart, T. G.; Davidovac, Z.; Botz, C. K.; Zingg, W.; Schipper, H.; Gander, R. Clinical Control of Diabetes by the Artificial Pancreas. *Diabetes*, **1974**, *23*, 397-404.
47. Nishida, K.; Shimoda, S.; Ichinose, K.; Araki, E.; Shichiri, M. What is the Artificial Endocrine Pancreas? Mechanism and History. *World J. Gastroenterol.*, **2009**, *15* (33), 4105-4110.

48. Shichiri, M.; Kawamori, R.; Goriya, Y.; Yamasaki, Y.; Nomura, M; Hakui, N.; Abe, H. Glycaemic Control in Pancreatectomized Dogs with a Wearable Artificial Endocrine Pancreas. *Diabetologia*, **1983**, *24* (3), 179-184.
49. Gale, E. A. M.; Gillespie, K. M. Diabetes and Gender. *Diabetologia*, **2001**, *44*, 3-15.
50. Ramachandran, A.; Ma, R. C. W.; Snehalatha, C. Diabetes in Asia. *Lancet*, **2010**, *375* (9712), 408-418.
51. Badugu, R.; Lakowicz, J. R.; Geddes, C. D. Fluorescence Sensors for Monosaccharides Based on the 6-Methylquinolinium Nucleus and Boronic Acid Moiety: Potential Application to Ophthalmic Diagnostics. *Talanta*, **2005**, *65*, 762-768.
52. Clark Jr., L. C.; Lyons, C. Electrode Systems for Continuous Monitoring in Cardiovascular Surgery. *Ann. N. Y. Acad. Sci.*, **1962**, *102*, 29-45.
53. Price, C. P. Point-of-Care Testing in Diabetes Mellitus. *Clin. Chem. Lab. Med.*, **2003**, *41*, 1213-1219.
54. D'Costa, E. J.; Higgins, I. J.; Turner, A. P. Quinoprotein Glucose Dehydrogenase and its Application in an Amperometric Glucose Sensor. *Biosensors*, **1986**, *2*, 71-87.
55. Heller, A.; Feldman, B. Electrochemical Glucose Sensors and their Applications in Diabetes Management. *Chem. Rev.*, **2008**, *108*, 2482-2505.
56. Bankar, S. B.; Bule, M. V.; Singhal, R. S.; Ananthanarayan, L. Glucose Oxidase - An Overview. *Biotechnol. Adv.*, **2009**, *27*, 489-501.
57. Guilbault, G. G.; Lubrano, G. J. An Enzyme Electrode for the Amperometric Determination of Glucose. *Anal. Chim. Acta.*, **1973**, *64*, 439-455.
58. Magers, T. A.; Tabb, D. L. A Composition and Test Device Based on a Benzidine-Type Indicator for Detecting the Presence of a Constituent in a Test Sample. EP19800106766, 4 November 1983.
59. Wang, J. Glucose Biosensors: 40 Years of Advances and Challenges. *Electroanalysis*, **2001**, *13* (12), 983-988.
60. Clark Jr., L. C. Monitor and Control of Blood and Tissue Oxygen Tensions. *Trans. Am. Soc. Artif. Intern. Organs*, **1956**, *2* (1), 41-48.
61. Hilditch, P.; Green, M. Disposable Electrochemical Biosensors. *Analyst*, **1991**, *116* (12), 1217-1220.
62. Matthews, D.; Holman, R.; Brown, E.; Streemson, J.; Watson, A.; Hughes, S. Pen-Sized Digital 30-Second Blood Glucose Meter. *Lancet*, **1987**, *1* (8536), 778-779.
63. Moreno-Bondi, M. C.; Wolfbeis, O. S. Oxygen Optrode for use in a Fiber-Optic Glucose Biosensor. *Anal. Chem.*, **1990**, *62*, 2377-2380.
64. Nathan, D. M. The Diabetes Control and Complications Trial/Epidemiology of Diabetes Interventions and Complications Study at 30 years: Overview. *Diabetes Care*, **2014**, *37*, 9-16.

65. O'Kelly, S.; Clarke, A. Glucose Monitoring Systems. <http://www.diabetes.ie/living-with-diabetes/educational-articles/diabetes-and-research-articles/continuous-glucose-monitoring-cgm-systems/>.
66. Newman, J.; Turner, A. P. F. Home Blood Glucose Biosensors: A Commercial Perspective. *Biosens. Bioelectron.*, **2005**, *20* (12), 2435-2453.
67. Boiroux, D.; Batora, V.; Hagdrup, M.; Tarnik, M.; Murgas, J.; Schmidt, S.; Norgaard, K.; Poulsen, N. K.; Madsen, H.; Jorgensen, J. B. Comparison of Prediction Models for a Dual-Hormone Artificial Pancreas. *IFAC-PapersOnLine*, **2015**, *48* (20), 7-12.
68. Bindra, D. S.; Zhang, Y.; Wilson, G. S.; Sternberg, R.; Thévenot, D. R.; Moatti, D.; Reach, G. Design and In Vitro Studies of a Needle-Type Glucose Sensor for Subcutaneous Monitoring. *Anal. Chem.*, **1991**, *63* (17), 1692-1696.
69. McGreevy, R. Flash Glucose Monitoring Latest Concept in Testing. *The Irish Times*, October 22 2013, **2013**, p 1.
70. Worsley, G. J.; Tourniaire, G. A.; Medlock, K. E. S.; Sartain, F. K.; Harmer, H. E.; Thatcher, M.; Horgan, A. M.; Pritchard, J. Continuous Blood Glucose Monitoring with a Thin-Film Optical Sensor. *Clin. Chem.*, **2007**, *53* (10), 1820-1826.
71. Fox, L. A.; Beck, R. W.; Xing, D.; Chase, H. P.; Gilliam, L. K.; Hirsch, I.; Kollman, C.; Laffel, L.; Lee, J.; Ruedy, K. J.; Tamberlane, W. V.; Tansey, M.; Wilson, D. M. Variation of Interstitial Glucose Measurements Assessed by Continuous Glucose Monitors in Healthy Nondiabetic Individuals. *Diabetes Care*, **2010**, *33* (6), 1297-1299.
72. Koschinsky T.; Heinemann, L. Sensors for Glucose Monitoring: Technical and Clinical Aspects. *Diabetes/Metab. Res. Rev.*, **2001**, *17* (2), 113-123.
73. Lee, H.; Song, C.; Hong, Y. S.; Kim, M. S.; Cho, H. R.; Kang, T.; Shin, K.; Choi, S. H.; Hyeon, T.; Kim, D. Wearable/Disposable Sweat-Based Glucose Monitoring Device with Multistage Transdermal Drug Delivery Module. *Sci. Adv.*, **2017**, *3*, e1601314.
74. Heikenfeld, J. Non-Invasive Analyte Access and Sensing Through Eccrine Sweat: Challenges and Outlook circa 2016. *Electroanalysis*, **2016**, *28*, 1242-1249.
75. Gupta, S.; Sandhu, V. S.; Bansal, H.; Sharma, D. Comparison of Salivary and Serum Glucose Levels in Diabetic Patients. *J. Diabetes Sci. Technol.*, **2014**, *9* (1), 91-96.
76. Baliga, S.; Muglikar, S.; Kale, R. Salivary pH: A Diagnostic Biomarker. *J. Indian Soc. Periodontol.*, **2013**, *17* (4), 461-465.
77. Jiang, C.; Sun, M.; Wang, Z.; Chen, Z.; Zhao, X.; Yuan, Y.; Li, Y.; Wang, C. A Portable Real-Time Ringdown Breath Acetone Analyser: Toward Potential Diabetic Screening and Management. *Sensors*, **2016**, *16*, 1199.
78. Hunt, J. Exhaled Breath Condensate pH Assays. *Immunol. Allergy Clin. North Am.*, **2007**, *27* (4), 597-605.
79. Vashist, S. K. Non-Invasive Glucose Monitoring Technology in Diabetes Management: A Review. *Anal. Chim. Acta*, **2012**, *750*, 16-77.

80. Jina, A.; Tierney, M. J.; Tamada, J. A.; McGill, S.; Desai, S.; Chua, B.; Chang, A.; Christiansen, M. Design, Development, and Evaluation of a Novel Microneedle Array-Based Continuous Glucose Monitor. *J. Diabetes Sci. Technol.*, **2014**, *8* (3), 483-487.
81. Zhi, Z.; Khan, F.; Pickup, J. C. Multilayer Nanoencapsulation: A Nanomedicine Technology for Diabetes Research and Management. *Diabetes Res. Clin. Pract.*, **2013**, *100*, 162-169.
82. Food and Drug Administration. GlucoWatch for Diabetes. *WHO Drug Information*, **2002**, *16* (3), 1.
83. Huang, X.; Li, S.; Schultz, J. S.; Wang, Q.; Lin, Q. A MEMS Affinity Glucose Sensor using a Biocompatible Glucose-Responsive Polymer. *Sens. Actuators, B.*, **2009**, *140*, 603-609.
84. Rao, G.; Guy, R. H.; Glikfeld, P.; LaCourse, W. R.; Leung, L.; Tamada, J.; Potts, R. O.; Azimi, N. Reverse Iontophoresis: Noninvasive Glucose Monitoring In Vivo in Humans. *Pharm. Res.*, **1995**, *12* (12), 1869-1873.
85. Bagavathiappan, S.; Saravanan, T.; Philip, J.; Jayakumar, T.; Raj, B.; Karunanithi, R.; Panicker, T. M. R.; Korath, M. P.; Jagadeesan, K. Infrared Thermal Imaging for Detection of Peripheral Vascular Disorders. *J. Med. Phys.*, **2009**, *34* (1), 43-47.
86. Oberli, M. A.; Schoellhammer, C. M.; Langer, R.; Blankschtein, D. Ultrasound-Enhanced Transdermal Delivery: Recent Advances and Future Challenges. *Ther. Deliv.*, **2014**, *5* (7), 843-857.
87. Hanashi, T.; Yamazaki, T.; Tsugawa, W.; Ikebukuro, K.; Sode, K. BioRadioTransmitter: A Self-Powered Wireless Glucose-Sensing System. *J. Diabetes Sci. Technol.*, **2011**, *5* (5), 1030-1035.
88. Russell, J. R.; Pishko, M. V.; Gefrides, C. C.; McShane, M. J.; Coté, G. L. A Fluorescence-Based Glucose Biosensor using Concanavalin A and Dextran Encapsulated in a Poly(ethylene glycol) Hydrogel. *Anal Chem.*, **1999**, *71* (15), 3126-3132.
89. Henderson, T. A.; Morries, L. D. Near-Infrared Photonic Energy Penetration: Can Infrared Phototherapy Effectively Reach the Human Brain? *Neuropsychiatry. Dis. Treat.*, **2015**, *11*, 2191-2208.
90. Zhang, W.; Du, Y.; Wang, M. L. On-Chip Highly Sensitive Saliva Glucose Sensing using Multilayer Films Composed of Single-Walled Carbon Nanotubes, Gold Nanoparticles, and Glucose Oxidase. *Sensing and Bio-Sensing Research*, **2015**, *4*, 96-102.
91. Yao, H.; Shum, A. J.; Cowan, M.; Lahdesmaki, I.; Parvis, B. A. A Contact Lens with Embedded Sensor for Monitoring Tear Glucose Level. *Biosensors and Bioelectronics*, **2011**, *26*, 3290-3296.
92. Glenon, T.; O'Quigley, C.; McCaul, M.; Matzeu, G.; Beirne, S.; Wallace, G. G.; Stroiescu, F.; O'Mahoney, N.; White, P.; Diamond, D. SWEATCH: A Wearable Platform for Harvesting and Analysing Sweat Sodium Content. *Electroanalysis*, **2016**, *28*, 1-8.



93. Heikenfeld, J. Technological Leap for Sweat Sensing. *Nature*, **2016**, 529, 475-476.
94. Heikenfeld, J. Let Them See You Sweat: Your Sweat May Bring Medical Diagnostics to Fitbits and Fuelbands. *IEEE Spectrum* November 2014, **2014**, pp 46-63.
95. Morris, D.; Coyle, S.; Wu, Y.; Lau, K. T.; Wallace, G.; Diamond, D. Bio-Sensing Textile based Patch with Integrated Optical Detection System for Sweat Monitoring. *Sens. Actuators, B.*, **2009**, 139, 231-236.
96. Mitsubayashi, K.; Suzuki, M.; Tamiya, E.; Karube, I. Analysis of Metabolites in Sweat as a Measure of Physical Condition. *Anal. Chim. Acta*, **1994**, 289 (1), 27-34.
97. Sempionatto, J. R.; Nakagawa, T.; Pavinatto, A.; Mensah, S. T.; Imani, S.; Mercier, P.; Wang, J. Eyeglasses Based Wireless Electrolyte and Metabolite Sensor Platform. *Lab on a Chip*, **2017**, 17, 1834-1842.
98. Bhandodkar, A. J.; You, J.-M.; Kim, N.-H.; Gu, Y.; Kumar, R.; Mohan, A. M. V.; Kurniawan, J.; Imani, S.; Nakagawa, T.; Parish, B.; Parthasarathy, M.; Mercier, P. P.; Xu, S.; Wang, J. Soft, Stretchable, High Power Density Electronic Skin-Based Biofuel Cells for Scavenging Energy from Human Sweat. *Energy Environ. Sci.*, **2017**, 10, 1581-1589.
99. Abellán-Llobregat, A.; Jeerapan, I.; Bhandodkar, A.; Vidal, L.; Canals, A.; Wang, J.; Morallón, E. A Stretchable and Screen-Printed Electrochemical Sensor for Glucose Determination in Human Perspiration. *Biosens. Bioelectron.*, **2017**, 91, 885-891.
100. Gao, W.; Emaminejad, S.; Nyein, H. Y. Y.; Challa, S.; Chen, K.; Peck, A.; Fahad, H. M.; Ota, H.; Shiraki, H.; Kiriya, D.; Lein, D.-H.; Brooks, G. A.; Davis, R. W.; Javey, A. Fully Integrated Wearable Sensor Arrays for Multiplexed In Situ Perspiration Analysis. *Nature*, **2016**, 529 (7587), 509-514.
101. Huang, X.; Liu, Y.; Chen, K.; Shin, W.-J.; Lu, C.-J.; Kong, G.-W.; Patnaik, D.; Lee, S.-H.; Cortes, J. F.; Rogers, J. A. Stretchable, Wireless Sensors and Functional Substrates for Epidermal Characterization of Sweat. *small*, **2014**, 10 (15), 3083-3090.
102. Jang, K.-I.; Jung, H. N.; Lee, J. W.; Xu, S.; Liu, Y. H.; Ma, Y.; Jeong, J.-W.; Song, Y. M.; Kim, J.; Kim, B. H.; Banks, A.; Kwak, J. W.; Yang, Y.; Shi, D.; Wei, Z.; Feng, X.; Paik, U.; Huang, Y.; Ghaffari, R.; Rogers, J. A. Ferromagnetic, Folded Electrode Composite as a Soft Interface to the Skin for Long-Term Electrophysiological Recording. *Adv. Funct. Mater.*, **2016**, 26, 7281-7290.
103. Rosenfeld, J. V.; Harvey, A. S.; Wrennall, J.; Zacharin, M.; Berkovic, S. F. Transcallosal Resection of Hypothalamic Hamartomas, with Control of Seizures, in Children with Gelastic Epilepsy. *Neurosurgery*, **2001**, 48 (1), 108-118.
104. Cram, J. R.; Steger, J. C. EMG Scanning in the Diagnosis of Chronic Pain. *Biofeedback and Self-regulation*, **1983**, 8 (2), 229-241.

105. Parkey, R. W.; Bonte, F. J.; Meyer, S. L.; Atkins, J. M.; Curry, J. L.; Stokely, E. M.; Willerson, J. T. A New Method for Radionuclide Imaging of Acute Myocardial Infarction in Humans. *Circulation*, **1974**, *50* (3), 540-546.
106. Staman, J. A.; Fitzgerald, C. R.; Dawson, W. W.; Barris, M. C.; Hood, C. I. The EOG and Choroidal Malignant Melanomas. *Doc. Ophthalmol.*, **1980**, *49* (2), 201-209.
107. Fishberg, E. H.; Beirman, W. Acid-Base Balance in Sweat. *J. Biol. Chem.*, **1932**, *97*, 433-441.
108. Wilson, A. D. Advances in Electronic-Nose Technologies for the Detection of Volatile Biomarker Metabolites in the Human Breath. *Metabolites*, **2015**, *5*, 140-163.
109. Xing, R.; Xu, L.; Song, J.; Zhou, C.; Li, Q.; Liu, D.; Song, H. W. Preparation and Gas Sensing Properties of In<sub>2</sub>O<sub>3</sub>/Au Nanorods for Detection of Volatile Organic Compounds in Exhaled Breath. *Sci. Rep.*, **2015**, *5*, 10717.
110. Shafiek, H.; Fiorentino, F.; Merino, J. L.; Lopez, C.; Oliver, A.; Segura, J.; de Paul, I.; Sibila, O.; Agusti, A.; Cosio, B. G. Using the Electronic Nose to Identify Airway Infection During COPD Exacerbations. *PLoS One*, **2015**, *10* (9), e0135199.
111. Pavlou, A.; Turner, A. P.; Magan, N. Recognition of Anaerobic Bacterial Isolates In Vitro using Electronic Nose Technology. *Lett. Appl. Microbiol.*, **2002**, *35* (5), 366-369.
112. Pavlou, A. K.; Magan, N.; Jones, J. M.; Brown, J.; Klatser, P.; Turner, A. P. Detection of Mycobacterium Tuberculosis (TB) In Vitro and In Situ using an Electronic Nose in Combination with a Neural Network System. *Biosens. Bioelectron.*, **2004**, *20* (3), 538-544.
113. Di Natale, C.; Macagnano, A.; Davide, F.; D'Amico, A.; Paolesse, R.; Boschi, T.; Faccio, M.; Ferri, G. An Electronic Nose for Food Analysis. *Sens. Actuators, B.*, **1997**, *44* (1-3), 521-526.
114. Xu, S.; Zhou, Z.; Li, K.; Jamir, S. M.; Luo, X. Recognition of the Duration and Prediction of Insect Prevalence of Stored Rough Rice Infested by the Red Flour Beetle (*Tribolium Castaneum Herbst*) using an Electronic Nose. *Sensors (Basel)*, **2017**, *17* (4), 688-696.
115. Bikov, A.; Hernadi, M.; Korosi, B. Z.; Kunos, L.; Zsamboki, G.; Sutto, Z.; Tarnoki, A. D.; Tarnoki, D. L.; Losonczy, G.; Horvath, I. Expiratory Flow Rate, Breath Hold and Anatomic Dead Space Influence Electronic Nose Ability to Detect Lung Cancer. *BMC Pulm. Med.*, **2014**, *14*, 202-211.
116. Plaza, V.; Crespo, A.; Giner, J.; Merino, J. L.; Ramos-Barbon, D.; Mateus, E. F.; Torrego, A.; Cosio, B. G.; Agusti, A.; Sibila, O. Inflammatory Asthma Phenotype Discrimination using an Electronic Nose Breath Analyzer. *J. Investig. Allergol. Clin. Immunol.*, **2015**, *25* (6), 431-437.
117. Chen-Kaminsky, S.; Nakhleh, M.; Perros, F.; Montani, D.; Girerd, B.; Garcia, G.; Simonneau, G.; Haick, H.; Humbert, M. A Proof of Concept for the Detection and Classification of Pulmonary Arterial Hypertension Through Breath Analysis with a Sensor Array. *Am. J. Respir. Crit. Care Med.*, **2013**, *188* (6), 756-759.

118. Liu, C.; Sheng, Y.; Sun, Y.; Feng, J.; Wang, S.; Zhang, J.; Xu, J.; Jiang, D. A Glucose Oxidase-Coupled DNAzyme Sensor for Glucose Detection in Tears and Saliva. *Biosens. Bioelectron.*, **2015**, *70*, 455-461.
119. Kim, J.; Valdes-Ramirez, G.; Bhandodkar, A. J.; Jia, W.; A. G.; Ramirez, J.; Mercier, P.; Wang, J. Non-Invasive Mouthguard Biosensor for Continuous Salivary Monitoring of Metabolites. *Analyst*, **2013**, *139*, 1632-1636.
120. Mannoor, M. S.; Tao, H.; Clayton, J. D.; A.; Kaplan, D. L.; Naik, R. R.; Verma, N.; Omenetto, F. G.; McAlpine, M. C. Graphene-Based Wireless Bacteria Detection on Tooth Enamel. *Nat. Commun.*, **2012**, *3* (763), 1-8.
121. Thomas, N.; Lahdesmaki, I.; Parvis, B. A. A Contact Lens with an Integrated Lactate Sensor. *Sens Actuators, B.*, **2012**, *162*, 128-134.
122. King, L. Google Smart Contact Lens Focuses on Healthcare Billions. *ForbesLife*, 15 July 2014, 2014.
123. Senior, M. Novartis Signs up for Google Smart Lens. *Nat. Biotechnol.*, **2014**, *32* (9), 856.
124. Scott, M. Novartis Joins with Google to Develop Contact Lens that Monitors Blood Sugar. *The New York Times* 15 July 2014, **2014**.
125. Tsukayama, H. Google's Smart Contact Lens: What it Does and How it Works. *The Washington Post* 17 January 2014, **2014**.
126. Kleinman, J. Google's Smart Contact Lenses Move One Step Closer to Launch. <https://www.technobuffalo.com/2014/07/15/google-smart-contact-lens/>. (accessed 15 July 2014).
127. Watt, B. E.; Proudfoot, A. T.; Vale, J. A. Hydrogen Peroxide Poisoning. *Toxicol. Rev.*, **2004**, *23* (1), 51-57.
128. Reid, R. C.; Minter, S. D.; Gale, B. K. Contact Lens Biofuel Cells Tested in a Synthetic Tear Solution. *Biosens. Bioelectron.*, **2015**, *68*, 142-148.
129. Lardinois, F. Google Unveils Smart Contact Lens That Lets Diabetics Measure Their Glucose Levels. *Techcrunch*, 16 January 2014.
130. Vincent, J. Google Contact Lenses: Tech Giant Licenses Smart Contact Lens Technology to Help Diabetics and Glasses Wearers. *The Independent*, 15 July 2014.
131. Iguchi, S.; Kudo, H.; Saito, T.; Ogawa, M.; Satio, H.; Otsuka, K.; Funakubo, A.; Mitsubayashi, K. A Flexible and Wearable Biosensor for Tear Glucose Measurement. *Biomed. Microdevices*, **2007**, *9*, 603-609.
132. Kagie, A.; Bishop, D. K.; Burdick, J.; La Belle, J. T.; Dymond, R.; Felder, R.; Wang, J. Flexible Rolled Thick-Film Miniaturized Flow-Cell For Minimally Invasive Amperometric Sensing. *Electroanalysis*, **2008**, *20* (14), 1610-1614.
133. Badugu, R.; Lakowicz, J. R.; Geddes, C. D. Wavelength-Ratiometric and Colorimetric Probes for Glucose Determination. *Dyes Pigm.*, **2006**, *68*, 159-163.
134. Badugu, R.; Lakowicz, J. R.; Geddes, C. D. A Glucose Sensing Contact Lens: A Non-Invasive Technique for Continuous Physiological Glucose Monitoring. *J. Fluoresc.*, **2003**, *13* (5), 371-374.

135. Jeong, J. W.; Arnob, M. P.; Baek, K.-M.; Lee, S. Y.; Shih, W.-C.; Jung, Y. S. 3D Cross-Point Plasmonic Nanoarchitectures Containing Dense and Regular Hot Spots for Surface-Enhanced Raman Spectroscopy Analysis. *Adv. Mater.*, **2016**, *28*, 8695-8704.
136. Moser, T.; Celma, C.; Lebert, A.; Charrault, E.; Brooke, R.; Murphy, P. J.; Browne, G.; Young, R.; Higgs, T.; Evans, D. Hydrophilic Organic Electrode on Flexible Hydrogels. *ACS Appl. Mater. Interfaces*, **2016**, *8*, 974-982.
137. Kell, M. Making Magic: The Smart Contact Lens. <https://www.mivision.com.au/making-magic-the-smart-contact-lens/>.
138. Lakowicz, J. R. *Principles of Fluorescence Spectroscopy*. 3rd Edition ed.; Springer Science and Business Media: **2006**; p 1-923.
139. Shimizu, Y.; T., Azumi, T. Mechanism of External Heavy Atom Effect on Intersystem Crossing in Fluid Solutions. Analysis Based on Fluorescence Decay Data. *J. Phys. Chem.*, **1982**, *86* (1), 22-26.
140. Koziar, J. C.; Cowan, D. O., Photochemical Heavy-Atom Effects. *Acc. Chem. Res.*, **1978**, *11* (9), 334-341.
141. de Silva, A. P.; Moody, T. S.; Wright, G. W. Fluorescent PET (Photoinduced Electron Transfer) Sensors as Potent Analytical Tools. *Analyst*, **2009**, *134*, 2385-2393.
142. Daly, B.; Ling, J.; de Silva, A. P. Current Developments in Fluorescent PET (Photoinduced Electron Transfer) Sensors and Switches. *Chem. Soc. Rev.*, **2015**, *44*, 4203-4211.
143. Kubo, K. *PET Sensors*. Plenum Press: New York, USA, **2005**; Vol. 9.
144. Hansen, J. S.; Christensen, J. B.; Petersen, J. F.; Hoeg-Jensen, T.; Norrild, J. C. Arylboronic Acids: A Diabetic Eye on Glucose Sensing. *Sens. Actuators, B.*, **2012**, *161*, 45-79.
145. Suri, J. T.; Cordes, D. B.; Cappuccio, F. E.; Wessling, R. A.; Singaram, B. Continuous Glucose Sensing with a Fluorescent Thin-Film Hydrogel. *Angew. Chem., Int. Ed.*, **2003**, *42*, 5857-5859.
146. Pappin, B.; Kiefel, M. J.; Houston, T. A. Boron-Carbohydrate Interactions. In *Carbohydrates - Comprehensive Studies on Glycobiology and Glycotechnology*, Chang, Chuan-Fa, Ed. Creative Commons Attribution: InTech, **2012**; pp 37-54.
147. Sun, X.; Zhai, W.; Fossey, J. S.; James, T. D. Boronic Acids for Fluorescence Imaging of Carbohydrates. *Chem. Commun.*, **2016**, *52*, 3456-3469.
148. Arimori, S.; Bell, M. L.; Oh, C. S.; James, T. D. A Modular Fluorescence Intramolecular Energy Transfer Saccharide Sensor. *Org. Lett.*, **2002**, *4* (24), 4249-4259.
149. Hansen, J. S.; Ficker, M.; Peterson, J. F.; Christensen, J. B.; Hoeg-Jensen, T. *Ortho*-Substituted Fluorescent Aryl Monoboronic Acid Displays Physiological Binding of D-Glucose. *Tetrahedron Lett.*, **2013**, *54*, 1849-1852.
150. Sun, X.; James, T. D. Glucose Sensing in Supramolecular Chemistry, *Chem. Rev.*, **2015**, *115*, 8001-8037.

151. Zhang, X. T.; Wang, S.; Xing, G. W. Aggregates-Based Boronlectins with Pyrene as Fluorophore: Multichannel Discriminative Sensing of Monosaccharides and Their Applications. *ACS Appl. Mater. Interfaces.*, **2016**, *8* (19), 12007-12017.
152. Yoon, J.; Czarnik, A. W. Fluorescent Chemosensors of Carbohydrates. A Means of Chemically Communicating the Building of Polyols in Water Based on Chelation-Enhanced Quenching. *J. Am. Chem. Soc.*, **1992**, *114*, 5874-5875.
153. Wu, X.; Li, Z.; Chen, X.-X.; Fossey, J. S.; James, T. D.; Jiang, Y.-B. Selective Sensing of Saccharides using Simple Boronic Acids and Their Aggregates. *Chem. Soc. Rev.*, **2013**, *42*, 8032-8048.
154. Hall, D. G. Structure, properties, and preparation of boronic acid derivatives. Overview of their reactions and applications, in *Boronic acids*, Vol. 2 (Eds: D. G. Hall), Wiley-VCH, Weinheim, **2005**, pp. 1-100.
155. Zhai, W.; Sun, X.; James, T. D.; Fossey, J. S. Boronic Acid-Based Carbohydrate Sensing. *Chem. Asian J.*, **2015**, *10*, 1836-1848.
156. Chapin, B. M.; Metola, P.; Lynch, V. M.; Stanton, J. F.; James, T. D.; Anslyn, E. V. Structural and Thermodynamic Analysis of a Three-Component Assembly Forming *Ortho*-Iminophenylboronate Esters. *J. Org. Chem.*, **2016**, *81*, 8319-8330.
157. James, T. D.; Samankumara Sandanayake, K. R. A.; Shinkai, S. Novel Saccharide-Photoinduced Electron Transfer Sensors Based on the Interaction of Boronic Acid and Amine. *J. Am. Chem. Soc.*, **1995**, *117* (35), 8982-8987.
158. Sun, X.; James, T. D.; Anslyn, E. V. Arresting "Loose Bolt" internal conversion from -B(OH)<sub>2</sub> groups is the mechanism for emission turn-on in *ortho*-aminomethylphenylboronic acid-based saccharide sensors, *J. Am. Chem. Soc.*, **2018**, *140*, 2348-2354.
159. Wulff, G. Selective Binding to Polymers via Covalent Bonds - The Construction of Chiral Cavities as Specific Receptor-Sites. *Pure. Appl. Chem.*, **1982**, *54*, 2093-2102.
160. Kowada, T.; Maeda, H.; Kikuchi, K. BODIPY-Based Probes for the Fluorescence Imaging of Biomolecules in Living Cells. *Chem. Soc. Rev.*, **2015**, *44*, 4953-4972.
161. Hansen, J. S.; Peterson, J. F.; Hoeg-Jensen, T.; Christensen, J. B. Buffer and Sugar Concentration Dependent Fluorescence Response of a BODIPY-Based Aryl Monoboronic Acid Sensor. *Tetrahedron Lett.*, **2012**, *53*, 5852-5855.
162. Zhai, J.; Pan, T.; Zhu, J.; Xu, Y.; Chen, J.; Xie, Y.; Qin, Y. Boronic Acid Functionalised Boron Dipyrromethane Fluorescent Probes: Preparation, Characterisation and Saccharide Sensing Applications. *Anal. Chem.*, **2012**, *84*, 10214-10220.
163. Vilozny, B.; Schiller, A.; Wessling, R. A.; Singaram, B. Multiwell Plates Loaded with Fluorescent Hydrogel Sensors for Measuring pH and Glucose Concentration. *J. Mater. Chem.*, **2011**, *21*, 7589-7595.

164. Li, Y.; Zhang, L.; Haung, J.; Liang, R.; Qiu, J. Fluorescent Graphene Quantum Dots with a Boronic Acid Appended Bipyridinium Salt to Sense Monosaccharides in Aqueous Solution. *Chem. Commun.*, **2013**, *49*, 5180-5182.
165. Cappuccio, F. E.; Suri, J. T.; Cordes, D. B.; Wessling, R. A.; Singaram, B. Evaluation of Pyranine Derivatives in Boronic Acid Based Saccharide Sensing: Significance of Charge Interaction Between Dye and Quencher in Solution and Hydrogel. *J. Fluoresc.*, **2004**, *14* (5), 521-533.
166. Suri, J. T.; Cordes, D. B.; Cappuccio, F. E.; Wessling, R. A.; Singaram, B. Monosaccharide Detection with 4,7-Phenanthroline Salts: Charge-Induced Fluorescence Sensing. *Langmuir*, **2003**, *19*, 5145-5152.
167. Feng, L.; Liang, F.; Wang, Y.; Xu, M.; Wang, X. A Highly Sensitive Water-Soluble System to Sense Glucose in Aqueous Solution. *Org. Biomol. Chem.*, **2011**, *9*, 2938-2942.
168. Camara, J. N.; Suri, J. T.; Cappuccio, F. E.; Wessling, R. A.; Singaram, B. Boronic Acid Substituted Viologen Based Optical Sugar Sensors: Modulated Quenching with Viologen as a Method for Monosaccharide Detection. *Tetrahedron Lett.*, **2002**, *43*, 1139-1141.
169. Sharrett, Z.; Gamsey, S.; Fat, J.; Cunningham-Bryant, D.; Wessling, R. A.; Singaram, B. The Effect of Boronic Acid Acidity on Performance of Viologen-Based Boronic Acids in a Two-Component Optical Glucose-Sensing System. *Tetrahedron Lett.*, **2007**, *48*, 5125-5129.
170. Feng, L.; Yin, N.; Wang, X.; Wang, Z. Fluorescence Probe for Monosaccharide Based Anionic Polyelectrolyte and Cationic Pyridine Quaternary Ammonium Salt. *Sens. Actuators, B*, **2013**, *181*, 730-734.
171. Karnati, V. V.; Gao, X.; Gao, S.; Yang, W.; Ni, W.; Sankar, S.; Wang, B. A Glucose-Selective Fluorescence Sensor Based on Boronic Acid-Diol Recognition. *Bioorg. Med. Chem. Letters*, **2002**, *12*, 3373-3377.
172. Axthelm, J.; Görles, H.; Schubert, U. S.; Schiller, A. Fluorinated Boronic Acid-Appended Bipyridinium Salts for Diol Recognition and Discrimination via <sup>19</sup>F NMR barcodes. *J. Am. Chem. Soc.*, **2015**, *137*, 15402-15405.
173. Larkin, J. D.; Fossey, J. S.; James, T. D.; Brooks, B. R.; Bock, C. W. A Computational Investigation of the Nitrogen-Boron Interaction in *o*-(*N,N*-Dialkylaminomethyl)arylboronate Systems. *J. Phys. Chem. A.*, **2010**, *114* (47), 12531-12539.
174. Lee, H.; Choi, T. K.; Lee, Y. B.; Cho, H. R.; Ghaffari, R.; Wang, L.; Choi, H. J.; Chung, T. D.; Lu, N.; Hyeon, T.; Choi, S. H.; Kim, D. A Graphene-Based Electrochemical Device with Thermoresponsive Microneedles for Diabetes Monitoring and Therapy. *Nat. Nanotechnol.*, **2016**, *11* (6), 566-572.
175. Shen, J.; Zhu, Y.; Yang, X.; Li, C. Graphene Quantum Dots: Emergent Nanolights for Bioimaging, Sensors, Catalysis and Photovoltaic Devices. *Chem. Commun. (Camb)*. **2012**, *48* (31), 3686-3699.
176. Dinis-Oliveira, R. J.; Duarte, J. A.; Sanchez-Navarro, A.; Remiao, F.; Bastos, M. L.; Carvalho, F. Paraquat Poisonings: Mechanisms of Lung Toxicity, Clinical Features, and Treatment. *Crit. Rev. Toxicol.*, **2008**, *38* (1), 13-71.

177. Sharrett, Z.; Gamsey, S.; Hirayama, L.; Viložny, B.; Suri, J. T.; Wessling, R. A.; Singaram, B. Exploring the Use of APTS as a Fluorescent Reporter Dye for Continuous Glucose Sensing. *Org. Biomol. Chem.*, **2009**, 7, 1461-1470.
178. Ziółkowski, B.; Florea, L.; Theobald, J.; Benito-Lopez, F.; Diamond, D. Porous Self-Protonating Spiropyran-Based NIPAAm Gels with Improved Reswelling Kinetics. *J. Mater. Sci.*, **2016**, 51 (3), 1392-1399.

## **Chapter 2**

---

### **Direct Glucose Sensing: Probing Interactions Between Glucose and Fluorescent Boronic Acids**

---



## Contents

### Chapter 2: Direct Glucose Sensing: Probing Interactions Between Glucose and Fluorescent Boronic Acids

<b>2.1 Abstract</b>	<b>85</b>
<b>2.2 Introduction</b>	<b>86</b>
<b>2.3 Experimental</b>	<b>88</b>
2.3.1 Materials and Methods	88
2.3.2 General Procedure for the Synthesis of Carboxylic Acid-BA sensors	89
2.3.3 Synthesis of 1-(2-boronobenzyl)-5-carboxyquinolin-1-ium bromide ( <i>o</i> -COOHBA)	90
2.3.4 Synthesis of 1-(3-boronobenzyl)-5-carboxyquinolin-1-ium bromide ( <i>m</i> -COOHBA)	91
2.3.5 Immobilisation of <i>o</i> -COOHBA on to a PDMS ‘Lens’-Like Polymeric Platform	92
<b>2.4 Results and Discussion</b>	<b>93</b>
2.4.1 Glucose Sensing Mechanism	93
2.4.2 Determining the Sensing Range of <i>o</i> -COOHBA and <i>m</i> -COOHBA	94
2.4.3 Fluorescence Glucose-Sensing Using <i>o</i> -COOHBA and <i>m</i> -COOHBA	96
2.4.4 Immobilisation of <i>o</i> -COOHBA on to a PDMS ‘Lens-Like’ Platform and Fluorescence Response to Glucose	98
<b>2.5 Conclusions</b>	<b>100</b>
<b>2.6 Future Work</b>	<b>101</b>
<b>2.6 References</b>	<b>103</b>

## 2.1 Abstract

Diabetes is an incurable disease known to have severe acute and chronic side effects, namely blindness, heart disease or kidney failure, among others. While monitoring the disease marker glucose in blood prolongs life expectancy, non-invasive continuous monitoring systems currently aren't available. The blood-glucose range for a healthy person is ~3-8 mM, increasing to up to 40 mM for people with diabetes, where the related glucose levels in the ocular fluid are approximately ten times smaller, between 0.05-0.5 mM increasing to up to 5 mM for diabetics. Consequently, there is considerable interest in using ocular fluid as a sample medium for tracking the disease marker.

Herein, boronic acid (BA) sugar sensors have been investigated for their ability to sense glucose in solution and when immobilised on to a polymeric polydimethylsiloxane (PDMS) 'lens'-like platform. The Lewis acidic BA moiety of the sensor is known for its strong interaction with diols. On interaction with glucose, the anionic boronate form is produced leading to a decrease in the fluorescence intensity of the BA sensor with increasing sugar concentrations. In this chapter, the synthesis and fluorescence studies of novel BA derivatives, *o*-COOHBA and *m*-COOHBA, for fluorescence sugar sensing are presented. These BA sensors have been synthesised via a one-step nucleophilic substitution reaction, where each sensor has a carboxylic acid group incorporated (-COOH). This COOH functionality would allow for these BA derivatives to be anchored on to flexible polymeric surfaces. The newly synthesised BA sensors were compared in terms of their fluorescence, sensitivity to glucose and their optimal pH sensing range. The sensors have proven efficient for glucose sensing in the relevant physiological range of blood and ocular fluid.

## 2.2 Introduction

In recent years the development of glucose sensors for diabetes has been an important focus of the medical device community, as stringent control of glucose levels can significantly minimize the risk of severe side effects and mortality.<sup>1-3</sup> Several approaches exist for glucose monitoring, based primarily on electrochemical enzymatic sensing.<sup>1, 2</sup> Although at present enzymatic glucose sensors remain commercially unchallenged, they are not readily available for non-invasive wearable technology integration.

Boronic acids (BAs) however have been acknowledged for their glucose sensing capabilities.<sup>4</sup> As a result of their Lewis acidic properties, they form strong but reversible interactions with diol-containing compounds, such as glucose.<sup>1</sup> Due to the  $pK_a$  of the BA and the sugar bound form, being  $\sim 9$  and  $\sim 6$  respectively, glucose detection is possible between a pH range of pH 6-9, which is well suited for physiological applications.<sup>5</sup>

Integration of BA moieties in to fluorescent frameworks, allows for BA-sugar binding interactions to be monitored by fluorescence.<sup>6</sup> James *et al.*, Badugu *et al.* and others, have published numerous articles in this area.<sup>1-23</sup> In the work of Badugu and co-workers, intramolecular charge transfer mechanisms account for a quenched state of fluorescence on increased glucose binding to the BA receptor.<sup>1,2,5</sup> They employed cationic quinolinium fluorophores with a phenylBA substituent attached through a methyl-linker. As glucose binds to the BA receptor, the BA moiety is transformed to the anionic boronate form. Consequently, the negative charge on  $B^-$  can interact with the positive  $N^+$  atom in the quinoline ring to quench the fluorescence.<sup>1,2,5</sup>

Badugu *et al.*<sup>5</sup> and March *et al.*<sup>24</sup> have previously introduced the idea of integrating chemosensors within a contact lens sensing platform. Conveniently a contact lens would allow for painless non-invasive continuous sensing since the lens would be in constant contact with the ocular fluid. When paired with ICT-technologies, optical changes in this functionalised lens captured by the smartphone integrated camera, would allow for personalised monitoring with the use of a mobile phone application (Figure 2.1). Moreover, since eye-damage and blindness are side effects of diabetes, this smart lens could also act as a form of corrective vision.<sup>5, 14, 25</sup>

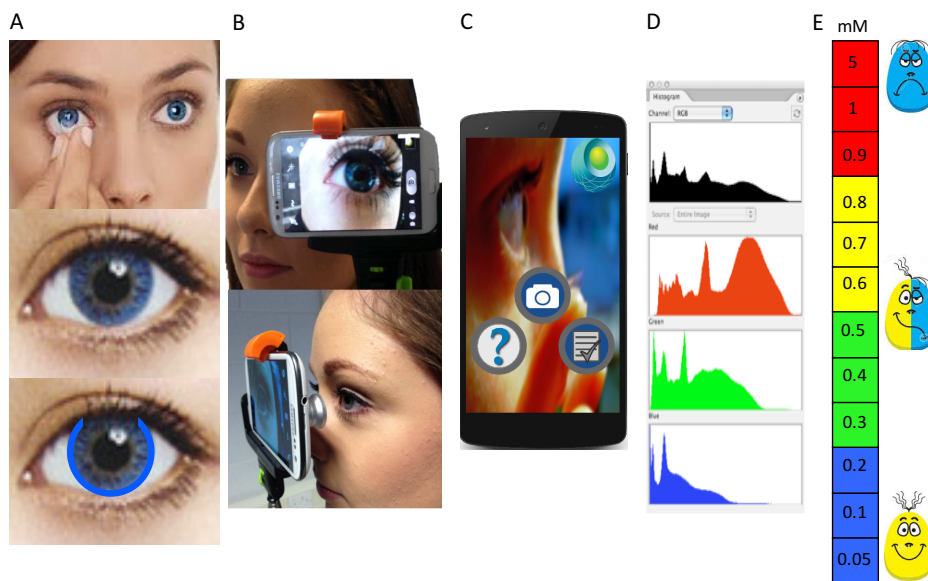


**Figure 2.1.** (A) Concept of a smart-contact lens, functionalised with BA sensor. (B) Mobile device is used to capture image of smart-lens while in eye. (C) Non-invasive and continuous glucose-sensing contact lens is coupled to an ICT application. (D) The application evaluates and maps an optical response in the lens to a specific glucose concentration. (E) Specific glucose concentrations can provide an indication of hypo- or hyperglycaemic levels in diabetic patients, allowing them to personally monitor their condition.

In this chapter, two novel BA probes have been synthesised and their response towards glucose characterised when in solution and when adsorbed to a ‘lens’-like material. The probe design is based on that of Badugu *et al.* which implements a quinoline fluorophore attached to a phenylBA ring.<sup>1, 2, 5, 14-16, 18</sup> The two novel sensors differ in the orientation of the BA group in the *ortho* and *meta* positions. Conversely, carboxylic acid substituents were employed in the 5-position on the quinoline ring, in contrast to the methyl- or methoxy-substituents in the 6-position employed by Badugu *et al.* The inclusion of the  $-\text{COOH}$  group allows for these BA-probes to be covalently immobilised on to a flexible polymeric platform, such as a hydrogel contact lens or sensing patch. The BA derivatives have shown to respond to glucose between a concentration range of 0-50 mM, corresponding to the reported ocular glucose levels (0.05-5 mM) and the blood glucose levels (2-40 mM) in diabetic patients. The BA sensors were also investigated in aqueous media of varying pH, confirming that the sensing range of the BA derivatives lies between pH 6-9, between the  $\text{pK}_a$  of the BA and sugar bound form. The aim of this research is to create a non-invasive continuous monitoring device for diabetics. By immobilizing a BA sensor on to a polymeric

platform it is possible to design wearable and conformable sensing devices for use as smart-contact lenses or sensing-patches.

## 2.3 Experimental

### 2.3.1 Materials and Methods

All reagents were purchased from Fluorochem UK or Sigma Aldrich Ireland and used as received. The polydimethylsiloxane (PDMS) elastomer (Sylgard 184) was purchased from Dow Corning. Solvents used were methanol (CH<sub>3</sub>OH), anhydrous acetonitrile (CH<sub>3</sub>CN) and anhydrous dimethylformamide (DMF). All reactions were conducted under an inert atmosphere of nitrogen.

pH measurements were carried out on a VWR sympHony SP70P pH meter. Structural <sup>1</sup>H, <sup>13</sup>C and <sup>11</sup>B NMR spectra were recorded on a Bruker Avance Ultrashield 600 MHz spectrometer or a Bruker Avance 400 MHz spectrometer, using deuterium oxide (D<sub>2</sub>O), deuterated methanol (*d*<sub>4</sub>-CH<sub>3</sub>OH) or deuterated dimethylformamide (*d*<sub>7</sub>-DMF) as solvents. <sup>11</sup>B NMR experiments used BF<sub>3</sub> in *d*<sub>4</sub>-CH<sub>3</sub>OH as an external standard. All reactions were monitored by thin layer chromatography (TLC) that used basic silica plates and CH<sub>3</sub>OH:CH<sub>2</sub>Cl<sub>2</sub> (5:95) as the mobile phase. High Resolution Mass spectrometry (HRMS) analysis was carried out on an electrospray ionisation (ESI) mass spectrometer in deionised (DI) water or CH<sub>3</sub>OH. All fluorescence measurements in solution and doped PDMS-‘lenses’ were carried out on a JASCO Spectrofluorometer FP-8300 in pH buffer solutions.

A range of buffers were prepared for solvents in spectroscopic analysis, where the buffer compositions can be found in Table 2.1. Acetate salts were used for acidic pH buffers (< pH 6), neutral buffers were prepared from phosphate and hydroxide salts (pH 6-8) and carbonate and hydroxide salts were required for basic pH buffers (> pH 8). All buffers were made up to 200 mL using deionised water.

**Table 2.1.** Buffer compositions for 200 mL of required pH buffer.

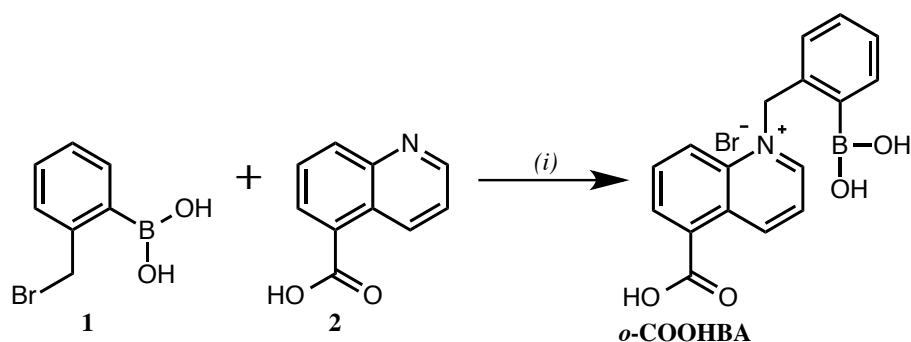
<b>Acetate Buffers</b>	CH <sub>3</sub> COOH 0.2 M (mL)	CH <sub>3</sub> COONa 0.2 M (mL)	DI H <sub>2</sub> O (mL)
pH 5.3	17.6	82.4	100
<b>Phosphate Buffers</b>	KH <sub>2</sub> PO <sub>4</sub> 0.1 M (mL)	NaOH 0.1 M (mL)	DI H <sub>2</sub> O (mL)
pH 6.3	100	19.4	80.6
pH 7.4	100	78.2	21.8
pH 8.12	100	93.4	6.6
<b>Carbonate Buffer</b>	Na <sub>2</sub> CO <sub>3</sub> 0.2 M (mL)	NaHCO <sub>3</sub> 0.2 M (mL)	DI H <sub>2</sub> O (mL)
pH 8.88	4	46	150
<b>Carbonate Buffer</b>	NaOH 0.1 M (mL)	NaHCO <sub>3</sub> 0.05 M (mL)	DI H <sub>2</sub> O (mL)
pH 11.12	45.4	100	54.6

### 2.3.2 General Procedure for the Synthesis of Carboxylic Acid-BA sensors

The carboxylic acid-BA sensors, *o*-COOHBA and *m*-COOHBA, were synthesised by a one-step nucleophilic substitution reaction, as depicted in Scheme 2.1 and 2.2, respectively. The phenylBA component was dissolved in anhydrous DMF and allowed to reflux before the addition of quinoline-5-carboxylic acid dropwise over ~30 minutes. On addition of quinoline-5-carboxylic acid, a colour change occurred from pale yellow to dark yellow to orange, where the final colour of the reaction was dark red. The reaction was left for 4 days and was monitored by TLC using basic silica TLC plates as the stationary phase and CH<sub>3</sub>OH: CH<sub>2</sub>Cl<sub>2</sub> (5:95) as the mobile phase. An iodine chamber was used to aid visualisation of the spots on the TLC plate.

Solubility tests were carried out on quinoline-5-carboxylic acid, where this material dissolved in most solvents in a large volume to solid ratio when vigorously heated; H<sub>2</sub>O, CH<sub>3</sub>OH, tetrahydrofuran (THF), CH<sub>3</sub>CN, DMF and toluene (tol.). Quinoline-5-carboxylic acid was found to be insoluble in CH<sub>2</sub>Cl<sub>2</sub> and diethyl ether.

### 2.3.3 Synthesis of 1-(2-boronobenzyl)-5-carboxyquinolin-1-ium bromide (*o*-COOHBA)



**Scheme 2.1.** Synthesis of novel BA sensor (*o*-COOHBA). (i) Anhydrous DMF, N<sub>2</sub>, 80 °C for 4 days.

*o*-[2-(Bromomethyl)phenylboronic acid] (compound **1**; 0.9926 g, 4.62 mmol, 1.8 eq.) was dissolved in anhydrous DMF (1 mL). Quinoline-5-carboxylic acid (compound **2**; 0.4596 g, 2.54 mmol, 1 eq.) was dissolved in anhydrous DMF and was added dropwise to compound **1** via a syringe, while refluxing over ~30 minutes. On addition of compound **2**, the reaction changed colour from pale yellow to a dark yellow and after an hour the reaction appeared orange. It was determined that the reaction reached completion once the mixture appeared a rosewood red colour. The reaction was refluxed at 80 °C for 4 days and kept under an atmosphere of N<sub>2</sub>.

The reaction mixture was dried under reduced pressure and column chromatography was performed using silica as the stationary phase and CH<sub>3</sub>OH:CH<sub>2</sub>Cl<sub>2</sub> (5:95) as the mobile phase. The product eluted last having the lowest R<sub>f</sub> value of 0.1. The fractions containing *o*-COOHBA were combined and concentrated under a reduced pressure before drying. *o*-COOHBA was collected in a 4% yield as a white/beige powder and its structure was confirmed by NMR. <sup>1</sup>H NMR spectrum (600 MHz, 20 °C, D<sub>2</sub>O) δ: 10.5 (1H, *d*, *J* = 7 Hz, CH – j), 9.5 (1H, *s*, CH – h), 8.5-8.6 (2H, *m*, CH – c, a), 8.1-8.2 (2H, *m*, CH – i, b), 7.6 (2H, *d*, *J* = 53 Hz, CH – e, f), 7.3 (2H, *s*, CH – d, g), 6.3 (2H, *s*, CH<sub>2</sub>) ppm (Figure 2.2). <sup>13</sup>C NMR (150 MHz, 20 °C, CD<sub>3</sub>OD, DEPT) δ: CH 123.9, 129.7, 130.2, 132.6, 133.4, 134.1, 135.8, 139.9, 147.8, 150.8, COOH 168.1, CH<sub>2</sub> 62.9 ppm. <sup>11</sup>B NMR (192 MHz, 20 °C, CD<sub>3</sub>OD) δ: B(OH)<sub>2</sub> 27.3 ppm. HRMS (ESI-MS, D<sub>2</sub>O) calculated for [C<sub>18</sub>H<sub>17</sub>BNO<sub>4</sub>]<sup>+</sup> (Figure 2.3), *m/z*, 322.1245, found 322.1290. FT-IR spectrum for *o*-COOHBA showed peaks at 3365.19

(C-OH), 2979.67, 2774.0 (B-OH, C=C-H), 1711.68 (C=O), 1607.95 (C=C)  $\text{cm}^{-1}$ .<sup>26</sup> UV-visible spectroscopy found an absorbance peak at 320 nm. Excitation wavelength was found at 380 nm with a corresponding fluorescence emission wavelength at 485 nm. For raw spectral data and supplementary information see Appendix A.

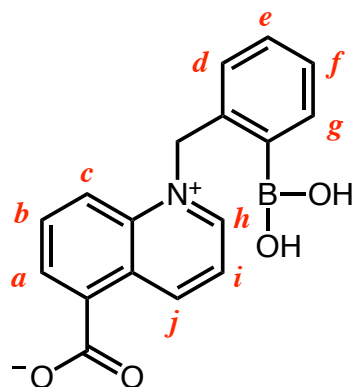


**Figure 2.2.**  $^1\text{H}$  NMR assignment for *o*-COOHBA.

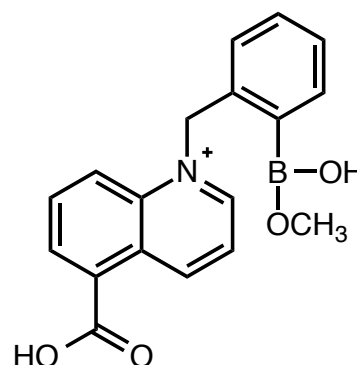
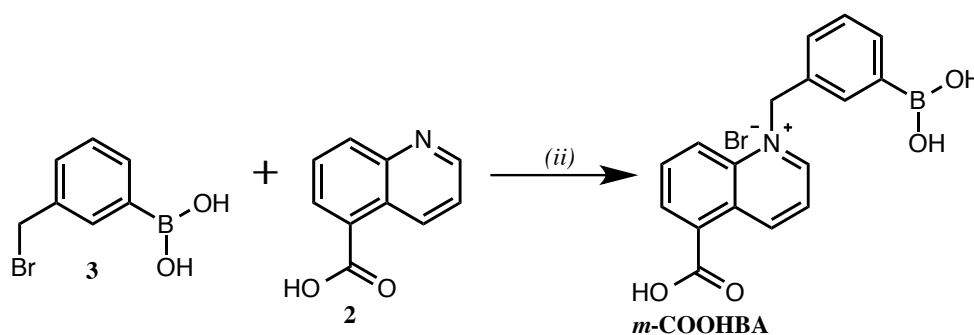


**Figure 2.3.** Structure of *o*-COOHBA found from mass spectrometry analysis,  $[\text{C}_{18}\text{H}_{17}\text{BNO}_4]^+$ .

### 2.3.4 Synthesis of 1-(3-boronobenzyl)-5-carboxyquinolin-1-ium bromide (*m*-COOHBA)



**Scheme 2.2.** Synthesis of novel BA sensor (*m*-COOHBA). (ii) Anhydrous DMF,  $\text{N}_2$ , 66  $^\circ\text{C}$  for 4 days (61%).

*m*-[3-(Bromomethyl)phenylboronic acid] (compound **3**; 0.2 g; 0.9 mmol, 1 eq.) was weighed in a glove box under  $\text{N}_2$  and dissolved in anhydrous DMF (~2 mL). Compound **3** was stirred under nitrogen and heated to 80  $^\circ\text{C}$ . The solution appeared colourless. Compound **2** (0.165 g; 0.95 mmol) was dissolved in anhydrous DMF (~30 mL) and the reaction was heated vigorously. Compound **2** dissolved after ~3h and appeared as a pale-yellow solution. Compound **2** was added sequentially via a pressure-equalised dropping funnel to compound **1**. The reaction appeared as a pale-



yellow solution, which evolved to a dark red colour on reaction completion. The reaction was left to reflux under N<sub>2</sub> at 66 °C overnight.

Compound **2** precipitated from the reaction and was filtered. The reaction mixture was then dried under reduced pressure and DI H<sub>2</sub>O was added to dissolve the desired product. Compound **2** possessed a very low solubility in water as determined from previous solubility tests. The mixture was filtered to yield compound **2** as a precipitate. The water filtrate was concentrated and dried under reduced pressure to yield *m*-COOHBA as a white/beige powder in a 61% yield. <sup>1</sup>H NMR (400 MHz, 20 °C, D<sub>2</sub>O), δ: 9.6 (1H, *d*, *J* = 9 Hz, CH – *j*), 9.2 (1H, *d*, *J* = 5 Hz, CH – *h*), 8.2 (1H, *d*, *J* = 9 Hz, CH – *i*), 7.8 (1H, *dd*, *J* = 3, 9 and 15 Hz, CH – *c*), 7.7 (1H, *d*, *J* = 7 Hz, CH – *a*), 7.6 (1H, *dd*, *J* = 1, 9 and 16 Hz, CH – *f*), 7.3 (1H, *d*, *J* = 7 Hz, CH – *d*), 7.3 (1H, *s*, CH – *b*), 7.1 (1H, *d*, *J* = 8 Hz, CH – *e*), 7.1–7.0 (1H, *m*, CH – *g*), 5.9 (2H, *s*, CH<sub>2</sub>) ppm (Figure 2.4). <sup>13</sup>C NMR (100 MHz, 20 °C, D<sub>2</sub>O), δ: CH 121.8, 122.7, 127.1, 128.4, 128.9, 129.3, 129.4, 131.8, 132.1, 132.3, 134.6, 135.0, 138.3, 146.8, 149.5, CH<sub>2</sub> 31.1, 34.5, 61.8, COOH 163.6, 164.3, 169.2 ppm. FT-IR spectrum for *m*-COOHBA showed peaks at 3248.49 (C-OH), 2921.71, 2851.57 (B-OH), 2372.06, 2152.91 (C=C-H), 1658.91 (C=O), 1469.53 (C=C) cm<sup>-1</sup>.<sup>26</sup> UV-visible spectroscopy found an absorbance peak at 320 nm. Excitation wavelength was found at 390 nm with a corresponding fluorescence emission wavelength at 465 nm. For raw spectral data and supplementary information see Appendix A.

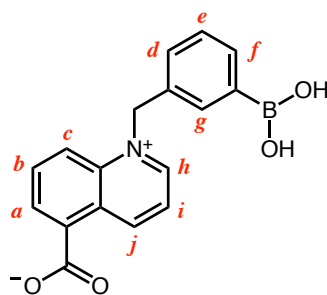
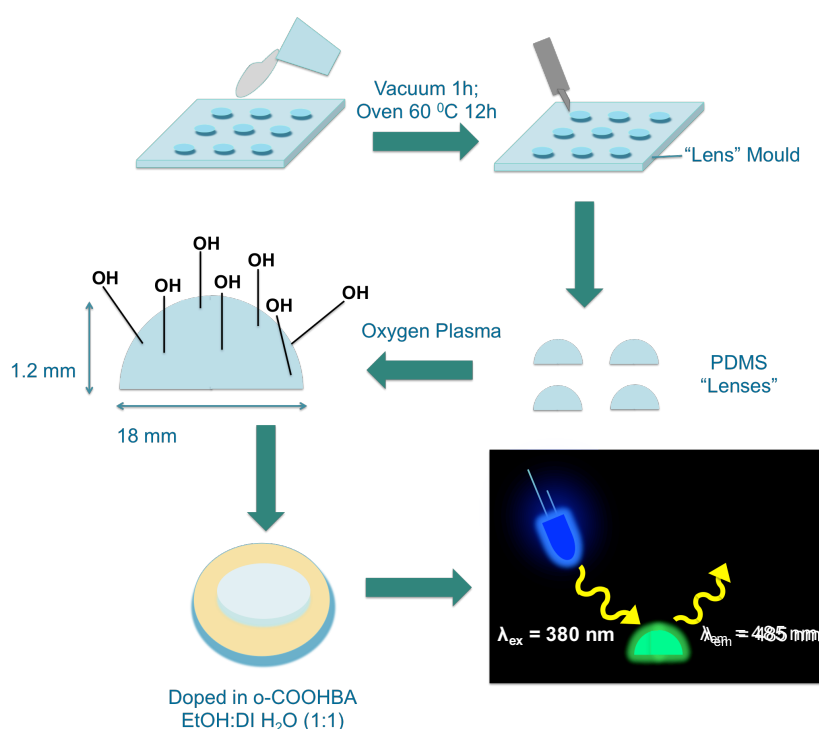


**Figure 2.4.** <sup>1</sup>H NMR assignment for *m*-COOHBA.

### 2.3.5 Immobilisation of *o*-COOHBA on to a PDMS ‘Lens’-Like Polymeric Platform

A PDMS-‘lens’ was fabricated as illustrated in Scheme 2.3. For producing this ‘lens’-like structure, PDMS elastomer (Sylgard 184) was mixed with a curing agent (10:1) and poured in to the desired ‘lens’ mould and cured at 60 °C for 12h. After this

time, the ‘lenses’ were removed from the mould. Oxygen plasma was then performed on the PDMS ‘lenses’ to cleanse the hydrogel and populate hydroxyl groups on its outer surface, which were required for adsorbing *o*-COOHBA. Immediately after performing oxygen plasma, the ‘lenses’ were immersed in a solution of *o*-COOHBA (30 mM) dissolved in ethanol and DI water (1:1). Ethanol was used to allow for increased diffusion of the BA sensing compound through the PDMS polymer structure. The doped ‘lenses’ were then air dried and their fluorescence was recorded using fluorometer. Alternatively, a light-emitting diode (LED) source could be used to excite the fluorescent “lens-like” platform (Scheme 2.3).



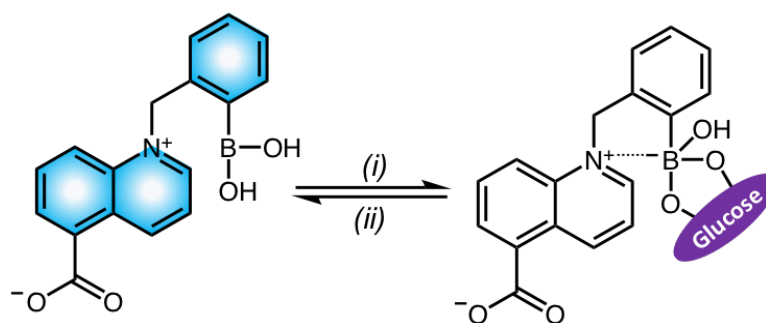
**Scheme 2.3.** Fabrication steps taken for producing a doped PDMS ‘lens’ with *o*-COOHBA.

## 2.4 Results and Discussion

### 2.4.1 Glucose Sensing Mechanism

The equilibrium of BA groups binding sugars is quite complex. The BA group is trigonal planar when neutral, however in basic pH solutions, the BA moiety is transformed to the anionic boronate form, which has a tetrahedral geometry.<sup>5</sup> As previously mentioned, BA derivatives can sense glucose within a pH range of pH 6-9, due to the  $pK_a$  of the BA and sugar bound form. On formation of the boronate-sugar complex, a conformational change around boron is induced. Sugar binding to the BA

group is preferential when the BA moiety exists in its anionic form. Since the  $pK_a$  of the BA group is  $\sim 9$ , using BA derivatives for glucose sensing in solutions close to physiological pH can be unfavourable. To overcome this challenge, electron-withdrawing groups can be incorporated in to the structure of BA derivatives to lower the  $pK_a$  of the BA group and enhance sugar binding in solutions of pH 7.4.<sup>22</sup> In this context, a positively charged  $N^+$  atom was included in the quinoline fluorophore, which possesses electron-withdrawing properties.<sup>12</sup> From the literature, this is known to reduce the  $pK_a$  of the BA sensors to  $< 7$ .<sup>14</sup> When glucose binds, the BA group is typically tetrahedral and anionic. Primarily as depicted in Scheme 2.4, the *ortho* positioning of the BA group to the  $N^+$  moiety is optimal for interaction with the cationic fluorescent component of the molecule, for an intramolecular charge-transfer interaction.<sup>5</sup> This  $B^-N^+$  interaction is known to neutralise the anionic charge on boron and also stabilise sugar binding.<sup>3</sup> Consequently, this fluorescence quenching is induced in the fluorescent-BA sensor on sugar binding, known as a charge neutralisation-stabilisation interaction (Scheme 2.4).<sup>1, 14</sup> As a result, glucose concentrations can be monitored by fluorescence quenching in the BA sensors. Since the tetrahedral form of boron can be induced in basic solutions, quenching can also be achieved by increasing the pH of the solution above the  $pK_a$  of the BA derivative.



**Scheme 2.4.** Charge neutralisation-stabilisation interaction on glucose binding to the fluorescent *o*-COOHBA sensor, forming the non-fluorescent boronate-sugar complex. (i) Addition of glucose. (ii) Removal of glucose or addition of acid.

#### 2.4.2 Determining the Sensing Range of *o*-COOHBA and *m*-COOHBA

The pH sensing range of BA sensors has been defined between pH 6-9, due to the  $pK_a$  of the BA group and sugar-bound form.<sup>5</sup> By investigating the fluorescence response of *o*-COOHBA and *m*-COOHBA towards glucose in solutions of varying pH, their sensing range can be determined. Consequently, when this interaction was

monitored in pH solutions of less than pH 6 and higher than pH 9, fluorescence quenching was not observed. As expected, in both COOHBA sensors, in pH solutions of  $\text{pH} < 6$  ( $\text{pH} 5.3$ ), corresponding to the  $\text{pK}_a$  of  $\sim 6$  for the sugar-bound BA form, the fluorescence intensity remained stable as the concentration of glucose was increased (Figure 2.5). Similarly, in pH solutions greater than pH 9 ( $\text{pH} 11.8$ ), corresponding to the  $\text{pK}_a \sim 9$  for the BA form, increasing glucose concentrations showed to have no effect on the fluorescence of the COOHBA derivatives. As expected, only within the defined sensing range of pH 6-9 (*e.g.* pH 7.4), a decrease in the fluorescence intensity was observed with increased concentrations of glucose (Figure 2.5). This demonstrates that sensing in solutions close to physiological pH is possible, highlighting that both COOHBA sensors could be implemented for biological sensing applications.

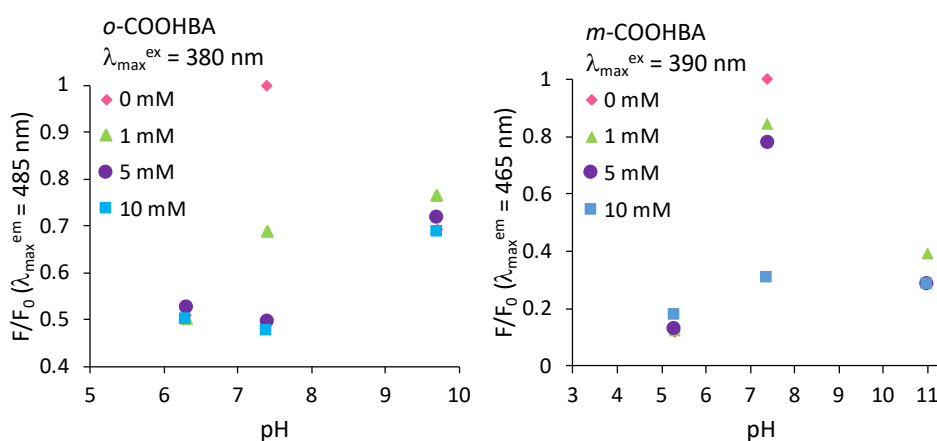


**Figure 2.5.** Glucose sensing using both *o*-COOHBA and *m*-COOHBA in various pH buffer solutions ranging between pH 5.3-11.8. Left: Fluorescence glucose-sensing using *o*-COOHBA (0.5 mM) with 10 mM glucose. Right: Fluorescence glucose-sensing employing *m*-COOHBA with 10 mM glucose, where  $F_0$  is the maximum fluorescence of the COOHBA derivatives in pH 7.4 buffer solution and  $F$  is the measured fluorescence of the COOHBA derivatives in all other solutions.

It was also notable that the fluorescence of *o*-COOHBA was greater outside of the sensing range in comparison to *m*-COOHBA. In pH solutions  $< 6$ , the  $F/F_0$  values for *o*-COOHBA and *m*-COOHBA were  $\sim 0.5$  and  $\sim 0.1$ , respectively and similarly, in pH solutions  $> 9$ , the  $F/F_0$  values were  $\sim 0.7$  and  $\sim 0.3$  respectively. The higher  $F/F_0$  for *o*-COOHBA suggest that the orientation of the BA group in the 2-position enables an optimal geometry for  $\text{B}^-\text{N}^+$  interaction to stabilise glucose binding. On forming this interaction, the conjugated  $\pi$ -system in the BA derivatives structure can be elongated to exhibit enhanced fluorescence in comparison to *m*-COOHBA, where the BA group

is slightly hindered for a maximised interaction. In this *meta* orientation, solvent molecules are required to bridge the spacial gap between B<sup>-</sup> and N<sup>+</sup> to permit this interaction.<sup>3, 22</sup> However, although optimised fluorescence quenching was expected with *o*-COOHBA, *m*-COOHBA exhibited the enhanced response possibly owed to steric hindrance effects on glucose binding. Fluorescence in both COOHBA derivatives however, is quickly quenched due to the intramolecular charge transfer fluorescence quenching mechanism.

Further observations denote that the fluorescence was higher in basic solutions in comparison to acidic pH solution. This result can be explained based on the high pK<sub>a</sub> of the BA moiety (~8-9).<sup>3, 22</sup> For this reason, BA derivatives bind diol-containing compounds in alkaline aqueous media more favourably than in acidic or neutral solutions.<sup>9</sup> This can be related to the tetrahedral conformation of the boronate moiety in basic solutions, which allows for sugars to bind rapidly. Recently, this has been an area of great interest, where many research groups have attempted to synthesise BA derivatives with a lower pK<sub>a</sub>.<sup>11</sup> Research has shown that by including EWGs into the BA-sensor structure, the BA derivative can become more receptive to glucose in neutral solutions.<sup>21</sup> This approach aims to optimise glucose-sensing using BA derivatives for physiological applications.

#### 2.4.3 Fluorescence Glucose-Sensing Using *o*-COOHBA and *m*-COOHBA

*o*-COOHBA and *m*-COOHBA have been investigated for their glucose sensing capabilities in solutions of pH 7.4, close to physiological pH. As glucose binds to the BA receptor, glucose concentrations can be measured by changes in fluorescence. An intramolecular charge transfer quenching mechanism induces a decrease in the fluorescence intensity as the glucose concentrations increase. The excitation of these sensors was just outside the visible range of the electromagnetic spectrum, where the excitation wavelength for *o*-COOHBA was 380 nm and the corresponding emission wavelength was 485 nm (Figure 2.6A). Similarly, for *m*-COOHBA the excitation wavelength was 390 nm and the emission wavelength was 465 nm (Figure 2.6B). Both of these sensors exhibit a large Stokes shift between the excitation and emission wavelength, which is desired for sensing applications. Moreover, since the excitation wavelengths are in the blue-UV region, low cost, readily available blue LEDs could be easily integrated as an excitation source into a sensing platform for the COOHBA sensors.

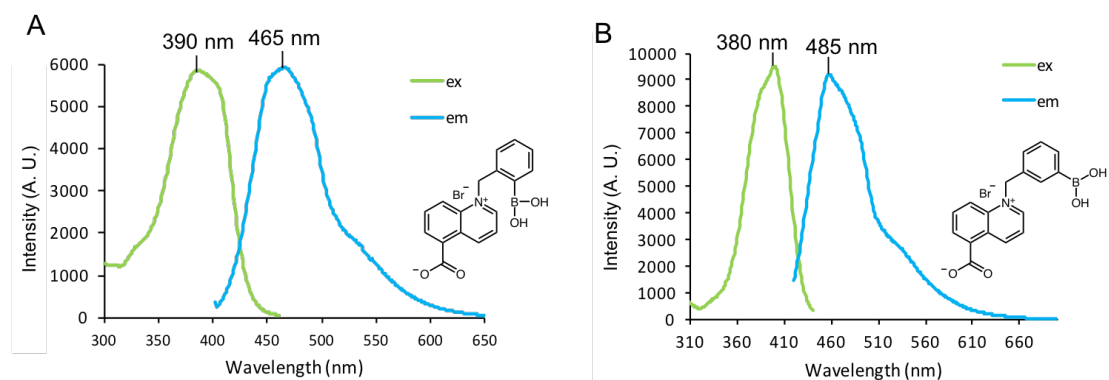


**Figure 2.6.** (A) Excitation (green) and emission (blue) fluorescence spectra for *o*-COOHBA, where the excitation wavelength is 380 nm and the corresponding emission wavelength is 485 nm. (B) Excitation (green) and emission (blue) fluorescence spectra for *m*-COOHBA, where the excitation wavelength is 390 nm and the corresponding emission wavelength is 465 nm.

*o*-COOHBA and *m*-COOHBA have shown that they are responsive to glucose within the clinically accepted physiological range for diabetic sugar concentrations. The blood-glucose range for a healthy individual is ~3-8 mM, varying greatly in people suffering with diabetes in a range of 2-40 mM.<sup>5, 21</sup> From Figure 2.7, a quenched state of fluorescence in *o*-COOHBA can be seen by 40% when 50 mM glucose is introduced. In the case of *m*-COOHBA (Figure 2.7A), the fluorescence is essentially switched-off as a decrease in fluorescence by 78% is observed in the presence of 50 mM glucose (Figure 2.7B). Moreover, these COOHBA sensors are particularly susceptible to the lower concentrations of glucose between 0-10 mM, where this is important for monitoring hypoglycaemic states. Monitoring these low glucose concentrations is particularly important in intensive care units in hospitals and also for detecting glucose in alternative physiological fluids, such as ocular fluid, where the glucose concentrations are approximately ten times smaller than the blood glucose levels (0.05-5 mM in diabetic patients).<sup>5, 27</sup> Since the emission wavelengths for the sensors are in the visible region of the electromagnetic spectrum, quenching by increased concentrations of glucose was visible by eye under a bench-top UV lamp. The BA derivatives were also designed to contain a carboxylic acid anchoring group, so that these sensors could be immobilised on to a flexible polymeric support, which would allow for efficient integration in to a device. Under these conditions, the sensors could be readily fabricated into a sensing platform for non-invasive and continuous glucose detection in alternative physiological fluids such as ocular fluid or sweat.

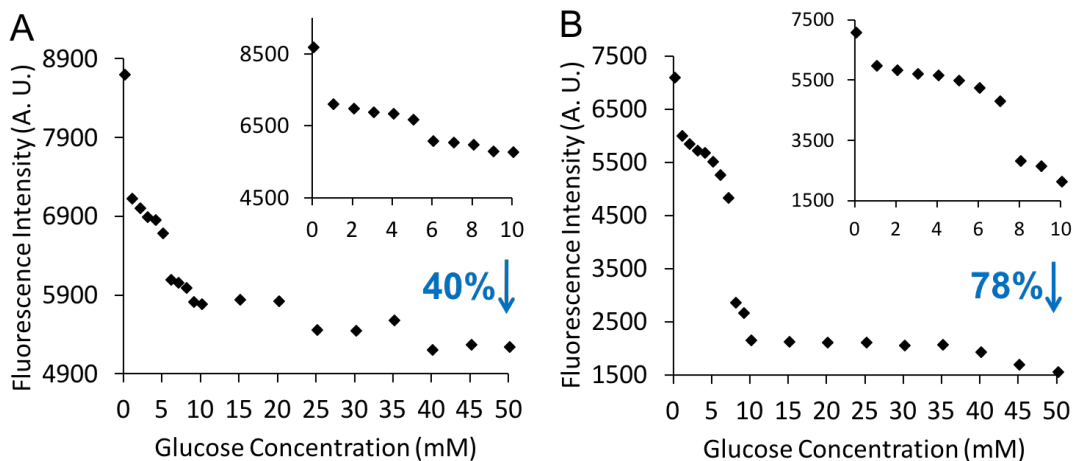
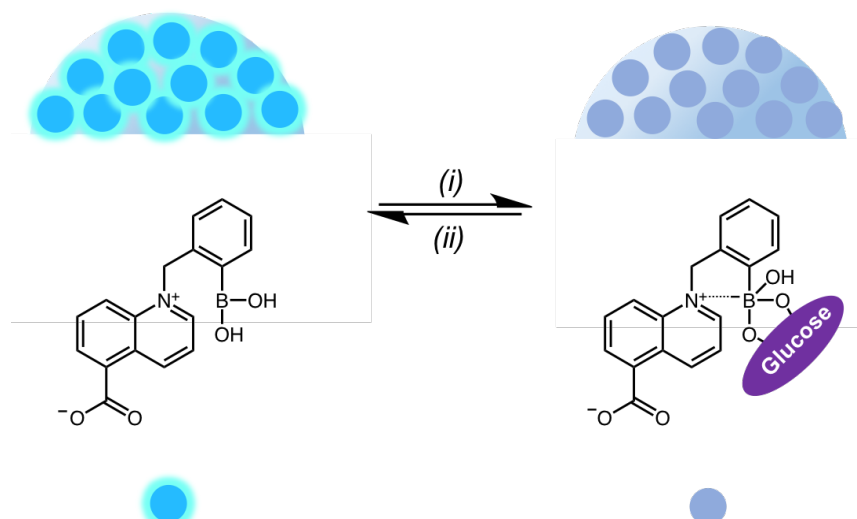


**Figure 2.7.** (A) Fluorescence quenching of *o*-COOHBA (0.5 mM) on sequential additions of glucose (0-50 mM) in pH 7.4 phosphate buffer solution. A decrease in fluorescence intensity by 40% was observed at the emission wavelength 485 nm in the presence of 50 mM glucose. The excitation wavelength was 380 nm. (B) Fluorescence quenching of *m*-COOHBA (0.5 mM) on sequential additions of glucose (0-50 mM) in pH 7.4 phosphate buffer solution. A decrease in fluorescence intensity by 78% was observed at the emission wavelength 460 nm in the presence of 50 mM glucose. The excitation wavelength was 390 nm. The insets for each graph show the COOHBA sensor response to glucose between the concentration range of 0-10 mM.

#### 2.4.4 Immobilisation of *o*-COOHBA on to a PDMS ‘Lens-Like’ Platform and Fluorescence Response to Glucose

*o*-COOHBA was chosen for immobilisation on to a PDMS ‘lens’-like polymeric platform since this material had a higher fluorescence intensity in comparison to *m*-COOHBA. A PDMS ‘lens’-like platform was fabricated as illustrated in Scheme 2.3 (Section 2.3.5). Upon *o*-COOHBA (30 mM) doping in DI water and ethanol (1:1), the ‘lens’ was fluorescent, due to the presence of the BA group in its neutral trigonal planar form.



**Scheme 2.5.** Doped PDMS ‘lens’ with *o*-COOHBA. The ‘lens’ is fluorescent due to the presence of neutral BA group. When the ‘lens’ is then immersed in a solution containing glucose, the ‘lens’ becomes non-fluorescent due to the conformational change in boron to the anionic boronate form producing the boronate-glucose complex. (i) Addition of glucose (ii) Removal of glucose or addition of acid.

On immersion of this ‘lens’ in solutions containing glucose, the fluorescence of the ‘lens’ became quenched (Scheme 2.5). The fluorescence of the ‘lens’ was initially measured using a fluorimeter in a pH 7.4 buffer solution and then recorded when the ‘lens’ was immersed in glucose solutions (0-5 mM) in the same buffer. The PDMS ‘lens’ was placed on a glass slide at a 30° angle inside the quartz cuvette and the fluorescence was recorded while the PDMS material was hydrated in solution. Concentrations of glucose were increased in increments of 1 mM and fluorescence measurements were recorded after each addition. When the ‘lens’ was placed in the solution containing 5 mM glucose, the fluorescence was practically switched off (Figure 2.8). The highest concentration of glucose employed was 5 mM glucose, since this concentration range can be correlated with the ocular glucose concentration range in diabetic patients.<sup>5, 17</sup> The aim of this research was to propose the applicability of the *o*-COOHBA sensor in a non-invasive and continuous sensing platform, such as a contact lens.



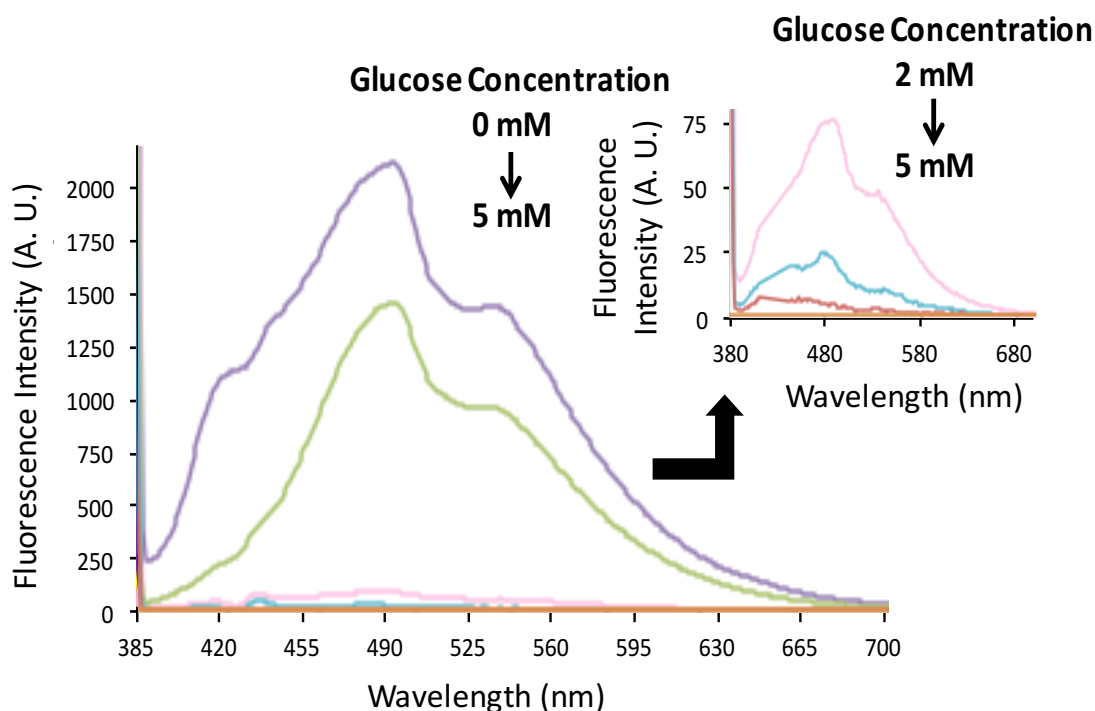


**Figure 2.8.** Fluorescence quenching in the *o*-COOHBA doped PDMS ‘lens’ on immersing the ‘lens’ in various pH 7.4 phosphate buffer solutions containing glucose concentrations between 0-5 mM. The excitation wavelength used was 380 nm and the corresponding emission wavelength was 485 nm.

## 2.5 Conclusions

In recent years, sugar detection has been exploited by an array of different sensing methods with an end goal of producing a non-invasive and continuous monitoring device for diabetics to control their glucose-levels. Currently, such a device does not exist. An optical approach, such as variations in colour or fluorescence, using chemosensors is thought as the solution for overcoming monitoring device challenges to reach this elusive goal.

BA derivatives can bind diol-containing molecules, like glucose, which is the reason many BA-containing compounds have been synthesised for glucose monitoring applications. It has been shown in this chapter that the *o*-COOHBA and *m*-COOHBA sensors can be used for monitoring glucose concentrations by a decrease in their fluorescence within the determined pH sensing range of pH 6-9. Moreover, these sensors have shown that glucose detection is possible in the lower glucose concentration ranges correlating to the accepted glucose levels for diabetic patients in the aqueous ocular humour (0.05-5mM). The *o*-COOHBA sensor was chosen for immobilisation on to a flexible polymeric platform, similar to that of a contact lens. In

comparison to the solution-based studies, the fluorescence of the *o*-COOHBA doped ‘lens’-like platform was quenched as the concentration of glucose was increased. The fluorescence of the ‘lens’ was practically switched off in the presence of 5 mM glucose in pH 7.4 phosphate buffer solution. These results demonstrate that the newly synthesised BA sensors have the potential to be employed in future physiological glucose-sensing devices for glucose monitoring in the aqueous ocular humour.

## 2.6 Future Work

Further research in this area currently involves investigating glucose binding efficiency between the *ortho* and *meta* derivatives. Due to the intramolecular  $N^+-B^-$  interaction that can occur, it would be expected that the *ortho* derivative would show the enhanced fluorescence response, however in this study the *meta* derivative showed a greater decrease in fluorescence. This can be explained by steric effects preventing desired binding of glucose. Further investigations by NMR and molecular modelling are underway to prove this theory.

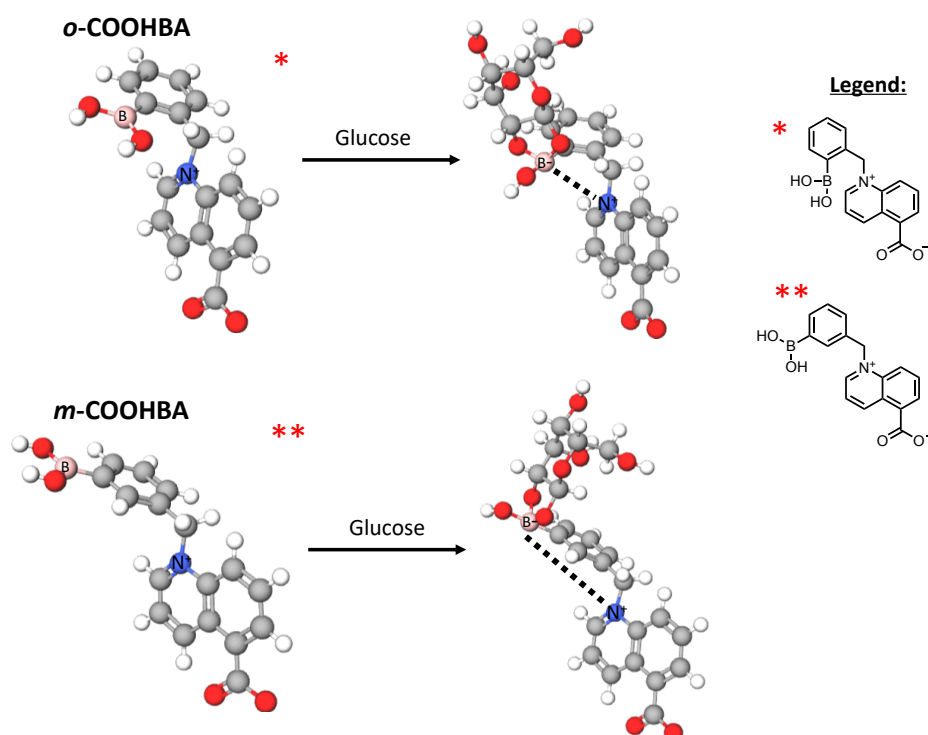


**Figure 2.9.** 3D molecular models of COOHBA derivatives, produced using free MolView software, shows the potential conformation of the COOHBA derivatives before and after sugar binding. The  $N^+-B^-$  interaction is represented by the dotted line.

The covalent immobilisation of the COOHBA sensing components on to the convex side of commercially available contact lenses is also being investigated. Badugu *et al.*, have introduced before the concept of attaching a BA fluorophore to a contact lens, for fluorescence sensing of glucose.<sup>1, 2, 5, 17</sup> Several immobilisation strategies involving a tether motif are likely to be employed to attach the COOHBA derivative to a polymeric surface, in order to study the influence of the fluorophore-surface interactions, the optimal spacer length and the optimal density of fluorophores. Polyethylene glycol derivatives are of interest in this context as anchoring spacers due to their hydrophilicity and biocompatibility. A polymeric brush approach, whereby multiple BA binding sites are available for glucose interaction is also envisioned, since it is known that glucose binds more favourably to *bis*-BA derivatives over mono-BA ones.

We would attempt to improve the system reported by Badugu *et al.* by selectively attaching the BA sensors in desired patterns on the convex side of the commercial contact lens, rather than non-covalent doping by absorption of the contact lens with the BA derivatives.<sup>1,2,5,17</sup> This aims to avoid important issues such as leaching of the dye and direct contact of the BA probes with the eye, minimizing potential toxicity effects of these sensing lenses, while simultaneously allowing diabetics to continuously and non-invasively track their glucose levels in real-time. The smart-contact lens aims to report obvious colour changes or changes in fluorescence and therefore provide continuous information on glucose levels in the ocular fluid. In conjunction with ICT-technologies this functionalised lens could evaluate and map an optical change in the lens to a specific glucose concentration, on capturing an image of the lens while in the eye. This could offer convenience and practicality when monitoring glucose levels. The ultimate goal would be to produce an application for smartphones to track glucose concentrations via optical changes in contact lenses captured using the smartphone's integrated camera. This application will allow data to become available to patients, doctors and careers, which would contribute to increased patient compliance<sup>1,2</sup> and citizen focused management of personal health through the use of a non-invasive optical sensor.

## 2.6 References

1. Badugu, R.; Lakowicz, J. R.; Geddes, C. D. Boronic acid fluorescent sensors for monosaccharide signaling based on the 6-methoxyquinolinium heterocyclic nucleus: progress toward noninvasive and continuous glucose monitoring, *Bioorg. Med. Chem.*, **2005**, *13*, 113-119.
2. Badugu, R.; Lakowicz, J. R.; Geddes, C. D. Ophthalmic glucose sensing: a novel monosaccharide sensing disposable and colorless contact lens, *Analyst*, **2004**, *129*, 516-521.
3. Sun, X.; James, T. D. Glucose sensing in supramolecular chemistry, *Chem. Rev.*, **2015**, *115*, 8001-8037.
4. Sun, X.; Zhai, W.; Fossey, J. S.; James, T. D. Boronic acids for fluorescence imaging of carbohydrates, *Chem. Commun.*, **2016**, *52*, 3456-3469.
5. Badugu, R.; Lakowicz, J. R.; Geddes, C. D. Ophthalmic glucose monitoring using disposable contact lenses - a review, *J. Fluoresc.*, **2004**, *14* (5), 617-633.
6. Zhai, W.; Sun, X.; James, T. D.; Fossey, J. S. Boronic acid-based carbohydrate sensing, *Chem. Asian J.*, **2015**, *10*, 1836-1848.
7. James, T. D.; Samanukumara Sandanayake, K. R. A.; Shinkai, S. Novel photoinduced electron-transfer sensor for saccharides based on the interaction of boronic acid and amine, *Chem. Commun.*, **1994**, 477-478.
8. Bull, S. D.; Davidson, M. G.; van den Elsen, J. M. H.; Fossey, J. S.; Jenkins, A. T. A.; Jiang, Y.; Kubo, Y.; Marken, F.; Sakurai, K.; Zhao, J.; James, T. D. Exploiting the reversible covalent bonding of boronic acids: recognition, sensing, and assembly, *Acc. Chem. Res.*, **2012**, *46* (2), 312-326.
9. Arimori, S.; Bell, M. L.; Oh, C. S.; James, T. D. A Modular fluorescence intramolecular energy transfer saccharide sensor, *Org. Lett.*, **2002**, *4* (24), 4249-4259.
10. Lacina, K.; Skládal, P.; James, T. D. Boronic acids for sensing and other applications - a mini-review of papers published in 2013, *Chem. Cent. J.*, **2014**, *8* (60).
11. James, T. D.; Samankumara Sandanayake, K. R. A.; Shinkai, S. Novel saccharide-photoinduced electron transfer sensors based on the interaction of boronic acid and amine, *J. Am. Chem. Soc.*, **1995**, *117* (35), 8982-8987..
12. Wu, X.; Li, Z.; Chen, X.; Fossey, J. S.; James, T. D.; Jiang, Y. Selective sensing of saccharides using simple boronic acids and their aggregates, *Chem. Soc. Rev.*, **2013**, *42*, 8032-8048.
13. Badugu, R.; Lakowicz, J. R.; Geddes, C. D. Wavelength-ratiometric and colorimetric robes for glucose determination, *Dyes Pigm.*, **2006**, *68*, 159-163.
14. Badugu, R.; Lakowicz, J. R.; Geddes, C. D. A glucose-sensing contact lens: from bench top to patient, *Curr. Opin. Biotechnol.*, **2005**, *16*, 100-107.
15. Badugu, R.; Lakowicz, J. R.; Geddes, C. D. Fluorescence sensors for monosaccharides based on the 6-methylquinolinium nucleus and boronic acid moiety: potential application to ophthalmic diagnostics, *Talanta*, **2005**, *65*, 762-768.

16. Geddes, C. D.; Badugu, R.; Lakowicz, J. R. Quaternary Nitrogen Heterocyclic Compounds for Detecting Aqueous Monosaccharides in Physiological Fluids. 2007.
17. Badugu, R.; Lakowicz, J. R.; Geddes, C. D. Noninvasive continuous monitoring of physiological glucose using a monosaccharide-sensing contact lens, *Anal. Chem.*, **2004**, *76*, 610-618.
18. Badugu, R.; Lakowicz, J. R.; Geddes, C. D. A glucose sensing contact lens: a non-invasive technique for continuous physiological glucose monitoring, *J. Fluoresc.*, **2003**, *13* (5), 371-374.
19. Fang, H.; Kaur, G.; Wang, B. Progress in boronic acid-based fluorescent glucose sensors, *J. Fluoresc.*, **2004**, *14* (5), 481-489.
20. Wang, J.; Jin, S.; Wang, B. A new boronic acid fluorescent reporter that changes emission intensities at three wavelengths upon sugar binding, *Tetrahedron Lett.*, **2005**, *46* (41), 7003-7006.
21. Hansen, J. S.; Ficker, M.; Peterson, J. F.; Christensen, J. B.; Hoeg-Jensen, T. *ortho*-Substituted fluorescent aryl monoboronic acid displays physiological binding of D-glucose, *Tetrahedron Lett.*, **2013**, *54*, 1849-1852.
22. Hansen, J. S.; Christensen, J. B.; Petersen, J. F.; Hoeg-Jensen, T.; Norrild, J. C. Arylboronic acids: A diabetic eye on glucose sensing, *Sens. Actuators, B*, **2012**, *161*, 45-79.
23. Springsteen, G.; Wang, B. A detailed examination of boronic acid-diol complexation, *Tetrahedron*, **2002**, *58* (26), 5291-5300.
24. March, W. F.; Rabinovitch, B.; Adams, R.; Wise, J. R.; Melton, M. Ocular glucose sensor, *Trans. Am. Soc. Artif. Intern. Organs*, **1982**, *28* (1), 232-235.
25. American Diabetes Association, Diagnosis and classification of diabetes mellitus, *Diabetes Care*, **2004**, *27* (1), 5-10.
26. Silverstein, R. M.; Bassler, G. C.; Morrill, T. C. *Spectroscopic identification of organic compounds*, 4th Ed.; Wiley and Sons, New York, 1981.
27. Crane, B. C.; Barwell, N. P.; Gopal, P.; Gopichand, M.; Higgs, T.; James, T. D.; Jones, C. M.; Mackenzie, A.; Mulavisala, K. P.; Paterson, W. The development of a continuous intravascular glucose monitoring sensor, *J. Diabetes Sci. Technol.*, **2015**, *9* (4), 751-761.

## **Chapter 3**

---

### **Intermolecular Quenching and Recovery of Fluorescence Using Cationic Boronic Acid Derivatives for Indirect Glucose Sensing**

---

## Contents

### Chapter 3: Intermolecular Quenching and Recovery of Fluorescence Using Cationic Boronic Acid Derivatives for Indirect Glucose Sensing

<b>3.1 Abstract</b>	<b>107</b>
<b>3.2 Introduction</b>	<b>108</b>
<b>3.3 Experimental</b>	<b>109</b>
3.3.1 Materials and Methods	109
3.3.2 Synthesis of 1-(2-boronobenzyl)-5-bromopyrimidin-1-ium bromide (BA1) and 1-(3-boronobenzyl)-5-(3-hydroxy-3-methylbut-1-yn-1-yl) pyrimidin-1-ium bromide (BA2)	111
3.3.2.1 <i>Synthesis of BA1</i>	111
3.3.2.2 <i>Synthesis of BA2</i>	112
<b>3.4 Results and Discussion</b>	<b>114</b>
3.4.1 Fluorescence Spectroscopy	114
3.4.1.1 <i>Fluorescence Spectroscopy of BA1</i>	116
3.4.2.2 <i>Fluorescence Spectroscopy of BA2</i>	119
<b>3.5 Conclusion</b>	<b>125</b>
<b>3.6 References</b>	<b>126</b>

### 3.1 Abstract

Lewis acidic boronic acids (BAs) are well known for their strong, but reversible interactions with diol-containing compounds like glucose. In this context, a two-component sensing system comprising of 7-hydroxycoumarin (7HC), a commercially available negatively-charged fluorophore and cationic BA molecules, have been investigated for indirect glucose sensing. In this system, the fluorescence of 7HC is monitored. On increased concentrations of the cationic BA derivative to the anionic fluorophore, the formation of a non-fluorescent ground-state complex results by electrostatic and  $\pi$ - $\pi$  stacking interactions. On glucose addition, dissociation in the complex is initiated to restore the fluorescence of 7HC, acting as a molecular switch.

In this chapter, the synthesis of novel cationic BA fluorescence quencher molecules, 1-(2-boronobenzyl)-5-bromopyrimidin-1-ium bromide (BA1) and 1-(3-boronobenzyl)-5-(3-hydroxy-3-methylbut-1-yn-1-yl) pyrimidin-1-ium bromide (BA2) is presented. BA1 and BA2, respectively, are then used in conjunction with 7HC in a two-component system to provide a fluorescence response to glucose. Both BA1 and BA2 induce a quenched state of fluorescence in 7HC. 125 equivalences of BA1 in pH 8.12 phosphate buffer caused a quenched state of fluorescence in 7HC by 24%, where this fluorescence was restored by 4% on introducing 5 mM glucose. On the other hand, 300 equivalences of BA2 induced a decrease in the fluorescence intensity of 7HC by 98% in a solution of pH 8.6, where 33% of this fluorescence could be recovered on sequential additions of glucose up to 100 mM. From these results, it was deduced that by working in a pH solution slightly more basic than the  $pK_a$  of the fluorophore ( $\sim 7.7$ ), fluorescence quenching interaction could be optimised. The glucose sensing range for BA1 was determined to be between 0-5 mM glucose, which lies within the clinical range for ocular-glucose concentrations in diabetic patients (0.05-5 mM). On the other hand, the glucose sensing range for BA2 is between 0-50 mM, which corresponds to the recognised range for blood-glucose concentrations in diabetics, known to be between 2-40 mM.



## 3.2 Introduction

Boronic acids (BAs) can act as sensors for recognising sugars. Due to their Lewis acidic properties,<sup>1,2</sup> BAs are capable of strong, reversible interactions with electron withdrawing diol-containing compounds, such as glucose.<sup>3</sup> This allows for the formation of *cis*-1,2- or *cis*-1,3-cyclic boronate diesters on sugar binding under alkaline conditions due to their basic pK<sub>a</sub>.<sup>1,4,5</sup> BAs typically have a pK<sub>a</sub> close to 9, however when situated close to an electron withdrawing group, such as a N<sup>+</sup> moiety or when bonded to hydroxyl groups in a saccharide molecule, the BA becomes more acidic with a reduced pK<sub>a</sub> to ~ 8 or ~6, respectively.<sup>3,5</sup> As a result, BAs are suitable for bio-sensing, as the pH of physiological fluids, such as blood, sweat or tears, lies within this range.<sup>6</sup>

In 2002 Singaram and co-workers were the first to introduce an indirect sugar sensing concept of monitoring glucose concentrations by changes in fluorescence.<sup>7</sup> In this research, the fluorescence quenching in pyranine was reported, on interacting with a cationic BA viologen compound to form a non-fluorescent ground state complex.<sup>7</sup> The fluorescence restoration was then accomplished by the addition of glucose, fructose or galactose, that induced a conformational change around boron to the anionic boronate species on saccharide binding.<sup>3,7</sup> Singaram and co-workers initially studied this sensing interaction in solution and more recently when the two-component system was immobilised inside a hydrogel matrix.<sup>2,5,7-11</sup> Feng *et al.*<sup>12-14</sup> and Li *et al.*<sup>1</sup> have also proposed two-component sensing systems utilising the same BA viologen compounds proposed by Singaram and co-workers. The main disadvantage to Singaram *et al.*'s approach is that viologen-compounds exhibit biological toxicity.<sup>15</sup> There are several advantages for indirect sensing over the direct sensing approach described in Chapter 2. The main benefit is that the BA component can be modified separately to obtain enhanced selectivity for glucose over other sugars, such as fructose, without altering the structure of the fluorophore reporter unit.<sup>5,8,12</sup>

Fluorescent dyes are complex organic molecules, which can be used to induce an optical response in a sensing system.<sup>5</sup> They are sensitive to discreet alterations in their chemical structure, which makes them desirable as fluorescent reporter units.<sup>5</sup> Therefore, the use of commercially available, well-studied fluorescent units in a two-component sensing approach, is considered an advantage over covalently attaching

BA components to fluorescent structures in a direct glucose-sensing approach.<sup>5</sup> Utilising two-components also allows for a screening process of other BA molecules with a chosen fluorophore and vice versa, to achieve an optimised quenching interaction and hence, to maximise fluorescence recovery in the presence of sugar molecules.<sup>8</sup>

In this context, the syntheses of two novel fluorescent BA-molecules, BA1 and BA2 are presented and the sensors are investigated for their ability to detect glucose in a two-component sensing system. In this case, the BA molecule acts as the glucose receptor and fluorescence quencher. The BA molecules contain a positively charged pyridinium nucleus to promote electrostatic interactions with an anionic fluorophore to induce fluorescence quenching.<sup>7</sup> This quenching process is achieved based on an electrostatic interaction, where an anionic fluorophore interacts with a cationic BA molecule.<sup>2</sup> Photophysical characterisation shows that upon increased concentrations of a cationic BA-derivative to 7HC, an efficient and sequential decrease in the fluorescence intensity of 7HC can be observed by the formation of a non-fluorescent ground state complex, through electrostatic and  $\pi$ - $\pi$  stacking interactions.<sup>5, 14</sup> In the presence of saccharides, the anionic boronate ester form is produced, which causes dissociation of the BA-molecule and fluorophore ground state complex, leading to a sequential restoration of fluorescence.<sup>1, 5, 11, 12, 14, 17</sup>

### 3.3 Experimental

#### 3.3.1 Materials and Methods

All BA reagents were purchased from Fluorochem, UK and all other reagents were acquired from Sigma Aldrich, Ireland. All reagents were used as received. Solvents used were methanol (CH<sub>3</sub>OH), anhydrous acetonitrile (CH<sub>3</sub>CN), anhydrous tetrahydrofuran (THF) and anhydrous dimethylformamide (DMF). All reactions were conducted under an inert atmosphere of nitrogen.

pH measurements were carried out on a VWR sympHony SP70P pH meter. <sup>1</sup>H and <sup>13</sup>C NMR spectra were recorded on a 400 MHz or 600 MHz Bruker NMR spectrometer, using deuterium oxide, deuterated methanol (*d*<sub>4</sub>-CH<sub>3</sub>OH) or deuterated dimethylformamide (*d*<sub>7</sub>-DMF) as solvents. <sup>11</sup>B NMR experiments were carried out on a Bruker Avance Ultrashield 600 MHz NMR spectrometer. BF<sub>3</sub> in deuterated methanol was used as an external standard for <sup>11</sup>B experiments. All reactions were

monitored by thin layer chromatography (TLC) that used basic silica plates and CH<sub>3</sub>OH: CH<sub>2</sub>Cl<sub>2</sub> (5:95) as the mobile phase. All fluorescence measurements were carried out on a JASCO Spectrofluorometer FP-8300 in pH buffer solutions using a quartz Suprasil cell with a pathlength of 10 mm and a volume of 1.4 mL. Parameters for fluorescence measurements were; medium sensitivity, 2.5 nm bandwidth, 1 nm data interval, 1 second response time and 500 nm/min scan speed.

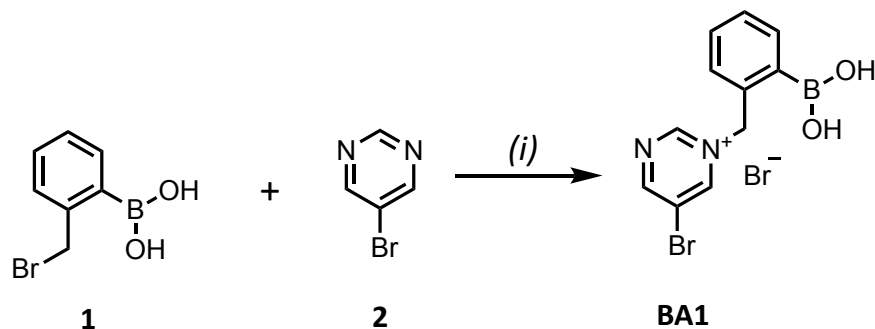
A range of buffers was prepared for spectroscopic analysis, where the buffer compositions can be found in Table 3.1. Both phosphate buffers were prepared for solutions of pH 7.4 and pH 8.12 and a carbonate buffer was prepared for the pH 8.88 solution. The phosphate buffers used were 0.1 M potassium dihydrogen phosphate (KH<sub>2</sub>PO<sub>4</sub>) and 0.1 M sodium hydroxide (NaOH) salts, while the carbonate buffer was composed of 0.2 M sodium carbonate (Na<sub>2</sub>CO<sub>3</sub>) and 0.2 M sodium hydrogen carbonate (NaHCO<sub>3</sub>) salts. All buffers were made up to 200 mL using deionised water. The pH of all solutions was measured using a VWR sympHony SP70P pH meter.

**Table 3.1.** Buffer compositions for 200 mL of required buffer.

<b>Phosphate Buffers</b>	KH <sub>2</sub> PO <sub>4</sub> 0.1 M (mL)	NaOH 0.1 M (mL)	DI H <sub>2</sub> O (mL)
pH 7.4	100	78.2	21.8
pH 8.12	100	93.4	6.6
<b>Carbonate Buffer</b>	Na <sub>2</sub> CO <sub>3</sub> 0.2 M (mL)	NaHCO <sub>3</sub> 0.2 M (mL)	DI H <sub>2</sub> O (mL)
pH 8.88	4	46	150

### 3.3.2 Synthesis of 1-(2-boronobenzyl)-5-bromopyrimidine-ium bromide (BA1) and 1-(3-boronobenzyl)-5-(3-hydroxy-3-methylbut-1-yn-1-yl) pyrimidine-1-ium bromide (BA2)

#### 3.3.2.1 Synthesis of BA1



**Scheme 3.1.** Synthesis of BA1. (i) Diethyl ether, 20 °C for 24h.

BA1 was prepared by a one-step nucleophilic substitution reaction, depicted by Scheme 3.1. *o*-[2-(Bromomethyl)phenylboronic acid] (compound **1**: 0.5069 g; 2.3593 mmol, 2 eq.) was dissolved in diethyl ether (2 mL). 5-Bromopyrimidine (compound **2**: 0.1875 g; 1.1791 mmol, 1 eq.) was dissolved in diethyl ether (2 mL) and was added drop-wise to compound **1** while stirring. The reaction was stirred at room temperature for 24h. The reaction was cooled to 0 °C and a white precipitate formed, affording BA1. The precipitate was collected via vacuum filtration and the white solid was washed with diethyl ether. BA1 was collected in a 44% yield as a white powder and its formation was confirmed via <sup>1</sup>H NMR (400 MHz, 20 °C, D<sub>2</sub>O), δ: 9.0 (1H, *s*, CH – c), 8.9 (2H, *s*, CH – b), 8.5 (2H, *s*, CH – a), 7.1 (2H, *s*, CH – a), 5.7 (2H, *s*, CH<sub>2</sub>) ppm (Figure 3.1). <sup>11</sup>B NMR (192 MHz, 20 °C, D<sub>2</sub>O), δ: 27.9 (B, *s*, B(OH)<sub>2</sub>) ppm. HRMS (*m/z*) calculated for [C<sub>12</sub>H<sub>13</sub>BBrN<sub>2</sub>O]<sup>+</sup> (monomethylether) 307.0250, found 307.0249. FT-IR for BA1 found peaks at 3166.17 (B-OH), 2832.65 and 2353.51 (C=C-H), 1574.05, 1445.0 (C=C) and 752.3 (C-Br) cm<sup>-1</sup>.<sup>18</sup> UV-visible spectroscopy found an absorbance peak at 285 nm. Fluorescence spectroscopy found an excitation peak at 338 nm and a corresponding emission peak at 380 nm. For raw spectral data and supplementary information see Appendix B.

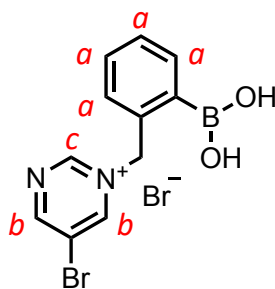
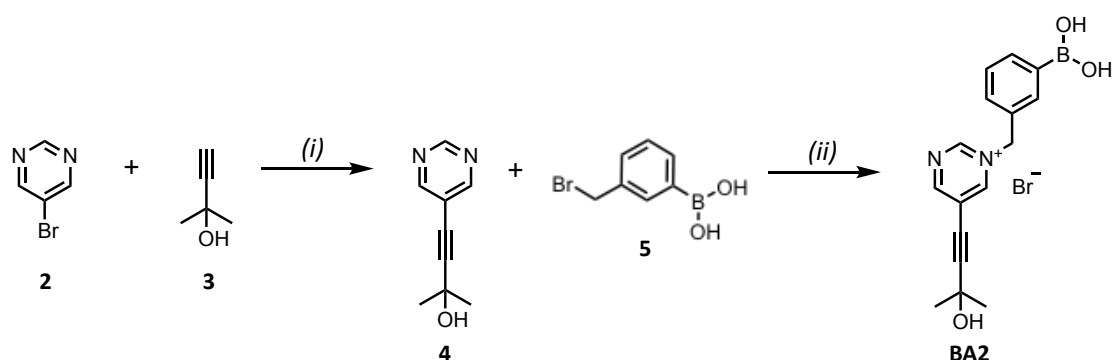


**Figure 3.1.** Chemical structure of BA1, with labelled  $^1\text{H}$  atom assignments.

### 3.3.2.2 Synthesis of BA2



**Scheme 3.2.** Synthesis of BA2. (i)  $\text{PdCl}_2(\text{PPh}_3)_2$ ,  $\text{CuI}$ , diethylamine, Ar, stirred at RT for 24h. (ii) Anhydrous THF,  $\text{N}_2$ , reflux at  $80\text{ }^\circ\text{C}$  for 5 days.

A two-step reaction process was required to synthesize BA2. A Sonogashira coupling reaction was first completed to produce 2-methyl-4-(pyrimidin-5-yl)but-3-yn-2-ol (compound **4**), which then underwent a nucleophilic substitution reaction to yield BA2 (Scheme 3.2). 5-bromopyrimidine (compound **2**; 6.09 g, 38.30 mmol, 11.3 eq.),  $\text{PdCl}_2(\text{PPh}_3)_2$  (0.30 g, 4.31 mmol, 1.3 eq.),  $\text{CuI}$  (65 mg, 3.40 mmol, 1 eq.) and 2-methyl-3-butyn-2-ol (compound **3**; 4.40 mL, 45.4 mmol, 13.4 eq.) were dissolved in diethylamine (90 mL) and bubbled under Ar. The reaction mixture was stirred under Ar overnight at room temperature. The solvent was then removed *in vacuo* and the mixture was dissolved in  $\text{CH}_2\text{Cl}_2$ . Addition of  $\text{CH}_3\text{OH}$  precipitated the desired product and the product was filtered and washed with  $\text{CH}_3\text{OH}$ . Compound **4** was collected as light brown crystals (66%). M.pt:  $114\text{--}118\text{ }^\circ\text{C}$ .  $^1\text{H}$  NMR (400 MHz,  $20\text{ }^\circ\text{C}$ ,  $\text{CDCl}_3$ )  $\delta$ : 9.16 (1H, s, CH – a), 8.79 (2H, s, CH – b), 2.17 (1H, s, OH), 1.67 (6H, s,  $\text{CH}_3$ ) ppm (Figure 3.2).  $^{13}\text{C}$  NMR: (150 MHz,  $20\text{ }^\circ\text{C}$ ,  $\text{CDCl}_3$ )  $\delta$ : 158.6 (2C, b), 156.6 (1C, a), 119.2 (1C,  $\text{C}_{\text{quat/aryl}}$ ), 100.9 (1C, Ar- $\text{C}\equiv\text{C}$ -), 75.3 (1C, Ar- $\text{C}\equiv\text{C}$ -), 65.4 (1C,  $\text{C}_{\text{quat/aryl}}$ ), 31.0 (2C,  $-\text{CH}_3$ ) ppm (Figure 3.2). HRMS (ESI-MS,  $\text{CHCl}_3$ ) calculated

for  $C_9H_{11}N_2O$ ,  $[M+H]^+$   $m/z$ , 163.0871, found 163.0866. FT-IR for compound **5** found peaks at 3256 (C-OH), 2932, 2671, 2489 (C=C-H), 2161 (Alkyne C-C-H), 1555, 1475 and  $1397\text{ cm}^{-1}$  (C=C).<sup>18</sup> UV-visible spectroscopy in methanol found an absorbance peak at 245 nm. Fluorescence spectroscopy found an excitation wavelength at 283 nm and the corresponding emission wavelength was 311 nm. For raw spectral data and supplementary information see Appendix B.

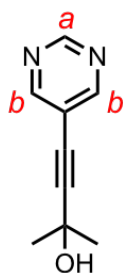


**Figure 3.2.** Chemical structure of compound **4**. H atoms are labelled.

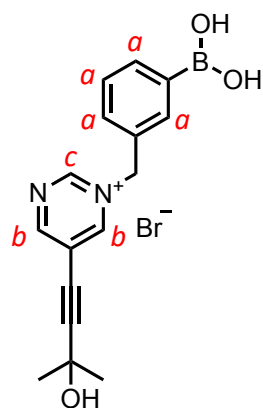


**Figure 3.3.** Chemical structure of BA2, with labelled  $^1H$  atom assignments.

BA2 was prepared by a nucleophilic substitution reaction, as depicted in Scheme 3.2. *m*-[3-(bromomethyl)phenylboronic acid] (compound **5**; 0.5116 g; 2.3813 mmol, 2.3 eq.) was dissolved in anhydrous THF (~5 mL). Compound **4** (0.1705 g; 1.0514 mmol, 1 eq.) was dissolved in anhydrous THF (~10 mL) and was added drop-wise via a pressure-equalised dropping funnel to compound **6** while refluxing over 30 minutes. The reaction was refluxed at 80 °C for 5 days and kept under  $N_2$ . After 5 days, the reaction appeared as a red/brown solution containing a tan precipitate. The tan precipitate was isolated via vacuum filtration as BA2 (30%) and washed with cold THF. NMR confirmed the structure of BA2 and the proton assignments can be seen in Figure 3.3.  $^1H$  NMR (600 MHz, 20 °C,  $DMF-d_7$ ),  $\delta$ : 8.7 (1H, *s*, CH – *c*), 8.2 (2H, *s*, CH – *b*), 7.9 (2H, *d*,  $J = 7$  Hz, CH – *a*), 7.7 (1H, *d*,  $J = 8$  Hz, CH – *a*), 7.4 (1H, *t*,  $J = 7$  and 14 Hz, CH – *a*), 3.6 (2H, *s*,  $CH_2$ ), 2.9 (3H, *s*,  $CH_3$ ), 2.7 (3H, *s*,  $CH_3$ ) ppm. (Figure 3.3).  $^{13}C$  NMR (150 MHz, 20 °C,  $DMF-d_7$ ),  $\delta$ : 28.8, 28.9, 29.0, 29.1, 29.2, 29.3, 29.5, 29.6 ( $CH_3$ ), 34.3, 34.4, 34.6, 34.7, 34.8 ( $C_{quat/aryl}$ ), 47.1, 47.1, 47.3, 47.4, 47.6, 47.7, 47.9, 48.3, 48.6 (Ar-C $\equiv$ C-), 162.6, 162.8, 163.0 (CH) ppm. FT-IR for BA2 found peaks at 3359.27 (B-OH), 3188.03 (C-OH), 2920.99, 2851.27 (C=C-H), 2020.05

(Alkyne C-C-H), 1645.55, 1632.29  $\text{cm}^{-1}$  (C=C).<sup>18</sup> UV-visible spectroscopy found an absorbance peak at 370 nm for 2.5 mM BA2 in  $\text{CH}_3\text{OH}$ . Excitation wavelength was at 430 nm and the corresponding fluorescence emission wavelengths were at 484 nm and 533 nm. For raw spectral data and supplementary information see Appendix B.

### 3.4 Results and Discussion

#### 3.4.1 Fluorescence Spectroscopy

To evaluate the effectiveness of fluorescence quenching of 7HC in the case of both BA sensors, BA1 and BA2, fluorescence measurements in different pH buffer solutions were carried out. 7HC is known to emit a strong blue fluorescence at  $\sim 460$  nm, when excited at  $\sim 328$  nm (in its neutral form) or  $\sim 370$  nm (in its anionic form). Solutions used for these fluorescence experiments included pH 7.4 phosphate buffer, pH 8.12 phosphate buffer and a mixture of pH 7.4 phosphate buffer with methanol (1:1) with a measured pH of 8.6. The pH of the buffer solutions was imperative for these tests due to the  $\text{pK}_a$  of 7HC being  $\sim 7.7$ .<sup>19</sup> In tests conducted at pH 7.4 the neutral form of 7HC (Figure 3.4, yellow) was predominantly present while in solutions of pH 8.12 and pH 8.88 the anionic form (Figure 3.4, blue) was dominant. Both forms of the fluorophore were determined spectroscopically, where in the excitation spectrum the neutral form of 7HC appeared at 328 nm and the anionic form at 367 nm, respectively (Figure 3.4).

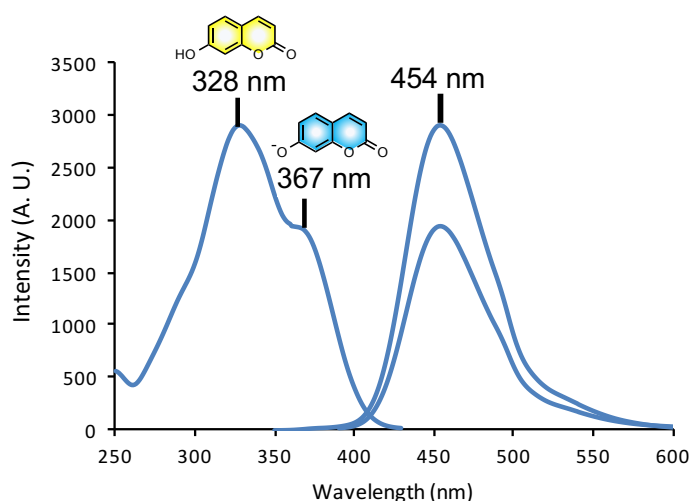


**Figure 3.4.** Excitation and fluorescence emission spectra for 7HC (4  $\mu\text{M}$ ) in pH 7.4 buffer solution, where the excitation wavelengths are 328 and 367 nm and the emission wavelength corresponding to both excitation wavelengths is 454 nm.

In this work, the cationic BA-components BA1 and BA2 were synthesised to contain a positively charged N atom, in order to promote electrostatic interactions with the anionic fluorophore 7HC, to form a photo-inactive ground-state complex.<sup>2, 5, 14</sup> On glucose additions to this two-component system, glucose bound to the BA moiety, which induced a conformational change around boron to the anionic boronate form. This resulted in the dissociation of the ground state complex, demonstrating the reversible restoration of fluorescence in 7HC.

Two types of quenching can occur when using a cationic BA molecule to decrease the fluorescence of an anionic fluorophore, namely static and dynamic quenching. Static quenching includes electrostatic and  $\pi$ - $\pi$  stacking interactions,<sup>12</sup> while dynamic quenching involves fluorescence deactivation due to collisions with other molecules in the excited state in solution.<sup>5</sup> Static quenching interactions are the main intermolecular interactions of interest in this two-component fluorescence quenching mechanism, due to the structure of the components containing conjugated  $\pi$ -systems and ionic charges.<sup>2, 5, 7, 12, 20</sup> At pH values above the  $pK_a$  of 7HC ( $> 7.7$ ), the 7HC fluorophore is anionic and the BA components are cationic, which allows for electrostatic interactions, as well as  $\pi$ - $\pi$  stacking interactions, as both compounds contain benzyl ring functionalities. A Stern-Volmer plot permits the study of an intermolecular deactivation process, such as fluorescence<sup>5, 20</sup> and when only one type of quenching process occurs, this is usually depicted by a linear Stern-Volmer plot in the fluorescence curve, corresponding to Equation 3.1.<sup>5, 20</sup> On the other hand, where two intermolecular interactions take place, *i.e.* both electrostatic and  $\pi$ - $\pi$  stacking quenching processes, this is represented by an exponential decreasing trend in the fluorescence curve, corresponding to Equation 3.2.<sup>5, 12, 14, 20</sup> In static quenching, the fluorophore is quenched based on the formation of a ground-state complex, which is not dependant on diffusion or molecular collisions. In order to achieve the optimal quenching parameters for this study, both electrostatic and  $\pi$ - $\pi$  stacking quenching interactions are required. This would ensure for an effective fluorescence decrease and hence fluorescence restoration, in order to maximise the fluorescence response for glucose detection.

$$F_0/F = 1 + K_Q[Q] \quad (3.1)$$

$$F_0/F = (1 + K_S[Q])e^{V[Q]} \quad (3.2)$$



### 3.4.1.1 Fluorescence Spectroscopy of BA1

The fluorescence of 7HC was measured in a pH 8.12 phosphate buffer solution. With increased concentrations of BA1 the fluorescence of 7HC became quenched (Figure 3.5A). Since the pH of the working solution was slightly higher than that of the  $pK_a$  of the fluorophore ( $\sim 7.7$ ), the fluorophore was present mostly in its anionic state.<sup>19</sup> Therefore, electrostatic quenching between the negatively charged fluorophore and cationic BA-derivative was permitted. From Figure 3.5 (B and C), the excitation and emission spectra for 7HC with increased concentrations of BA1 is illustrated, where the excitation wavelength of 7HC was 367 nm and the corresponding emission was at 454 nm, corresponding to literature reported values.<sup>19</sup> From the excitation spectrum, it can be confirmed that the fluorophore is present largely in its anionic state by displaying one predominant peak at 367 nm. A slight shoulder can be seen at  $\sim 328$  nm, characteristic for the neutral form of 7HC (Figure 3.5B).<sup>5, 19</sup>

From the fluorescence curve in Figure 3.5D, a linear trend ( $R^2 = 0.999$ ) can be seen, which denotes a single type of quenching resulting from the ground state complex formation between the fluorophore and BA-derivative. This type of quenching is most likely a result of electrostatic interactions between the fluorophore and BA derivative, since the pH of the solution is slightly higher than the  $pK_a$  of the fluorophore, meaning the fluorophore is mainly in its anionic form. It is believed that the bulky electron withdrawing  $-Br$  substituent attached to the pyrimidine ring, in this case prevents efficient overlap between the fluorophore and BA-quencher molecules for sufficient  $\pi$ - $\pi$  stacking interactions to result in an exponential decrease of fluorescence.

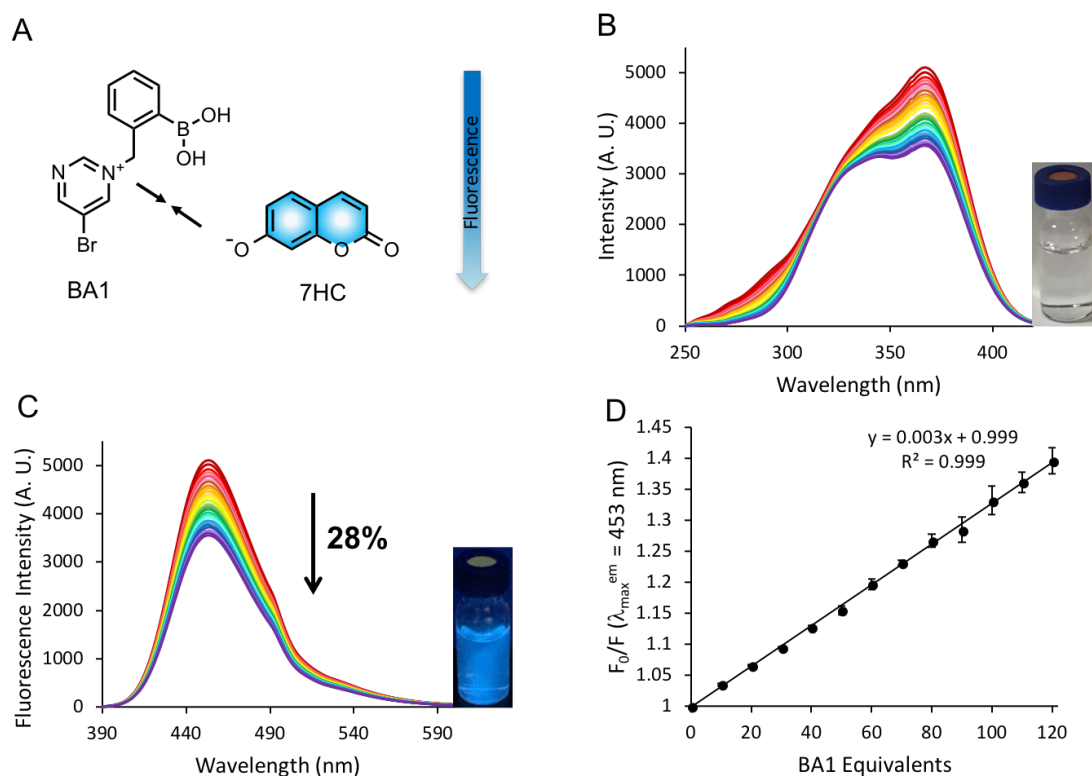


**Figure 3.5.** (A). Schematic for the fluorescence quenching of 7HC with BA1. (B) Excitation spectrum of 7HC (4  $\mu\text{M}$ ) with increased concentrations of BA1 (up to 0.48 mM; 120 eq.) in pH 8.12 phosphate buffer solution, showing an excitation wavelength of 367 nm and a shoulder at 328 nm, corresponding to the emission wavelength at 454 nm. (C) Emission spectrum of 7HC with increased concentrations of BA1, displaying an emission at 454 nm when excited at 367 nm. (D) Linear curve of 7HC ( $R^2 = 0.999$ ), where each point on the curve represents the average maximum emission point ( $n = 3$ ) at 454 nm with increased additions of BA1.

When this same interaction, between 7HC and BA1 was investigated in a more basic buffer solution of pH 8.88, an enhanced quenching result was obtained. From Figure 3.6, the excitation and emission spectra for 7HC (left) in the higher pH 8.88 buffer solution can be seen, where the excitation was at 367 nm and the emission was at 454 nm, similar to fluorescence measurements at pH 8.12. The fluorescence quenching profile was also similar to that at pH 8.12, since the fluorophore was present mostly in its anionic form, corresponding to the peak at 367 nm in the excitation spectrum. A non-linear quenching trend ( $R^2 = 0.980$ ) in 7HC by BA1 was observed indicating an enhanced interaction between 7HC and BA1 at the higher pH of 8.88 (Figure 3.6C). As the fluorophore was present in its anionic form, it was expected that electrostatic interaction with BA1 would be enhanced. Similarly, by incorporating an electron-withdrawing bromo group, the electron density around the

$N^+$  atom was expected to decrease, to render the BA derivative more electron accepting. However, on comparing both of the fluorescence quenching experiments at pH 8.12 and pH 8.88 at 120 equivalents of BA1, a decrease in fluorescence in 7HC by 28% and 56% were observed, respectively. As a result, by working in a buffer solution slightly above the  $pK_a$  of the fluorophore ( $\sim 7.7$ ), a more enhanced fluorescent quenching interaction can be observed. Moreover, it was deduced that the bulky bromo group in the BA molecule sterically hindered the quenching interaction with 7HC by preventing efficient  $\pi$ - $\pi$  stacking overlap.

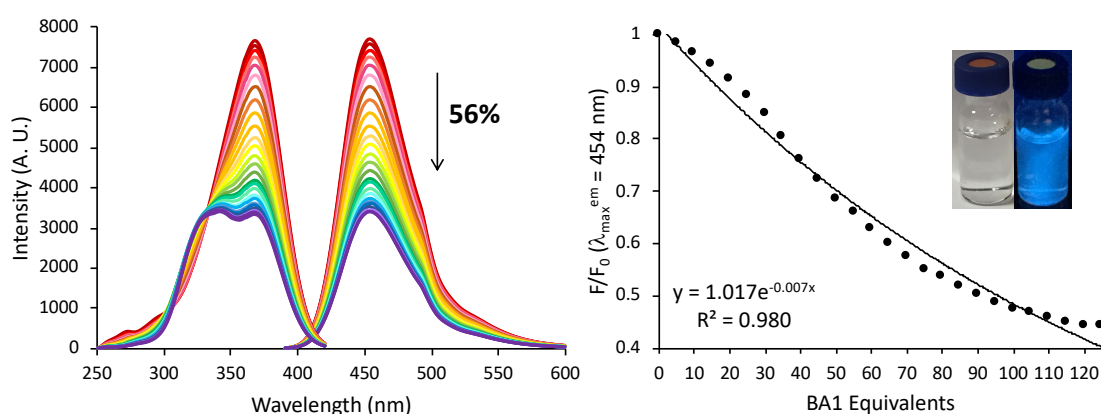


**Figure 3.6.** (A) Excitation spectrum of 7HC (4  $\mu$ M) with increased concentrations of BA1 (up to 0.8 mM; 200 eq.) in pH 8.88 phosphate buffer solution, showing an excitation wavelength of 367 nm, corresponding to the emission wavelength of 454 nm (B) Emission spectrum of 7HC, showing an emission wavelength at 454 nm, with increased additions of BA1, when excited at 367 nm. Non-linear curve of 7HC with increased concentrations of BA1 ( $R^2 = 0.980$ ) is shown, where each point on the curve was the maximum emission at 454 nm after each addition of BA1.

Glucose addition to the system resulted in the dissociation of the ground-state complex formed between 7HC and BA1, restoring the fluorescence in 7HC (Figure 3.7A). Since the most effective fluorescence quenching in 7HC by BA1 was 28%, which was represented by a linear static quenching trend in Figure 3.5D, it wasn't surprising to find that the recovery of fluorescence was also limited to 4%, when 5 mM glucose was employed at pH 8.12 (Figure 3.7C). In order to improve this recovery, the quenching interaction between 7HC and BA1 would need to depict an exponential trend in the quenching curve, *i.e.* representing both electrostatic and  $\pi$ - $\pi$  stacking interactions. A possible reason for only one type of static quenching occurring could be due to the bulky electron withdrawing  $-Br$  substituent attached to the pyrimidine ring. It's possible that this halogen group is preventing effective  $\pi$ - $\pi$

stacking interactions between 7HC and BA1 due to steric hindrance and as a result, only electrostatic interactions are permitted. For this reason, in place of the  $-Br$  substituent, the second BA-derivative, BA2, was designed to contain an extended pyrimidine  $\pi$ -system, consisting of an alkyne group, which would enhance  $\pi$ - $\pi$  stacking interactions with 7HC for an exponential quenching of fluorescence.

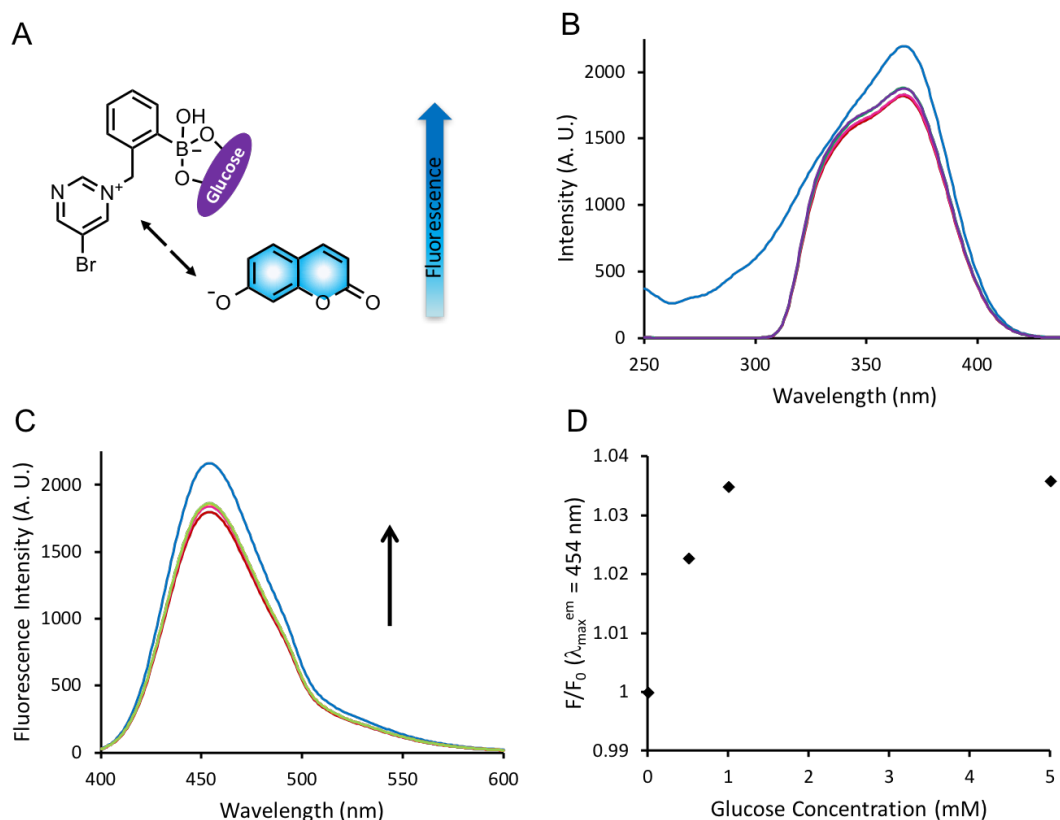


**Figure 3.7.** (A) Schematic of fluorescence recovery in 7HC, on dissociation of 7HC:BA1-complex in the presence of glucose. (B) Excitation spectrum of 7HC (4  $\mu$ M) with BA1 (175 eq.; 0.7 mM) and increased concentrations of glucose (0-5 mM) in pH 8.12 phosphate buffer solution, where the pink line indicates the original excitation of 7HC before any BA1 additions. The peak in the excitation spectrum was found at 367 nm, corresponding to an emission at 454 nm. (C) Emission spectrum of 7HC and BA1 (1:175 eq.) with increased additions of glucose (0-5 mM), displaying an increase in emission intensity by 4%, where the emission wavelength was 454 nm, corresponding to an excitation wavelength of 367 nm. (D) Fluorescence curve of 7HC and BA1 (1:175 eq.) with increased concentrations of glucose (0-5 mM). Each data point curve was taken as the maximum intensity at 454 nm after each addition of glucose.

#### 3.4.2.2 Fluorescence Spectroscopy of BA2

In order to improve the quenching interactions between 7HC and BA1 and hence fluorescence recovery, a second BA molecule was synthesised, BA2 (Figure 3.8). BA1 contained a  $-Br$  substituent that was thought to sterically hinder effective  $\pi$ - $\pi$

overlap between 7HC and BA1 to produce an exponential decrease in fluorescence. BA2 was synthesised to overcome this challenge by replacing the -Br group in the 3-position on the pyrimidine ring with a 2-methylbut-3-yn-2-ol substituent. The alkyne substituent was expected to allow for efficient  $\pi$ - $\pi$  stacking interactions, since this group extended the  $\pi$ -conjugation from the pyrimidine ring. BA2 also differs in the positioning of the BA groups from *ortho* to *meta*. The sugar selectivity is dependent on the orientation of the BA groups.

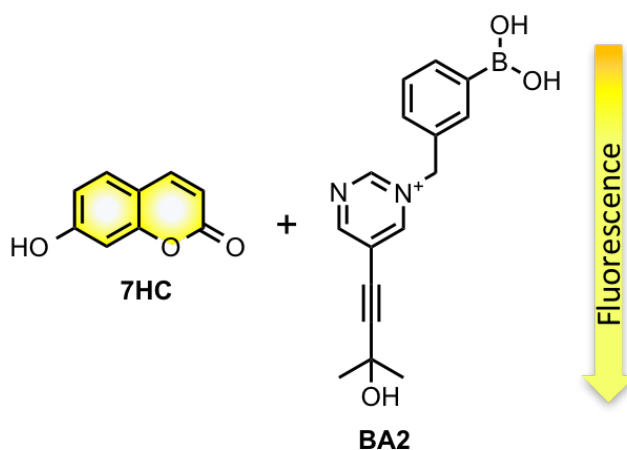


**Figure 3.8.** Fluorescence quenching in neutral 7HC on increased additions of BA2.

On determining the quenching efficiency of BA2 with 7HC, in a pH buffer solution of pH 7.4, it was clear that both the neutral form (Figure 3.9, yellow) and the anionic form (Figure 3.9, blue) of the fluorophore were present, as shown by the two peaks observed in the excitation spectrum in Figure 3.9A.<sup>5,19</sup> The two forms co-exist because the  $pK_a$  of 7HC is approximately 7.7 and the pH of the solution was pH 7.4. When the pH of the solution is equal to the  $pK_a$  of the fluorophore, it can be said that half of the concentration of the fluorophore exists in its anionic form and the other half is present in its neutral form.<sup>4</sup> Since the pH of the solution (pH 7.4) is slightly lower than that of the  $pK_a$  of 7HC (~7.7), the neutral form of the fluorophore is dominant and this is observed as the more prevailing peak in the excitation spectrum at 328 nm.

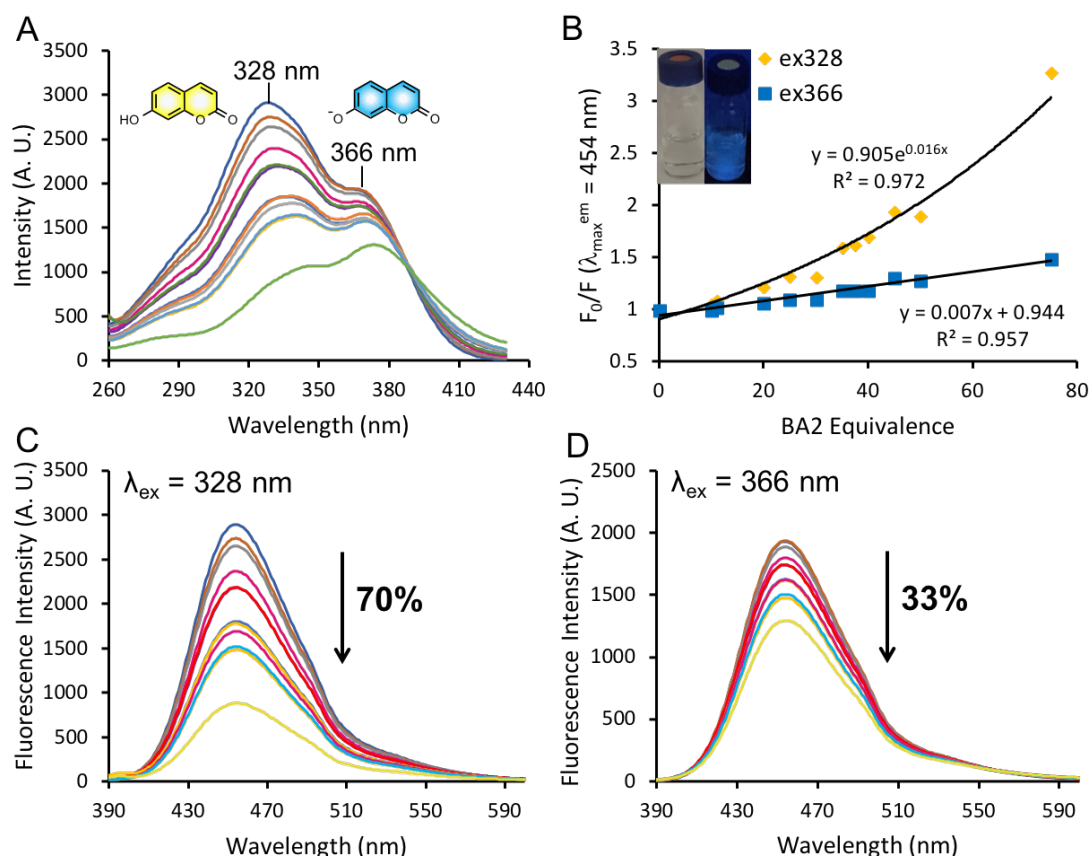


**Figure 3.9.** (A) Excitation spectrum of 7HC (4 μM) with increased concentrations of BA2 (up to 0.3 mM; 75 eq.) in pH 7.4 phosphate buffer solution (containing 40 μL CH<sub>3</sub>OH in each 1.5 mL sample). The peak at 328 nm represents the neutral form of 7HC (yellow) and the peak at 366 nm represents the anionic form of 7HC (blue). Both excitation wavelengths correspond to the same emission wavelength at 454 nm. (B) Fluorescence response of 7HC with increased additions of BA2, excited at 328 and 366 nm. Each data point was taken at 454 nm corresponding to the maximum emission after addition of BA2 ( $R^2 = 0.972$  and  $0.957$  at 328 and 366 nm, respectively). (C) Emission spectrum of 7HC showing an emission maximum at 454 nm, with increased concentrations of BA2 when excited at 328 nm. (D) Emission spectrum of 7HC showing an emission maximum at 454 nm, with increased additions of BA2 when excited at 366 nm.

The solutions containing both 7HC (4 μM) and BA2 (up to 75 eq.) were then excited at both excitation wavelengths to determine the optimal excitation wavelength to monitor the fluorescence quenching by the BA molecule. When the samples were excited at 328 nm, corresponding to the neutral form of 7HC,<sup>19</sup> a quenched state of fluorescence by 70% was observed (Figure 3.9C). This was represented by a decreasing non-linear trend ( $R^2 = 0.972$ ) (Figure 3.9B). In comparison, when the samples were excited at 366 nm, corresponding to the anionic form of the fluorophore,<sup>19</sup> a linear decrease of fluorescence by 33% was observed ( $R^2 = 0.957$ ) (Figure 3.9D). From these results, it could be concluded that both  $\pi$ - $\pi$  stacking interactions and electrostatic interactions between 7HC and BA2 were enhanced to

exhibit a 70% decrease in fluorescence at pH 7.4. In contrast, the maximised quenching response using BA1 at pH 8.12, showed a 28% decrease in fluorescence intensity. This enhanced quenching ability of BA2 was thought to depend on the elongated alkyne  $\pi$ -system in BA2 in comparison to the bromo group in BA1. This experiment also supported that under these pH conditions,  $\pi$ - $\pi$  stacking interactions play an important role in the quenching interaction between 7HC and BA2, since the neutral form of 7HC demonstrated the most effective quenching when the samples were excited at 328 nm.

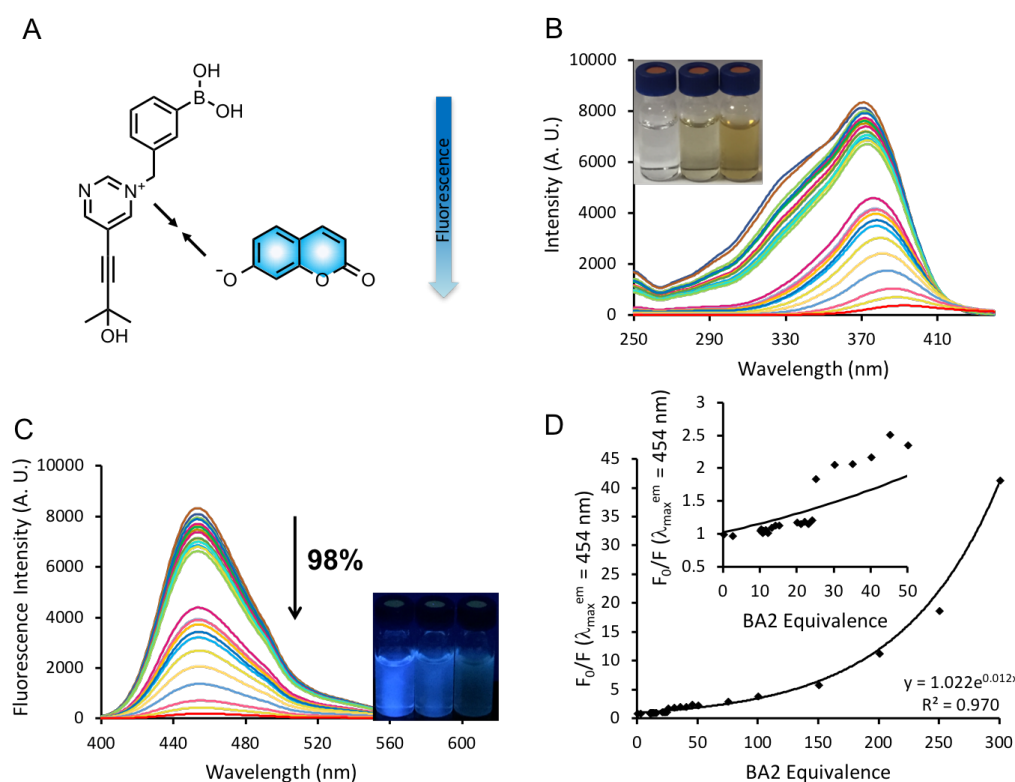


**Figure 3.10.** (A) Schematic of fluorescence quenching in anionic 7HC on increased interactions with BA2. (B) Excitation spectrum of 7HC (4  $\mu$ M) with increased concentrations of BA2 (up to 1.2 mM; 300 eq.) in pH 7.4 phosphate buffer solution and CH<sub>3</sub>OH (1:1) (measured pH 8.6). The excitation wavelength is shown as 370 nm with a shoulder at 328 nm, corresponding to the emission wavelength 454 nm. (C) Emission spectrum of 7HC with increased additions of BA2, showing an emission wavelength at 454 nm, corresponding to the excitation wavelength at 370 nm. (D) Fluorescence quenching of 7HC with increased concentrations of BA2, where each point on the curve was taken as the maximum fluorescence intensity at 454 nm after the addition of BA2 ( $R^2 = 0.970$ ).

The effect of BA2 on the fluorescence of the anionic form of 7HC was then investigated in a pH 8.6 solution (Figure 3.10A). As the pH of the solution is higher than the pK<sub>a</sub> of 7HC (~7.7), the anionic form of 7HC is dominant. By employing the anionic form of 7HC it was expected to optimise the quenching interaction between



7HC and BA2 by favouring both electrostatic interactions, as well as  $\pi$ - $\pi$  stacking interactions, to observe an exponential decreasing trend in the Stern-Volmer plot. The excitation spectrum of 7HC in Figure 3.10B confirms this, where one prominent absorption peak can be seen at 370 nm representing the anionic form of 7HC.<sup>19</sup> The shoulder at  $\sim$ 328 nm represents the small presence of the neutral form of 7HC. The exponential decreasing trend in Figure 3.10D ( $R^2 = 0.970$ ) denotes that both electrostatic and  $\pi$ - $\pi$  stacking quenching interactions are occurring. As a result, the fluorescence of 7HC is switched off, on quenching the fluorescence by 98% with up to 300 equivalents of BA2 (Figure 3.10C). This change in fluorescence was visible by eye under a UV lamp (Figure 3.10C, inset).

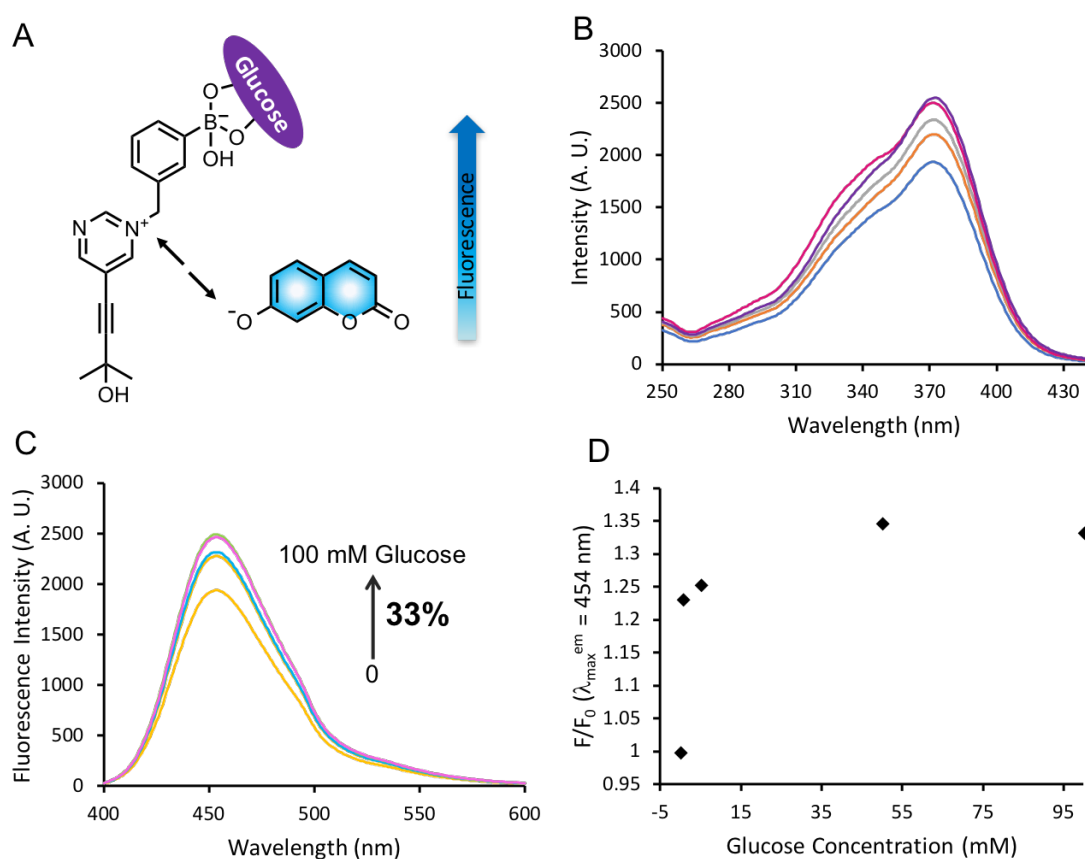


**Figure 3.11.** (A) Schematic of the fluorescence recovery in 7HC, on dissociation of fluorophore:BA2-quencher ground-state complex in the presence of glucose. (B) Excitation spectrum of 7HC (4  $\mu$ M) with BA2 (20 eq.; 80  $\mu$ M) and increased concentrations of glucose (up to 100 mM) in pH 7.4 phosphate buffer solution and CH<sub>3</sub>OH (1:1) (measured pH 8.6). The excitation wavelength was 370 nm with a shoulder at 328 nm, corresponding to an emission at 454 nm. (C) Emission spectrum of 7HC and BA2 (1:20 eq.) with increased concentrations of glucose. The emission wavelength was 454 nm. (D) Fluorescence curve of 7HC and BA2 (1:20 eq.) with increased concentrations of glucose, where each point on the curve was taken as the maximum intensity at 454 nm after the addition of glucose.



As anticipated, a greater increase in fluorescence could be observed with BA2 compared to the employment of BA1 in a similar system. On glucose addition, the conformational change around boron to the anionic boronate form,<sup>21</sup> initiated dissociation in the fluorophore:BA photo-inactive complex, to restore the fluorescence intensity in 7HC (Figure 3.11A).<sup>2, 5, 7</sup> As a result of an exponential decrease of fluorescence in 7HC when using BA2 at pH 8.6 (Figure 3.10D), a greater recovery of fluorescence was predicted on glucose additions to this system when compared to the use of BA1. 300 equivalents of BA2 were required to effectively switch-off the fluorescence of 7HC and 50 mM glucose was used to partially recover this fluorescence by 33% at pH 8.6 (Figure 3.11C and D). BA2 compared to BA1 proved to be superior, where 125 equivalents of BA1 (0.5 mM) was required to quench the fluorescence of 7HC by 28% and 5 mM glucose was used to partially restore the fluorescence by 4% at pH 8.12. Conveniently, a lower concentration of BA2 (0.1 mM; 25 eq.) was required to induce a quenching effect of 45% in 7HC, in comparison to a decrease of 28% by BA1. Therefore, by employing BA2 this fluorescence quenching interaction can be enhanced.

To summarise, a two-component sensing system was described that can be used for glucose detection in solution. This bimolecular switch operates by initially quenching the fluorescence of a known fluorophore using a cationic BA molecule, to then restore the fluorescence with increased glucose concentrations.<sup>2, 5, 7</sup> On increased concentrations of the BA-molecules (BA1 and BA2, respectively) to 7HC, a non-fluorescent ground state complex is formed by either electrostatic or  $\pi$ - $\pi$  stacking interactions or both. This complex formation is dependent on the pH of the buffer solution, which deems the fluorophore in its neutral state when working below the  $pK_a$  of 7HC ( $\sim 7.7$ ) or anionic when working in more basic solutions. When glucose is then added to the system, the fluorescence can be recovered.<sup>2, 5, 7</sup>

This two-component glucose sensing system has several advantages over the direct approach described in Chapter 2. In indirect glucose sensing, an increase in fluorescence is detected as opposed to a decrease in fluorescence using a direct sensing approach. By recovering the fluorescence, this sensing system can also offer better means of visualising the fluorescence response compared to a quenched state of fluorescence for direct sensing.

Compared to a direct sensing approach, an indirect sensing system can much more efficiently be tailored towards the detection of saccharides. In an indirect sensing

system, the fluorescent component or the BA moiety can be interchanged with other similar molecules to enhance the optical response.<sup>5</sup> This allows for an independent screening process for the fluorophore and the BA derivative to determine the optimum sensing conditions,<sup>5</sup> as opposed to a direct sensing approach, where the single sensing component must fulfil all functionalities, such as an efficient fluorescent species, effective B<sup>-</sup>-N<sup>+</sup> interaction and selective glucose binding.<sup>3</sup> A two-component sensing system can be better configured towards a certain application, for example where pH or biocompatibility are sensitive factors.

### 3.5 Conclusion

The two-component system presented functions in an aqueous buffer solution, where the fluorophore and dicationic BA compounds are water-soluble. The sensors operate over important physiological glucose concentration ranges, where BA1 is more suited towards ocular glucose sensing because of its sensitivity to glucose in a range of 0-5 mM corresponding to the ocular fluid glucose concentration ranges of diabetic patients.<sup>3, 22</sup> On the other hand, BA2 is desired for blood-glucose or interstitial fluid sensing in a glucose range of 0-50 mM, corresponding to diabetic blood-glucose levels.<sup>3, 22</sup> When combined with the anionic water-soluble fluorescent dye 7HC in the absence of glucose, the novel BA molecules formed a photo-inactive complex in the ground state by static interactions, which greatly reduced the fluorescence intensity of 7HC. Upon glucose binding to the BA molecules, a negatively charged boronate diester was formed. This weakened the association between 7HC and the BA molecule to restore the fluorescence intensity. The recovery of fluorescence was dependant on glucose concentration. BA2 showed a greater ability to quench and recover the fluorescence of 7HC compared to BA1. Further studies are underway to evaluate the binding ratio of BA2 with glucose, as well as screening these BA molecules with other anionic fluorophores, such as fluorescein or pyranine, for optimum performance in physiological pH conditions. Future work in this area is described in Chapter 6, which involves the immobilisation of the sensing components inside a hydrogel matrix.

### 3.6 References

1. Li, Y.; Zhang, L.; Huang, J.; Liang, R.; Qiu, J. Fluorescent graphene quantum dots with a boronic acid appended bipyridinium salt to sense monosaccharides in aqueous solution, *Chem. Commun.*, **2013**, *49*, 5180-5182.
2. Sharrett, Z.; Gamsey, S.; Fat, J.; Cunningham-Bryant, D.; Wessling, R. A.; Singaram, B. The effect of boronic acid acidity on performance of viologen-based boronic acids in a two-component optical glucose-sensing system, *Tetrahedron Lett.*, **2007**, *48*, 5125-5129.
3. Badugu, R.; Lakowicz, J. R.; Geddes, C. D. Ophthalmic glucose monitoring using disposable contact lenses - A review, *J. Fluoresc.*, **2004**, *14* (5), 617-633.
4. Brooks, W. L. A.; Sumerlin, B. S. Synthesis and applications of boronic acid-containing polymers: From materials to medicine, *Chem. Rev.*, **2016**, *116*, 1375-1397.
5. Suri, J. T.; Cordes, D. B.; Cappuccio, F. E.; Wessling, R. A.; Singaram, B. Monosaccharide detection with 4,7-phenanthroline salts: Charge-induced fluorescence sensing, *Langmuir*, **2003**, *19*, 5145-5152.
6. Corrie, S. R.; Coffey, J. W.; Islam, J.; Markey, K. A.; Kendall, M. A. F. Blood, sweat, and tears: Developing clinically relevant protein biosensors for integrated body fluid analysis, *Analyst*, **2015**, *140* (13), 4350-4364.
7. Camara, J. N.; Suri, J. T.; Cappuccio, F. E.; Wessling, R. A.; Singaram, B. Boronic acid substituted viologen based optical sugar sensors: Modulated quenching with viologen as a method for monosaccharide detection, *Tetrahedron Lett.*, **2002**, *43*, 1139-1141.
8. Viložny, B.; Schiller, A.; Wessling, R. A.; Singaram, B. Multiwell plates loaded with fluorescent hydrogel sensors for measuring pH and glucose concentration, *J. Mater. Chem.*, **2011**, *21*, 7589-7595.
9. Cappuccio, F. E.; Suri, J. T.; Cordes, D. B.; Wessling, R. A.; Singaram, B. Evaluation of pyranine derivatives in boronic acid based saccharide sensing: Significance of charge interaction between dye and quencher in solution and hydrogel, *J. Fluoresc.*, **2004**, *14* (5), 521-533.
10. Sharrett, Z.; Gamsey, S.; Hirayama, L.; Viložny, B.; Suri, J. T.; Wessling, R. A.; Singaram, B. Exploring the use of APTS as a fluorescent reporter dye for continuous glucose sensing, *Org. Biomol. Chem.*, **2009**, *7*, 1461-1470.
11. Suri, J. T.; Cordes, D. B.; Cappuccio, F. E.; Wessling, R. A.; Singaram, B. Continuous glucose sensing with a fluorescent thin-film hydrogel, *Angew. Chem., Int. Ed.*, **2003**, *42*, 5857-5859.
12. Feng, L.; Liang, F.; Wang, Y.; Xu, M.; Wang, X. A highly sensitive water-soluble system to sense glucose in aqueous solution, *Org. Biomol. Chem.*, **2011**, *9*, 2938-2942.
13. Wang, Z.; Lei, H.; Feng, L. A facile channel for D-glucose detection in aqueous solution, *Spectrochim. Acta, Part A*, **2013**, *114*, 293-297.

14. Feng, L.; Yin, N.; Wang, X.; Wang, Z. Fluorescence probe for monosaccharide based anionic polyelectrolyte and cationic pyridine quaternary ammonium salt, *Sens. Actuators, B*, **2013**, *181*, 730-734.
15. Dinis-Oliveira, R. J.; Duarte, J. A.; Sanchez-Navarro, A.; Remiao, F.; Bastos, M. L.; Carvalho, F. Paraquat poisonings: Mechanisms of lung toxicity, clinical features, and treatment, *Crit. Rev. Toxicol.*, **2008**, *38* (1), 13-71.
16. James, T. D.; Samankumara Sandanayake, K. R. A.; Shinkai, S. Novel saccharide-photoinduced electron transfer sensors based on the interaction of boronic acid and amine, *J. Am. Chem. Soc.*, **1995**, *117* (35), 8982-8987.
17. Yao, H.; Shum, A. J.; Cowan, M.; Lahdesmaki, I.; Parvis, B. A. A contact lens with embedded sensor for monitoring tear glucose level, *Biosens. Bioelectron.*, **2011**, *26*, 3290-3296.
18. Silverstein, R. M.; Bassler, G. C.; Morrill, T. C.; *Spectroscopic identification of organic compounds*, 4th Ed., Wiley and Sons, New York, 1981.
19. Fink, D. W.; Koehler, W. R. pH effects on fluorescence of Umbelliferone, *Anal. Chem.*, **1970**, *42* (9), 990-993.
20. Lakowicz, J. R. *Principles of Fluorescence Spectroscopy*, 3<sup>rd</sup> Edition ed.; Springer Science and Business Media: **2006**; p 1-923.
21. Fang, H.; Kaur, G.; Wang, B. Progress in boronic acid-based fluorescent glucose sensors, *J. Fluoresc.*, **2004**, *14* (5), 481-489.
22. Bruen, D.; Delaney, C.; Florea, L.; Diamond, D. Glucose Sensing for Diabetes Monitoring: Recent developments, *Sensors*, **2017**, *17*, 1866-1887.

## Chapter 4

---

### **Water-Soluble Polymerisable Boronic Acids: Combining an Adaptable One-Step Synthesis with an In-Depth Understanding of pH and Glucose Response\***

---

\*This chapter has been submitted for publication as “Water-Soluble Polymerisable Boronic Acids: Combining an Adaptable One-Step Synthesis with an In-Depth Understanding of pH and Glucose Response”, Danielle Bruen, Colm Delaney, Dermot Diamond and Larisa Florea, *Org. Lett.*, **2018**.

\*\*The boronic acid compounds synthesised in this chapter are covered under GB Patent, GB1805226.6, “Boronic Acid Derivatives for Sugar-Sensing Hydrogels”, Colm Delaney, Larisa Florea, Danielle Bruen and Dermot Diamond, March **2018**.

## Contents

### Chapter 4: Water-Soluble Polymerisable Boronic Acids: Combining an Adaptable One-Step Synthesis with an In-Depth Understanding of pH and Glucose Response

<b>4.1 Abstract</b>	<b>130</b>
<b>4.2 Introduction</b>	<b>131</b>
<b>4.3 Experimental</b>	<b>133</b>
4.3.1 Materials and Methods	133
4.3.2 Synthesis of BA Monomers ( <i>o</i> -BA, <i>m</i> -BA and <i>p</i> -BA)	134
4.3.2.1 General Synthesis of BA Monomers	134
4.3.2.2 Synthesis of <i>o</i> -BA ( <i>N</i> -(2-boronobenzyl)-2-(methacryloyloxy)- <i>N,N</i> -dimethylethan-1-ammonium bromide)	134
4.3.2.3 Synthesis of <i>m</i> -BA ( <i>N</i> -(3-boronobenzyl)-2-(methacryloyloxy)- <i>N,N</i> -dimethylethan-1- ammonium bromide)	135
4.3.2.4 Synthesis of <i>p</i> -BA ( <i>N</i> -(4-boronobenzyl)-2-(methacryloyloxy)- <i>N,N</i> -dimethylethan-1- ammonium bromide)	136
4.3.3 <sup>11</sup> B NMR Titrations	137
4.3.4 Fluorescence Titrations	138
<b>4.4 Results and Discussion</b>	<b>139</b>
4.4.1 Synthesis of BA Monomers	139
4.4.2 NMR Spectroscopy	139
4.4.2.1 <sup>1</sup> H NMR Spectroscopy	139
4.4.2.2 <sup>11</sup> B NMR Spectroscopy	140
4.4.3 Fluorescence Spectroscopy	143
4.4.3.1 pH Titrations	143
4.4.3.2 Glucose Titrations	145
<b>4.5 Conclusions and Future Work</b>	<b>148</b>
<b>4.6 References</b>	<b>149</b>

## 4.1 Abstract

Diabetes is one of the leading causes of death every year due to the associated chronic complications including heart disease, kidney failure, blindness and amputation. It is well accepted that these risks can be reduced by monitoring physiological glucose levels, where glucose monitors account for approximately 85% of the global biosensor market. Chemical sensing using boronic acids (BAs) has attracted much attention over the last few decades, where most of these BAs have been paired with fluorophores to exhibit dramatic optical changes directly related to glucose concentrations. More recently, fluorescent BA derivatives with a propensity to aggregate have offered a viable solution to small-molecule chemical glucose detectors for real-time monitoring of glucose. Only a handful of groups have developed charged saccharide sensors in this regard, where they have all been coupled with fluorescent moieties, such as pyrene.

In this chapter, three monomeric BA derivatives (*o*-BA, *m*-BA and *p*-BA) are described that display an innate fluorescence on aggregation in the presence of glucose. These monomers contain no fluorescent moieties in their acetylcholine-like structure, where the increased fluorescence is based solely on aggregation of the zwitterionic monomers on glucose binding. An adaptable methodology for synthesising polymerisable boronic acids is described through which we have generated this new family of fluorescent, water-soluble, zwitterionic BA monomers. The glucose binding ability of these monomers has been characterised using fluorescence and  $^{11}\text{B}$  NMR spectroscopy.  $^{11}\text{B}$  NMR spectroscopy allowed for characterisations of the neutral and anionic form of BA, across a pH range of 3-13, in the absence and presence of glucose. Similarly, fluorescence spectroscopy allowed for the  $\text{pK}_a$  of each BA monomer to be estimated for optimised glucose sensing. The *p*-BA monomer exhibited the largest fluorescence increase upon glucose addition, of 177% at pH 7.4 in the presence of 150 mM glucose. Using these novel polymerisable BA derivatives would enable charged boronic acid monomers to be produced that are tailored for the incorporation in to glucose responsive polymeric matrices.

## 4.2 Introduction

Boronic acids (BAs) are abiotic compounds that can be considered ‘green compounds’ with low-toxicity.<sup>1</sup> As a result, BAs have been widely studied for their chemo-sensing abilities under physiological conditions.<sup>2,3</sup> BAs are electron deficient, thereby rendering the boron atom Lewis acidic.<sup>4</sup> The trigonal planar geometry in the BA group, arising from the low energy *p*-orbital orthogonal to the boron atom, supports the formation of strong, reversible interactions with diol-containing compounds, such as saccharides, neurotransmitters like dopamine, other bio-analytes including amino alcohols,  $\alpha$ -amino acids and  $\alpha$ -hydroxyl acids, as well as anions such as cyanide and fluoride.<sup>1,5-8</sup> This binding is reversible and consequently has attracted much attention over the last decade for glucose sensing applications.<sup>9-13</sup>

Typically, the  $pK_a$  of a phenyl-BA moiety is approximately 8.7.<sup>14</sup> When the BA group is close to electron-withdrawing groups, the  $pK_a$  can be reduced and similarly, when the BA group is near electron-donating groups, the  $pK_a$  can be increased.<sup>4</sup> A reduction in the  $pK_a$  of phenyl-BA moieties is favoured for sensing glucose close to physiological pH. Binding glucose allows for the formation of *cis*-1,2- or *cis*-1,3-cyclic boronate diesters, preferably under alkaline conditions due to the basic  $pK_a$  of the phenyl-BA moiety.<sup>11-13</sup> Due to the mild electron-withdrawing capability of diols, the  $pK_a$  of the BA-ester is reduced typically by 2-3 units, upon sugar complexation.<sup>4</sup> As sugar binding preferentially occurs close to the  $pK_a$  of the BA-ester, performing measurements around this pH is optimum for sensing applications.<sup>13</sup>

Variations in the molecular structure of BA derivatives upon sugar binding, can be used to probe saccharide-BA interactions using various spectroscopic approaches, such as infra-red,<sup>15</sup> UV-visible,<sup>16,17</sup> fluorescence,<sup>18,19</sup> Raman<sup>20</sup> and nuclear magnetic resonance spectroscopy.<sup>17,21</sup> Some of these approaches are also being investigated for use in continuous non-invasive sensing platforms.<sup>22</sup> In particular, <sup>11</sup>B NMR spectroscopy has been used by Anslyn *et al.*<sup>21,23</sup> for rapid understanding of diol-binding to BAs, by monitoring the B-N interaction in protic and aprotic media.

Other recent related investigations have involved monitoring changes in fluorescence to track BA-sugar interactions. Primarily, this type of sensing has been carried out in solution, using direct (in which the fluorophore is a component of the BA derivative) and indirect (in which the fluorophore is a separate entity from the BA derivative) sensing approaches.<sup>11,19,20,24</sup> In a direct sensing approach as described in



Chapter 2, the BA moiety and the fluorophore are incorporated within the same structure, and the fluorescence of the fluorophore is modulated by the presence of the diol moiety.<sup>11, 19, 20, 24</sup>

In contrast, with the indirect sensing approach, the BA moiety and fluorophore exist as two distinct molecules, as described in Chapter 3.<sup>25</sup> Commonly, a cationic BA is used to induce quenching in an anionic fluorophore through the formation of a non-fluorescent ground-state complex. Upon the introduction of glucose, this electrostatic interaction is inhibited, thereby initiating dissociation of the ground-state complex and restoration of the fluorescence.<sup>26</sup> Singaram and co-workers have pioneered this idea, and have successfully immobilised this sensing arrangement within a hydrogel.<sup>27</sup>

Recently, several groups have also turned to supramolecular interactions, through the intelligent design of boronic acids with a propensity to aggregate, as a means to generate excimer formation in the presence of saccharides. Liu *et al.*,<sup>28</sup> used a polythiophene matrix, containing a zwitterionic boronic acid appended to a C<sub>6</sub> chain, to exploit saccharide-induced changes in fluorescence caused by multivalent binding. Similarly, Yam *et al.*,<sup>29</sup> employed a combination of a water soluble boronic acid polymer and a pyrene-based fluorophore substituted with a quaternized ammonium chain. Upon glucose binding, creation of a polyanion within the boronic acid chains induced aggregation via electrostatic interactions, thereby resulting in a strong excimer fluorescence. The 1:2 glucose:BA interaction was a significant factor favouring aggregation as this brought the BA moieties into close proximity. Extending this multi-linkage interaction between saccharide and boronic acid was achieved very elegantly by Jiang *et al.*<sup>30</sup> using a pyrene fluorophore attached to a cationic pyridinium BA via a short alkyl amide linker. Pyrene excimer emission occurred in the presence of glucose, leading to a significant increase in fluorescence. Measurement of the hydrodynamic diameter confirmed that in the presence of glucose, rather than fructose, a higher degree of aggregation occurred, which was attributed to the 1:2 glucose:BA interaction.

Comparatively, few examples exist of BA-fluorescence sensing in gel matrices, most likely due to the scarcity of polymerisable fluorophores and charged BA monomers.<sup>27, 31</sup> This has motivated us to investigate new approaches for creating building blocks of fluorescent BA polymeric materials that respond to glucose. Herein, we report facile and highly-adaptable, one-step procedures for producing

cationic, water-soluble, monomeric BA derivatives (*o*-BA, *m*-BA and *p*-BA, see Figure 4.1) that exhibit an innate fluorescent response to glucose.

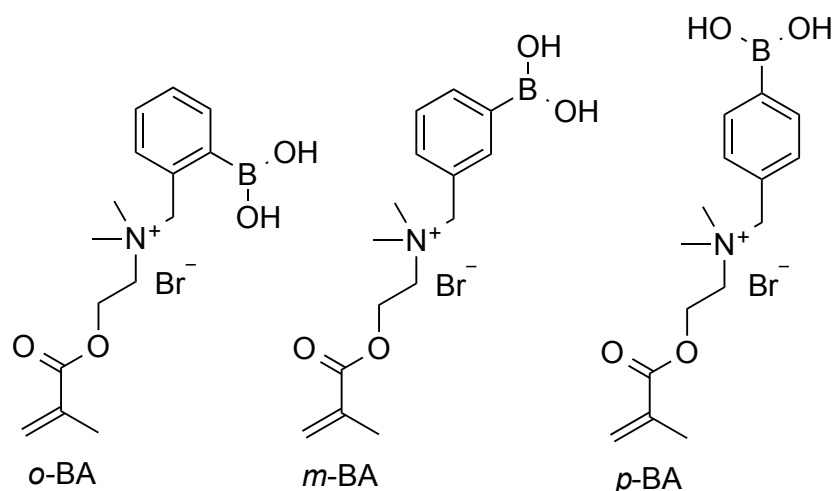


**Figure 4.1.** Monomeric BA derivatives *o*-BA, *m*-BA and *p*-BA.

## 4.3 Experimental

### 4.3.1 Materials and Methods

2-(Bromomethylphenyl)boronic acid (100%), 3-(bromomethylphenyl)boronic acid (95%) and 4-(bromomethylphenyl)boronic acid (95%) were acquired from Fluorochem, UK and used as received. 2-(Dimethylamino)ethyl methacrylate (98%), anhydrous acetonitrile (CH<sub>3</sub>CN) and anhydrous dichloromethane (CH<sub>2</sub>Cl<sub>2</sub>) were purchased from Sigma Aldrich, Ireland and used as received. Solvents used were methanol (CH<sub>3</sub>OH), acetonitrile (CH<sub>3</sub>CN) and dichloromethane (CH<sub>2</sub>Cl<sub>2</sub>). Deionised water (18.2 MΩ·cm<sup>-1</sup>) (DI H<sub>2</sub>O) used was purified using a Milli-Q Water Purification System (Merck Millipore, Darmstadt, Germany). All reactions were conducted under an inert atmosphere of nitrogen.

Structural <sup>1</sup>H, <sup>13</sup>C and <sup>11</sup>B NMR studies were carried out on a Bruker Avance Ultrashield 600 MHz spectrometer. <sup>11</sup>B NMR experiments used BF<sub>3</sub> in deuterated methanol as an external standard. Deuterium oxide (D<sub>2</sub>O) was the solvent used for all NMR measurements. The fluorescence of the BA monomers was recorded using a JASCO FP-8300 spectrofluorometer at 20 °C and UV-visible measurements were carried out on a Varian Cary 50 Probe spectrophotometer, in a precision cell made from Quartz Suprasil that had a path length of 10 mm and a volume of 1.4 mL.

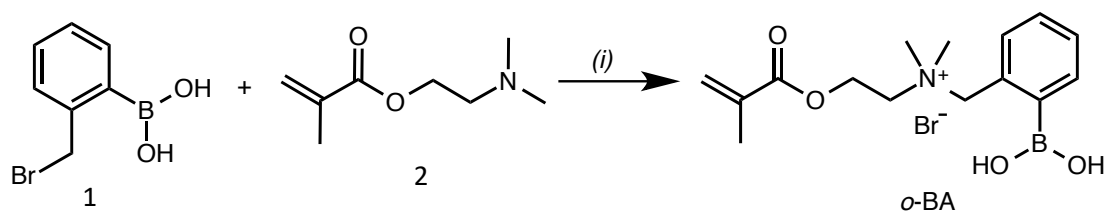
Fourier Transform Infrared (FT-IR) spectroscopy measurements were carried out on a Perkin Elmer Spectrum GX. All pH measurements were carried out using a VWR sympHony SP70P pH meter. The phosphate buffer solution at pH 7.4 was prepared from 0.1 M potassium dihydrogen phosphate (KH<sub>2</sub>PO<sub>4</sub>; 100 mL) and 0.1 M sodium hydroxide (NaOH; 78 mL) salts and was made up to 200 mL using deionised water.

#### 4.3.2 Synthesis of BA Monomers (o-BA, m-BA and p-BA)

##### 4.3.2.1 General Synthesis of BA Monomers

The BA monomers, *o*-BA, *m*-BA and *p*-BA were synthesised according to this general procedure. First the phenylBA starting material was dissolved in anhydrous CH<sub>2</sub>Cl<sub>2</sub> or CH<sub>3</sub>CN and 2-(dimethylamino)ethyl methacrylate was added dropwise. The mixture was left to stir for 24h between 20-35 °C. After this time, the solvent was evaporated in *vacuo* and the resulting white solid material was washed with cold diethyl ether or CH<sub>2</sub>Cl<sub>2</sub> (60-65%).

##### 4.3.2.2 Synthesis of *o*-BA (*N*-(2-boronobenzyl)-2-(methacryloyloxy)-*N,N*-dimethylethan-1- ammonium bromide)

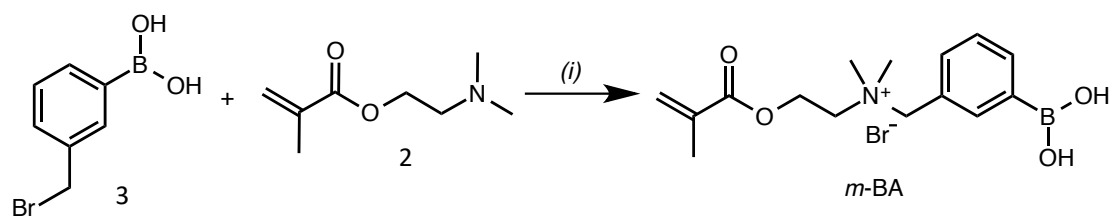


**Scheme 4.1.** Synthesis of *o*-BA. (i) CH<sub>2</sub>Cl<sub>2</sub>, N<sub>2</sub>, 35 °C, 24h (60%).

*o*-BA was prepared via a one-step nucleophilic substitution reaction, depicted by Scheme 4.1. 2-(Bromomethylphenyl)boronic acid (compound **1**; 1.00 g, 4.6 mmol) was stirred at 35 °C in anhydrous CH<sub>2</sub>Cl<sub>2</sub> (30 mL) under an inert atmosphere of N<sub>2</sub>. 2-(Dimethylamino)ethyl methacrylate (compound **2**; 0.86 mL, 5.1 mmol) was added dropwise to the BA while stirring. The reaction was stirred for a further 24h at 35 °C. The reaction was monitored by thin layer chromatography (TLC) using hexane:ethyl acetate (1:10) as the mobile phase. The reaction mixture was concentrated under reduced pressure and dried. The resulting yellow oil was washed with diethyl ether (100 mL) and CH<sub>2</sub>Cl<sub>2</sub> (100 mL) and filtered, to retrieve a white crystalline solid. This solid was dried in a desiccator overnight. A sample of the white crystalline solid was

taken for NMR analysis in D<sub>2</sub>O, which confirmed that *o*-BA was produced in 60% yield. <sup>1</sup>H NMR (600 MHz, 20 °C, D<sub>2</sub>O), δ: 7.7 (1H, *dd*, *J* = 3 and 8 Hz, CH, H2), 7.5 (3H, *m*, CH, H-3,4,5), 6.1 (1H, *s*, CH<sub>2</sub>, H11), 5.7 (1H, *s*, CH<sub>2</sub>, H12), 4.8 (2H, *s*, CH<sub>2</sub>, H7), 4.6 (2H, *s*, CH<sub>2</sub>, H9), 3.8 (2H, *m*, CH<sub>2</sub>, H8), 3.0 (6H, *s*, CH<sub>3</sub>, H6), 1.9 (3H, *s*, CH<sub>3</sub>, H9), ppm (Figure C1). <sup>13</sup>C NMR (150 MHz, 20 °C, D<sub>2</sub>O), δ: 168.4 (C=O), 134.4 (C-H2), 133.9 (C-H4), 130.3 (C-H3), 127.7 (CH<sub>2</sub>-Vinyl), 130.0, 68.0 (C-H5), 63.4 (CH<sub>2</sub>, H8), 58.4 (CH<sub>2</sub>, H9), 50.0 (CH<sub>3</sub>-Amine), 17.2 (CH<sub>3</sub>-Vinyl) ppm (Figure C2). <sup>11</sup>B NMR (192 MHz, 20 °C, D<sub>2</sub>O), δ: 29.24 (1B, B(OH)<sub>2</sub>) ppm (Figure C3). HRMS (m/z) calculated for [M-Br]<sup>+</sup> C<sub>15</sub>H<sub>23</sub>BNO<sub>4</sub><sup>+</sup> calculated 292.1717, found 292.1715. FT-IR: 3355 (B-OH), 3228 (B-OH), 2971 (C=C-H), 1726 (C=O), 1638 (C=C), 1598 (C=C) and 1489 (C=C) cm<sup>-1</sup> (Figure C4). UV-visible spectroscopy: 270 nm in DI H<sub>2</sub>O (Figure C5). Fluorescence spectroscopy: 327 nm (low pH), 367 nm (high pH) as excitation wavelengths and the emission wavelength at 460 nm (Figure C6). *o*-BA is soluble in H<sub>2</sub>O, CH<sub>3</sub>OH and (CH<sub>3</sub>)<sub>2</sub>SO and is insoluble in other organic solvents.

#### 4.3.2.3 Synthesis of *m*-BA (*N*-(3-boronobenzyl)-2-(methacryloyloxy)-*N,N*-dimethylethan-1-ammonium bromide)

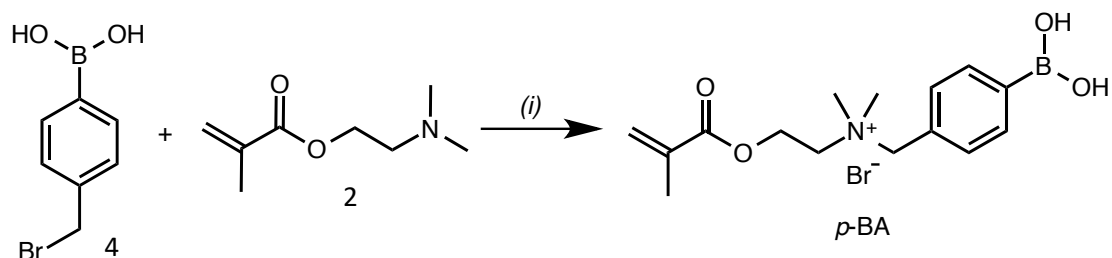


**Scheme 4.2.** Synthesis of *m*-BA. (i) CH<sub>3</sub>CN, N<sub>2</sub>, 20 °C, 24h (63%).

*m*-BA was synthesised by a nucleophilic substitution reaction, depicted by Scheme 4.2. 3-(Bromomethylphenyl)boronic acid (compound **3**; 1.01 g, 4.7 mmol) was stirred at room temperature in anhydrous CH<sub>3</sub>CN (40 mL) and anhydrous CH<sub>3</sub>OH (1 mL) to dissolve. 2-(Dimethylamino)ethyl methacrylate (compound **2**; 0.86 mL, 5.1 mmol) was added dropwise to the BA while stirring. The reaction was stirred under N<sub>2</sub> for 24h. The reaction was monitored by TLC using CH<sub>3</sub>OH:CH<sub>2</sub>Cl<sub>2</sub> (1:4) as the mobile phase. The reaction mixture was concentrated under a reduced pressure and dried and CHCl<sub>2</sub> was added. The mixture was sonicated and filtered. The precipitate was washed and sonicated with CH<sub>2</sub>Cl<sub>2</sub> and dried under vacuum. A sample of the white crystalline solid was taken for NMR analysis in D<sub>2</sub>O, which confirmed that *m*-BA was

produced in 63% yield.  $^1\text{H}$  NMR (600 MHz, 20 °C,  $\text{D}_2\text{O}$ ) for *m*-BA,  $\delta$ : 7.7 (1H, *dd*,  $J$  = 3 and 8 Hz, CH, H1), 7.5 (3H, *m*, CH, H-3,4,5), 6.1 (1H, *s*,  $\text{CH}_2$ , H11), 5.7 (1H, *s*,  $\text{CH}_2$ , H12), 4.8 (2H, *s*,  $\text{CH}_2$ , H9), 4.6 (2H, *s*,  $\text{CH}_2$ , H7), 3.8 (2H, *m*,  $\text{CH}_2$ , H8), 3.0 (6H, *s*,  $\text{CH}_3$ , H6), 1.9 (3H, *s*,  $\text{CH}_3$ , H10), ppm (Figure C7).  $^{13}\text{C}$  NMR (150 MHz, 20 °C,  $\text{D}_2\text{O}$ ),  $\delta$ : 168.3 (C=O), 137.7 (C-H1), 135.6 (C-H3), 135.1 (C-H5), 134.5 (CH-4), 128.6 (CH-Vinyl), 126.2 ( $\text{CH}_2$ -Vinyl), 69.4 ( $\text{CH}_2$ -Amine), 62.5 ( $\text{CH}_2$ -Amine), 58.3 (CH-9), 50.1 ( $\text{CH}_3$ -Amine), 17.2 ( $\text{CH}_3$ -Vinyl) ppm (Figure C8).  $^{11}\text{B}$  NMR (192 MHz, 20 °C,  $\text{D}_2\text{O}$ ),  $\delta$ : 24.0 (1B, *s*, B-(OH) $_2$ ) ppm (Figure C9). HRMS (*m/z*) calculated for  $[\text{M-Br}]^+$   $\text{C}_{15}\text{H}_{23}\text{BNO}_4^+$  calculated 292.1717, found 292.1718. FT-IR: 3355 (B-OH), 2959 (C=C-H), 1717 (C=O), 1635 (C=C), 1603 (C=C) and 1437 (C=C)  $\text{cm}^{-1}$  (Figure C10). UV-visible spectroscopy: 270 nm in DI  $\text{H}_2\text{O}$  and  $\text{CH}_3\text{OH}$  (Figure C11). Fluorescence spectroscopy: 328 nm (low pH), 372 nm (high pH) and the emission wavelength at 466 nm (Figure C12). *m*-BA is soluble in  $\text{H}_2\text{O}$ ,  $\text{CH}_3\text{OH}$  and  $(\text{CH}_3)_2\text{SO}$  and is insoluble in other organic solvents.

#### 4.3.2.4 Synthesis of *p*-BA (*N*-(4-boronobenzyl)-2-(methacryloyloxy)-*N,N*-dimethylethan-1- ammonium bromide)



**Scheme 4.3.** Synthesis of *p*-BA. (i)  $\text{CH}_2\text{Cl}_2$ ,  $\text{N}_2$ , 20 °C, 24h (65%).

*p*-BA was prepared by a nucleophilic substitution reaction, as depicted in Scheme 4.3. 4-(bromomethylphenyl)boronic acid (compound **4**; 1.00 g, 4.6 mmol) was stirred at room temperature in anhydrous  $\text{CH}_2\text{Cl}_2$  (30 mL) to dissolve. 2-(Dimethylamino)ethyl methacrylate (compound **2**; 0.86 mL, 5.1 mmol) was added dropwise to the BA while stirring. The reaction was stirred under  $\text{N}_2$  for 24h. The reaction was monitored by TLC using hexane:ethyl acetate (1:10) as the mobile phase. To the reaction mixture diethyl ether (50 mL) was added, which turned the mixture cloudy. The mixture was sonicated and the diethyl ether was then decanted off. This was repeated three more times. The material was dried under vacuum to

retrieve a white crystalline solid. A sample of the white crystalline solid was taken for NMR analysis in D<sub>2</sub>O, which confirmed that *p*-BA was produced in 65% yield. <sup>1</sup>H NMR (600 MHz, 20 °C, D<sub>2</sub>O), δ: 7.7 (2H, *d*, *J* = 8 Hz, CH-2,3), 7.4 (2H, *d*, *J* = 8 Hz, CH-1,4), 6.0 (1H, *s*, CH-10), 5.6 (1H, *t*, *J* = 1 and 2 Hz, CH-11), 4.5 (2H, *s*, CH<sub>2</sub>-8), 4.5 (2H, *d*, *J* = 5 Hz, CH<sub>2</sub>-5), 3.6 (2H, *m*, CH<sub>2</sub>-7), 3.0 (6H, *s*, CH<sub>3</sub>-6), 1.81 (3H, *s*, CH<sub>3</sub>-9) ppm (Figure C13). <sup>13</sup>C NMR (150 MHz, 20 °C, D<sub>2</sub>O), δ: 168.3 (C=O), 135.1 and 134.0 (C-H<sub>2</sub>,4), 133.0 and 132.3 (C-H<sub>1</sub>,5), 127.7 (CH<sub>2</sub>-Vinyl), 69.0 (CH<sub>2</sub>, H7), 62.6 (CH<sub>2</sub>, H8), 58.3 (CH<sub>2</sub>, H9), 50.2 (CH<sub>3</sub>-Amine), 17.2 (CH<sub>3</sub>-Vinyl) ppm (Figure C14). <sup>11</sup>B NMR (192 MHz, 20 °C, D<sub>2</sub>O), δ: 29.2 (1B, B(OH)<sub>2</sub>) ppm (Figure C15). HRMS (*m/z*) calculated for [M-Br]<sup>+</sup> C<sub>15</sub>H<sub>23</sub>BNO<sub>4</sub><sup>+</sup> calculated 292.1717, found 292.1716. FT-IR: 3332 (B-OH), 2960 (C=C-H), 1716 (C=O), 1613 (C=C), 1635 (C=C) and 1414 (C=C) cm<sup>-1</sup> (Figure C16). UV-visible spectroscopy: 270 nm in DI H<sub>2</sub>O (Figure C17). Fluorescence spectroscopy: 325 nm (low pH), 370 nm (high pH) and emission wavelength at 460 nm (Figure C18). *p*-BA is soluble in H<sub>2</sub>O, CH<sub>3</sub>OH and (CH<sub>3</sub>)<sub>2</sub>SO and is insoluble in other organic solvents.

#### 4.3.3 <sup>11</sup>B NMR Titrations

For <sup>11</sup>B NMR measurements, a quartz thin walled NMR sample tube was used, which was acquired from Fluorochem, UK (W507-pp-QTZ 7" 5 mm). BF<sub>3</sub>.OCH<sub>3</sub> in CDCl<sub>3</sub> was used as an external reference for <sup>11</sup>B NMR spectra. Processing for <sup>11</sup>B NMR spectra included line broadening by 10 Hz.

Samples for <sup>11</sup>B NMR pH titrations were prepared using 30.5 mg of the appropriate BA dissolved in D<sub>2</sub>O (995 μL) with acetic acid (5 μL; 17.4 M). For pH titrations containing ten equivalences of glucose, the samples were prepared using 30.5 mg of the appropriate BA dissolved in D<sub>2</sub>O (826 μL) with acetic acid (5 μL; 17.4 M) and glucose (164 μL; 5 M in D<sub>2</sub>O), so that the final concentrations of the BA was 82 mM, glucose was 820 mM and the pH was ~pH 3. The initial pH was measured using a VWR sympHony SP70P pH meter and the samples were titrated with various stock solutions of NaOH. In all <sup>11</sup>B NMR spectra, a peak corresponding to boric acid was found at 19 ppm in acidic pH solutions and at 2 ppm in basic solutions as seen in Figure 4.2.

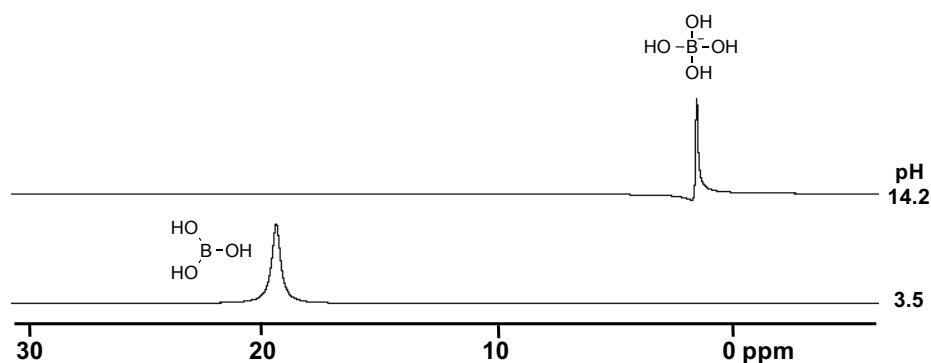


**Figure 4.2.**  $^{11}\text{B}$  NMR of boric acid in  $\text{D}_2\text{O}$  at pH 3.5 (bottom) and pH 14.2 (top).

#### 4.3.4 Fluorescence Titrations

The fluorescence of the BA monomers was recorded using a JASCO FP-8300 spectrofluorometer at 20 °C in a precision cell made from Quartz Suprasil that had a path length thickness of 10 mm and a volume of 1.4 mL.

Samples were prepared from stock solutions of the appropriate BA, so that the final concentration of the BA was 1 mM in  $\text{D}_2\text{O}$ . Acetic acid (10  $\mu\text{L}$ ; 17.4 M) was then added so that the pH was pH 2.9 and the total volume was 3 mL. The pH was measured using a VWR sympHony SP70P pH meter. The sample was titrated with various concentrations of NaOH and the pH of the sample was measured after each addition. For pH titrations containing glucose, a glucose stock solution of 5 M in DI  $\text{H}_2\text{O}$  was prepared. The samples contained the appropriate BA (1 mM), acetic acid (10  $\mu\text{L}$ ; 17.4 M) and glucose (6  $\mu\text{L}$ ; 5 M in DI  $\text{H}_2\text{O}$ ) made up to 3 mL with DI  $\text{H}_2\text{O}$ . For the glucose titrations, the samples contained the appropriate BA (1 mM) in DI  $\text{H}_2\text{O}$ , where the pH was pH 8 for *o*-BA and *p*-BA and pH 7.5 for *m*-BA.

The  $\text{pK}_a$  for each BA derivative in the absence and presence of glucose was estimated via fluorescence pH titrations using Equation 4.1, where  $Y$  is the increase in the normalised intensity,  $a$  is the sigmoid height,  $b$  is the slope coefficient,  $c$  is the  $x$ -value at the inflection of the sigmoid,  $d$  is the baseline offset,  $e$  is the symmetry parameter for the sigmoid and  $x$  is the pH value. The data was analysed using Excel Solver from Microsoft Excel 2016.

$$Y = \left[ \frac{a}{(1 + \exp[b(x-c)])^e} \right] + d \quad (4.1)$$

## 4.4 Results and Discussion

### 4.4.1 Synthesis of BA Monomers

These cationic BA monomers were synthesised by quaternisation of 2-(dimethylamino)ethyl methacrylate with a bromomethyl substituted phenylboronic acid to form the BA-ammonium bromide salts. This synthesis can very easily be adapted to produce a wide range of monomeric BA derivatives by simply interchanging the polymerisable chain. In this way, a library of monomeric BAs can be easily produced. Upon quaternization of the nitrogen atom, the BA monomers are rendered water-soluble, which is an advantage for subsequent polymerisation strategies and for solution-based sensing applications in aqueous media.

### 4.4.2 NMR Spectroscopy

#### 4.4.2.1 <sup>1</sup>H NMR Spectroscopy

In the <sup>1</sup>H NMR spectrum for *o*-BA, proton H2 appears furthest downfield (Figure 4.3). This proton experiences the most deshielding effect due to the adjacent B atom. Similarly, H1 and H3 in the *m*-BA spectrum and H2 and H4 in the *p*-BA spectrum, appear the furthest downfield. The multiplicity of these chemical shifts also differs due to the substitution of the BA group. In the *o*-BA NMR spectrum, protons H3, H4 and H5 are all equivalent and appear at the same chemical shift. In the *m*-BA NMR spectrum the protons sit in different chemical environments, which allows us to see individual shifts for each proton. In the *p*-BA <sup>1</sup>H NMR spectrum, the BA group is orientated *para* to the CH<sub>2</sub>-linker, creating a symmetry through the phenyl ring. Protons H2 and H4, and H1 and H5 therefore appear as a pair of doublets.



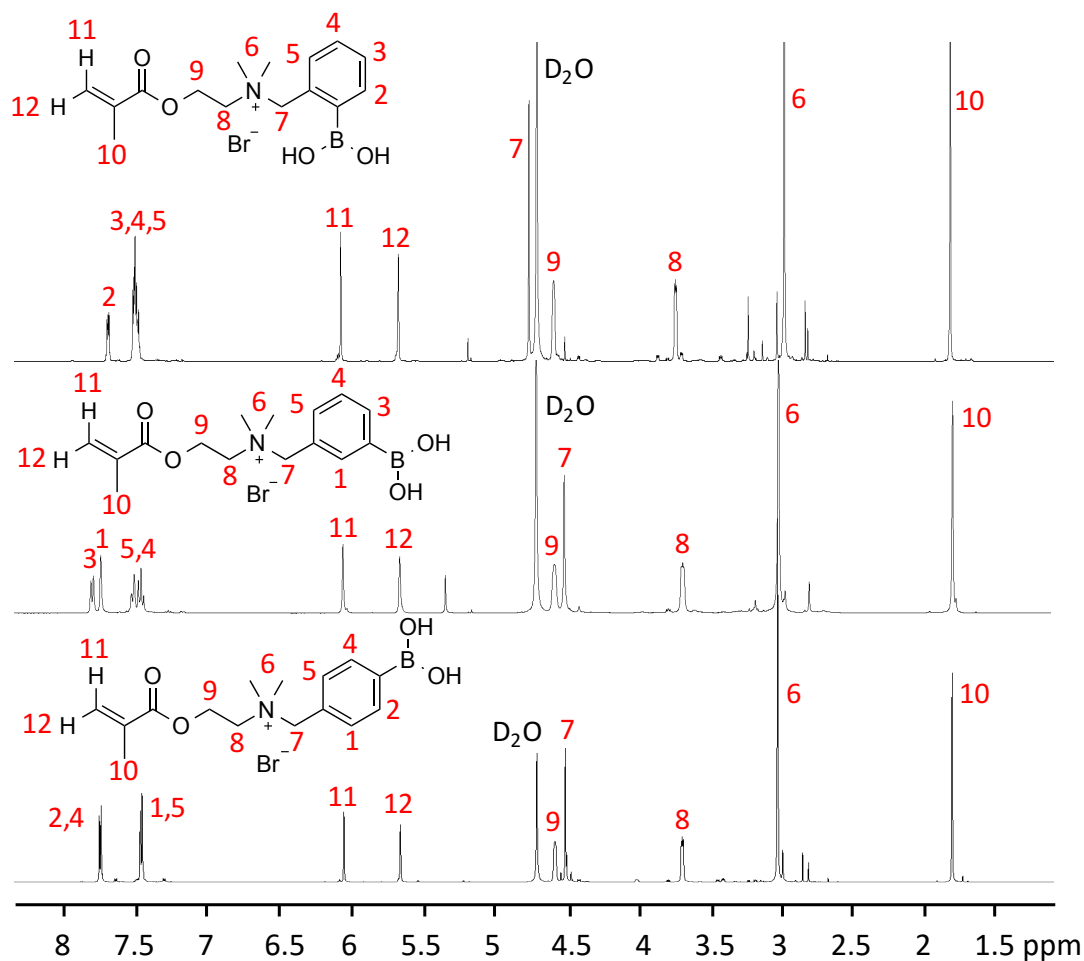


**Figure 4.3.**  $^1\text{H}$  NMRs for all three BA monomers in  $\text{D}_2\text{O}$ , *o*-BA (top), *m*-BA (middle) and *p*-BA (bottom).

#### 4.4.2.2 $^{11}\text{B}$ NMR Spectroscopy

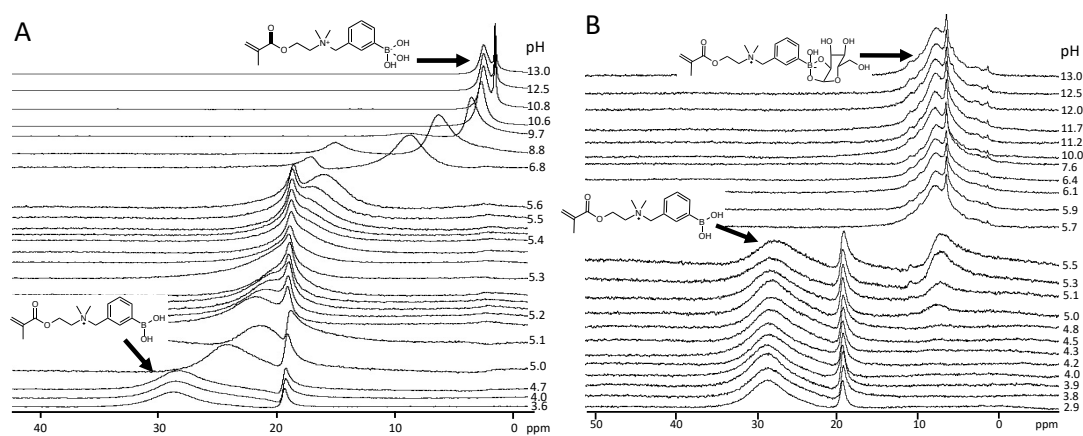


**Figure 4.4.**  $^{11}\text{B}$  NMR pH titration in  $\text{D}_2\text{O}$  for *m*-BA (82 mM) in the absence of glucose (A) and in the presence of 10 equivalents glucose (820 mM) (B). The peak at  $\sim 19$  ppm is the impurity boric acid. For details regarding the boric acid peak refer to Figure 4.2.

$^{11}\text{B}$  NMR proved a useful and convenient characterisation tool to provide insights into the mechanism of glucose binding, and to probe the effect of pH on the BA-derivatives.  $^{11}\text{B}$  NMR spectra clearly show that in acidic pH media the neutral  $\text{sp}^2$  hybridised boron atom is favoured, whereas at a basic pH, the anionic  $\text{sp}^3$  hybridised form predominates. This can be seen in Figure 4.4, which depicts the  $^{11}\text{B}$  NMR pH titration for *m*-BA before (A) and after (B) glucose addition, with the first spectrum recorded at  $\sim\text{pH}$  3. The pH was sequentially increased to  $\sim\text{pH}$  13 by addition of NaOH in  $\text{D}_2\text{O}$ . In Figure 4.4A between pH 3.6 and 4.7, the BA group is in the neutral  $\text{sp}^2$  hybridised form, seen as the broad singlet at 28.6 ppm. As the pH of the solution is gradually raised, this peak shifted to 2.5 ppm, which is indicative of the anionic  $\text{sp}^3$  hybridised form of *m*-BA. Repeating this experiment in the presence of 10 equivalents of glucose enabled the  $^{11}\text{B}$  chemical shift for the anionic boronate-ester form of *m*-BA to be tracked (Figure 4.4B). Initially, the neutral BA form appeared between pH 2.9-5.5. However, at pH 5.0 a peak at 6.4 ppm attributed to the anionic boronate form appeared along with the neutral BA form at 28.6 ppm. The anionic boron peak appears at a lower pH in the presence of glucose (Figure 4.4B). This can be rationalised by the reduced  $\text{pK}_a$  of the boronate-ester form compared to the boronate form (Figure 4.4A).<sup>4</sup> Results for  $^{11}\text{B}$  NMR titrations for *o*-BA and *p*-BA are shown in Figure 4.5. From Table 4.1, the  $^{11}\text{B}$  shifts for each form of the BAs can be found.

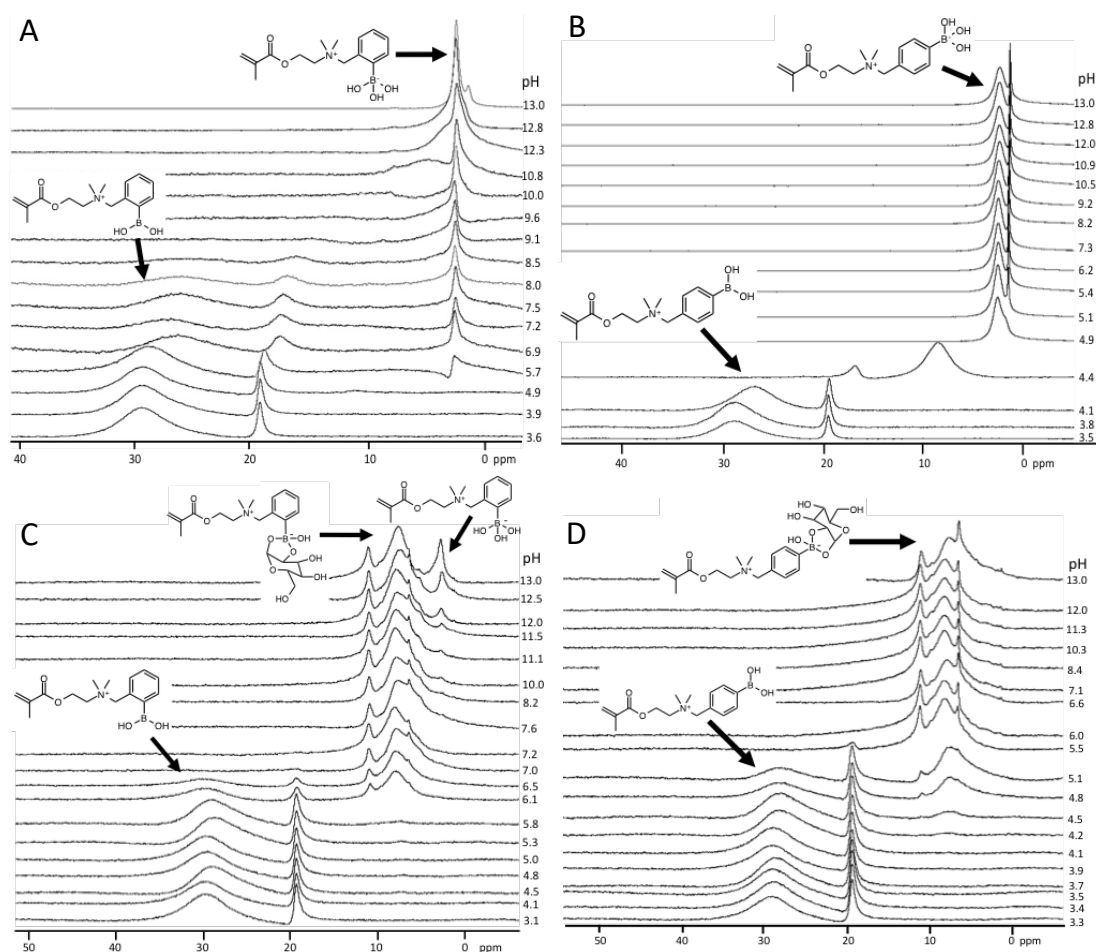


**Figure 4.5.** (A)  $^{11}\text{B}$  NMR pH titration in the absence of glucose for *o*-BA (82 mM). (B)  $^{11}\text{B}$  NMR pH titration in the absence of glucose for *p*-BA (82 mM). (C)  $^{11}\text{B}$  NMR pH titration in the presence of 10 equivalents of glucose (820 mM) for *o*-BA. (D)  $^{11}\text{B}$  NMR pH titration in the presence of 10 equivalents of glucose (820 mM) for *p*-BA. The solvent for all titrations was  $\text{D}_2\text{O}$ .

**Table 4.1.**  $^{11}\text{B}$  NMR shifts (ppm) for the neutral BA, anionic BA and anionic BA-ester for all BA monomers.

$^{11}\text{B}$ NMR Chemical Shifts	<i>o</i> -BA	<i>m</i> -BA	<i>p</i> -BA
BA	29.5	28.6	28.6
Boronate	2.8	2.5	2.6
Boronate-Ester	7.8	6.4	8.0

#### 4.4.3 Fluorescence Spectroscopy

Once it was established that the BA monomers could successfully bind glucose through  $^{11}\text{B}$  NMR studies, the monomers were investigated for their ability to bind glucose by an optical fluorescence approach. In order to choose the optimum pH for glucose binding, the  $\text{pK}_a$  of each BA derivative was determined.

##### 4.4.3.1 pH Titrations

Figure 4.6 compares the fluorescence of the BA monomers in solutions of pH 4, 7.4 and 11.5. *m*-BA was the most fluorescent, being 14 times more fluorescent than *p*-BA and 3 times more fluorescent than *o*-BA at pH 11.5. *o*-BA was 5 times more fluorescent than *p*-BA. The difference in fluorescence between the compounds could be attributed to the BA group substitution. The other group directly attached to the phenyl ring is the  $\text{CH}_2$  linker in all BA molecules. This linker can be considered slightly electron-donating, where it can activate the ring in the *ortho/para* position.<sup>32</sup> Consequently, as a result of resonance effects it's possible that the electron density around the ring could be slightly increased at these locations, which quenches the fluorescence of *o*-BA and *p*-BA more in comparison to *m*-BA.

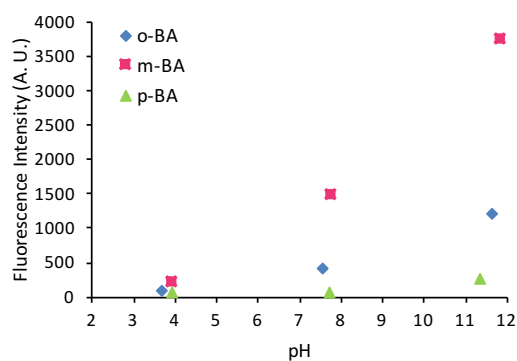


**Figure 4.6.** Fluorescence emission in  $\text{H}_2\text{O}$  of the three BA monomers (1 mM) at approximately pH 4.0 7.7 and 11.5, where the excitation wavelength was 367, 372 and 370 nm for *o*-BA, *m*-BA and *p*-BA, respectively, corresponding to the anionic form of each BA.

At low pH, all three BAs were non-emissive. When the pH of the solution was increased to above pH 7, a new excitation band at  $\sim 370$  nm was observed, with an isosbestic point centred at 335 nm. This excitation band resulted in a strong fluorescence centred at  $\sim \lambda_{\text{max}} = 460$  nm (Figure 4.7, Figures C19-C23). This is likely attributed to the formation of a boronic acid zwitterion that serves to promote aggregation, thereby producing a fluorescent excimer. The  $\text{pK}_a$  for each BA monomer

system was determined by pH titrations, using the fluorescence maximum at each pH value to construct a sigmoidal plot.

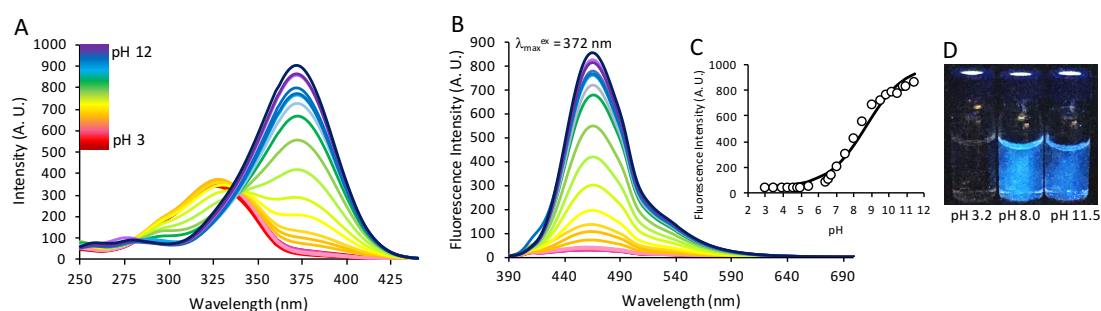


**Figure 4.7.** Excitation and fluorescence emission spectra for *m*-BA (1 mM) in H<sub>2</sub>O. (A) Excitation spectra as a function of pH showing maxima at 329 nm (low pH) and 372 nm (high pH), and an isosbestic point at 335 nm. (B) Emission spectra as a function of pH with  $\lambda_{\text{ex}} = 372$  nm, showing fluorescence emission intensity increasing with pH, with maximum emission at 466 nm. (C) The  $\text{pK}_a$  for *m*-BA was estimated to be 8.7 from the emission spectra taken at 466 nm. (D) Photo showing the fluorescence increase for *m*-BA solutions under 365 nm irradiation at pH 3.2, 8.0 and 11.5.

Using excitation of the lower energy band at 372 nm, the emission spectra at various pH values were obtained (Figure 4.7C). From the sigmoid plot of Figure 4.7C, the  $\text{pK}_a$  was estimated to be approximately 8.7. This fluorescence change with pH could be observed by eye under a bench-top UV lamp, where the blue fluorescence of the solution could be seen close to the  $\text{pK}_a$  of *m*-BA at pH 8.0 and in more basic solutions at pH 11.0 (Figure 4.7D). The same experiment was carried out in the presence of 10 equivalents of glucose (Figure 4.8), which enabled the boronate-ester  $\text{pK}_a$  to be estimated as ca. 8.5. The equivalent spectral data for *o*-BA and *p*-BA pH titrations is provided in Appendix C, Figures C19-C23, Figure 4.9 and Table 4.2.

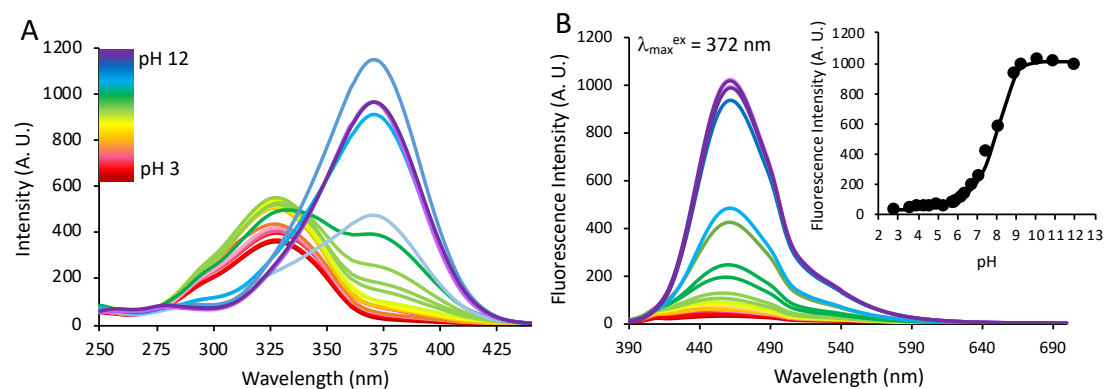


**Figure 4.8.** Excitation and fluorescence emission spectra for *m*-BA (1 mM) in H<sub>2</sub>O. (A) The excitation wavelengths were 329 nm (low pH) and 372 nm (high pH). (B) The emission wavelength was 466 nm. The  $\text{pK}_a$  calibration for *m*-BA (inset B) was estimated to be 8.5.

Decreases in the  $pK_a$  values for all BA derivatives were observed in the presence of glucose (Table 4.2 and Figure 4.9). This effect arises due to the sugar molecule acting as a more efficient electron withdrawing group in comparison to the hydroxyl groups on boron. Charge separation in the *p*-BA is likely to form a more efficient zwitterion, resulting in enhanced aggregation.<sup>33</sup> In contrast, close proximity of the  $N^+$  and  $B^-$  charges in the *o*-BA and *m*-BA can permit  $N^+ \cdots B^-$  through-space electrostatic interactions, thereby offering the possibility of a charge-neutralisation stabilisation effect.<sup>24, 34</sup> This interpretation was supported in the *o*-BA  $^{11}\text{B}$  NMR titrations, which showed both the neutral and anionic boron forms to be simultaneously present (Figure 4.5A).

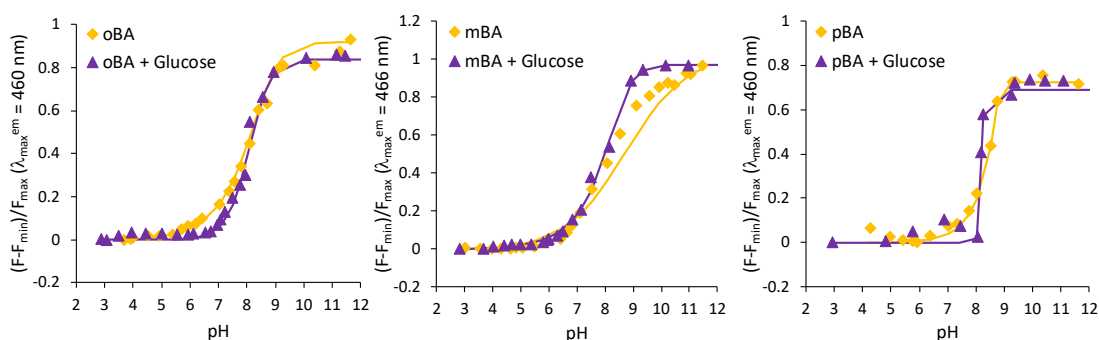


**Figure 4.9.** Experimental emission values taken at the emission wavelengths for *o*-BA, *m*-BA and *p*-BA at 460, 466 and 460 nm respectively, as a function of pH and fit to a sigmoid model, to estimate the  $pK_a$  for each BA derivative (1 mM) in  $\text{H}_2\text{O}$ ;  $F$  is the measured fluorescence intensity at excitation wavelengths 367, 372 and 370 nm for the BA derivatives, respectively, in the presence of glucose (10 mM),  $F_{\min}$  and  $F_{\max}$  are the minimum and maximum fluorescence intensities measured in each case.

**Table 4.2.** Estimated  $pK_a$  values for the BA and BA-ester forms of the BA monomers.

	<i>o</i> -BA	<i>m</i> -BA	<i>p</i> -BA
<b>BA</b>	8.6	8.7	8.8
<b>BA-Ester</b>	8.1	8.5	8.0

#### 4.4.3.2 Glucose Titrations

Glucose titrations were carried out on all three BA monomers close to the  $pK_a$  of their BA-ester, to investigate their fluorescence response to glucose. *o*-BA showed a marginal increase of 13% in fluorescence at  $\lambda_{\max}^{\text{em}} = 460$  nm upon addition of 150

mM glucose (Figure 4.10A and B, and Figure C24). *m*-BA showed an enhanced response of 47% (Figure 4.10C and D, and Figures C25-27). This limited increase of excimer emission demonstrated by *o*-BA and *m*-BA can be accounted for by the closer proximity of the boron atom to the cationic N<sup>+</sup> moiety. In its anionic form, the boron atom is likely to interact intramolecularly (*o*-BA) or solvent-assisted (*m*-BA) with the adjacent cation. The conformation of *p*-BA allows the aggregation mechanism to prevail in the presence of glucose, resulting in an enhanced fluorescence at  $\lambda_{\text{max}}^{\text{em}} = 460$  of 177% (Figure 4.10E and F, and Figure C28). As the concentration of glucose increased, the appearance of a shoulder at 490 and 520 nm in the emission emerged. This resulted in a fluorescence colour change from blue to green, which would be desired for glucose-sensing applications. The orientation of the BA group in the *para* position in *p*-BA also minimises steric interactions with the CH<sub>2</sub> linker attached the phenyl ring, to allow for glucose to bind more readily in comparison to the BA group in *o*-BA and *m*-BA. This aids to explain the more enhanced fluorescence increase by aggregation in *p*-BA compared to the other monomers. This observation also supports the increased fluorescence in *m*-BA over *o*-BA (Figure 4.10).

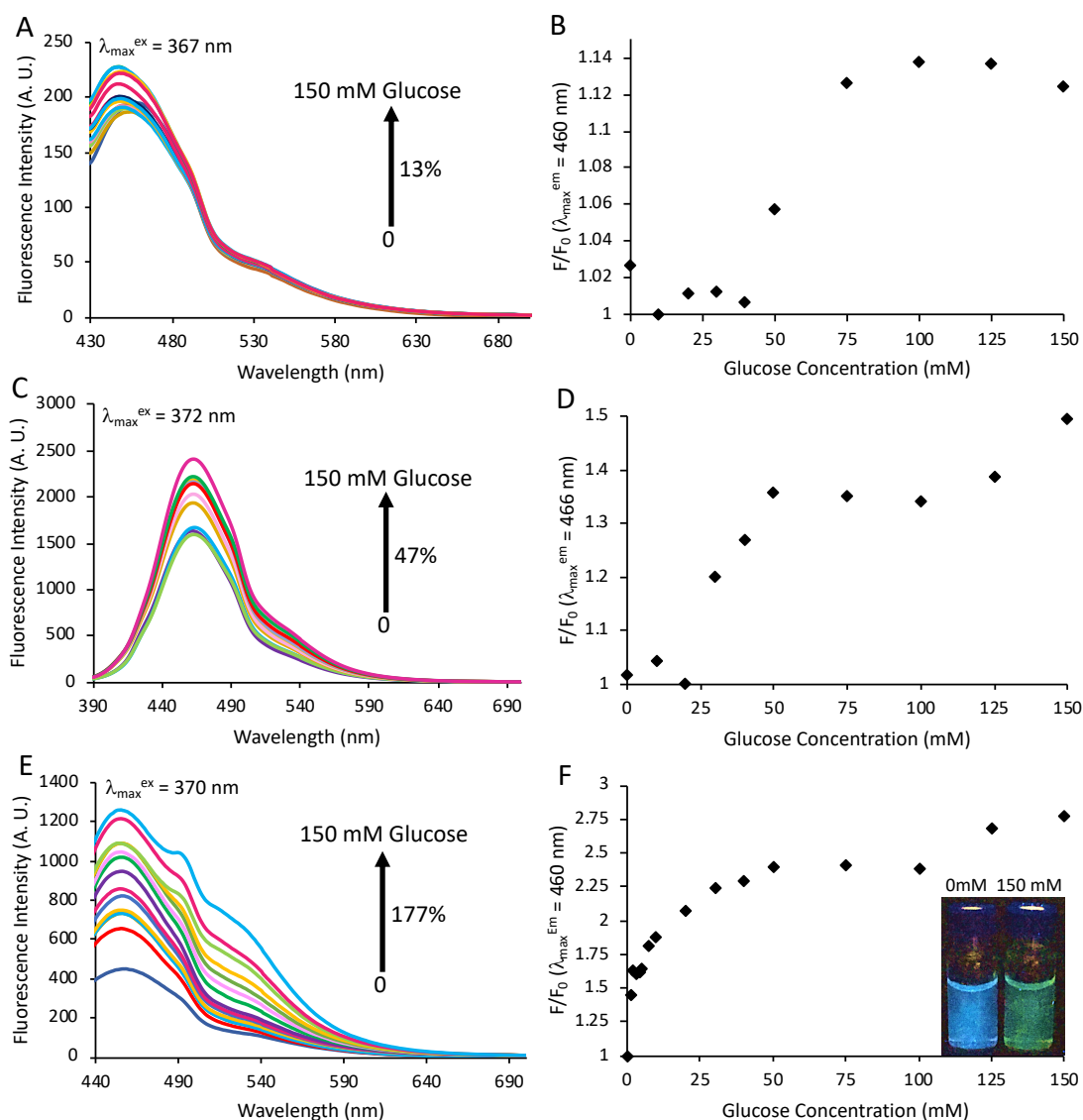


**Figure 4.10.** Fluorescence emission spectra (A) and relative fluorescence increase (B) for *o*-BA (1 mM) with glucose (0-150 mM) in H<sub>2</sub>O at pH 8.0; The emission at 460 nm was recorded using the corresponding excitation wavelength ( $\lambda_{\max}^{\text{ex}}$ ) of 367 nm, showing a fluorescence increase of 13% in the presence of 150 mM glucose. Fluorescence emission spectra (C) and relative fluorescence increase (D) for *m*-BA (1 mM) with glucose (0-150 mM) in H<sub>2</sub>O at pH 7.5; The emission at 466 nm was recorded using the corresponding excitation wavelength ( $\lambda_{\max}^{\text{ex}}$ ) of 372 nm, showing a fluorescence increase of 47% in the presence of 150 mM glucose. Fluorescence emission spectra (E) and relative fluorescence increase (F) for *p*-BA (1 mM) with glucose (0-150 mM) in H<sub>2</sub>O at pH 8.0; The emission at 460 nm was recorded using the corresponding excitation wavelength ( $\lambda_{\max}^{\text{ex}}$ ) of 370 nm, showing a fluorescence increase of 177% in the presence of 150 mM glucose. Inset F Shows a photo of the samples before (blue fluorescent) and after the addition of 150 mM glucose (green fluorescent).  $F_0$  is the initial fluorescence of the BA in the absence of glucose and  $F$  is the measured fluorescence intensity of the BA in the presence of glucose (0-150 mM).



## 4.5 Conclusion and Future Work

In summary, a new class of polymerisable, water soluble, BA derivatives has been produced. Their structures and binding ability towards glucose have been characterised by  $^{11}\text{B}$  NMR and fluorescence, which have been shown to serve as a useful tool to probe their binding behaviour and structural interactions with glucose. The  $\text{pK}_a$  values of the BA and BA-ester forms of the monomers were estimated by tracking changes in fluorescence emission spectra as a function of pH. The *p*-BA was found to be the most responsive derivative towards glucose, exhibiting the highest increase in excimer fluorescence around physiological pH. Furthermore, the high-yielding synthetic procedure is a facile, one-step, methodology for the generation of a library of polymerisable boronic acids. Moreover, these BA derivatives contain polymerisable handles in their structures, which would allow for simple covalent attachment in a polymer matrix. Next, these monomers were investigated in a two-component fluorescence sensing system in solution and within hydrogel matrices (Chapter 5).

## 4.6 References

1. Hall, D. G. Structure, properties, and preparation of boronic acid derivatives. Overview of their reactions and applications, in *Boronic acids*, Vol. 2 (Eds: D. G. Hall), Wiley-VCH, Weinheim, 2005, pp. 1-100.
2. Zhang, A.; Liu, Q.; Lei, Y.; Hong, S.; Lin, Y. Synthesis and antimicrobial activities of acrylamide polymers containing quaternary ammonium salts on bacteria and phytopathogenic fungi, *React. Funct. Polym.*, **2015**, *88*, 39-46.
3. Pappin, B.; Kiefel, M. J.; Houston, T. A. Boron-Carbohydrate Interactions, in *Carbohydrates - comprehensive studies on glycobiology and glycotecnology*, Creative Commons Attribution, InTech, 2012, pp 37-54.
4. Hansen, J. S.; Christensen, J. B.; Petersen, J. F.; Hoeg-Jensen, T.; Norrild, J. C. Arylboronic Acids: A Diabetic Eye on Glucose Sensing, *Sens. Actuators, B*, **2012**, *161*, 45-79.
5. Badugu, R.; Lakowicz, J. R.; Geddes, C. D. Enhanced fluorescence cyanide detection at physiologically lethal levels: reduced ICT-based signal transduction, *J. Am. Chem. Soc.*, **2004**, *127*, 3635-3641.
6. Jin, S.; Li, M.; Zhu, C.; Tran, V.; Wang, B. Computer-based de novo design, synthesis and evaluation of boronic acid-based artificial receptors for selective recognition of dopamine, *ChemBioChem*, **2008**, *9*, 1431-1438.
7. Springsteen, G.; Wang, B. A detailed examination of boronic acid-diol complexation, *Tetrahedron*, **2002**, *58*, 5291-5300.
8. Axthelm, J.; Askes, S. H. C.; Elstner, M.; Reddy, G. U.; Görls, H.; Bellstedt, P.; Schiller, A. Fluorinated boronic acid-appended pyridinium salts and <sup>19</sup>F NMR spectroscopy for diol sensing, *J. Am. Chem. Soc.*, **2017**, *139*, 11413-11420.
9. Fang, H.; Kaur, G.; Wang, B. Progress in boronic acid-based fluorescent glucose sensors, *J. Fluoresc.*, **2004**, *14*, 481-489.
10. Sun, X.; Zhai, W.; Fossey, J. S.; James, T. D. Boronic acids for fluorescence imaging of carbohydrates, *Chem. Commun.*, **2016**, *52*, 3456-3469.
11. Arimori, S.; Bell, M. L.; Oh, C. S.; James, T. D. A Modular Fluorescence Intramolecular Energy Transfer Saccharide Sensor, *Org. Lett.*, **2002**, *4*, 4249-4259.
12. Hansen, J. S.; Ficker, M.; Peterson, J. F.; Christensen, J. B.; Hoeg-Jensen, T. *ortho*-Substituted fluorescent aryl monoboronic acid displays physiological binding of D-glucose, *Tetrahedron Lett.*, **2013**, *54*, 1849-1852.
13. Sun, X.; James, T. D. Glucose sensing in supramolecular chemistry, *Chem. Rev.*, **2015**, *115*, 8001-8037.
14. Yan, J.; Springsteen, G.; Deeter, S.; Wang, B. The relationship among pK<sub>a</sub>, pH, and binding constants in the interactions between boronic acids and diols - It is not as simple as it appears, *Tetrahedron*, **2004**, *60*, 11205-11209.
15. Brewer, S. H.; Allen, A. M.; Lappi, S. E.; Chasse, T. L.; Briggman, K. A.; Gorman, C. B.; Franzen, S. Infrared detection of a phenylboronic acid terminated alkane thiol monolayer on gold surfaces, *Langmuir*, **2004**, *20*, 5512-5520.

16. DiCesare, N.; Lakowicz, J. R. New colour chemisensors for monosaccharides based on azo dyes, *Org. Lett.*, **2001**, *3*, 3891-3893.
17. Boduroglu, S.; El Khoury, J. M.; Reddy, D. V.; Rinaldi, P. L.; Hu, J. A colorimetric titration method for quantification of millimolar glucose in a pH 7.4 aqueous phosphate buffer, *Bio. Med. Chem.*, **2005**, *15*, 3974-3977.
18. James, T. D.; Samankumara Sandanayake, K. R. A.; Shinkai, S. Novel Photoinduced Electron-Transfer Sensors for Saccharides Based on the Interaction of Boronic Acid and Amine, *J. Chem. Soc., Chem. Commun.*, **1994**, *0*, 477-478.
19. Yoon, J.; Czarnik, A. W. Fluorescent Chemosensors of Carbohydrates. A Means of Chemically Communicating the Building of Polyols in Water Based on Chelation-Enhanced Quenching, *J. Am. Chem. Soc.*, **1992**, *114*, 5874-5875.
20. Bi, X.; Du, X.; Jiang, J.; Huang, X. Facile and sensitive glucose sandwich assay using in situ-generated Raman reporters, *Anal. Chem.*, **2015**, *87*, 2016-2021.
21. Chapin, B. M.; Metola, P.; Lynch, V. M.; Stanton, J. F.; James, T. D.; Anslyn, E. V. Structural and thermodynamic analysis of a three-component assembly forming *ortho*-iminophenylboronate esters, *J. Org. Chem.*, **2016**, *81*, 8319-8330.
22. Bruen, D.; Delaney, C.; Florea, L.; Diamond, D. Glucose sensing for diabetes monitoring: recent developments, *Sensors*, **2017**, *17*, 1866-1887.
23. Collins, B. E.; Sorey, S.; Hargrove, A. E.; Shabbir, S. H.; Lynch, V. M.; Anslyn, E. V. Probing Intramolecular B-N Interactions in *ortho*-Aminomethyl Arylboronic Acids, *J. Org. Chem.*, **2009**, *74*, 4055-4060.
24. Badugu, R.; Lakowicz, J. R.; Geddes, C. D. Ophthalmic glucose monitoring using disposable contact lenses - a review, *J. Fluoresc.*, **2004**, *14*, 617-633.
25. Camara, J. N.; Suri, J. T.; Cappuccio, F. E.; Wessling, R. A.; Singaram, B. Boronic Acid Substituted Viologen Based Optical Sugar Sensors: Modulated Quenching with Viologen as a Method for Monosaccharide Detection, *Tetrahedron Lett.*, **2002**, *43*, 1139-1141.
26. Gamsey, S.; Baxter, N. A.; Sharrett, Z.; Cordes, D. B.; Olmstead, M. M.; Wessling, R. A.; Singaram, B. The effect of boronic acid-positioning in an optical glucose-sensing ensemble, *Tetrahedron*, **2006**, *62*, 6321-6331.
27. Suri, J. T.; Cordes, D. B.; Cappuccio, F. E.; Wessling, R. A.; Singaram, B. Continuous glucose sensing with a fluorescent thin-film hydrogel, *Angew. Chem. Int. Ed.*, **2003**, *42*, 5857-5859.
28. Xue, C.; Cai, F.; Liu, H. Ultrasensitive fluorescent responses of water-soluble, zwitterionic, boronic acid-bearing, regioregular head-to-tail polythiophene to biological species, *Chem. Eur. J.*, **2008**, *14*, 1648-1653.
29. Yu, C.; Yam, V. W. Glucose sensing via polyanion formation and induced pyrene excimer emission, *Chem. Comm. (Camb)*, **2009**, *11*, 1347-1349.
30. Huang, Y.; Ouyang, W.; Wu, X.; Li, Z.; Fossey, J. S.; James, T. D.; Jiang, Y. Glucose sensing via aggregation and the use of "knock-out" binding to improve selectivity, *J. Am. Chem. Soc.*, **2013**, *135*, 1700-1703.

31. Vancoillie, G.; Hoogenboom, R. Synthesis and polymerization of boronic acid containing monomers, *Polym. Chem.*, **2016**, *7*, 5484-5495.
32. Carey, F.A. Reactions of arenes. Electrophilic aromatic substitution, in *Organic chemistry*, 4th ed.; Kane, K.T., Ed. McGraw-Hill Companies: Boston, MA, 2000; p 457.
33. Wang, Y.; Huang, X.; Li, Y.; Wang, J.; Wang, Y. Aggregation properties of zwitterionic surfactants with different ionic headgroups, hydrophobic chain length and inter-charge spacers, *Colloids Surf., A*, **2009**, *333*, 108-114.
34. Rios, A.; Amyes, T. L.; Richard, J. P. Formation and stability of organic zwitterions in aqueous solution: Enolates of the amino acid glycine and its derivatives, *J. Am. Chem. Soc.*, **2000**, *122*, 9373-9385.

## Chapter 5

---

### A Two-Component Fluorescent System for Sugar-Sensing\*

---

\*This chapter has been submitted as “A Two-Component Fluorescent System for Sugar-Sensing”, Danielle Bruen, Colm Delaney, Dermot Diamond and Larisa Florea, *J. Am. Chem. Soc.*, **2018**.

## Contents

### Chapter 5: A Two-Component Fluorescent System for Sugar-Sensing

<b>5.1 Abstract</b>	<b>154</b>
<b>5.2 Introduction</b>	<b>155</b>
<b>5.3 Experimental</b>	<b>157</b>
5.3.1 Materials and Methods	157
5.3.2 Fluorescence Titrations with Hydrogel Cocktails	158
5.3.3 Synthesis of Glucose-Responsive Hydrogels	159
5.3.4 Calculating the Fluorescence Quenching and Sugar Binding Constants	160
<b>5.4 Results and Discussion</b>	<b>161</b>
5.4.1 Fluorescence Quenching of Pyranine with <i>o</i> -BA, <i>m</i> -BA and <i>p</i> -BA	161
5.4.2 Fluorescence Recovery of Pyranine with Monosaccharides	164
<b>5.5 Conclusions</b>	<b>167</b>
<b>5.6 References</b>	<b>169</b>

## 5.1 Abstract

Boronic acids have been widely exploited for their ability to interact with diol-containing compounds. By combining boronic acid molecules with fluorophores, interactions with saccharides can be detected. In this context, an indirect glucose-sensing system is described, by monitoring the fluorescence of an anionic fluorophore, 8-hydroxypyrene-1,3,6-trisulfonic acid. When this fluorophore is introduced to cationic boronic acid monomers (*o*-BA, *m*-BA and *p*-BA), its fluorescence becomes quenched, due to the formation of a non-fluorescent boronic acid-fluorophore complex. Upon addition of saccharides, a boronic acid-saccharide complex is formed, with simultaneous dissociation of the non-fluorescent complex, and recovery of the fluorescence. This response of this system was examined in solution with common monosaccharides, such as glucose, fructose and galactose. Polymerisation of the boronic acid monomers yielding cross-linked hydrogels, which showed similar reversible recovery of fluorescence in the presence of glucose.

## 5.2 Introduction

Boronic acids (BAs) have been investigated for many potential applications, such as purification of glycoproteins by affinity chromatography,<sup>1</sup> protecting groups in carbohydrate chemistry<sup>2</sup> and as coupling reagents in the formation of new C-C bonds.<sup>3</sup> This versatility originates from their trigonal planar geometry and vacant orthogonal *p*-orbital, which consequently renders them Lewis acidic.<sup>3</sup> This Lewis acidity also enables BA groups to form strong and reversible interactions with saccharides, anions,<sup>4</sup> neurotransmitters such as dopamine<sup>5</sup> and  $\alpha$ -amino acids.<sup>3</sup> Arylboronic acids typically have a  $pK_a$  around 8,<sup>6</sup> which can be reduced by 2-3 units when bound to saccharides, due to the electron-withdrawing capability of the sugar molecule.<sup>7</sup> As a result, BAs are suitable for sensing bioanalytes within the pH range of physiological fluids.<sup>8</sup> The fabrication of BA-substituted fluorophores for the detection of glucose has significant clinical potential, in particular for the detection, diagnosis and monitoring of diseases, such as diabetes.<sup>9-15</sup>

To date, most BA-based fluorescent sensors have focused on exploiting well-characterised quenching mechanisms associated with discrete molecules. Appropriate covalent attachment of a BA moiety to a fluorophore exhibiting internal charge transfer (ICT) or photoinduced electron transfer (PET) can produce systems which exhibit restored fluorescence upon saccharide binding. For the past ten years, this approach has been championed by groups, such as James *et al.*<sup>10, 13, 16-18</sup> and Badugu, *et al.*<sup>4, 19</sup> In solution, demonstration of this effect is relatively straightforward, but upon transitioning to a polymeric matrix, maintaining the response can be significantly challenging.<sup>20</sup>

In an indirect fluorescent sensing system, as pioneered by Singaram and co-workers,<sup>21-28</sup> the fluorophore is typically anionically charged and the BA group is appended to a separate cationic molecule.<sup>23</sup> These molecules interact electrostatically to form a non-fluorescent ground-state complex.<sup>24, 25</sup> Upon saccharide binding, a conformational change around boron is induced and the anionic boronate form is generated.<sup>19, 25</sup> This structural change leads to the dissociation of the ground-state complex, thereby restoring fluorescence.<sup>24</sup>

This indirect sensing system is dependent on through-space electrostatic interactions between two molecules. Conversely, in a direct sensing approach, all sensing components are incorporated into a single structure. By employing a two-



component system, the sensing approach can be simplified through the design of small cationic BA derivatives. The resulting fluorescence response therefore relies on both the ability of the BA molecule to interact with the fluorophore and the subsequent binding of saccharides, to sufficiently disrupt this fluorescence quenching mechanism. Singaram *et al.*<sup>26</sup> have demonstrated that for BA-substituted bipyridinium, and phenanthroline viologens, the substitution of the phenylboronic acid has a significant bearing on both fluorescence quenching and recovery. In particular, the ability of the cationic nitrogen to interact with the boron centre, can have a profound effect on the fluorescent response.<sup>26</sup> Upon N<sup>+</sup>-B<sup>-</sup> interaction, fluorescence recovery to dissociate the ground-state complex was thought to occur more rapidly.<sup>26</sup>

Using the same family of viologens, other groups have expanded on this work by variation of the fluorophore. Feng *et al.*<sup>29, 30</sup> demonstrated two-component sensing systems in solution by interchanging the fluorophore with a substituted naphthalene dye or a fluorescent BINOL-containing polymer. Both approaches were most sensitive to glucose at lower concentrations (<10 mM). Li *et al.*<sup>31</sup> have also proposed a two-component sensing system utilising the same BA-viologen salts with fluorescent quantum dots. The fluorescence in this case, could be quenched by 80% on addition of the BA-viologen (0.5 mM) and restored by 33% on sequential additions of glucose (0-60 mM). Although all of these systems showed excellent fluorescence quenching and recovery, the BA viologen compounds employed exhibit biological toxicity.<sup>32</sup> This two-component system has also been extended to a hydrogel matrix. Optimisation of cross-linkers and polymerisable sensing moieties by Singaram *et al.*,<sup>23-25, 29</sup> yielded a system comprising a diboronic viologen with acrylate tethers, coupled with a substituted pyrene fluorophore containing multiple anionic groups and cross-linked with a polyethylene glycol crosslinker. The resulting hydrogel showed a fluorescent response to physiological relevant concentrations of glucose (5 mM), showing a stable fluorescence signal for glucose diffusion in to the gel after ~2h.<sup>22-24, 28</sup>

Recently, we have reported a new family of cationic BA monomers that can be synthesised via a one-step, easily adaptable methodology.<sup>33, 34</sup> Advantageously, these small cationic monomers bear structural similarities to acetylcholine, which is biologically significant for peptide synthesis<sup>35</sup> and receptor agonists.<sup>36</sup> BAs are also considered as 'green compounds' with low toxicity.<sup>3</sup> Herein, we use polymerisable

BA derivatives in conjunction with the anionic fluorophore 8-hydroxypyrene-1,3,6-trisulfonic acid (pyranine) in a two-component sensing system (Figure 5.1), for the detection of monosaccharides. This indirect system was optimised first in solution by interchanging the BA monomers to determine the most efficient quencher. Thereafter, the fluorescence recovery was studied using three monosaccharides; glucose, fructose and galactose. The system was then integrated in to a hydrogel matrix, which showed good reproducibility for sensing glucose within physiological relevant concentration ranges.

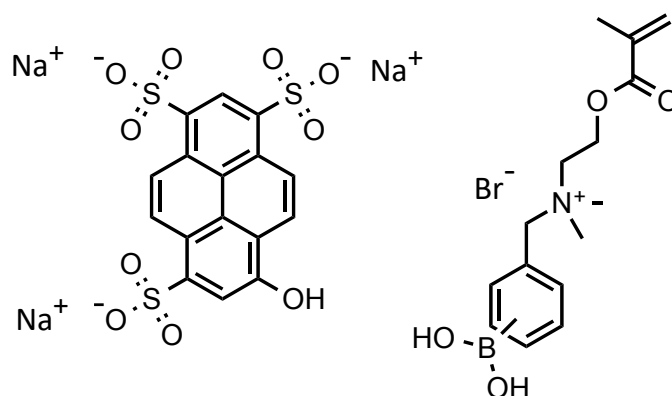


**Figure 5.1.** Indirect sensing system components; pyranine (left) and the general structure of the BA monomers (right).

## 5.3 Experimental

### 5.3.1 Materials and Methods

2-(Bromomethylphenyl)boronic acid (100%), 3-(bromomethylphenyl)boronic acid (95%) and 4-(bromomethylphenyl)boronic acid (95%) were acquired from Fluorochem, UK and used as received. 2-(Dimethylamino)ethyl methacrylate (98%), 8-hydroxypyrene-1,3,6-trisulfonic acid trisodium salt (pyranine; >97%), acrylamide (>99%), *N,N'*-methylenebis(acrylamide) (MBIS; 99%), 2-hydroxy-2-methylpropiophenone (HMPP; 97%), D-(+)-glucose (>99.5%), D-(-)-fructose (>99%), D-(+)-galactose (>98%), anhydrous acetonitrile (CH<sub>3</sub>CN; 99.8%), anhydrous dichloromethane (CH<sub>2</sub>Cl<sub>2</sub>; >99.8%) and deuterium oxide (D<sub>2</sub>O; 99.9%, atom D) were purchased from Sigma Aldrich, Ireland and used as received. Structural <sup>1</sup>H, <sup>13</sup>C and <sup>11</sup>B NMR studies were carried out on a Bruker Avance Ultrashield 600 MHz spectrometer. D<sub>2</sub>O was used for all NMR measurements. The fluorescence of the BA

monomers was recorded using a JASCO FP-8300 spectrofluorometer at 20 °C and UV-vis absorption measurements were carried out on a Varian Cary 50 Probe spectrophotometer, in a precision cell made from quartz Suprasil that had a path length of 10 mm and a volume of 1.4 mL. All pH measurements were carried out using a VWR sympHony SP70P pH meter. Deionised water (18.2 M $\Omega$ .cm<sup>-1</sup>) (DI H<sub>2</sub>O) used was purified using a Milli-Q Water Purification System (Merck Millipore, Darmstadt, Germany).

### 5.3.2 Fluorescence Titrations with Hydrogel Cocktails

Fluorescence recovery titrations were carried out by monitoring the fluorescence of pyranine (100  $\mu$ M; 0.001 mol%) in the hydrogel cocktail containing acrylamide (100 mol%) and MBIS (1 mol%) in DI H<sub>2</sub>O (2 mL), with increasing concentrations of BA monomers. Additions of BA monomer were made using automated pipettes. Each BA stock solution was dissolved in DI H<sub>2</sub>O. Following each addition of saccharide, the fluorescence was measured in a quartz Suprasil 1.4 mL cuvette with a path length of 10 mm, on a JASCO FP3800 Spectrophotometer. Excitation and emission spectra were recorded from the characteristic wavelengths of pyranine, where the excitation wavelengths were 374 nm, 404 nm and 454 nm, and the emission wavelength was 515 nm. A fluorescence curve was plotted by taking the maximum intensity of the fluorescence emission, when excited at all wavelengths. The parameters used for fluorescence measurements were as follows; 280 V sensitivity, 5 nm bandwidth, 1 nm data interval, 1 second response time and 500 nm/min scan speed, unless otherwise stated.

### 5.3.3 Synthesis of Glucose-Responsive Hydrogels

**Table 5.1.** Recipe for fluorescent acrylamide-*o*BA hydrogels.

Materials	Mass (g)	Volume ( $\mu$ L)	Density ( $\rho$ )	$M_r$	mmol	Molar %
Acrylamide	1.000	-	-	71.0	14.0	100
MBIS	0.0216	-	-	154.1	0.14	1
Pyranine	-	250.0	-	524.3	0.0002	0.001
<i>o</i> BA	-	37.5	-	372.0	0.003	0.02
HMPP	0.0231	21.5	1.077	164.2	0.14	1.0

\* The final concentration of pyranine in the cocktail solution was 0.1 mM and the final concentration of *o*-BA was 1.5 mM (15 eq.).

The hydrogels were prepared by adding the reagents as described in Table 5.1 and Table 5.2 and dissolved in 2 mL DI H<sub>2</sub>O. Thin hydrogel films were achieved using a home-made cell consisting of a glass slide (bottom), poly(methyl methacrylate) (top) and a pressure-sensitive adhesive (120  $\mu$ m) spacer. The films were polymerised inside a CL-1000 Ultraviolet Crosslinker UVP chamber at 365 nm for 30 minutes. Once polymerised the films were cut, to produce 13 mm diameter hydrogel disks with a thickness of 120  $\mu$ m. The hydrogel disks were placed in pH 7.4 buffer solution after cutting.

The fluorescence of the hydrogel disks was measured first after polymerisation and immersion in buffer (3 mL) for at least an hour. The fluorescent hydrogel disks were then placed in to glucose solutions of various concentrations between 0-100 mM. The experiment was carried out in triplicate by measuring the fluorescence of at least three gels in the same glucose concentration. Similar to the solution-based studies, the fluorescence of pyranine (100  $\mu$ M; 0.001 mol%) in the hydrogels was monitored. Two different hydrogels were polymerised. Hydrogels containing pyranine:*o*-BA (1:15) and pyranine:*m*-BA (1:10) with the same mol% of the other hydrogel components; acrylamide 100 mol% and MBIS 1 mol%. Initially, the hydrogels exhibited low fluorescence and when in the presence of glucose, the fluorescence increased. The excitation and emission spectra for the hydrogels were measured using

the JASCO FP8300 spectrophotometer on a high precision glass cover slide while hydrated at an angle of 30°. A fluorescence curve was plotted by taking the maximum intensity of the fluorescence emission, when excited at the wavelengths stated. The parameters used for fluorescence measurements were as follows; 500 V sensitivity, 2.5 nm bandwidth, 1 nm data interval, 1 second response time and 500 nm/min scan speed, unless otherwise stated.

**Table 5.2.** Recipe for fluorescent acrylamide-mBA hydrogels.

Materials	Mass (g)	Volume ( $\mu\text{L}$ )	Density ( $\rho$ )	$M_r$	mmol	Molar %
Acrylamide	1.000	-	-	71.0	14.0	100
MBIS	0.0216	-	-	154.1	0.14	1
Pyranine	-	250.0	-	524.3	0.0002	0.001
mBA	-	20.0	-	372.0	0.002	0.01
HMPP	0.0231	21.5	1.077	164.2	0.14	1.0

\* The final concentration of pyranine in the cocktail solution was 0.1 mM and the final concentration of m-BA was 1 mM (10 eq.).

#### 5.3.4 Calculating the Fluorescence Quenching and Sugar Binding Constants

The static and dynamic quenching constants for the decrease in pyranine fluorescence were determined for both *o*-BA and *m*-BA, using Equation 5.1.<sup>23,24</sup>  $F_0$  is the initial fluorescence of pyranine,  $F$  is the measured fluorescence after the addition of BA monomer,  $V$  is the dynamic quenching constant,  $K_s$  is the static quenching constant and  $[Q]$  is the concentration of the BA quencher molecule. The apparent binding constants for each saccharide were also determined via fluorescence titrations with glucose, fructose and galactose and calculated using Equation 5.2,<sup>22-24</sup> where  $F_0$  is the fluorescence intensity of the quenched dye,  $F$  is the fluorescence intensity after sugar addition,  $F_{max}$  is the intensity at which the fluorescence increase reaches its maximum,  $[S]$  is the concentration of the sugar and  $K_b$  is the apparent binding constant. The data was analysed with a non-linear least squares method using Solver from Microsoft Excel 2016.

**Equation 5.1 for fluorescence quenching:**

$$F_0/F = (1 + K_s[Q])e^{V[Q]} \quad (5.1)$$

**Equation 5.2 for fluorescence recovery:**

$$F/F_0 = (1 + (F_{max}/F_0)K_b[S])/(1 + K_b[S]) \quad (5.2)$$

## 5.4 Results and Discussion

The adaptable, one-step synthesis was used to produce a series of polymerisable BA derivatives. Pyranine was chosen as the anionic fluorophore because of its water solubility, large Stokes shift, resistance to photobleaching and the breadth of previous research detailing its application in sensing.<sup>4, 23, 24, 37-39</sup> Photophysical characterisation of pyranine in solution showed that in the presence of the cationic BA monomers, *o*-BA, *m*-BA and *p*-BA, a ground state complex was formed. Figure 5.2 shows the absorbance of pyranine (blue spectrum) and the change in this absorbance upon formation of the ground-state complex between pyranine and *o*-BA (pink spectrum). The absorption of pyranine was then partially restored on introducing glucose (green spectrum).

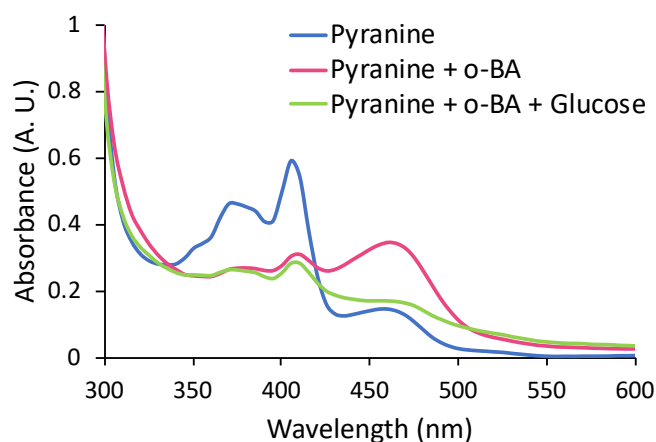


**Figure 5.2.** Absorbance spectra for pyranine (4  $\mu$ M) (blue), pyranine and *o*-BA (1:50) (pink) and pyranine, *o*-BA (1:50) and glucose (100 mM) (green) in pH 7.4 buffer.

### 5.4.1 Fluorescence Quenching of Pyranine with *o*-BA, *m*-BA and *p*-BA

To optimise this two-component sensing system, the BA monomers were initially screened in solution for their ability to quench the fluorescence of pyranine. Pyranine was dissolved in pH 7.4 phosphate buffer solution and quenching titrations were

carried out with each BA monomer (Figure 5.3 and Figures D1-D5 in Appendix D). The pyranine fluorescence showed a characteristic excitation spectrum with absorption bands ( $\lambda_{\max}^{\text{ex}}$ ) at 374 nm, 404 nm and 454 nm, which all resulted in a single emission ( $\lambda_{\max}^{\text{em}}$ ) centred at 515 nm. Figure 5.3 shows the excitation and emission spectra for the fluorescence titration of pyranine (4  $\mu\text{M}$ ) with *o*-BA (0-200  $\mu\text{M}$ ), *m*-BA (0-160  $\mu\text{M}$ ) and *p*-BA (0-1000  $\mu\text{M}$ ), where the fluorescence showed a decrease of 96% with *m*-BA. This change from strongly fluorescent (green) to weakly fluorescent (blue) was clearly observed by eye under UV light.

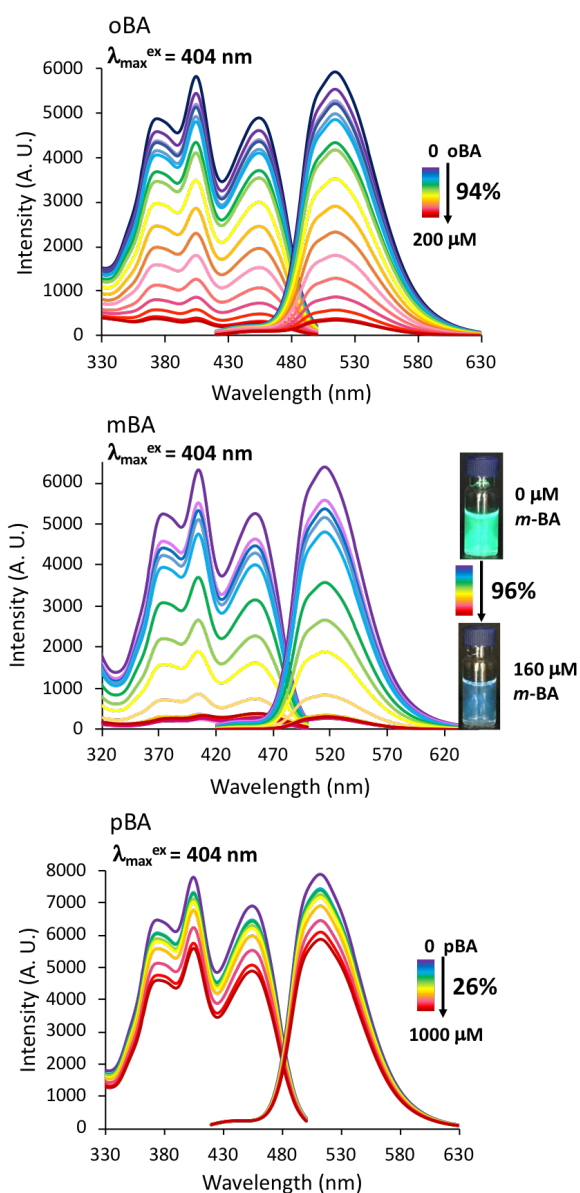


**Figure 5.3.** Excitation and emission spectra for pyranine (4  $\mu\text{M}$ ) with increasing concentrations of *o*-BA (0-200  $\mu\text{M}$ ), *m*-BA (0-160  $\mu\text{M}$ ) and *p*-BA (0-1000  $\mu\text{M}$ ) in pH 7.4 buffer solution. The inset for *m*-BA shows an image of this change under 365 nm UV irradiation.

*o*-BA also quenched the fluorescence by 94% with 50 equivalents (Figure 5.4, blue), more efficiently than the *p*-BA which generated only 10% quenching up to 40 equivalents (Figure 5.4, purple). The static and dynamic quenching constants were estimated for *o*-BA and *m*-BA, using Equation 5.1 (Table 5.3) and are comparable to bipyridinium substituted bisboronic acids (BBV) presented by Singaram *et al.*, in which the *o*-BBV and *m*-BBV derivatives have static quenching constants of 16,000 M<sup>-1</sup> and 8749 M<sup>-1</sup> and dynamic quenching constants of 21,000 M<sup>-1</sup> and 1549 M<sup>-1</sup>, respectively.<sup>23</sup> In contrast to Singaram *et al.* the *m*-BA shown here quenched the fluorescence more efficiently in comparison to *o*-BA.

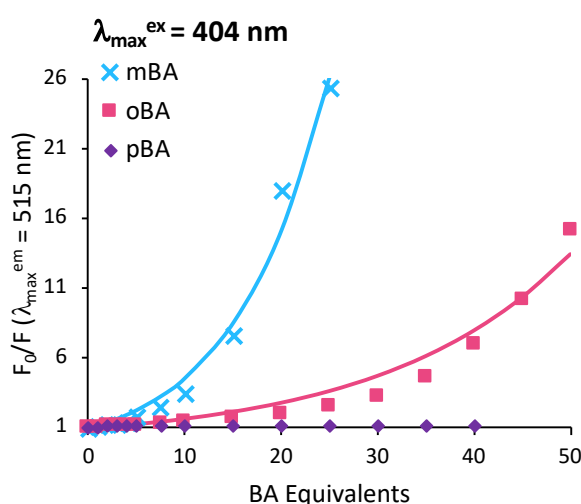


**Figure 5.4.** Fluorescence quenching of pyranine (4  $\mu$ M) with *o*-BA (0-200  $\mu$ M), *m*-BA (0-100  $\mu$ M) and *p*-BA (0-160  $\mu$ M).

Considering the values obtained in Table 5.3, our interpretation is that *o*-BA acts as a weaker quencher molecule in comparison to *m*-BA, due to the close proximity of the BA group *ortho* to the N<sup>+</sup> moiety, which facilitates N<sup>+</sup>-B<sup>-</sup> interactions. If an intramolecular N<sup>+</sup>-B<sup>-</sup> interaction occurs in *o*-BA, electrostatic interactions between the N<sup>+</sup> moiety and the anionic sulphonate groups in pyranine are weakened, leading to an enhanced emission.

**Table 5.3.** Quenching constants for *o*-BA and *m*-BA.

Quenching Constants (M <sup>-1</sup> )	<i>o</i> -BA	<i>m</i> -BA
Static (K <sub>s</sub> )	12993	19205
Dynamic (V)	0	28526



#### 5.4.2 Fluorescence Recovery of Pyranine with Monosaccharides

The recovery of fluorescence in solution was investigated for the *o*-BA and *m*-BA systems, since both of these monomers exhibited the most efficient quenching interactions with pyranine. The ratios between pyranine and the BA monomers of 1:20 for *m*-BA and 1:50 for *o*-BA, were chosen by close examination of the fluorescence quenching curves (Figure 5.4). Upon sugar binding to the BA molecule, a conformational change around boron is induced from the neutral trigonal planar BA to the anionic tetrahedral boronate ester form. This change results in a zwitterionic BA molecule, inducing instability in the electrostatically bound ground-state complex. This dissociation between the BA molecule and pyranine generates a recovery in pyranine fluorescence.

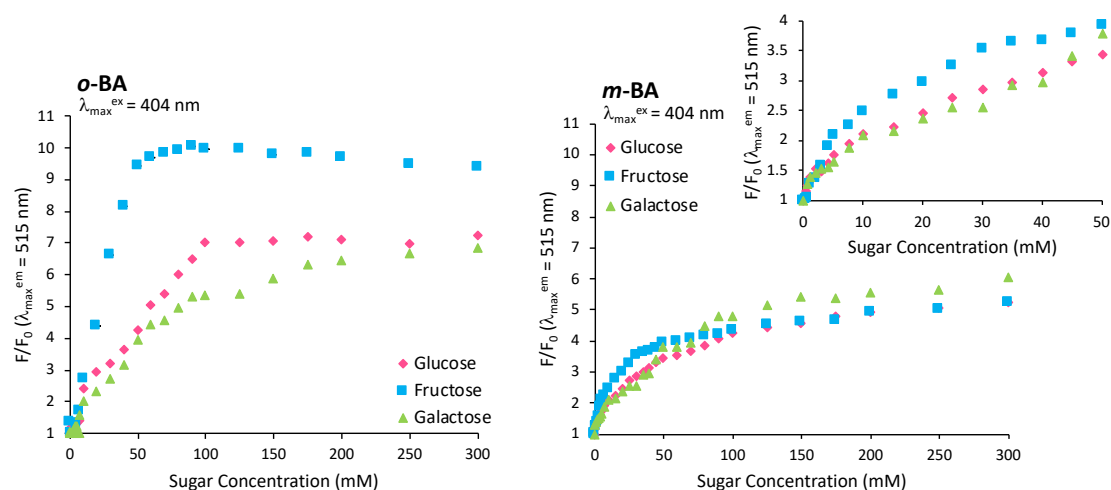


**Figure 5.5.** Left: Fluorescence recovery of pyranine (4  $\mu\text{m}$ ) and *o*-BA (1:50), Right: Fluorescence recovery of pyranine and *m*-BA (1:20).

*o*-BA showed the greatest fluorescence recovery response for all three sugars, with the most significant response (9-fold) seen upon binding fructose. *m*-BA showed a markedly lower restoration of fluorescence for the same sugars, with a 6-fold fluorescence increase on complexing galactose and a 5-fold increase with glucose and fructose (Figure 5.5). (For spectral data on all of the fluorescence recovery titrations, the reader is directed to Figures D6-D11 in Appendix D). The apparent binding constants were also determined from this data for *o*-BA and *m*-BA with each monosaccharide (Table 5.4). From these binding constants, the BA derivatives show a higher selectivity for fructose over glucose and galactose, similar to other reported BA derivatives.<sup>17, 26</sup>

**Table 5.4.** Binding constants ( $K_s$ ) for *o*-BA and *m*-BA with all three monosaccharides.

<b>Binding Constants (<math>M^{-1}</math>)</b>	<b><i>o</i>-BA</b>	<b><i>m</i>-BA</b>
<b>Glucose</b>	33.0	29.0
<b>Fructose</b>	61.6	44.9
<b>Galactose</b>	23.1	23.4

The fluorescence recovery reported here, displaying between three- and ten-fold growth is notably higher than previously reported similar two-component pyranine systems (Singaram *et al.* show a maximum of  $F/F_0 = \sim 2.2$  in solution).<sup>23</sup> Interestingly, the *o*-BBV derivative employed by Singaram showed a higher binding constant value in comparison to the *meta* and *para* counterparts.<sup>26</sup> For the compounds presented here, both *o*-BA and *m*-BA showed very similar binding constants for all three monosaccharides. Overall, the greatest fluorescence recovery for each monosaccharide was observed with the *o*-BA system. It is likely that this would result from enhanced intramolecular stabilisation in *o*-BA on saccharide binding from the adjacent  $N^+$  moiety.

With a view to optimising ratios of quencher and fluorophore within a hydrogel matrix, the gel cocktail was titrated with the BA monomers (Figure 5.6). Acrylamide, methylenebis(acrylamide) and pyranine (0.1 mM) were dissolved in  $H_2O$ . From Figure 5.6, it can be seen that similar to the solution-based studies, *m*-BA quenches the fluorescence more efficiently than *o*-BA. From this quenching study (Figure 5.6, Figures D12-D13), it was deduced that the favoured ratios of pyranine to the BA monomers for polymerisation were 1:15 for *o*-BA and 1:10 for *m*-BA. Since the BA monomers contained polymerisable handles in their structures they were co-polymerised in the hydrogel matrix. The presence of cationic  $N^+$  groups within the polymeric chains enables pyranine to be electrostatically bound in the hydrogel matrix.

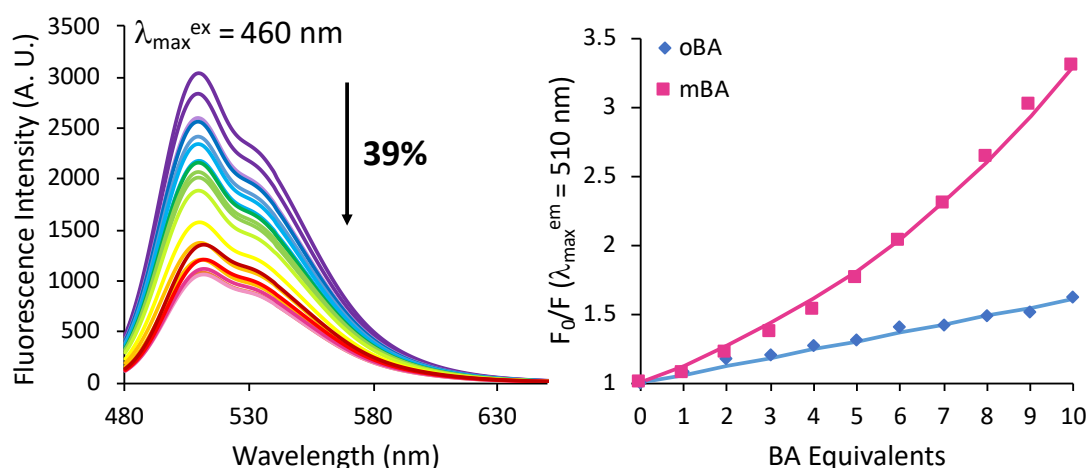


**Figure 5.6.** Left: Fluorescence emission spectra of the hydrogel cocktail; containing acrylamide (100 mol%), MBIS (1 mol%) and pyranine (0.001 mol%) after titration with *o*-BA (0-5 mM) and right: normalised ( $F_0/F$ ) fluorescence emission of both hydrogel cocktails after titrations with *o*-BA (0-1.5 mM) and *m*-BA (0-1.5 mM) in DI H<sub>2</sub>O fitted with a model using Equation 5.1.

The BA monomers were photo-polymerised in to thin hydrogel films, which were then cut in to circular disks. The fluorescent disks were hydrated in pH 7.4 buffer solution before being immersed in various glucose concentrations ranging between 0-100 mM. From the emission spectra, quenching curves were plotted (Figure 5.7) and the apparent binding constants ( $K_b$ ) with glucose were determined. The  $K_b$  value for the hydrogels containing *o*-BA was  $40.6 \text{ M}^{-1}$  and the  $K_b$  value for the *m*-BA gels was  $100.6 \text{ M}^{-1}$ , where both  $K_b$  values are higher than the calculated values for the solution-based studies (Table 5.4).

Similar to the solution-based studies, the fluorescence of the hydrogels increased with glucose concentration. Figure 5.7 shows the changes in fluorescence for the *o*-BA and *m*-BA hydrogels in varying glucose concentration, where an overall increase of 45% was observed for *m*-BA with 100 mM glucose. Similarly, for *o*-BA hydrogels, the fluorescence is recovered by  $\sim 35\%$ .

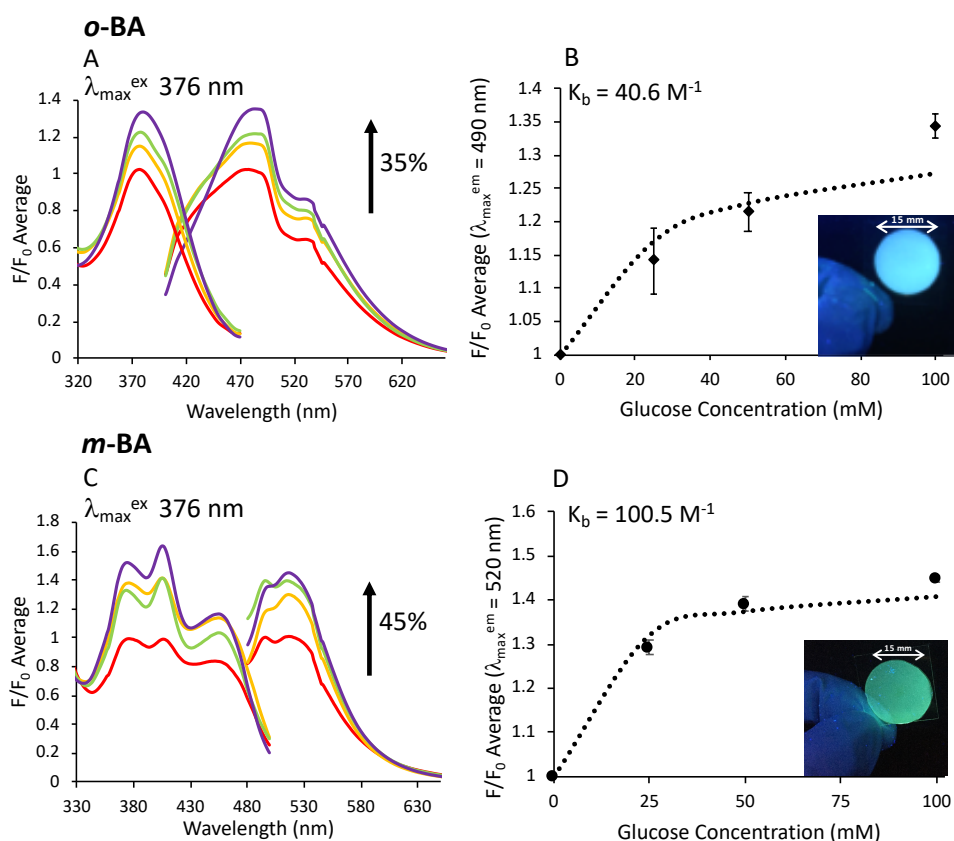


**Figure 5.7.** Normalised emission data ( $n = 3$ ) of hydrogel disks containing pyranine (0.0001 mol%) and *o*-BA (15 eq.) or *m*-BA (10 eq.) with varied glucose concentrations (0-100 mM). (A) Shows the excitation and emission spectra for the *o*-BA hydrogels with increased fluorescence by 35% with 100 mM glucose and (B) shows the emission at 490 nm. (C) Shows the excitation and emission spectra for the *m*-BA hydrogels with increased fluorescence by 45% with 100 mM glucose and (D) shows the emission at 520 nm. The insets in (B) and (D) show images of the quenched hydrogel under 365 nm UV light. The points on the curve represent the mean  $\pm$  standard deviation.

## 5.5 Conclusions

In summary, a new class of polymerisable, water soluble, BA derivatives has been synthesized and characterised. Their cationic nature was exploited to quench the fluorescence of an anionic fluorophore. In the presence of saccharides, the formation of a cyclic boronate ester resulted in dissociation of this non-fluorescent complex, thereby enabling fluorescence recovery. The presence of polymerizable groups within the BA structure enabled their incorporation within hydrogel matrices. The resulting hydrogels were shown to respond to glucose within concentration ranges relevant for physiological sensing (up to 50 mM). These small, cationic BA monomeric units offer an adaptable approach for the production of soft hydrogel sensors, in which they can

be co-polymerised (up to 100%) with a wide range of available monomers. We believe these results can provide great potential for the creation of hydrogel saccharide sensors.

## 5.6 References

1. Hageman, J. H.; Kuehn, G. D. Boronic Acid Matrices for the Affinity Purification of Glycoproteins and Enzymes. In *Practical Protein Chromatography*; Kenney, A.; Fowell, S.; Eds. The Humana Press Inc., Totowa, New Jersey, 1992; Vol. 11, pp 45-71.
2. Duggan, P. J.; Tyndall, E. M. Boron Acids as Protective Agents and Catalysts in Synthesis, *J. Chem. Soc., Perkin Trans.*, **2002**, *1*, 1325-1339.
3. Hall, D. G. Structure, properties, and preparation of boronic acid derivatives. Overview of their reactions and applications. In *Boronic Acids: Preparation and application in organic synthesis, medicine and materials*, 2<sup>nd</sup> Ed.; Hall, D. G., Ed.; Wiley-VCH, Weinheim, 2005; Vol. 2, pp 1-100.
4. Badugu, R.; Lakowicz, J. R.; Geddes, C. D. Enhanced Fluorescence Cyanide Detection at Physiologically Lethal Levels: Reduced ICT-Based Signal Transduction, *J. Am. Chem. Soc.*, **2005**, *127*, 3635-3641.
5. Jin, S.; Li, M.; Zhu, C.; Tran, V.; Wang, B. Computer-Based de Novo Design, Synthesis and Evaluation of Boronic Acid-Based Artificial Receptors for Selective Recognition of Dopamine, *ChemBioChem*, **2008**, *9*, 1431-1438.
6. Yan, J.; Springsteen, G.; Deeter, S.; Wang, B. The Relationship Among pK<sub>a</sub>, pH, and Binding Constants in the Interactions Between Boronic Acids and Diols - It is not as Simple as it Appears, *Tetrahedron*, **2004**, *60*, 11205-11209.
7. Hansen, J. S.; Christensen, J. B.; Petersen, J. F.; Hoeg-Jensen, T.; Norrild, J. C. Arylboronic Acids: A Diabetic Eye on Glucose Sensing, *Sens. Actuators, B*, **2012**, *161*, 45-79.
8. Corrie, S. R.; Coffey, J. W.; Islam, J.; Markey, K. A.; Kendall, M. A. F. Blood, Sweat, and Tears: Developing Clinically Relevant Protein Biosensors for Integrated Body Fluid Analysis, *Analyst*, **2015**, *140* (13), 4350-4364.
9. Yoon, J.; Czarnik, A. W. Fluorescent Chemosensors of Carbohydrates. A Means of Chemically Communicating the Building of Polyols in Water Based on Chelation-Enhanced Quenching, *J. Am. Chem. Soc.*, **1992**, *114*, 5874-5875.
10. Lacina, K.; Skládel, P.; James, T. D. Boronic Acids for Sensing and Other Applications - A Mini-Review of Papers Published in 2013, *Chem. Cent. J.*, **2014**, *8* (60).
11. Fang, H.; Kaur, G.; Wang, B. Progress in Boronic Acid-Based Fluorescent Glucose Sensors, *J. Fluoresc.*, **2004**, *14* (5), 481-489.
12. Pappin, B.; Kiefel, M. J.; Houston, T. A. Boron-Carbohydrate Interactions. In *Carbohydrates - Comprehensive Studies on Glycobiology and Glycotechnology*, Creative Commons Attribution, InTech, 2012, pp 37-54.
13. Crane, B. C.; Barwell, N. P.; Gopal, P.; Gopichand, M.; Higgs, T.; James, T. D.; Jones, C. M.; Mackenzie, A.; Mulavisala, K. P.; Paterson, W. The Development of a Continuous Intravascular Glucose Monitoring Sensor, *J. Diabetes Sci. Technol.*, **2015**, *9* (4), 751-761.
14. Sharma, B.; Bugga, P.; Madison, L. R.; Henry, A.-I.; Blaber, M. G.; Greenelch, N. G.; Chiang, N.; Mrksich, M.; Schatz, G. C.; Van Duyne, R. P. Bisboronic

- Acids for Selective, Physiological Relevant Direct Glucose Sensing with Surface-Enhanced Raman Spectroscopy, *J. Am. Chem. Soc.*, **2016**, *138*, 13952-13959.
15. Bruen, D.; Delaney, C.; Florea, L.; Diamond, D. Glucose Sensing for Diabetes Monitoring: Recent Developments, *Sensors*, **2017**, *17*, 1866-1887.
  16. Badugu, R.; Lakowicz, J. R.; Geddes, C. D. Ophthalmic Glucose Monitoring Using Disposable Contact Lenses - A Review. *J. Fluoresc.*, **2004**, *14* (5), 617-633.
  17. Wu, X.; Li, Z.; Chen, X.-X.; Fossey, J. S.; James, T. D.; Jiang, Y.-B. Selective Sensing of Saccharides Using Simple Boronic Acids and Their Aggregates, *Chem. Soc. Rev.*, **2013**, *42*, 8032-8048.
  18. Sun, X.; James, T. D. Glucose Sensing in Supramolecular Chemistry, *Chem. Rev.*, **2015**, *115*, 8001-8037.
  19. James, T. D.; Samankumara Sandanayake, K. R. A.; Shinkai, S. A Glucose-Selective Molecular Fluorescence Sensor, *Angew. Chem., Int. Ed. Engl.*, **1994**, *33*, 2207-2209
  20. Appleton, B.; Gibson, T. D. Detection of total sugar concentration using photoinduced electron transfer materials: development of operationally stable, reusable optical sensors, *Sens. Actuators, B*, **2000**, *65*, 302-304.
  21. Suri, J. T.; Cordes, D. B.; Cappuccio, F. E.; Wessling, R. A.; Singaram, B. Monosaccharide Detection with 4,7-Phenanthroline Salts: Charge-Induced Fluorescence Sensing, *Langmuir*, **2003**, *19*, 5145-5152.
  22. Lakowicz, J. R., *Principles of Fluorescence Spectroscopy*, 3rd Ed.; Springer Science+Business Media, 2006, pp 1-923.
  23. Vilozny, B.; Schiller, A.; Wessling, R. A.; Singaram, B. Multiwell Plates Loaded with Fluorescent Hydrogel Sensors for Measuring pH and Glucose Concentration, *J. Mater. Chem.*, **2011**, *21*, 7589-7595.
  24. Cappuccio, F. E.; Suri, J. T.; Cordes, D. B.; Wessling, R. A.; Singaram, B. Evaluation of Pyranine Derivatives in Boronic Acid Based Saccharide Sensing: Significance of Charge Interaction Between Dye and Quencher in Solution and Hydrogel. *J. Fluoresc.*, **2004**, *14* (5), 521-533.
  25. Sharrett, Z.; Gamsey, S.; Hirayama, L.; Vilozny, B.; Suri, J. T.; Wessling, R. A.; Singaram, B. Exploring the Use of APTS as a Fluorescent Reporter Dye for Continuous Glucose Sensing, *Org. Biomol. Chem.*, **2009**, *7*, 1461-1470.
  26. Camara, J. N.; Suri, J. T.; Cappuccio, F. E.; Wessling, R. A.; Singaram, B. Boronic Acid Substituted Viologen Based Optical Sugar Sensors: Modulated Quenching with Viologen as a Method for Monosaccharide Detection, *Tetrahedron Lett.*, **2002**, *43*, 1139-1141.
  27. Gamsey, S.; Baxtor, N. A.; Sharrett, Z.; Cordes, D. B.; Olmstead, M. M.; Wessling, R. A.; Singaram, B. The Effect of Boronic Acid-Positioning in an Optical Glucose-Sensing Ensemble, *Tetrahedron*, **2006**, *62*, 6321-6331.
  28. Sharrett, Z.; Gamsey, S.; Fat, J.; Cunningham-Bryant, D.; Wessling, R. A.; Singaram, B. The Effect of Boronic Acid Acidity on Performance of Viologen-

- Based Boronic Acids in a Two-Component Optical Glucose-Sensing System, *Tetrahedron Lett.*, **2007**, *48*, 5125-5129.
29. Suri, J. T.; Cordes, D. B.; Cappuccio, F. E.; Wessling, R. A.; Singaram, B. Continuous Glucose Sensing with a Fluorescent Thin-Film Hydrogel. *Angew. Chem., Int. Ed.*, **2003**, *42*, 5857-5859.
  30. Wang, Z.; Lei, H.; Feng, L. A Facile Channel for D-Glucose Detection in Aqueous Solution, *Spectrochim. Acta, Part A*, **2013**, *114*, 293-297.
  31. Feng, L.; Liang, F.; Wang, Y.; Xu, M.; Wang, X. A Highly Sensitive Water-Soluble System to Sense Glucose in Aqueous Solution, *Org. Biomol. Chem.*, **2011**, *9*, 2938-2942.
  32. Li, Y.; Zhang, L.; Haung, J.; Liang, R.; Qiu, J. Fluorescent Graphene Quantum Dots with a Boronic Acid Appended Bipyridinium Salt to Sense Monosaccharides in Aqueous Solution, *Chem. Commun.*, **2013**, *49*, 5180-5182.
  33. Dinis-Oliveira, R. J.; Duarte, J. A.; Sanchez-Navarro, A.; Remiao, F.; Bastos, M. L.; Carvalho, F. Paraquat Poisonings: Mechanisms of Lung Toxicity, Clinical Features, and Treatment, *Crit. Rev. Toxicol.*, **2008**, *38* (1), 13-71.
  34. Bruen, D.; Delaney, C.; Diamond, D.; Florea, L. A New Family of Monomeric Fluorescent Boronic Acids - Synthesis and Glucose Binding Studies, *Chem. Commun.*, **2018** (under review).
  35. Delaney, C.; Florea, L.; Bruen, D.; Diamond, D. Boronic Acid Derivatives for Sugar-Sensing Hydrogels, GB1805226.6, 29 March 2018.
  36. GörmerHerbert Waldmann, K.; Brunsveld, L. Amino Acids, Peptides and Proteins. In *Comprehensive Natural Products II*; Lew Mander, Hung-Wen (Ben) Liu, Ed.; Elsevier Ltd., Amsterdam, Netherlands, 2010; Vol. 5, pp 531-585.
  37. O'Shaughnessy, K. M. Cholinergic and Antimuscarinic (Anticholinergic) Mechanisms and Drugs. In *Clinical Pharmacology*, 11<sup>th</sup> Ed.; Elsevier Ltd., Amsterdam, Netherlands, 2012; pp 372-381.
  38. Schulman, S.; Chen, S.; Bai, F.; Leiner, M.; Weis, L.; Wolfbeis, O. Dependence of the Fluorescence of Immobilized 1-Hydroxypyrene-3,6,8-trisulfonate on Solution pH: Extension of the Range of Applicability of a pH Fluorosensor, *Analyt. Chima. Acta.*, **1995**, *304*, 165-170.
  39. Mohr, G. J.; Werner, T.; Wolfbeis, O. S. Application of a Novel Lipophilized Fluorescent Dye in an Optical Nitrate Sensor, *J. Fluoresc.*, **1995**, *5* (2), 135-138.
  40. Kano, K.; Fendler, J. Pyranine as a Sensitive pH Probe for Liposome Interiors and Surfaces, *Biochim. Biophys. Acta*, **1978**, *509*, 289-299.



## **Chapter 6**

---

**Future Work: Sugar Sensing Using Boronic Acid  
Polymers**

---

## Contents

### Chapter 6: Future Work: Sugar Sensing Using Boronic Acid Polymers

6.1 Abstract	175
<b><u>Part A – Indirect Glucose Sensing in Ionogels</u></b>	<b>176</b>
6.2 Introduction	176
6.3 Experimental	179
6.3.1 Materials and Methods	179
6.3.2 Synthesis of Ionogel 1	180
6.3.2.1 <i>Synthesis of Di(trihexyltetradecyl phosphonium) Fluorescein Ionic Liquid (P<sub>6,6,6,14</sub> Fluorescein IL)</i>	180
6.3.2.2 <i>Synthesis of Tetrabutylphosphonium Sulfopropyl Methacrylate (P<sub>4,4,4,4</sub>SPMA) IL Monomer</i>	181
6.3.2.3 <i>Preparation of Ionogel 1</i>	182
6.3.2.4 <i>Synthesis of Cationic BA Derivatives, 1-(3-Boronobenzyl)-6-methylquinolin-1-ium bromide (m-MethylBA) and 5-Amino-1-(2-boronobenzyl)quinolin-1-ium bromide (o-AminoBA)</i>	183
6.3.4 Ionogel 1 – Probing Interactions with BAs	184
6.3.5 Synthesis of Ionogel 2	185
6.3.6 Ionogel 2 – Probing Interactions with Glucose	186
6.4 Results and Discussion	187
6.4.1 Ionogel 1	187
6.4.2 Ionogel 2	192
6.5 Conclusions and Future Work	194
<b><u>Part B – Fluorescence Quenching and Recovery Studies in Hydrogel Cocktails</u></b>	<b>195</b>
6.6 Introduction	195
6.7 Experimental	195
6.7.1 Materials and Methods	195
6.7.2 Preparation of Fluorescent Monomeric Cocktails	196
6.8 Results and Discussion	197
6.8.1 Monomer Quenching Effect on Pyranine Fluorescence	197
6.8.2 Fluorescence Titrations	200

6.8.2.1 <i>Fluorescence Quenching</i>	200
6.8.2.2 <i>Fluorescence Recovery</i>	203
<b>6.9 Conclusions and Future Work</b>	<b>204</b>
<b><u>Part C - Layer-by-Layer Films Composed of BA Linear Polymers and Poly(vinyl sulfonate)</u></b>	<b>205</b>
<b>6.10 Introduction</b>	<b>205</b>
<b>6.11 Experimental</b>	<b>210</b>
6.11.1 Materials and Methods	210
6.11.2 Preparation of BA Linear Polymers	211
6.11.3 LbL Films	211
6.11.3.1 <i>LbL Assembly</i>	211
6.11.3.2 <i>Sugar-Induced LbL Disassembly</i>	212
<b>6.12 Results and Discussion</b>	<b>213</b>
<b>6.13 Conclusion and Future Work</b>	<b>215</b>
<b>6.14 References</b>	<b>216</b>

## 6.1 Abstract

Over recent years, Boronic acids (BAs) have been exploited for their ability to sense saccharides. BAs are Lewis acidic since they possess a vacant *p*-orbital, which allows them to form strong, but reversible interactions with diol-containing compounds, thus forming an anionic boronate-saccharide complex. This interaction can be probed intramolecularly, via interactions with the fluorophore moiety incorporated in a BA sensor, or intermolecularly, via through space interactions with a separate fluorophore molecule. Previous chapters have focussed on the design and synthesis of single molecule fluorescent sensors (Chapters 2 and 4) or two-component sensing systems (Chapters 3 and 5) and their characterisation in solution. Consideration of long term stability and reliability of point-of-care devices highlights the need to incorporate these sensing systems in solid-state polymeric membranes. Therefore, in this future work chapter, several strategies for potential incorporation of two-component sensing systems (BA–Fluorophore) in gel matrices are investigated (Part A and B).

Boronic acid derivatives have piqued interest not only for the development of sensors but also as stimuli-responsive materials that can be incorporated into drug delivery platforms. In particular, BA-containing linear polymers have been used in layer-by-layer (LbL) assemblies to trigger the release of drugs in the presence of saccharides. Part C of this future work chapter describes a novel LbL system based on cationic BA-homopolymers, their assembly and sugar-induced disassembly in aqueous solutions.

## Part A – Indirect Glucose Sensing in Ionogels

### 6.2 Introduction

In Chapter 3 and 5, an indirect sensing approach was described for novel cationic BA derivatives whose interaction with known fluorophores can be used to measure glucose concentrations. A fluorescence decrease of the fluorophore emission upon increased concentrations of the BA component was first detected, followed by the restoration of fluorescence in the presence of glucose. To date, few examples of this two-component sensing system exist in solid state,<sup>1-7</sup> where our group has shown great expertise in the incorporation of sensing molecules in polymer gel structures.<sup>8,9</sup>

Recently, the use of fluorescence-based molecular sensors for glucose-monitoring applications has been a research area of interest. Fluorophores, such as anthracene, have demonstrated long-term *in vivo* glucose-monitoring for up to 140 days in mice models.<sup>10</sup> Although there are known disadvantages for the use of fluorophores, such as necessary UV-light irradiation, immune responses towards the fluorescent probes and photo-bleaching of the fluorophore, most of these challenges could be overcome by implementing the sensing system inside a hydrogel.<sup>10</sup> This is due to the fact that owing to their high water content, hydrogels display biomimetic properties.<sup>7</sup> Interchanging 7-hydroxycoumarin (7HC) (Chapter 3) for fluorescein could eliminate health concerns raised by the need of UV-light irradiation,<sup>10</sup> since the excitation wavelength for dianionic fluorescein is ~500 nm,<sup>11</sup> which is of a higher excitation wavelength compared to ~370 nm for anionic 7HC.<sup>12</sup> Fluorescein is also known to be non-toxic and has been previously used in biomedical applications.<sup>13</sup>

Hydrogels are three-dimensionally cross-linked hydrophilic polymer networks which are capable of retaining high quantities of water in their structures.<sup>7, 10</sup> Physiochemical properties of hydrogels are comparable with living tissues, due to their high water content, which makes these materials biocompatible.<sup>7, 14</sup> By fabricating a BA-containing hydrogel, both the benefits of hydrogels and BAs can be combined.<sup>7</sup> Incorporating BA components in to a hydrogel framework would allow for integration of these sensing gels in to smart sensing platforms, while retaining robustness, sensitivity and ease of handling of the sensing components.<sup>14</sup>

Singaram *et al.*<sup>2-5</sup> and others<sup>6</sup> have investigated two-component sensing in the solid-state for glucose detection. Predominantly pyranine was used as the

fluorescence reporter unit and BA-viologen compounds acting simultaneously as the fluorescence quenchers and BA receptor units. As it stands, the most advanced two-component hydrogel sensing system developed by Singaram *et al.* relies on local interactions between the fluorophore and BA-viologen units, where these components are co-polymerized within the gel matrix. Instead, herein we propose electrostatic immobilisation of the fluorophore by employing fluorescent ionic liquids (ILs). This would allow for the fluorophore to remain mobile within the gel matrix, which could be beneficial for BA-fluorophore interactions.

The use of ILs in materials science is a relatively new concept that has attracted substantial interest in recent years.<sup>8</sup> Integrating an ionic liquid inside a polymer gel merges the favourable features associated with both materials in a novel matrix.<sup>15, 16</sup> ILs are liquid salts below 100 °C that have paved applications in many fields of chemistry and materials science, as well as industry, due to their chemical and thermal stability, low vapour pressure and high ionic conductivity.<sup>8, 15-17</sup> Being a liquid salt, ILs are therefore composed of an anion and a cation.<sup>17</sup> As a result, these materials are hydrophilic, but can also be tailored for hydrophobic properties.<sup>15, 17</sup> Conveniently, many have labelled these liquids as ‘designer solvents’ where they are easily tuned for a variety of specific functions such as electrochemical materials in green chemistry, electrolytes for electrochemical devices, including double layer capacitors, solar cells and rechargeable lithium batteries, as well as solvents for organic synthesis (*e.g.* for Diels-Alder, Grignard reaction, Suzuki or Heck cross-coupling reactions).<sup>17</sup> Simply by interchanging the anionic or cationic component combinations of up to one trillion ionic liquids can be produced.<sup>8, 15-17</sup> Conveniently, this allows for a range of ILs that can be made responsive to numerous stimuli, including temperature, pressure, magnetic and electric fields, pH and light, among others, on incorporation of stimuli-responsive species available for local interaction.<sup>8, 16, 18</sup>

Ionogels are a new class of polymeric materials, where an ionic liquid is generally used to solvate the polymeric chains. Poly(ionic liquid)s (PILs) comprise a subclass of ILs, where they are synthesised from ILs containing polymerizable groups.<sup>8</sup> Several ionogels have been fabricated by us and others, where these have been modified to contain functional units, such as photochromic or fluorescent dyes, which enabled the gel to be photo-responsive.<sup>8, 18</sup> Within the IL field, phosphonium cation-based ionic liquids possess some advantageous properties that can be exploited. When compared

to their imidazolium based counterparts, for example, phosphonium ILs show higher thermal stability, lack acidic protons and are often less dense than water, which can be beneficial in complex organic chemistry work-up stages that involve decanting aqueous layers containing undesired by-products.<sup>15, 17</sup> By modifying the anionic or cationic components, the physical and chemical properties of polymerizable phosphonium ILs can be modified, to elicit control over the design of novel polymeric materials.<sup>15</sup>

In this section, an indirect sensing method for glucose detection using a di(trihexyltetradecyl phosphonium) Fluorescein ionic liquid (P<sub>6,6,6,14</sub> Fluorescein IL) is described. Two fluorescein-containing ionogels, Ionogel 1 and Ionogel 2, have been synthesised for a two-component glucose detection system. In Chapter 3, it was determined that by working in a solution close to the pK<sub>a</sub> of the fluorophore, the fluorescence response could be optimised for glucose detection. Fluorescein was chosen for this reason because it has been widely studied<sup>11</sup> and for its pK<sub>a</sub> close to ~7,<sup>7</sup> which would permit glucose detection in pH solutions close to physiological pH.

In Ionogel 1, both the P<sub>6,6,6,14</sub> fluorescein IL and the BA derivatives were electrostatically bound within the ionogel matrix. In pH 7.4 conditions, the anionic fluorescein and cationic BA molecules formed a non-fluorescent ground-state complex by electrostatic interactions within the ionogel. On introducing glucose, a change in hybridization in boron was induced to the anionic boronate form. This initiated dissociation in the ground-state complex to restore the fluorescence in fluorescein. Ionogel 1 was used to screen two phenyl-BA derivatives, *m*-MethylBA and *o*-AminoBA, in an attempt to optimise the system for glucose sensing. Two cationic BA derivatives of different design were synthesised to determine the most favourable BA structure, in terms of the positioning of substituents on the quinoline rings and the orientation of the BA group for glucose binding and hence, fluorescence recovery.

In Ionogel 2, the P<sub>6,6,6,14</sub> fluorescein IL was electrostatically bound inside the gel matrix, while the 3-(acrylamido)phenylBA was co-polymerised together with acrylamide and *N*-[3-(dimethylamino)propyl] methacrylamide in a 1:3:1 molar ratio. The fluorescence of Ionogel 2 was monitored upon glucose addition.

## 6.3 Experimental

### 6.3.1 Materials and Methods

Fluorescein disodium salt ( $\text{Na}_2\text{Fl}$ ), trihexyltetradecyl phosphonium chloride 95% ( $\text{P}_{6,6,6,14}\text{Cl}$ ), potassium 3-sulfopropyl methacrylate salt, magnesium sulphate ( $\text{MgSO}_4$ ), polypropylene oxide diacrylate (PPO800; crosslinker), 2,2-dimethoxy-2-phenacetophenone (DMPA; photoinitiator), 3-(acrylamido)phenylboronic acid, *N*-[3-(dimethylamino)propyl] methacrylamide, polyethylene glycol (PEG) diacrylate-258 (crosslinker), 2-hydroxy-2-methylpropiophenone (photoinitiator), D-glucose and 6-methylquinoline were purchased from Sigma Aldrich and used as received. 2-(Bromomethyl)phenylboronic acid, 3-(bromomethyl)phenylboronic acid and 5-aminoquinoline were purchased from Fluorochem UK. Tetrabutylphosphonium chloride ( $\text{P}_{4,4,4,4}\text{Cl}$ ) was kindly donated by Cytec<sup>®</sup> Industries. Solvents used were methanol ( $\text{CH}_3\text{OH}$ ), anhydrous acetonitrile ( $\text{CH}_3\text{CN}$ ). Deionized water ( $18.2 \text{ M}\Omega \cdot \text{cm}^{-1}$ ) (DI water) was made using a Merck Millipore Milli-Q Water Purification System. pH measurements were carried out on a VWR symphony SP70P pH meter.  $^1\text{H}$  and  $^{13}\text{C}$  NMR spectra were recorded on a 400 MHz or 600 MHz Bruker NMR spectrometer, using deuterium oxide ( $\text{D}_2\text{O}$ ) or deuterated methanol ( $d_4\text{-CH}_3\text{OH}$ ).  $^{11}\text{B}$  NMR experiments were carried out on a 600 MHz NMR spectrometer that used  $\text{BF}_3$  in deuterated methanol as an external standard. All reactions employing BA derivatives were monitored by thin layer chromatography (TLC) that used basic silica plates and 5:95%  $\text{CH}_3\text{OH}:\text{CH}_2\text{Cl}_2$  as the mobile phase. All fluorescence measurements were carried out on a JASCO Spectrofluorometer FP-8300 in pH buffer solutions.

The fluorescence of the gels was measured in a customised 3D printed holder (Figure 6.1). All measurements were carried out at room temperature. The parameters set were as follows; bandwidth: 5 nm, sensitivity: high. Approximately 20 scans were taken at 20 second intervals before the emission spectrum was stabilised, previous to glucose additions. All fluorescence measurements were carried out in pH 7.4 phosphate buffer solution, where the buffer composition was as follows; 0.1 M potassium dihydrogen phosphate ( $\text{KH}_2\text{PO}_4$ ; 100 mL) and 0.1 M sodium hydroxide ( $\text{NaOH}$ ; 78.2 mL) salts. The buffer was made up to 200 mL using deionised water.



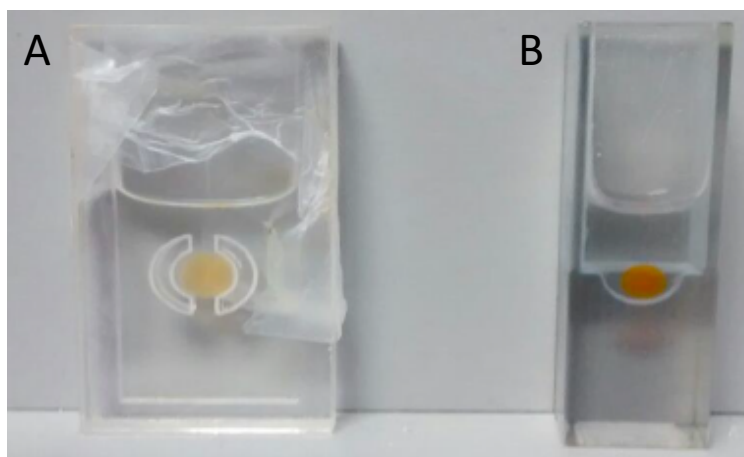
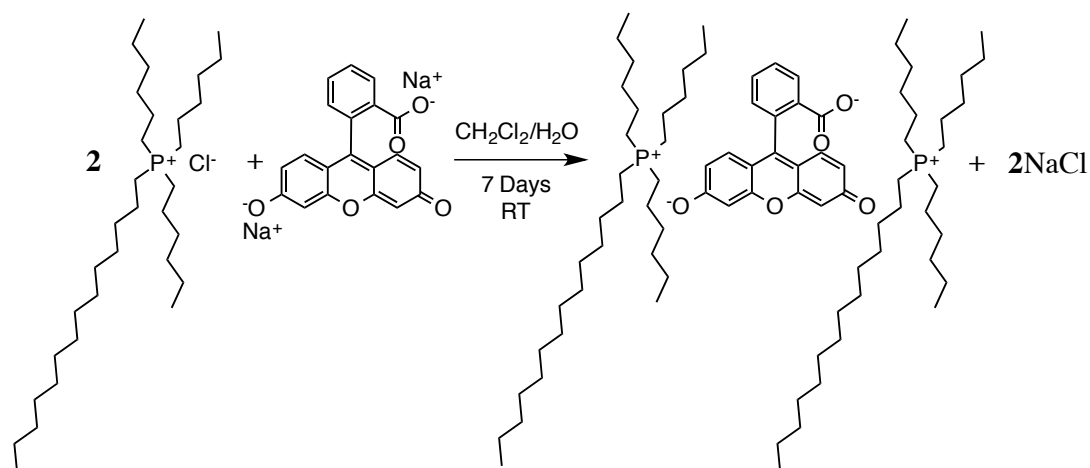


**Figure 6.1.** (A) Prototype holder; plastic slide holder with glass coverslip sealed with parafilm, the ionogel sits inside with pH 7.4 phosphate buffer. (B) 3D-printed cuvette style holder with fluorescein ionogel in pH 7.4 phosphate buffer solution.

### 6.3.2 Synthesis of Ionogel 1

Prior to ionogel synthesis, tetrabutylphosphonium sulfopropyl methacrylate (monomeric IL) and the di(trihexyltetradecyl phosphonium) fluorescein ( $P_{6,6,6,14}$  fluorescein IL) were synthesised as described below.

#### 6.3.2.1 Synthesis of Di(trihexyltetradecyl phosphonium) Fluorescein Ionic Liquid ( $P_{6,6,6,14}$ Fluorescein IL)

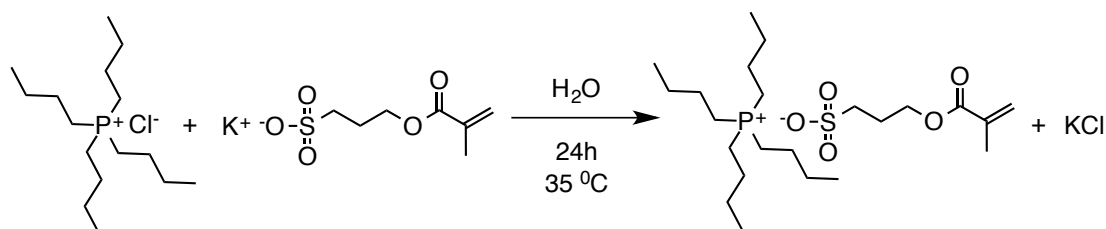


**Scheme 6.1.** Synthesis of  $P_{6,6,6,14}$  fluorescein ionic liquid.

$P_{4,4,4,16}$  Fluorescein IL was synthesised as indicated in Scheme 6.1, according to a previously published procedure.<sup>19, 20</sup> Briefly, fluorescein disodium salt ( $\text{Na}_2\text{Fl}$ ) (3.34 g; 8.95 mmol; 1.5 eq.) was dissolved in DI  $\text{H}_2\text{O}$  (200 mL).  $P_{6,6,6,14}\text{Cl}$  (3.1 g; 5.96 mmol; 1 eq.) was dissolved in  $\text{CH}_2\text{Cl}_2$  (40 mL) and was added to the  $\text{H}_2\text{O}$  solution.

The mixture was kept under vigorous stirring at room temperature for 7 days. In this case the reaction was taking place at the boundary of the two immiscible solvents, hence the need for vigorous stirring to ensure the surface area between the two liquids is maximized. The product was obtained in the organic phase. The organic phase was washed with excess DI H<sub>2</sub>O few times to remove unreacted fluorescein salt. After the washing was complete, the organic phase was concentrated under reduced pressure until a deep red and very viscous liquid was obtained. The final purification step consisted of drying the liquid overnight using a high vacuum pump (0.5 mBar). The result was a deep red, tar-like liquid, produced in a 70% yield.

### 6.3.2.2 Synthesis of Tetrabutylphosphonium Sulfopropyl Methacrylate ( $P_{4,4,4,4}$ SPMA) IL Monomer



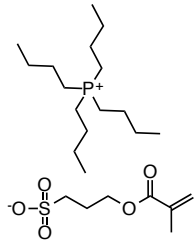
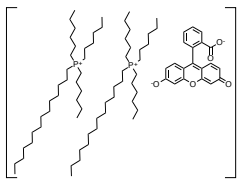
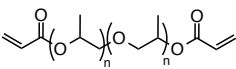
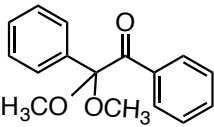
**Scheme 6.2.** Synthesis of tetrabutylphosphonium sulfopropyl methacrylate IL monomer.

Tetrabutylphosphonium sulfopropyl methacrylate ( $P_{4,4,4,4}$ SPMA) IL monomer was synthesised as indicated in Scheme 6.2, according to a previously published procedure.<sup>8</sup> Briefly, potassium 3-sulfopropyl methacrylate salt (6.26 g, 25.43 mmol, 1.5 eq.) and  $P_{4,4,4,4}$ Cl (5 g, 16.96 mmol, 1 eq.) were dissolved in DI H<sub>2</sub>O (20 mL) and the mixture was stirred for 24h at 35 °C. The reaction product was extracted three times with 40 ml of CH<sub>2</sub>Cl<sub>2</sub>. Following this, the organic phase was dried over MgSO<sub>4</sub> and the solvent was removed under reduced pressure. The IL product was left to dry further on the high vacuum line (0.5 mBar) for 4h to ensure all the CH<sub>2</sub>Cl<sub>2</sub> was removed. The desired IL was obtained as a viscous transparent liquid in a 70% yield. <sup>1</sup>H NMR (400 MHz, 20 °C), δ: 6.0 (1H, *dd*, *J* = 1, 2 and 3 Hz, CH – SPMA), 5.4 (1H, *t*, *J* = 1 and 3 Hz, CH – SPMA), 4.2 (2H, *t*, *J* = 6 and 12 Hz, CH<sub>2</sub> – SPMA), 2.8 (2H, *m*, CH<sub>2</sub> – SPMA), 2.3 (8H, *m*, CH<sub>2</sub> – P<sub>4,4,4,4</sub>), 2.2 (2H, *m*, CH<sub>2</sub> – SPMA), 1.8 (3H, *t*, *J* = 1 and 2 Hz, CH<sub>3</sub> – SPMA), 1.4 (16H, *t*, *J* = 4 and 8 Hz, CH<sub>2</sub> – P<sub>4,4,4,4</sub>), 0.9 (12H, *t*, *J* = 7 and 14 Hz, CH<sub>3</sub> – P<sub>4,4,4,4</sub>) ppm. For raw spectral data and supplementary information see Appendix E.

### 6.3.2.3 Preparation of Ionogel 1

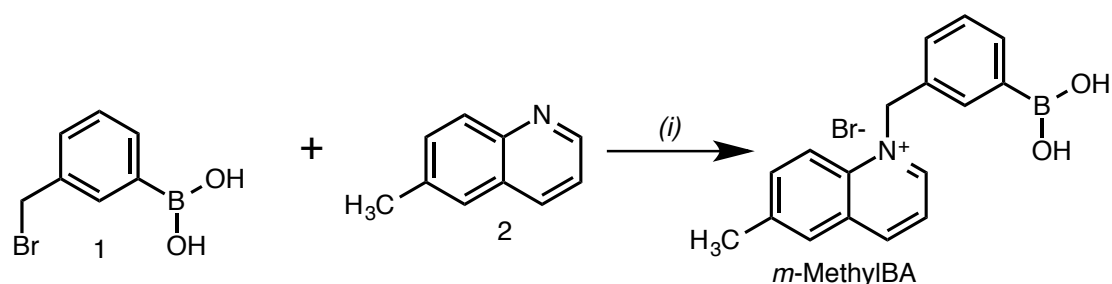
For Ionogel 1 synthesis, the polymerizable phosphonium IL, P<sub>4,4,4,4</sub>SPMA (0.187 g, 0.400 mmol, 100 eq.) and the P<sub>6,6,6,14</sub> Fluorescein IL (0.0052 g, 0.004 mmol, 1 eq.) were dissolved in CH<sub>3</sub>OH (100 mg) in a plastic vial. The cross-linker, PPO800 (0.018 g, 0.02 mmol, 5 eq.) and the photo-initiator, DMPA (0.002 g; 0.008 mmol; 2 eq.) were then added (Table 6.1). The mixture was stirred at room temperature until all components were dissolved. Once dissolved, the mixture was pipetted in to the desired mould and placed in the CL-1000 UV Crosslinker UVP chamber (365 nm) for 30 minutes.

**Table 6.1.** Reagents used for Ionogel 1 synthesis.

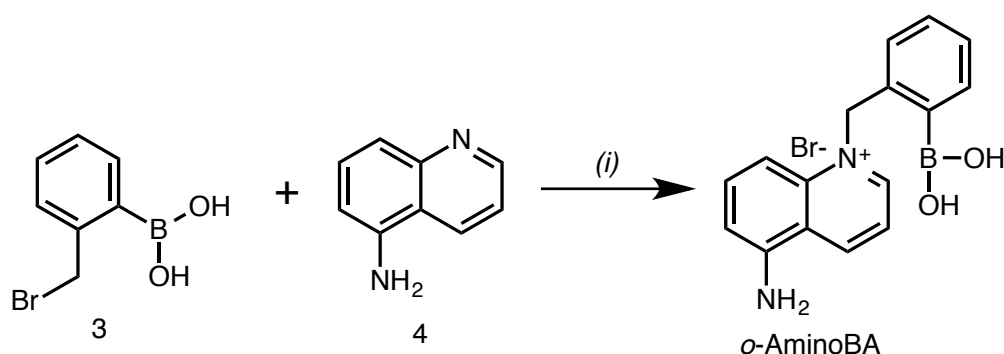
Materials		g	M <sub>r</sub> (g/mol)	mmol	Eq.
Tetrabutylphosphonium Sulfopropyl Methacrylate (P <sub>4,4,4,4</sub> SPMA)		0.187	466.6	0.4	100
Fluorescein IL		0.0052	1298	0.004	1
Polypropylene oxide diacrylate (PPO800) (Cross-linker)		0.018	926.0	0.02	5
2,2-dimethoxy-2-phenacetophenone (DMPA) (Initiator)		0.002	256.3	0.008	2

6.3.2.4 Synthesis of Cationic BA Derivatives, 1-(3-Boronobenzyl)-6 methylquinolin-1-ium bromide (*m*-MethylBA) and 5-Amino-1-(2-boronobenzyl)quinolin-1-ium bromide (*o*-AminoBA)

*m*-MethylBA and *o*-AminoBA were synthesised following the procedure outlined by Badugu *et al.*,<sup>21</sup> via a one-step nucleophilic substitution reaction (Scheme 6.3 and 6.4). This generic procedure involved the addition of equimolar amounts of the corresponding *o*- or *m*-boronobenzyl bromide (compounds 1 or 3) with the appropriate -CH<sub>3</sub> or -NH<sub>2</sub> substituted quinoline derivative (compounds 2 or 4) to form the boronic acid products *m*-MethylBA and *o*-AminoBA, respectively. The boronobenzyl bromide and quinoline moiety were dissolved in dry acetonitrile and stirred under an inert atmosphere for 24h at 70 °C. This reaction occurred rapidly to precipitate the quaternized nitrogen salt out of solution. The white precipitate (*m*-MethylBA) or orange precipitate (*o*-AminoBA) was then filtered and washed using dry acetonitrile and dried under vacuum for 12h. These resulting compounds were characterised by <sup>1</sup>H NMR, in CD<sub>3</sub>OD or D<sub>2</sub>O.



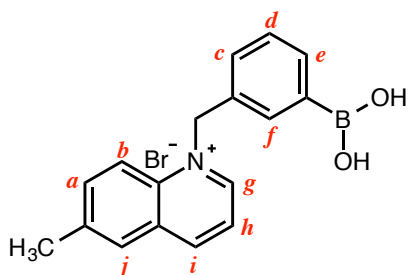
**Scheme 6.3.** Synthesis of *m*-MethylBA. (i) Anhydrous acetonitrile, N<sub>2</sub>, 24h.



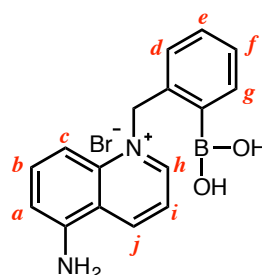
**Scheme 6.4.** Synthesis of *o*-AminoBA. (i) Anhydrous acetonitrile, N<sub>2</sub>, 24h.

*m*-MethylBA was produced as a white powder in an 83% yield (0.14823 g; 0.414 mmol). <sup>1</sup>H NMR (600 MHz, CD<sub>3</sub>OD, 20 °C) δ: 9.2 (1H, *d*, *J* = 6 Hz, CH – j), 9.0 (1H, *d*, *J* = 8 Hz, CH – i), 8.1 (1H, *d*, *J* = 9 Hz, CH – h), 8.0 (1H, *s*, CH – g), 7.9 (1H, *dd*, *J* = 2, 5, 8 and 14 Hz, CH – f), 7.8 (1H, *dd*, *J* = 1, 7, 9 and 10 Hz, CH – e), 7.7 (1H, *d*, *J* = 7 Hz, CH – d), 7.6 (1H, *s*, CH – c), 7.3-7.4 (2H, *m*, CH – a, b), 2.5 (3H, *s*, CH<sub>3</sub>), 6.2 (2H, *s*, CH<sub>2</sub>) ppm (Figure 6.2).

*o*-AminoBA was produced as an orange powder in an 83% yield (0.2722 g; 0.758 mmol). <sup>1</sup>H NMR (600 MHz, CD<sub>3</sub>OD, 20 °C) δ: 9.0 (1H, *d*, *J* = 9 Hz, CH – j), 8.8 (1H, *d*, *J* = 6 Hz, CH – h), 7.7 (2H, *m*, CH – g, i), 7.5 (1H, *dd*, *J* = 2, 5 and 7 Hz, CH – c), 7.3 (1H, *d*, *J* = 9 Hz, CH – b), 7.2 (2H, *m*, CH – e, f), 7.0 (1H, *d*, *J* = 8 Hz, CH – d), 6.8 (1H, *m*, CH – a), 6.1 (2H, *s*, CH<sub>2</sub>) ppm (Figure 6.3). <sup>11</sup>B NMR (192 MHz, CD<sub>3</sub>OD, 20 °C), δ: 4.9 (1B, B(OH)<sub>2</sub>) ppm. FT-IR spectroscopy found peaks at 3343, 3109 (B-OH), 2752, 2380 (C=C-H), 1922, 1836 (C=C), 1623, 1567 (Amine N-H), 1331 cm<sup>-1</sup>.<sup>22</sup> UV-visible spectroscopy found an absorbance wavelength at 269 nm. For raw spectral data and supplementary information see Appendix E.



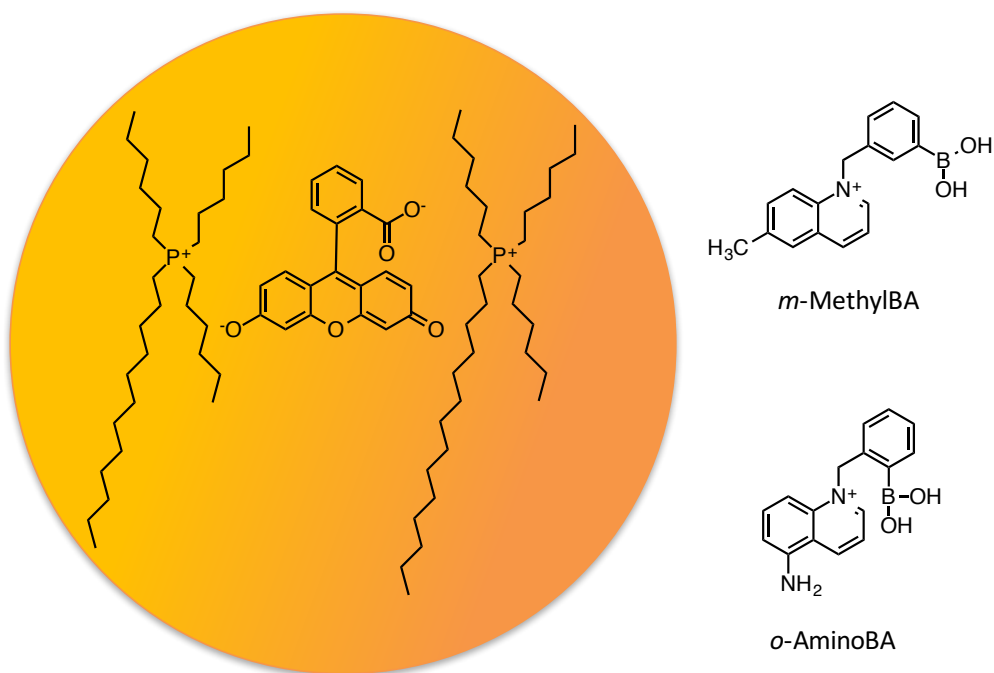
**Figure 6.2.** <sup>1</sup>H NMR assignment for *m*-MethylBA.



**Figure 6.3.** <sup>1</sup>H NMR assignment for *o*-AminoBA.

### 6.3.3 Ionogel 1 – Probing Interactions with BAs

Both BA derivatives described above, *m*-MethylBA and *o*-AminoBA were screened with the fluorescent Ionogel 1, in order to understand the effect attached substituents to the quinoline ring had on the quenching interaction and how the positioning of the BA group affected fluorescence restoration. As P<sub>6,6,6,14</sub> fluorescein IL was only held inside Ionogel 1 by electrostatic interactions (Figure 6.4), this meant that the P<sub>6,6,6,14</sub> fluorescein IL was not covalently appended to the gel matrix but was mobile within. This allowed for dynamic interactions with the BA derivatives, *m*-MethylBA or *o*-AminoBA, as they diffused in to the ionogel matrix.

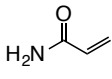
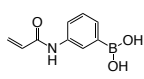
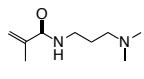
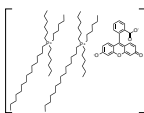
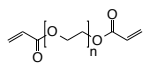
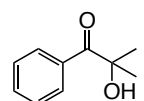


**Figure 6.4.** Ionogel 1 mobile components: P<sub>6,6,6,14</sub> fluorescein IL and cationic BA derivatives used for screening.

#### 6.3.4 Synthesis of Ionogel 2

For Ionogel 2 synthesis, acrylamide (106.5 mg, 1.5 mmol, 60 eq.), 3-(acrylamido)phenylboronic acid (95 mg, 0.5 mmol, 20 eq.), *N*-[3-(dimethylamino)propyl] methacrylamide (89.7  $\mu$ L, 0.5 mmol, 20 eq.) and the P<sub>6,6,6,14</sub> fluorescein IL (0.019 mg, 0.015 mmol, 1 eq.) were dissolved in DMSO (500  $\mu$ L). Once dissolved, the crosslinker (polyethylene glycol (PEG) diacrylate-258; 7  $\mu$ L, 0.03 mmol, 2 eq.) and the photo-initiator (2-hydroxy-2-methylpropiophenone; 4.6  $\mu$ L, 0.03 mmol, 2 eq.) were added. Once dissolved, the mixture was pipetted in to the desired mould (circles of 1 mm depth and 4 mm diameter) and placed in the CL-1000 UV Crosslinker UVP chamber (365 nm) for 40 minutes.

**Table 6.2.** Reagents used for Ionogel 2 synthesis.

Materials		g	V ( $\mu\text{L}$ )	Density ( $\rho$ ;g/mL)	$M_r$ (g/mol)	mmol	Eq.
Acrylamide		0.107	-	-	71.08	1.5	60
3-(Acrylamido)phenylboronic acid		0.095	-	-	190.99	0.5	20
<i>N</i> -[3-(Dimethylamino)propyl]methacrylamide		0.085	89.7	0.949	170.25	0.5	20
Fluorescein IL		0.019	-	-	1298	0.015	1
Polyethylene Glycol Diacrylate-258		7.74	7	1.11	258.0	0.03	2
2-Hydroxy-2-methylpropio phenone		0.005	4.6	1.077	164.2	0.03	2

### 6.3.5 Ionogel 2 – Probing Interactions with Glucose

In the case of Ionogel 2, the BA component was co-polymerised inside the polymer matrix together with acrylamide and *N*-[3-(dimethylamino)propyl]methacrylamide in a 1:3:1 molar ratio. This meant that the BA was immobilised and cannot therefore leave the system. The P<sub>6,6,6,14</sub> fluorescein IL was immobilised inside the ionogel framework by electrostatic interactions. Similarly to Ionogel 1, since fluorescein was not physically attached to the gel framework, it remained mobile inside the ionogel, allowing for dynamic interactions with the BA derivative that was co-polymerised within the ionogel matrix (Figure 6.5).

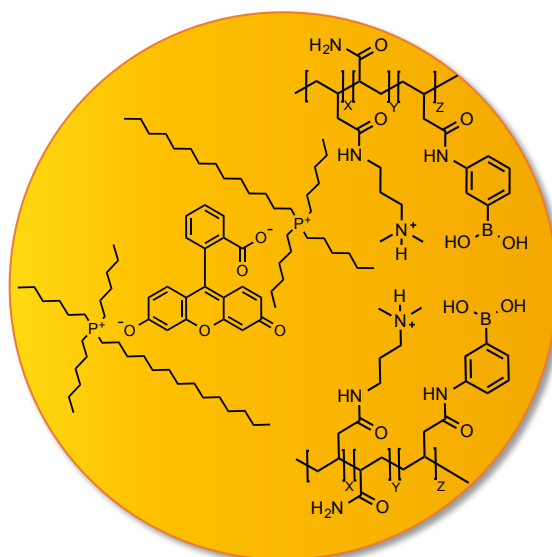


**Figure 6.5.** Structure of Ionogel 2 in pH 7.4 conditions, where X:Y:Z is 1:3:1.

## 6.4 Results and Discussion

The two novel fluorescent ionogels, Ionogel 1 and Ionogel 2, were investigated for their indirect glucose sensing capabilities at pH 7.4. In Ionogel 1, based on P<sub>4,4,4,4</sub>SPMA PIL, the BA solution was initially absorbed inside the gel and the fluorescence was monitored. This ionogel was screened with two cationic BA derivatives, *m*-MethylBA and *o*-AminoBA, to better understand the BA-sensor design for optimising glucose detection. A decrease in fluorescence of the fluorophore was observed, probably due to electrostatic interactions with the cationic BA component. Following this, glucose was added to the hydration solution, and the fluorescence recovery was monitored.

In the case of Ionogel 2, the 3-(acrylamido)phenyl-BA derivative was secured inside the hydrogel based on acrylamide by co-polymerisation. Ionogel 2 was initially fluorescent. With increased concentrations of glucose, the fluorescence in the fluorescein component became quenched. This quenched state of fluorescence resulted from a conformational change in the hybridisation of boron by a charge transfer mechanism on glucose binding.<sup>23</sup>

### 6.4.1 Ionogel 1

This indirect glucose-sensing mechanism is illustrated in Figure 6.6, similar to the indirect sensing mechanism described in Chapter 3. When the P<sub>6,6,6,14</sub> fluorescein Ionogel 1 was placed in a solution of the BA derivative, the fluorescence in the



ionogel became quenched. Fluorescence quenching occurred due to the formation of a non-fluorescent ground state complex due to electrostatic and  $\pi$ - $\pi$  stacking interactions between the anionic fluorescein and cationic BA derivatives. Glucose addition to this two-component sensing system, formed a BA-saccharide complex on binding to the BA group. Glucose binding induced a conformational change in the BA moiety transforming it from the neutral  $sp^2$  hybridised BA form to the anionic  $sp^3$  hybridised boronate form. The negatively charged boron atom could then form a dative bond with the  $N^+$  moiety of the BA derivative to neutralise the anionic charge on boron and stabilise glucose binding. Consequently, the electrostatic attraction between fluorescein and the BA derivative was weakened, as a result of increased electron density around  $N^+$ . This led to dissociation of the BA-fluorophore ground state complex to recover the fluorescence in fluorescein.

Two cationic BA derivatives were screened with Ionogel 1 in an attempt to optimise glucose detection in a pH 7.4 phosphate buffer. The design of the BA derivatives structures was investigated to determine how it affected the quenching of fluorescence, as well as the fluorescence recovery with glucose. In the BA derivatives structure, an  $N^+$  moiety was incorporated to promote electrostatic interactions with the anionic fluorophore. Consequently, the effect of electron-withdrawing groups (EWGs) and electron-donating groups (EDGs) was investigated, where a methyl substituent was employed in the *m*-MethylBA derivative and an electron donating amine group was present in the *o*-AminoBA compound. Moreover, these compounds also contain phenyl rings, which can further enhance communication with fluorescein by  $\pi$ - $\pi$  stacking interactions to quench its fluorescence. The positioning of the BA groups was also investigated to maximise fluorescence recovery with glucose. The  $pK_a$  of the BA moieties in these compounds are slightly lower than 9, at  $\sim 8.5$ , due to the electron-withdrawing  $N^+$  atom in the methyl-linked quinoline ring.<sup>21, 24</sup> By including EWGs, the acidity of the BA groups can be increased, particularly in the *ortho* position, which is beneficial for binding sugars at a lower pH, so that sensing closer to physiological pH is possible.<sup>1, 21, 24, 25</sup>

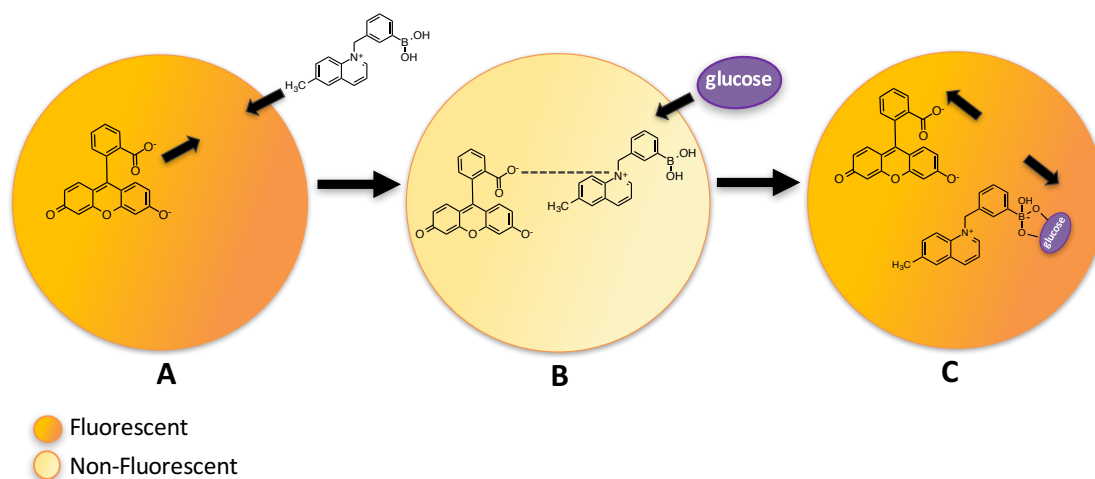


**Figure 6.6.** Proposed two-component glucose-sensing mechanism using Ionogel 1. (A) Ionogel 1 in its initial fluorescent state; (B) Cationic BA derivative diffuses into Ionogel 1 to form a non-fluorescent ground-state complex by electrostatic and  $\pi$ - $\pi$  stacking interactions; (C) Glucose diffuses inside Ionogel 1 and binds to the BA derivative. BA group binds glucose, leading to dissociation in BA-fluorophore complex to recover fluorescence.

*o*-AminoBA was first investigated with Ionogel 1 for its ability to quench the fluorescence of fluorescein and recover the fluorescence with glucose (Figure 6.7). The amine group (-NH<sub>2</sub>) attached to the quinoline ring in this BA derivative has electron-donating properties. The N atom in this group possesses a lone pair of electrons that can be donated into the quinoline ring. Consequently, by mesomeric and inductive effects in the quinoline ring, an increase in electron density around the N<sup>+</sup> atom can occur. Thus, weakening the electrostatic attraction with fluorescein to only slightly quench its fluorescence. As a result, a fluorescence decrease of 26% in the presence of 10 mM *o*-AminoBA was observed (Figure 6.8). The BA group however was present in the *ortho* position, which is in the optimal orientation for favourable interaction with the N<sup>+</sup> moiety. On glucose binding to the BA group, the anionic boronate formation was triggered. The negative charge on boron was then stabilised by the N<sup>+</sup> atom. When the BA group is in the *ortho* position, the B-N<sup>+</sup> interaction is optimised, which allows for more stable interaction on glucose binding. Glucose binding rendered the BA derivative zwitterionic, resulting in dissociation from the fluorophore. As a result, the fluorescence recovered by 16%, in the presence of 10 mM glucose (Figure 6.8).

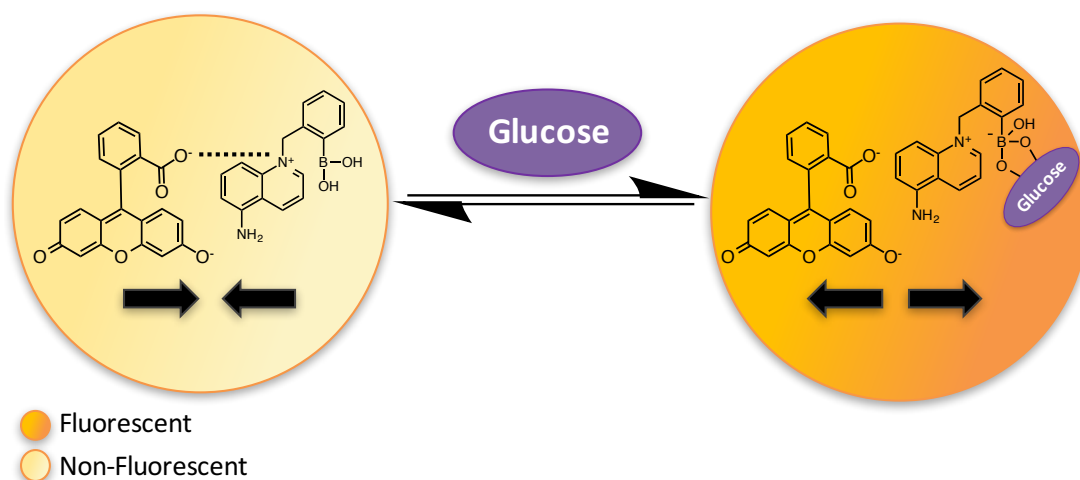


**Figure 6.7.** Immersion of Ionogel 1 in a solution of *o*-AminoBA (10 mM) in pH 7.4 phosphate buffer, resulted in a decrease in fluorescence (left). Sequential addition of a glucose containing solution in pH 7.4 phosphate buffer (10 mM) caused restoration of fluorescence (right).

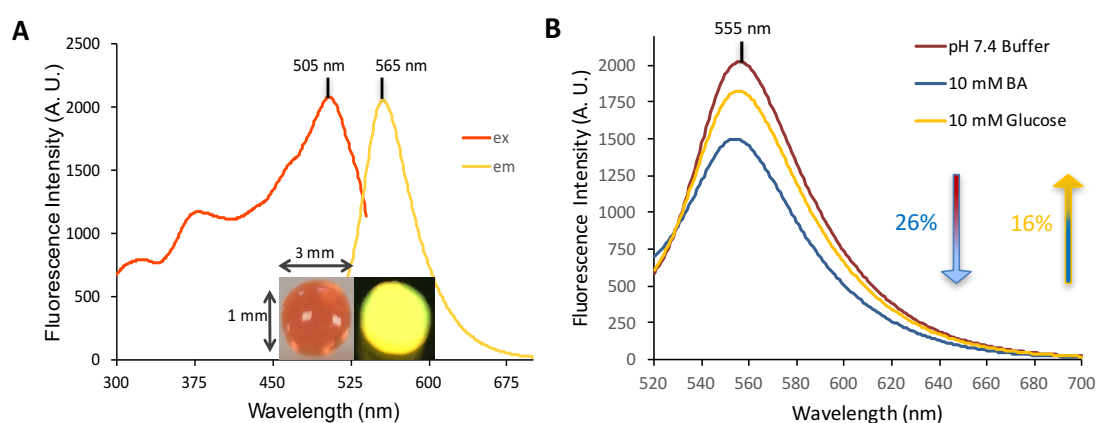


**Figure 6.8.** (A) Excitation and emission spectra of Ionogel 1 in pH 7.4 phosphate buffer solution, where the excitation wavelength is 505 nm and the corresponding emission wavelength is 565 nm. (B) Initial emission spectrum for Ionogel 1 in pH 7.4 phosphate buffer solution (red); Ionogel 1 was immersed in a solution of *o*-AminoBA in pH 7.4 phosphate buffer (10 mM), demonstrating a decrease in the emission intensity by 26% after 12h (blue); Following this, Ionogel 1 was placed in a solution of glucose in pH 7.4 phosphate buffer (10 mM), exhibiting an increase in fluorescence intensity by 16% after 12h (yellow).

*m*-MethylBA was also screened with Ionogel 1. *m*-MethylBA differs to *o*-AminoBA in that a methyl substituent is present in the 6-position on the quinoline ring, compared to an amine group in the 5-position in *o*-AminoBA. *m*-MethylBA has its BA group in the *meta* position, in contrast to the *ortho* orientation in *o*-AminoBA. Since the amine group is electron donating, it can increase the electron density around the N<sup>+</sup> moiety more in comparison to the methyl substituent. Consequently, the

methyl group in *m*-MethylBA has little effect on the N<sup>+</sup> atom in the quinoline ring. As a result, the N<sup>+</sup> atom in *m*-MethylBA can be considered more cationic in comparison to the N<sup>+</sup> atom in *o*-AminoBA. Therefore, the electrostatic attraction between *m*-MethylBA and fluorescein is enhanced compared to *o*-AminoBA. Subsequently, a decrease of 72% in the fluorescence intensity was observed for Ionogel 1 on immersion in a pH 7.4 buffer solution containing *m*-MethylBA (10 mM) (Figure 6.9). *m*-MethylBA exhibited enhanced fluorescence quenching in Ionogel 1 in comparison to *o*-AminoBA, which demonstrated only a 26% decrease in fluorescence. The BA group in *m*-MethylBA was present in the *meta* position. It is known that when the BA group is in the *ortho* orientation fluorescence recovery can be optimised, due to the ease of interaction between the N<sup>+</sup> moiety and the anionic B atom on glucose binding. In the *meta* orientation however, the B-N interaction is slightly sterically hindered, where solvent molecules are required to bridge the gap to permit B-N interactions, in order to neutralise the anionic charge on B on glucose binding and stabilise the boronate-sugar complex.<sup>26</sup> Consequently, fluorescence recovery with glucose when the BA group is in the *meta* position is less favoured compared to when this group in the *ortho* position.<sup>25</sup> A recovery of fluorescence by 32% was observed with 44 mM glucose (Figure 6.9).

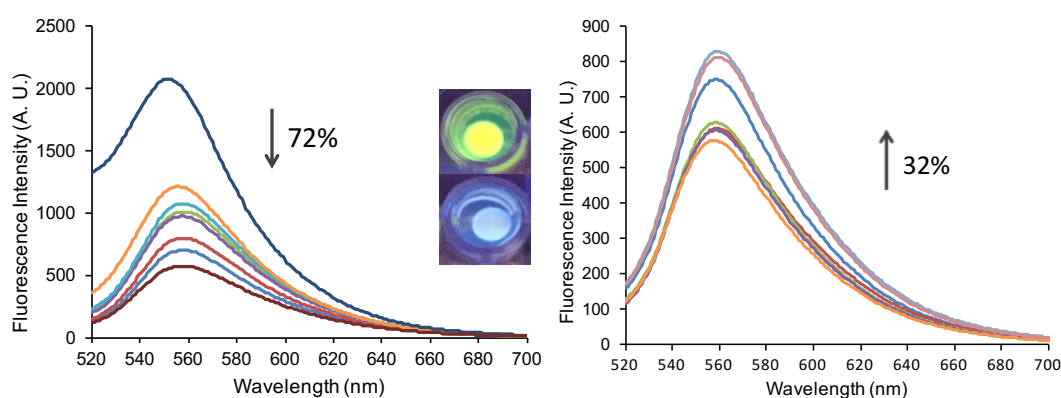


**Figure 6.9.** Emission spectrum of Ionogel 1 when immersed in a solution of *m*-MethylBA in pH 7.4 phosphate buffer (10 mM) at room temperature, showing a fluorescence decrease by 72% over 4h (left) when excited at 505 nm. Emission spectrum of Ionogel 1 when placed in a solution of glucose in pH 7.4 phosphate buffer (44 mM) showing a fluorescence increase by 32% (right).

Overall, the design of the BA derivative in a two-component sensing system is important when attempting to optimise both fluorescence quenching and recovery for glucose detection. Herein, the BA derivatives were designed to employ a cationic charge in order to quench the fluorescence of the anionic fluorophore electrostatically.

The BA compounds also contained phenyl rings to favour this quenching process by  $\pi$ - $\pi$  stacking interactions. It is also recommended that EWGs are incorporated close to an electron-accepting group or cationic atom, such as the  $N^+$  atom, in order to promote electrostatic interactions with the anionic fluorophore. This simply pulls electron density away from the  $N^+$  moiety by inductive effects to further enhance electrostatic interactions with the fluorophore.<sup>1</sup> Moreover, EWGs may also be included close to the BA moiety to increase the binding affinity for glucose to aid fluorescence recovery.<sup>1</sup> Future developments in this area include the covalent immobilisation of the ionogel components in order to avoid leaching of the sensing system through diffusion.

#### 6.4.2 Ionogel 2

A second approach using Ionogel 2 was designed and investigated for indirect glucose sensing. This second ionogel, based on a two-component sensing system, was fabricated to have the BA molecule covalently immobilised. In this case a neutral BA derivative was employed as the glucose receptor, which was co-polymerised in to the ionogel matrix (Figure 6.10). The presence of a neutral BA eliminated the possibility of electrostatic quenching interactions with the anionic fluorescein derivative. Therefore, a nitrogen-containing tertiary amine was also co-polymerised. This serves two purposes; the first is to lower the  $pK_a$  of the boronic acid. The association between the lone pair on the nitrogen and the unfilled  $sp^2$  orbital on the boron was shown to lower the  $pK_a$  to around pH 7, thereby improving glucose sensitivity at physiological pH.<sup>27</sup> Secondly, at neutral pH 7.0, this association could result in the formation of a dative bond with strong dipolar character.<sup>27</sup>

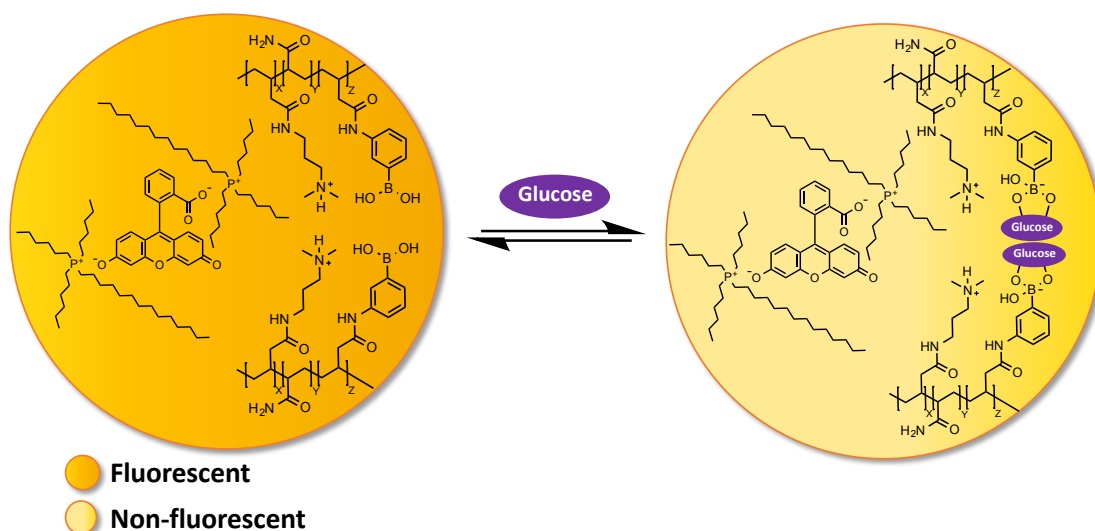


**Figure 6.10.** Immersion of Ionogel 2 (initially fluorescent, left) in a glucose containing solution of pH 7.4 phosphate buffer (100 mM) resulted in a decrease in fluorescence (right), where X:Y:Z is 1:3:1.

Figure 6.11 shows the fluorescence quenching trend by 44% in Ionogel 2, when the gel was immersed in a pH 7.4 phosphate buffer solution containing glucose (100 mM). This result correlates well with previously reported examples in the literature, where glucose has been shown to quench the fluorescence of BA-fluorophore systems by a maximum of 32% in solution.<sup>28</sup>

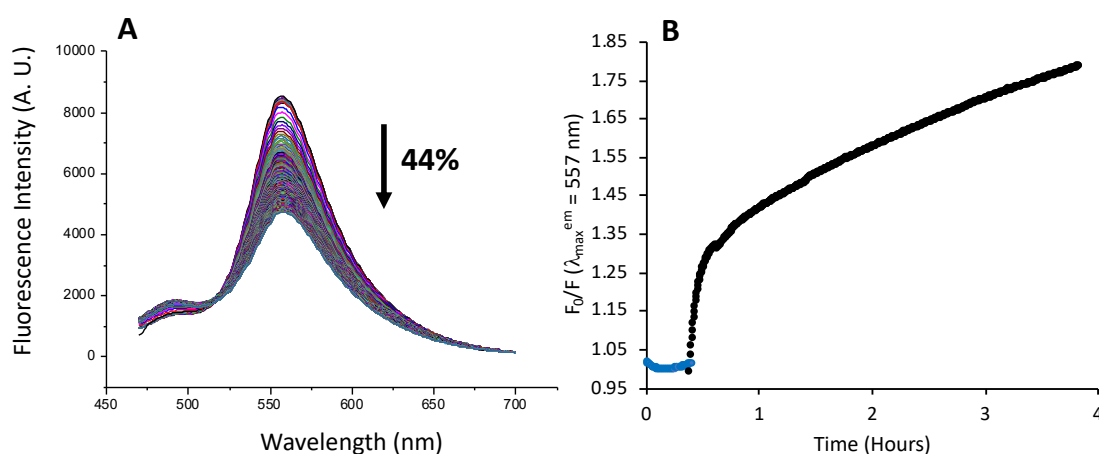


**Figure 6.11.** (A) Emission spectrum of Ionogel 2 when immersed in 100 mM glucose solution in pH 7.4 phosphate buffer over ~4h; the excitation wavelength was 448 nm and the corresponding emission wavelength was 557 nm. (B) Evolution of the emission at 557 nm in the presence of 100 mM glucose over ~4h, where the initial blue points represent stabilisation of the hydrogel in buffer before the addition of glucose. A decrease in fluorescence intensity by 44% was recorded.  $F_0$  represents the initial fluorescence of fluorescein and  $F$  corresponds to the measured fluorescence after the addition of glucose.

## 6.5 Conclusions and Future Work

There are some advantages to both indirect sensing approaches described in this chapter. By covalently immobilising the BA components within Ionogel 2, this two-component sensing system could be more easily incorporated into a sensing platform to fulfil an application, since all sensing components are readily available in the gel. Examples of such devices include a contact lens or wearable sensing-patch, to act as a non-invasive and continuous glucose-monitoring device. On the other hand, by electrostatically immobilising both the fluorophore and BA components inside the gel matrix, as in the case of Ionogel 1, this gel can be used to screen a range of different BA derivatives, to optimise the sensing process. This type of system allows for the design of a range of BA derivatives to later be immobilised inside the gel for fluorescence response optimisation. As in the case for Ionogel 2, the BA component can be co-polymerised into the ionogel matrix. A disadvantage of this approach is the fine tuning of the ratios and spacing between the individual components involved in the sensing mechanism, which can require extensive optimisation. Moreover, as seen from the results presented in this chapter, the response times are slow (up to several hours) as they are dependent on diffusion of sugar molecules inside the hydrogel matrix. Attempts to modify the size of the gel to smaller dimensions and increase the pore density will be made in order to minimise response times.

Future work in this area will include the screening of other BA derivatives with the P<sub>6,6,6,14</sub> fluorescein ionogel and covalent immobilisation of both sensing units (BA and fluorophore) inside a hydrogel/ionogel matrix. In this context, the synthesis of polymerizable sensing components is under investigation in our group, such as polymerizable fluorophores (*e.g.* rhodamine and pyranine derivatives) as well as other polymerizable BA units.

## **Part B – Fluorescence Quenching and Recovery Studies in Hydrogel Cocktails**

### **6.6 Introduction**

In Chapter 5, a novel two-component sensing system was described in solution. Singaram *et al.*<sup>4</sup> were the first to describe a two-component sensing system in solution and then later immobilised it inside a hydrogel.<sup>2, 3, 5</sup> In this system, the fluorescence was initially quenched on introducing the BA derivative, to form a non-fluorescent ground-state complex. The fluorescence was later recovered in the presence of saccharides inside the hydrogel matrix.

This chapter section outlines preliminary studies for the incorporation of the two-component sensing system described in Chapter 5 inside a hydrogel matrix. As the BA derivatives described in Chapter 5 contain polymerisable groups, they can be copolymerised in to a hydrogel matrix together with common, commercially available acrylic monomers, such as acrylic acid (AA), 2-hydroxyethyl acrylate (HEA), methacrylic acid (MAA), *N*-(2-(diethylamino)ethyl)methacrylate (DMAEMA), *N*-(3-(diethylamino)propyl)methacrylamide (DMAPMA) and sodium acrylate (Na-Acrylate). In contrast, the anionic fluorophore pyranine was electrostatically immobilised inside the gel, on interacting with the cationic BA derivatives.

The optimum ratio between the two sensing components (BA unit and pyranine) was investigated in the presence of different acrylic monomers. For this purpose, the fluorescence of pyranine was monitored for each of the hydrogel cocktails, with increasing concentrations of the BA monomeric unit. The effect of the acrylic monomer on pyranine fluorescence was also investigated.

### **6.7 Experimental**

#### 6.7.1 Materials and Methods

Acrylamide, acrylic acid (AA), *N*-(2-(diethylamino)ethyl)methacrylate (DMAEMA), *N*-(3-(diethylamino)propyl)methacrylamide (DMAPMA), 2-hydroxyethyl acrylate (HEA), methacrylic acid (MAA), sodium acrylate (Na-Acrylate), methylenebis(acrylamide) (MBIS) and D-glucose were purchased from Sigma Aldrich, Ireland and used as received. BA monomers *o*-BA, *m*-BA and *p*-BA were employed, and their synthesis is as described in Chapter 4. Deionized water



(18.2 M $\Omega$ ·cm<sup>-1</sup>) (DI water) was made using a Merck Millipore Milli-Q Water Purification System. All fluorescence measurements were carried out on a JASCO Spectrofluorometer FP-8300 in DI H<sub>2</sub>O.

### 6.7.2 Preparation of Fluorescent Monomeric Cocktails for Fluorescence Titrations

The fluorescent cocktails contained a commercially available monomer, the cross-linker methylenebis(acrylamide) (MBIS) and pyranine dissolved in DI H<sub>2</sub>O. The cocktails were prepared as outlined in Tables 6.3 and 6.4 and were titrated with *o*-BA (80 mM) and *m*-BA (100 mM) stock solutions in DI H<sub>2</sub>O. The initial excitation and fluorescence emission of each cocktail mixture was measured before ( $F_0$ ) and upon addition of increased concentrations of BA monomers ( $F$ ). The emission maximum for the green fluorescent cocktails was at 510 nm and the emission maximum for blue fluorescent cocktails was at 490 nm (Figure 6.12). The emission maxima upon each BA addition was recorded.

**Table 6.3.** Recipe for hydrogel cocktails.

<b>Materials</b>	<b>Mass (g)</b>	<b>Volume (<math>\mu</math>L)</b>	<b>Molecular Mass (g.mol<sup>-1</sup>)</b>	<b>mmol</b>	<b>Mol%</b>
<b>Monomer*</b>	-	-	-	14.06	100
<b>MBIS</b>	0.022	-	154.17	0.14	1
<b>Pyranine (0.1 mM from 1 mM Stock Solution)</b>	-	200	524.37	0.0002	0.001
<b>Solvent H<sub>2</sub>O</b>	1.8	1800	-	-	-

\*See Table 6.4 for monomer quantities.

**Table 6.4.** Monomer quantities for hydrogel cocktail recipes.

<b>Monomers</b>	<b>Mass (g)</b>	<b>Volume (<math>\mu\text{L}</math>)</b>	<b>Density (<math>\text{g.mL}^{-1}</math>)</b>	<b>Molecular Mass (<math>\text{g.mol}^{-1}</math>)</b>	<b>mmol</b>	<b>Mol%</b>
<b>AA</b>	1.01	966	1.05	72.06	14.06	100
<b>Acrylamide</b>	1.00	-	-	71.08	14.06	100
<b>DMAEMA</b>	2.21	2371	0.933	157.21	14.06	100
<b>DMAPMA</b>	2.39	2548	0.94	170.25	14.06	100
<b>HEA</b>	1.63	1616	1.011	116.12	14.06	100
<b>MAA</b>	1.21	1187	1.02	86.06	14.06	100
<b>NA-Acrylate</b>	1.32	-	-	94.05	14.06	100

## 6.8 Results and Discussion

### 6.8.1 Monomer Quenching Effect on Pyranine Fluorescence

In Chapter 5 a two-component sensing system was described. Initially, in this system, the fluorescence quenching of pyranine with increased concentrations of BA monomers was investigated before the fluorescence recovery could be achieved in the presence of monosaccharides. This system was later integrated inside an acrylamide hydrogel matrix, where the BA monomers were co-polymerised inside the matrix and pyranine was electrostatically bound.

In this chapter section, additional acrylic monomers were investigated in terms of their effect on pyranine fluorescence in the absence and presence of the BA co-monomer. A series of fluorescence measurements on the hydrogel cocktails were performed upon titration with increasing concentration of the BA monomer.

Firstly, it was observed that common monomers could shift the fluorescence of pyranine from green to blue in the absence of the BA co-monomer under UV light irradiation (Figure 6.12).<sup>29-31</sup> Consequently, fluorescence titrations on these monomeric cocktails with increased BA concentrations were performed to determine which acrylic monomer could promote optimisation of the electrostatic interactions between pyranine and the BA monomer within the hydrogel.

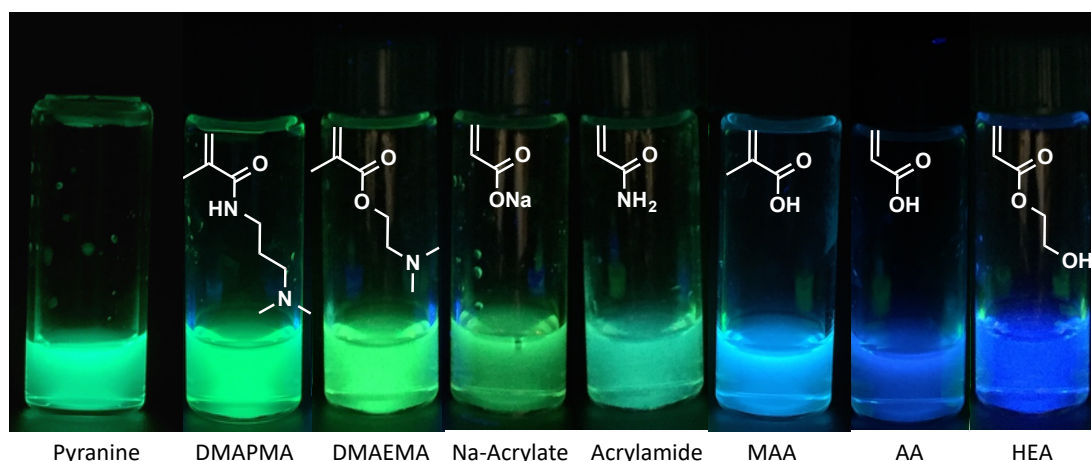


**Figure 6.12.** Fluorescent pyranine monomeric cocktails in DI H<sub>2</sub>O, where the colours range from green to blue depending on the acidic nature of the solution. Left to right: pyranine, *N*-(3-(dimethylamino)propyl)methacrylamide (DMAPMA), *N*-(2-(dimethylamino)ethyl)methacrylate (DMAEMA), sodium acrylate (Na-Acrylate), acrylamide, methacrylic acid (MAA), acrylic acid (AA) and 2-hydroxyethylacrylate (HEA).

It was observed that the monomeric cocktails ranged in colour from fluorescent green to fluorescent blue (Figure 6.12). Two fluorescent forms of pyranine exist due to an acid-base equilibrium that can occur in pyranine's excited-state, when the -OH group of pyranine becomes protonated or deprotonated. The fluorescent green form of pyranine corresponds to the deprotonated form showing an emission band centred at ~510 nm and the fluorescent blue form displays an emission centred at ~430 nm, correlating to the protonated form of pyranine (Figure 6.13).<sup>29</sup> This acid-base equilibrium takes place in protic aqueous media and has been extensively studied in water, protic solvents and acetate buffer solutions.<sup>29-31</sup> In an acetic acid buffer solution (4 M), Nibbering *et al.*<sup>31, 32</sup> showed that this excited-state proton transfer occurs very quickly in <150 fs. It has also been noted that this excited-state proton transfer can be facilitated when solvent and hydrogen bonding interactions are involved. Fang *et al.*<sup>33</sup> used time-resolved vibrational spectroscopy to show that water molecules are responsible for bringing the excited-state pyranine and the acetate ion together by bridging the spacial gap for the excited-state proton transfer. Moreover, water molecules enhance stabilisation in the pyranine excited-state.<sup>29, 31</sup>

This acid-base equilibrium is an example of an excited-state reaction since a structural change in pyranine is induced on photoexcitation.<sup>34</sup> Deprotonation of pyranine's -OH group is possible in the excited state due to alterations in electron distribution on light absorption.<sup>34</sup> Photoexcitation of phenol is a well-known example.

On absorbing light, the electron density around the phenolic group is shifted towards the benzene ring, rendering a reduced  $pK_a$  in phenol and donation of the proton.<sup>34</sup> Similarly, this resulting increased acidity in pyranine is enhanced in the excited-state on transitioning from the  $\pi$ - $\pi^*$  state.<sup>35,36</sup> In the case of pyranine, the  $pK_a$  is reduced by approximately 7 units, from  $\sim 7.3$  to  $\sim 0.4$ ,<sup>37</sup> on photoexcitation from the  $S_0$  ground state (PA) to the excited  $S_1$  state (PA\*) in Figure 6.13.<sup>37,38</sup> Consequently, this results in a change in the physical properties of pyranine by a bathochromic shift in the emission wavelength from 430 nm to 510 nm.

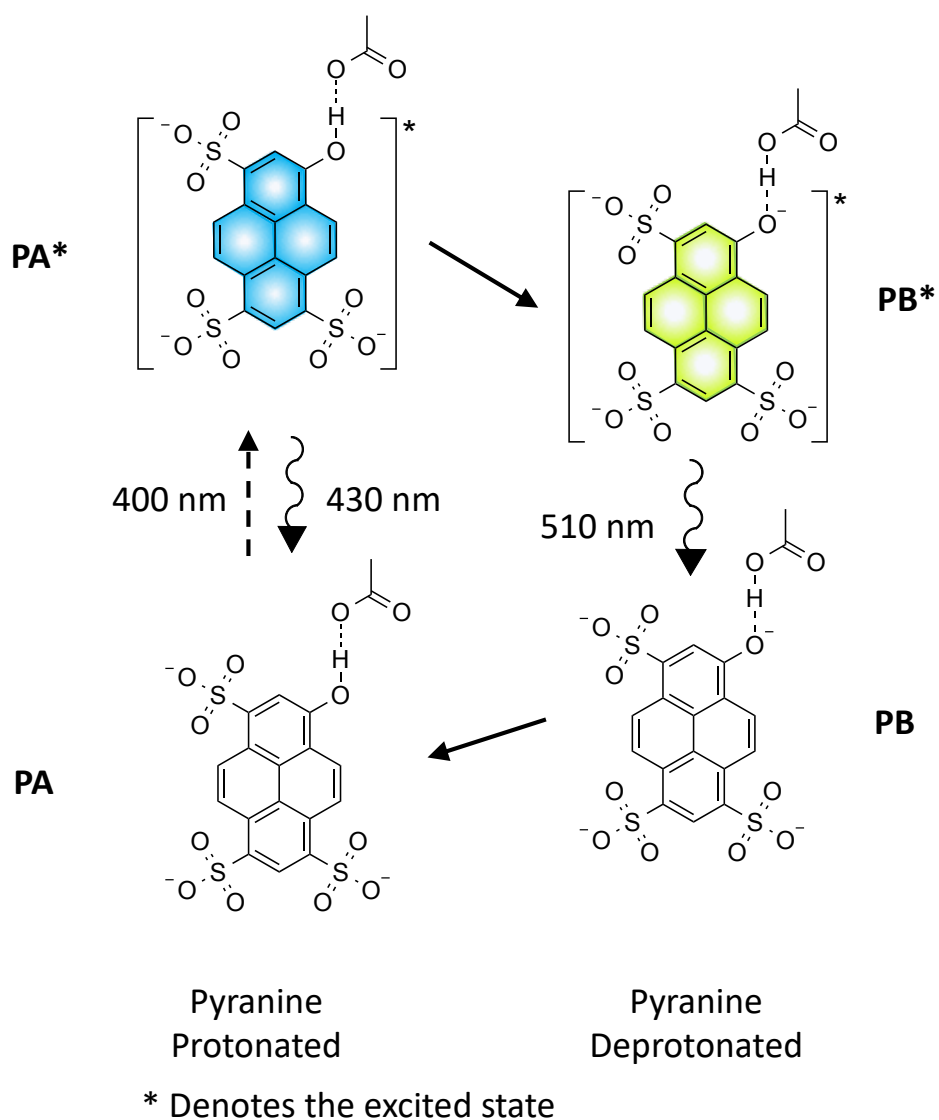


**Figure 6.13.** Pyranine acid-base equilibrium indicating switching from blue to green fluorescent state. Adapted from reference 29.

## 6.8.2 Fluorescence Titrations

### 6.8.2.1 Fluorescence Quenching

In the fluorescent pyranine monomeric cocktails, the cocktails that appeared blue under UV light irradiation contained monomers that could donate a proton. These monomeric cocktails included acrylic acid (AA), methacrylic acid (MAA) and 2-hydroxyethyl acrylate (HEA), and all showed an emission centred at ~440 nm and a shoulder at ~500 nm, indicating both forms of pyranine were present. The acrylamide-based cocktails appeared to exhibit green fluorescence, displaying an emission at 510 nm. The blue fluorescence at ~440 nm was thought to result from a hydrogen bonding interaction that may occur between the -OH groups in AA, MAA and HEA and the O<sup>-</sup> atom in the -OH group of pyranine. All monomeric cocktails (Figure 6.12) were investigated by fluorescence titrations to optimise their role in a two-component sensing mechanism in a hydrogel matrix.

In order to maximise fluorescence recovery in this two-component sensing system, the quenching interactions between all components of the hydrogels was first studied. The cocktails containing pyranine (0.1 mM, 0.0014 mol%), the cross-linker MBIS (1 mol%) and the acrylic monomer (100 mol%) were titrated with the BA co-monomers to determine the optimum cocktail composition. Figure 6.14 shows the fluorescence quenching curves of the hydrogel cocktails with *o*-BA and *m*-BA.

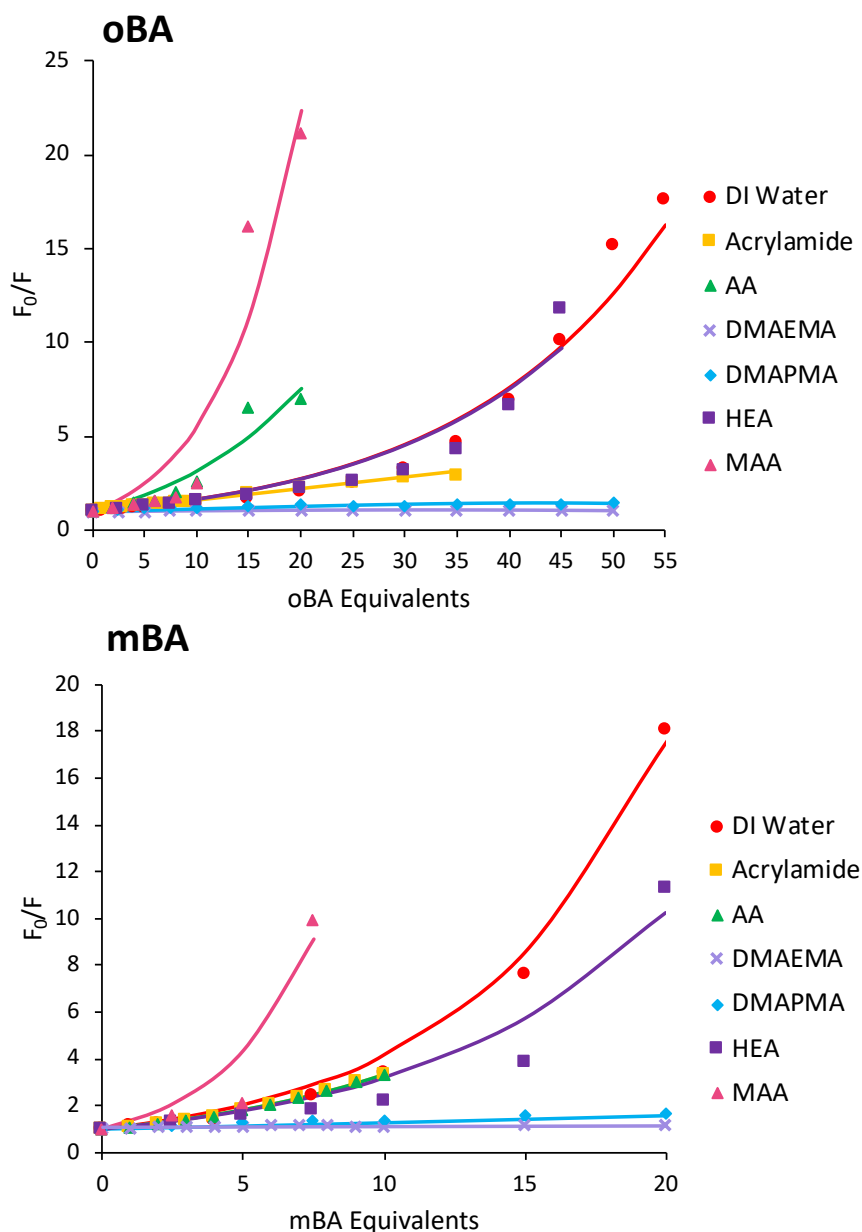


**Figure 6.14.** Fluorescence quenching of pyranine (0.1 mM) in monomeric cocktails with cross-linker MBIS (1 mol%) and acrylic monomers (100 mol%); acrylamide, DMAEMA, DMAPMA, HEA and MAA, with increased concentrations of *o*-BA (top) and *m*-BA (bottom) in DI H<sub>2</sub>O, fitted with a model using Equation 5.1. The solution sample contains pyranine (0.1 mM) and increased equivalents of the BA co-monomer only in DI water. The emission wavelengths for the monomeric cocktails were; 510, 440, 517, 515, 436 and 440 nm for acrylamide, AA, DMAEMA, DMAPMA, HEA and MAA cocktails, respectively. For spectral data on the excitation and emission wavelengths see Appendix E.

From Figure 6.14, the fluorescence quenching in pyranine was enhanced with the BA monomers in the presence of acrylamide, AA, HEA and MAA. The fluorescence could be quenched by 86% and by 90% with 2 mM *o*-BA and 0.8 mM *m*-BA, respectively, in the AA and MAA cocktails. Similarly, the fluorescence was quenched by 92% with 4.5 mM *o*-BA and by 92% with 2 mM *m*-BA, respectively, in the HEA

cocktails. In the acrylamide cocktails the fluorescence was decreased by 66% with 3.5 mM *o*-BA and by 70% with 1 mM *m*-BA. Overall, *m*-BA, in comparison to *o*-BA, showed to induce the most effective fluorescence quenching in pyranine in the monomeric cocktails (represented by the diamond in Figure 6.15). A lower concentration of the *m*-BA monomer, in comparison to *o*-BA, was required to reduce the fluorescence intensity. *o*-BA is thought to act as a weaker quencher, in contrast to *m*-BA, since it is possible that a competing N<sup>+</sup>-B<sup>-</sup> intramolecular interaction can form due to the close proximity of the B atom to the cationic nitrogen.<sup>39</sup> In this case, the intramolecular N<sup>+</sup>-B<sup>-</sup> interaction potentially competes with the electrostatic interaction between *o*-BA and pyranine when forming the non-fluorescent ground-state complex. The second observation was that, the acrylic monomers capable of donating a proton to pyranine provided the most efficient environment for fluorescence quenching in pyranine with the BA monomers. This resulted from the enhanced electrostatic and hydrogen bonding interactions that could be permitted between pyranine and the BA co-monomers.

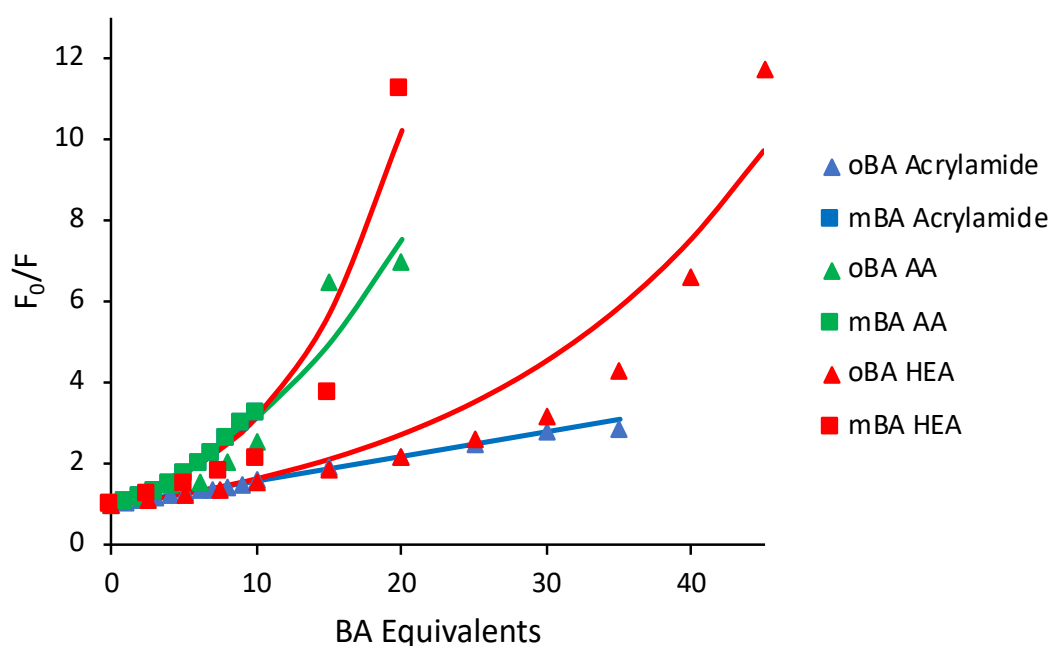


**Figure 6.15.** Fluorescence emission curves for the acrylamide, AA and HEA cocktails comparing the *o*-BA and *m*-BA monomer fluorescence quenching efficiency in pyranine (0.1 mM) in H<sub>2</sub>O. The acrylamide cocktail is shown in blue, the AA cocktail is shown in green and the HEA cocktail is shown in red. The *o*-BA equivalents to pyranine is represented by the triangle and the *m*-BA equivalents is represented by the square. The emission wavelengths were 510, 440 and 436 nm for the acrylamide, AA and HEA cocktails, respectively. The data is fitted with a model using Equation 5.1.

### 6.8.2.2 Fluorescence Recovery

The HEA, MAA and AA cocktails, in comparison to other monomeric cocktails studied, exhibited the most desired fluorescent quenching responses. Consequently, the HEA cocktail was investigated with glucose for its ability to restore the fluorescence. In this two-component sensing system when glucose was introduced at pH 7.4, a change around boron in the BA co-monomer occurred to form the anionic boronate form, which resulted in the zwitterionic BA co-monomer. As a result, dissociation in the ground-state complex was initiated to release the fluorophore and recover the fluorescence. With 100 mM glucose, the fluorescence in the acrylamide-based hydrogels, from Chapter 5, increased by 35% and 45% with 15 equivalents of *o*-BA and 10 equivalents of *m*-BA, respectively. In the case of the HEA-based monomeric cocktails studied here, the fluorescence increased by 52% and 25% with 50 equivalents of *o*-BA and 20 equivalents of *m*-BA, respectively (Figure 6.16).

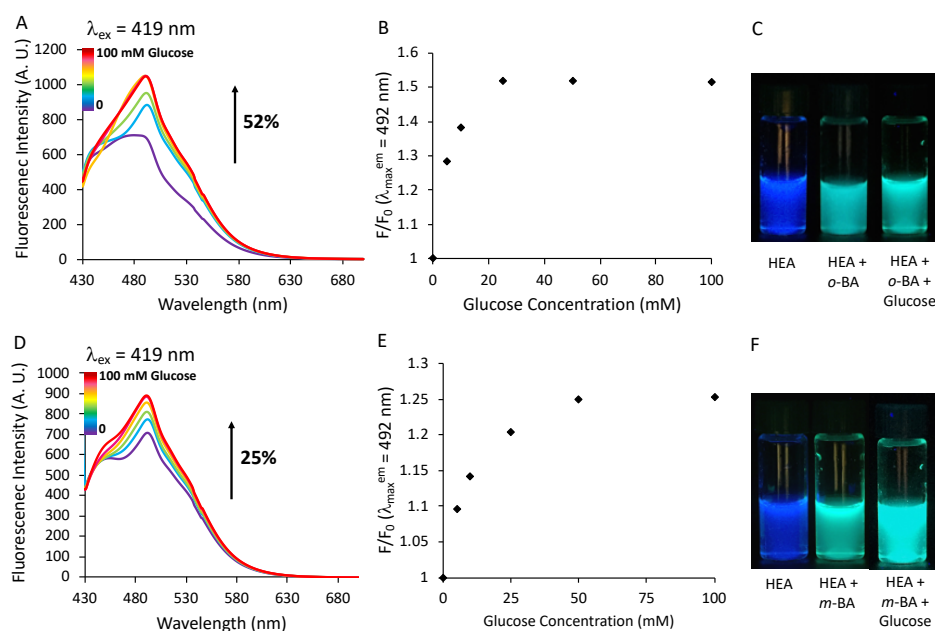


**Figure 6.16.** Fluorescence recovery in HEA cocktails with *o*-BA (5 mM; top, A-C) and *m*-BA (2 mM; bottom, D-F) in DI H<sub>2</sub>O. (A) Fluorescence emission spectrum with emission peak at 492 nm, corresponding to an excitation wavelength of 419 nm, showing fluorescence increase by 52% with 100 mM glucose. (B) Fluorescence emission curve at 492 nm, where  $F_0$  is the initial fluorescence of the cocktail before the addition of *o*-BA and  $F$  is the measured fluorescence after the addition of 5 mM *o*-BA. (C) Shows an image of the HEA cocktail before (left) and after the addition of *o*-BA (middle) and after the addition of 100 mM glucose (right). (D) Fluorescence emission spectrum with emission peak at 492 nm, corresponding to an excitation wavelength of 419 nm, showing fluorescence increase by 25% with 100 mM glucose. (E) Fluorescence emission curve at 492 nm. (F) Shows an image of the HEA cocktail before (left) and after the addition of 2 mM *m*-BA (middle) and after the addition of 100 mM glucose (right).



## 6.9 Conclusions and Future Work

To conclude, by conducting fluorescence titrations in the monomeric cocktail the desired concentrations and ratio between the BA derivatives and the fluorophore, pyranine, could be determined. With increased concentrations of the BA monomers to the acrylic cocktails, containing pyranine (0.1 mM) and the crosslinker MBIS, the fluorescence was quenched. Two forms of pyranine fluorescence could be detected by two characteristic emission wavelengths, one at ~440 nm corresponding to the blue fluorescent protonated form of pyranine and the second at ~510 nm correlating to the green fluorescent deprotonated form of pyranine. This change in pyranine fluorescence resulted from an acid-base excited-state equilibrium that occurs in aqueous media. It was observed that the acrylamide, HEA, AA and MAA cocktails, exhibiting mostly blue fluorescence, showed the most efficient fluorescence quenching with increased equivalents of the BA monomers to pyranine. This enhanced response was believed to be due to the hydrogen bonding interactions that can occur between the acrylic monomer and pyranine.

Overall, lower concentrations of the *m*-BA monomer were required to quench the fluorescence of pyranine more efficiently in comparison to *o*-BA. The fluorescence was decreased by ~90% in the presence of AA, MAA and HEA cocktails with 0.8 mM, 0.8 mM and 2 mM *m*-BA, respectively. The glucose fluorescence recovery response was thereafter investigated in the HEA cocktail, where the fluorescence could be restored by 52% with 5 mM *o*-BA and by 25% with 2 mM *m*-BA in the presence of 100 mM glucose. Although the *m*-BA monomer shows optimal fluorescence quenching, the *o*-BA monomer exhibits desired fluorescence recovery due to the proximity of the N<sup>+</sup> moiety to boron enabling an intramolecular N<sup>+</sup>-B<sup>-</sup> interaction in the presence of glucose.

In this section a range of acrylic monomeric cocktails were investigated for a two-component saccharide response detection system. The cocktails permitting hydrogen bonding interactions between the acrylic monomers and pyranine, showed the most efficient fluorescence quenching responses with the BA co-monomers. Future work in this area involves the polymerisation of the HEA and AA cocktails in to hydrogels for investigation in a two-component sensing system.

## **Part C - Layer-by-Layer Films Composed of BA Linear Polymers and Poly(vinyl sulfonate)**

### **6.10 Introduction**

Multilayer films composed of organic, inorganic, polymeric, metallic or biological components have been studied since the 1930s primarily for modifying surfaces.<sup>40, 41</sup> These multilayer systems are typically adsorbed to solid supports, such as glass slides, colloids or any hard, solid material with larger dimensions reaching several centimetres.<sup>40, 42, 43</sup> Initially, Langmuir-Blodgett approaches were used. In this case, monolayers were built upon a water-surface and later transferred on to a solid support.<sup>40</sup> The disadvantages associated include necessary specialised equipment, limitations regarding substrate sizes and topology, film size and stability of the resulting films.<sup>40</sup> In the 1960s Iler<sup>42</sup> introduced a layer-by-layer (LbL) concept and Decher<sup>40</sup> later established the method in the late 1990s. This simplistic approach exploited natural intermolecular reactions that could overcome the challenges associated with the Langmuir-Blodgett method, allowing for rapid formation of polymeric pairs directly on to solid substrates.<sup>40</sup>

The LbL technique works best when using polymeric materials with opposing ionic charges. Typically, a polycation and a polyanion are employed and the solid substrate is sputter coated or dipped in to each solution with a water washing step in between. This cycle is repeated until the desired number of layers have been deposited.<sup>40, 41</sup> The washing step becomes important to avoid issues such as contamination between the aqueous polyelectrolyte solutions and encourage stabilisation of weakly electrostatically bonded monolayers.<sup>40, 44</sup> The layers overlap in a 1:1 stoichiometry of polycation to polyanion by approximately 50%, due to the system attempting to achieve neutralisation of charges between the polyion layers. The type of substrate doesn't just affect this procedure, other variables such as weight average molecular weight, concentrations of the polyelectrolyte solutions, deposition times, temperature and agitation of the solutions also play a role.<sup>40, 45</sup> Consequently, linear polymers with similar weight average molecular weights, absolute zeta potentials and solution concentrations provide optimal polyion films.<sup>40</sup> Adsorption times of the polymeric pairs range from minutes when using glass slides, to hours on building up multilayer films on to for example gold colloid particles.

Secondary intermolecular interactions can also be exploited for LbL film fabrication.<sup>45</sup> These typically include  $\pi$ - $\pi$  stacking interactions, hydrogen-bond bridges and Van der Waals forces. Other interactions that can be employed include reversible covalent bonds, polymeric systems employing an electron donor and acceptor and biological interactions, such as between proteins-vitamins and sugars-lectin.<sup>40, 41, 43, 44, 46</sup> Conveniently, this intermolecular adsorption process can be achieved not only on 2D platforms to produce planar films, but also on 3D scaffolds, leading to the production of multi-layered capsules, nanotubes and other 3D templates.<sup>41</sup> Advantageously, a wealth of materials can be used to fabricate a variety of functional LbL films. Applications of such films can be useful for photovoltaics, conductive electrochemical sensing as robust coatings, micro- or nano-porous functional patterning surfaces and nanoscopic devices. LbL films for biological applications have also piqued interest, for example for drug delivery, as antifouling agents, gene therapy and nanovaccines.<sup>40, 41, 44, 45</sup> Advantageously, disassembly of the multilayer films can be stimulated by numerous triggers, such as pH, ionic strength, temperature, light, magnetic field and by small bio-molecules, such as glucose.<sup>43, 45, 47</sup> Typically, all of these stimuli initiate weakened electrostatic interactions between the layers to disassemble the LbL film.<sup>46</sup>

Developing drug delivery systems using LbL films is of particular interest, since many medications require encapsulation and controlled release of the drug.<sup>41, 43, 48</sup> LbL is fortuitous in this regard, where a multitude of polymeric materials can be used for film assembly. This provides a vast range of desirable properties that can be achieved in the LbL film. For example, to enhance biological compatibility or to facilitate drug delivery of hydrophobic medications, proteins, peptides, nucleic acids, antibodies, bioactive molecules or liposomes are usually incorporated. For optical monitoring of controlled drug release and efficacy, fluorophores or chromophores can be employed and for conducting materials polyelectrolytes are typically incorporated.<sup>40, 41, 49</sup> These systems can then be easily controlled to disassemble and release the desired encapsulated drug in the presence of specific triggers. Great achievements in recent years have attracted researchers to LbL fabrication techniques, where LbL films can be cost effective and rapid to produce, reliable, high loading capacity, improved biointegrity, low toxicity, specificity for biological receptor sites

and independent time scales, which is desirable for releasing a drug within a therapeutic window.<sup>40, 41, 44</sup>

In particular, researchers have been drawn to LbL systems using glucose to stimulate disassembly, as these materials hold great promise for use in targeted insulin delivery therapies for diabetes.<sup>43, 44, 45-51</sup> For drug delivery, LbL films can be used to embed drugs between the monolayers for controlled drug administration (Figure 6.17A) or templated upon nano- or micro-structured hollow capsules or tubes containing a drug, such as insulin, for an immediate burst release of insulin (Figure 6.17B).<sup>41, 45</sup>

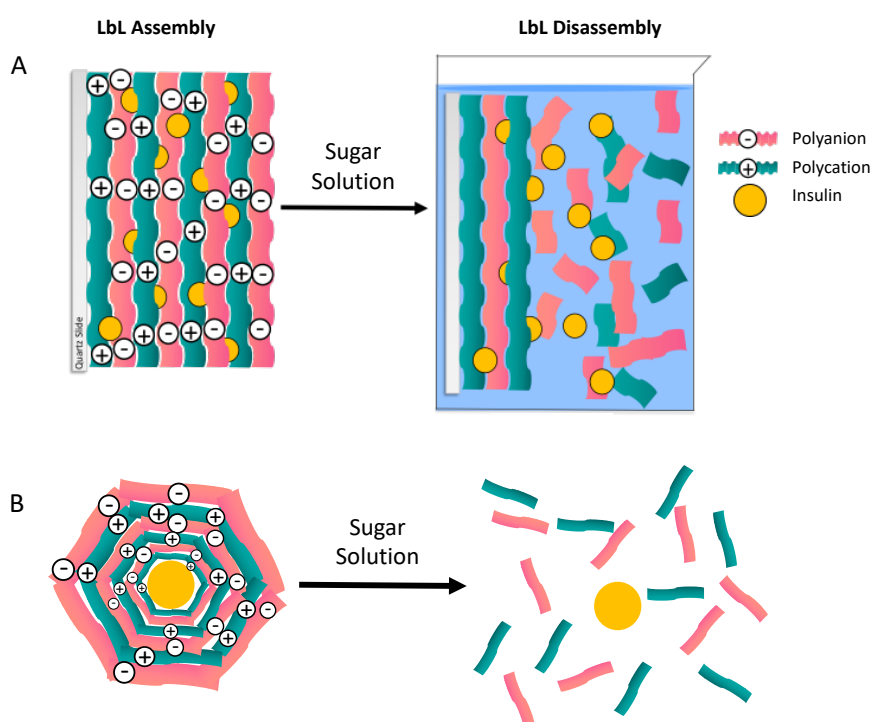


**Figure 6.17.** LbL assembly (A) and disassembly (B) processes for insulin drug delivery systems stimulated by glucose.

Glucose-responsive BA linear polymers (LPs) have gained much attention in LbL systems. Levy *et al.*<sup>43</sup> reported using BA LPs in this regard by constructing layers on to a flat quartz crystal with a gold modified surface and on to colloidal  $\text{CaCO}_3$  templates.  $\text{CaCO}_3$  templates were acquired since they can be dissolved over almost the entire pH range and they allow for the encapsulation of bovine serum, employed as the culture media in the majority of vaccines.<sup>43</sup> These colloidal particles were also fluorescently labelled with fluorescein isothiocyanate-dextran, so that the bovine release process could be monitored by increases in fluorescence intensities.<sup>43</sup> Seven bilayers of a poly(acrylic acid)-phenylacrylamido-BA LP and the polysaccharide

mannan were built upon each template and the response towards common monosaccharides, such as glucose, fructose, galactose and mannose, was investigated using a quartz crystal microbalance in the case of the quartz crystal and by fluorescence for the templated capsules.<sup>43</sup> The layers were assembled in aqueous solutions close to the pK<sub>a</sub> of the BA at pH 9-11. The layers formed based on the reversible formation of the boronate ester with mannan. Mannan was used to enhance stabilisation of the monolayers, since a conformational change around boron to the anionic cyclic boronate ester form resulted on binding.<sup>43</sup> The monosaccharides introduced to dismantle the LbL film, competed with mannan for the BA binding sites. Consequently, on the BA-polymer chains binding glucose, the layers disassembled. Levy and co-workers showed that the film could be destroyed above the critical saccharide concentration with 25 mM of all monosaccharides after 5 minutes. Overall, the LbL film was most responsive to fructose, due to the binding of fructose being an order of magnitude higher than that of glucose, galactose and mannose, where the layers could be completely disassembled after 2 minutes with 5 mM fructose.<sup>43</sup> Similarly, the capsules released the bovine serum with 10 mM fructose and 100 mM glucose, galactose and mannose after 15 minutes. Below the critical sugar concentration, the films took hours to disassemble. Moreover, since this system was pH sensitive, Levy *et al.* also showed that the film could be disassembled in pH solutions of pH 1-8 after less than a minute.<sup>43</sup>

Kim *et al.*<sup>48</sup> reported block co-BA LPs, containing a N<sup>+</sup> moiety, for use in drug releasing platforms and sugar sensing. This saccharide-responsive polymer could be exploited for its BA charge-switching ability on binding glucose or fructose, resulting in the anionic boronate ester form. This induced negative charge on boron rendered the polymer zwitterionic with increased water solubility.<sup>48</sup> The N<sup>+</sup> moiety in the polymer structure provide stabilisation on sugar binding through a N<sup>+</sup>-B<sup>-</sup> intramolecular interaction. This interaction was confirmed by x-ray crystallography and resulted in increased acidity around boron, to lower the pK<sub>a</sub> of the BA group. This allowed for solubilisation of the polymer at a lower pH in the presence of glucose and fructose.<sup>48</sup> Initially, the polymer was only soluble in moderately basic solutions and insoluble at pH 7.4. It was only on the addition of glucose or fructose, that the polymer could be dissolved in solution at pH 7.4.<sup>48</sup> The authors demonstrated that this block co-BA polymer could be used as a glucose-responsive material at physiological pH to potentially aid the monitoring of glucose for diabetes.<sup>48</sup> The

RAFT method used mild conditions to produce longer chain linear polymers with narrow molecular weight distributions, in contrast to traditional radical polymerisation approaches resulting in random sized polymer chains.<sup>50</sup> This controlled polymerisation strategy is desired in the case of LbL films held by electrostatic interactions. By using uniform linear polymers, a 1:1 stoichiometry of the cationic and anionic polyelectrolyte layers can be established to aid efficient assembly of the LbL film.<sup>40, 51</sup>

Watahiki *et al.*<sup>44</sup> produced multilayer films composed of BA dendrimers and poly(vinyl alcohol) that could stimulate disassembly in the presence of glucose. Using BA dendrimers over linear chain polymers allowed for the enhanced glucose response at physiological pH 7.4 compared to other reported systems.<sup>44</sup> The polymer layers were adsorbed on to quartz slides by subsequent dipping in to the aqueous polymer solutions for 20 minutes each.<sup>44</sup> The layers were assembled by covalent interactions forming cyclic boronate ester bonds between the BA dendrimers and the diol groups in poly(vinyl alcohol). Two different BA dendrimers, 3CPBA-D (3-carboxyphenylboronic acid-dendrimer) and 3C5NPBA-D (3-carboxy-5-nitrophenylboronic acid-dendrimer), were studied to investigate the effect of the electron-withdrawing nitro group on the  $pK_a$  of the BA. 3CPBA-D acted as a control containing no nitro group and 3C5NPBA-D had the nitro group meta to the BA group. The disassembly of the layers was monitored by absorbance under gentle stirring for 90 minutes.<sup>44</sup> The film decomposition was investigated with up to 100 mM glucose in different pH buffer solutions by immersing the slide in solutions of pH 4.0-8.0 for 30 minutes. The LbL films were stable in basic solutions of pH 7.0 or higher and decomposed in weakly acidic solutions of pH 4.0-6.0 by ~80%.<sup>44</sup> This decomposition was stimulated due to the predominant formation of trigonal planar boronate bonds in acidic media. The layers were more stable in basic solutions due to the higher concentration of anionic tetragonal boronate ester bonds, which increase the stability of boron. The films could be successfully disassembled by ~50% in the presence of glucose at 37 °C in pH 7.4 solutions at a critical concentration above 15 mM.<sup>44</sup> The disassembly of the layers was dependant on the competitive binding nature of glucose over the diol groups in poly(vinyl alcohol), where the layers could be completely disassembled within 30 minutes with 100 mM glucose.<sup>44</sup> Overall, the 3C5NPBA-D films exhibited optimal responses to glucose, owned to the electron-withdrawing

properties of the nitro substituent by reducing the  $pK_a$  of the BA group. Increased acidity of this BA moiety allowed for glucose binding at a lower pH, more suited towards physiological glucose sensing applications, where these layers could be completely disassembled within 30 minutes. On the other hand, the 3CPBA-D films were recommended for sustained release, with slower disassembly times of up to 4 days.<sup>44</sup>

Taking inspiration from this work, cationic LPs were polymerised from the BA monomers introduced in Chapter 4 (*o*-BA, *m*-BA and *p*-BA) and paired with anionic poly(vinyl sulfonate) (PVS), to afford thin LbL films on quartz slides. The assembly and disassembly of the layers was tracked by absorbance spectroscopy. Initially, the BA LPs were studied in Chapter 4, where it was observed that the *p*BA isomer could stack the most efficiently. *p*BA LP when deposited on to LbL films with PVS showed optimum results for assembly and disassembly with monosaccharides. Employing this concept, future work in this area could involve interchanging the polyanion with a dye molecule to produce an optical glucose-responsive insulin-drug delivery system.

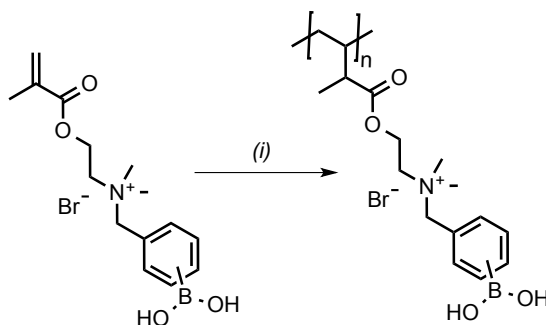
## 6.11 Experimental

### 6.11.1 Materials and Methods

Hydrogen peroxide (30 w% in H<sub>2</sub>O), poly(ethyleneimine) (PEI, branched), poly(vinyl sulfonic acid, sodium salt) solution (PVS) (25 wt.% in H<sub>2</sub>O), phenylbis(2,4,6-trimethylbenzoyl)phosphine oxide (PBPO), acetic acid, sodium hydroxide, D-glucose and D-fructose were purchased from Sigma Aldrich and used as received. 2-(Bromomethyl)phenylboronic acid, 3-(bromomethyl)phenylboronic acid and 4-(bromomethyl)phenylboronic acid were purchased from Fluorochem UK and used as received. Deionized water (18.2 M $\Omega$ ·cm<sup>-1</sup>) (DI water) was made using a Merck Millipore Milli-Q Water Purification System. pH measurements were carried out on a VWR symphony SP70P pH meter. <sup>1</sup>H and <sup>13</sup>C NMR spectra were recorded on a 400 MHz or 600 MHz Bruker NMR spectrometer, using deuterium oxide (D<sub>2</sub>O) or deuterated methanol (*d*<sub>4</sub>-CH<sub>3</sub>OH). <sup>11</sup>B NMR experiments were carried out on a 600 MHz NMR spectrometer that used BF<sub>3</sub> in deuterated methanol as an external standard. Fourier Transform Infrared (FT-IR) spectroscopy measurements were carried out on a Perkin Elmer Spectrum GX. All UV-vis spectroscopic measurements were carried out on a Varian Cary 50 Probe spectrophotometer, using a quartz slide in

a quartz Suprasil cell that had a path length of 10 mm and a volume of 3 mL. The phosphate buffer solution at pH 7.4 was prepared from 0.1 M potassium dihydrogen phosphate ( $\text{KH}_2\text{PO}_4$ ; 100 mL) and 0.1 M sodium hydroxide ( $\text{NaOH}$ ; 78 mL) salts and was made up to 200 mL using DI water.

### 6.11.2 Preparation of BA Linear Polymers



**Scheme 6.5.** Radical polymerisation of the BA monomers to form the linear polymers. (i) DMSO, PBPO (2 mol%) and THF, white light irradiation for 1h.

The BA monomer was polymerised by a radical polymerisation procedure (Scheme 6.5). The BA monomer (260 mg; 0.699 mmol) was dissolved in DMSO (500  $\mu\text{L}$ ) in a 1 mL glass vial. The photoinitiator PBPO (2 mg; 0.005 mmol) was added with THF (100  $\mu\text{L}$ ). The vial was placed under high intensity white light irradiation for 1h to polymerise the monomer. Cold diethyl ether was added to the polymerised mixture to precipitate the polymer. The polymer was filtered and washed with diethyl ether and collected as a white solid.

### 6.11.3 LbL Films

#### 6.11.3.1 LbL Assembly

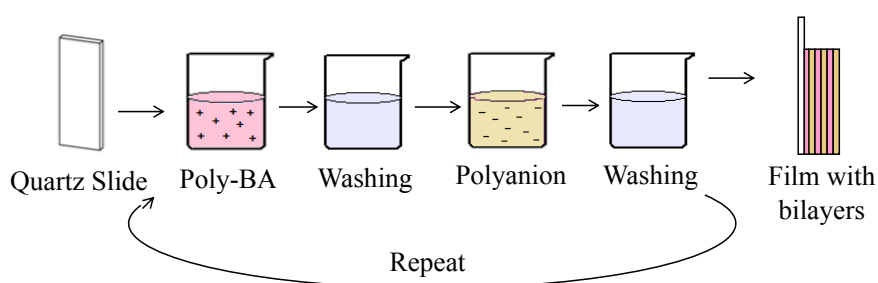


**Figure 6.18.** Assembly process of bilayers on to a quartz slide, where the poly-BA is the BA linear polymer and the polyanion is PVS.



The LbL films were assembled on to quartz slides (40 x 10 x 1 mm). The slide was primed using  $\text{NH}_4\text{OH}/\text{H}_2\text{O}_2/\text{H}_2\text{O}$  (1:1:5, v:v:v) and  $\text{HCl}/\text{H}_2\text{O}_2/\text{H}_2\text{O}$  (1:1:6, v:v:v) hydrophilization solutions at 75 °C for 10 min. PEI and PVS solutions were prepared at concentrations of 1  $\text{mg}\cdot\text{mL}^{-1}$  and 4  $\mu\text{L}\cdot\text{mL}^{-1}$ , respectively. The BA-LPs were dissolved in DI  $\text{H}_2\text{O}$  at a concentration of 1  $\text{mg}\cdot\text{mL}^{-1}$  and the pH was altered to pH 7.3 using acetic acid and sodium hydroxide and measured using a SympHony pH meter. Figure 6.18 depicts the assembly process of the LbL films;  $(\text{PEI}/\text{PVS})_2(\text{BA-LP}/\text{PVS})_5$ . Each slide was dipped in to the respective polymer solutions for approximately 5 mins to deposit the linear chains. The polymer solutions during LbL assembly for all films were kept at room temperature. A washing step using DI water was performed to avoid contamination between the polyelectrolyte solutions. This cyclic process was repeated until all desired 5 or 15 bilayers were afforded. A UV-vis spectrum of the slide after air drying was recorded after each bilayer deposition, where the absorbance of the poly-BA at 230 nm was monitored as the number of layers increased.

### 6.11.3.2 Sugar-Induced LbL Disassembly

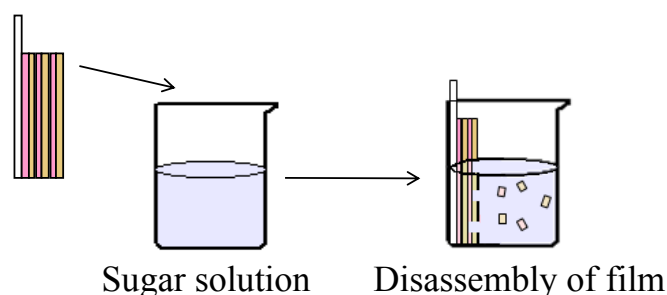


**Figure 6.19.** Disassembly process of the LbL films in saccharide containing solutions.

The disassembly of the LbL films is illustrated in Figure 6.19. The slide was simply dipped in the pH 7.4 buffer solution at 36 °C with gentle stirring to equilibrate and stabilise the layers in the LbL film. Once stabilised, the slide was placed in glucose (up to 100 mM) or fructose (up to 100 mM) solutions at pH 7.4 at 36 °C and stirred for 5 minutes to disassemble the film. The slide was air dried and this disassembly process was monitored by UV-Vis spectroscopy.

## 6.12 Results and Discussion

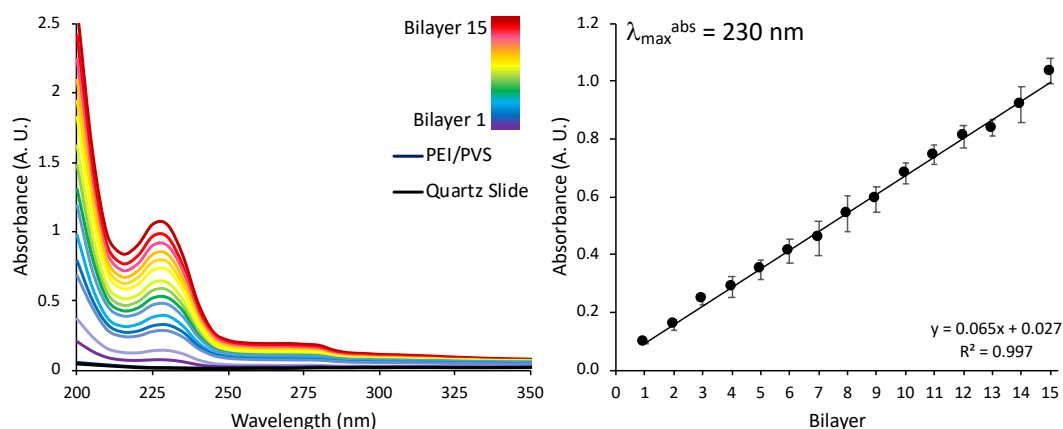


**Figure 6.20.** Absorbance spectra for the assembly of the (PEI/PVS)<sub>2</sub>(pBA LP/PVS)<sub>15</sub> film (left) and the average ( $n = 3$ ) linear growth at 230 nm (right).

The assembly and disassembly of the LbL films on quartz substrates was monitored by UV-Vis spectroscopy (Figure 6.20). The (PEI/PVS)<sub>*n*</sub> and (pBA LP/PVS)<sub>*n*</sub> films were deposited simply by dipping the substrate in alternating solutions containing the polyelectrolytes. Two bilayers of (PEI/PVS)<sub>2</sub> polyelectrolytes were initially adsorbed on to the slides to reduce any influence of substrate morphology on the film growth and enhance the assembly of subsequent bilayers.<sup>49</sup> The deposition of each bilayer was monitored by UV-Vis spectroscopy. The absorbance of pBA LP was followed at a detection wavelength of 230 nm. This wavelength was chosen to allow monitoring to be carried out at the lowest limit of detection.<sup>49</sup> The absorbance of the layers increased linearly as the film growth increased. From Figure 6.20, this assembly process can be visualised by the assembly of 15 bilayers in the (PEI/PVS)<sub>2</sub>(pBA LP/PVS)<sub>15</sub> film. The linear deposition means that multiple layers can be deposited with the same efficiency as the previous added layer. This is advantageous if a thicker film is desired. Similar results were obtained for the assembly of the (PEI/PVS)<sub>2</sub>(oBA LP/PVS)<sub>5</sub> and (PEI/PVS)<sub>2</sub>(mBA LP/PVS)<sub>5</sub> LbL films, where Figure 6.21 compares the assembly of 5 bilayers for each oBA, mBA and pBA film.

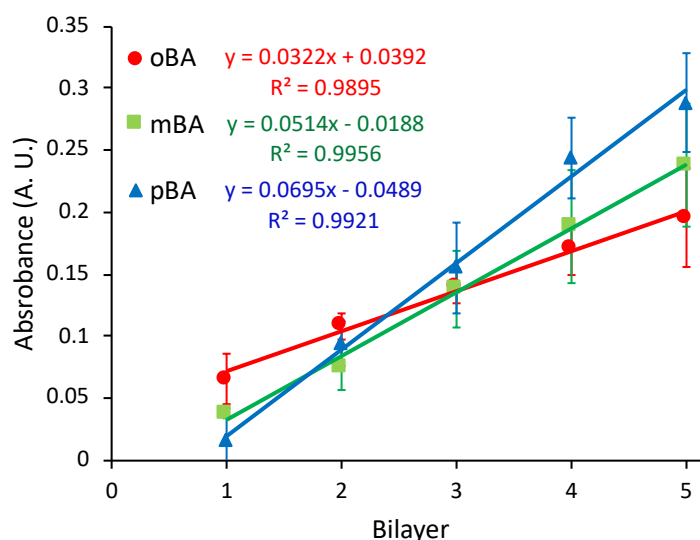


**Figure 6.21.** Assembly of the  $(\text{PEI/PVS})_2(\text{oBA LP/PVS})_5$  film (Red circle ●),  $(\text{PEI/PVS})_2(\text{mBA LP/PVS})_5$  (green square ■), and the  $(\text{PEI/PVS})_2(\text{pBA LP/PVS})_5$  film (blue triangle square ▲), in triplicate, when monitored at 230 nm (left).

On exposing the LbL films to a solution containing fructose, a release assay could be performed. The conformation of the deposited BA LP was trigonal planar. On introducing glucose, a conformational change around boron could be triggered to the tetrahedral form, rendering boron negatively charged. This change in boron leads to a zwitterionic BA LP. Consequently, the electrostatic interactions between the BA LP and PVS can become weakened to initiate disassembly in the LbL film. In order to study fructose-induced disassembly of the  $(\text{PEI/PVS})_2(\text{pBA LP/PVS})_5$ ,  $(\text{PEI/PVS})_2(\text{mBA LP/PVS})_5$  and  $(\text{PEI/PVS})_2(\text{oBA LP/PVS})_5$  films, the quartz substrates were placed in to sugar containing solutions at pH 7.4 and 36 °C with gentle stirring. A rapid release profile was observed when the  $(\text{PEI/PVS})_2(\text{BA LP/PVS})_5$  LbL films were immersed in fructose solutions (10 mM). In this case, the oBA film and mBA film was disassembled by 65% and 71%, respectively. The pBA layers were disassembled by 93% after 3 minutes in the presence of 10 mM fructose (Figure 6.22). This rapid response to fructose, can be explained by the binding constant of fructose with phenylBA. It is known that phenylBA binds fructose more readily in comparison to other sugars such as glucose. James *et al.*<sup>52</sup> have reported the binding constant of phenylBAs as  $110 \text{ M}^{-1}$  with glucose and  $4370 \text{ M}^{-1}$  with fructose. The furanose ring form of fructose binds with almost a 40 times greater affinity to phenylBAs in contrast to the pyranose form of glucose, since 99% of glucose exists in the pyranose form and less than 1% of glucose exists in the furanose form.<sup>52</sup> This low concentration of the furanose form of glucose accounts for the discrepancies between

these binding constants. To monitor the disassembly with fructose more closely, the release assay profile was monitored in 5 seconds intervals (Figure 6.22). This figure illustrates that the pBA film was disassembled by 27% after 5 seconds, by 71% after 30 seconds and disassembled by 93% with 10 mM fructose after ~60 seconds.

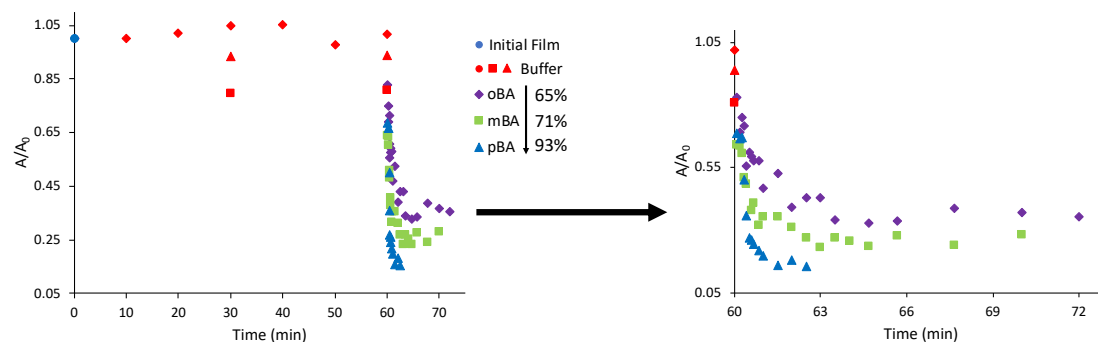


**Figure 6.22.** Normalised absorbance ( $A/A_0$ ) at 230 nm for the disassembly of the BA films; oBA ( $\blacklozenge$ ), mBA ( $\blacksquare$ ) and pBA ( $\blacktriangle$ ) with 10 mM fructose at pH 7.4, where the blue circle ( $\bullet$ ) is the initial measurement for each film. The red points represent stabilisation of the films in buffer before the addition of fructose, where  $A_0$  is the last stable measurement in buffer and  $A$  is the measured absorbance after the addition of fructose.

### 6.13 Conclusions and Future Work

In summary, three similar LbL films were constructed,  $(PEI/PVS)_2(oBA LP/PVS)_5$ ,  $(PEI/PVS)_2(mBA LP/PVS)_5$  and  $(PEI/PVS)_2(pBA LP/PVS)_5$ . All films were investigated for their response towards fructose.  $(PEI/PVS)_2(oBA LP/PVS)_5$  disassembled by 65% in the presence of 10 mM fructose,  $(PEI/PVS)_2(mBA LP/PVS)_5$  disassembled by 71% with 10 mM fructose and  $(PEI/PVS)_2(pBA LP/PVS)_5$  showed increased disassembly by 93% in the presence of 10 mM fructose.

Future work investigations will comprise of disassembly assays in the presence of other saccharides, such as glucose or galactose. Advantageously by interchanging the polyanion for an anionic dye or fluorescent molecule, the assembly and disassembly processes can be better tracked by optical means and the anionic dye could act as a potential drug model. In this case, the dye or drug could be released in the presence of a sugar. By intercalating the drug between the layers of the polymer film, a drug delivery system can be produced that is sugar-responsive.

## 6.14 References

1. Brooks, W. L. A.; Sumerlin, B. S. Synthesis and applications of boronic acid-containing polymers: from materials to medicine, *Chem. Rev.*, **2016**, *116*, 1375-1397.
2. Viložny, B.; Schiller, A.; Wessling, R. A.; Singaram, B. Multiwell plates loaded with fluorescent hydrogel sensors for measuring pH and glucose concentration, *J. Mater. Chem.*, **2011**, *21*, 7589-7595.
3. Suri, J. T.; Cordes, D. B.; Cappuccio, F. E.; Wessling, R. A.; Singaram, B. Continuous glucose sensing with a fluorescent thin-film hydrogel, *Angew. Chem., Int. Ed.*, **2003**, *42*, 5857-5859.
4. Sharrett, Z.; Gamsey, S.; Hirayama, L.; Viložny, B.; Suri, J. T.; Wessling, R. A.; Singaram, B. Exploring the use of APTS as a fluorescent reporter dye for continuous glucose sensing, *Org. Biomol. Chem.*, **2009**, *7*, 1461-1470.
5. Cappuccio, F. E.; Suri, J. T.; Cordes, D. B.; Wessling, R. A.; Singaram, B. Evaluation of pyranine derivatives in boronic acid based saccharide sensing: significance of charge interaction between dye and quencher in solution and hydrogel, *J. Fluoresc.*, **2004**, *14* (5), 521-533.
6. Feng, L.; Liang, F.; Wang, Y.; Xu, M.; Wang, X. A highly sensitive water-soluble system to sense glucose in aqueous solution, *Org. Biomol. Chem.*, **2011**, *9*, 2938-2942.
7. Guan, Y.; Zhang, Y. Boronic acid-containing hydrogels: synthesis and their applications, *Chem. Soc. Rev.*, **2013**, *42*, 8106-8121.
8. Tudor, A.; Florea, L.; Gallagher, S.; Burns, J.; Diamond, D. Poly(ionic liquid) semi-interpenetrating network multi-responsive hydrogels, *Sensors*, **2016**, *16*, 219.
9. B. Ziółkowski, L. Florea, J. Theobald, F. Benito-Lopez, D. Diamond, Porous self-protonating spiropyran-based NIPAAm gels with improved reswelling kinetics. *J. Mater. Sci.*, **2016**, *51* (3), 1392-1399.
10. Srinivasan, G.; Chen, J.; Parisi, J.; Bruckner, C.; Yao, X.; Lei, Y. An injectable PEG-BSA-Coumarin-GOx hydrogel for fluorescence turn-on glucose detection, *Appl. Biochem. Biotechnol.*, **2015**, *177*, 1115-1126.
11. Margulies, D.; Meiman, G.; Shanzer, A. Fluorescein as a model molecular calculator with reset capability, *Nature Materials*, **2005**, *4*, 768-771.
12. Fink, D. W.; Koehler, W. R. pH effects on fluorescence of Umbelliferone, *Analyt. Chem.*, **1970**, *42* (9), 990-993.
13. Srivastava, R.; Jayant, R. D.; Chaudhary, A.; McShane, M. J. "Smart tattoo" glucose biosensors and effect of coencapsulated anti-inflammatory agents, *J. Diabetes Sci. Technol.*, **2011**, *5* (1), 76-85.
14. Lacina, K.; Skladal, P.; James, T. D. Boronic acids for sensing and other applications - a mini-review of papers published in 2013, *Chem. Cent. J.*, **2014**, *8* (60).

15. Benito-Lopez, F.; Byrne, R.; Raduta, A. M.; Vrana, N. E.; McGuinness, G.; Diamond, D. Ionogel-based light-actuated valves for controlling liquid flow in micro-fluidic manifolds, *Lab on a Chip*, **2010**, *10*, 195-201.
16. Gallagher, S.; Florea, L.; Fraser, K. J.; Diamond, D. Swelling and shrinking properties of thermo-responsive polymeric ionic liquid hydrogels with embedded linear pNIPAAm, *Int. J. Mol. Sci.*, **2014**, *15*, 5337-5349.
17. Fraser, K. J.; MacFarlane, D. R.; Phosphonium-based ionic liquids: an overview, *Aust. J. Chem.*, **2009**, *62*, 309-321..
18. Gallagher, S.; Kavanagh, A.; Florea, L.; MacFarlane, D. R.; Fraser, K. J.; Diamond, D. Temperature and pH triggered release characteristics of water/fluorescein from 1-ethyl-3-methylimidazolium ethylsulfate based ionogels, *Chem. Commun.*, **2013**, *49*, 4613-4615.
19. Sanderson, W. M.; Johnson, R. D. Spectroscopic behaviour of fluorescein as a constituent anion in a phosphonium-based ionic liquid material, *Mater. Chem. Phys.*, **2012**, *132*, 239-243.
20. Das, S.; Magut, P. K. S.; de Rooy, S. L.; Hasan, F.; Warner, I. M. Ionic liquid-based fluorescein colorimetric pH nanosensors, *RSC Adv.*, **2013**, *3* (43), 21054-21061.
21. Badugu, R.; Lakowicz, J. R.; Geddes, C. D. Boronic acid fluorescent sensors for monosaccharide signaling based on the 6-methoxyquinolinium heterocyclic nucleus: progress toward noninvasive and continuous glucose monitoring, *Bioorg. Med. Chem.*, **2005**, *13*, 113-119.
22. Silverstein, R. M.; Bassler, G. C.; Morrill, T. C. *Spectroscopic identification of organic compounds*, 4th Ed.; Wiley and Sons, New York, 1981.
23. Fang, H.; Kaur, G.; Wang, B. Progress in boronic acid-based fluorescent glucose sensors, *J. Fluoresc.*, **2004**, *14* (5), 481-489.
24. Badugu, R.; Lakowicz, J. R.; Geddes, C. D. Fluorescence sensors for monosaccharides based on the 6-methylquinolinium nucleus and boronic acid moiety: potential application to ophthalmic diagnostics, *Talanta*, **2005**, *65*, 762-768.
25. Zhai, W.; Sun, X.; James, T. D.; Fossey, J. S. Boronic acid-based carbohydrate sensing, *Chem. Asian J.*, **2015**, *10*, 1836-1848.
26. Larkin, J. D.; Fossey, J. S.; James, T. D.; Brooks, B. R.; Bock, C. W. A computational investigation of the nitrogen-boron interaction in *o*-(*N,N*-dialkylaminomethyl)arylboronate systems, *J. Phys. Chem. A.*, **2010**, *114* (47), 12531-12539.
27. Kim, A.; Mujumdar, S. K.; Siegel, R. A. Swelling properties of hydrogels containing phenylboronic acids, *Chemosensors*, **2014**, *2*, 1-12.
28. Badugu, R.; Lakowicz, J. R.; Geddes, C. D. Ophthalmic glucose monitoring using disposable contact lenses - a review, *J. Fluoresc.*, **2004**, *14* (5), 617-633.
29. Heo, W.; Uddin, N.; Park, J. W.; Rhee, Y. M.; Choi, C. H.; Joo, T. Coherent intermolecular proton transfer in the acid-base reaction of excited state pyranine, *Phys. Chem. Chem. Phys.*, **2017**, *19*, 18243-18251.

30. Cox, M. J.; Bakker, H. J. Parallel proton transfer pathways in aqueous acid-base reactions, *J. Chem. Phys.*, **2008**, *128* (17), 174501-174510.
31. Rini, M.; Pines, D.; Magnes, B.-Z.; Pines, E.; Nibbering, E. T. J. Bimodal proton transfer in acid-base reactions in water, *J. Chem. Phys.*, **2004**, *121* (19), 9593-9610.
32. Rini, M.; Magnes, B.-Z.; Pines, E.; Nibbering, E. T. J. Real-time observation of bimodal proton transfer in acid-base pairs in water, *Science*, **2003**, *301* (5631), 349-352.
33. Liu, W.; Han, F.; Smith, C.; Fang, C. Ultrafast conformational dynamics of pyranine during excited state proton transfer in aqueous solution revealed by femtosecond stimulated Raman spectroscopy, *J. Chem. Phys. B.*, **2012**, *116* (35), 10353-10550.
34. Lakowicz, J. R. Excited-State Reactions in *Principles of Fluorescence Spectroscopy*, Springer, Boston, MA, **1999**, 3<sup>rd</sup> Ed, pp 515-530.
35. Zimmerman, H. E.; Sandel, V. R. Mechanistic organic photochemistry. II.<sup>1,2</sup> solvolytic photochemical reactions, *J. Am. Chem. Soc.*, **1963**, *85* (7), 915-922.
36. Zimmerman, H. E. Meta-ortho effect in organic photochemistry: Mechanistic and exploratory organic photochemistry<sup>1,2</sup>, *J. Phys. Chem. A.*, **1998**, *102* (28), 5616-5621.
37. Smith, K. K.; Kaufmann, K. J.; Huppert, D.; Gutman, M. Picosecond proton ejection: An ultrafast pH jump, *Chem. Phys. Lett.*, **1979**, *64* (3), 522-527.
38. Pines, E.; Huppert, D. Geminate recombination in excited-state proton-transfer reactions: Numerical solution of the Debye–Smoluchowski equation with backreaction and comparison with experimental results, *J. Chem. Phys.*, **1988**, *88* (9), 5620-5630.
39. Cordes, D. B.; Singaram, B. A Unique, Two-Component Sensing System for Fluorescence Detection of Glucose and Other Carbohydrates, *Pure. Appl. Chem.*, **2012**, *84* (11), 2183-2202.
40. Decher, G. Fuzzy nanoassemblies: Towards layered polymeric multicomposites, *Science*, **1997**, *277*, 1232-1237.
41. Costa, R. R.; Alatorre-Meda, M.; Mano, J. F. Drug nano-reservoirs synthesized using layer-by-layer technologies, *Biotechnol. Adv.*, **2015**, *33*, 1310-1326.
42. Iler, R. K. Multilayers of colloidal particles, *J. Colloid Interface Sci.*, **1966**, *21* (6), 569-594.
43. Levy, T.; Déjugnat, C.; Sukhorukov, G. B. Polymer Microcapsules with carbohydrate-sensitive properties, *Adv. Funct. Mater.*, **2008**, *18*, 1586-1594.
44. Watahiki, R.; Sato, K.; Suwa, K.; Niina, S.; Egawa, Y.; Seki, T.; Anzai, J. Multilayer films composed of phenylboronic acidmodified dendrimers sensitive to glucose under physiological conditions, *J. Mater. Chem., B*, **2014**, *2*, 5809-5817.
45. Choi, D.; Hong, J. Layer-by-layer assembly of multilayer films for controlled drug release, *Arch. Pharm. Res.*, **2014**, *37*, 79-87.

46. Wang, B.; Yoshida, K.; Sato, K.; Anzai, J. Phenylboronic acid-functionalized layer-by-layer assemblies for biomedical applications, *Polymers*, **2017**, *9*, 202-218.
47. Guan, Y.; Zhang, Y. Dynamically bonded layer-by-layer films: dynamic properties and applications, *J. Appl. Polym. Sci.*, **2014**, *131* (19), 40918-40929.
48. Kim, K. T.; Cornelissen, J. J. L. M.; Nolte, R. J. M.; van Hest, J. C. M. Polymeric monosaccharide receptors responsive at neutral pH, *J. Am. Chem. Soc.*, **2009**, *131*, 13908-13909.
49. Campos, P. P.; Fernandes Fraceto, L.; Ferreira, M. Layer-by-layer films containing emodin or emodin encapsulated in liposomes for transdermal applications, *Colloids Surf., B*, **2018**, *162*, 69-75.
50. Chen, Q.; Hill, M. R.; Brooks, W. L. A.; Zhu, A.; Sumerlin, B. S.; An, Z. Boronic acid linear homopolymers as effective emulsifiers and gelators, *ACS Appl. Mater. Interfaces*, **2015**, *7*, 21668-21672.
51. Roy, D.; Sumerlin, B. S. Glucose-sensitivity of boronic acid block copolymers at physiological pH, *ACS Macro Lett.*, **2012**, *1*, 529-532.
52. Wu, X.; Li, Z.; Chen, X.-X.; Fossey, J. S.; James, T. D.; Yun-Bao Jiang, Y.-B. Selective sensing of saccharides using simple boronic acids and their aggregates, *Chem. Soc. Rev.*, **2013**, *42*, 8032-8048.
53. <http://www.chem.ucalgary.ca/courses/351/Carey5th/Ch25/ch25-3-3.html> (Accessed online: 14<sup>th</sup> February 2018).



---

# Appendix A

---

Supporting Information for Chapter 2

## **Direct Glucose Sensing: Probing Interactions Between Glucose and Fluorescent Boronic Acids**

*Danielle Bruen, Colm Delaney, Larisa Florea and Dermot Diamond*

*Insight Centre for Data Analytics, National Centre for Sensor Research (NCSR),  
School of Chemical Sciences, Dublin City University, Dublin 9, Ireland*

## A.1 Methods

**Nuclear Magnetic Resonance Spectroscopy (NMR)** spectra were recorded on a Bruker Avance 400 MHz or Bruker Avance Ultrashield 600 MHz NMR spectrometer. Splitting patterns are designated as *s*, singlet; *d*, doublet; *dd*, double doublet; *t*, triplet and *m*, multiplet.  $^1\text{H}$  and  $^{13}\text{C}$  NMR spectra were recorded using deuterium oxide ( $\text{D}_2\text{O}$ ) or deuterated methanol ( $d_4\text{-CH}_3\text{OH}$ ) as solvents, with corresponding reference peaks of  $^1\text{H}$ : 4.87 ( $\text{D}_2\text{O}$ ), 3.31 and 3.34 ( $d_4\text{-CH}_3\text{OH}$ ) and 2.85, 3.01 and 7.92 ( $d_7\text{-DMF}$ ) ppm.  $^{11}\text{B}$  NMR experiments were recorded using  $\text{BF}_3$  in deuterated methanol as an external standard.

**Mass Spectrometry** measurements were carried out on a MALDI/ESI-Q-TOF (time-of-flight) electrospray ionisation mass spectrometer, where the samples were dissolved in deionised water, pH 7.4 phosphate buffer, methanol or chloroform.

**Fluorescence Spectroscopy** measurements were carried out on a JASCO Spectrofluorometer FP-8300 at 20 °C in a precision cell made from Quartz Suprasil that had a path length thickness of 10 mm and a total volume of 1.4 mL. The same cell was used for all fluorescence and UV-visible absorption experiments. Samples were dissolved in either pH 7.4 phosphate buffer, methanol or a mixture of both. Parameters used for fluorescence measurements were as follows; high sensitivity, 2.5 nm bandwidth, 1 second response time, 1 nm data interval and 500 nm/min scan speed.

**Ultraviolet-Visible (UV-Vis) Spectroscopy** was used to determine the excitation wavelength for fluorescence measurements. Measurements were carried out on a Varian Cary 50 Probe spectrophotometer.

**Fourier Transform Infrared (FT-IR) Spectroscopy** measurements were carried out on a Perkin Elmer Spectrum GX.

## A.2 NMR Spectroscopy

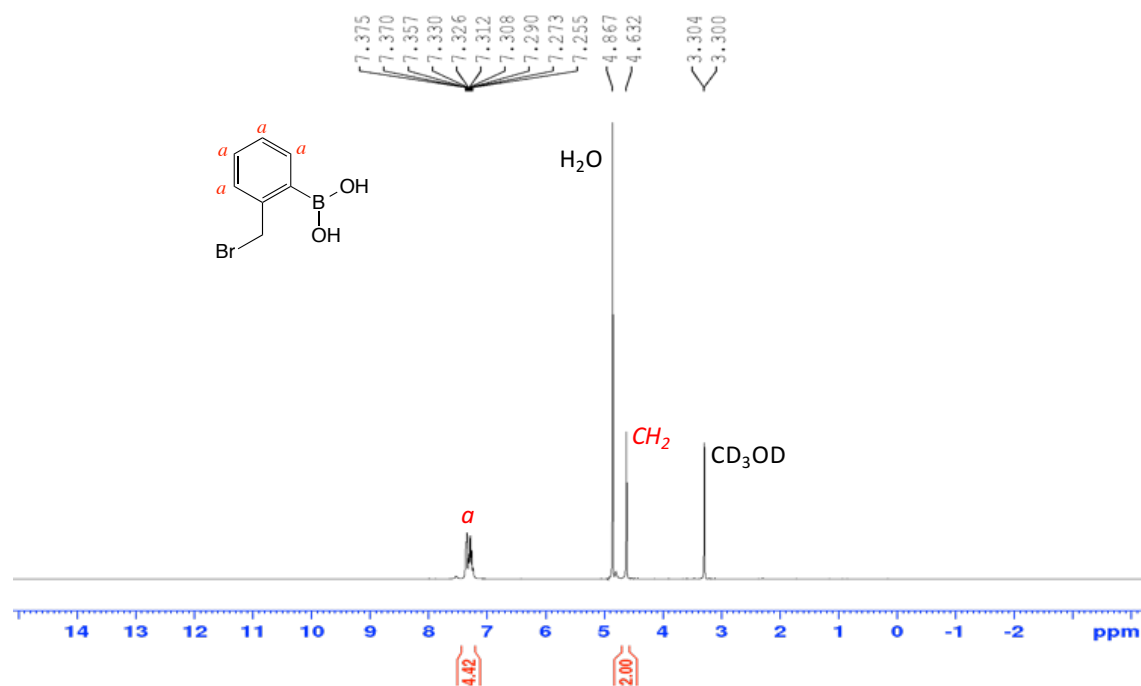


**Figure A1.** <sup>1</sup>H NMR spectrum for 2-(bromomethyl)phenylboronic acid. <sup>1</sup>H NMR (400 MHz, 20 °C, CD<sub>3</sub>OD), δ: 7.3 (4H, *m*, CH – *a*), 4.6 (2H, *s*, CH<sub>2</sub>) ppm.

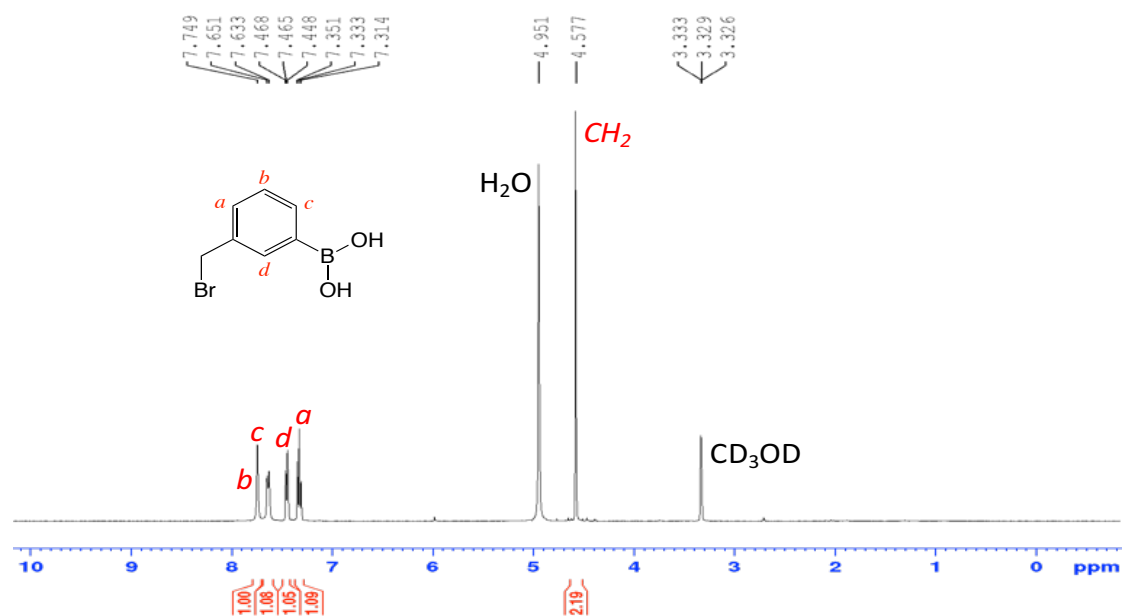


**Figure A2.** <sup>1</sup>H NMR spectrum for 3-(bromomethyl)phenylboronic acid. <sup>1</sup>H NMR (400 MHz, 20 °C, CD<sub>3</sub>OD), δ: 7.7 (1H, *s*, CH – *c*), 7.6 (1H, *d*, *J* = 7 Hz, CH – *d*), 7.4 (1H, *d*, *J* = 7 Hz, CH – *b*), 7.3 (1H, *t*, *J* = 7 Hz, CH – *a*), 4.7 (2H, *s*, CH<sub>2</sub>) ppm.

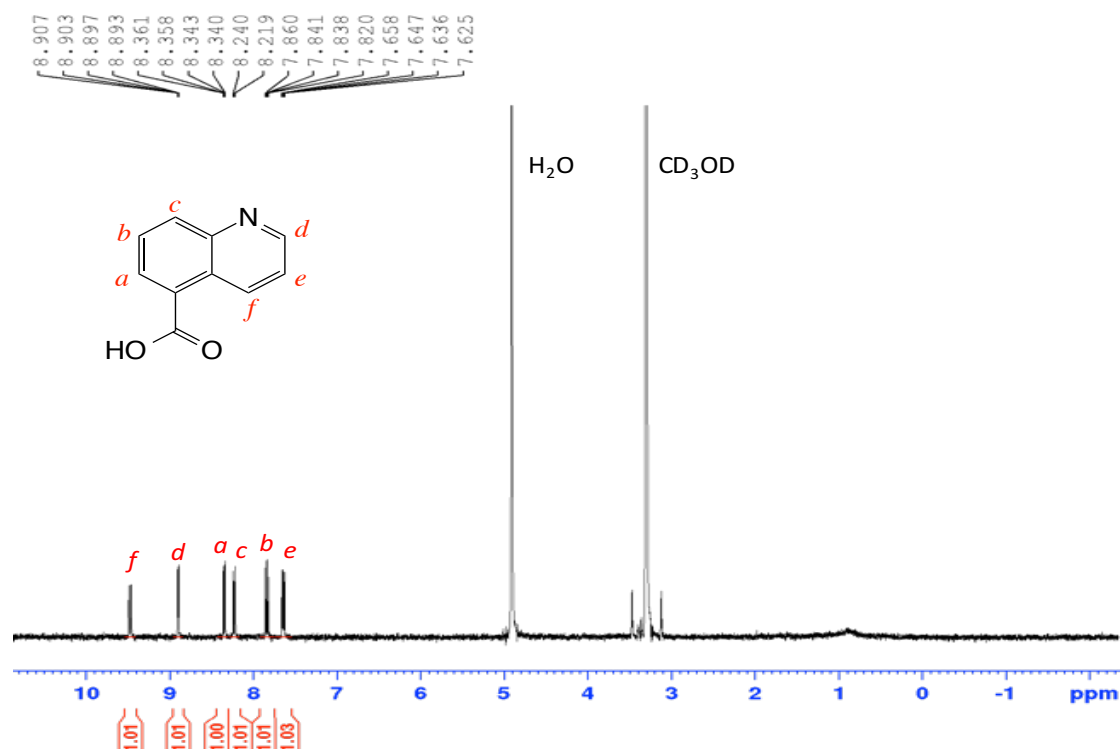


**Figure A3.**  $^1\text{H}$  NMR spectrum for 5-quinoline carboxylic acid.  $^1\text{H}$  NMR (400 MHz,  $20^\circ\text{C}$ ,  $\text{CD}_3\text{OD}$ ),  $\delta$ : 9.4 (1H, *d*,  $J = 9$  Hz, CH – *f*), 8.9 (1H, *dd*,  $J = 2, 3, 4$  and  $6$  Hz, CH – *d*), 8.3 (1H, *dd*,  $J = 1, 6, 7$  and  $9$  Hz, CH – *a*), 8.2 (1H, *d*,  $J = 9$  Hz, CH – *c*), 7.8 (1H, *dd*,  $J = 1, 8, 9$  and  $16$  Hz, CH – *b*), 7.6 (1H, *dd*,  $J = 5, 9$  and  $13$  Hz, CH – *e*) ppm.

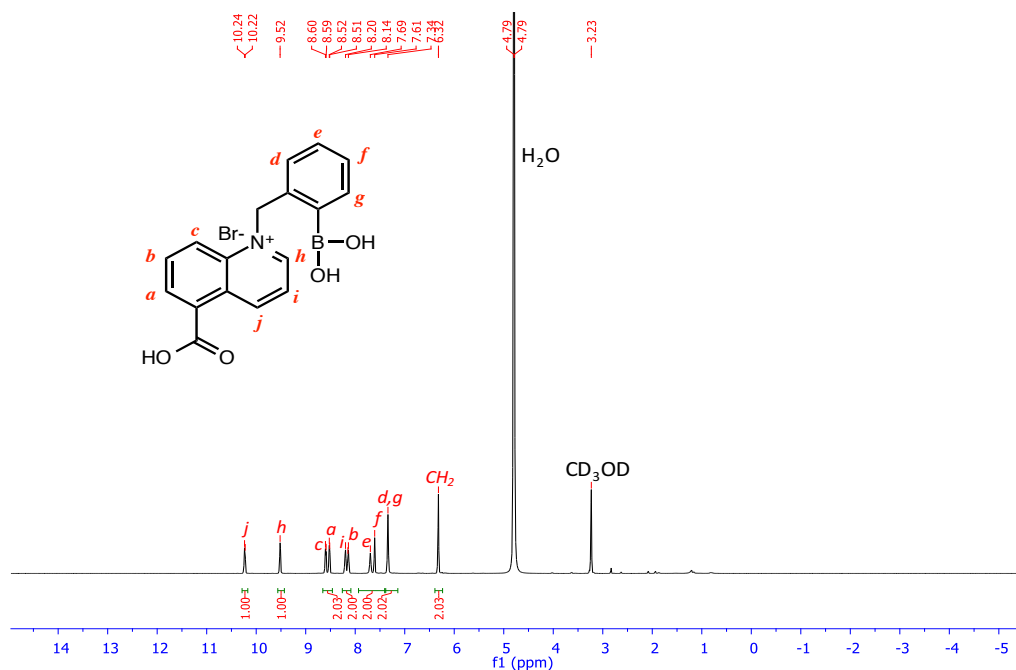


**Figure A4.**  $^1\text{H}$  NMR spectrum for 1-(2-boronobenzyl)-5-carboxyquinolin-1-ium bromide.  $^1\text{H}$  NMR (600 MHz,  $\text{D}_2\text{O}$ ,  $20^\circ\text{C}$ )  $\delta$ : 10.5 (1H, *d*,  $J = 7$  Hz, CH – *j*), 9.5 (1H, *s*, CH – *h*), 8.5–8.6 (2H, *m*, CH – *c*, *a*), 8.1–8.2 (2H, *m*, CH – *i*, *b*), 7.6 (2H, *d*,  $J = 53$  Hz, CH – *e*, *f*), 7.3 (2H, *s*, CH – *d*, *g*), 6.3 (2H, *s*,  $\text{CH}_2$ ) ppm.

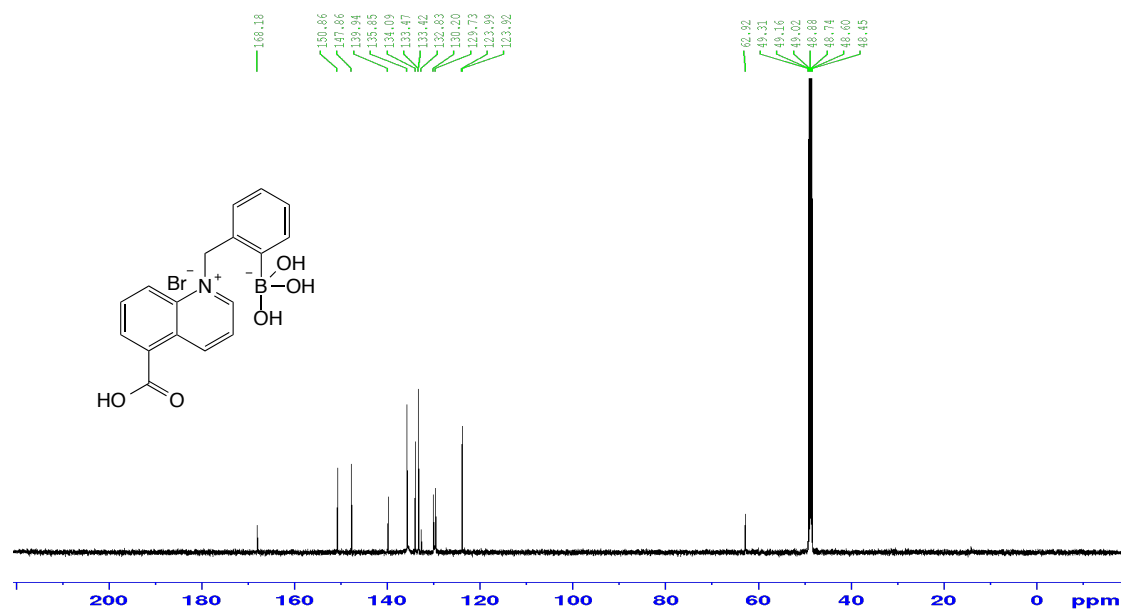


**Figure A5.** <sup>13</sup>C NMR spectrum for 1-(2-boronobenzyl)-5-carboxyquinolin-1-ium bromide. <sup>13</sup>C NMR (150 MHz, 20 °C, CD<sub>3</sub>OD) δ: CH 123.9, 129.7, 130.2, 132.6, 133.4, 134.1, 135.8, 139.9, 147.8, 150.8, COOH 168.1, CH<sub>2</sub> 62.9 ppm.

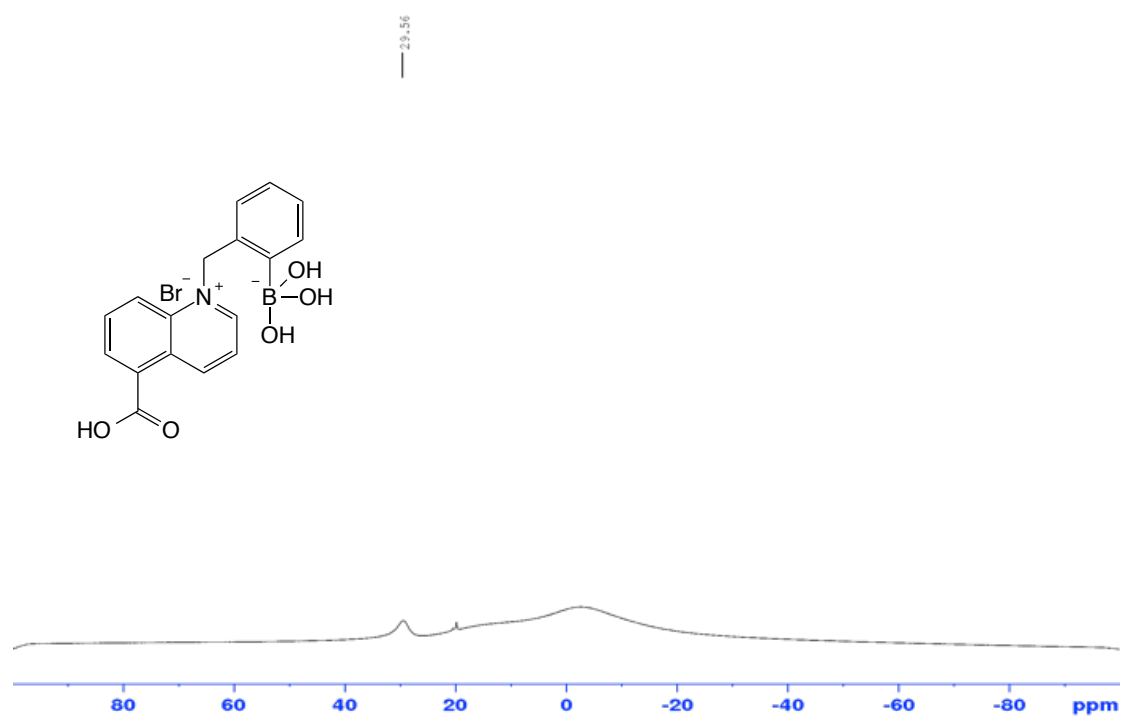


**Figure A6.** <sup>11</sup>B NMR spectrum for 1-(2-boronobenzyl)-5-carboxyquinolin-1-ium bromide. <sup>11</sup>B NMR (192 MHz, 20 °C, CD<sub>3</sub>OD) δ: B(OH)<sub>2</sub> 27.3 ppm. The chemical shift at 19 ppm corresponds to boric acid and the broad peak centred at -2 ppm corresponds to borate in the glass of the NMR tube.

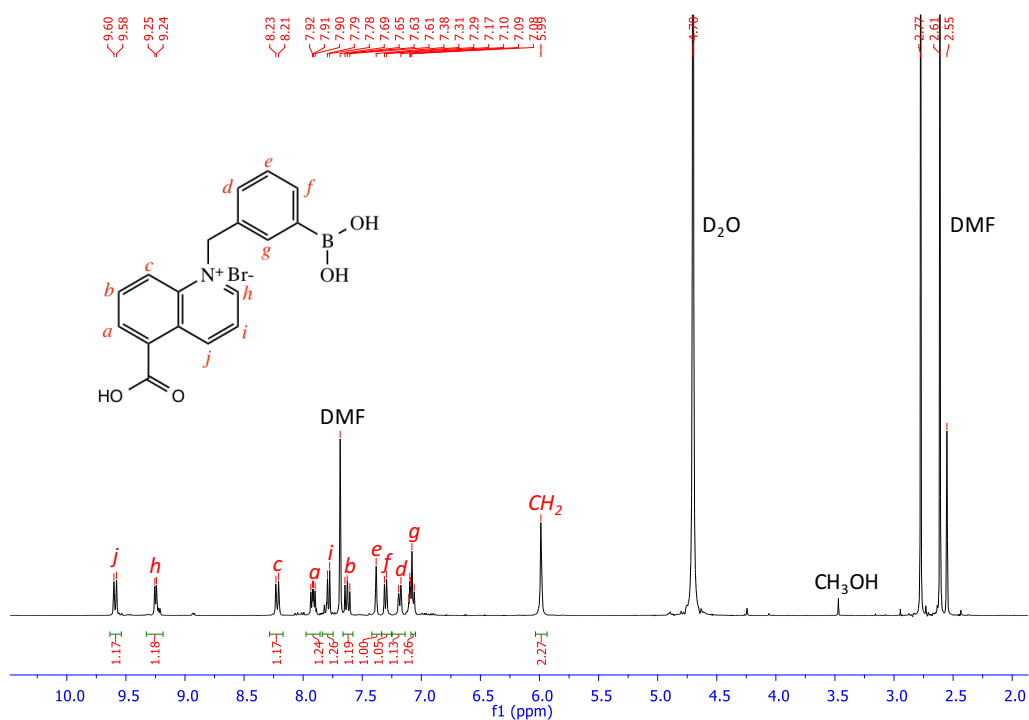


**Figure A7.**  $^1\text{H}$  NMR spectrum for 1-(3-boronobenzyl)-5-carboxyquinolin-1-ium bromide  $^1\text{H}$  NMR (400 MHz, 20 °C,  $\text{D}_2\text{O}$ ),  $\delta$ : 9.6 (1H, *d*,  $J = 9$  Hz, CH – *j*), 9.2 (1H, *d*,  $J = 5$  Hz, CH – *h*), 8.2 (1H, *d*,  $J = 9$  Hz, CH – *c*), 7.8 (1H, *dd*,  $J = 3, 9$  and 15 Hz, CH – *a*), 7.7 (1H, *d*,  $J = 7$  Hz, CH – *i*), 7.6 (1H, *dd*,  $J = 1, 9$  and 16 Hz, CH – *b*), 7.3 (1H, *d*,  $J = 7$  Hz, CH – *f*), 7.3 (1H, *s*, CH – *e*), 7.1 (1H, *d*,  $J = 8$  Hz, CH – *d*), 7.0 – 7.1 (1H, *m*, CH – *g*), 5.9 (2H, *s*,  $\text{CH}_2$ ), ppm.

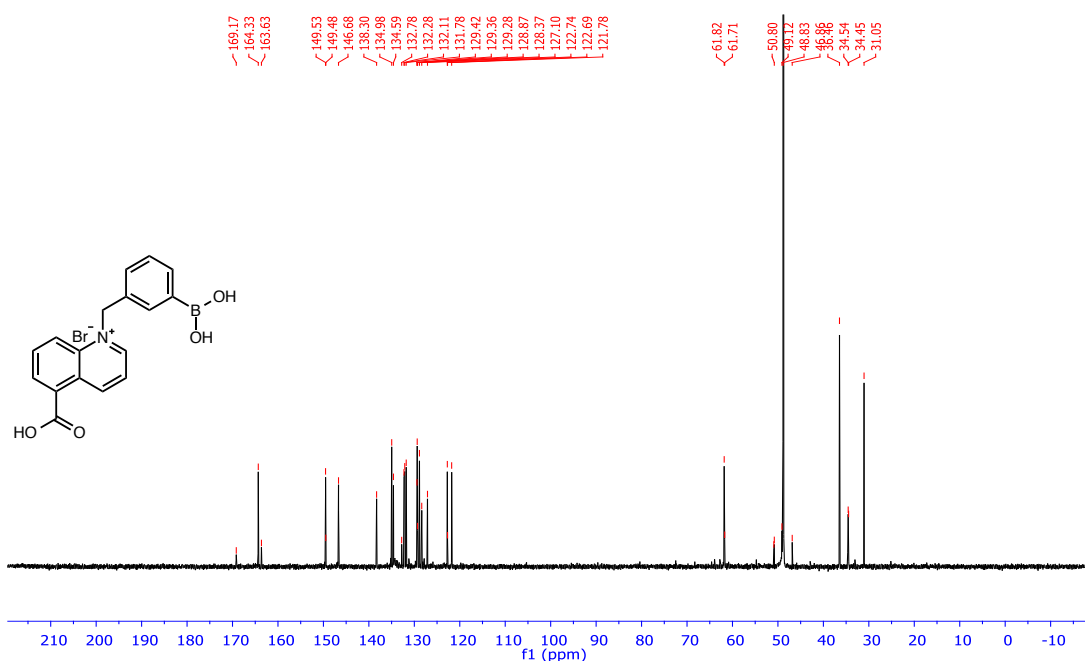


**Figure A8.**  $^{13}\text{C}$  NMR spectrum for 1-(2-boronobenzyl)-5-carboxyquinolin-1-ium bromide.  $^{13}\text{C}$  NMR (150 MHz, 20 °C,  $\text{CD}_3\text{OD}$ )  $\delta$ : COOH 169.2, 164.3, 163.6,  $\text{CH}_2$  61.8, 34.5, 31.1, CH 149.5, 146.8, 138.3, 135.0, 134.6, 132.3, 132.1, 131.8, 129.4, 129.3, 128.9, 128.4, 127.1, 122.7, 121.8 ppm.

### A.3 Mass Spectrometry

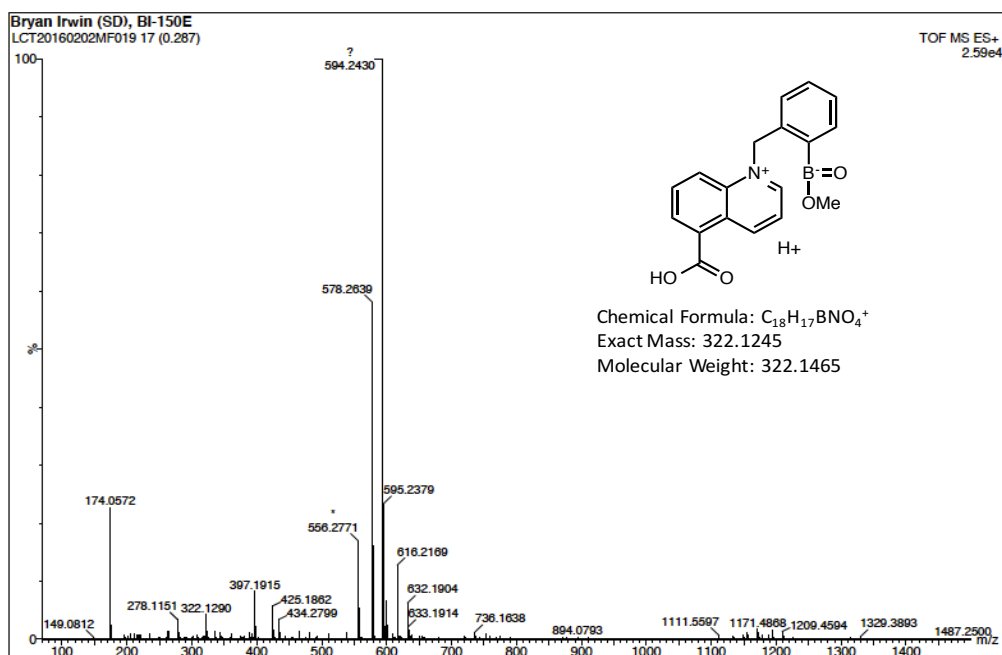


**Figure A9.** Mass spectrometry spectrum for *o*-COOHBA. *o*-COOHBA: Chemical formula:  $C_{17}H_{15}BBrNO_4$ ; Exact Mass: 387.0278; Molecular Weight: 388.0240. *m/z* found:  $[C_{18}H_{17}BNO_4^+]$ , Exact Mass: 322.1245, Molecular Weight: 322.1465.

### A.4 UV-Vis Spectroscopy Spectra

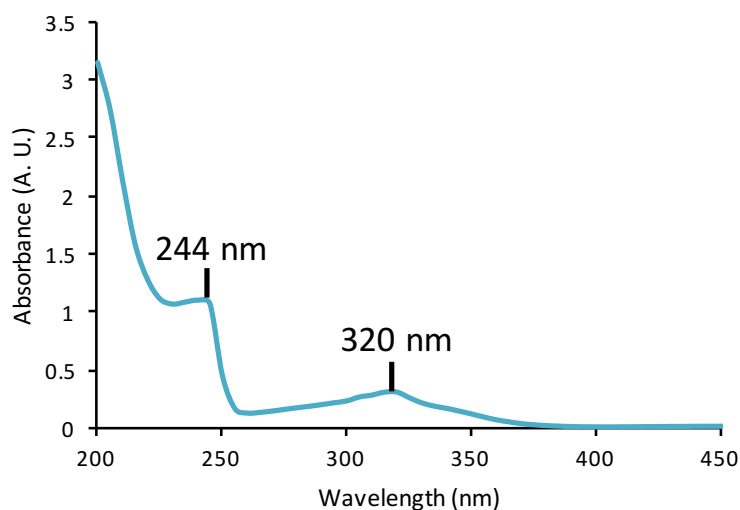


**Figure A10.** Absorbance spectrum for *m*-COOHBA in pH 7.4 phosphate buffer, where the main absorbance peak can be seen at 320 nm.

## A.5 FT-IR Spectroscopy

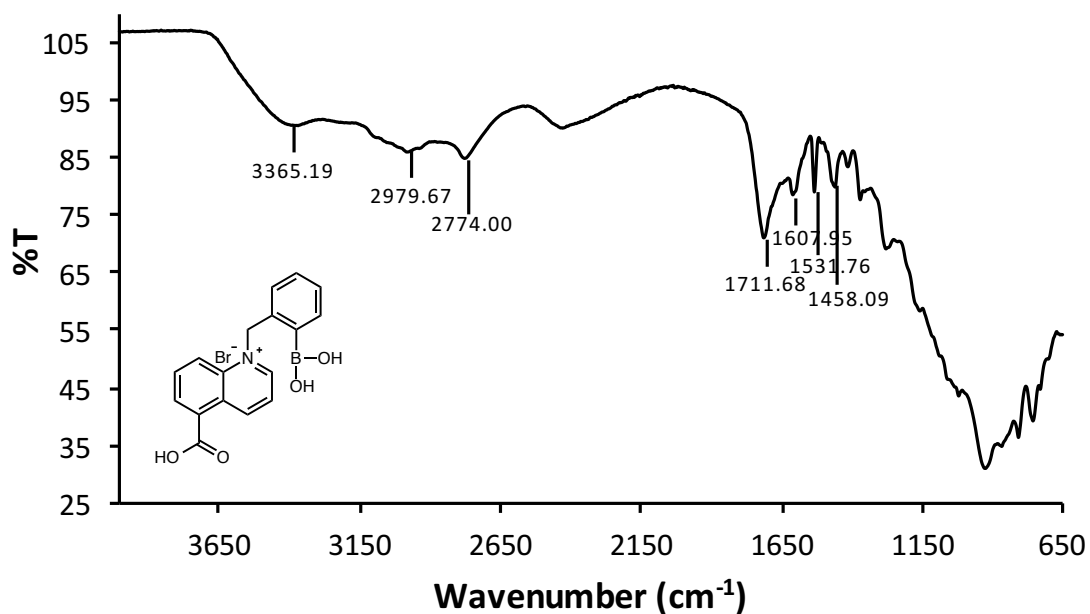


**Figure A11.** FT-IR spectrum for *o*-COOHBA, where peaks were found at 3365.19 (C-OH), 2979.67 and 2774.0 (B-OH, C=C-H), 1711.68 (C=O), 1607.95 (C=C) cm<sup>-1</sup>.

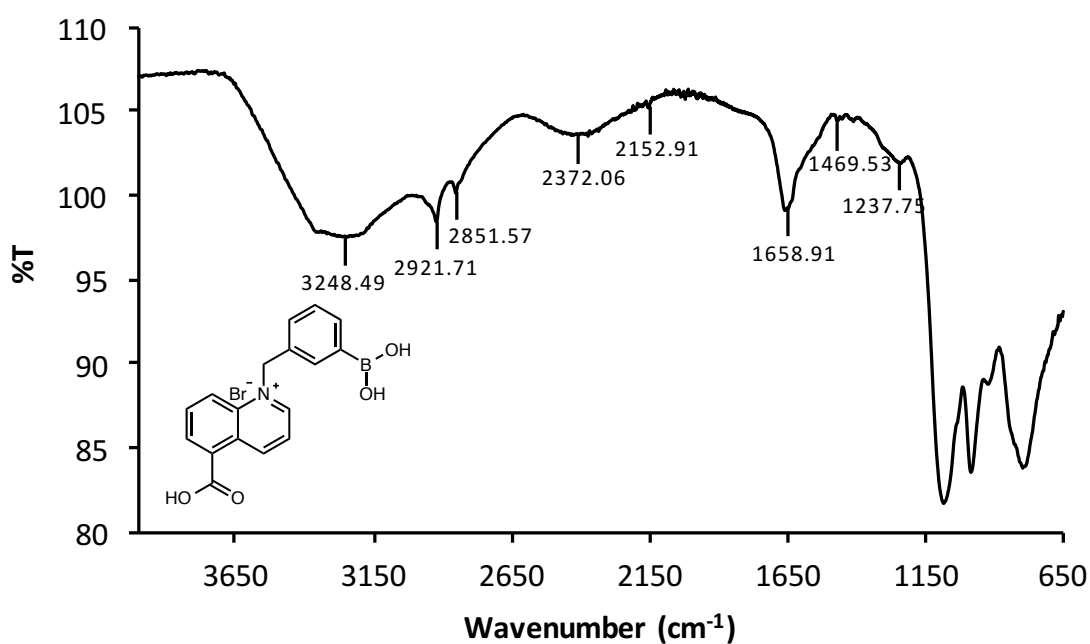


**Figure A12.** FT-IR spectrum for *m*-COOHBA, where peaks were found at 3248.49 (C-OH), 2921.71 and 2851.57 (B-OH), 2372.06 and 2152.91 (C=C-H), 1658.91 (C=O), 1469.53 (C=C) cm<sup>-1</sup>.



---

## Appendix B

---

Supporting Information for Chapter 3

### **Intermolecular Quenching and Recovery of Fluorescence Using Cationic Boronic Acid Derivatives for Indirect Glucose Sensing**

*Danielle Bruen, Colm Delaney, Larisa Florea and Dermot Diamond*

*Insight Centre for Data Analytics, National Centre for Sensor Research (NCSR),  
School of Chemical Sciences, Dublin City University, Dublin 9, Ireland*

## B.1 Methods

**Nuclear Magnetic Resonance Spectroscopy (NMR)** spectra were recorded on a Bruker Avance 400 MHz or Bruker Avance Ultrashield 600 MHz NMR spectrometer. Splitting patterns are designated as *s*, singlet; *d*, doublet; *dd*, double doublet; *t*, triplet and *m*, multiplet.  $^1\text{H}$  and  $^{13}\text{C}$  NMR spectra were recorded using deuterium oxide ( $\text{D}_2\text{O}$ ), deuterated methanol ( $d_4\text{-CH}_3\text{OH}$ ) or deuterated dimethylformamide ( $d_7\text{-DMF}$ ) as solvents, with corresponding reference peaks of  $^1\text{H}$ ,  $\delta$ : 4.87 ( $\text{D}_2\text{O}$ ), 3.31 and 3.34 ( $d_4\text{-CH}_3\text{OH}$ ) and 2.85, 3.01 and 7.92 ( $d_7\text{-DMF}$ ) ppm.  $^{11}\text{B}$  NMR experiments were recorded using  $\text{BF}_3$  in deuterated methanol as an external standard.

**Fluorescence Spectroscopy** measurements were carried out on a JASCO Spectrofluorometer FP-8300 at 20 °C in a precision cell made from Quartz Suprasil that had a path length thickness of 10 mm. The same cell was used for all fluorescence experiments. Samples were dissolved in either pH 7.4 phosphate buffer, methanol or a mixture of both. Parameters for fluorescence measurements were; medium sensitivity, 2.5 nm bandwidth, 1 nm data interval, 1 second response time and 500 nm/min scan speed, unless otherwise stated.

**Ultraviolet-Visible (UV-Vis) Spectroscopy** was used to determine the excitation wavelength for fluorescence measurements. Measurements were carried out on a Varian Cary 50 Probe spectrophotometer.

**Fourier Transform Infrared (FT-IR) Spectroscopy** measurements were carried out on a Perkin Elmer Spectrum GX.

## B.2 NMR Spectroscopy

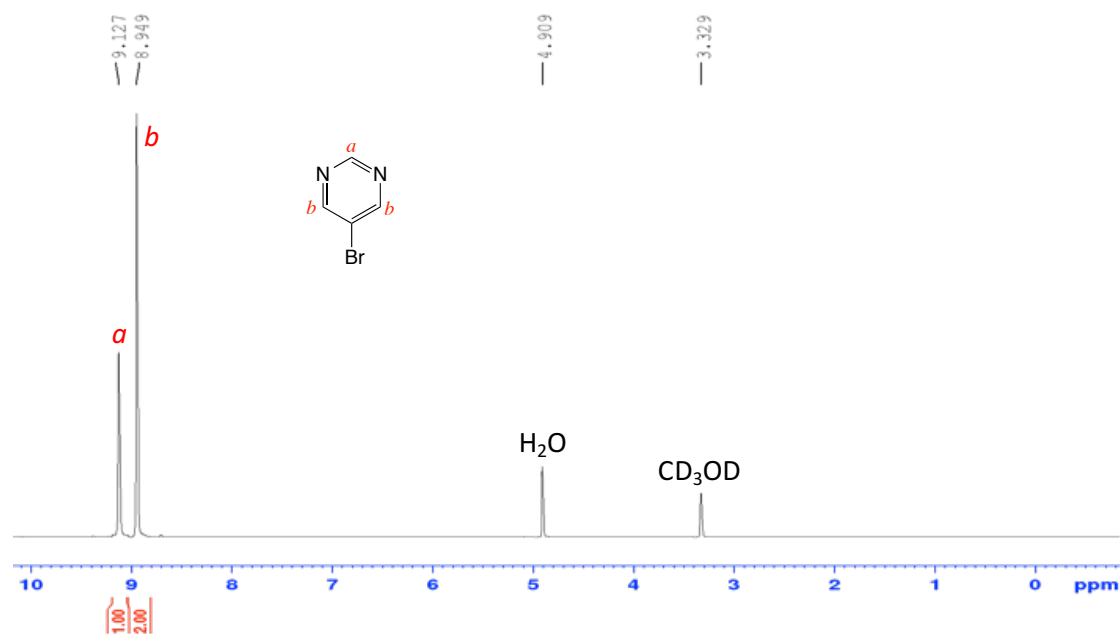


**Figure B1.**  $^1\text{H}$  NMR spectrum for 5-bromopyrimidine.  $^1\text{H}$  NMR (400 MHz, 20 °C,  $\text{CD}_3\text{OD}$ ),  $\delta$ : 9.1 (1H, s, CH – a), 8.9 (2H, s, CH – b) ppm.

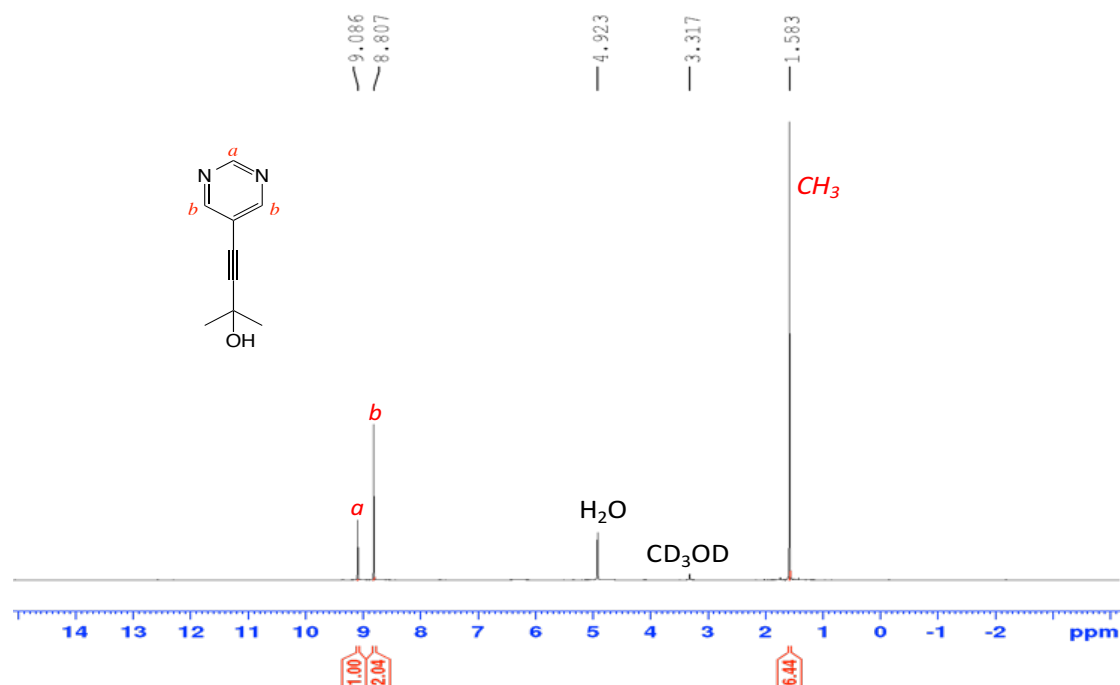


**Figure B2.**  $^1\text{H}$  NMR spectrum for compound **5** (2-(methyl-4-pyrimidin-5-yl)but-3-yn-2-ol).  $^1\text{H}$  NMR (400 MHz, 20 °C,  $\text{CDCl}_3$ )  $\delta$ : 9.08 (1H, s, CH – a), 8.80 (2H, s, CH – b), 1.58 (6H, s,  $\text{CH}_3$ ) ppm.  $^{13}\text{C}$  NMR (150 MHz, 20 °C,  $\text{D}_2\text{O}$ ),  $\delta$ : 158.6 (2C, b), 156.6 (1C, a), 119.2 (1C,  $\text{C}_{\text{quat/aryl}}$ ), 100.9 (1C, Ar- $\text{C}\equiv\text{C}$ -), 75.3 (1C, Ar- $\text{C}\equiv\text{C}$ -), 65.4 (1C,  $\text{C}_{\text{quat/aryl}}$ ), 31.0 (2C, - $\text{CH}_3$ ) ppm.

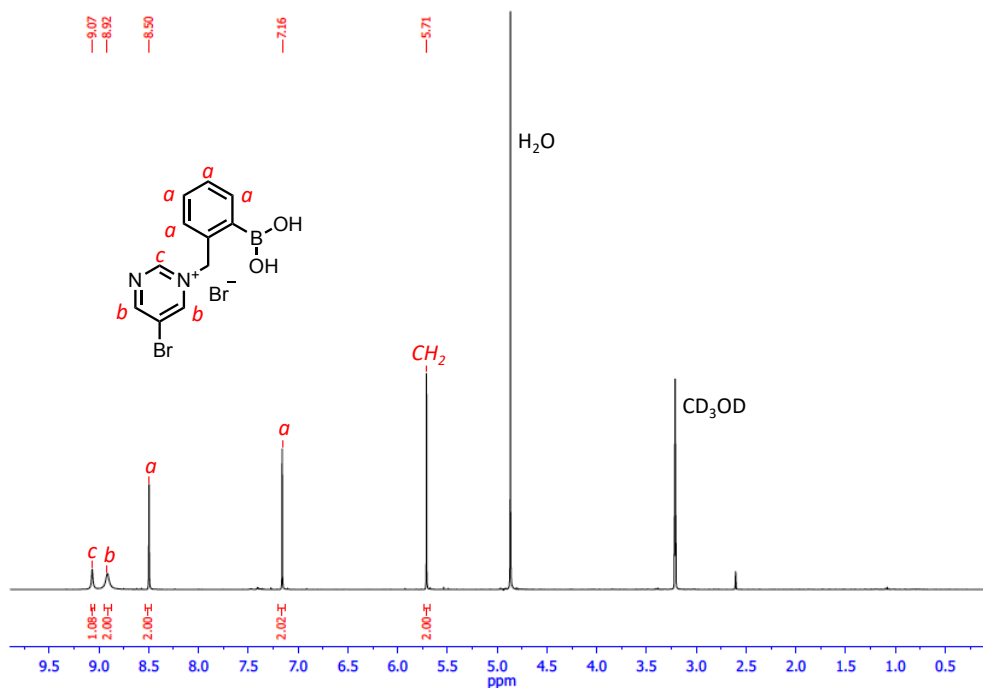


**Figure B3.** <sup>1</sup>H NMR spectrum for 1-(2-bromobenzyl)-5-bromopyrimidine-1-ium bromide (BA1). <sup>1</sup>H NMR (400 MHz, 20 °C, D<sub>2</sub>O), δ: 9.07 (1H, *s*, CH - c), 8.92 (2H, *s*, CH - b), 8.50 (2H, *s*, CH - a), 7.16 (2H, *s*, CH - a), 5.71 (2H, *s*, CH<sub>2</sub>) ppm. <sup>11</sup>B NMR (192 MHz, 20 °C, CD<sub>3</sub>OD), δ: 27.9 (B, *s*, B(OH)<sub>2</sub>) ppm.

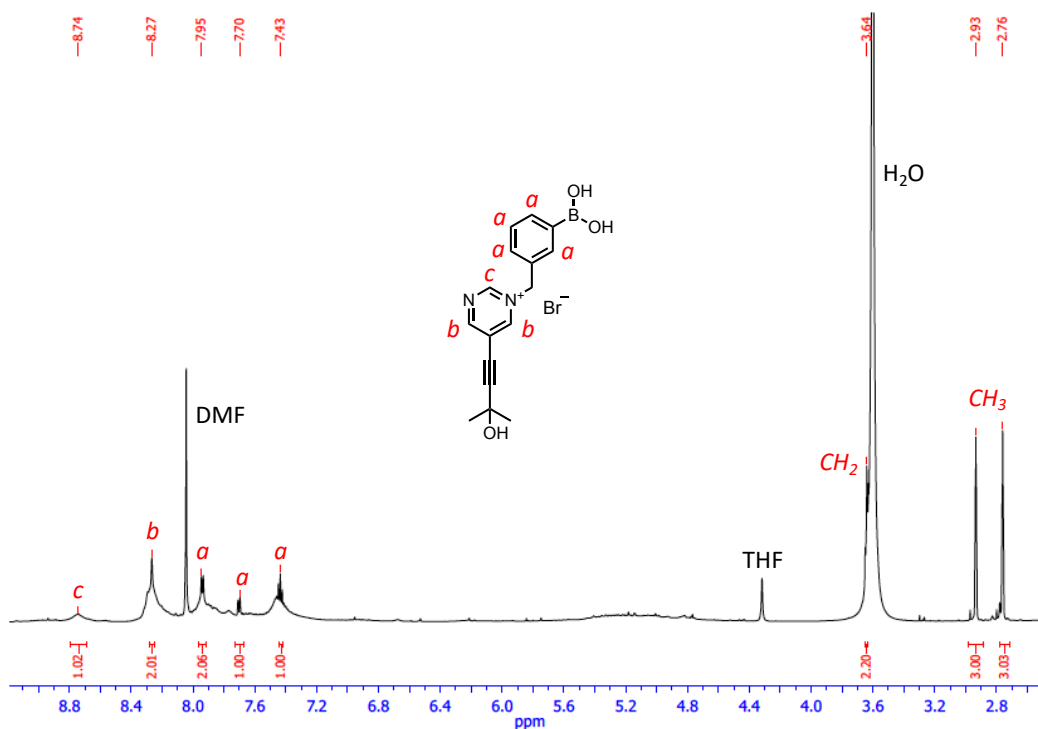


**Figure B4.** <sup>1</sup>H NMR spectrum for 1-(3-boronobenzyl)-5-(3-hydroxy-3-methylbut-1-yn-1-yl)pyrimidine-1-ium bromide (BA2). <sup>1</sup>H NMR (600 MHz, 20 °C, DMF-*d*<sub>7</sub>), δ: 8.74 (1H, *s*, CH - c), 8.27 (2H, *s*, CH - b), 7.95 (2H, *d*, *J* = 7 Hz, CH - a), 7.70 (1H, *d*, *J* = 8 Hz, CH - a), 7.43 (1H, *t*, *J* = 7 and 14 Hz, CH - a), 3.64 (2H, *s*, CH<sub>2</sub>), 2.93 (3H, *s*, CH<sub>3</sub>), 2.76 (3H, *s*, CH<sub>3</sub>) ppm.

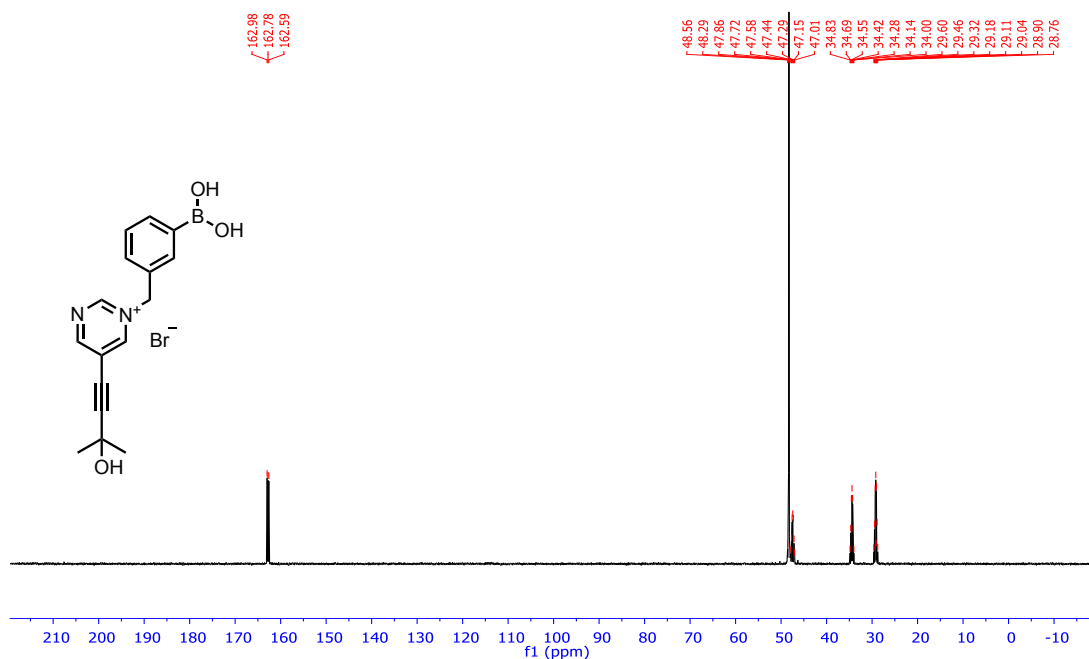


**Figure B5.**  $^{13}\text{C}$  NMR spectrum for BA2.  $^{13}\text{C}$  NMR (150 MHz, 20 °C,  $d_7$ -DMF),  $\delta$ : 163.0, 162.8, 162.6 (CH), 48.6, 48.3, 47.9, 47.7, 47.6, 47.4, 47.3, 47.1 (Ar-C $\equiv$ C-), 34.8-34.6, 34.4, 34.3, ( $\text{C}_{\text{quat/aryl}}$ ), 29.6, 29.5, 29.3-28.8 ( $\text{CH}_3$ ), ppm.

### B.3 Mass Spectroscopy

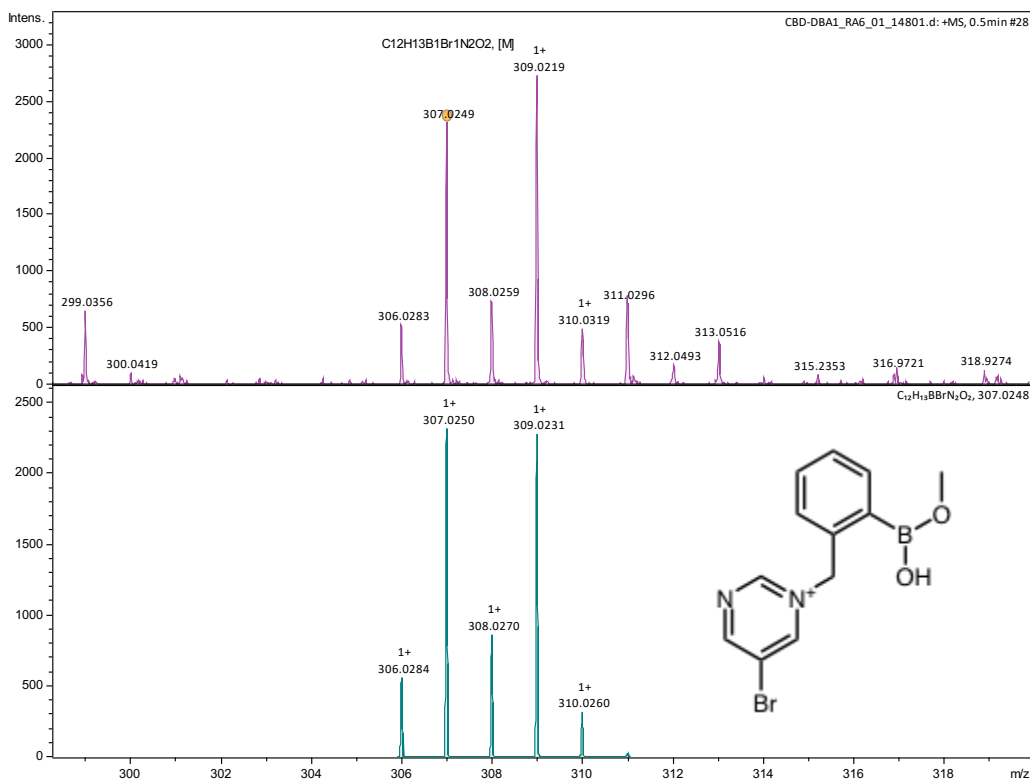


**Figure B6.** High Resolution Mass Spectrometry (HRMS) for BA1 in methanol, where the ( $m/z$ ) calculated for  $[\text{C}_{12}\text{H}_{13}\text{BBBrN}_2\text{O}]^+$  (monomethylether) was 307.0250, found 307.0249.

## B.4 UV-Vis Spectroscopy

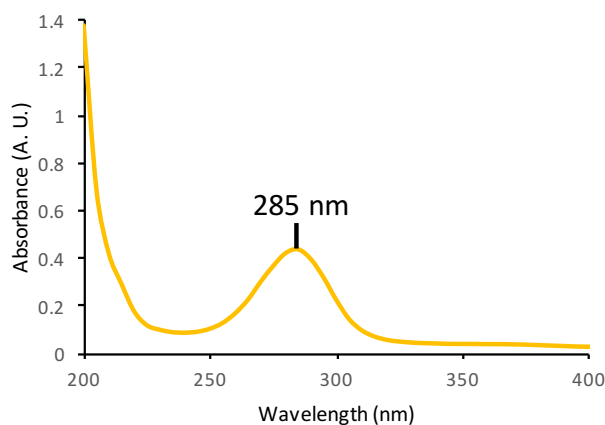


**Figure B7.** Absorbance spectrum for BA1 in pH 7.4 phosphate buffer at a concentration of 0.03 mM, showing an absorbance peak centred at 285 nm.

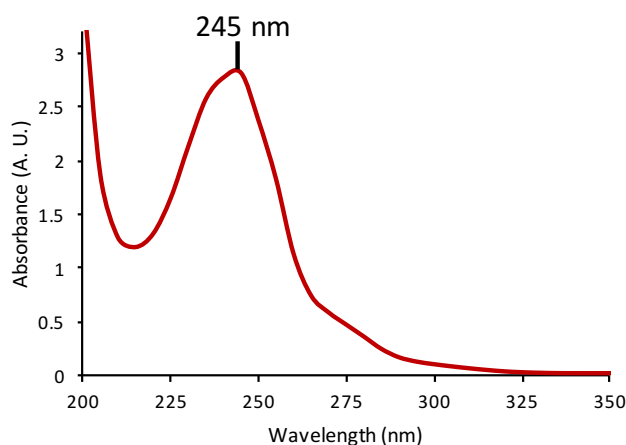


**Figure B8.** Absorbance spectrum for compound 5 (2-(methyl-4-pyrimidin-5-yl)but-3-yn-2-ol) (0.125 mM) in CH<sub>3</sub>OH, showing an absorbance peak centred at 245 nm.

## B.5 Fluorescence Spectroscopy

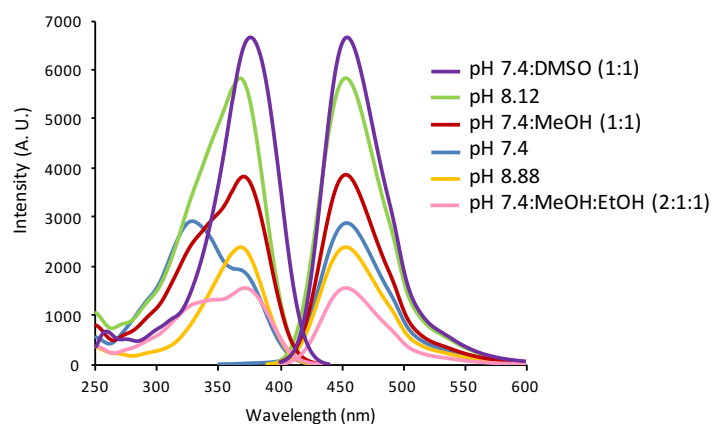


**Figure B9.** Fluorescence excitation and emission spectra for 7HC (7-hydroxycoumarin) solutions (4 μM) in pH buffers and various solvents.

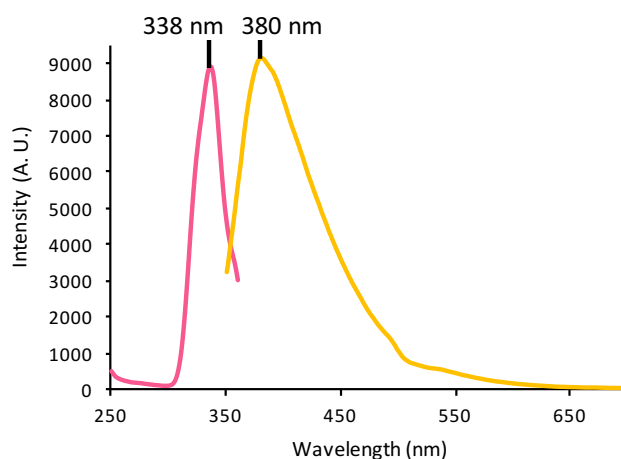


**Figure B10.** Fluorescence excitation and emission spectra for BA1, where the excitation peak is at 338 nm and the corresponding emission peak is at 380 nm. Fluorescence parameters: manual sensitivity at 690 V, 2.5 nm bandwidth, 1 second response time, 1 nm data interval, 500 nm/min scan speed.

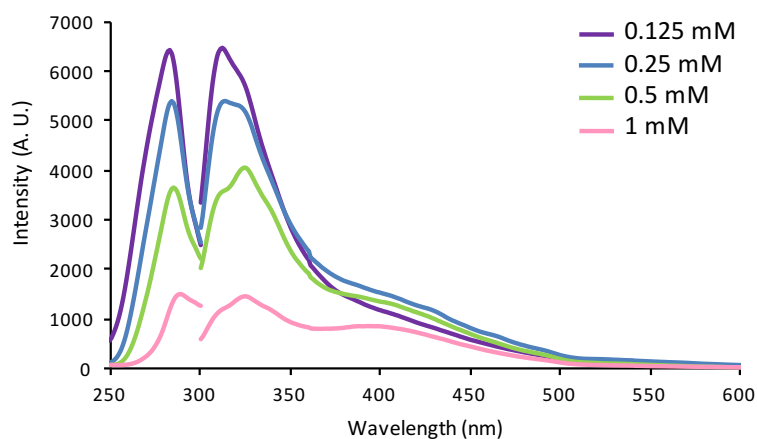


**Figure B11.** Fluorescence spectra for compound **5** (2-(methyl-4-pyrimidin-5-yl)but-3-yn-2-ol) in CH<sub>3</sub>OH, where the excitation wavelength was 283 nm and the corresponding emission was at 311 nm. Fluorescence parameters: high sensitivity, 2.5 nm bandwidth, 1 second response time, 1 nm data interval, 500 nm/min scan speed.

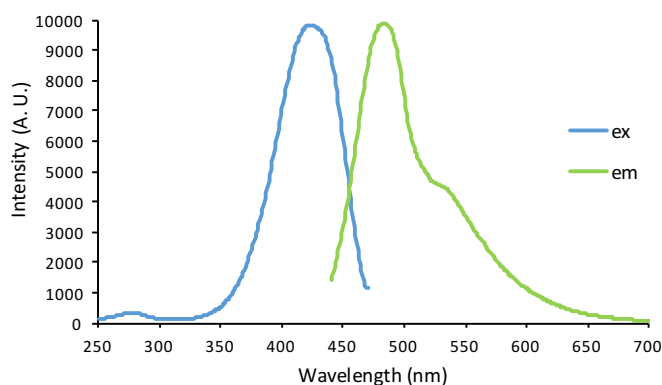


**Figure B12.** Excitation and emission fluorescence spectrum for BA2 (0.5 mM) in CH<sub>3</sub>OH, excitation 430 nm and emission 484 nm, 533 nm; fluorescence parameters: high sensitivity, 2.5 nm bandwidth, 500 nm/min scan rate, data interval at 1 nm.

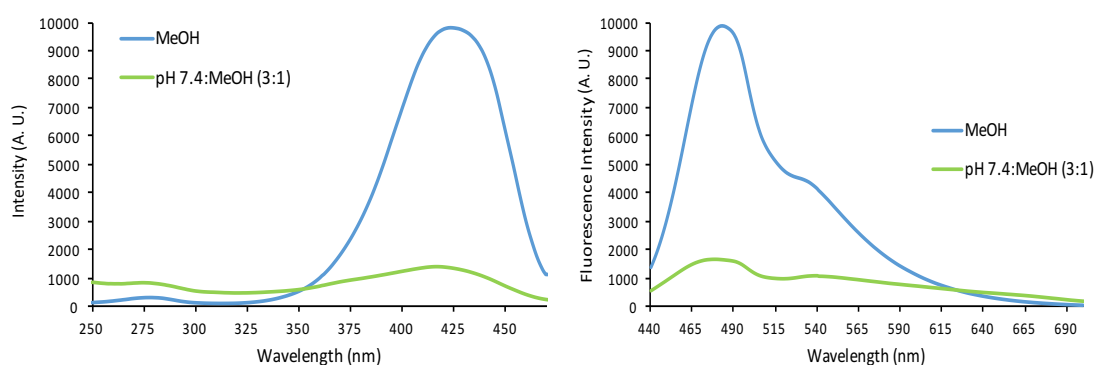


**Figure B13.** Excitation and emission spectra for BA2 in CH<sub>3</sub>OH and pH 7.4 phosphate buffer:CH<sub>3</sub>OH (3:1). The excitation band shifts from 430 nm (CH<sub>3</sub>OH) to 420 nm (pH 7.4 buffer:CH<sub>3</sub>OH 3:1). The emission peak remains at 484 nm and 533 nm in both cases, with a dramatic decrease in the more polar solvent mixture. This indicates that the  $n \rightarrow \pi^*$  transition can be identified at around 275 nm and the  $\pi \rightarrow \pi^*$  transition can be identified at around 430 nm.

## B.6 FT-IR Spectroscopy

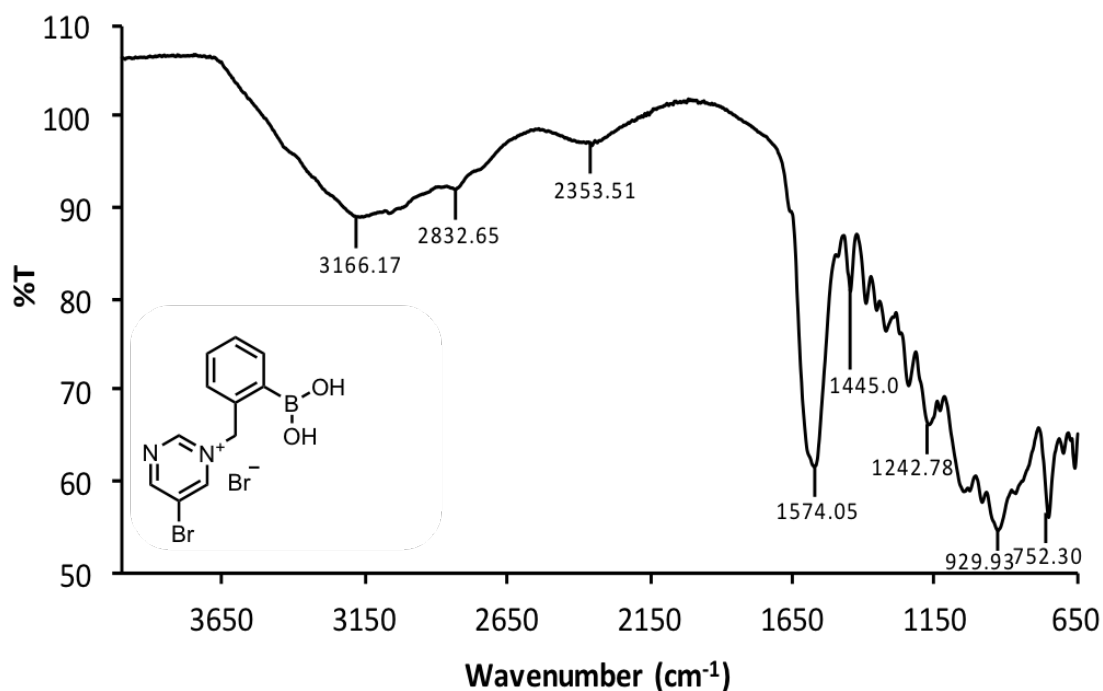


**Figure B14.** FT-IR for BA1, where peaks were found at 3166.17 (B-OH), 2832.65 and 2353.51 (C=C-H), 1574.05, 1445.0 (C=C), 752.3 cm<sup>-1</sup> (C-Br) corresponding to functional groups observed in BA1.



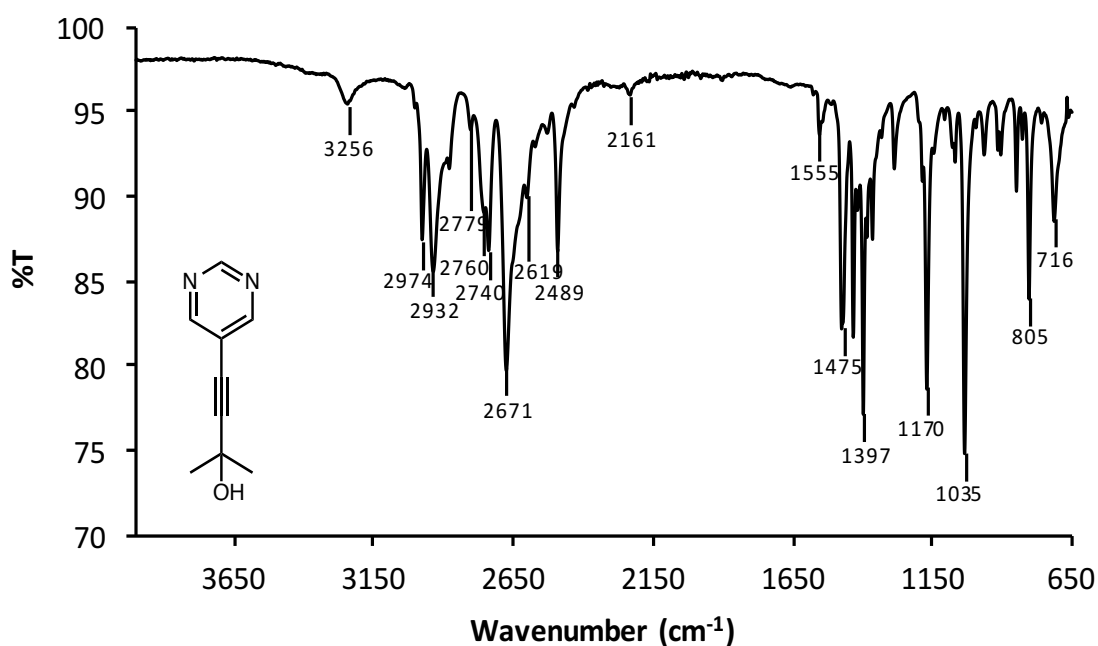


**Figure B15.** FT-IR for compound **5** (2-(methyl-4-pyrimidin-5-yl)but-3-yn-2-ol), where peaks were found at 3256 (C-OH), 2974, 2932, 2779, 2760, 2740, 2671, 2619, 2489 (C=C-H), 2161 (Alkyne C-C-H), 1555, 1475, 1397 cm<sup>-1</sup> (C=C) corresponding to functional groups observed in compound **5**.

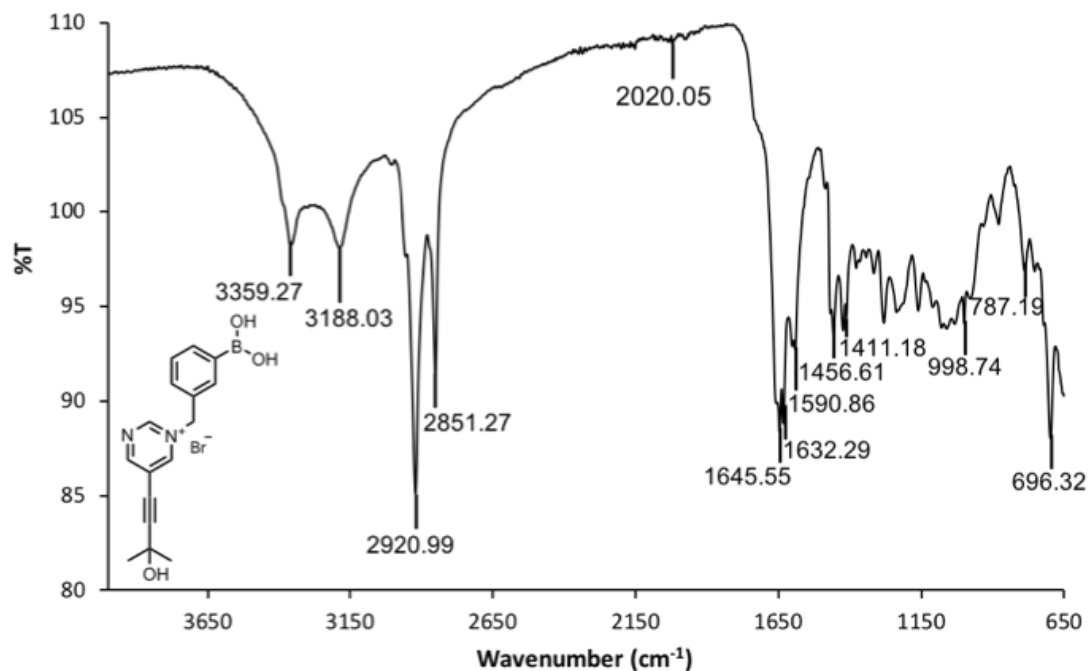


**Figure B16.** FT-IR for BA2, where peaks were found at 3359.27 (B-OH), 3188.03 (C-OH), 2920.99, 2851.27 (C=C-H), 2020.05 (Alkyne C-C-H), 1645.55, 1632.29, 1590.86, 1456.61, 1411.18 cm<sup>-1</sup> (C=C) corresponding to functional groups observed in BA2.

---

## Appendix C

---

Supporting Information for Chapter 4

### **Water-Soluble Polymerisable Boronic Acids: Combining an Adaptable One-Step Synthesis with an In-Depth Understanding of pH and Glucose Response\***

*Danielle Bruen, Colm Delaney, Dermot Diamond and Larisa Florea*

*Insight Centre for Data Analytics, National Centre for Sensor Research (NCSR),  
School of Chemical Sciences, Dublin City University, Dublin 9, Ireland*

\*This chapter has been submitted for publication as “Water-Soluble Polymerisable Boronic Acids: Combining an Adaptable One-Step Synthesis with an In-Depth Understanding of pH and Glucose Response”, [Danielle Bruen](#), Colm Delaney, Larisa Florea and Dermot Diamond, *Org. Lett.*, **2018**.

\*\*The boronic acid compounds synthesised in this chapter are covered under GB Patent, GB1805226.6, “Boronic Acid Derivatives for Sugar-Sensing Hydrogels”, Colm Delaney, Larisa Florea, [Danielle Bruen](#) and Dermot Diamond, March **2018**.

## C.1 Characterisations for BA monomers

### C.1.1 Spectroscopic Characterisations for *o*-BA

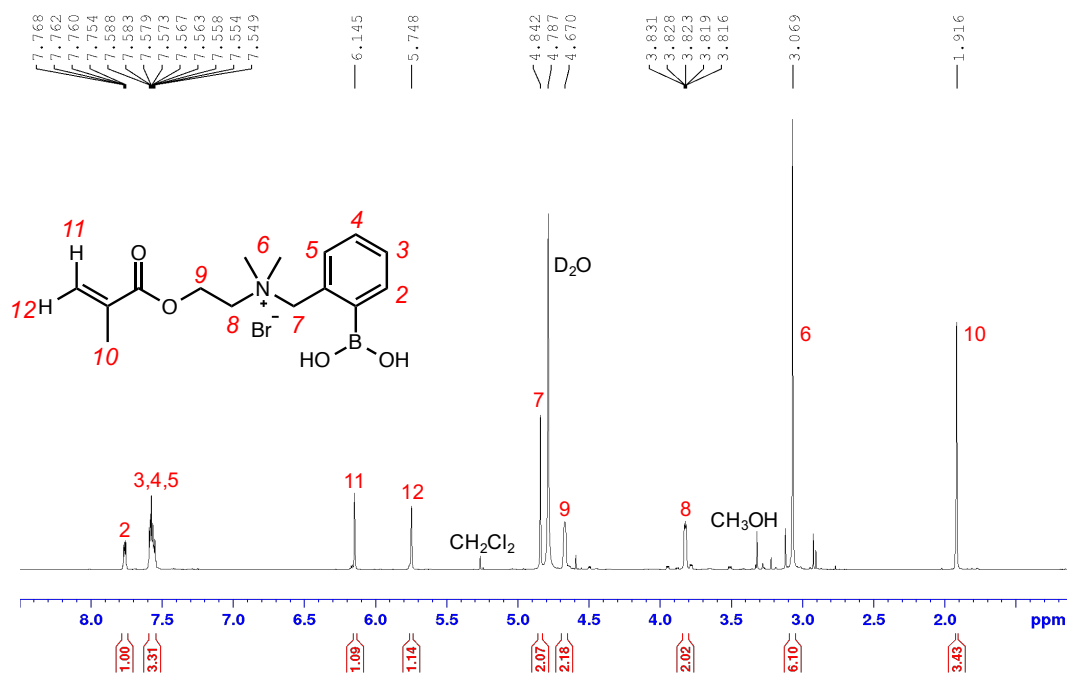


**Figure C1.** <sup>1</sup>H NMR for *o*-BA in D<sub>2</sub>O. <sup>1</sup>H NMR (600 MHz, 20 °C, D<sub>2</sub>O), δ: 7.7 (1H, *dd*, *J* = 3 and 8 Hz, CH, H2), 7.5 (3H, *m*, CH, H-3,4,5), 6.1 (1H, *s*, CH<sub>2</sub>, H11), 5.7 (1H, *s*, CH<sub>2</sub>, H12), 4.8 (2H, *s*, CH<sub>2</sub>, H7), 4.6 (2H, *s*, CH<sub>2</sub>, H9), 3.8 (2H, *m*, CH<sub>2</sub>, H8), 3.0 (6H, *s*, CH<sub>3</sub>, H6), 1.9 (3H, *s*, CH<sub>3</sub>, H9), ppm.

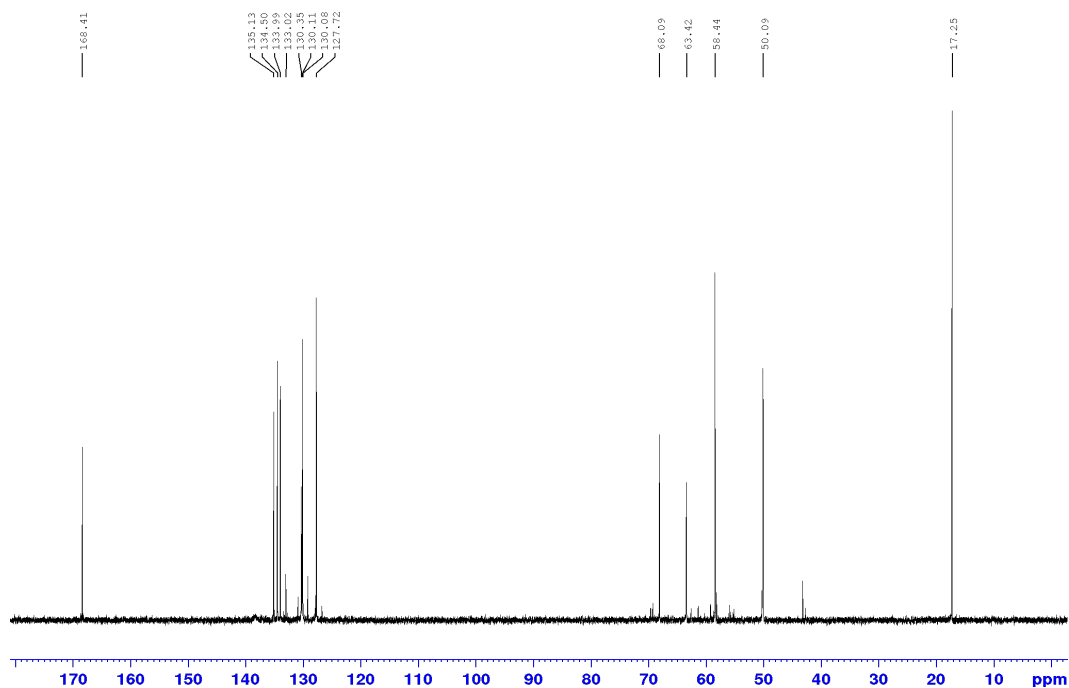


**Figure C2.** <sup>13</sup>C NMR for *o*-BA in D<sub>2</sub>O. <sup>13</sup>C NMR (150 MHz, 20 °C, D<sub>2</sub>O), δ: 168.4 (C=O), 134.4 (C-H<sub>2</sub>), 133.9 (C-H<sub>4</sub>), 130.3 (C-H<sub>3</sub>), 127.7 (CH<sub>2</sub>-Vinyl), 130.0, 68.0 (C-H<sub>5</sub>), 63.4 (CH<sub>2</sub>, H8), 58.4 (CH<sub>2</sub>, H9), 50.0 (CH<sub>3</sub>-Amine), 17.2 (CH<sub>3</sub>-Vinyl) ppm.

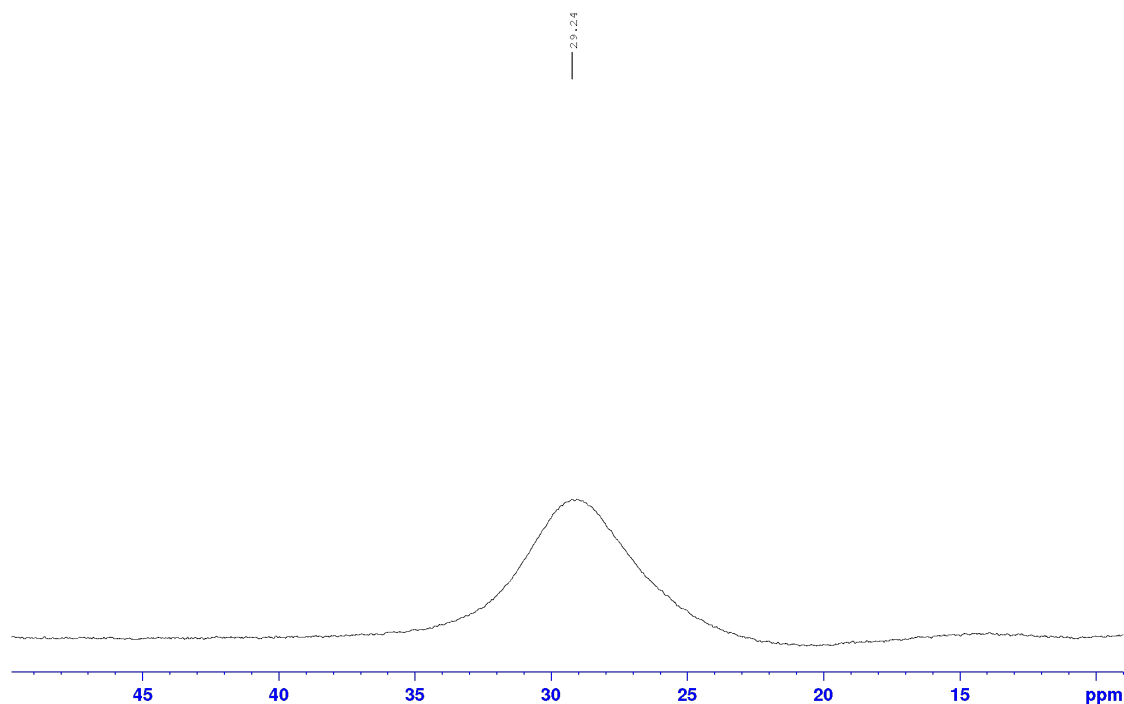


**Figure C3.**  $^{11}\text{B}$  NMR for *o*-BA in  $\text{D}_2\text{O}$ .  $^{11}\text{B}$  NMR (192 MHz, 20 °C,  $\text{D}_2\text{O}$ ),  $\delta$ : 29.24 (1B,  $\text{B}(\text{OH})_2$ ) ppm. (Line broadening by 10 Hz).

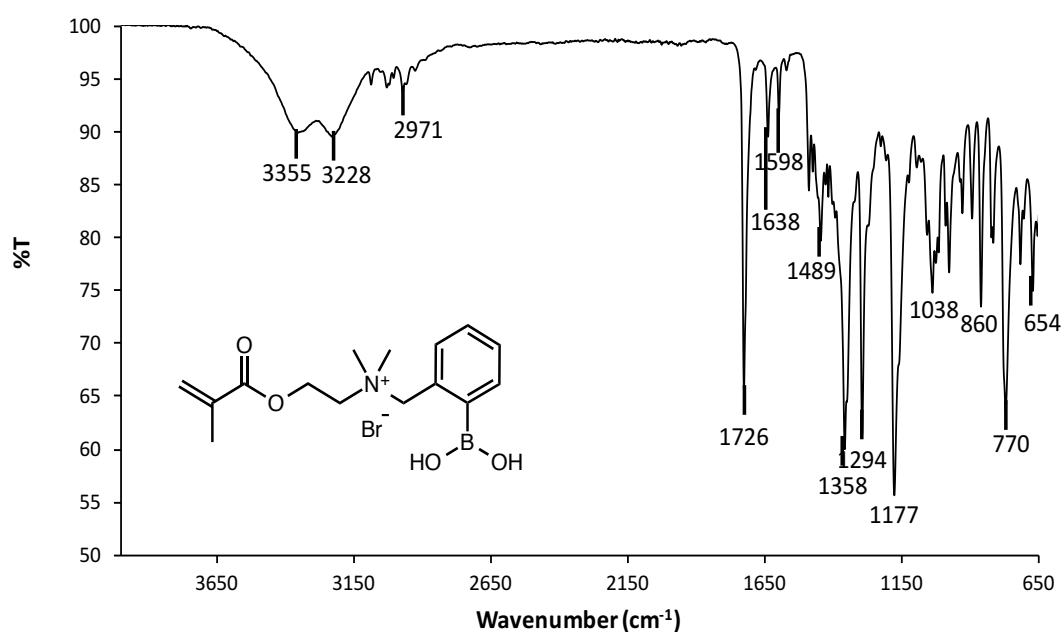


**Figure C4.** IR spectrum for *o*-BA. FT-IR: 3355 (B-OH), 3228 (B-OH), 2971 (C=C-H), 1726 (C=O), 1638 (C=C), 1598 (C=C) and 1489 (C=C)  $\text{cm}^{-1}$ .

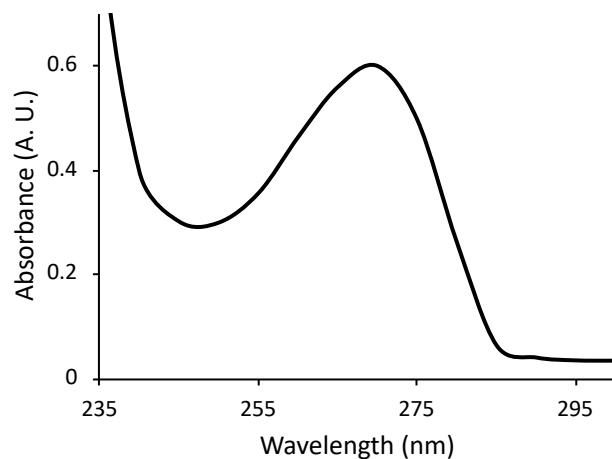


**Figure C5.** UV-visible spectrum for *o*-BA (1 mM), where the absorbance peak is at 270 nm at pH 7.4.

### C.1.2 Spectroscopic Characterisations for *m*-BA

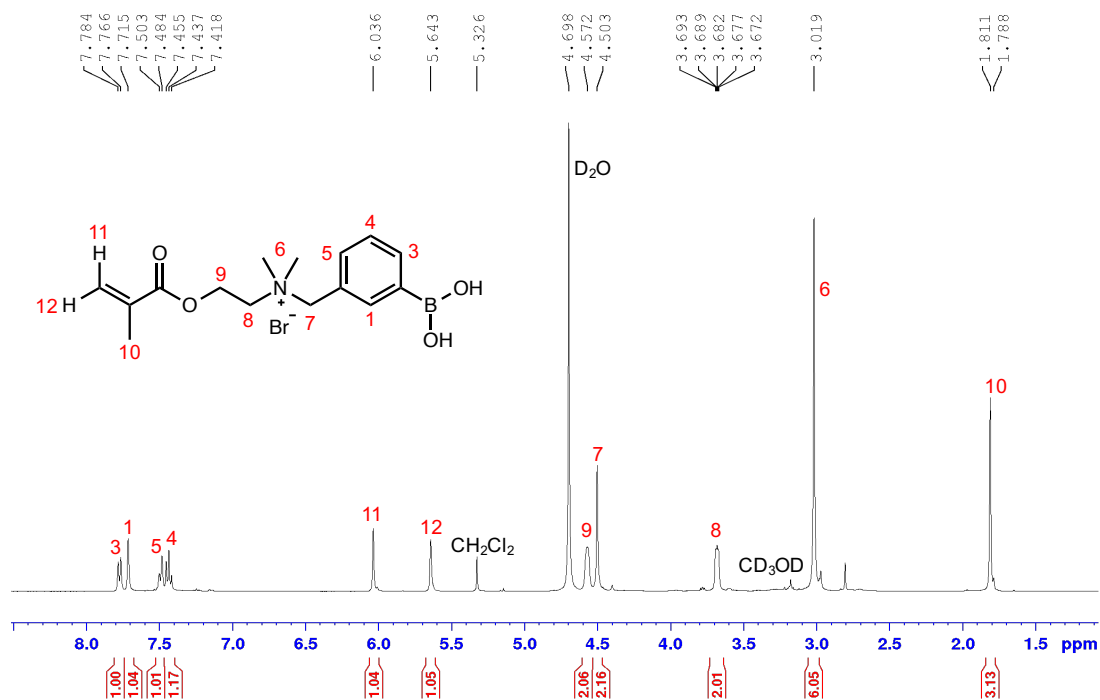


**Figure C6.** <sup>1</sup>H NMR for *m*-BA in D<sub>2</sub>O. <sup>1</sup>H NMR (600 MHz, 20 °C, D<sub>2</sub>O) for *m*-BA, δ: 7.7 (1H, *dd*, *J* = 3 and 8 Hz, CH, H1), 7.5 (3H, *m*, CH, H-3,4,5), 6.1 (1H, *s*, CH<sub>2</sub>, H11), 5.7 (1H, *s*, CH<sub>2</sub>, H12), 4.8 (2H, *s*, CH<sub>2</sub>, H9), 4.6 (2H, *s*, CH<sub>2</sub>, H7), 3.8 (2H, *m*, CH<sub>2</sub>, H8), 3.0 (6H, *s*, CH<sub>3</sub>, H6), 1.9 (3H, *s*, CH<sub>3</sub>, H10) ppm.

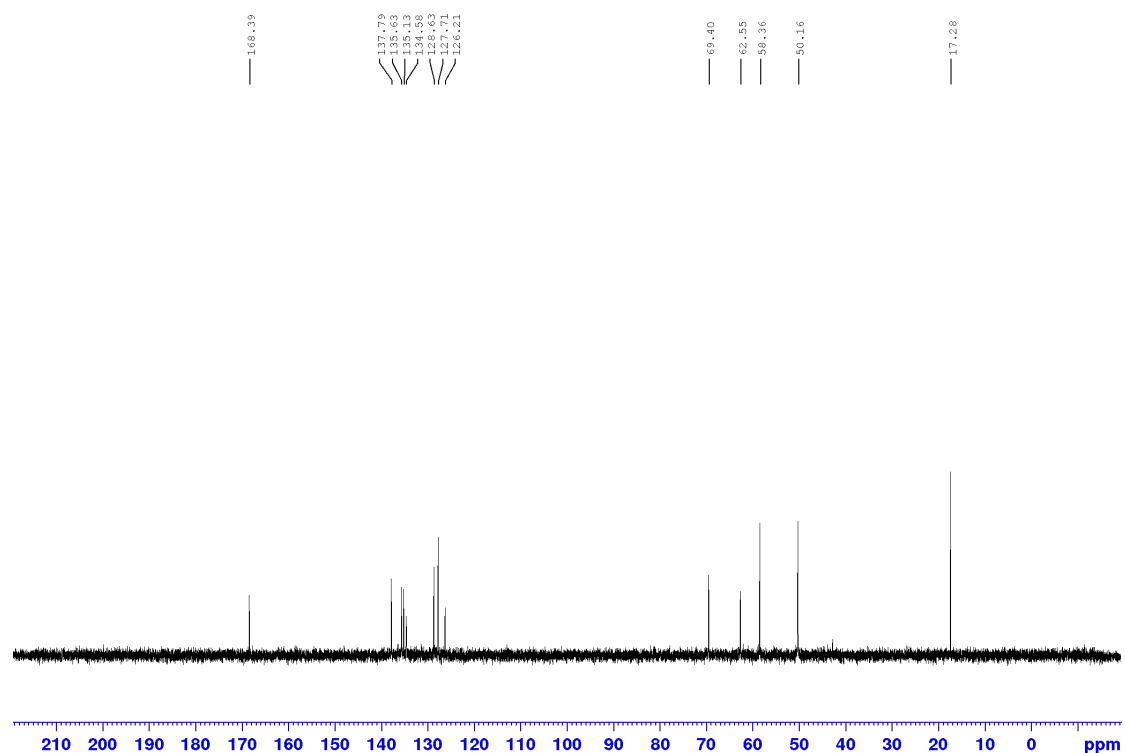


**Figure C7.**  $^{13}\text{C}$  NMR for *m*-BA in  $\text{D}_2\text{O}$ .  $^{13}\text{C}$  NMR (150 MHz, 20 °C,  $\text{D}_2\text{O}$ ),  $\delta$ : 168.3 (C=O), 137.7 (C-H1), 135.6 (C-H3), 135.1 (C-H5), 134.5 (CH-4), 128.6 (CH-Vinyl), 126.2 (CH<sub>2</sub>-Vinyl), 69.4 (CH<sub>2</sub>-Amine), 62.5 (CH<sub>2</sub>-Amine), 58.3 (CH-9), 50.1 (CH<sub>3</sub>-Amine), 17.2 (CH<sub>3</sub>-Vinyl) ppm

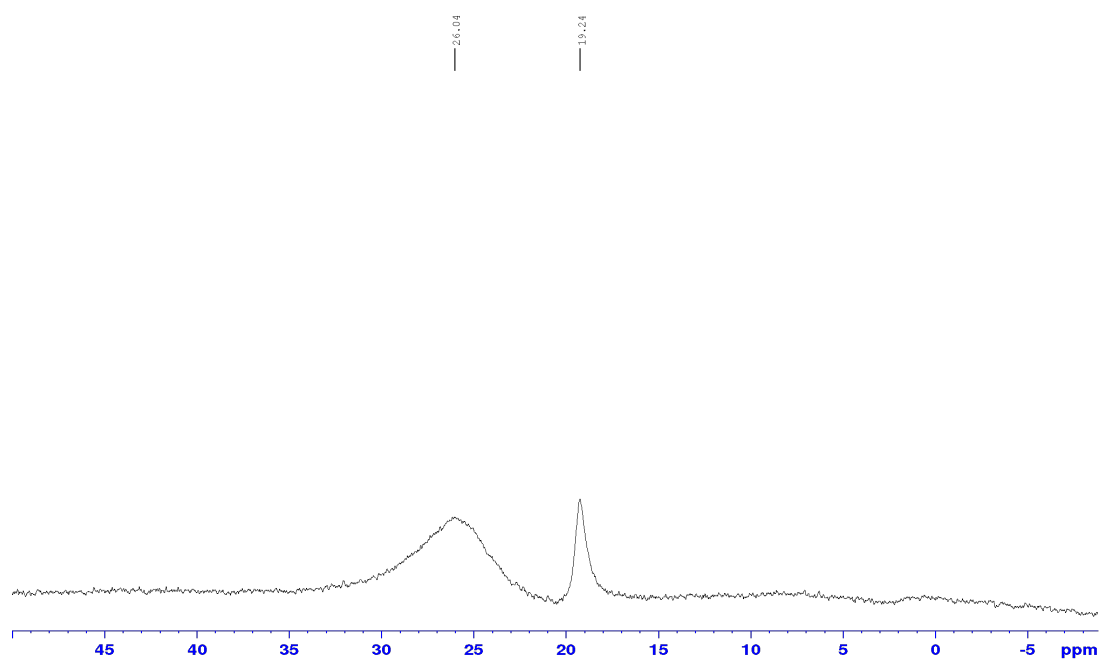


**Figure C8.**  $^{11}\text{B}$  NMR for *m*-BA in  $\text{D}_2\text{O}$ .  $^{11}\text{B}$  NMR (192 MHz, 20 °C,  $\text{D}_2\text{O}$ ),  $\delta$ : 24.0 (1B, s, B-(OH)<sub>2</sub>) ppm. (Line broadening by 10 Hz).

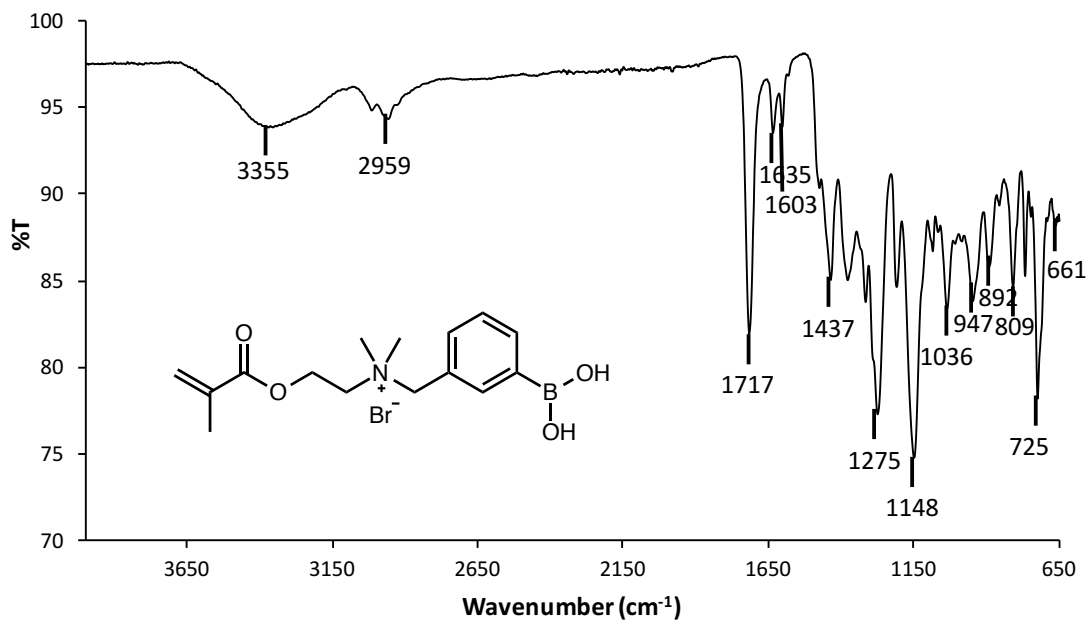


**Figure C9.** IR spectrum for *m*-BA. FT-IR: 3355 (B-OH), 2959 (C=C-H), 1717 (C=O), 1635 (C=C), 1603 (C=C) and 1437 (C=C) cm<sup>-1</sup>.

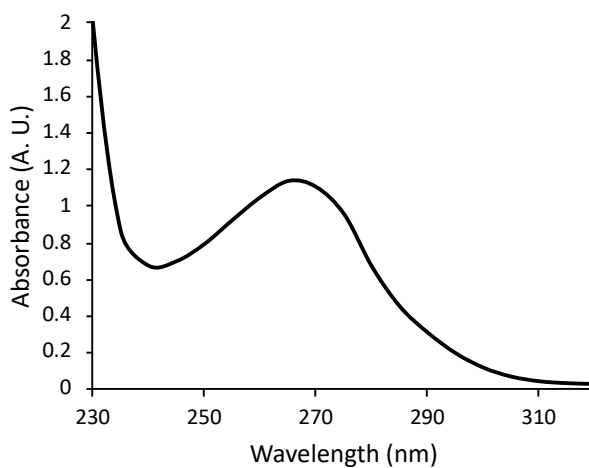


**Figure C10.** UV-visible spectrum for *m*-BA (1 mM), where the main absorbance peak is at 265 nm at pH 7.4.

### C.1.3 Spectroscopic characterisations for *p*-BA

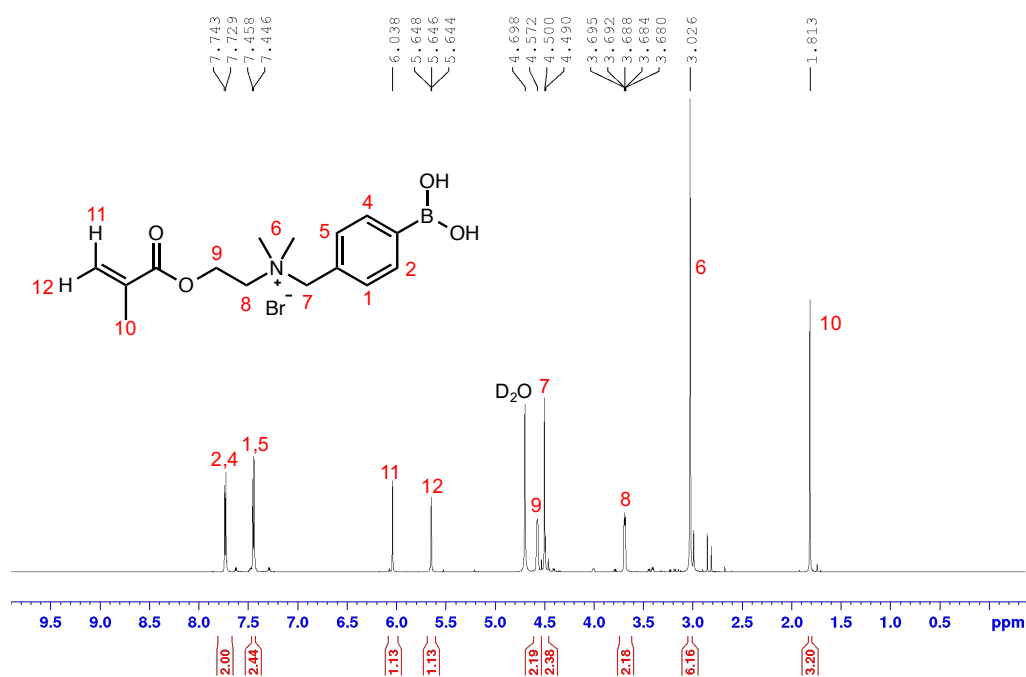


**Figure C11.** <sup>1</sup>H NMR for *p*-BA in D<sub>2</sub>O. <sup>1</sup>H NMR (600 MHz, 20 °C, D<sub>2</sub>O), δ: 7.7 (2H, *d*, *J* = 8 Hz, CH-2,3), 7.4 (2H, *d*, *J* = 8 Hz, CH-1,4), 6.0 (1H, *s*, CH-10), 5.6 (1H, *t*, *J* = 1 and 2 Hz, CH-11), 4.5 (2H, *s*, CH<sub>2</sub>-8), 4.5 (2H, *d*, *J* = 5 Hz, CH<sub>2</sub>-5), 3.6 (2H, *m*, CH<sub>2</sub>-7), 3.0 (6H, *s*, CH<sub>3</sub>-6), 1.81 (3H, *s*, CH<sub>3</sub>-9) ppm.

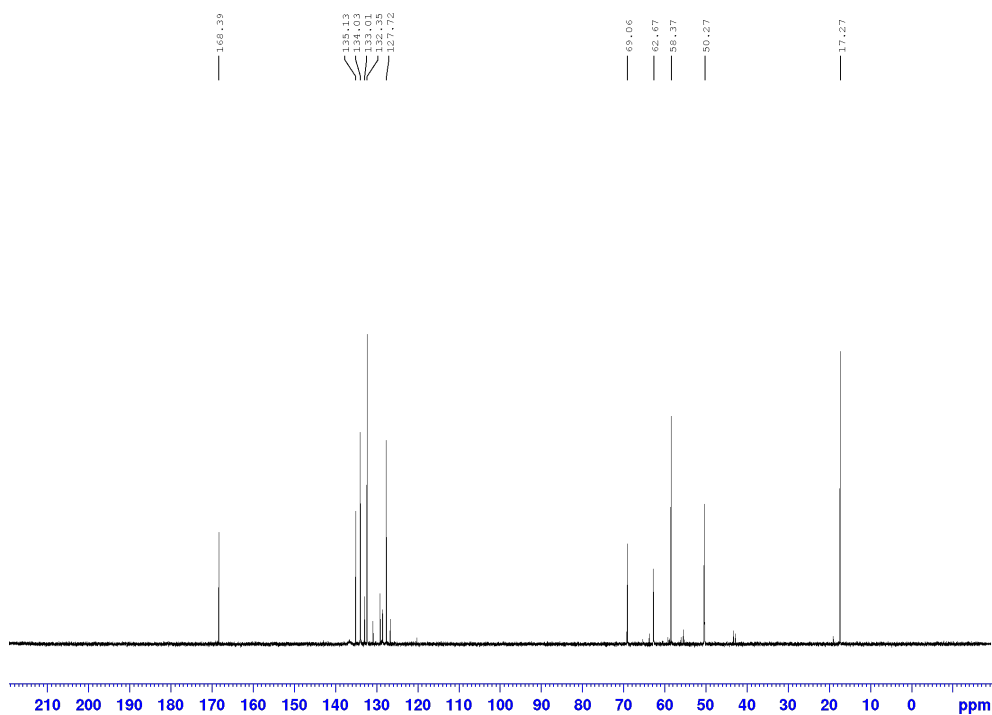


**Figure C12.** <sup>13</sup>C NMR for *p*-BA in D<sub>2</sub>O. <sup>13</sup>C NMR (150 MHz, 20 °C, D<sub>2</sub>O), δ: 168.3 (C=O), 135.1 and 134.0 (C-H<sub>2</sub>,4), 133.0 and 132.3 (C-H<sub>1</sub>,5), 127.7 (CH<sub>2</sub>-Vinyl), 69.0 (CH<sub>2</sub>, H<sub>7</sub>), 62.6 (CH<sub>2</sub>, H<sub>8</sub>), 58.3 (CH<sub>2</sub>, H<sub>9</sub>), 50.2 (CH<sub>3</sub>-Amine), 17.2 (CH<sub>3</sub>-Vinyl) ppm.



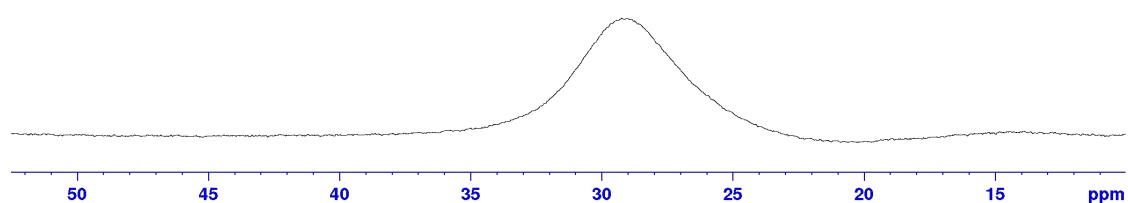


**Figure C14.**  $^{11}\text{B}$  NMR for *p*-BA in  $\text{D}_2\text{O}$ .  $^{11}\text{B}$  NMR (192 MHz, 20 °C,  $\text{D}_2\text{O}$ ),  $\delta$ : 29.2 (1B,  $\text{B}(\text{OH})_2$ ) ppm. (Line broadening by 10 Hz).

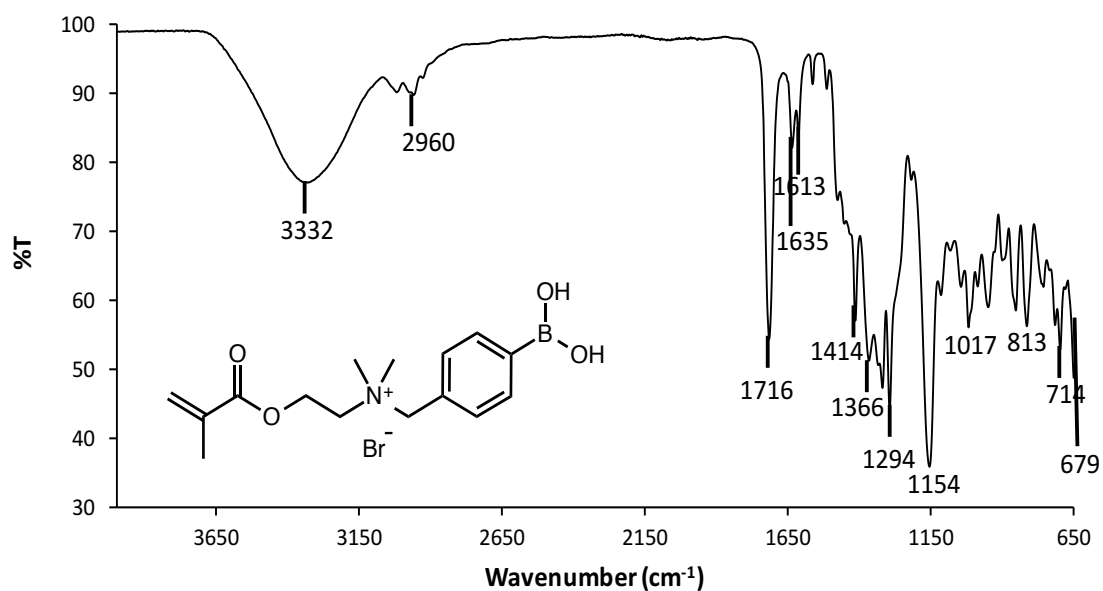


**Figure C15.** IR spectrum for *p*-BA. FT-IR: 3332 (B-OH), 2960 (C=C-H), 1716 (C=O), 1613 (C=C), 1635 (C=C) and 1414 (C=C)  $\text{cm}^{-1}$ .

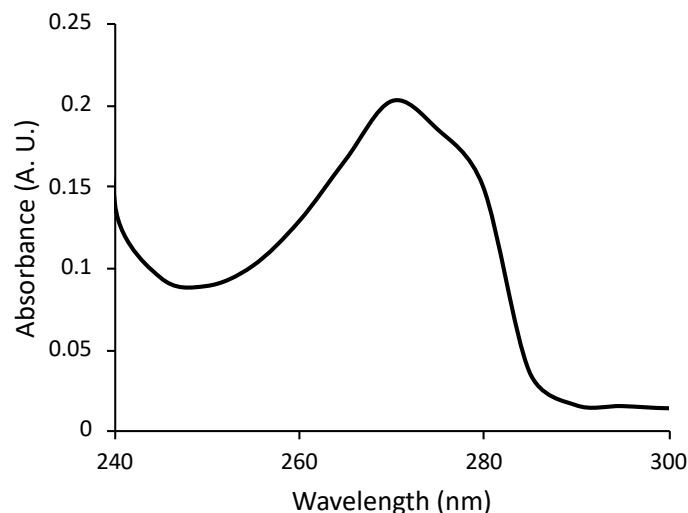


**Figure C16.** UV-visible spectrum for *p*-BA (0.2 mM), where the main absorbance peak is at 270 nm in H<sub>2</sub>O.

## C.2 Fluorescence pH and Glucose Titrations

### C.2.1 Fluorescence pH Titrations

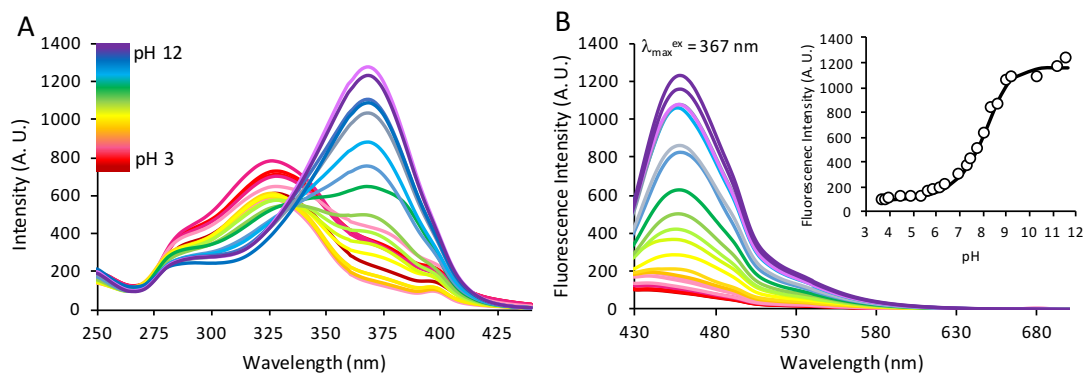


**Figure C17.** Excitation and fluorescence emission spectra for *o*-BA (1 mM) in H<sub>2</sub>O titrated with acetic acid and sodium hydroxide. The excitation wavelengths were at 327 nm and 367 nm (A) and the emission peak was at 460 nm (B). The pK<sub>a</sub> for *o*-BA was determined to be 8.6, showing experimental emission values at 460 nm as a function of pH and fit to sigmoid model (Inset B). Parameters used for these fluorescence measurements; 400 V sensitivity, 5 nm bandwidth, 1 nm data interval, 1 second response time, 500 nm/min scan/speed.

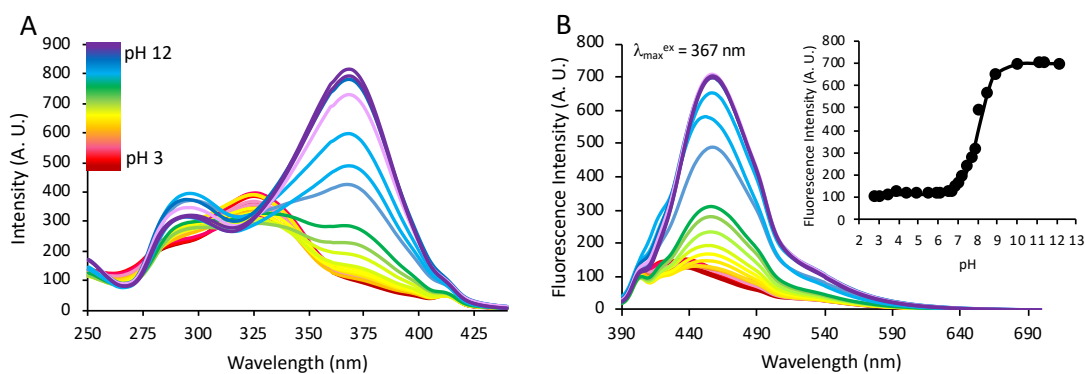


**Figure C18.** Excitation and fluorescence emission spectra for *o*-BA (1 mM) in H<sub>2</sub>O with glucose (10 mM) titrated with acetic acid and sodium hydroxide. The excitation wavelengths were at 327 nm and 367 nm (A) and the emission peak was at 460 nm (B). The  $pK_a$  for *o*-BA was determined to be 8.1, showing experimental emission values at 460 nm as a function of pH and fit to sigmoid model (Inset B). Parameters used for these fluorescence measurements; 400 V sensitivity, 5 nm bandwidth, 1 nm data interval, 1 second response time, 500 nm/min scan/speed.

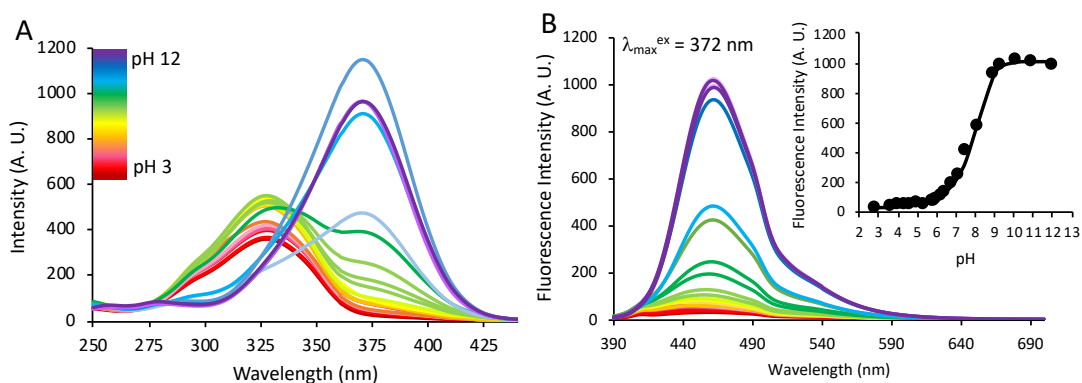


**Figure C19.** Excitation and fluorescence emission spectra for *m*-BA (1 mM) in H<sub>2</sub>O with glucose (10 mM) titrated with acetic acid and sodium hydroxide. The excitation wavelengths were at 329 nm and 372 nm (A) and the emission peak was at 466 nm (B). The  $pK_a$  for *m*-BA was determined to be 8.5, showing experimental emission values at 466 nm as a function of pH and fit to sigmoid model (Inset B). Parameters used for these fluorescence measurements; 300 V sensitivity, 5 nm bandwidth, 1 nm data interval, 1 second response time, 500 nm/min scan/speed.

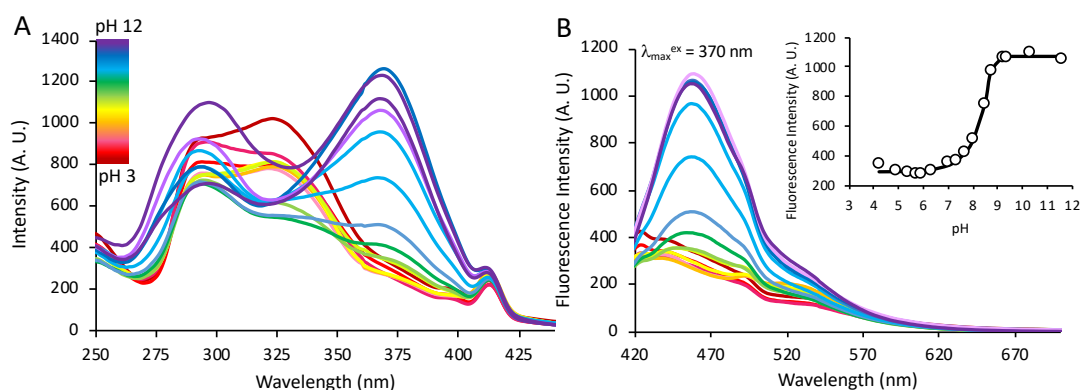


**Figure C20.** Excitation and fluorescence emission spectra for *p*-BA (1 mM) in H<sub>2</sub>O titrated with acetic acid and sodium hydroxide. The excitation wavelengths were at 325 nm and 370 nm (A) and the emission peak was at 460 nm (B). The pK<sub>a</sub> for *p*-BA was determined to be 8.8, showing experimental emission values at 460 nm as a function of pH and fit to sigmoid model (Inset B). Parameters used for these fluorescence measurements; 500 V sensitivity, 5 nm bandwidth, 1 nm data interval, 1 second response time, 500 nm/min scan/speed.

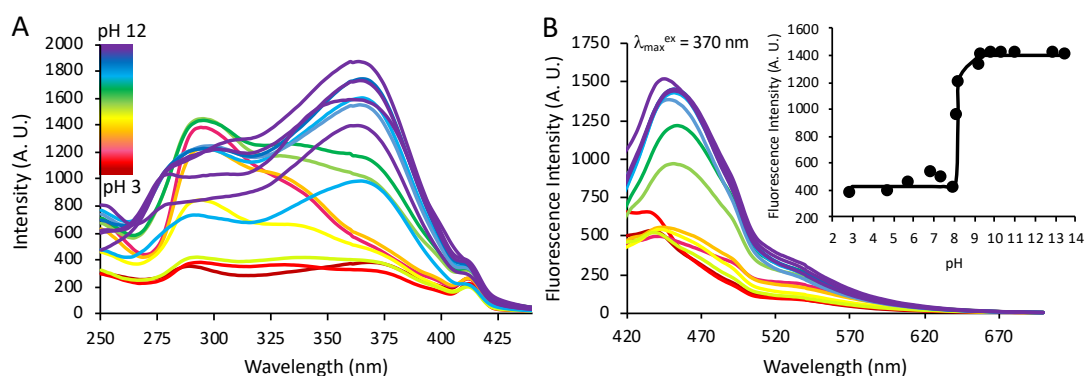


**Figure C21.** Excitation and fluorescence emission spectra for *p*-BA (1 mM) in H<sub>2</sub>O with glucose (10 mM) titrated with acetic acid and sodium hydroxide. The excitation wavelengths were at 325 nm and 370 nm (A) and the emission peak was at 460 nm (B). The pK<sub>a</sub> for *p*-BA was determined to be 8.0, showing experimental emission values at 460 nm as a function of pH and fit to sigmoid model (Inset B). Parameters used for these fluorescence measurements; 500 V sensitivity, 5 nm bandwidth, 1 nm data interval, 1 second response time, 500 nm/min scan/speed.

## C.2.2 Fluorescence Glucose Titrations

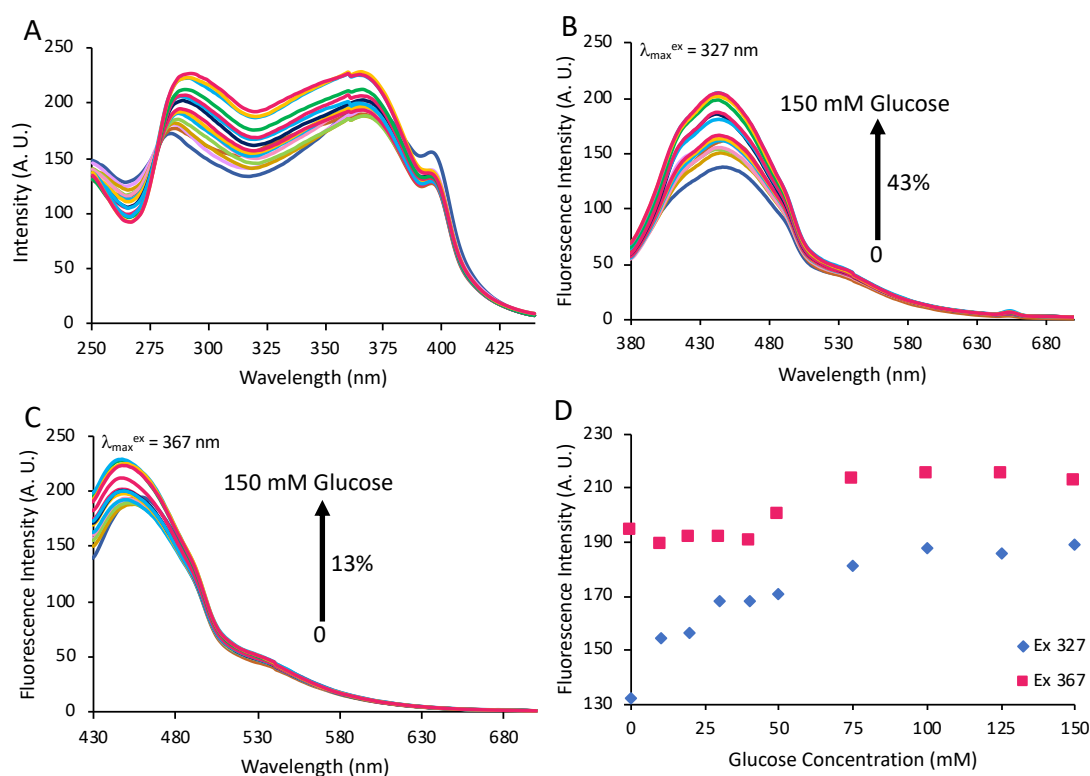


**Figure C22.** Excitation and fluorescence emission spectra for *o*-BA (1 mM) at pH 8 titrated with glucose (0-150 mM). (A) The excitation wavelengths for *o*-BA were at 327 nm and 367 nm. (B) The emission of *o*-BA at 460 nm when excited at 327 nm, where the fluorescence increases by 43% with 150 mM glucose. (C) The emission of *o*-BA at 460 nm when excited at 367 nm, where the fluorescence increases by 13% with 150 mM glucose. (D) Experimental emission values at 460 nm as a function of pH and fit to sigmoid model for *o*-BA at  $\lambda_{\max}^{\text{ex}} = 327 \text{ nm}$  (blue diamond) and 367 nm (pink square) showing the fluorescence increase with 150 mM glucose. Parameters used for these fluorescence measurements; 400 V sensitivity, 5 nm bandwidth, 1 nm data interval, 1 second response time, 500 nm/min scan/speed.

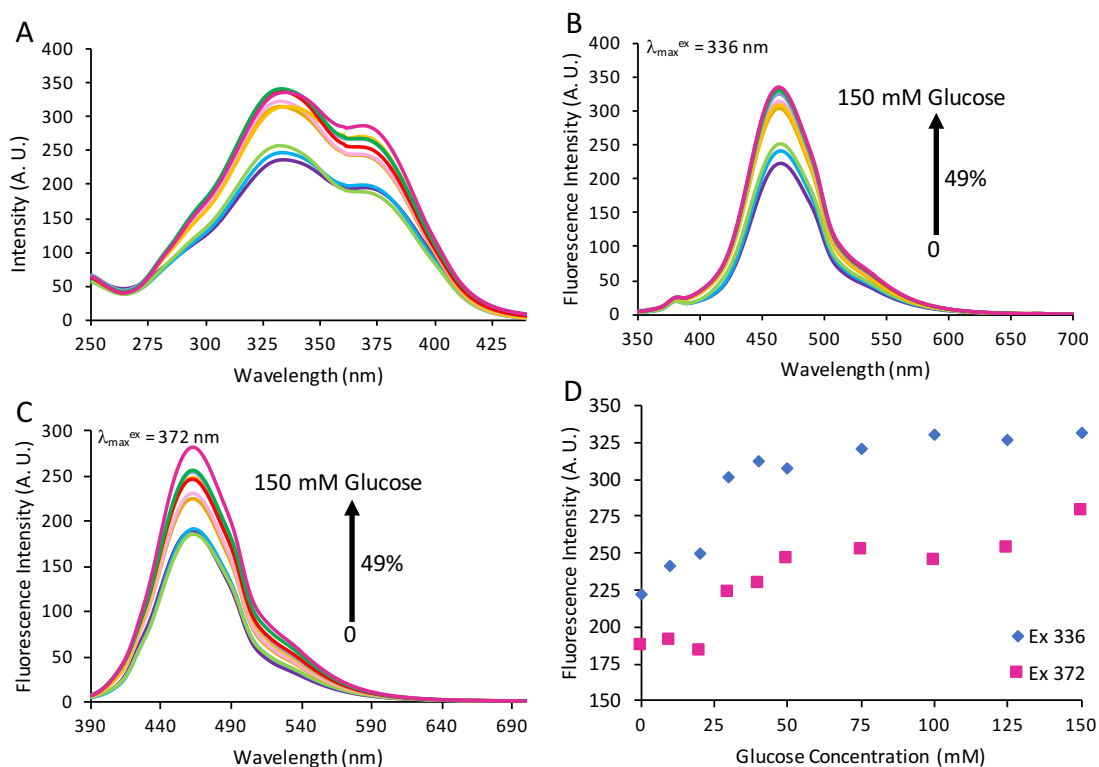


**Figure C23.** Excitation and fluorescence emission spectra for *m*-BA (1 mM) at pH 7.5 titrated with glucose (0-150 mM). (A) The excitation wavelengths for *m*-BA were at 336 nm and 372 nm. (B) The emission of *m*-BA at 466 nm when excited at 336 nm, where the fluorescence increases by 49% with 150 mM glucose. (C) The emission of *m*-BA at 460 nm when excited at 372 nm, where the fluorescence increases by 49% with 150 mM glucose. (D) Experimental emission values at 466 nm as a function of pH and fit to sigmoid model for *m*-BA at  $\lambda_{\text{max}}^{\text{ex}} = 336 \text{ nm}$  (blue diamond) and 372 nm (pink square) showing the fluorescence increase with 150 mM glucose. Parameters used for these fluorescence measurements; 300 V sensitivity, 5 nm bandwidth, 1 nm data interval, 1 second response time, 500 nm/min scan/speed.

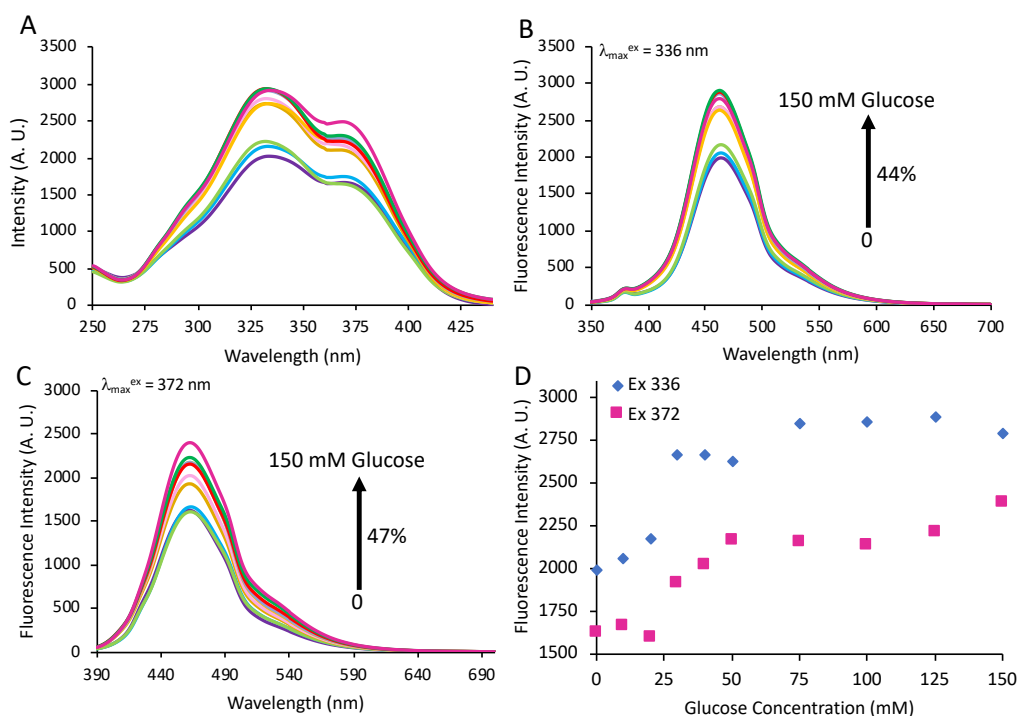


**Figure C24.** Excitation and fluorescence emission spectra for *m*-BA (1 mM) at pH 7.5 titrated with glucose (0-150 mM). (A) The excitation spectra for *m*-BA were at 336 nm and 372 nm. (B) The emission of *m*-BA at 466 nm when excited at 336 nm, where the fluorescence increases by 44% with 150 mM glucose. (C) The emission of *m*-BA at 466 nm when excited at 372 nm, where the fluorescence increases by 47% with 150 mM glucose. (D) Experimental emission values at 466 nm as a function of pH and fit to sigmoid model *m*-BA at  $\lambda_{\max}^{\text{ex}} = 336$  nm (blue diamond) and 372 nm (pink square) showing the fluorescence increase with 150 mM glucose. Parameters used for these fluorescence measurements; 400 V sensitivity, 5 nm bandwidth, 1 nm data interval, 1 second response time, 500 nm/min scan/speed.

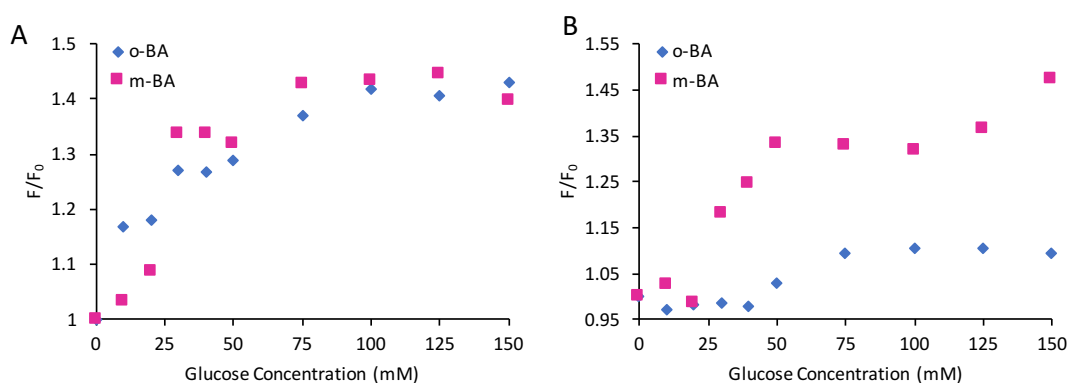


**Figure C25.** Fluorescence emission spectra for glucose titrations with *o*-BA and *m*-BA close to the  $\text{pK}_a$  for each BA, pH 8 and pH 7.5, respectively. (A) The emission when  $\lambda_{\max}^{\text{ex}} = 327$  nm and 336 nm for *o*-BA and *m*-BA, respectively. (B) The emission when  $\lambda_{\max}^{\text{ex}} = 367$  nm and 372 nm for *o*-BA and *m*-BA, respectively.  $F_0$  is the measured fluorescence intensity of the BA derivatives in the absence of glucose and  $F$  is the measured fluorescence intensity in the presence of glucose. Parameters used for these fluorescence measurements; 400 V sensitivity, 5 nm bandwidth, 1 nm data interval, 1 second response time, 500 nm/min scan/speed.

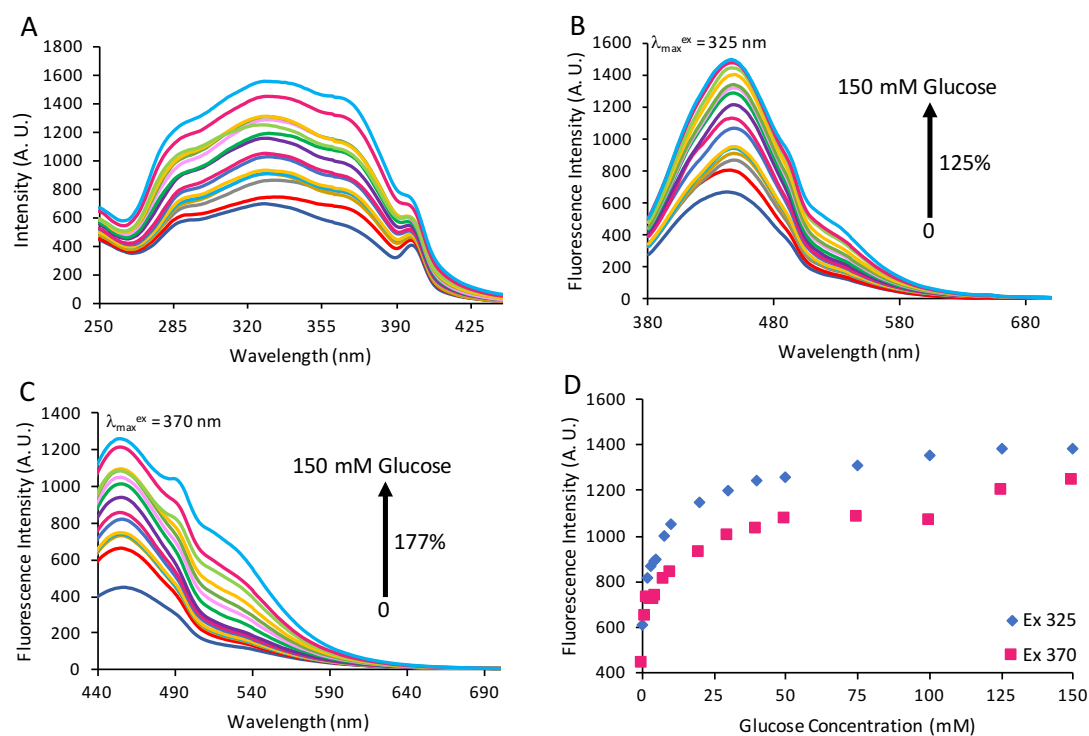


**Figure C26.** Excitation and fluorescence emission spectra for *p*-BA (1 mM) at pH 8 titrated with glucose (0-150 mM). (A) The excitation wavelengths for *p*-BA were at 325 nm and 370 nm. (B) The emission of *p*-BA at 460 nm when excited at 325 nm, where the fluorescence increases by 125% with 150 mM glucose. (C) The emission of *p*-BA at 460 nm when excited at 370 nm, where the fluorescence increases by 177% with 150 mM glucose. (D) Experimental emission values at 460 nm as a function of pH and fit to sigmoid model for *p*-BA at  $\lambda_{\text{max}}^{\text{ex}} = 325$  nm (blue diamond) and 370 nm (pink square) showing the fluorescence increase with 150 mM glucose. Parameters used for these fluorescence measurements; 500 V sensitivity, 5 nm bandwidth, 1 nm data interval, 1 second response time, 500 nm/min scan/speed.



---

## Appendix D

---

Supporting Information for Chapter 5

### **A Two-Component Fluorescent System for Sugar-Sensing\***

*Danielle Bruen, Colm Delaney, Dermot Diamond and Larisa Florea*

*Insight Centre for Data Analytics, National Centre for Sensor Research (NCSR),  
School of Chemical Sciences, Dublin City University, Dublin 9, Ireland*

\*This chapter has been submitted as “A Two-Component Fluorescent System for Sugar-Sensing”, Danielle Bruen, Colm Delaney, Dermot Diamond and Larisa Florea, *J. Am. Chem. Soc.*, **2018**.

## D.1 Materials and Methods

### D.1.1 Materials

2-(Bromomethylphenyl)boronic acid (100%), 3-(bromomethyl-phenyl)boronic acid (95%) and 4-(bromomethylphenyl)boronic acid (95%) were acquired from Fluorochem, UK and used as received. 2-(Dimethylamino)ethyl methacrylate (98%), 8-hydroxypyrene-1,3,6-trisulfonic acid trisodium salt (pyranine; >97%), acrylamide (>99%), N,N'-methylenebis(acrylamide) (MBIS; 99%), 2-hydroxy-2-methylpropiophenone (HMPP; 97%), D-(+)-glucose (>99.5%), D-(-)-fructose (>99%), D-(+)-galactose (>98%), anhydrous acetonitrile (CH<sub>3</sub>CN; 99.8%), anhydrous dichloromethane (CH<sub>2</sub>Cl<sub>2</sub>; >99.8%) and deuterium oxide (D<sub>2</sub>O; 99.9%, atom D) were purchased from Sigma Aldrich, Ireland and used as received. Structural <sup>1</sup>H, <sup>13</sup>C and <sup>11</sup>B NMR studies were carried out on a Bruker Avance Ultrashield 600 MHz spectrometer. D<sub>2</sub>O was the solvent used for all NMR measurements. The fluorescence of the BA monomers was recorded using a JASCO FP-8300 spectrofluorometer at 20 °C and UV-visible absorbance measurements were carried out on a Varian Cary 50 Probe spectrophotometer, in a precision cell made from Quartz Suprasil that had a path length of 10 mm and a volume of 1.4 mL. All pH measurements were carried out using a VWR sympHony SP70P pH meter. Deionised water (18.2 MΩ.cm<sup>-1</sup>) (DI H<sub>2</sub>O) was purified using a Milli-Q Water Purification System (Merck Millipore, Darmstadt, Germany).

### D.1.2 Synthesis of Fluorescent Acrylamide-BA Hydrogels

**Table D1.** Recipe for Fluorescent Acrylamide-oBA Hydrogels

Materials	Mass (g)	Volume (μL)	Density (ρ)	M <sub>r</sub>	mmol	Molar %
Acrylamide	1.0	-	-	71.08	14.0	100
MBIS	0.021	-	-	154.16	0.14	1
Pyranine	-	250	-	524.37	0.0002	0.001
oBA	-	37.5	-	372.06	0.003	0.02
HMPP	0.023	0.02	1.077	164.20	0.14	1

\* The final concentration of pyranine in the cocktail solution was 0.1 mM and the final concentration of o-BA was 1.5 mM (15 eq.).

**Table D2.** Recipe for Fluorescent Acrylamide-mBA Hydrogels

Materials	Mass (g)	Volume ( $\mu\text{L}$ )	Density ( $\rho$ )	$M_r$	mmol	Molar%
Acrylamide	1.0	-	-	71.08	14.0	100
MBIS	0.0216	-	-	154.169	0.14	1
Pyranine	-	250	-	524.371	0.0002	0.001
mBA	-	20	-	372.066	0.002	0.01
HMPP	0.023	0.02	1.077	164.204	0.14	1

\* The final concentration of pyranine in the cocktail solution was 0.1 mM and the final concentration of m-BA was 1 mM (10 eq.).

The hydrogels were prepared by adding the reagents as described in Table S1 and Table S2 and dissolving in 2 mL DI H<sub>2</sub>O. The hydrogel cocktail was sonicated and vortexed until all components of the mixture dissolved. Once dissolved, the hydrogel cocktail was pipetted in to a homemade cell composed of a glass slide (bottom) and a layer of poly(methyl methacrylate) (top) with a pressure-sensitive adhesive spacer (120  $\mu\text{m}$ ) between them, to polymerise the cocktail mixture as a thin film. The films were polymerised inside a CL-1000 Ultraviolet Crosslinker UVP chamber at 254 nm for 30 minutes. Once polymerised the films were cut using 13 mm cutters, to produce thin film circular hydrogels. The hydrogels were placed in pH 7.4 buffer solution after cutting. It was noted that the hydrogels swelled slightly in the buffer solution from 13 mm to ~15 mm. Once the initial fluorescence of each gel was measured, the gels were placed in various solutions of different glucose concentrations ranging between 0-100 mM. After at least 10 hours in the glucose solutions, the fluorescence of each gel was measured.

## D.2 Fluorescence

### D.2.1 Fluorescence Quenching Titrations in Solution

Fluorescence quenching titrations were carried out by monitoring the fluorescence of pyranine (4  $\mu\text{M}$ ) in pH 7.4 buffer solution (2 mL), with increasing concentrations of the BA monomers. Additions of each BA monomer were made using automated pipettes. Each BA stock solution was dissolved in DI H<sub>2</sub>O. Following each addition of BA monomer, the fluorescence was measured in a quartz Suprasil 1.4 mL cuvette with a path length of 10 mm, on a JASCO FP3800 Spectrophotometer. Excitation and emission spectra were recorded from the characteristic wavelengths of pyranine, where the excitation wavelengths were 374 nm, 404 nm and 454 nm, and the emission wavelength was 515 nm. A fluorescence curve was plotted by taking the maximum intensity of the fluorescence emission, when excited at 404 nm. The parameters used for fluorescence measurements were as follows; 280 V sensitivity, 5 nm bandwidth, 1 nm data interval, 1 second response time and 500 nm/min scan speed, unless otherwise stated.

From the fluorescence quenching curves, the static and dynamic quenching constants for *o*-BA and *m*-BA were determined by Equation D1, for their ability to quenching the fluorescence of pyranine, where  $F_0$  is the initial fluorescence of pyranine,  $F$  is the measured fluorescence after the addition of BA monomer,  $V$  is the dynamic quenching constant and  $K_s$  is the slope coefficient correlating to the static quenching constant.

Equation D1 for fluorescence quenching:

$$F_0/F = (1 + K_s[Q])e^{V[Q]} \quad (1)$$

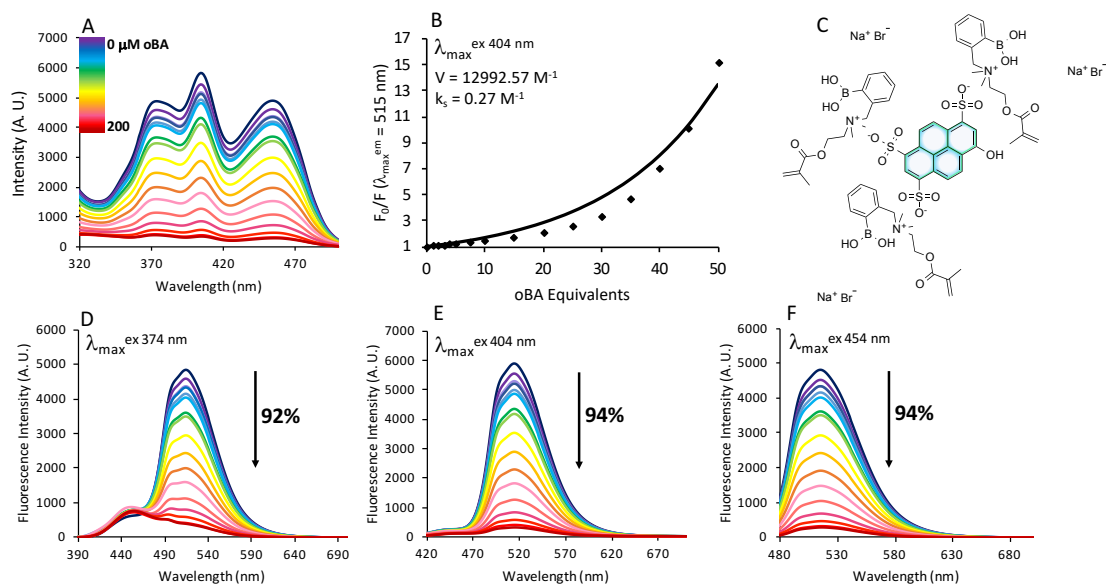


**Figure D1.** (A) Excitation spectrum for pyranine (4  $\mu\text{M}$ ) titrated with *o*-BA (0-0.2 mM) in pH 7.4 phosphate buffer corresponding to the emission wavelength 515 nm. (B) Fluorescence emission quenching curve, corresponding to the excitation wavelength at 404 nm, showing dynamic ( $V$ ) and static ( $K_s$ ) quenching constants, where  $F_0$  is the initial fluorescence of pyranine and  $F$  is the measure fluorescence of pyranine after the addition of *o*-BA. (C) Structural schematic diagram of the quenching interaction between pyranine and *o*-BA in solution. (D) Fluorescence emission spectrum of pyranine with increased concentrations of *o*-BA, corresponding to the excitation wavelength at 374 nm. (E) Fluorescence emission spectrum of pyranine with increased concentrations of *o*-BA, corresponding to the excitation wavelength at 404 nm. (F) Fluorescence emission spectrum of pyranine with increased concentrations of *o*-BA, corresponding to the excitation wavelength at 454 nm.

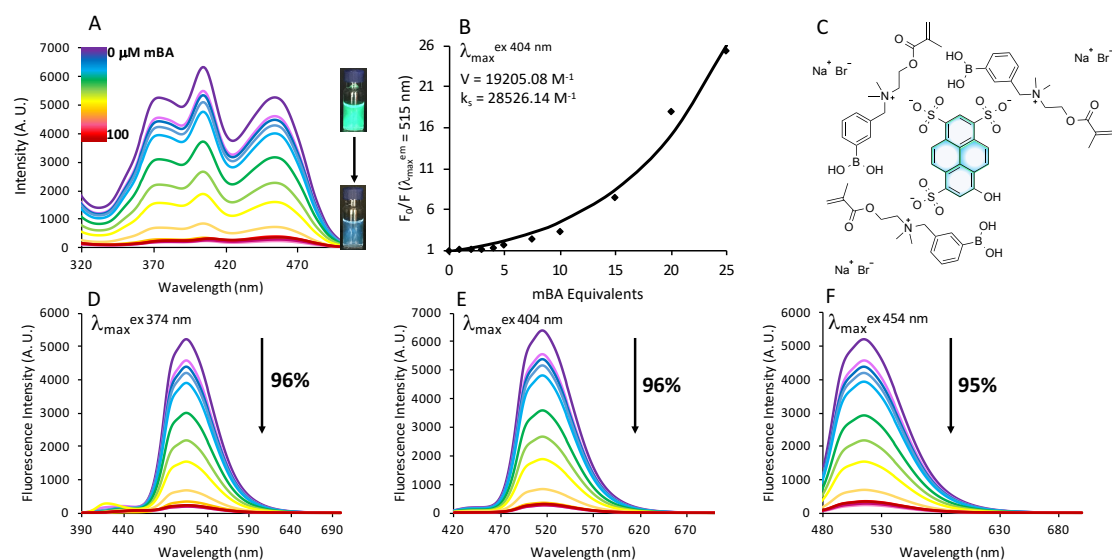


**Figure D2.** (A) Excitation spectrum for pyranine (4  $\mu\text{M}$ ) titrated with *m*-BA (0-0.1 mM) in pH 7.4 phosphate buffer corresponding to the emission wavelength 515 nm. (B) Fluorescence emission quenching curve, corresponding to the excitation wavelength at 404 nm, showing dynamic ( $V$ ) and static ( $K_s$ ) quenching constants, where  $F_0$  is the initial fluorescence of pyranine and  $F$  is the measure fluorescence of pyranine after the addition of *m*-BA. (C) Structural schematic diagram of the quenching interaction between pyranine and *m*-BA in solution. (D) Fluorescence emission spectrum of pyranine with increased concentrations of *m*-BA, corresponding to the excitation wavelength at 374 nm. (E) Fluorescence emission spectrum of pyranine with increased concentrations of *m*-BA, corresponding to the excitation wavelength at 404 nm. (F) Fluorescence emission spectrum of pyranine with increased concentrations of *m*-BA, corresponding to the excitation wavelength at 454 nm.

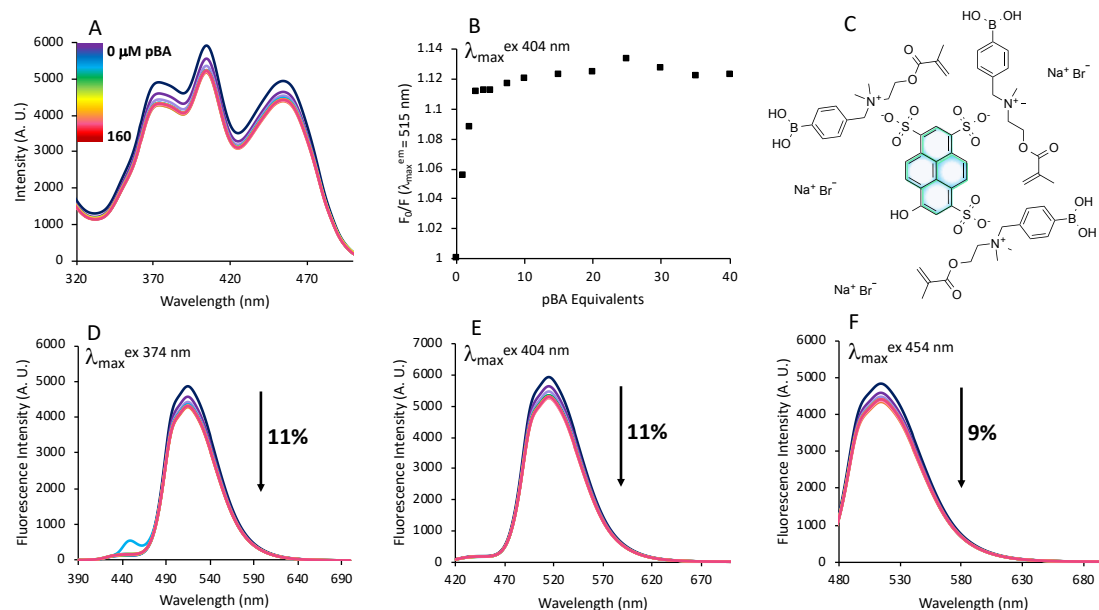


**Figure D3.** (A) Excitation spectrum for pyranine (4 μM) titrated with *p*-BA (0-0.08 mM) in pH 7.4 phosphate buffer corresponding to the emission wavelength 515 nm. (B) Fluorescence emission quenching curve, corresponding to the excitation wavelength at 404 nm, where  $F_0$  is the initial fluorescence of pyranine and  $F$  is the measure fluorescence of pyranine after the addition of *p*-BA. (C) Structural schematic diagram of the quenching interaction between pyranine and *p*-BA in solution. (D) Fluorescence emission spectrum of pyranine with increased concentrations of *p*-BA, corresponding to the excitation wavelength at 374 nm. (E) Fluorescence emission spectrum of pyranine with increased concentrations of *p*-BA, corresponding to the excitation wavelength at 404 nm. (F) Fluorescence emission spectrum of pyranine with increased concentrations of *p*-BA, corresponding to the excitation wavelength at 454 nm.

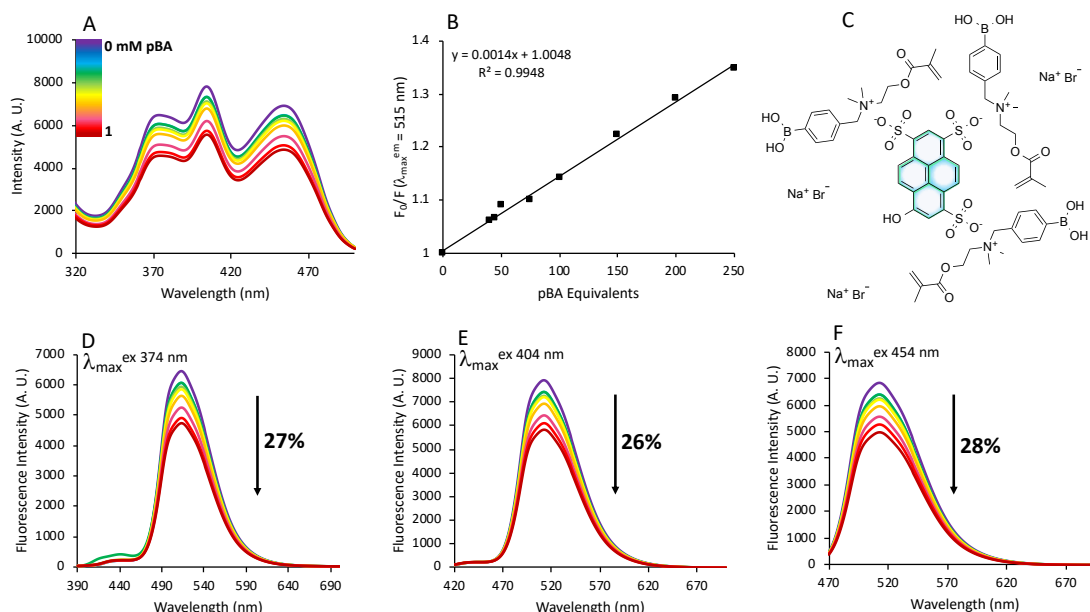


**Figure D4.** (A) Excitation spectrum for pyranine (4  $\mu$ M) titrated with *p*-BA (0-1 mM) in pH 7.4 phosphate buffer corresponding to the emission wavelength 515 nm. (B) Fluorescence emission quenching curve, corresponding to the excitation wavelength at 404 nm, where  $F_0$  is the initial fluorescence of pyranine and  $F$  is the measure fluorescence of pyranine after the addition of *p*-BA. (C) Structural schematic diagram of the quenching interaction between pyranine and *p*-BA in solution. (D) Fluorescence emission spectrum of pyranine with increased concentrations of *p*-BA, corresponding to the excitation wavelength at 374 nm. (E) Fluorescence emission spectrum of pyranine with increased concentrations of *p*-BA, corresponding to the excitation wavelength at 404 nm. (F) Fluorescence emission spectrum of pyranine with increased concentrations of *p*-BA, corresponding to the excitation wavelength at 454 nm.

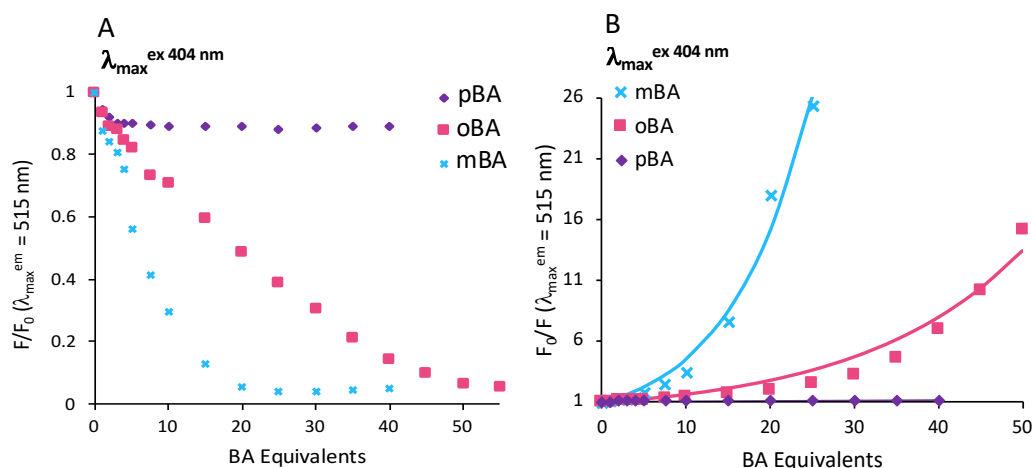


**Figure D5.** Fluorescence quenching trends for all BAs with pyranine (4  $\mu$ M). (A) shows decreasing fluorescence intensity trends, where the fluorescence of pyranine with *o*-BA (0-0.22 mM) decreased by 94%, with *m*-BA (0-0.16 mM) decreased by 96% and with *p*-BA (0-0.16 mM) decreased by 10%. (B) Shows the same curve with fluorescence-fold quenching of pyranine with *o*-BA (0-0.2 mM) showing a decrease by 16-fold, with *m*-BA a decrease by 26-fold and with *p*-BA a decrease by 0.1-fold in pH 7.4 buffer solution.



### D.2.2 Fluorescence Recovery Titrations in Solution

Fluorescence recovery titrations were carried out by monitoring the fluorescence of pyranine (4  $\mu\text{M}$ ) in pH 7.4 buffer solution (2 mL), with increasing concentrations of monosaccharides, glucose, fructose or galactose. Additions of each sugar were made using automated pipettes. Each sugar stock solution was dissolved in pH 7.4 buffer. Following each addition of saccharide, the fluorescence was measured in a quartz Suprasil 1.4 mL cuvette with a path length of 10 mm, on a JASCO FP3800 Spectrophotometer. Excitation and emission spectra were recorded from the characteristic wavelengths of pyranine, where the excitation wavelengths were 374 nm, 404 nm and 454 nm, and the emission wavelength was 515 nm. A fluorescence curve was plotted by taking the maximum intensity of the fluorescence emission, when excited at all wavelengths. The parameters used for fluorescence measurements were as follows; 280 V sensitivity, 5 nm bandwidth, 1 nm data interval, 1 second response time and 500 nm/min scan speed, unless otherwise stated.

From the fluorescence recovery curves, the apparent binding constants for each saccharide were also determined via fluorescence titrations with glucose, fructose and galactose and calculated using Equation 2, where  $a$  is the concentration of the sugar (M) and  $K_b$  is the apparent binding constant. The data was analysed with a non-linear least squares method using Solver from Microsoft Excel 2016.

Equation 2 for fluorescence recovery:

$$F/F_0 = a(1 - e^{-(K_b)(F/F_{0_{\max}})}) + F/F_{0_{\min}} \quad (2)$$

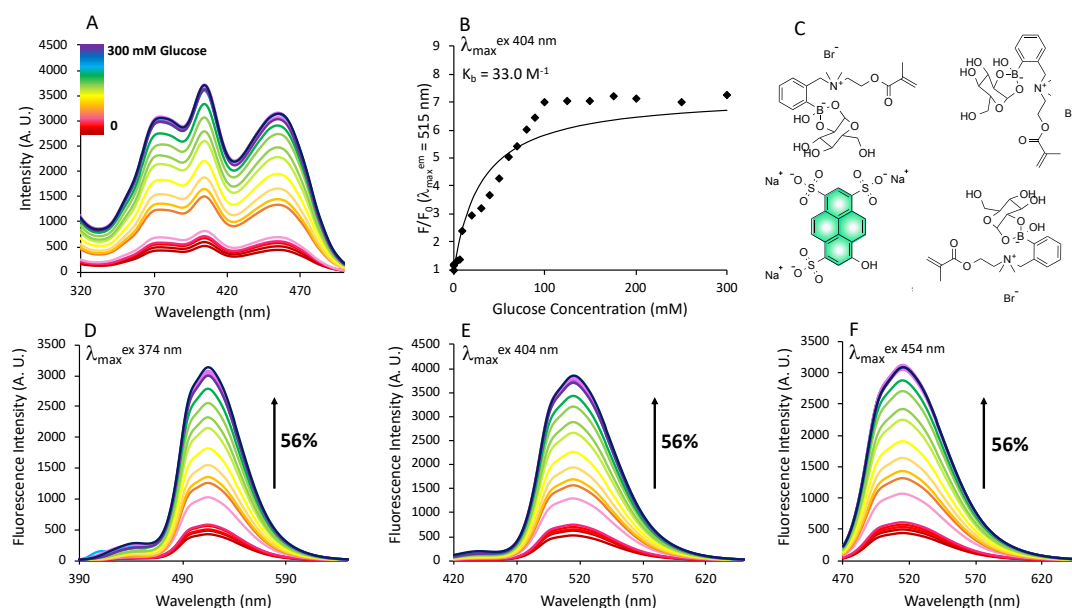


**Figure D6** (A) Excitation spectrum for pyranine (4  $\mu$ M) and *o*-BA (0.2 mM) titrated with glucose (0-300 mM), where the corresponding emission wavelength was 515 nm. (B) Fluorescence emission curve corresponding the excitation wavelength of 404 nm, for pyranine:*o*-BA (1:50) with increased glucose concentrations (0-300 mM), showing the apparent binding constant ( $K_b$ ) as 33.0  $\text{M}^{-1}$ .  $F_0$  is the initial fluorescence of pyranine:*o*-BA (1:50) and  $F$  is the measured fluorescence after each glucose addition. (C) A schematic diagram illustrating dissociation of the ground-state complex formed between pyranine and *o*-BA to recover the fluorescence on glucose addition. (D) The emission spectrum for pyranine:*o*-BA (1:50) with increasing glucose concentrations corresponding to the excitation wavelength of 374 nm. (E) The emission spectrum for pyranine:*o*-BA (1:50) with increasing glucose concentrations corresponding to the excitation wavelength of 404 nm. (F) The emission spectrum for pyranine:*o*-BA (1:50) with increasing glucose concentrations corresponding to the excitation wavelength of 454 nm.

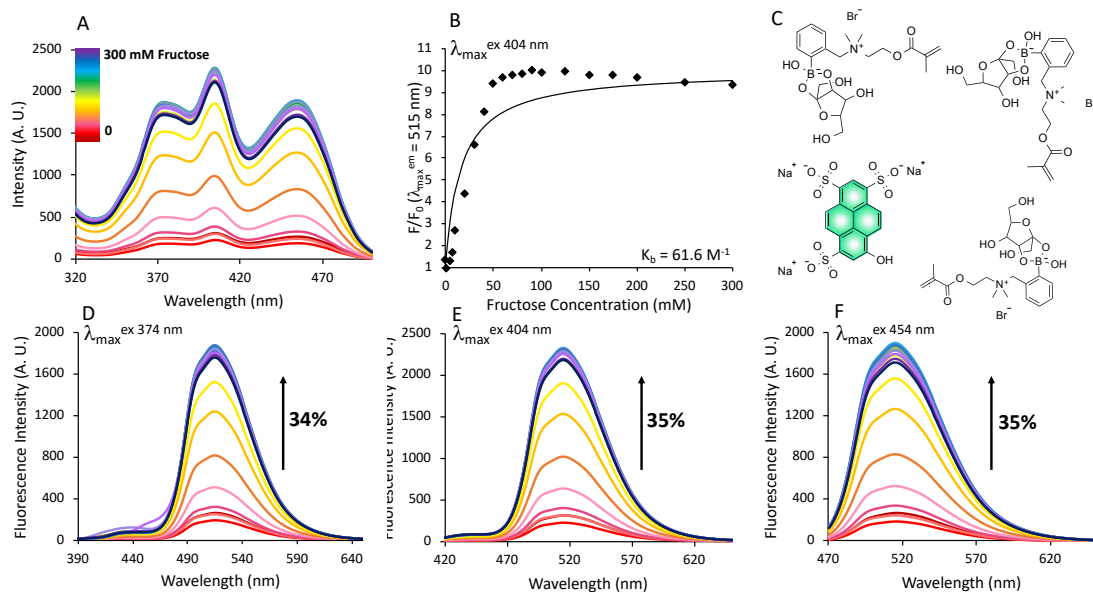


**Figure D7.** (A) Excitation spectrum for pyranine (4 μM) and *o*-BA (0.2 mM) titrated with fructose (0-300 mM), where the corresponding emission wavelength was 515 nm. (B) Fluorescence emission curve corresponding the excitation wavelength of 404 nm, for pyranine:*o*-BA (1:50) with increased fructose concentrations (0-300 mM), showing the apparent binding constant ( $K_b$ ) as  $61.6 \text{ M}^{-1}$ .  $F_0$  is the initial fluorescence of pyranine:*o*-BA (1:50) and  $F$  is the measured fluorescence after each fructose addition. (C) A schematic diagram illustrating dissociation of the ground-state complex formed between pyranine and *o*-BA to recover the fluorescence on fructose addition. (D) The emission spectrum for pyranine:*o*-BA (1:50) with increasing fructose concentrations corresponding to the excitation wavelength of 374 nm. (E) The emission spectrum for pyranine:*o*-BA (1:50) with increasing fructose concentrations corresponding to the excitation wavelength of 404 nm. (F) The emission spectrum for pyranine:*o*-BA (1:50) with increasing fructose concentrations corresponding to the excitation wavelength of 454 nm.

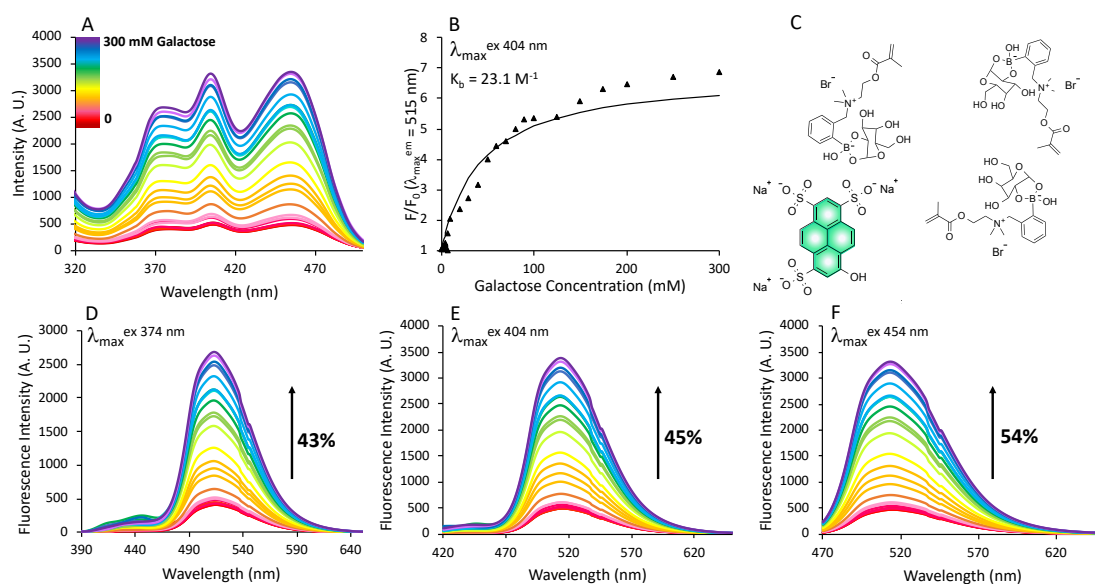


**Figure D8.** (A) Excitation spectrum for pyranine (4 μM) and *o*-BA (0.2 mM) titrated with galactose (0-300 mM), where the corresponding emission wavelength was 515 nm. (B) Fluorescence emission curve corresponding the excitation wavelength of 404 nm, for pyranine:*o*-BA (1:50) with increased galactose concentrations (0-300 mM), showing the apparent binding constant ( $K_b$ ) as  $23.1 \text{ M}^{-1}$ .  $F_0$  is the initial fluorescence of pyranine:*o*-BA (1:50) and  $F$  is the measured fluorescence after each galactose addition. (C) A schematic diagram illustrating dissociation of the ground-state complex formed between pyranine and *o*-BA to recover the fluorescence on galactose addition. (D) The emission spectrum for pyranine:*o*-BA (1:50) with increasing galactose concentrations corresponding to the excitation wavelength of 374 nm. (E) The emission spectrum for pyranine:*o*-BA (1:50) with increasing galactose concentrations corresponding to the excitation wavelength of 404 nm. (F) The emission spectrum for pyranine:*o*-BA (1:50) with increasing galactose concentrations corresponding to the excitation wavelength of 454 nm.

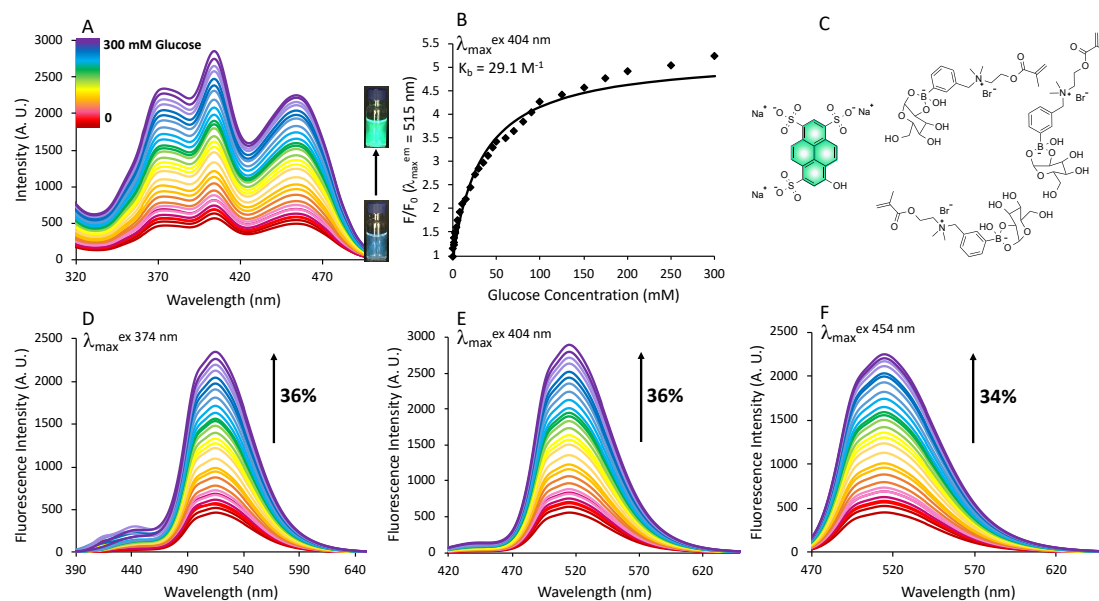


**Figure D9.** (A) Excitation spectrum for pyranine (4  $\mu\text{M}$ ) and *m*-BA (0.08 mM) titrated with glucose (0-300 mM), where the corresponding emission wavelength was 515 nm. (B) Fluorescence emission curve corresponding the excitation wavelength of 404 nm, for pyranine:*m*-BA (1:20) with increased glucose concentrations (0-300 mM), showing the apparent binding constant ( $K_b$ ) as 29.1  $\text{M}^{-1}$ .  $F_0$  is the initial fluorescence of pyranine:*m*-BA (1:20) and  $F$  is the measured fluorescence after each glucose addition. (C) A schematic diagram illustrating dissociation of the ground-state complex formed between pyranine and *m*-BA to recover the fluorescence on glucose addition. (D) The emission spectrum for pyranine:*m*-BA (1:20) with increasing glucose concentrations corresponding to the excitation wavelength of 374 nm. (E) The emission spectrum for pyranine:*m*-BA (1:20) with increasing glucose concentrations corresponding to the excitation wavelength of 404 nm. (F) The emission spectrum for pyranine:*m*-BA (1:20) with increasing glucose concentrations corresponding to the excitation wavelength of 454 nm.

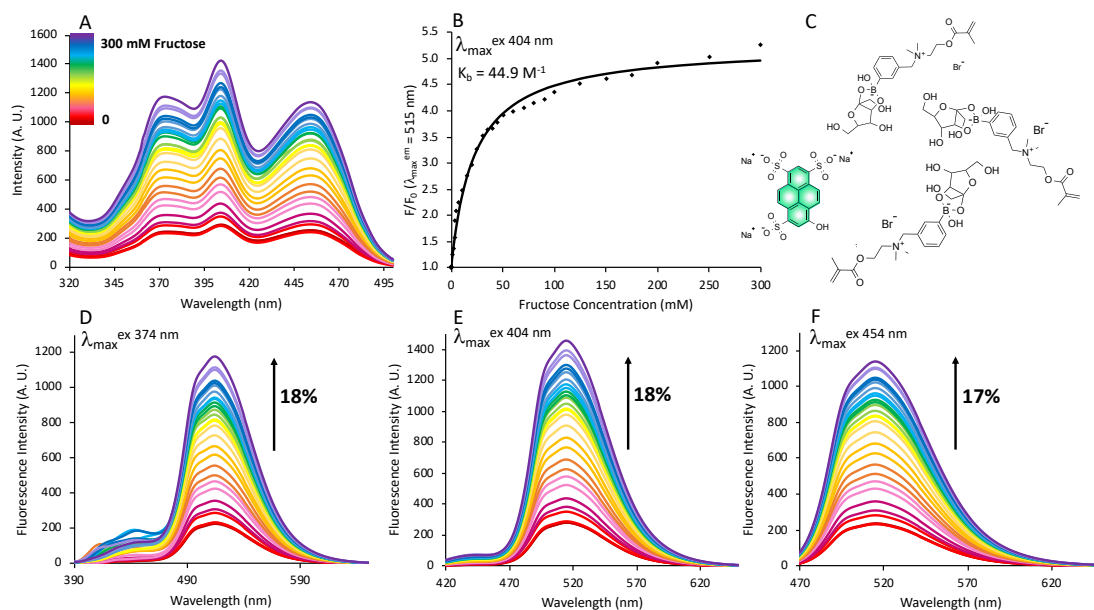


**Figure D10.** (A) Excitation spectrum for pyranine (4  $\mu\text{M}$ ) and *m*-BA (0.08 mM) titrated with fructose (0-300 mM), where the corresponding emission wavelength was 515 nm. (B) Fluorescence emission curve corresponding the excitation wavelength of 404 nm, for pyranine:*m*-BA (1:20) with increased fructose concentrations (0-300 mM), showing the apparent binding constant ( $K_b$ ) as 44.9  $\text{M}^{-1}$ .  $F_0$  is the initial fluorescence of pyranine:*m*-BA (1:20) and  $F$  is the measured fluorescence after each fructose addition. (C) A schematic diagram illustrating dissociation of the ground-state complex formed between pyranine and *m*-BA to recover the fluorescence on fructose addition. (D) The emission spectrum for pyranine:*m*-BA (1:20) with increasing fructose concentrations corresponding to the excitation wavelength of 374 nm. (E) The emission spectrum for pyranine:*m*-BA (1:20) with increasing fructose concentrations corresponding to the excitation wavelength of 404 nm. (F) The emission spectrum for pyranine:*m*-BA (1:20) with increasing fructose concentrations corresponding to the excitation wavelength of 454 nm.

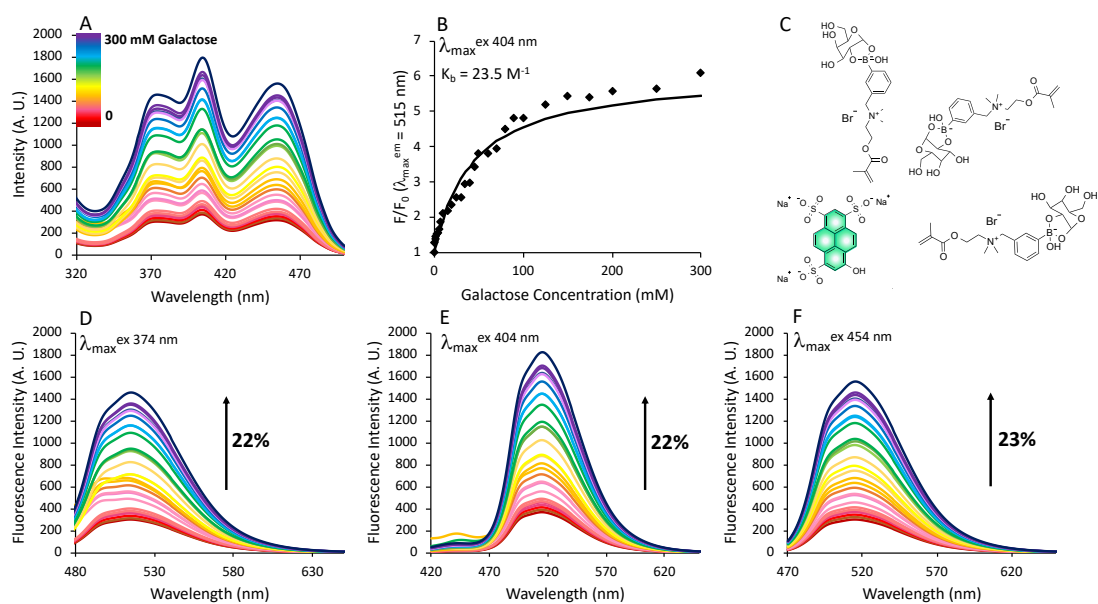


**Figure D11.** (A) Excitation spectrum for pyranine (4  $\mu\text{M}$ ) and *m*-BA (0.08 mM) titrated with galactose (0-300 mM), where the corresponding emission wavelength was 515 nm. (B) Fluorescence emission curve corresponding the excitation wavelength of 404 nm, for pyranine:*m*-BA (1:20) with increased galactose concentrations (0-300 mM), showing the apparent binding constant ( $K_b$ ) as  $23.5 \text{ M}^{-1}$ .  $F_0$  is the initial fluorescence of pyranine:*m*-BA (1:20) and  $F$  is the measured fluorescence after each galactose addition. (C) A schematic diagram illustrating dissociation of the ground-state complex formed between pyranine and *m*-BA to recover the fluorescence on galactose addition. (D) The emission spectrum for pyranine:*m*-BA (1:20) with increasing galactose concentrations corresponding to the excitation wavelength of 374 nm. (E) The emission spectrum for pyranine:*m*-BA (1:20) with increasing galactose concentrations corresponding to the excitation wavelength of 404 nm. (F) The emission spectrum for pyranine:*m*-BA (1:20) with increasing galactose concentrations corresponding to the excitation wavelength of 454 nm.

### D.2.3 Fluorescence Titrations with Hydrogel Cocktails

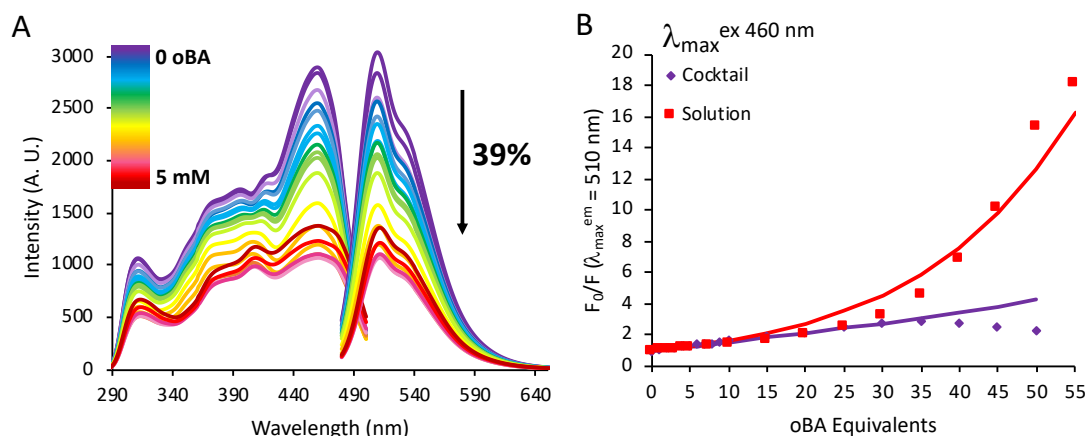


**Figure D12.** Fluorescence titration of the hydrogel cocktail, containing pyranine (0.1 mM) with *o*-BA (0-5 mM). (A) Shows the excitation spectrum correlating to the emission at 520 nm, with increasing concentrations of *o*-BA (0-5 mM). (B) Shows the decreasing fluorescence emission for pyranine in the hydrogel cocktail, corresponding to the excitation wavelength at 460 nm, with increasing concentrations of *o*-BA (0-5 mM) and illustrates the fluorescence emission from the titration with the hydrogel cocktail (♦) and the titration from the solution-based studies (■) corresponding to an excitation wavelength at 460 nm. Both curves in (B) are fitted with a model using Equation 5.1.

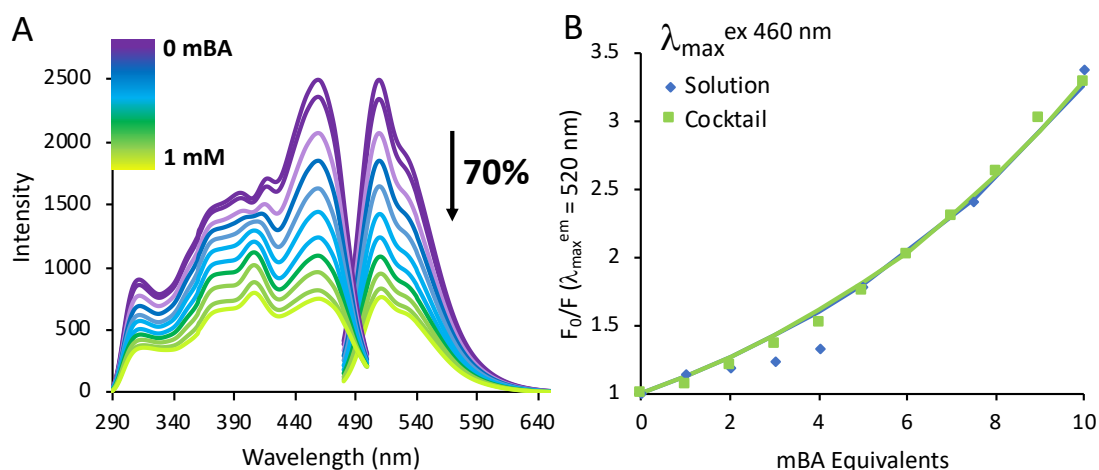


**Figure D13.** Fluorescence titration of the hydrogel cocktail, containing pyranine (0.1 mM) with *m*-BA (0-5 mM). (A) Shows the excitation spectrum correlating to the emission at 520 nm, with increasing concentrations of *m*-BA (0-5 mM). (B) Shows the decreasing fluorescence emission for pyranine in the hydrogel cocktail, corresponding to the excitation wavelength at 460 nm, with increasing concentrations of *m*-BA (0-5 mM) and illustrates the fluorescence emission from the titration with the hydrogel cocktail (■) and the titration from the solution-based studies (♦) corresponding to an excitation wavelength at 460 nm. Both curves in (B) are fitted with a model using Equation 5.1.



---

## Appendix E

---

### Supporting Information for Chapter 6

#### **Future Work: Sugar Sensing Using Boronic Acid Polymers**

**Part A – Indirect Sensing in Ionogels**, Danielle Bruen,<sup>1</sup> Colm Delaney,<sup>1</sup> Adam McColgan,<sup>1</sup> Larisa Florea,<sup>1</sup> Dermot Diamond<sup>1</sup>

**Part B – Fluorescence of Pyranine in the Presence of Acrylic Monomers**, Danielle Bruen,<sup>1</sup> Colm Delaney,<sup>1</sup> Dermot Diamond,<sup>1</sup> Larisa Florea<sup>1</sup>

**Part C – Layer-by-Layer Films Composed of BA Linear Polymers and Poly(vinyl sulfonate, sodium salt)**, Danielle Bruen,<sup>1\*</sup> Paula P. Campos,<sup>2\*</sup> Colm Delaney,<sup>1</sup> Marystela Ferreira,<sup>2</sup> Dermot Diamond,<sup>1</sup> Larisa Florea<sup>1</sup>

<sup>1</sup>*Insight Centre for Data Analytics, National Centre for Sensor Research, School of Chemical Sciences, Dublin City University.*

<sup>2</sup>*Sao Paulo State University (UNESP), Bauru School of Science, POSMAT, SP, Brazil*

\* *Authors who contributed equally to this work*

## Part A – Indirect Glucose Sensing in Ionogels

### E.1 Methods

**Nuclear Magnetic Resonance Spectroscopy (NMR)** spectra were recorded on a Bruker Avance 400 MHz or Bruker Avance Ultrashield 600 MHz NMR spectrometer. Splitting patterns are designated as *s*, singlet; *d*, doublet; *dd*, double doublet; *t*, triplet and *m*, multiplet.  $^1\text{H}$  and  $^{13}\text{C}$  NMR spectra were recorded using deuterium oxide ( $\text{D}_2\text{O}$ ) or deuterated methanol ( $d_4\text{-CH}_3\text{OH}$ ) as solvents, with corresponding reference peaks of  $^1\text{H}$ ,  $\delta$  4.87 ( $\text{D}_2\text{O}$ ), 3.31 and 3.34 ( $d_4\text{-CH}_3\text{OH}$ ) and 3.92 ( $d_6\text{-DMSO}$ ) ppm.  $^{11}\text{B}$  NMR experiments were recorded using  $\text{BF}_3$  in deuterated methanol as an external standard.

**Fluorescence Spectroscopy** measurements were carried out on a JASCO Spectrofluorometer FP-8300 at 20 °C in a precision cell made from Quartz Suprasil that had a path length thickness of 10 mm. The same cell was used for all fluorescence experiments. Samples were dissolved in either pH 7.4 phosphate buffer, methanol or a mixture of both.

**Ultraviolet-Visible (UV-Vis) Spectroscopy** was used to determine the absorbance spectra of the BA derivatives. Measurements were carried out on a Varian Cary 50 Probe spectrophotometer.

**Fourier Transform Infrared (ATR FT-IR) Spectroscopy** measurements were carried out on a Perkin Elmer Spectrum GX.

**Dynamic Light Scattering** measurements were carried out to determine the zeta potential of the BA linear polymers and were recorded on a Malvern Zetasizer Nano ZS. A specialised Malvern cell, DTS1070 folded capillary cell was purchased from Malvern Instruments, UK for these measurements. The BA linear polymers was dissolved in various buffer solutions ranging from pH 5.4 to 12.1 at a concentration of 1 mg.mL<sup>-1</sup>.

## E.2 NMR Spectroscopy

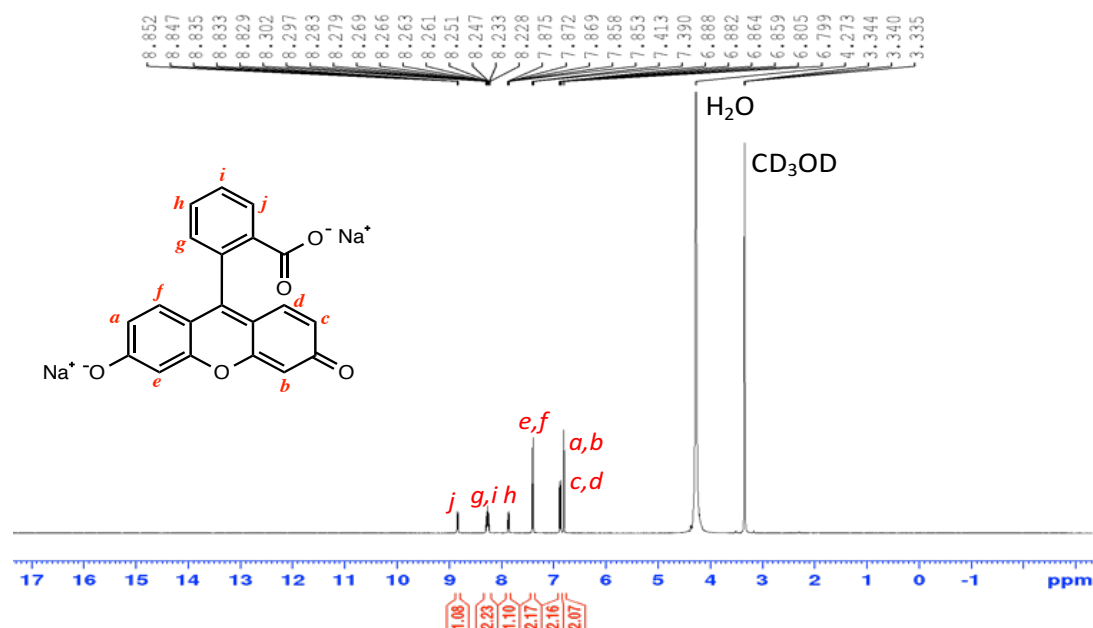


**Figure E1.**  $^1\text{H}$  NMR spectrum for Fluorescein disodium salt.  $^1\text{H}$  NMR (400 MHz, 20 °C,  $\text{CD}_3\text{OD}$ ),  $\delta$ : 8.0 (1H, *m*, CH – j), 7.4 (2H, *m*, CH – h, i), 7.0 (1H, *m*, CH – g), 6.6 (1H, *s*, CH – f), 6.5 (1H, *s*, CH – e), 6.0 (2H, *dd*,  $J = 2, 7, 9$  and 11 Hz, CH – c, d), 5.9 (2H, *d*,  $J = 2$  Hz, CH – a, b) ppm.

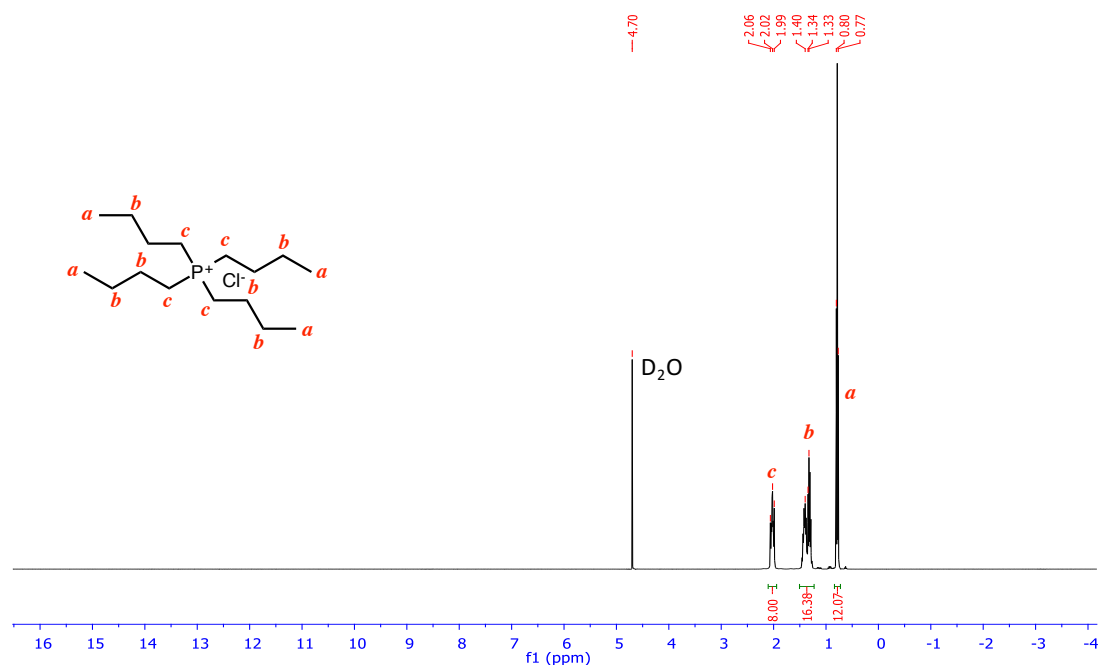


**Figure E2.**  $^1\text{H}$  NMR spectrum for tetrabutylphosphonium chloride ( $\text{P}_{4,4,4,4}\text{Cl}$ ).  $^1\text{H}$  NMR (400 MHz, 20 °C,  $\text{D}_2\text{O}$ ),  $\delta$ : 1.9-1.0 (8H, *m*,  $\text{CH}_2$  – c), 1.2-1.4 (16H, *m*,  $\text{CH}_2$  – b), 0.7 (12H, *t*,  $J = 7$  and 14 Hz,  $\text{CH}_3$  – a) ppm.

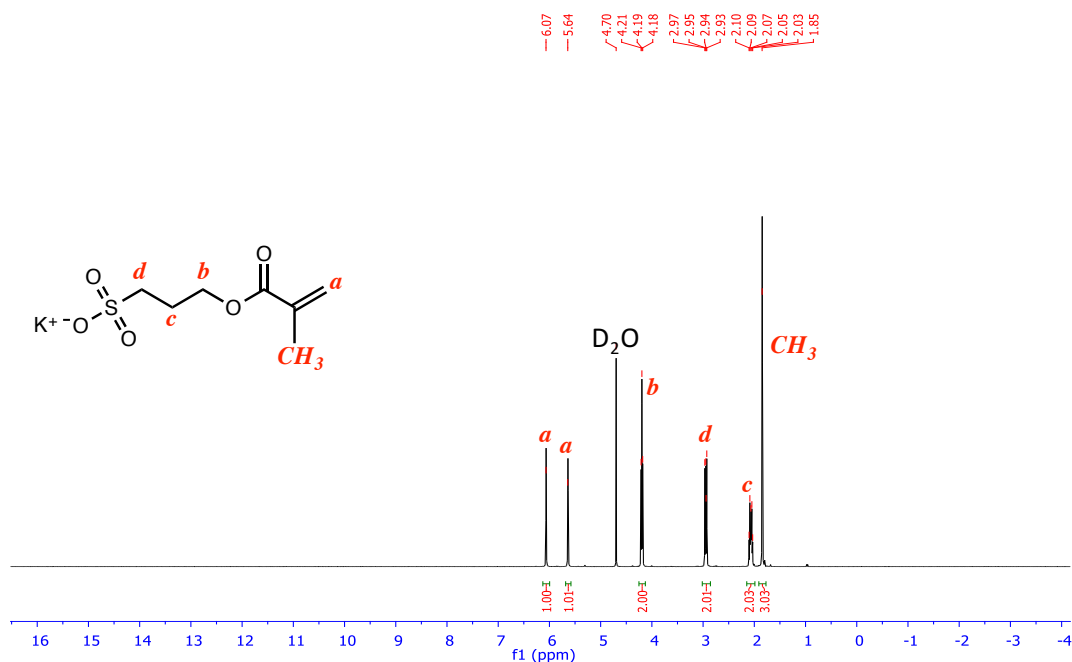


**Figure E3.** <sup>1</sup>H NMR spectrum for potassium sulfopropyl methacrylate (SPMA). <sup>1</sup>H NMR (400 MHz, 20 °C, D<sub>2</sub>O), δ: 6.0 (1H, *t*, *J* = 1 and 2 Hz, CH<sub>2</sub> – a), 5.6 (1H, *t*, *J* = 1 and 3 Hz, CH<sub>2</sub> – a), 4.1 (2H, *t*, *J* = 6 and 12 Hz, CH<sub>2</sub> – b), 2.9 (2H, *q*, *J* = 2, 4, 5, 7, 9, 10 and 15 Hz, CH<sub>2</sub> – d), 2.0 (2H, *m*, CH<sub>2</sub> – c), 1.8 (3H, *s*, CH<sub>3</sub>) ppm.

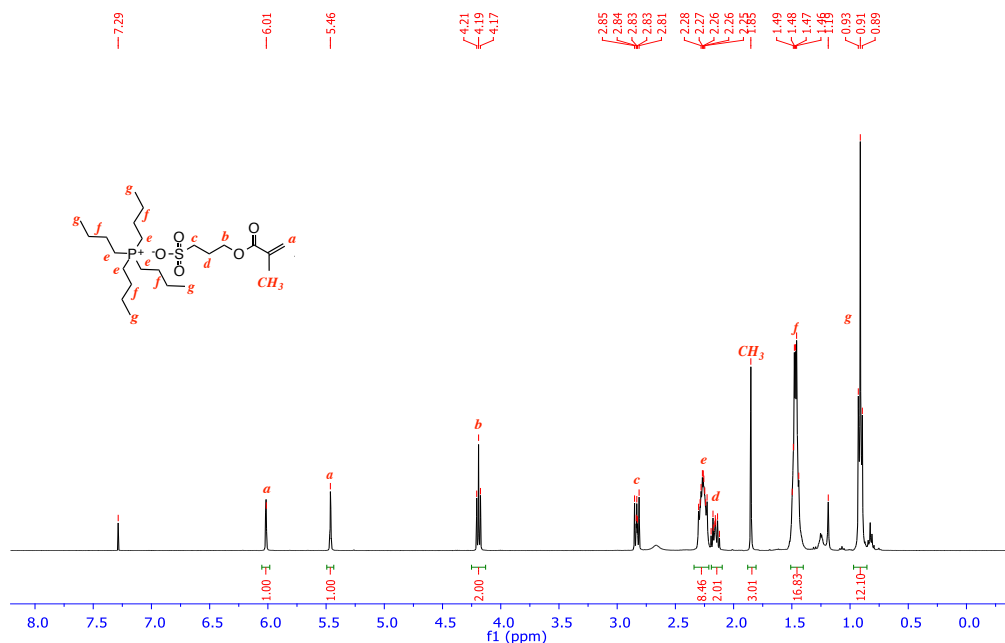


**Figure E4.** <sup>1</sup>H NMR spectrum for P<sub>4,4,4,4</sub>SPMA monomeric IL (tetrabutylphosphonium sulfopropyl methacrylate IL monomer). <sup>1</sup>H NMR (400 MHz, 20 °C), δ: 6.0 (1H, *dd*, *J* = 1, 2 and 3 Hz, CH – a), 5.4 (1H, *t*, *J* = 1 and 3 Hz, CH – a), 4.2 (2H, *t*, *J* = 6 and 12 Hz, CH<sub>2</sub> – b), 2.8 (2H, *m*, CH<sub>2</sub> – c), 2.3 (8H, *m*, CH<sub>2</sub> – e), 2.2 (2H, *m*, CH<sub>2</sub> – d), 1.8 (3H, *t*, *J* = 1 and 2 Hz, CH<sub>3</sub> – SPMA), 1.4 (16H, *t*, *J* = 4 and 8 Hz, CH<sub>2</sub> – P<sub>4,4,4,4</sub>, f), 0.9 (12H, *t*, *J* = 7 and 14 Hz, CH<sub>3</sub> – g) ppm.

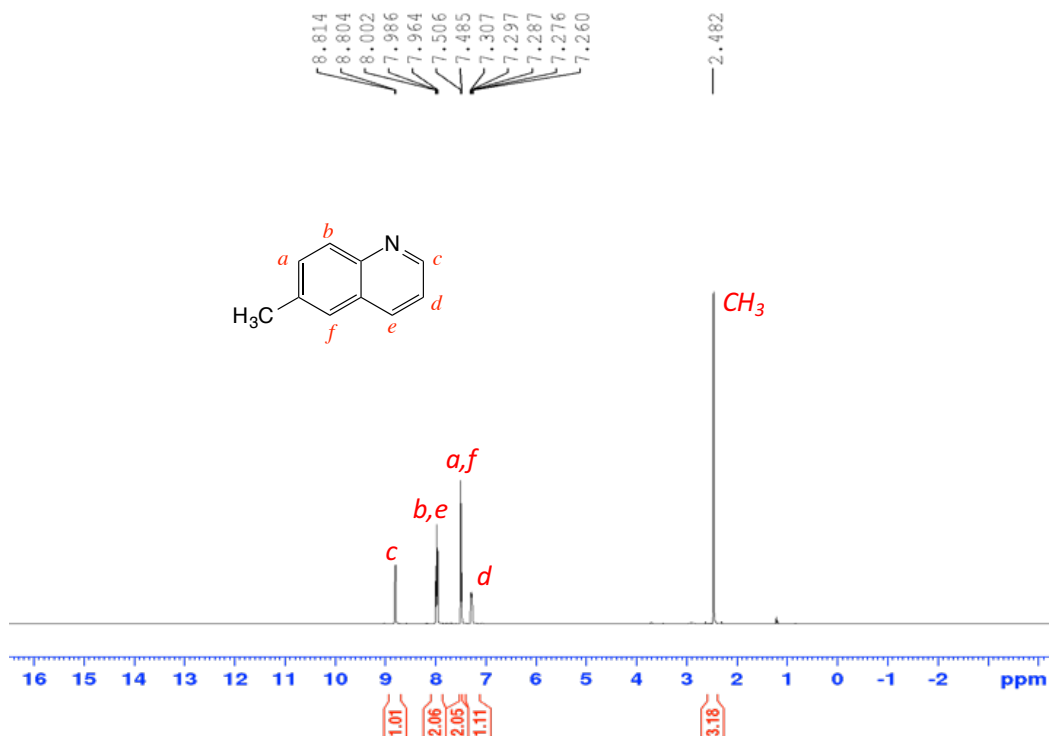


**Figure E5.**  $^1\text{H}$  NMR spectrum for 6-methylquinoline.  $^1\text{H}$  NMR (400 MHz,  $20^\circ\text{C}$ ,  $\text{CDCl}_3$ )  $\delta$ : 8.8 (1H, *d*,  $J = 4$  Hz, CH – c), 7.9 (2H, *m*, CH – b, e), 7.5 (2H, *d*,  $J = 8$  Hz, CH – a), 7.3 (1H, *q*,  $J = 4, 8$  and  $12$  Hz, CH – a), 2.5 (3H, *s*,  $\text{CH}_3$ ), ppm.

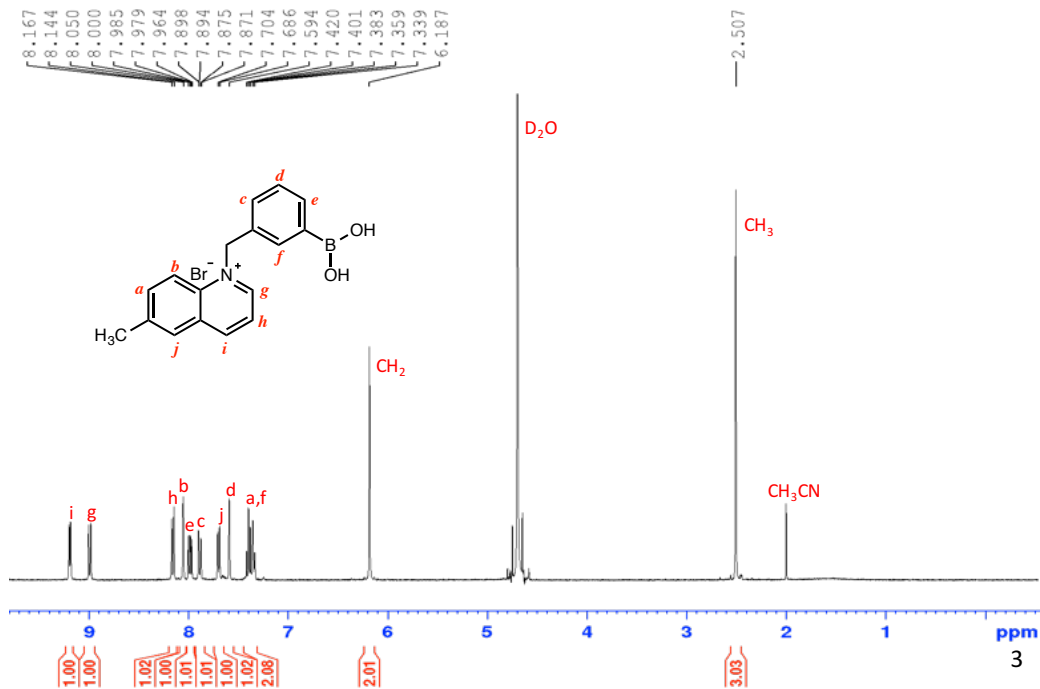


**Figure E6.**  $^1\text{H}$  NMR for 1-(3-Boronobenzyl)-6-methylquinolin-1-ium bromide (*m*-MethylBA).  $^1\text{H}$  NMR (600 MHz,  $20^\circ\text{C}$ ,  $\text{D}_2\text{O}$ )  $\delta$ : 9.2 (1H, *d*,  $J = 6$  Hz, CH – j), 9.0 (1H, *d*,  $J = 8$  Hz, CH – i), 8.1 (1H, *d*,  $J = 9$  Hz, CH – h), 8.0 (1H, *s*, CH – g), 7.9 (1H, *dd*,  $J = 2, 5, 8$  and  $14$  Hz, CH – f), 7.8 (1H, *dd*,  $J = 1, 7, 9$  and  $10$  Hz, CH – e), 7.7 (1H, *d*,  $J = 7$  Hz, CH – d), 7.6 (1H, *s*, CH – c), 7.3-7.4 (2H, *m*, CH – a, b), 6.2 (2H, *s*,  $\text{CH}_2$ ), 2.5 (3H, *s*,  $\text{CH}_3$ ) ppm.

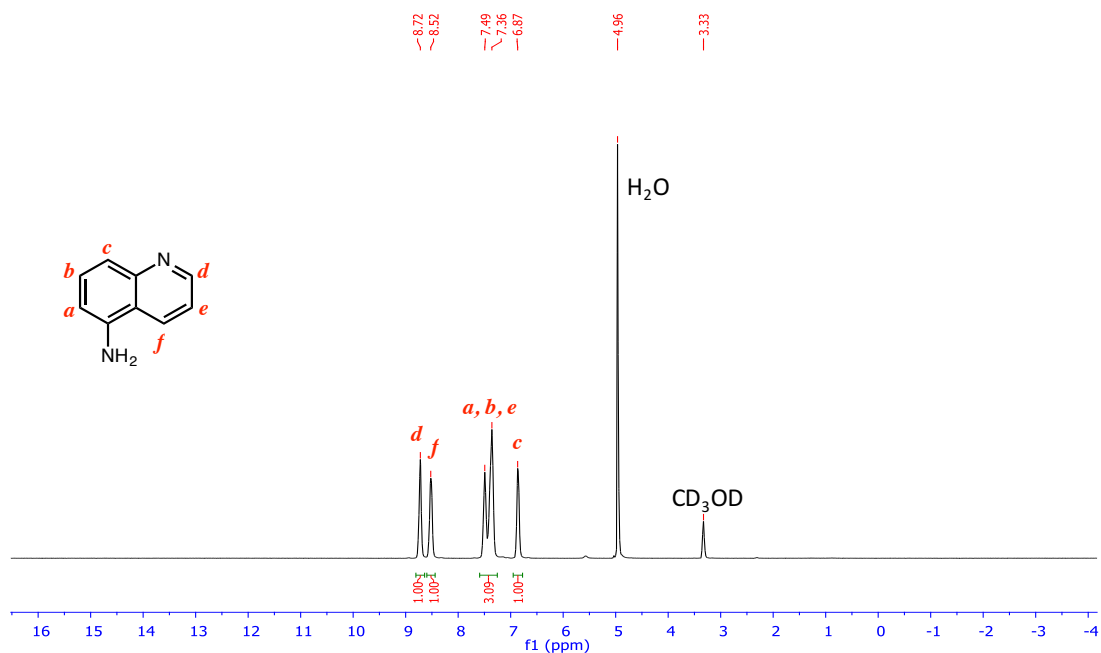


**Figure E7.** <sup>1</sup>H NMR for 5-aminoquinoline. <sup>1</sup>H NMR (400 MHz, 20 °C, CD<sub>3</sub>OD), δ: 8.7 (1H, s, CH – d), 8.5 (1H, s, CH – f), 7.4 (3H, d, J = 7 Hz, CH – a, b, e), 6.8 (1H, s, CH – c) ppm.

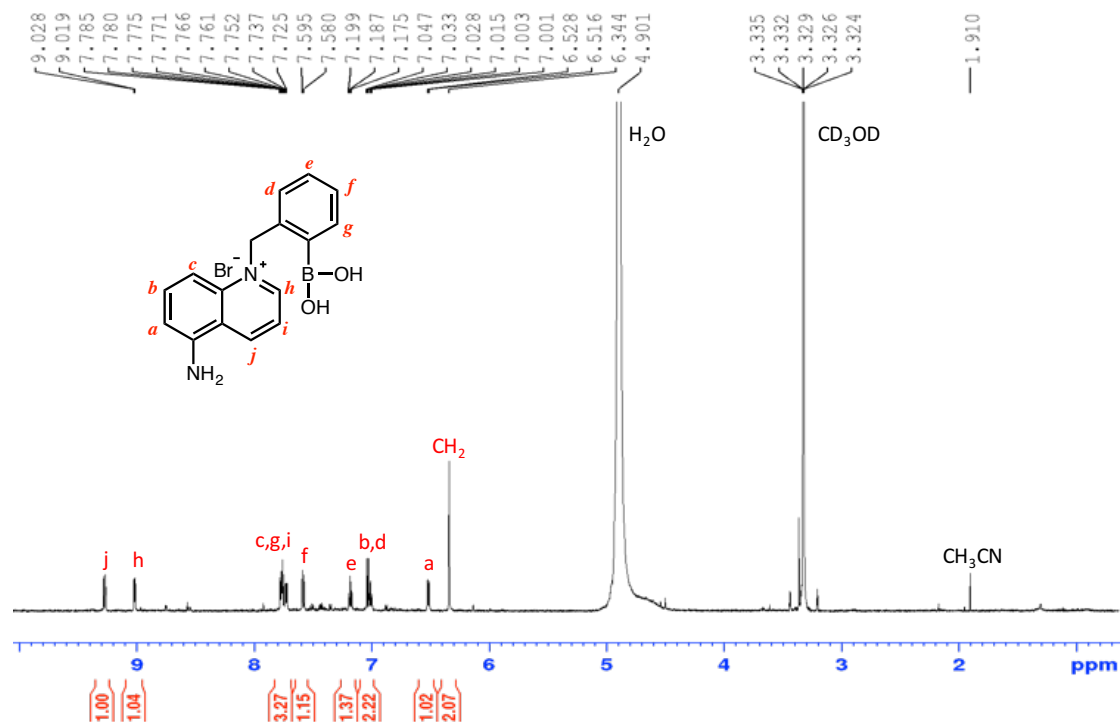


**Figure E8.** <sup>1</sup>H NMR for 5-Amino-1-(2-boronobenzyl)quinolin-1-ium bromide (*o*-AminoBA). <sup>1</sup>H NMR (600 MHz, 20 °C, CD<sub>3</sub>OD), δ: 9.2 (1H, d, J = 9 Hz, CH – j), 9.0 (1H, d, J = 5 Hz, CH – h), 7.7 (3H, m, CH – c, g, i), 7.5 (1H, d, J = 10 Hz, CH – f), 7.1 (1H, t, J = 7 and 14 Hz, CH – e), 7.0 (2H, m, CH – b, d), 6.5 (1H, d, J = 7 Hz, CH – a), 6.3 (2H, s, CH<sub>2</sub>) ppm.

### E.3 Fluorescence Spectroscopy

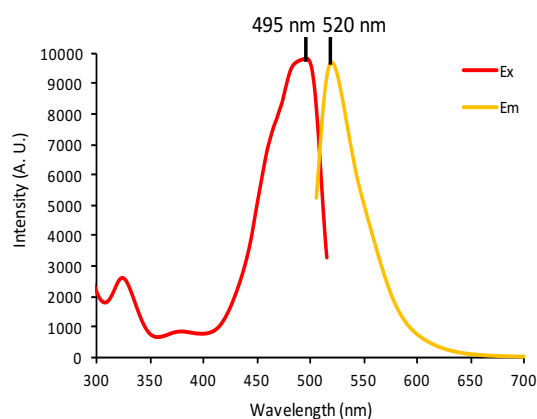


**Figure E9.** Excitation and fluorescence emission spectra for fluorescein disodium salt in pH 7.4 phosphate buffer, where the excitation wavelength was 495 nm and the corresponding emission wavelength was 520 nm. Fluorescence parameters: medium sensitivity, 2.5 nm bandwidth, 1 second response time, 1 nm data interval and 500 nm/min scan speed.

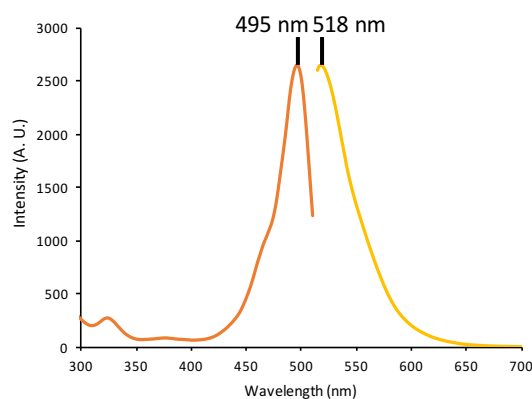


**Figure E10.** Excitation and fluorescence emission spectrum for Fluorescein IL (4  $\mu\text{M}$ ) in MeOH, where the excitation wavelength is 495 nm and the corresponding emission wavelength is 518 nm. Fluorescence parameters: high sensitivity, 2.5 nm bandwidth, 500 nm/min scan rate, data interval at 1 nm and response time 1 second.

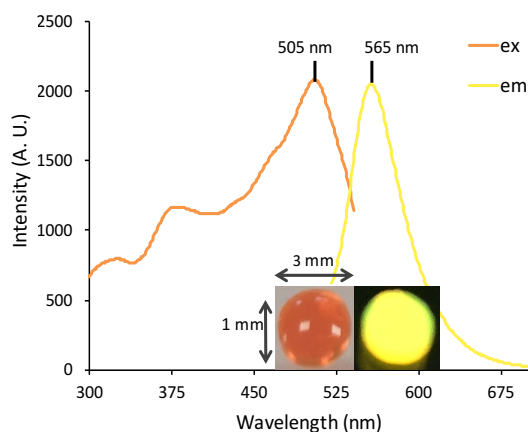


**Figure E11.** Excitation and fluorescence emission spectra for Ionogel 1 in pH 7.4 phosphate buffer, where the excitation wavelength is 505 nm and the corresponding emission wavelength is 565 nm.

## E.4 Fourier Transform Infrared Spectroscopy

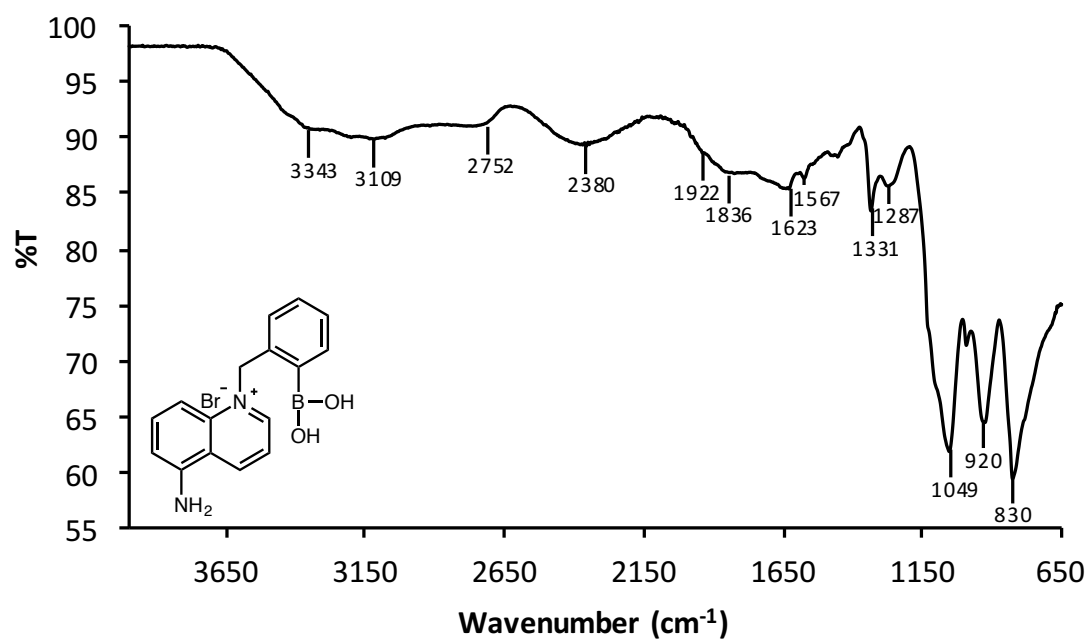


**Figure E12.** FT-IR spectrum for *o*-AminoBA, where the following peaks were found; 3343, 3109 (B-OH), 2752, 2380 (C=C-H), 1922, 1836 (C=C), 1623, 1567 (Amine N-H), 1331 cm<sup>-1</sup>.



## Part B – Fluorescence Quenching and Recovery Studies in Hydrogel Cocktails

### E.5 Fluorescence Spectroscopy

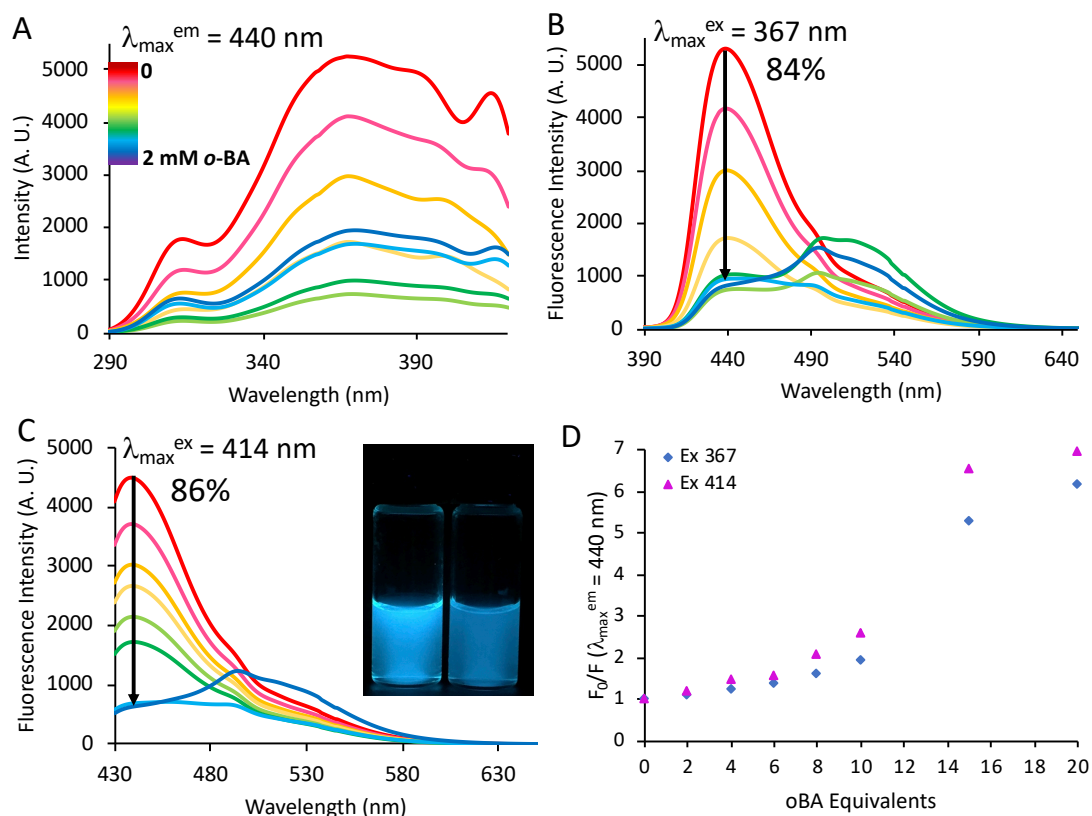


**Figure E13.** (A) Excitation spectrum for the acrylic acid (AA) cocktail in  $\text{H}_2\text{O}$ , containing pyranine (0.1 mM) and methylenebis(acrylamide) (MBIS) crosslinker titrated with *o*-BA (0-2 mM), corresponding to an emission wavelength of 440 nm. (B) Fluorescence emission spectrum with *o*-BA (0-2 mM) exhibiting a decrease in fluorescence by 84%, corresponding to an excitation wavelength of 367 nm. (C) Fluorescence emission showing a decrease by 86% titrated with *o*-BA (0-2 mM), corresponding to an excitation wavelength of 414 nm. The inset shows a photo of the AA-based cocktail before (left) and after (right) the addition of 2 mM *o*-BA, under 365 nm UV light. (D) Fluorescence emission at 440 nm as a function of *o*-BA equivalents present. Fluorescence parameters: 5 nm bandwidth, 250 V sensitivity, 1 nm data interval, 1 second response time, 500 nm/min scan speed.

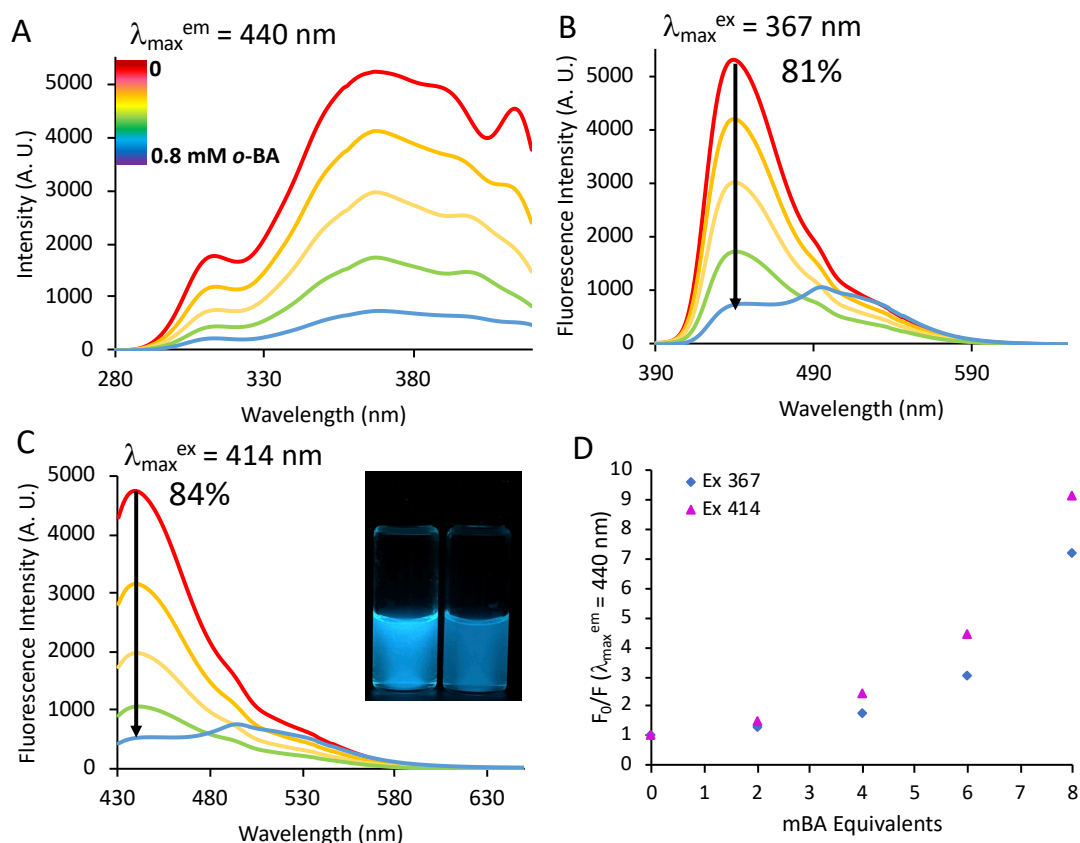


**Figure E14.** (A) Excitation spectrum for the AA cocktail in H<sub>2</sub>O, containing pyranine (0.1 mM) and methylenebis(acrylamide) (MBIS) crosslinker titrated with *m*-BA (0-0.8 mM), corresponding to an emission wavelength of 440 nm. (B) Fluorescence emission spectrum with *m*-BA (0-0.8 mM) exhibiting a decrease in fluorescence by 81%, corresponding to an excitation wavelength of 367 nm. (C) Fluorescence emission showing a decrease by 84% titrated with *m*-BA (0-0.8 mM), corresponding to an excitation wavelength of 414 nm. The inset shows a photo of the AA-based cocktail before (left) and after (right) the addition of 1 mM *m*-BA, under 365 nm UV light. (D) Fluorescence emission at 440 nm, as a function of *m*-BA equivalents present. Fluorescence parameters: 5 nm bandwidth, 250 V sensitivity, 1 nm data interval, 1 second response time, 500 nm/min scan speed.

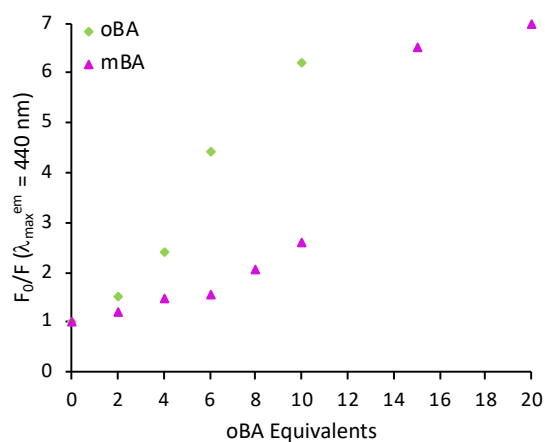


**Figure E15.** Fluorescence emission of the AA-based cocktail in the presence of increasing equivalents of *o*-BA and *m*-BA, respectively, when excited at 414 nm.

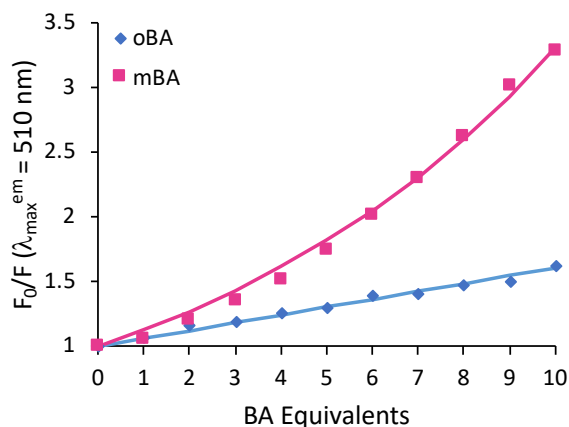


**Figure E16.** Fluorescence emission of the acrylamide-based cocktail in the presence of increasing equivalents of *o*-BA and *m*-BA, respectively, when excited at 460 nm.

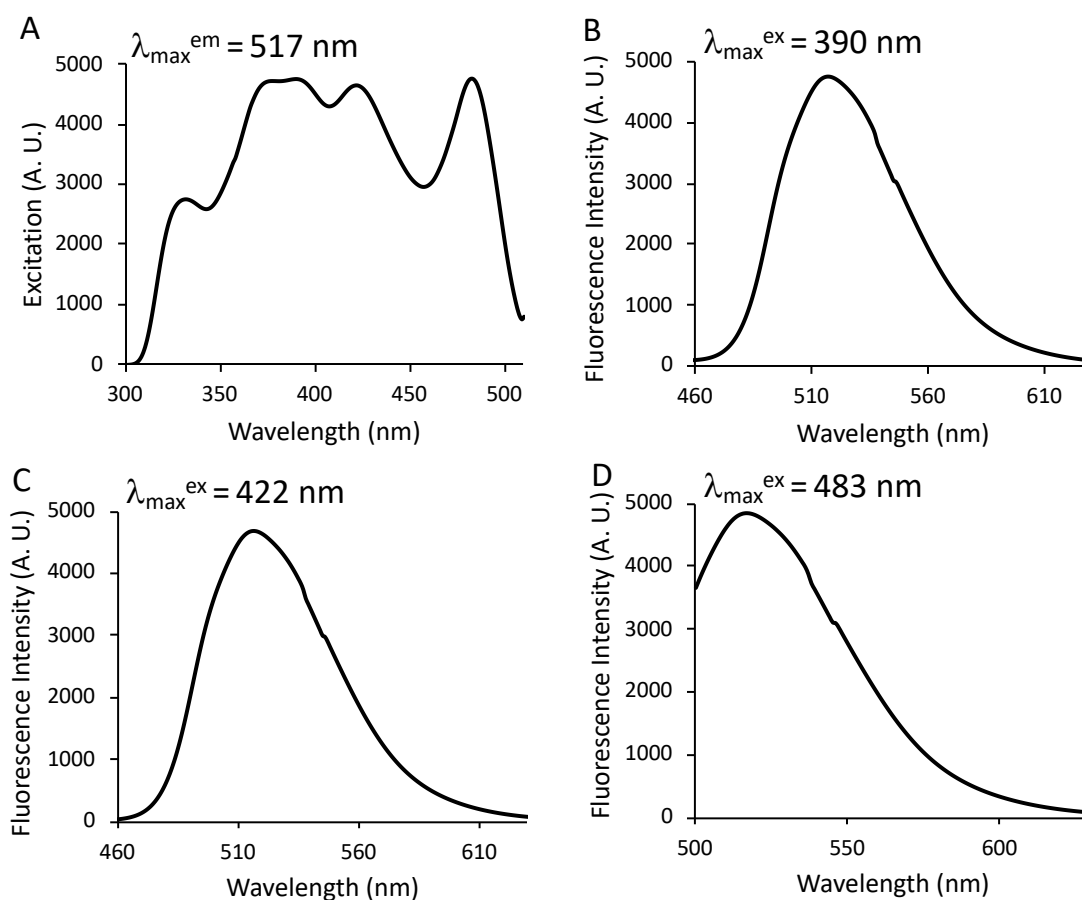


**Figure E17.** (A) Excitation spectrum for the 2-(dimethylaminoethyl)methacrylate (DMAEMA) cocktail in H<sub>2</sub>O, containing pyranine (0.1 mM) and MBIS crosslinker, corresponding to an emission wavelength of 517 nm. (B) Fluorescence emission spectrum, corresponding to an excitation wavelength of 390 nm. (C) Fluorescence emission spectrum, corresponding to an excitation wavelength of 422 nm. (D) Fluorescence emission spectrum, corresponding to an excitation wavelength of 483 nm. Fluorescence parameters: 5 nm bandwidth, 250 V sensitivity, 1 nm data interval, 1 second response time, 500 nm/min scan speed.

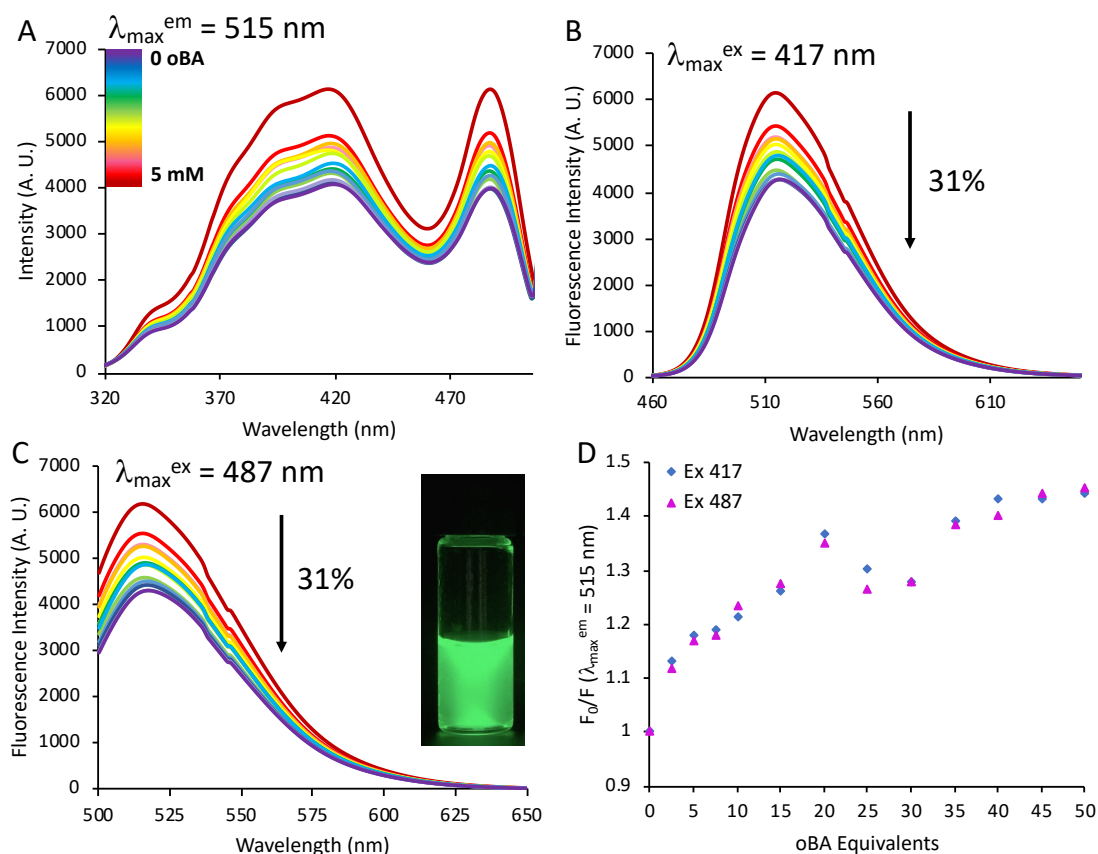


**Figure E18.** (A) Excitation spectrum for the 3-(dimethylaminopropyl)methacrylamide (DMAPMA) cocktail in  $\text{H}_2\text{O}$ , containing pyranine (0.1 mM) and MBIS crosslinker titrated with *o*-BA (0-5 mM), corresponding to an emission wavelength of 515 nm. (B) Fluorescence emission spectrum with *o*-BA (0-5 mM) exhibiting a decrease in fluorescence by 31%, corresponding to an excitation wavelength of 417 nm. (C) Fluorescence emission showing a decrease by 31% titrated with *o*-BA (0-5 mM), corresponding to an excitation wavelength of 487 nm. The inset shows a photo of the DMAPMA-based cocktail before (left) and after (right) the addition of 5 mM *o*-BA under 365 nm UV light. (D) Fluorescence emission at 515 nm, as a function of *o*-BA equivalents present. Fluorescence parameters: 5 nm bandwidth, 230 V sensitivity, 1 nm data interval, 1 second response time, 500 nm/min scan speed.

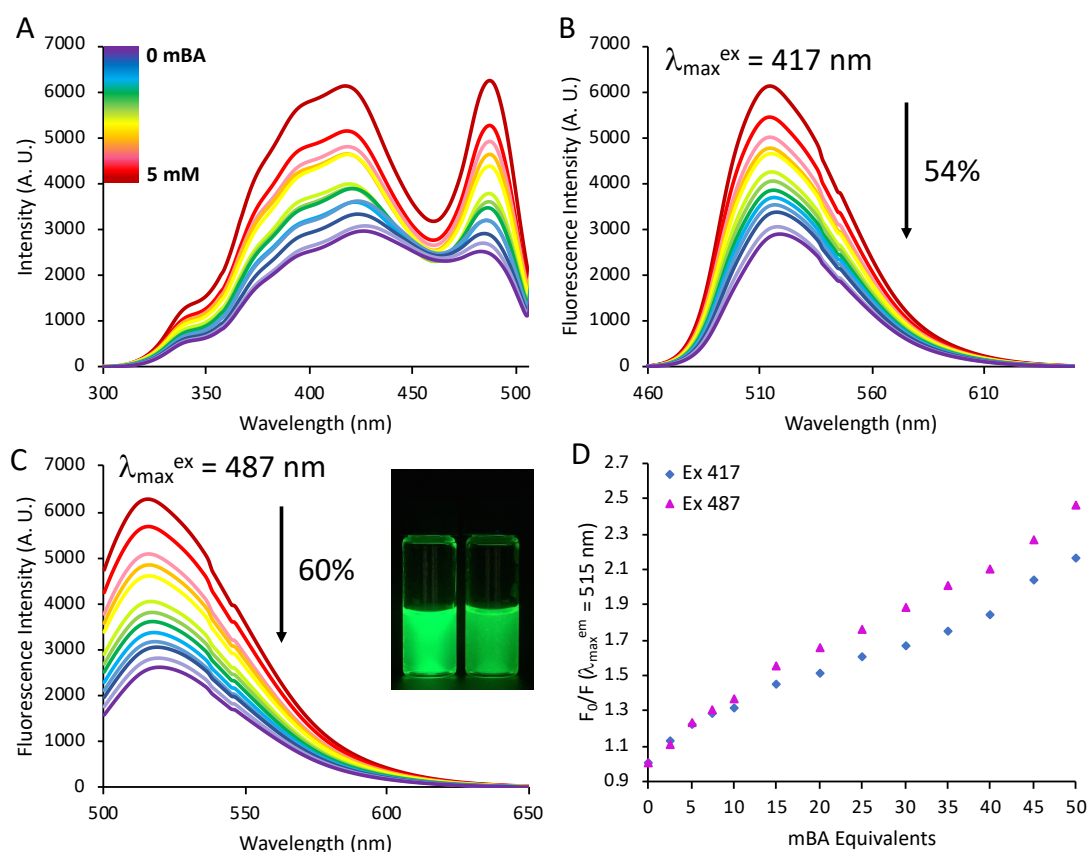


**Figure E19.** (A) Excitation spectrum for the DMAPMA cocktail in H<sub>2</sub>O, containing pyranine (0.1 mM) and MBIS crosslinker titrated with *m*-BA (0-5 mM), corresponding to an emission wavelength of 515 nm. (B) Fluorescence emission spectrum with *m*-BA (0-5 mM) exhibiting a decrease in fluorescence by 54%, corresponding to an excitation wavelength at 417 nm. (C) Fluorescence emission showing a decrease by 60% titrated with *m*-BA (0-5 mM), corresponding to an excitation wavelength at 487 nm. The inset shows a photo of the DMAPMA-based cocktail before (left) and after (right) the addition of 5 mM *m*-BA, under 365 nm UV light. (D) Fluorescence emission at 515 nm, as a function of *m*-BA equivalents present. Fluorescence parameters: 5 nm bandwidth, 230 V sensitivity, 1 nm data interval, 1 second response time, 500 nm/min scan speed.

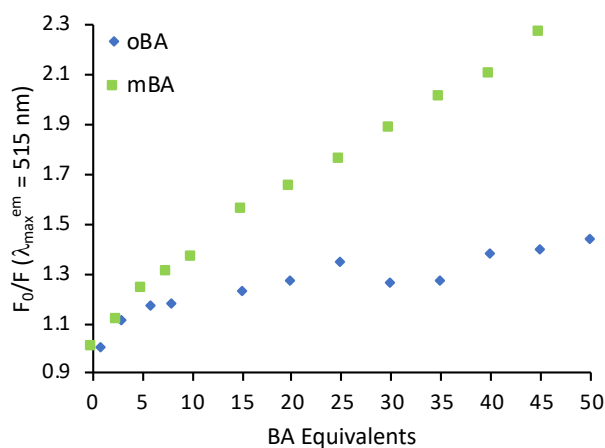


**Figure E20.** Fluorescence emission of the DMAPMA-based cocktail in the presence of increasing equivalents of *o*-BA and *m*-BA, respectively, when excited at 487 nm.

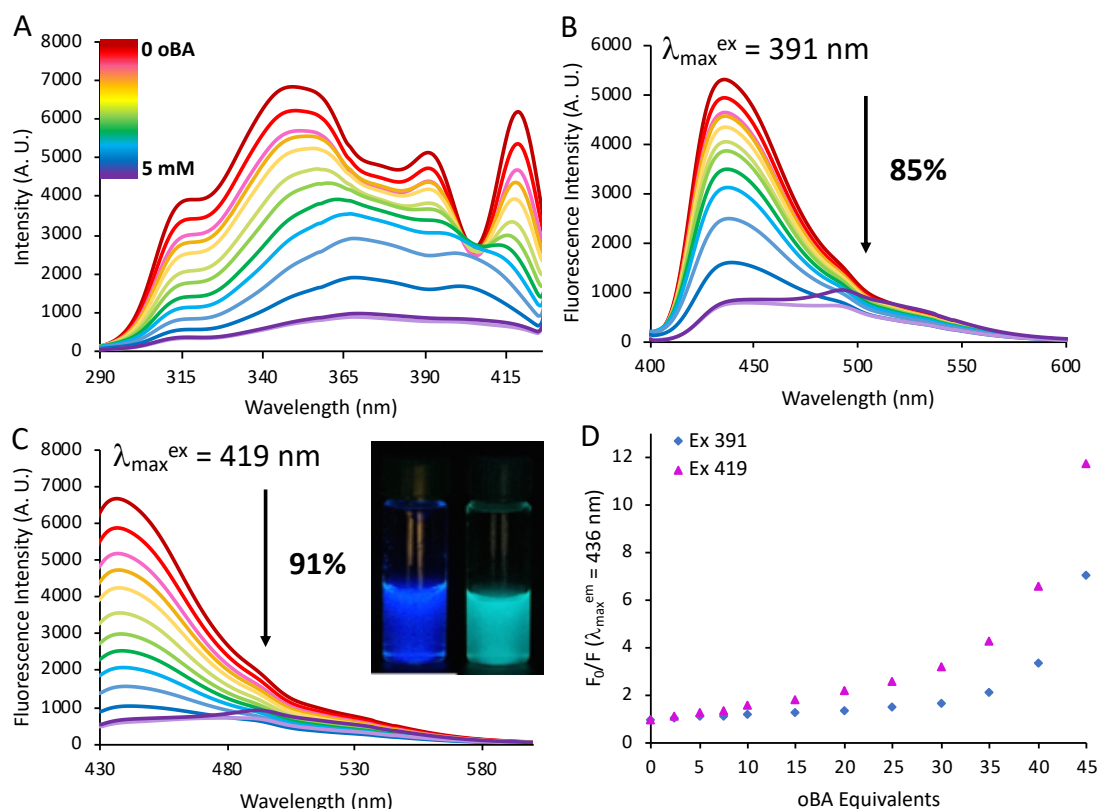


**Figure E21.** (A) Excitation spectrum for the 2-hydroxyethylmethacrylate (HEA) cocktail in H<sub>2</sub>O, containing pyranine (0.1 mM) and MBIS crosslinker titrated with *o*-BA (0-5 mM), corresponding to an emission wavelength of 436 nm. (B) Fluorescence emission spectrum with *o*-BA (0-5 mM) exhibiting a decrease in fluorescence by 85%, corresponding to an excitation wavelength of 391 nm. (C) Fluorescence emission showing a decrease by 91% titrated with *o*-BA (0-5 mM), corresponding to an excitation wavelength of 419 nm. The inset shows a photo of the HEA-based cocktail before (left) and after (right) the addition of 5 mM *o*-BA, under 365 nm UV light. (D) Fluorescence emission at 436 nm, as a function of *o*-BA equivalents present. Fluorescence parameters: 5 nm bandwidth, 250 V sensitivity, 1 nm data interval, 1 second response time, 500 nm/min scan speed.

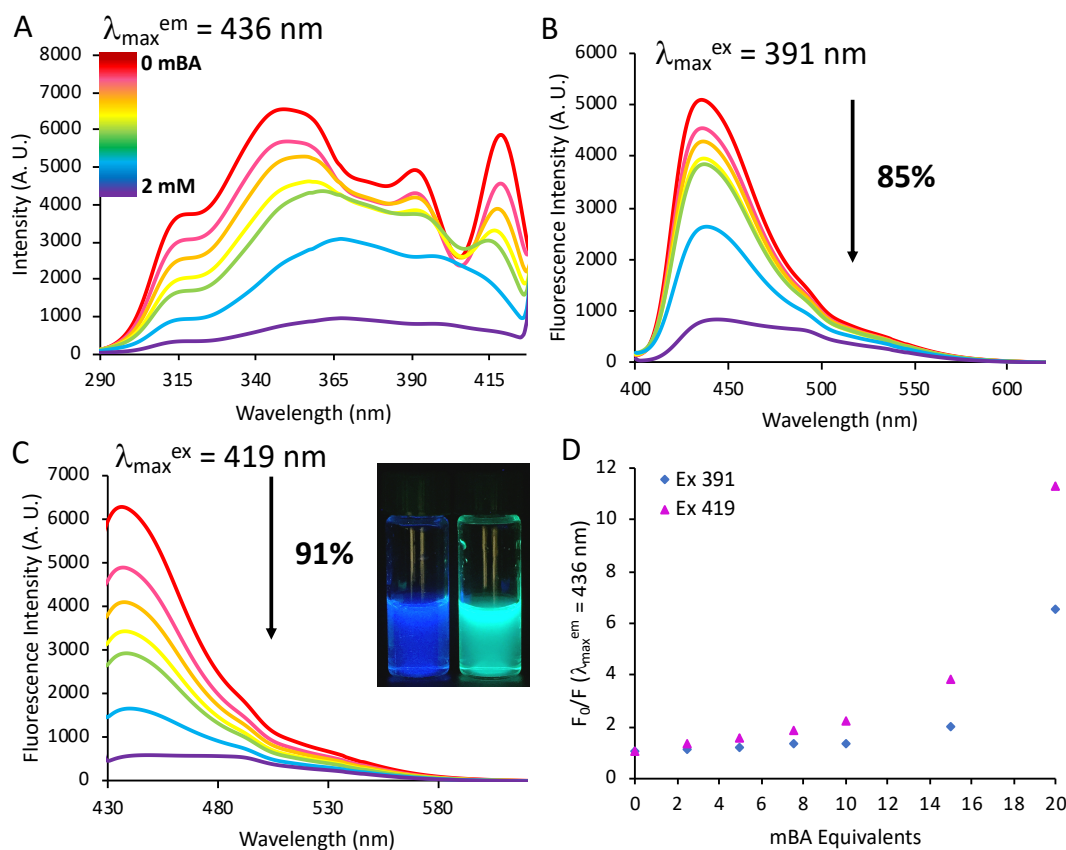


**Figure E22.** (A) Excitation spectrum for the HEA cocktail in H<sub>2</sub>O, containing pyranine (0.1 mM) and MBIS crosslinker titrated with *m*-BA (0-2 mM), corresponding to an emission wavelength of 436 nm. (B) Fluorescence emission spectrum with *m*-BA (0-2 mM) exhibiting a decrease in fluorescence by 85%, corresponding to an excitation wavelength of 391 nm. (C) Fluorescence emission showing a decrease by 91% titrated with *m*-BA (0-2 mM), corresponding to an excitation wavelength at 419 nm. The inset shows a photo of the HEA-based cocktail before (left) and after (right) the addition of 2 mM *m*-BA, under 365 nm UV light. (D) Fluorescence emission at 436 nm, as a function of *m*-BA equivalents present. Fluorescence parameters: 5 nm bandwidth, 250 V sensitivity, 1 nm data interval, 1 second response time, 500 nm/min scan speed.

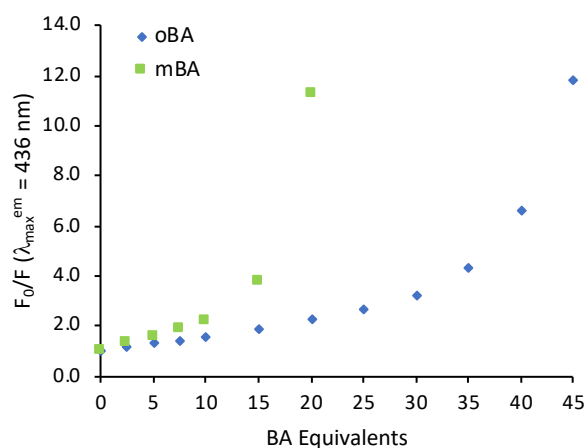


**Figure E23.** Fluorescence emission of the HEA-based cocktail in the presence of increasing equivalents of *o*-BA and *m*-BA, respectively, when excited at 419 nm.

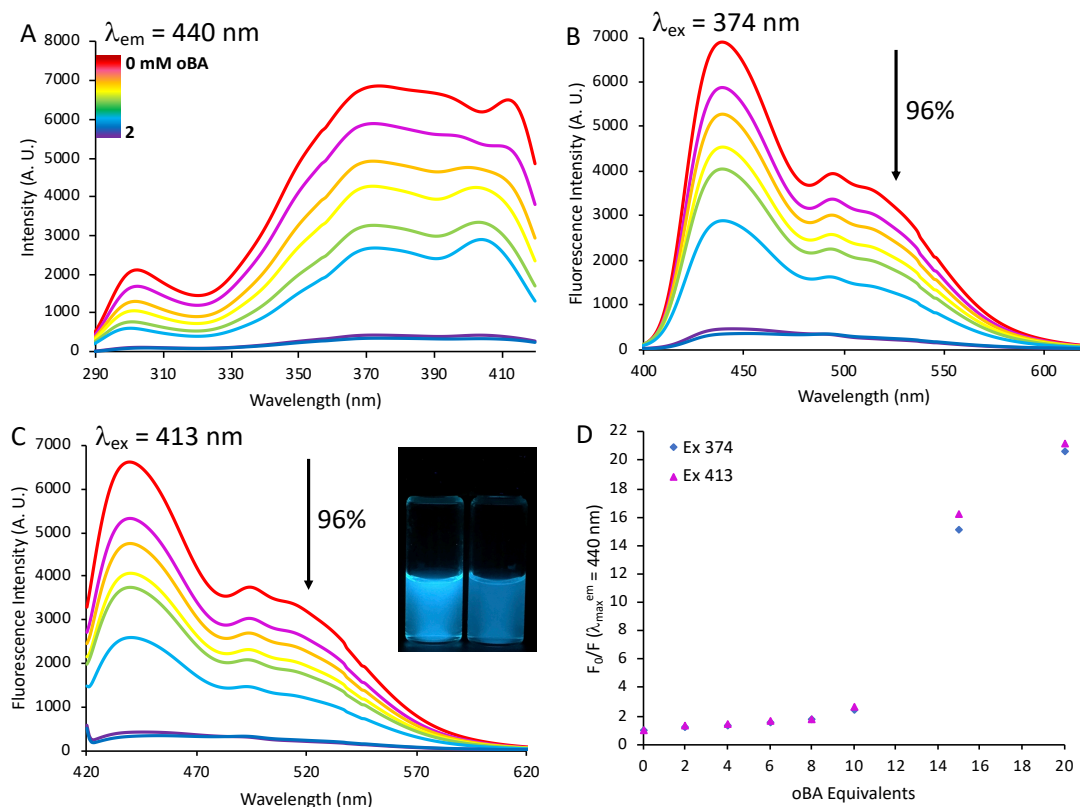


**Figure E24.** (A) Excitation spectrum for the methacrylic acid (MAA) cocktail in H<sub>2</sub>O, containing pyranine (0.1 mM) and MBIS crosslinker titrated with *o*-BA (0-2 mM), corresponding to an emission wavelength of 440 nm. (B) Fluorescence emission spectrum with *o*-BA (0-2 mM) exhibiting a decrease in fluorescence by 96%, corresponding to an excitation wavelength of 374 nm. (C) Fluorescence emission showing a decrease of 96% titrated with *o*-BA (0-2 mM), corresponding to an excitation wavelength at 413 nm. The inset shows a photo before (left) and after (right) the addition of 2 mM *o*-BA, under 365 nm UV light. (D) Fluorescence emission at 440 nm, as a function of *o*-BA equivalents present. Fluorescence parameters: 5 nm bandwidth, 250 V sensitivity, 1 nm data interval, 1 second response time, 500 nm/min scan speed.



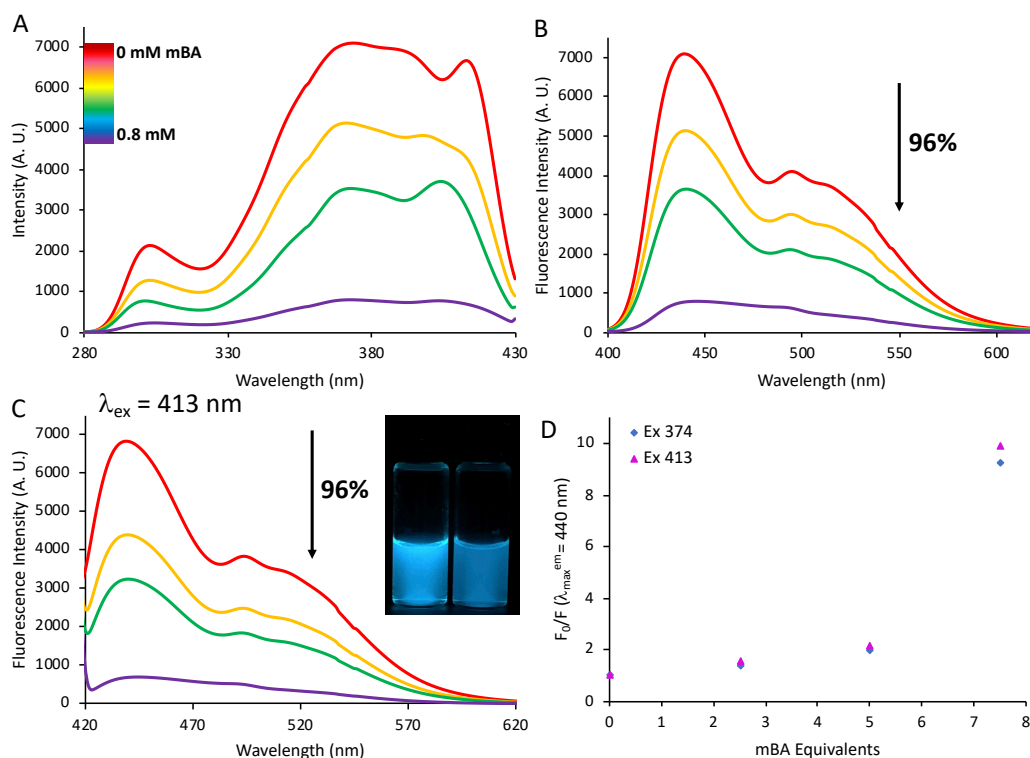


**Figure E25.** (A) Excitation spectrum for the MAA cocktail in H<sub>2</sub>O, containing pyranine (0.1 mM) and MBIS crosslinker titrated with *m*-BA (0-1 mM), corresponding to an emission wavelength of 440 nm. (B) Fluorescence emission spectrum with *m*-BA (0-1 mM) exhibiting a decrease in fluorescence by 90%, corresponding to an excitation wavelength of 374 nm. (C) Fluorescence emission showing a decrease by 90% titrated with *m*-BA (0-1 mM), corresponding to an excitation wavelength of 413 nm. The inset shows a photo before (left) and after (right) the addition of 1 mM *m*-BA, under 365 nm UV light. (D) Fluorescence emission at 440 nm, as a function of *m*-BA equivalents present. Fluorescence parameters: 5 nm bandwidth, 250 V sensitivity, 1 nm data interval, 1 second response time, 500 nm/min scan speed.

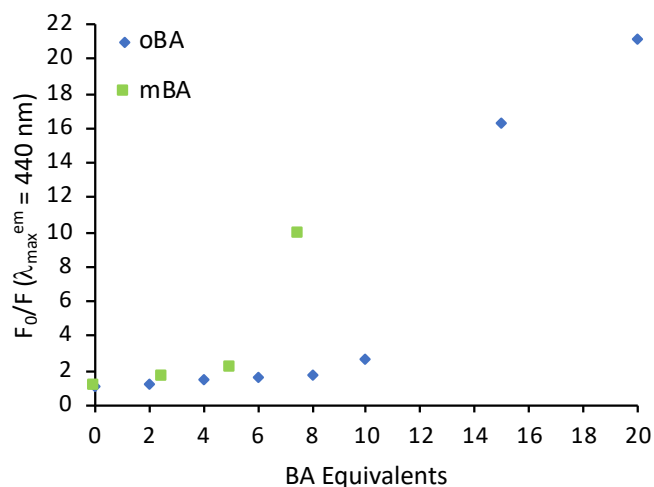


**Figure E26.** Fluorescence emission of the MAA-based cocktail in the presence of increasing equivalents of *o*-BA and *m*-BA, respectively, when excited at 413 nm.

## Part C – Layer-by-Layer Films Composed of BA Linear Polymers and Poly(vinyl sulfonate)

### E.6 Characterisation of BA Linear Polymers

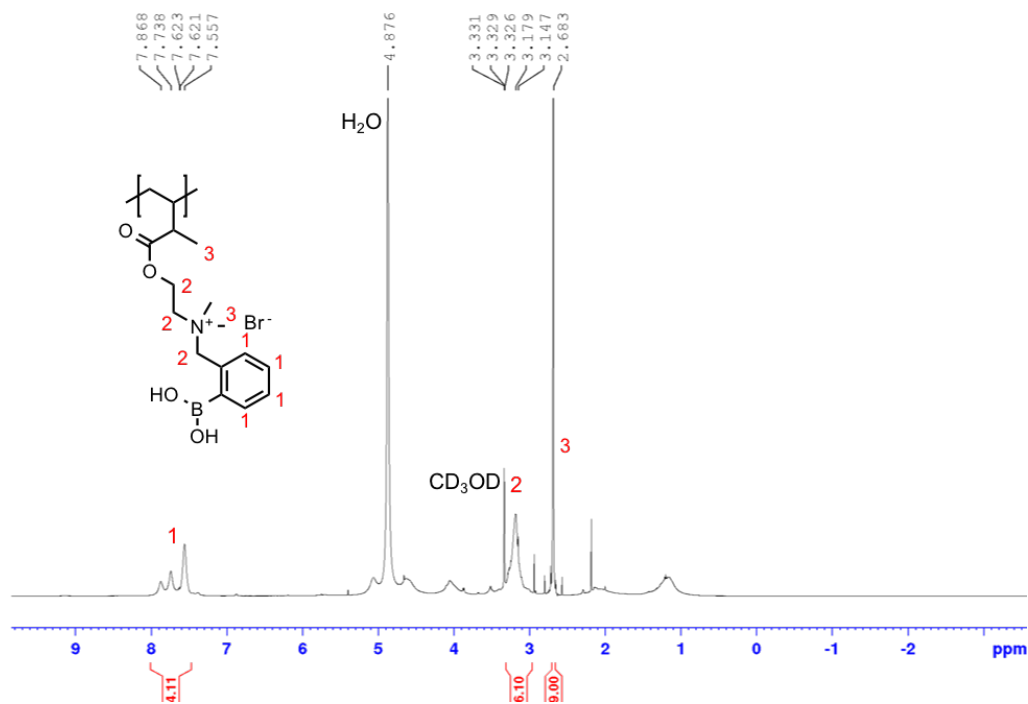


**Figure E27.** <sup>1</sup>H NMR for oBA LP, (600 MHz, 20 °C, CD<sub>3</sub>OD),  $\delta$ : 7.8-7.5 (4H, *m*, CH-1), 3.1 (6H, *m*, CH<sub>2</sub>-2), 2.6 (9H, *s*, CH<sub>3</sub>-3) ppm.

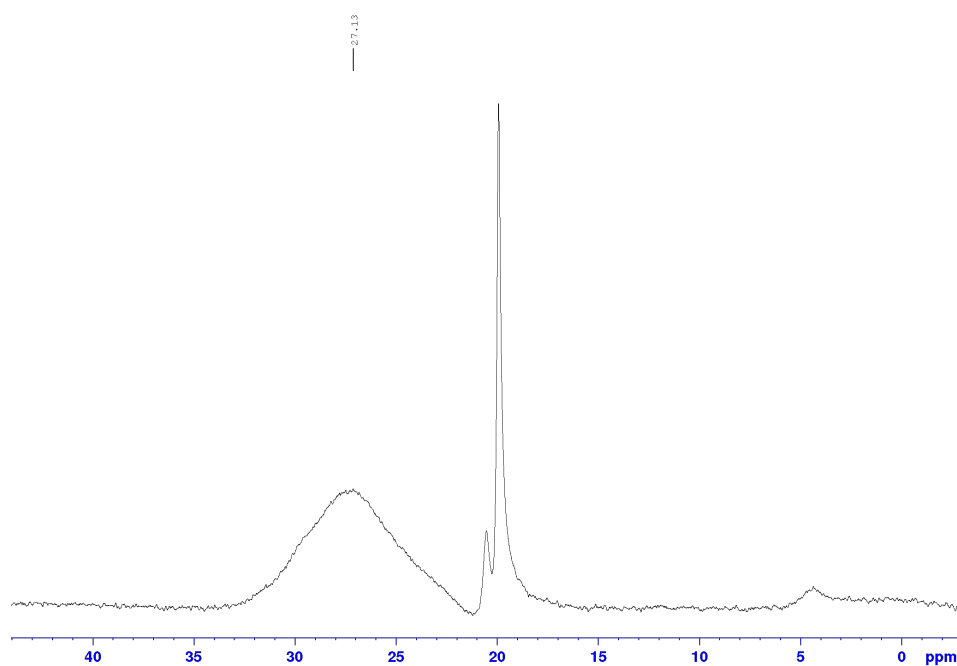


**Figure E28.** <sup>11</sup>B NMR for oBA LP, (192 MHz, 20 °C, D<sub>2</sub>O),  $\delta$ : 27.1 (1B, *s*, B(OH)<sub>2</sub>) ppm. Boric acid at 19.0 ppm. Line broadening by 10 Hz.

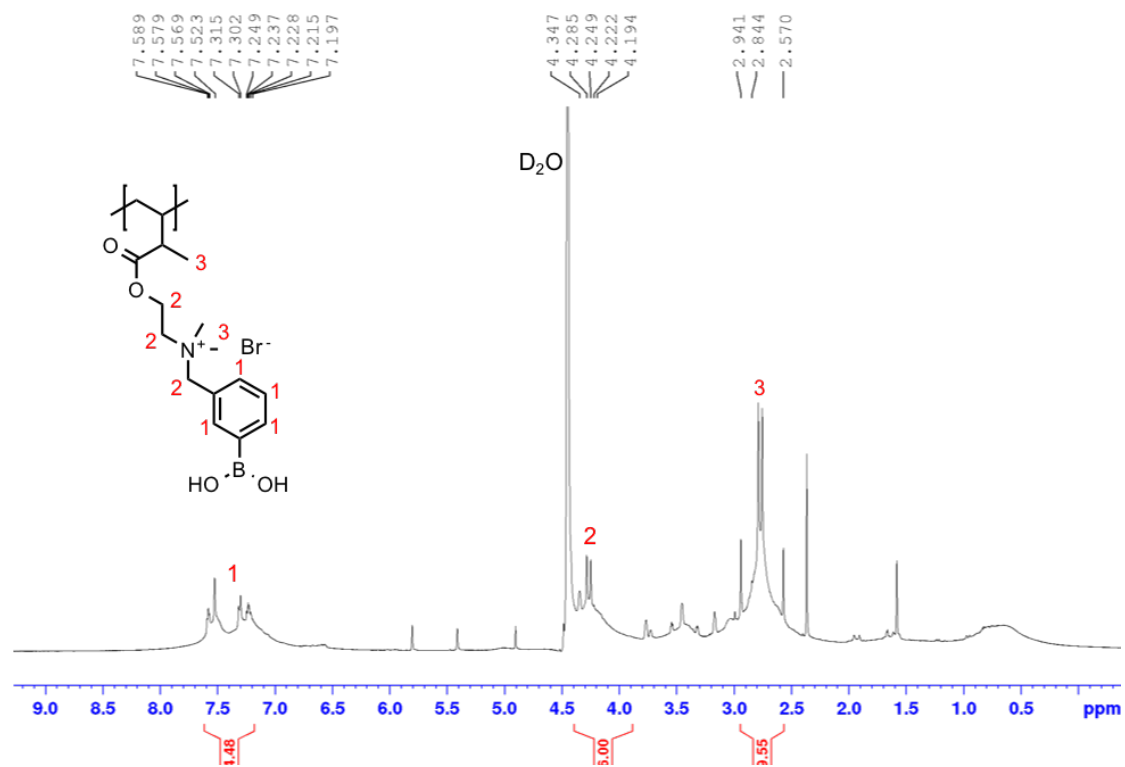


**Figure E29.**  $^1\text{H}$  NMR for mBA LP, (600 MHz, 20 °C,  $\text{D}_2\text{O}$ ),  $\delta$ : 7.6 (4H, *m*, CH-1), 3.2-3.1 (6H, *m*,  $\text{CH}_2$ -2), 2.5 (9H, *s*,  $\text{CH}_3$ -3) ppm.

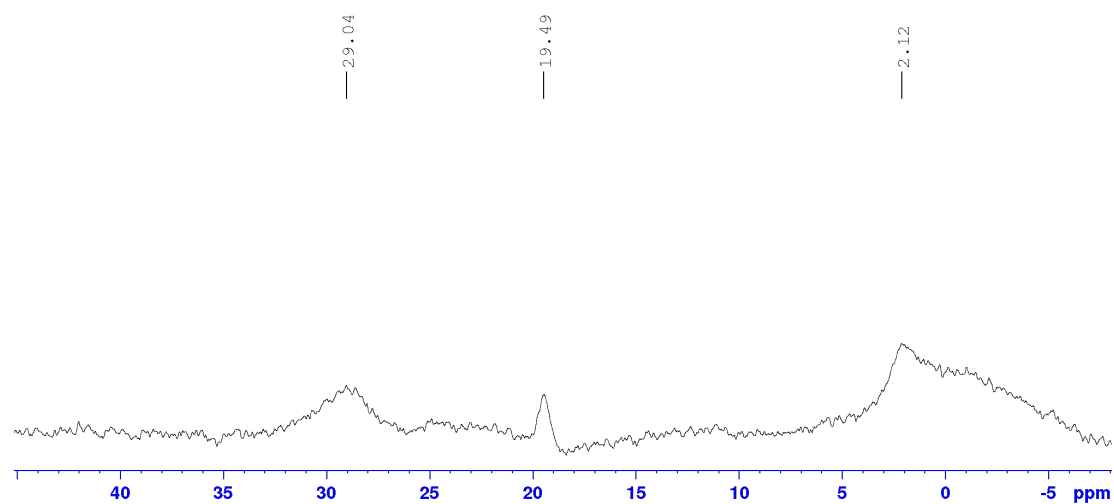


**Figure E30.**  $^{11}\text{B}$  NMR for pBA LP, (192 MHz, 20 °C,  $\text{D}_2\text{O}$ ),  $\delta$ : 29.0 (1B, *s*,  $\text{B}(\text{OH})_2$ ), 2.1 (*s*,  $\text{B}(\text{OH})_3$ ) ppm. Boric acid at 19.4 ppm. Line broadening by 10 Hz.

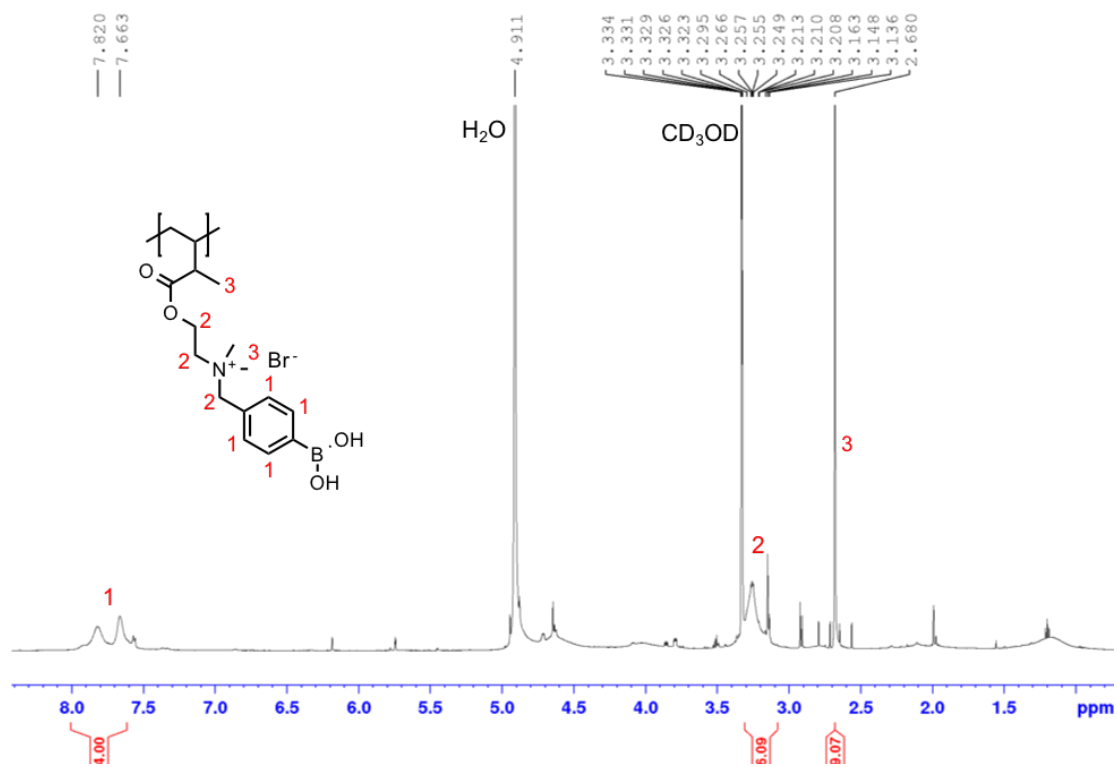


**Figure E31.**  $^1\text{H}$  NMR for pBA LP, (600 MHz, 20 °C,  $\text{CD}_3\text{OD}$ ),  $\delta$ : 7.6 (4H, *m*, CH-1), 3.2-3.1 (6H, *m*,  $\text{CH}_2$ -2), 2.5 (9H, *s*,  $\text{CH}_3$ -3) ppm.

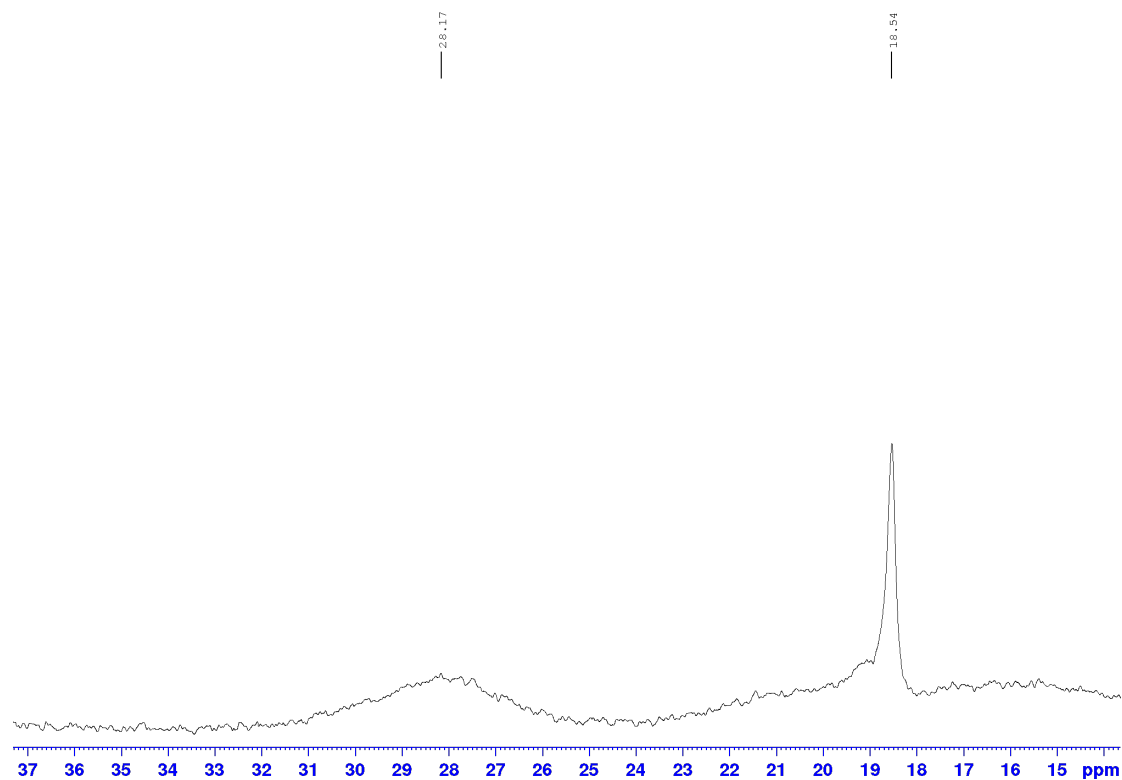


**Figure E32.**  $^{11}\text{B}$  NMR for pBA LP, (192 MHz, 20 °C,  $\text{CD}_3\text{OD}$ ),  $\delta$ : 28.1 (1B, *s*,  $\text{B}(\text{OH})_2$ ) ppm. Boric acid at 18.5 ppm. Line broadening by 20 Hz.

## E.7 Assembly and Disassembly of (PEI/PVS)<sub>2</sub>(BA LPs/PVS)<sub>5</sub> Films

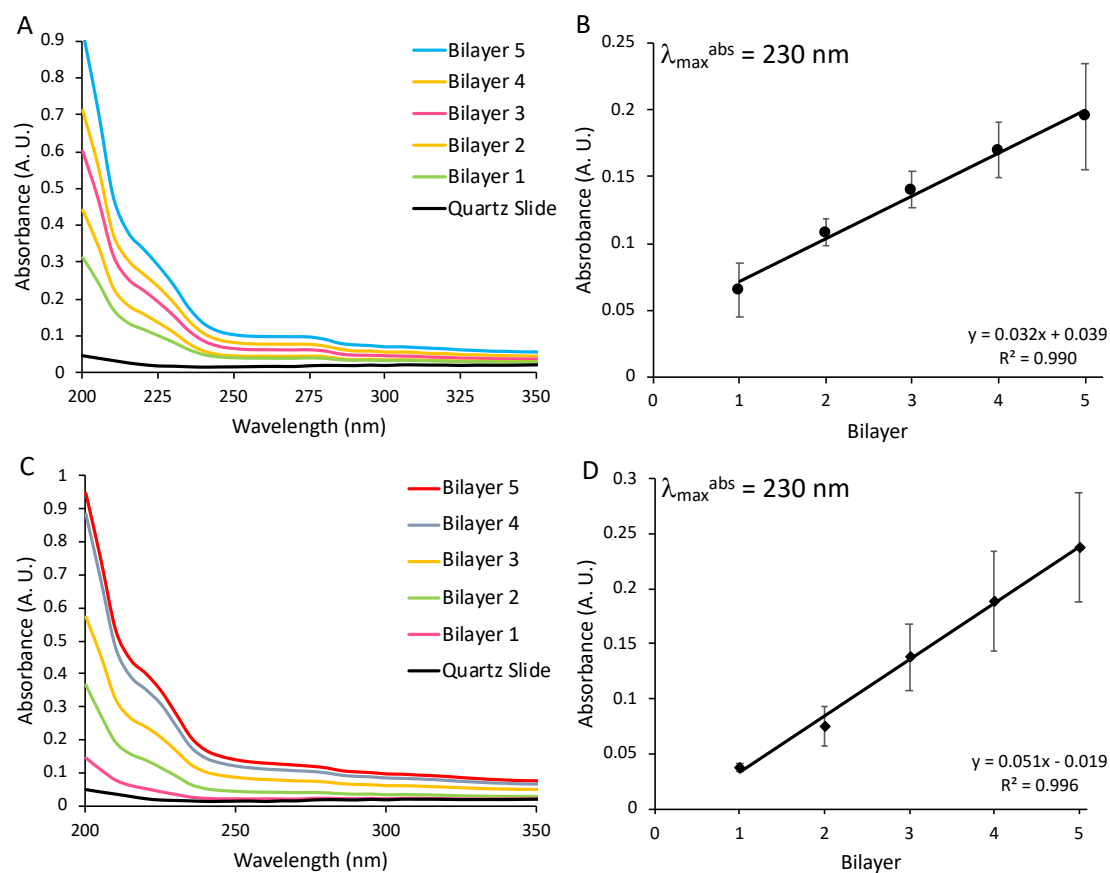


**Figure E33.** Left: Absorbance spectra for the assembly of the (PEI/PVS)<sub>2</sub>(oBA LP/PVS)<sub>5</sub> film (top) and the (PEI/PVS)<sub>2</sub>(mBA LP/PVS)<sub>5</sub> film (bottom). Right: Linear increase of the absorbance at 230 nm vs. the bilayer number. The points on the curve represent the mean ( $n = 3$ )  $\pm$  the standard deviation.

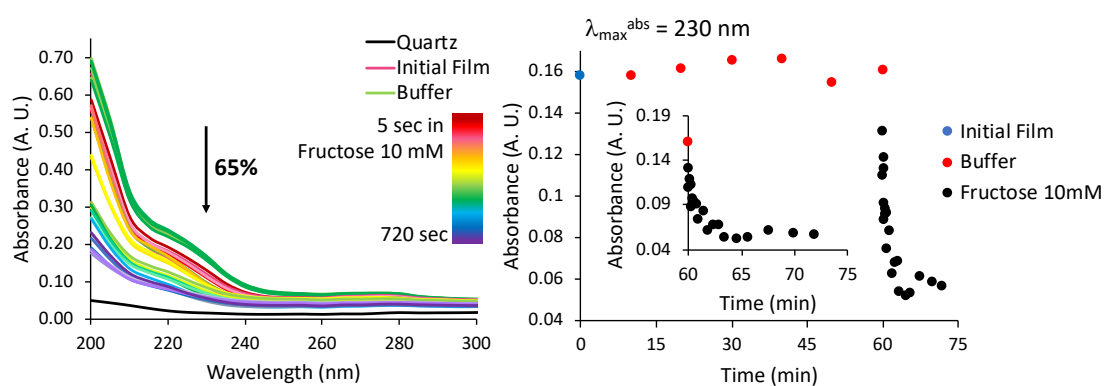


**Figure E34.** Absorbance spectra for the disassembly of the (PEI/PVS)<sub>2</sub>(oBA LP/PVS)<sub>5</sub> film with 10 mM fructose at pH 7.4 (left) and the absorbance curve when monitored at a detection wavelength of 230 nm (right), where the blue circle is the initial absorbance of the film, the red circles indicate the equilibrium time in pH 7.4 buffer and the black dots represent the film disassembly.

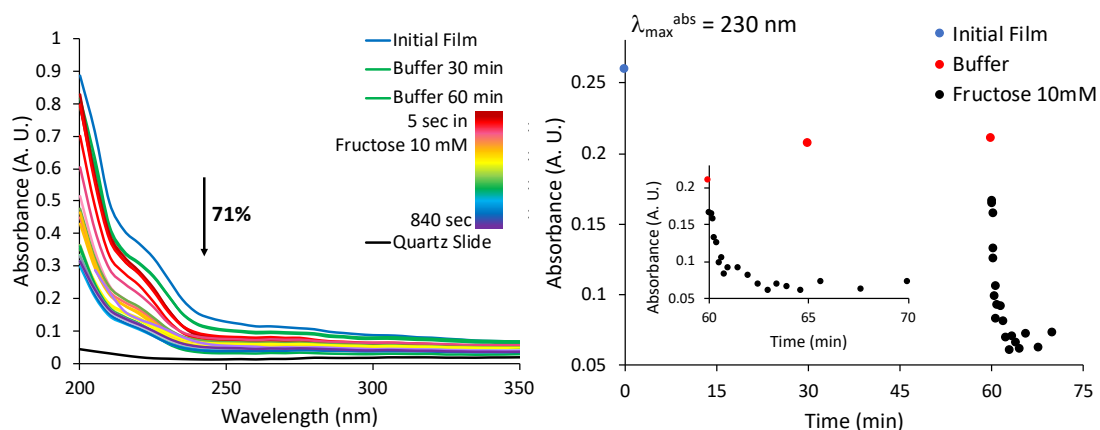


**Figure E35.** Absorbance spectra for the disassembly of the  $(\text{PEI/PVS})_2(\text{mBALP/PVS})_5$  film with 10 mM fructose at pH 7.4 (left) and the absorbance curve when monitored at a detection wavelength of 230 nm (right), where the blue circle is the initial absorbance of the film, the red circles indicate the equilibrium time in pH 7.4 buffer and the black dots represent the film disassembly.

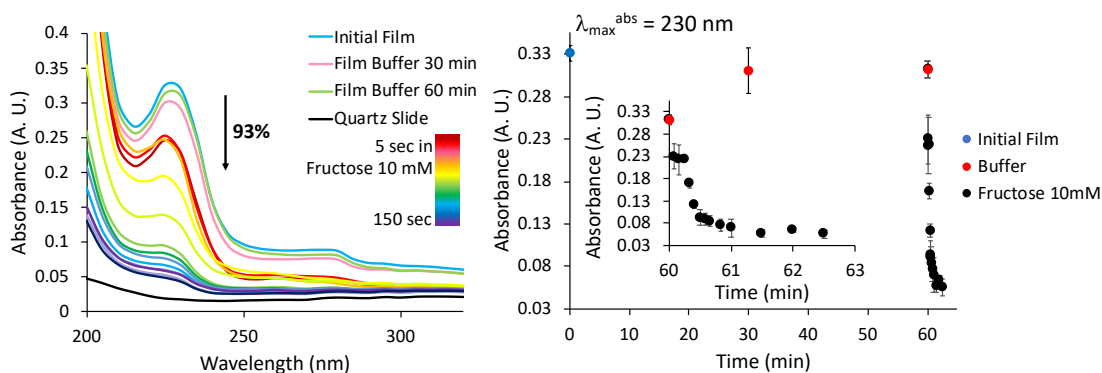


**Figure E36.** Absorbance spectra for the disassembly of the  $(\text{PEI/PVS})_2(\text{pBALP/PVS})_5$  film in 10 mM fructose (left) and the average absorbance on the curve ( $n = 3$ ) was taken at 230 nm, illustrating the disassembly of the LbL film. The points on the curve represent the mean  $\pm$  the standard deviation.